Nonlinear Finite Element Analysis of Reinforced Concrete Slab-Column Connections with Headed Stud/Bolt Shear Reinforcement Subjected to Punching Shear

by

Patrick Michel Beaulieu

A thesis
presented to the University of Waterloo
in fulfillment of the
thesis requirement for the degree of
Master of Applied Science
in
Civil Engineering

Waterloo, Ontario, Canada, 2022

© Patrick Michel Beaulieu 2022

Author’s Declaration

I hereby declare that I am the sole author of this thesis. This is a true copy of the thesis, including any required final revisions as accepted by my examiners.

I understand that my thesis may be made electronically available to the public.

Abstract

While many experimental tests have been conducted by various researchers on the punching behaviour of reinforced concrete flat slabs supported on columns with headed stud/bolt shear reinforcement, there are still many parameters which have not been adequately studied in the laboratory due to cost or time constraints. As a result much of the current code provisions for designing slab-column connections against punching shear are based on empirically derived formulations based on tests of partial scale isolated slab-column specimens. Researchers such as Genikomsou and Polak (2015), Navarro et al (2018), and Lapi et al (2020) have proven that these experimental tests can be supplemented using properly calibrated nonlinear finite element analysis (NLFEA) models in the commercial software ABAQUS.

In this thesis a three-dimensional NLFEA model is calibrated using interior slab-column connection specimens tested by Adetifa and Polak (2005) in concentric punching and exterior slab-column connection specimens tested by El-Salakawy et al (1998, 2000) in punching with unbalanced moment. This calibration uses the concrete damaged plasticity (CDP) model in ABAQUS, and includes discussion of the main parameters which influence the CDP model and values used in this calibration. The calibration also includes a study conducted to determine how to effectively model the shear reinforcement and shear reinforced area based on the "stem-star" method used by Genikomsou and Polak (2016). This includes a detailed analysis of the modelling of the shear stud star (S3) diameter to ensure enough rotational capability was provided in the shear reinforced region of the slab without significantly reducing the predicted capacity of the model. Through this study it was determined that a gap of 6-10mm should be provided between the column face and the first S3, and that the S3 diameter of subsequent rows of shear reinforcement had a negligible effect on connection behaviour. Additional effects such as changing the moment-shear ratio and the effect of adding openings near the column were also considered during calibration.

These calibrated models are then used to conduct several parametric studies on parameters related to the shear reinforcement in the specimens. Three parametric studies are presented in this thesis. The first study investigates the effect of changing the number of shear reinforcement rows and the spacing between adjacent rows of shear reinforcement. In this study it was determined that the total shear reinforced area has a larger effect on the connection than the number of reinforcement rows, and that when spaced between 0.75d and 1.5d no inter-stud punching could occur in any of the models.

The second study investigated the effect of changing the size and number of openings adjacent to the column, and the change in placement of shear reinforcement which must occur as a result of the opening changes. This study determined that 90% of the connection capacity was maintained when the opening width to column width ratio was 0.6 for two openings and 0.33 for four openings. This study also determined that providing stud rails outside of the openings in a double-cruciform arrangement has no significant effect on the behaviour of the shear reinforcement when compared to their usual placement.

Finally, the third study investigated the impact of anchorage-controlled shear reinforcement, which was proposed by Topuzi et al (2017) to increase the ductility of slab-column connections under cyclic loading without inducing higher lateral stresses in the connection, on the overall capacity of the connections. In this study it was determined that the inclusion of anchorage-controlled shear reinforcement results in less than a 10% drop in concentric punching connection capacity for all considered connections, and therefore could be suitable for inclusion in slab-column connections as proposed by Topuzi et al (2017).

Acknowledgements

Firstly, I would like to thank my supervisor and mentor Dr. Marianna Polak. When I was finishing my undergraduate degree and was completely unprepared for the world of graduate research she was gracious enough to discuss potential projects, ideas, and eventually to take me onto her team. Throughout these two years of research she has been instrumental in keeping me on track and helping me think through problems in interesting and useful ways.

I would like to acknowledge the funding for my research which was provided by the Natural Sciences and Engineering Research Council (NSERC).

I would like to thank the Polak Army members that were with me as we completed this journey: Graeme Milligan, Ryan Barrage, Katherine Liu, Leila Miri, Amin Izadi, Phillip Lochan, Dr. Shenglin Wang, and Dr. Pejoohan Tavassoti. The team have been instrumental at giving me feedback at all points of my research and helping me navigate graduate life. I would especially like to thank Graeme, for answering all of the (too many) questions I had about ABAQUS and slabs in general, and Ryan, for helping me automate my models through many lines of Python code.

I would like to thank my thesis reviewers, Dr. Marianna Polak, Dr. Trevor Hrynyk, and Dr. Stanislav Potapenko for taking the time to read my thesis and providing me with useful feedback.

I also would like to extend my gratitude to all of the professors at the University of Waterloo who have helped me get into the wonderful world of concrete throughout my undergraduate and graduate degrees. I would like to thank Richard Morrison, for all for all of the hands-on concrete experience that he's given me during my schooling and as a part of the Concrete Canoe/Toboggan Team.

Finally, I would like to thank my friends and family for all of their support over the last two years. My parents, Mike and Terri, for all of the emotional and financial support they have given me. My brother Cameron, for not making fun of me too much for making more money than me. My roommates and close friends: Robel Berhane, Brody Gartner, Juan Nino, Lukas Heppenstrijdt, Jacob Runstedler, and Sean Begy, for distracting me enough to keep me sane but not enough to prevent me from finishing this on time. My civil engineering friends: Rachel McMullan, Rudi Rendel, Sam Sherlock, Sam Chum, and Fook-Ye Yang, for being there to talk to about masters work, industry, and for just being great people. And lastly my uncle, Dr. Tarek Saleh, by who's guidance I started on this journey in the first place. This thesis would not have been responsible without all of their support.

Table of Contents

List of Figures

List of Tables

1.0 Introduction

1.1 Research Significance

Reinforced concrete flat slabs supported directly on columns are one of the most common structural systems in reinforced concrete buildings. They provide several benefits over slab supported on beams, including increased story height, decreased construction cost and ease of constructability. One of the most important considerations when designing this type of structural system is the existence of a complicated three-dimensional stress state near the connection of the slab and the supporting columns. If not reinforced correctly, this stress state can lead to a punching failure of the slab. Punching failures are typically brittle and can lead to the progressive collapse of an entire structure, which makes the safe design against punching shear imperative. Increasing the punching shear capacity of a slab-column connection can be done in many ways; such as increasing the size of the column or depth of the slab, increasing the strength of the concrete, or increasing the flexural reinforcement ratio of the slab (which is not accounted for in American design codes).

Possibly the most effective method of increasing the punching capacity is to outfit the slab with shear reinforcement in the punching zone. Various methods of (typically steel) shear reinforcement have been developed to combat punching and increase the ductility of slab-column connections. One popular method is the inclusion of headed stud rails in new construction, or post-installed headed bolts for retrofitting a structure. When properly designed these studs/bolts prevent shear cracks from opening within the slab near the columns, thereby increasing the punching resistance beyond the load required to fully yield the slab's flexural reinforcement. Failure of the slab through yielding of the flexural reinforcement is ductile, and therefore ensuring that flexural failure occurs prior to shear failure guarantees the ductility of the system. For many connections, the inclusion of shear reinforcement is imperative for the safe design of concrete flat slabs.

Reinforced concrete slab-column connections have been studied for many years, and several researchers have conducted extensive test programs to assess the behaviour of these connections under various loading conditions with and without shear reinforcement (ie. Elstner and Hognestad, 1956; Moe, 1961; Mowrer and Vanderbilt, 1967; Long and Masterson, 1974; Corley and Hawkins, 1968; Elgabry and Ghali, 1987; and Yamada et al, 1992). However, conducting a test on a full-scale slab column connection requires a significant cost and time investment, and because of this many parameters have not been adequately addressed in tests. As a result, much of the current code provisions for designing slab-column connections against punching shear are based on empirically derived formulations based on tests of partial scale isolated slab-column specimens.

More recently, researchers have started to investigate non-linear finite element analysis (NLFEA) as an alternative testing method to supplement experimental databases and allow for the measurement of quantities that would be difficult or costly to measure in the laboratory. The earliest attempts at using NLFEA to assess the punching behaviour of slab-column connections were fairly basic and utilized one dimensional elements (ie. Masterson and Long, 1974). Later, researchers developed two dimensional formulations using basic elements perpendicular to the slab direction (ie. González-Vidosa et al, 1988; Hallgren, 1996; Menétrey et al, 1997) or layered shell elements which capture the three-dimensional behaviour of the slab were subsequently used for the analyses (ie. Polak, 1998; Guan and Polak, 2007). Recently, many researchers have utilized three-dimensional NLFEA models of full-scale slab-column connections and have been able to accurately predict the punching behaviour of slab-column connections

when compared to experimental results (ie. Winkler and Stangenberg, 2008; Eder et al, 2010, Genikomsou and Polak, 2015; Navarro et al, 2018, Lapi et al, 2020). However, utilizing NLFEA requires calibration of an adopted material model for concrete and the selection of proper modelling parameters based on selected experimental results.

1.2 Research Objectives

This thesis presents a rational method for the modelling of reinforced concrete slab-column connections subjected to punching shear with headed stud or bolt shear reinforcement in the commercial finite element software ABAQUS using the software's concrete damaged plasticity (CDP) model to model the concrete connection. The CDP model has been successfully calibrated and used by many researchers to model concrete in various applications, including by previous researchers at the University of Waterloo (Genikomsou, 2015; Stoner, 2015; Barrage, 2017; Milligan, 2018).

In this thesis the calibration of the NLFEA model in ABAQUS was conducted based on the results of two experimental programs which investigated the effect of shear stud/bolt reinforcement at the University of Waterloo. In 2005, Adetifa and Polak tested six interior slab-column connections with shear bolt reinforcement in concentric punching, and observed that the shear bolts successfully prevented the propagation of shear cracks and improved the ductility of slab-column connections with and without openings. Between 1998 and 2000, El-Salakawy et al tested many edge slab-column connections subjected to concentric load and unbalancing moment with shear studs and shear bolts. Several parameters were observes such as the effect of openings and the effect of moment-shear ratio. Eight of these specimens were chosen for the calibration of this NLFEA model.

Once calibrated, the NLFEA model presented in this thesis was used to conduct several parametric studies based on the calibrated specimens. The first study investigates the effect of changing the number of shear reinforcement rows and the spacing between adjacent rows of shear reinforcement in the specimen series. The second study investigates the effect of changing the size and number of openings adjacent to the column, and the change in placement of shear reinforcement which must occur as a result of the opening changes. Finally the third study investigates the impact of anchorage-controlled reinforcement, which was proposed by Topuzi et al (2017) to increase the ductility of slab-column connections under cyclic loading without inducing higher lateral stresses in the connection, on the overall capacity of the connections. The specific objectives of this thesis are to:

1. Summarize the history of slab-column connection tests in punching shear with and without shear reinforcement, and the history of finite element analysis of slab-column connections in punching shear. Also summarize previous mechanical models and code provisions related to punching shear in reinforced concrete slabs supported on columns;

2. Develop a calibrated three-dimensional NLFEA model using the CDP model in ABAQUS which accurately predicts the behaviour of slab-column connections with shear stud/bolt reinforcement under various loading conditions;

3. Investigate the effect of the number and spacing of shear stud/bolt rows on the punching behaviour of a slab-column connection under various loading conditions;

4. Investigate the effect of the number and size of openings on the punching behaviour of a slab-column connection reinforced with stud/bolt reinforcement and;

5. Investigate the effect of the inclusion of anchorage-controlled reinforcement on the capacity and ductility of slab-column connections compared to those outfitted with traditional stud/bolt reinforcement under various loading conditions.

1.3 Thesis Outline

This thesis is presented as follows:

Chapter 1 provides a brief introduction to the research problem, the objectives which this thesis aims to address, and the outline of the thesis structure. Chapter 2 begins by discussing the punching shear phenomenon, and then provides a literature review of existing tests of slab-column connections in punching shear both with and without shear reinforcement. The literature review continues by discussing previous applications of finite element analysis to slab-column connections in punching shear, outlining previous mechanical models used to describe punching shear, and finally concludes by outlining several current design code provisions for punching shear in reinforced concrete slabs. Chapter 3 provides background knowledge necessary for understanding the NLFEA calibration methodology, including a discussion of the mechanics of the CDP model in ABAQUS and a description of the two series of test specimens used to calibrate the NLFEA model. Chapter 4 provides the methodology used to calibrate the NLFEA model, including discussions of material parameters, CDP parameters, mesh parameters and boundary conditions. The main parameter discussed is the method used to model the shear reinforcement, and specifically a calibration of the amount of confinement provided by the shear studs/bolts is presented. Chapter 5 presents several methods which were used to confirm the capability of the model in predicting the punching behaviour of the test specimens it was calibrated on. Chapter 6 presents the three parametric studies which were conducted using the calibrated models; the number and spacing of shear reinforcement rows study, the number and size of openings study, and the inclusion of anchorage-controlled reinforcement study. For each study an overview of the study objectives is presented, and then a detailed discussion of the study results is provided. Finally, Chapter 7 presents a summary of the research and conclusions based on the calibration and parametric study results, and finishes with guidance for future work to be conducted in this area.

2.0 Punching Shear in Reinforced Concrete Slabs

2.1 Introduction to the History of Punching Shear in Concrete Slabs

The structural system of a concrete flat slab supported on monolithic concrete columns was first presented by George M. Hill in 1900. This system was then first put into practice for the construction of various buildings for the Central Railroad of New York, at Elizabethport New Jersey in 1901 (Gasparini, 2002). Another interpretation of this system was patented by Orlando W. Norcross in 1902. This system contained four-way steel reinforcement and aimed to exist without any need for horizontal members such as beams or joists. However, this system was deemed impractical for construction, and no buildings using the system were ever built (Gasparini, 2002).

Two of the major contributors to early reinforced concrete flat slab systems were Robert Maillart in Switzerland, and Claude A. P. Turner in the USA, who invented very similar flat slab systems independently of each other. Turner designed his first reinforced concrete flat slab building, the Johnson-Bovey building in Minneapolis, in 1906. The flat slab contained four-way longitudinal steel reinforcement and large "mushroom" column capitals that were almost half a span in diameter for shear reinforcement (Gasparini, 2002). These large "mushroom" capitals would become a staple of early flat slab construction to mitigate the known deficiencies of concrete in shear and tension.

Following the success of the Johnson-Bovey building, Turner would go on to design and build 34 reinforced concrete flat slab buildings between 1906 and 1910 (Gasparini, 2002). By 1913, over 1000 of these systems had been constructed worldwide (Milligan, 2018). Eventually, concrete technology would progress enough to eliminate the need for the large capitals, and capital-less slab systems would begin to be constructed in the 1950's (Genikomsou, 2015). Today, reinforced concrete flat slab systems are a practical and efficient option due to their ease of construction, reduced construction cost, and increased vertical clearance per floor. This has come about due to years of research and optimization of the system by many researchers worldwide. Much of this research revolves around a core failure mode of the system known as punching shear, which is brittle and can lead to progressive collapse of the system.

In this chapter, the phenomenon of punching shear will first be discussed. Then, a summary of the research that has been conducted on punching shear in reinforced concrete flat slabs will be provided including: a discussion of punching shear tests that have been conducted, a review of research done on finite element modelling of reinforced concrete flat slabs, an outline of mechanical models developed to design flat slab systems for punching shear, and an overview of code provisions currently used to design flat slab systems for punching shear.

2.2 Punching Shear Mechanics

Punching shear in concrete flat slabs is a phenomenon that can occur in the D region at the connections of a concrete flat slab and its supporting columns. This region is subjected to a complex three-dimensional state of stress due to the significant flexural and shear loading in the region. In brief, when the shear stresses near the slab column connection (but not directly adjacent due to confining stresses provided by the column) exceed the shear strength of the slab, the column and a truncated conical portion of the slab

push through the slab resulting in failure of the connection. Punching shear is a very brittle failure mode, and can lead to progressive collapse of a structure if not adequately designed for. A typical punching shear failure surface is shown in Figure 1.

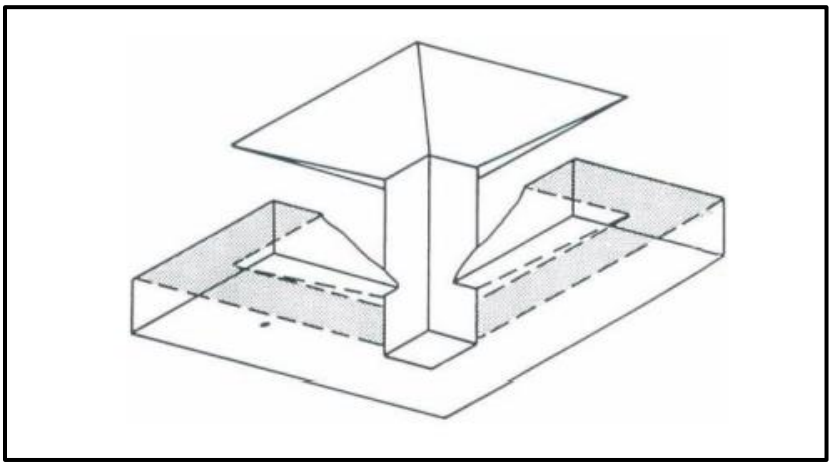

Figure 1: Punching Shear Failure Surface (MacGregor and Bartlett, 2000)

Punching shear failure is generally preceded by initial radial cracking of the slab due to flexural load. As the load increases, cracking similar to that considered in a yield-line analysis of the slab begin to appear and internal diagonal shear cracks which will form the conical failure surface begin to form within the slab (MacGregor and Bartlett, 2000). These cracks extend to reach the compressive surface of the slab causing the shear resistance of the slab concrete to deplete. At this point the shear forces are carried by diagonal struts in the un-cracked concrete to the slab reinforcement at the top of the slab. The horizontal component of these struts eventually causes loss of bond at the flexural slab reinforcement and the shear resistance of the connection, which is comprised of the shear strength of the compressive concrete, dowel action of the flexural reinforcement, and aggregate interlock, becomes less than the shear demand resulting in punching (Alexander and Simmonds, 1987). Examples of punching shear failure are shown in Figure 2.

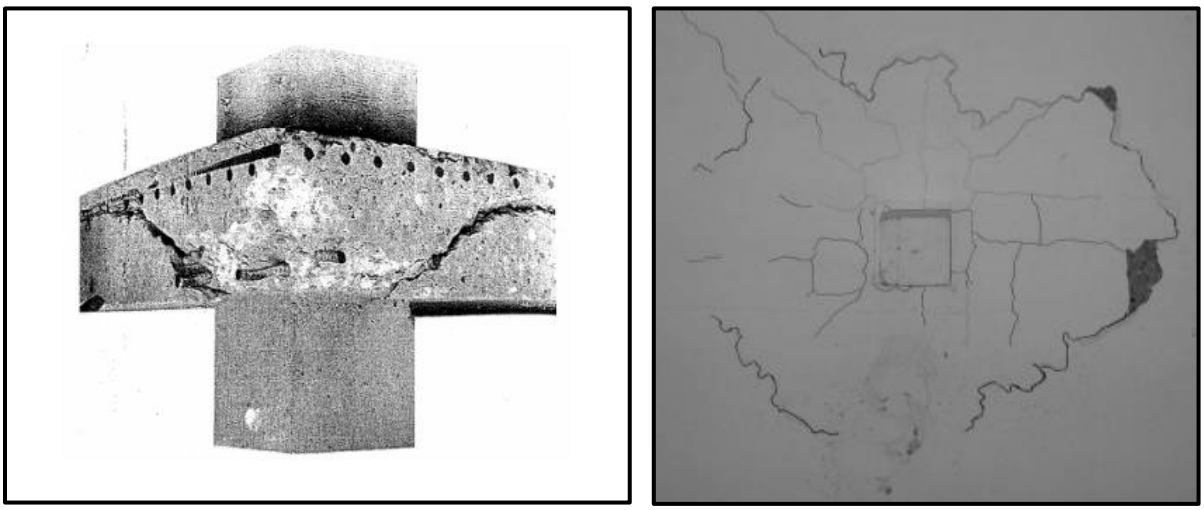

Figure 2: Punching Shear Inclined Cracking (MacGregor and Bartlett, 2000) and Surface Cracking (Adetifa and Polak, 2005)

2.3 Review of Punching Shear Tests and Finite Element Analysis

2.3.1 Introduction to the History of Punching Shear Tests

The first recorded testing program for slabs and footings with the objective of studying their shear strength was published by Arthur N. Talbot in 1913. Talbot (1913) tested 114 wall footings and 83 column footings to failure and found that the shear strength of the footings increased when a larger tensile reinforcement ratio was provided (Moe, 1961). Later, in 1915, Bach and Graf performed a large testing program of concrete slabs, of which several failed in shear. Later in 1933, Graf concluded that the shear strength of the slabs increased with the concrete strength, but at a reduced rate than the compressive and tensile strengths. He also predicted that the degree of flexural cracking in the slab had an impact on its shear strength (Moe, 1961). Other early punching shear research included that of Richart and Kluge, who conducted an investigation of slabs subject to concentrated loads in 1939 and concluded that an increase in flexural strength would also result in an increase in shear strength of the slab. In 1946, Forsell and Holmberg reported on many punching shear tests conducted from 1926 to 1928, and theorized that shear stresses varied parabolically through a slab's depth (Moe, 1961).

Since these initial tests and studies, many researchers have produced testing programs with the aim of studying different aspects of the punching shear behaviour of reinforced concrete slabs. Several databases, including those curated by the American Concrete Institute (ACI), or the International Federation for Structural Concrete (fib), now include much of the research and punching shear tests. More recently, research is being conducted on NLFEA of reinforced concrete slab-column specimens with the aim of supplementing these databases. In this section, some of the research on reinforced concrete slabs in punching shear will be presented and discussed for slabs with and without shear reinforcement, as well as research regarding NLFEA of these specimens.

2.3.2 Punching Shear Tests on Specimens without Shear Reinforcement

Elstner and Hognestad (1956) tested thirty-nine slab-column specimens to determine the impact of several key parameters, such as concrete compressive strength, tensile reinforcement ratio, compressive reinforcement ratio, column size, support conditions, and load conditions on the slab's behaviour when subjected to punching. Most of the slabs were simply supported on all four edges while a concentric load was applied to the central column stub. Thirty-four of the thirty-nine slabs failed in punching shear. Test results showed that concrete compressive strength played a significant role in punching strength of the slabs. Increasing the tensile reinforcement ratio near the column in the slabs had a negligible effect on the punching behaviour. The compressive reinforcement ratio also had a negligible effect on the punching behaviour. The effect of applying a concentric or eccentric load on the column was negligible. Finally, the test results helped revaluate analysis criteria for reinforced concrete slabs, which previously had been determined from a footing study conducted by Richart (1948) despite footings being differently reinforced and supported (Elstner and Hognestad, 1956).

Moe (1961) tested forty-three slab-column specimens in concentric punching. In this testing program, parameters such as column size, eccentricity of load, presence of openings, tensile reinforcement concentrations, and use of shear reinforcement. The specimens were supported on all four sides with the

corners free to lift. Test results showed that the flexural strength of the slab had an impact on its shear strength. The punching capacity of the connection was shown to be highest when the column width to slab depth ratio was low. Openings were found to significantly decrease the punching capacity of the connection. Based on these findings Moe (1961) suggested that that the column perimeter be used as the critical perimeter when determining shear strength and developed an equation that could be used to calculate the punching capacity of a slab-column connection. This work would become the bases of the ACI 218 provisions on punching shear (Moe, 1961).

Mowrer and Vanderbilt (1967) tested fifty-one slab-column specimens in concentric punching. The specimens had varying column size to slab depth ratios, reinforcement ratios, edge constraints, and concrete weights. The purpose of the study was to assess the predictive capabilities of design equations proposed by Elstner and Hognestad (1956) and Moe (1961) for varying specimens. Specimens were supported on either two or four edges and a concentric load was applied to their column stubs. The test results showed that the punching capacities of the slabs were best predicted by a revised version of Moe's (1961) equation. A new type of test specimen that better simulates a slab-column connection was also proposed from this research (Mowrer and Vanderbilt, 1967).

Hanson and Hanson (1968) tested seventeen slab-column specimens. Interior specimens with square and rectangular columns were investigated along with edge specimens with square columns. Specimens were tested using three different methods. In all of the methods the specimens were supported on their columns, where a hinge connection was simulated at the column ends. Method one involved applying an upwards line load at one end of the slab and a downwards line load at the other, thereby simulating moment transfer from the slab to the column. Method two involved applying equal downward line loads on both ends of the slab thereby simulating downwards gravity loading. Method three involved applying a downward line load to one end of the slab, thereby simulating combined gravity loading and moment transfer. Test results were influential in assessing design methods proposed for reinforced concrete slabs subjected to punching, and showed that the method proposed by Moe (1961) was accurate and simple in application (Hanson and Hanson, 1968).

In 1974, Hawkins et al conducted a critical analysis of available test data for slab specimens containing no reinforcement to investigate the effect of parameters such as concrete compressive strength, column size, slab thickness, scale effects, tensile reinforcement strength, tensile reinforcement pattern, slab restraints, column shape, and rate of loading. Tests of lightweight slabs, perforated slabs, prestressed slabs, and slab systems were all considered. This analysis suggested that circular columns provide higher slab strengths than square columns. Code values at the time were generally conservative for slabs with c/d ratios between two and eight and concrete strengths below 4000psi (28MPa). Shear capacity was found to be insensitive to tensile reinforcement strength. Recommendations for capacity calculations were also made for lightweight slabs, perforated slabs, and prestressed slabs (Hawkins et al, 1974).

Long and Masterson (1974) tested twelve slab-column specimens under combined shear and moment loading. The specimens were clamped along two edges while a uniformly distributed load was simulated through sixteen point loads on the slab's top surface and a moment couple was applied to the column using two hydraulic jacks. Half of the specimens were scaled versions of those tested by Long (1967), and the other half scaled versions of those tested by Moe (1961). Test results showed agreement between the

results for the specimens and their older counterparts, but with enhanced punching strengths. These strengths were attributed to the arching action developed in the specimens tested using this particular test setup. The arching action was increased for the first half of samples as they were larger. This improved testing procedure was seen as a more realistic representation of slab-column connections (Long and Masterson, 1974).

Swamy and Ali (1982) tested nineteen slab-column specimens, some of which were constructed using fibre reinforced concrete. The specimens were simply supported along all four edges with the corners free to rise, while a concentric load was applied to the central column. Test results showed that the fibre reinforced concrete had a significant effect on the punching behaviour of the speciemns. Deflections at service loads were decreased by approximately 30%, whereas the ultimate behaviour and failure mode became significantly more ductile. The overall capacity of the connections were also increased by up to 40%. It was also shown that providing fibre reinforcement within the area within 3d from the column was as effective as providing if throughout the slab. Fibre reinforcement was successful in pushing the critical perimeter away from the column and could support equal loads with a reduction in tensile reinforcement (Swamy and Ali, 1982).

Pan and Moehle (1989) conducted a study on test data from various researchers who tested interior slab-column specimens subjected to gravity and lateral loading, and in addition tested four interior slab-column specimens in this way themselves. Using this test data, relations were developed for gravity load and lateral load capacity, biaxial load and lateral load capacity, and inter-story drift and lateral load capacity. Based on this work it was suggested that lateral inter-story drift not exceed 1.5% of the inter-story height in interior slab-column connections (Pan and Moehle, 1989).

Robertson and Durrani (1991) tested three slab-column subassemblies containing two exterior slab-column connections and one interior slab-column connection under varying slab loads. The subassemblies were pinned at the bottom of the three columns and fixed to a distribution beam at the top of the columns. Lateral load was applied through the distribution beam while varying gravity loads were applied to the slab using weights hung from the top slab surface. The two subassemblies with the highest gravity loads failed at the interior slab-column connection prior to reaching the maximum prescribed lateral loads, whereas the other specimen failed at the exterior column at a higher drift percentage. The test results showed that desired drift capacity of 1.5% could be reached if the shear force applied to the slab is limited. The exterior connections reached their peak rotation capacity regardless of the applied shear force, whereas the interior connection did not. This shows that the interior connection is more critical in terms of punching strength and drift capacity (Robertson and Durrani, 1991) (Robertson and Durrani, 1993).

Marzouk and Hussein (1992) tested seventeen slab-column specimens using various different high strength concretes to assess the punching behaviour of reinforced high strength concrete slabs. Specimens were simply supported along all four of their edges on rubber pieces and were loaded axially though their column stubs. Fifteen of the seventeen specimens failed in shear, with five of the slabs experiencing distinct punching behaviour. Test results showed that the high strength specimens showed a more brittle failure mode than traditional specimens. The stiffness of the slabs was increased with increased slab

thickness and reinforcement ratio, while the slab ductility decreased. Finally, the code contribution of the concrete strength in relation to punching strength was found to be too high (Marzouk and Hussein, 1992).

Gardner and Shao (1996) tested one multi-bay (two by two slab and nine column) slab system specimen to test whether the analysis of an individual slab-column specimen is representative of that slab's punching behaviour in a continuous slab system. To test the slab system, a uniformly distributed load was simulated through forty point loads distributed across the slab's top face. The slab was initially supported on its nine columns and two to four supplementary supports near each of the columns. The slab was first loaded to a predetermined load while supported by all columns and supplementary supports, then the slab was unloaded, the simple supports were removed, and the slab was reloaded to failure. Test results showed that the interior slab-column connections are more critical than the edge or corner connections in a properly designed slab system. Isolated slab tests were effective in representing the punching shear behaviour of the interior slab-column connection in the slab system. Finally, supplementary supports at the edge slab-column connections increased punching shear capacity by about thirty percent when located a distance equal to the effective slab depth from the column (Gardner and Shao, 1996).

Teng et al (2004) tested twenty slab-column specimens that contained rectangular columns with varying aspect ratios and differently placed openings near to the columns. The specimens were tested in concentric punching where the specimens were supported on their columns and loaded through eight point loads around the slab perimeter. Test results allowed the authors to develop equations for accurately determining the punching strength of slab-column connections with rectangular columns in the presence of openings. The equations were verified using 223 specimens from literature and were shown to be very accurate in representing punching behaviour for these type of specimens (Teng et al, 2004).

Naaman et al (2007) tested ten slab specimens, nine of which being high performance fibre reinforced concrete, in concentric punching. The specimens were supported on four edges while a load was applied through a plate in the slab centers. The effect of different reinforcement ratios in addition to the fibre reinforcement was also investigated, as was the performance of different high-performance fibres. Test results showed that the punching capacity of the connection was increased by between 15 and 100 percent when fibres were provided at the level where tensile strain hardening was achieved. The ductility of the connection also increased significantly (between 90 and 280 percent) when fibres were provided. The effect of removing reinforcement layers in lieu of fibre reinforcement had little negative effect and often a positive effect on the punching performance of the connection. Spalling under large deformations was completely eliminated when fibre reinforcement was provided. Finally, it was suggested that the contribution of concrete strength to punching shear could safely be doubled when high performance fibre reinforcement is included in the concrete mix (Naaman et al, 2007).

Alam et al (2009) tested fifteen slab specimens in concentric punching, twelve of which containing an edge beam to simulate slab continuity. The slabs were simply supported along two edges and a displacement was applied through a loading cell in the slab center. Slab thickness and flexural reinforcement ratio were varied in the specimens. The test results found that the punching strength of the slab was increased when edge restraint was provided, and that the punching strength increased as the degree of edge restraint increased, suggesting that code provisions based on tests of individual simply supported slab specimens were conservative when applied to multi-bay construction. The tests also

showed that while changing the level of flexural reinforcement has minimal effect of heavily reinforced slabs, it has can have a significant influence on lightly reinforced slabs. (Alam et al, 2009).

Guandalini et al (2009) tested eleven slab specimens of varying sizes with varying flexural reinforcement ratios within a low range. The specimens were loaded through eight concentrated points along the column perimeter and supported in their centers. The load increased at a constant speed up until punching failure occurred. The test results showed that due to size effect, the punching strength of the specimen decreases with increasing slab thickness and the deformation at failure also decreases with increasing slab thickness. The test results also validated the principles of critical shear crack theory including the development of the critical shear crack leading to failure, and the failure criteria provided (Guandalini et al, 2009).

Sagaseta et al (2011) tested seven slab-column specimens under one way and two way gravity loading. The specimens contained different reinforcement ratios in each orthogonal direction and aimed to investigate if specimens with vastly different reinforcement ratios in the orthogonal directions would behave axis-symmetrically. The specimens were supported on their columns and load was applied through eight loading cables (two way loading) or four loading cables (one way loading) along the specimen perimeters. Test results showed that the tensile reinforcement ratio has an effect on the punching strength and symmetry of the response. Based on these findings, a version of critical shear crack theory (Muttoni, 2008) was proposed to account for the asymmetry of responses, considering non-uniform shear strength on the critical perimeter (Sagaseta et al, 2011).

Inacio et al (2015) tested four slab-column specimens with different longitudinal reinforcement ratios under concentric punching. Three of the slab specimens were constructed with high strength concrete with a compressive strength of 130MPa. The specimens were restrained in a diagonal formation at the suspected line of zero moment while load was applied vertically from underneath the specimens' column stubs. Test results showed that concrete strength has a direct influence on the punching strength of a slab, with the high strength slab outperforming the normal strength slab by 42% for the same reinforcement ratio. The increase of longitudinal reinforcement ratio increased the punching capacity but also caused a more brittle failure mechanism. Finally, the punching capacity for the tested slab-column specimens tended to be lower than predicted values from codes, although the compressive strength of the tested slabs was out of the range recommended for code use (Inacio et al, 2015).

Fick et al (2017) tested a three-story, two-bay, reinforced concrete flat slab structure under gravity loads and cyclic lateral loads. This was the first test of a full-scale concrete flat slab specimen of this magnitude and would fully validate the applicability of reduced scale and isolated test behaviour on actual structure behaviour. The specimen was first loaded on all three slabs using water barrels resulting in uniform loads, lateral loads were then applied using wall rams in both orthogonal directions. The specimen failed at one of the edge slab-column connections on the third story at 2.9% drift with the failure mode being combined shear and flexure. The test results showed that at the required drift ratio of 1.5% the structure was without fault with no shear reinforcement. The drift capacity of the connection was consistent with what had been predicted from isolated and reduced scale tests (Fick et al, 2017).

Santos et al (2022) tested eight full-scale slab-column specimens in concentric punching. The specimens contained rectangular columns, varying numbers of openings with various sizes and in different

configurations. The specimens were supported on their columns while load was applied at eight points along the slab's perimeter. Test results showed that the reduction in the critical perimeter for determining punching capacity of connections with openings should consider the position of the opening and geometry of the opening/column in addition to the distance of the opening from the column. The consideration of bending moment transfer in asymmetric opening configurations was also deemed as an important factor in judging the connection punching capacities (Santos et al, 2022)

2.3.3 Punching Shear Tests on Specimens with Shear Reinforcement

Corley and Hawkins (1968) investigated the applicability of using lightweight steel sections as shearhead reinforcement including the testing of twenty-one slab-column specimens with varying concrete types and shearhead sizes. Shearhead sizes included "over-reinforcing" and "under-reinforcing" shearheads depending on if the predicted failure mode was via shear or flexure. Loads were applied at eight points along the slab's perimeter incrementally using a hydraulic system while the slab was supported on its central column. The test results showed that shearhead reinforcement from structural steel sections was effective for thin slabs. Increased capacity by up to 75% was experienced in the tests and there was some indication that higher capacities could have been achieved. Based on the results of this testing a design methodology for shearhead reinforcement in concrete flat slabs was developed (Corley and Hawkins, 1968).

In 1974, Hawkins conducted a critical analysis of slab specimens containing shearhead reinforcement and bent bar reinforcement tested by several other researchers. Through this analysis, it was concluded that both reinforcing methods could be valid for increasing the shear capacity of the slabs, however for bent bars considerable reinforcement was required before such an increase was reached. Hawkins (1974) also made recommendations for detailing of shearhead and bent bar reinforcement, and suggested limites for possible shear strength increases using the methods. He also suggested that when transferring moment and shear, shearhead reinforcement may only be effective for shear stresses caused by shear transfer (Hawkins, 1974).

Sieble et al (1980) tested seven slab-column specimens outfitted with different types of preassembled shear reinforcing units. Specimens contained shear reinforcing units made out of wire meshes, stud rails, and I sections, all designed to not interfere with the placement of longitudinal reinforcement within the slab. Specimens were simply supported along all edges and loaded through their central columns. The specimens underwent ten cycles of load varying between 100 and 300 kN to simulate service loading conditions. Test results showed that it is possible to achieve the desired ductility and capacity through the use of prefabricated shear reinforcing units. The I section unit had the best anchorage performance, however the shear stud reinforcing unit was the easiest to install. The wire units were only able to provide significant anchorage when a top and bottom unit were utilized, which presented additional installation difficulty. In general, prefabricated shear reinforcing units could result in simple and accurate reinforcement placement and could be highly mechanized, resulting in lower costs (Sieble et al, 1980).

Pillai et al (1982) tested four slab-column subassemblies containing an exterior and an interior slab-column connection and framing columns. The subassemblies were reinforced around the columns using conventional stirrups. The subassemblies were supported at both ends of the columns while a uniformly

distributed load was applied to the slab at twenty-four different points. This uniform load was applied to service levels, at which point four cycles of lateral loading were applied. Once lateral loads had finished cycling, the exterior and then interior connections were loaded to failure. Test results showed that microcracking near the connections due to load cycles have an impact on subsequent moment capacity. The shear reinforcement in the specimens was found to be effective improving the ductility of the connections and preventing punching failures (Pillai et al, 1982).

Elgabry and Ghali (1987) tested five interior slab-column specimens under vertical load and unbalanced moment to assess the applicability of shear stud reinforcement to slabs undergoing unbalanced moment and adjust code recommendations for shear reinforcement made by Dilger and Ghali (1981) regarding shear stud rows. Four of the specimens contained shear stud rows of different lengths and spacings. The specimens were simply supported along their perimeters while vertical load and an unbalancing force couple were applied to the specimen's columns, which extended 700mm above and below the slab. Once service loads were reached, the moment was cycled to simulate reapplication of live loads. Test results proved that shear stud reinforcement could be effective in reinforcing slabs undergoing unbalanced moment. The tests also verified several of the code provisions suggested by Dilger and Ghali (1981) and provided additional guidance for dimensioning the top anchor heads and bottom anchor strips of the shear stud rows (Elgabry and Ghali, 1987).

Yamada et al (1992) tested thirteen slab-column specimens in concentric punching. The specimens were supported at their column bases while load was applied at eight symmetric points around the specimens' perimeters. Specimens contained either stirrup reinforcement or hooked bar reinforcement to resist punching shear in different configurations. Test results showed that anchorage of the shear reinforcement was very important in ensuring ductility of the connection. Frequent reinforcement spacing was required in order to intercept shear cracks with steep angles. The presence of shear reinforcement was not always successful in increasing punching capacity, but always was successful in increasing the specimen's ductility (Yamada et al, 1992).

El-Salakawy et al (1998) tested eight edge slab-column specimens subjected to vertical load and unbalanced moment. The specimens were divided into two series, four specimens with shear reinforcement and four specimens without shear reinforcement. Each series contained three specimens with openings adjacent to one of the column faces. The goal of the testing was to assess the opening effect on edge slabs with unbalanced moments and assess the ability of shear stud reinforcement in edge slabs with openings subjected to unbalanced moments. The specimens were simply supported along their three non-column edges and vertical load and the unbalancing moment couple were applied to the columns. The moment to shear ratio was kept constant at 0.3 throughout the tests and the loads were applied cyclically after service loads were reached in testing to simulate reapplication of live loads. Test results showed that while all openings decreased the stiffness of the connection, the most significant effect was that of the opening located in front of the column (in line with the moment couple). It was also shown that shear reinforcement is ineffective at stiffening connections in flat slabs where opening the same size as the column are provided, and that the opening width should be smaller than the column width (El-Salakawy et al, 1998).

Broms (2000) tested seven slab specimens with shear reinforcement provided in five specimens through the use of bent bars and a combination of bent bars and stirrups. The specimens were simply supported at eight points at their edges and load was applied vertically in the slab centers. The test results of this study showed that it was possible to achieve a ductile failure mode in a reinforced concrete flat slab system through the use of bent bars and stirrups, and that constructing such a system would still be economical when compared to a slab on beam system in many scenarios (Broms, 2000).

Megally and Ghali (2000) tested five edge slab-column specimens with shear reinforcement under simulated earthquake loading. Specimens were reinforced with five to seven peripheral rows of shear studs. Specimens were supported in a steel test frame so that the slab is vertical and the column is horizontal. The slabs are suoorted at three edges while loads are applied. The specimens were tested in three stages. First, shearing force and unbalanced moment are applied to the column simultaneously with a constant shear to moment ratio of 12in until a target value of shear force is reached. Next, cyclic lateral displacements were applied to the column ends with gradually increasing amplitudes. Finally, the specimen is completely unloaded and reloaded to the target shear force to examine the specimen's residual strength. Test results showed that without shear reinforcement may fail in punching at relatively low drift ratios if the shear force they experience is high. In specimens with shear reinforcement, ductility and maximum drift were significantly increased, and no limit on the shear force applied need be required to achieve appropriate ductility in the connection. The ability of the shear studs to resist gravity loads was also maintained in the post-earthquake portion of the loading. Finally, recommendations for the detailing of shear stud reinforcement in earthquake zones were suggested (Megally and Ghali, 2000).

Sherif and Dilger (2000) tested two slab-column subassemblies containing one exterior and one interior slab-column connection. One of the subassemblies was tested three times after twice being repaired. The test setup used a system of boundary frames to accurately simulate slab continuity beyond the subassemblies. Several of the tests contained shear stud reinforcement at the two connections. The results of this test were used to validate the equivalent frame method in the ACI/CSA codes. Test results showed good agreement between the tests and results obtained using the equivalent frame method, especially at low load levels, although moments at the edge connection were sometimes underestimated with the presence of shear reinforcement. The test of the subassemblies also showed that tests of isolated specimens could be used to predict the behaviour of continuous slabs when properly restrained (Sherif and Dilger, 2000).

Robertson et al (2002) tested four interior slab-column connections under cyclic lateral loading while maintaining a constant gravity load. Shear stud reinforcement, as well as single and double ls, were considered within the specimens. The specimens were pinned at the bottom of their columns while lateral load was applied to the top of the columns. The slab was supported on two roller supports at midspan in the direction of loading. Test results showed that the shear-reinforced specimens all reached eight percent lateral drift without failure, whereas the control specimen failed prior to four percent drift was reached. The lateral load experienced by the shear-reinforced specimens also reached a value twenty-two percent greater than the control specimen. Since all types of shear reinforcement easily reached drift ratios specified by ACI codes, a more relaxed maximum spacing was suggested. Shear stud reinforcement was chosen as the most desirable reinforcement type due to its ease of placement (Robertson et al, 2002).

Adetifa and Polak (2005) tested six interior slab-column specimens in concentric punching. The specimens were supported on neoprene pads near its edges while a displacement was applied through a 150mm square column stub in the specimen's center. Five of the specimens contained between two and four rows of shear bolts, which were added to the specimens post-casting through drilled holes as would be done in a retrofit. Two of the specimens also contained openings near the column stub. The test results showed that the shear bolt retrofit system performed adequately to prevent punching failure of the slabs and transition the failure mode to flexural failure. The bolts also performed effectively in the specimens with openings. (Adetifa and Polak, 2005).

Kang and Wallace (2005) conducted shaketable tests of two slab-column frames reinforced with stud rails to assess their seismic performance. One specimen was reinforced with standard steel reinforcement while the other specimen was reinforced with post-tensioned steel reinforcement. The test results showed that relatively little damage occurred in the specimens when compared to similar tests of slab-column frames without shear reinforcement, thus concluding that the presence of shear reinforcement decreases damage experienced during seismic punching. Even less damage was observed in the specimen with post-tensioned longitudinal reinforcement. While moment transfer degraded in the systems during testing, lateral drift ratios of only 3% and 4% were experienced in the specimens and lateral load capacity was mostly maintained throughout the test, possibly due to the shear reinforcement enhancing the specimens' post punching deformation capacity (Kang and Wallace, 2005).

Tan and Teng (2005) tested five interior slab-column specimens under a combination of gravity load and biaxial unbalanced moment. The specimens were subject to the loads in varying gravity/shear ratios and several of the specimens contained shear stud reinforcement. The specimen columns also had an aspect ratio of five for all specimens to test the effect of column rectangularity on the specimen response. The specimens were supported at the base of their columns while gravity load was applied via steel weights placed on the slab and a hydraulic jack at the base of the column. Once gravity load was applied, a set routine of biaxial lateral loads were applied to the top of the column based on desired drift ratios for the specimens. Test results showed that when the column aspect ratio is five, the target drift capacity of 1.5% us unlikely to be reached under biaxial loading, which decreased the drift capacity of slab-column connections significantly. The effect of biaxial loading and column rectangularity was observed to be much more significant than the effect of gravity/shear ratio on the shear capacity of the specimens. The presence of shear studs was also observed to increase the drift capacity, ductility, and strength of the connections (Tan and Teng, 2005).

Broms (2007) tested four octagonal slab specimens in concentric punching. Two of the specimens contained shear reinforcement in the form of shear studs. One of these specimens contained shear studs arranged in an orthogonal "double-cross" pattern whereas the other specimen contained shear studs arranged in a radial pattern. The other two specimens had shear reinforcement in the form of stirrup grids of two different sizes attached to four large bent bar anchors. The specimens were supported by eight anchor rods with spreader bars around the slab perimeter and load/displacement was applied to the slab center in 80kN or 8mm increments. The test results showed that while using stirrups as shear reinforcement even if the punching capacity exceeds the column reaction corresponding to yielding of the flexural reinforcement, there is still potential for brittle failure to occur before flexural failure if flexural reinforcement is not well designed. The test results also showed that the stirrup grid method of shear

reinforcement guarantees a ductile failure mode suggesting a good ability to endure accidental loads, although is significantly more expensive than shear reinforcement via studs (Broms, 2007).

Birkle and Dilger (2008) tested nine octagonal slab-column specimens in concentric punching grouped into three series: specimens without shear reinforcement, specimens designed to fail within shear reinforced zone, and specimens designed to fail outside the shear reinforced zone. The goal of the tests was to investigate the effect of slab depth on punching strength. In each series, specimens with a slab depth of 160mm, 230mm, and 300mm were considered. The test results showed that for unreinforced slabs, there was a significant decrease in the percentage of predicted punching capacity reached as the slab depth increased. For the 300mm unreinforced slab, only 89% of the punching capacity predicted by ACI 318-05 was reached. For specimens with shear reinforcement, only a small decrease in the predicted punching capacity was shown for the larger slab depth specimens (Birkle and Dilger, 2008).

Bu and Polak (2009) tested five slab-column specimens under constant gravity loading and cyclic horizontal loading. The specimens were identical to those tested by Adetifa and Polak (2005) but with different amounts of shear bolts and no openings. Vertical and lateral load were applied to the central column stubs of the specimens while the outer edges were supported on neoprene pads. The test results showed that peak lateral load capacity, slab-column drift ratio, drift ductility, and number of lateral drift cycles all increased when shear bolts were provided in the specimen, although shear bolts located at a distance of 4d had little impact on the test results. This research showed the applicability of shear bolts as a retrofitting option for concrete flat slab systems in seismic zones (Bu and Polak, 2009).

Lips et al (2012) tested sixteen full scale slab specimens reinforced with shear studs or stirrup cages. The objective of the research was to provide systematic data for shear reinforcements in full scale specimens to remove scale effects from the tests, as little such data previously existed. Different column sizes and slab thicknesses were also considered in the testing program. Specimens were supported at eight points along their perimeters while a concentric load was applied to the slab center from below. Test results showed that the crushing of the concrete strut near the support region is heavily dependent on the shear reinforcement detailing, including anchorage and distance to the column. Very little yielding was experienced in the shear reinforcement up until failure. Finally, the test results showed that the influence of size and slenderness effects on punching shear tests is similar for specimens with and without shear reinforcement (Lips et al, 2012).

Borges et al (2013) tested thirteen slabs with rectangular supports in their center. Several of the slabs contained opening near the short sides of the support in either a concentric or eccentric arrangement. Several of the slabs also contained shear stud rails in several different patterns. Load was applied in an upwards direction by a jack below the middle rectangular support, and the slabs were supported by tie bars on all four of the slab's edges. The test results showed that straight projection of the openings onto the critical perimeter outside of the shear reinforcement was the most accurate method of determining the shear capacity of the samples. Also, the test results showed that a critical perimeter of 1.5d beyond the final peripheral row of shear reinforcement was preferable to the 2d suggested in EC2 (Borges et al, 2013).

Einpaul et al (2016) tested twelve slab specimens with different types of shear reinforcement and different methods of incorporation the shear reinforcement types into the slab. Specimens with double headed studs, single and double leg stirrups, stirrup cages, bent bars, concrete screws and shear bolts were tested with various anchorage and location conditions. The test results showed that the type or shear reinforcement, its spacing, and its anchorage conditions have a significant impact on the punching performance of the slab up to a certain level of reinforcement where the punching capacity becomes dependent on the failure of the concrete between the column and the closest shear reinforcing element. Specimens with shear reinforcement in a radial or cruciform arrangement showed very similar punching capacity. Finally, for failures outside of the shear reinforced region, the area of resisting concrete in the critical perimeter may only be valid between anchorage locations according to the test results (Einpaul et al, 2016).

Topuzi et al (2017) tested six slab-column connections under constant vertical loading and cyclic lateral loading until failure. The specimens were retrofitted with flexible shear bolts which aimed to increase the ductility of the connection/failure mode without making the connection significantly stronger or stiffer initially which would attract more forces to the connection in a seismic event. Vertical and lateral load were applied to the central column stubs of the specimens while the outer edges were supported on neoprene pads. The test results showed that the flexible shear bolts were able to increase the ductility of the specimens to near the same levels as those with traditional shear bolts without significantly increasing the capacity. It was suggested that the same effect could be gained through flexible shear studs installed in new construction as well (Topuzi et al, 2017).

Hussein and El-Salakawy (2018) tested six slab-column connections in combined vertical load and unbalanced moment. Several of the specimens contained high strength concrete and glass fibre reinforced polymer (GFRP) flexural reinforcement. These specimens aimed to assess the effect of reinforcement ratio of GFRP reinforced high strength slabs. The other specimens contained normal strength concrete, GFRP longitudinal reinforcement, and GFRP shear reinforcement in the form of headed studs and corrugated bars. These specimens aimed to address the effect of GFRP shear reinforcement on punching behaviour. Specimens were supported along their perimeters while a load was applied to the top of the columns. Unbalanced moment was applied through a force couple on the column as well. Test results showed that the high strength specimens failed in brittle punching. Changing the flexural reinforcement in these specimens increased the punching capacity and post-cracking stiffness. The use of high strength concrete enhanced the pre-cracking performance of the specimens, but decreased the overall ductility. Both types of shear reinforcement enhanced the post-cracking ductility of the specimens. It was found that code predictions for GFRP shear-reinforced connections often underestimated capacities, and adjustments were suggested (Hussein and El-Salakawy, 2018).

Salama et al (2019) tested four full-size edge slab-column specimens under combined vertical load and unbalanced moment. Specimens were reinforced with steel tensile and compressive reinforcing grids, and several specimens contained different amounts of GFRP closed or spiral stirrups. Specimens were supported on three edges while vertical load and the unbalanced moment couples were applied to the column. Test results showed that specimens with GFRP stirrups which spanned 4.25d experienced a capacity increase of almost 40% and a ductility increase of over 100%. Spiral stirrups were found to result in better performance and easier installation than closed stirrups. Specimens were found to fail outside of

the shear reinforced zone. Specimens where the stirrups spanned only 2.25d experienced a much more brittle failure mode. Proposed code requirements were also found to be quite conservative when compared to test capacities (Salama et al, 2019).

Marques et al (2020) tested nine slab-column specimens with different arrangements of circular openings and shear stud reinforcement in a radial pattern. Specimens were supported upside-down using tie rods and beams along the perimeter while a concentric load was applied to the column stub from below. Test results showed that there were slight increases and decreases in punching capacity caused by the shear studs and openings respectively. The specimens with larger openings experienced a greater loss in stiffness than specimens with more, smaller openings. The specimens with more lines of shear reinforcement appeared to fail within the shear reinforced zone whereas the specimens with less lines of shear reinforcement failed outside the shear reinforced zone (Marques et al, 2020).

Polo et al (2021) tested six full-scale slab column specimens in concentric punching. The specimens contained shear stud rails arranged in cruciform and radial patterns, as well as two different flexural reinforcement ratios (1% and 1.4%). The specimens were supported at eight points in a 10ft circular pattern centered on the slabs while load was applied vertically on the column stubs. All of the specimens failed in either punching or a combination of punching and flexure. Test results showed that the punching response of the specimens was less dependent on the shear stud pattern than the differing flexural reinforcement ratios, as the specimens with more tensile reinforcement failed in a more brittle fashion. The capacity and ductility increase due to the presence of shear studs was the same for both flexural reinforcement ratios (Polo et al, 2021).

2.3.4 Finite Element Analysis of Slabs-Columns in Punching Shear

One of the earliest attempts at analyzing the punching behaviour of slab-column connections via finite element analysis was that of Masterson and Long (1974). Masterson and Long (1974) used a linear rectangular grid of sixteen degree of freedom finite elements and elastic plate bending theory to develop equations that could be used to model slab-column behaviour. This model was used to predict the baviour of slab-column specimens with varying column dimensions, loading conditions, and boundary conditions with reasonable accuracy (Masterson and Long, 1974).

González-Vidosa et al (1988) modelled two series specimens, the first of which being four circular slabs tested by Kinnunen et al (1978), and the second being five square slabs tested by Elstner and Hognestad (1956). The specimens were modelled using a nonlinear 2D finite element model based on the work of Bédard and Kotsovos (1985), with cracking being modelled using a modified Newton-Raphson method and residual force concept. The models were created using eight node isoparametric elements to model the slabs and three node truss elements to model the reinforcement. The modelling results predicted the test capacities of the first series within 10% and the second series within 20%, however the second series of square slabs were approximated as equivalent circular slabs due to the formulation of the model, which could explain the error (González-Vidosa et al, 1988).

Hallgren (1996) calibrated a nonlinear 2D finite element model in ABAQUS for three circular high strength reinforced concrete slab-column specimens tested by the author and one normal strength

reinforced concrete slab-column specimen tested by Tolf (1988). Cracking was modelled using a smeared crack approach based on a fixed orthogonal cracking model, and a shear retention model was used to account for the resulting drop in shear stiffness. The specimens were modelled with eight node isoparametric elements for concrete and three node linear truss elements for reinforcement. A modified Riks method was used in order for convergence to be achieved in the models. The finite element models were found to be in general agreement with test results. Cracks were found to be normal to tensile strains as expected and failure was found to occur at the expected position (Hallgren, 1996).

Menétrey et al (1997) used the nonlinear 2D finite element model calibrated by Menétrey et al (1994) to model several interior slab-column specimens with circular columns using four node quadrilateral elements. The model utilized a smeared crack approach and strain softening formulation through the fictitious crack model developed by Hillerborg et al (1976). Parametric studies were conducted using the model, investigating the effect of concrete tensile strength, concrete compressive strength, flexural reinforcement layouts, reinforcement ratios, and size effect. Based on the modelling results it was concluded that concrete tensile strength had a key role in the punching behvaiour of the specimens. Increasing the flexural reinforcement ratio was found to increase punching capacities, and size effect was found to be detrimental to punching capacity (Menétrey et al, 1997).

Polak (1998) utilized layered quadratic isoparametric shell elements to create a nonlinear 2D finite element model capable of considering the out-of-plane response of the slab. The model was created based on modified compression field theory (Vecchio and Collins, 1986). Longitudinal reinforcement was modelled as one of the element layers whereas shear reinforcement was taken into account through the modification of material properties on a per-element basis in the affected layers. A smeared crack approach was utilized to account for cracking in the model. The model was shown to accurately predict the punching behaviour of specimens with and without shear reinforcement through calibration on specimens tested by Yamada et al (1992) and Elstner and Hognestad (1956) (Polak, 1998).

Guan and Polak (2007) calibrated a nonlinear 2D finite element model using the technique of layered shell elements in the software ABAQUS. Models were created for twelve specimens tested by El-Salakawy et al (1999, 2000). Six of the specimens contained shear reinforcement in the form of shear stud rails, and ten of the specimens contained openings. The specimens were modelled with ten layers of eight node shell elements, with eight layers accounting for the varying stresses within the concrete and two layers accounting for flexural steel reinforcement regions. The models were shown to be able to predict load-deflection behaviour, ultimate capacities, and crack patterns up until failure for the specimens. Based on the modelling, it was also determined that the influence of the openings in the specimens is small when openings are less than 70% of the column size, and that openings have less effect when not located in the direction of the unbalanced moment (Guan and Polak, 2007).

Winkler and Stangenberg (2008) proposed a nonlinear 3D finite element model in the software ABAQUS using the concrete damaged plasticity model by Lubliner et al (1989). The model utilized a post-peak tensile relationship between stress and crack width by Hordijk (1992). The concrete was modelled using eight node or twenty node solid elements while the reinforcing steel was modelled by eight node three-dimensional truss elements. The model was verified on several slab-column specimens tested by Li (2000). A modified Riks method was used for load incrementation in the model. The model accurately

predicted the capacity of the specimens, but the overall load deflection response and ductility of the specimens experienced some error (Winkler and Stangenberg, 2008).

Eder et al (2010) calibrated a nonlinear 3D finite element model in the software DIANA using a slab-column specimen tested by Vollum et al (2009), and one tested by the authors. The model made use of the total strain model in DIANA, which is based on modified compression field theory (Vecchio and Collins, 1986). The slab and loading plates were modelled using twenty node isoparametric brick elements while the reinforcement was modelled using three node truss elements. Calibration studies were conducted for several parameters involved in the total strain model. After calibration was complete, the model was used to model three slab-column specimens with shearhead reinforcement. The modelling results showed that the calibrated model was able to accurately predict the load-deflection response of a slab-column specimen in punching shear without shear reinforcement. For specimens with shear reinforcement, agreement between test and model results were also good, and improved if a finer mesh was used to model the area of the slab up to 2d from the end of the shearhead (Eder et al, 2010).

Silva Mamede et al (2013) calibrated a nonlinear 3D finite element model in the software ATENA based on thirteen interior slab-column specimens tested by various researchers. The model utilized ATENA's *CC3DNonLinCementitious2* model, which uses a smeared crack fracture model and Rankine failure surface for concrete in tension and a plastic model and Menétrey-William failure surface for concrete in compression. Load incrementation was handled by the Newton-Raphson method. The slabs were modelled using eight node isoparametric brick elements. A finer mesh was used in the region near the column than in the rest of the slab. Modelling results were found to compare fairly well to experimental results and capacities predicted by Model Code 2010. After model calibration was completed, parametric studies were run with variations of the slab depth, reinforcement ratio, concrete strength, and column dimensions. Based on these studies it was found that increasing the reinforcement ratio increased the capacity closely according to EC2 predictions, but with less ductility. Increasing the concrete strength increased cracking loads, but had little effect on post-cracking behaviour. Finally, an increase in slab depth and column dimensions also increased the punching capacity (Silva Mamede et al, 2013).

Genikomsou and Polak (2015) calibrated a nonlinear 3D finite element model using an interior slab-column connection without shear reinforcement tested in concentric punching by Adetifa and Polak (2005). The finite element model was created in the software ABAQUS using the concrete damaged plasticity model based on the work of Lubliner et al (1989). Calibration studies were conducted for several important parameters in the concrete damaged plasticity model such as dilation angle, fracture energy, and damage parameters. Mesh type and sensitivity analyses were also conducted, and a 20mm mesh of eight node linear brick elements was used for the models. After calibration, the model was used to model four additional slab-column specimens in approximated seismic loading or combined shear and moment loading. The modelling results showed the applicability of the concrete damaged plasticity model for nonlinear 3D finite element modelling of slab-column connections in punching shear, and results were accurate to the tests for all of the specimens modelled (Genikomsou and Polak, 2015).

Mahmoud (2015) calibrated a nonlinear 3D finite element model in ANSYS 10, and used it to model twenty slab-column specimens with varying types of shear reinforcement tested by Ruiz et al (2012). The specimens were modelled using eight node solid cubic elements, reinforcement was modelled using two

node truss elements, and shear reinforcement was modelled using three node beam elements. A Newton-Raphson method was used to increment loading in the models. Modelling results showed good agreement between model and test capacities, however rotations were under-predicted by the models. A parametric study was conducted using the calibrated model on the addition of openings to the specimens. Openings were found to have reduced effects on the models when shear reinforcement was present (Mahmoud, 2015).

Genikomsou and Polak (2016) used their calibrated nonlinear 3D finite element model from their previous research (Genikomsou and Polak, 2015) to model three existing slab-column connections with shear stud reinforcement tested by Adefifa and Polak (2005), and thirteen iterations of the slabs with varying shear stud layouts. Modelling results were compared to capacities predicted using ACI318-14 and EC2-2004, which were both found to be conservative in all cases. A radial arrangement of the shear studs was found to result in a more ductile failure mode than a cruciform arrangement in the models (Genikomsou and Polak, 2016).

Navarro et al (2018) calibrated their own nonlinear 3D finite element model based on specimens tested by Adetifa and Polak (2005) in ABAQUS. The concrete damaged plasticity model within ABAQUS was used, incorporating the cracking behaviour from Hillerborg et al (1976) and a Drucker Prager failure criterion. The model was created using a 20mm mesh of eight node isoparametric brick elements, four node shell elements for the flexural reinforcement, and three node beam elements for the shear reinforcement. Using these calibrated models, various parametric studies were conducted on the models. Parameters investigated include: yield strength of flexural reinforcement, compressive strength of concrete, flexural reinforcement ratio, column/slab width ratio, column width/slab thickness ratio, shear bolt diameter, number of shear bolts, shear bolt layout, column-first bolt distance, and bolt-bolt spacing. Modelling results showed that increasing yield strength of flexural steel, the flexural reinforcement ratio, or the compressive strength of the concrete increases capacity but decreases ductility. Increasing the column width/slab thickness ratio decreases capacity and increases ductility. Bolt-bolt spacing and bolt diameter had proportional effects. The column-first bolt distance was more influential than the bolt-bolt spacing on the punching behaviour of the models. Finally a radial arrangement of bolts was found to be the best compromise between capacity and ductility (Navarro et al, 2018).

Lapi et al (2020) developed a procedure for calibrating 3D nonlinear finite element models in ABAQUS using a combination of experimental results and theory. The procedure assumes default values for every parameter within the concrete damaged plasticity model in ABAQUS except for the dilation angle and fracture energy. The dilation angle is first estimated based on common values used in other punching models, and the fracture energy is calibrated to an experimental specimen (in this case a test performed by Guandalini et al, 2009). Calibrating these values based on the experimental results alone showed a slight over-prediction of punching capacity when most specimens were modelled. Therefore a calibration of the fracture energy based on Critical Shear Crack Theory was introduced and a formula for estimating the fracture energy based on this theory was developed. When the fracture energy was calculated in this way, and the dilation angle was estimated from the experimental results, the agreement of the model and experimental output for a variety of specimens was very good, however it is expected that the procedure would only be valid for the experimental test setup used for the specimens considered in this work (Lapi et al, 2020).

Jiang et al (2021) calibrated a thermo-mechanical 3D nonlinear finite element model using layered shell elements to capture the behaviour of reinforced concrete flat slabs subjected to fire loads. The model utilized layered shell elements in OpenSEES including a layer accounting for thermal properties of the concrete, a smeared reinforcement layer, and a concrete damaged plasticity layer accounting for the mechanical behaviour of the concrete. The model was validated using two reinforced concrete slab specimens tested using ISO834 fire curves in BRANZ lab and one composite reinforced concrete slab specimen tested using the cardington corner test. The model was shown to accurately predict thermo-mechanical behaviour of flat slab specimens with little parameter calibration, however some difficulty was experienced in modelling the composite slab specimen (Jiang et al, 2021).

Panahi and Genikomsou (2021) compared the performance of the concrete damaged plasticity and concrete smeared cracking constitutive models for concrete in 3D nonlinear finite element modelling. The models were compared using plain concrete and reinforced concrete specimens. In plain concrete, both models showed good agreement for the uniaxial stress states and biaxial compression, however the concrete smeared cracking model showed better agreement for the tension-compression stress state. However the concrete smeared cracking model was unable to capture the behaviour of a cyclic test. For reinforced concrete, the concrete damaged plasticity model showed good agreement over a variety of stress states. The concrete smeared cracking model however had convergence issues when nonlinearity ensued. This suggests that the concrete damaged plasticity model, when properly calibrated with regards to mesh size, dilation angle etc. is more capable for 3D nonlinear finite element analysis (Panahi and Genikomsou, 2021).

2.4 Review of Punching Shear Mechanical Models

Based on the many tests of slab-column specimens in punching shear and finite element analyses of slab-column specimens in punching shear described previously, several researchers have developed mechanical models that can be utilized to estimate the punching capacity of a slab-column connection through hand calculations. Several of such mechanical models are briefly described in this section, however many other models exist outside of those presented in this thesis.

Alexander and Simmonds (1987) observed that all of the pre-existing models that described the punching behaviour of slab-column connections assumed that shear resistance was provided along some critical section. However, they observed through analysis of many test results that this critical section varied significantly between tests, and as a result they developed a model which was independent of a fixed critical section. They also suggested that the strength of a critical section be confined to the uncracked compression zone of the slab's cross-section, and that flexural reinforcement should play a role in determining the punching strength of a connection. The resulting model made use of three-dimensional concrete compression struts and steel tension ties, with the struts being divided into anchoring struts, which act as a couple between adjacent flexural bars to simulate unbalanced moment acting on a connection, and shear struts, which act parallel to the applied shear force to provide shear resistance at a strut inclination angle α. Shear struts are further divided into uplift and gravity struts depending on whether they resist the upward or downward motion of the slab relative to the column. These struts are illustrated in Figure 3.

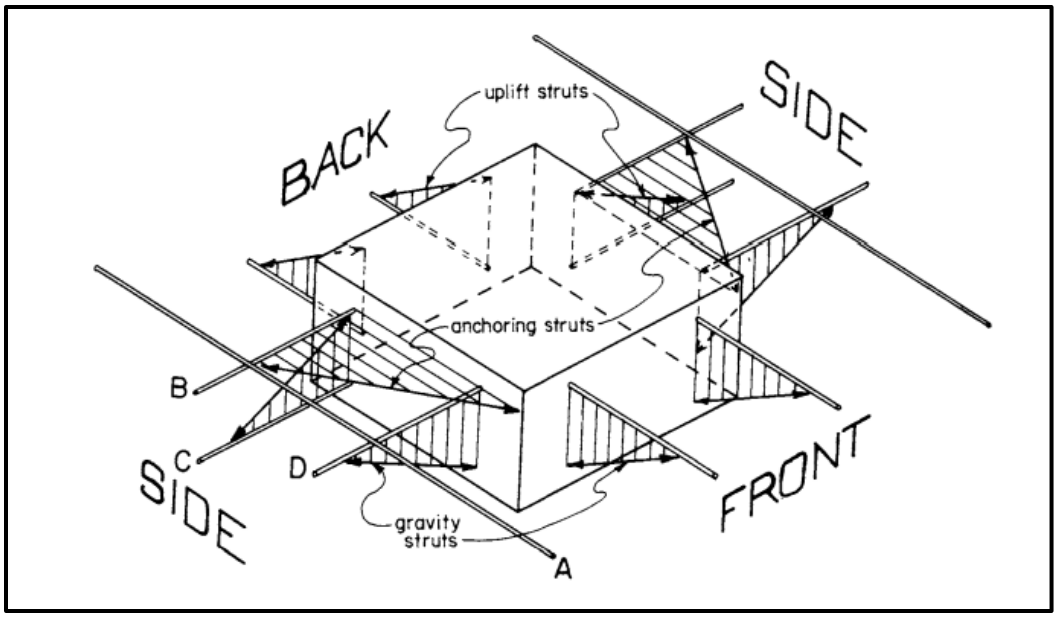

Figure 3: Slab-column connection struts and ties (Alexander and Simmonds, 1987)

The steel involved in the ties that define the struts was defined as any steel passing through the column and part of the steel that lies within one effective depth d from the column. It was assumed based on test data that the failure mode that would occur first in this type of connection was yielding of the tie steel, and not crushing of the strut concrete. Crushing of the strut concrete was not considered in the model. The strength of the tension ties is related to the in-plane stress component that they experience, which is easily calculated, and the out-of-plane stress component that they experience, which is related to their neighboring struts and is dependent on the strut inclination angle α. Alexander and Simmonds (1987) conducted a study on existing test data which related the tangent of the strut inclination angle through Equation 1, where K is defined based on other slab parameters according to Equation 2.

$$tan(\alpha) = 1 - e^{-2.25K} \tag{1}$$

$$K = {s_{eff} d' \sqrt{f_c'}} \Big/ {A_{bar} f_y (c/d)^{0.25}} \tag{2}$$

In Equation 2, s_{eff} is the tributary width of the tie, d' is the depth of the tie in the slab, and c/d is the ratio of the column dimension perpendicular to the bar to the effective depth. This model had several advantages, including the ability to explain the load path around the column, and the ability to account for the role of flexural reinforcement in punching strength. However, the model did not account for openings near the column or shear reinforcement in the slab, and the method for positioning the anchorage and shear struts was sometimes unclear (Alexander and Simmonds, 1987).

Rankin and Long (1987) observed that three separate failure modes can occur in a slab-column connection depending on the degree to which the connection is reinforced flexurally. If the connection has a low flexural reinforcement ratio, it is likely to fail in shear after extensive yielding of the flexural reinforcement in a ductile manner with yield lines coinciding with the tensile reinforcing grid. If the connection has a high flexural reinforcement ratio, the concrete on the compressive face of the slab near

the column will crush prior to any other failure occurring, and the failure will be localized to that area. For connections with reinforcement ratios in between the two extremes, the failure will be due to the opening of inclined shear cracks some critical distance from the column. Based on this observation, upper and lower limits were defined for the shear capacity of the column based on the connection strength with respect to the other two failure modes. The capacity of the slab in fully flexural shear failure is defined according to Equation 3.

$$P_{flex} = 8\left({}^{s}/_{(a-c)} - 0.172\right)M_b \tag{3}$$

In Equation 3, *s* is the side length of an isolated slab-column specimen (which usually approximates the area of negative moment around a column), *c* is the length of the column dimension (assuming a square column), and *a* is the distance between supports in the isolated slab-column connection. M_b is the flexural capacity of the slab. The capacity of the slab in localized compression failure is defined according to Equation 4.

$$P = \left({}^{25}/_{\left(ln(2.5a/c)\right)^{1.5}}\right)0.333f_c'd^2 \tag{4}$$

Between these two limits, the shear capacity of the connection is divided into two scenarios. Flexural punching is defined as a punching failure that occurs after partial yielding of the flexural reinforcement and is defined according to Equation 5.

$$P_{vf} = \left(8\left(\frac{s}{(a-c)} - 0.172\right) - \left(8\left(\frac{s}{(a-c)} - 0.172\right) - \frac{\frac{25}{\left(ln(2.5a/c)\right)^{1.5}}}{r_f}\right)\frac{M_b}{0.333f_c'd^2}\right)M_b \tag{5}$$

In Equation 5, r_f is a factor that adjusts for stress concentrations in the column. This factor is equal to 1 for circular columns and 1.15 for square columns. Shear punching is defined as a punching failure which occurs prior to any yielding of the flexural reinforcement. This capacity can be calculated according to Equation 6.

$$P_{vs} = 1.66\sqrt{f_c'}(c+d)d(100\rho)^{0.25} \tag{6}$$

In Equation 6, *d* is the effective slab depth and ρ is the flexural reinforcement ratio. The equations provided in this model are relatively easy to use and accurate in predicting the punching capacity for connections with simple geometries (Rankin and Long, 1987).

Shehata and Regan (1989) made improvements to a preexisting model by Kinnunen and Nylander (1960) to address concerns with some of the assumptions made in that model. As in the Kinnunen and Nylander (1960) model, the connection was divided into radial segments centered on the column's center of rotation, and a rigid wedge element was assumed to break from each element when punching failure occurs (Figure 4).

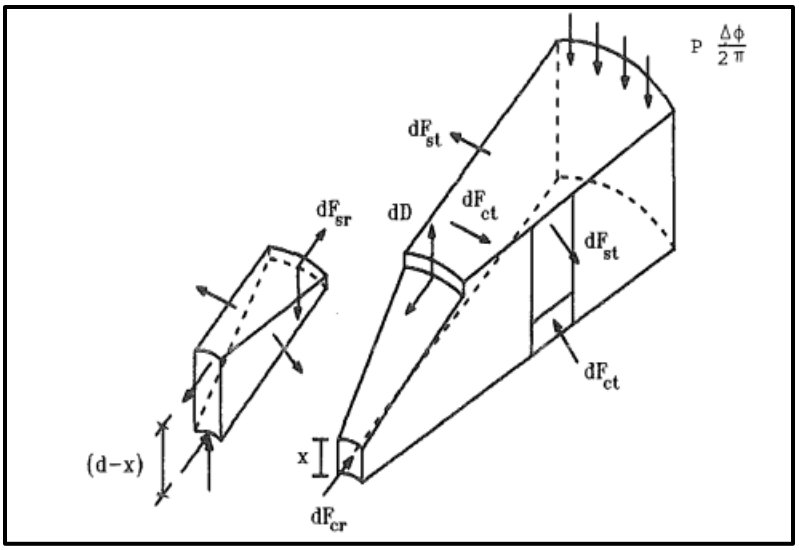

Figure 4: Radial element and Rigid Wedge Element (Shehata and Regan, 1989)

On this wedge element, equilibrium was used to develop expressions for various useful parameters for determining failure of the connection, such as neutral axis depth, inclination of the compression force, and the slab curvature. Forces considered include the reaction force at the supports, tangential forces in the flexural steel crossing the radial element boundaries, forces in the steel crossing the inclined wedge crack (longitudinal and dowel action), forces in the concrete normal to the radial boundaries, and forces in the concrete at the column. Three failure modes were defined in the model: when the inclination of the compressive force reaches 20° and causes tensile splitting of the element, when the strain on the compressive face of the element reaches the crushing strain of concrete (0.0035), or when the tangential strain reaches the crushing strain of concrete (0.0035) one neutral axis depth from the column. This model addresses the assumptions made by Kinnunen and Nylander (1960) with respect to dowel action forces, the failure mode, and the size of the slab/column (Shehata and Regan, 1989).

Muttoni (2008) more recently developed a model for estimating the punching strength of slab-column connections called critical shear crack theory. This model assumes failure results from a critical shear crack that propagates within the slab into the inclined compression strut transferring the shear force from the slab to the column. The width of this crack was shown to be proportional to the product of the slab rotation ψ and the effective depth of flexural reinforcement d. The amount of shear that can be transferred across this crack at a given crack width is also dependent on the roughness of the crack, as described in the following relationship (Equation 7, SI units).

$$\frac{V_R}{b_0 d^3 \sqrt{f_c}} = \frac{0.75}{\left(1 + 15\,\frac{\Psi d}{(d_{g0} + d_g)}\right)} \tag{7}$$

In Equation 7, d_g is the maximum aggregate size, d_{g0} is equal to 16mm, and b_0 is the perimeter of the critical section d/2 from the slab. Failure of a slab-column connection occurs at the intersection of the connection's load-rotation curve and the failure criterion shown in Equation 7. Thus it is necessary to determine the load-rotation curve for a connection to predict its failure. One presented approach to determining the load-rotation relationship is defined by the following Equations (8-10).

$$V = \frac{2\pi}{r_q - r_c} EI_1 \Psi \left(1 + ln\frac{r_s}{r_0}\right) \ (Elastic\ Regime) \tag{8}$$

$$V = \frac{2\pi}{r_q - r_c} EI_1 \Psi \left(1 + ln\frac{r_s}{r_y}\right) \ (Elasto - Plastic\ Regime) \tag{9}$$

$$V_{flex} = 2\pi m_R \frac{r_s}{r_q - r_c} \ (Plastic\ Regime) \tag{10}$$

The radius r_0 is located d from the column, the radius r_y is the yielded radius, the radius r_q is the radius of the slab supports, and the radius r_s is the full radius of the slab. Also, m_R is equal to the moment per unit length acting on the radius r_0. For use in codes, the radius of the slab is assumed to be 0.22L (22% of the span) and V_{flex} is assumed to be $8m_R$. The failure criterion can be simplified by assuming its shape to be that described in Equation 11.

$$\Psi = 1.5 \frac{r_s f_y}{d E_s} \left(\frac{V}{V_{flex}}\right)^{3/2} \tag{11}$$

However, while using simplified methods for the failure criteria and load-rotation relationship size effect was shown to affect capacity predictions. This model was shown to be useful because it gave accurate predations of both a slab-column's punching and rotation capacities. The simplified load-rotation relationship (or even a more simple bi-linear approximation) was shown to be accurate for thin slabs with regular reinforcement ratios. The model also effectively shows the effect of size/slenderness effect on punching behaviour of slab-column connections, and was proven effective when compared to code approximations and test data (Muttoni, 2008).

2.5 Review of Punching Shear Code Provisions

The design of a reinforced concrete flat slab supported on columns to resist punching shear is handled in slightly different manners by different governing bodies that produce design codes. Three of the most commonly used codes: ACI 318M-19, Eurocode 2, and Model Code 2010, have slightly different design procedures for punching shear which will be presented in this section. These codes consider many different parameters which have been determined to have an effect on the punching strength of a slab-column connection, however many of these parameters are not accounted for in every code. One thing that is common in these codes is that each of them assume that the strength of the connection should be determined at some critical section a certain distance away from the column. This critical perimeter concept was first introduced by Talbot (1913), and typically assumes uniform shear stresses along the (typically rectangular or circular) perimeter. Because of its simplicity and elegance, this concept has stood the test of time and is still used in design in current codes.

ACI 318M-19 is the most current design code released by the American Concrete Institute (ACI), formerly known as the National Association of Cement Users (NACU), and is based on over 100 years of research since their first code publication in 1908 (Milligan, 2018). The first provisions for punching shear in the ACI codes were added in ACI Standard Specification 1920 (Milligan, 2018) and since then have undergone several iterations to reach the current provisions, with particularly large changes being seen in the 1963 version of the code released after the work done by Moe (1961). The critical perimeter is

assumed to be located at a distance of d/2 from the column face or outer edge of the shear reinforced zone to account for the diagonal failure surface shown through various punching shear tests. On this failure surface the shear stress resisting capacity is determined as the minimum of Equations 12, 13, and 14.

$$v_c = 0.33\lambda_s\lambda\sqrt{f_c'} \tag{12}$$

$$v_c = 0.17\left(1 + {}^{2}/_{\beta}\right)\lambda_s\lambda\sqrt{f_c'} \tag{13}$$

$$v_c = 0.083\left(2 + \alpha_s\, {}^{d}/_{b_0}\right)\lambda_s\lambda\sqrt{f_c'} \tag{14}$$

In these equations, λ is a factor that adjusts for concrete density and λ_s is a factor that adjusts for size effect for beams with d > 250mm. The shear strength of the concrete is assume to be a third of the square root of the concrete compressive strength based on tests, as this is a more accessible parameter to test. Equation 13 accounts for non-uniform stresses resulting from column rectangularity through parameter β, which is the ratio of the column dimensions. Equation 14 accounts for the size effect of larger slabs through the ratio of effective depth to critical perimeter length b_0. α_s is a constant dependent on the column location in an assembly (interior, edge, or corner). After determining the shear stress resistance on the critical perimeter, the punching capacity is simply calculated according to Equation 15.

$$V_R = {}^{v_{c,min} b_0 d}/_{1000} \tag{15}$$

When unbalanced moments are present at the connection, they can be accounted for according to ACI 421.1R-20 (Equation 16).

$$V_R = \left(v_{c,min} - {}^{(\gamma_{vy} M_{u-y})}/_{J_{cy}}\, x - {}^{(\gamma_{vx} M_{u-x})}/_{J_{cx}}\, y\right) b_0 d \tag{16}$$

In Equation 16, $M_{u\text{-}x}$ and $M_{u\text{-}y}$ are the moments about the centroidal axis of the column, γ_{vx} and γ_{vy} are factors that determine the portion of the moments transferred by shear stress at the critical perimeter, J_{cx} and J_{cy} are properties of the critical perimeter based on its second moments of area, and x and y are coordinates of the critical point on the critical perimeter.

Eurocode 2 is the second iteration of a unified code meant to allow the same design framework to be used across Europe, while allowing individual nations to retain control of certain parameters, such as load levels (Johnson, 2009). Eurocode 2 uses a critical perimeter 2d from the column face or the edge of the shear reinforced area, primarily because at this perimeter the shear stress distribution was found to be almost uniform regardless of column rectangularity, allowing for the removal of column rectangularity parameters. The stress resistance along the critical perimeter is calculated according to Equation 17.

$$v_{Rd,c} = C_{Rd,c} k (100\rho_l f_{ck})^{\frac{1}{3}} \tag{17}$$

In Equation 17, f_{ck} is the characteristic concrete strength, k is a factor dependent on the effective depth that adjusts for size effect of the slab, ρ_l is based on the flexural reinforcement ratio in each orthogonal direction, and $C_{RD,c}$ is a constant based on the concrete safety factor common in most national codes. This

equation has been found to be fairly accurate for typical connections, however its accuracy decreases for connections with low or high reinforcement ratios. Therefore a lower and upper bound is set to the shear stress resistance on the critical perimeter according to Equations 18 and 19.

$$v_{Rd,min} = 0.035k^{\frac{3}{2}}f_{ck}^{\frac{3}{2}} \tag{18}$$

$$v_{Rd,max} = 0.4\big(0.6(1 - f_{ck}/250)\big)f_{cd} \tag{19}$$

In Equation 19 f_{cd} is the design concrete strength adjusted to account for long term effects. The punching capacity is calculated based on the minimum of the capacity along the critical perimeter and the column perimeter, calculated according to Equation 20.

$$V_R = min\begin{cases} v_{Rd,max}ud \\ v_{Rd,c}u_1 d \end{cases} \tag{20}$$

In Equation 20 u is the column perimeter length and u_1 is the critical perimeter length. When unbalanced moment occurs at the connection the applied shear force is adjusted by a constant β to account for the moment which is calculated according to Equation 21.

$$\beta = 1 + k\,{Mu_1}/{VW_1} \tag{21}$$

In Equation 21, k is the ratio of the column dimensions, M and V are the applied moment and shear, and W_1 is a factor that adjusts for non-uniformity of the shear stresses on the critical perimeter based on the column dimensions.

Model Code 2010 is the third iteration of a code published by the International Federation for Structural Concrete (fib), and is meant to be a starting point for which others can build their codes, providing them with state-of-the-art knowledge of the analysis and design of concrete structures (federation internationale du béton, 2013). The punching shear provisions in Model Code 2010 are based on Critical Shear Crack Theory (Muttoni, 2008), and as such are based on the rotational behaviour of the connection. The critical perimeter adopted in Model Code 2010 is located at a distance of d/2 from the column face. The punching capacity is calculated according to Equation 22.

$$V_{R,c} = k_\psi \sqrt{f_{ck}} b_0 d \tag{22}$$

In Equation 22, k_ψ is related to the rotational behaviour of the slab according to Equation 23.

$$k_\psi = \frac{1}{1.5 + 0.9\psi d k_{dg}} \leq 0.6 \tag{23}$$

In Equation 23, k_{dg} is a factor dependent on the maximum aggregate size in the concrete, and ψ is the slab rotation. Model Code 2010 adopts a level of approximation (LOA) approach to estimating the rotational behaviour of the connection, depending on how accurate the estimate is required for the desired application (Genikomsou, 2015). For the first and second LOA, the slab rotation can be estimated using Equations 24 and 25 respectively. For the third and fourth LOA, the slab rotation must be determined through linear or non-linear finite element analysis.

$$\psi = 1.5\, {r_s f_{yd}}\Big/{dE_s} \tag{24}$$

$$\psi = 1.5\, {r_s f_{yd}}\Big/{dE_s}\left({m_{Ed}}/{m_{Rd}}\right)^{1.5} \tag{25}$$

In these equations, r_s, f_{yd}, and E_s are the same parameters described earlier in Equation 11, m_{Ed} is the moment per unit length required in the support strip and m_{Rd} is the moment per unit length resistance provided in the support strip.

3.0 Calibration Background – the CDP Model and Test Specimens

3.1 Introduction to the Calibration Background Material

In this section, a brief overview of the CDP model is given, and a synopsis of the two series of test specimens that were used for the calibration of the NLFEA model are provided. This knowledge will be necessary for understanding the calibration procedure presented in Chapter 4.

3.2 The Concrete Damaged Plasticity Model

The NLFEA models presented in this thesis were calibrated in the commercial finite element software ABAQUS using the concrete damaged plasticity (CDP) model as the material model for the behavior of the slab concrete. The CDP model was first introduced by Lubliner et al (1989), and was further developed by Lee and Fenves (1998) to decouple the degradation damage from the effective stress determination (Jiang et al, 2021). The CDP model is composed of four main components: the determination of effective stresses via Hooke's law from trial strains, the test of a resulting stress state against a yield surface to determine yielding, the relation of plastic strains to the change in plastic potential via a plastic flow rule, and damage evolution with incrementation of stress and strain states (Jiang et al, 2021). In the CDP model, tensile and compressive responses are treated independently in terms of damage, as tensile damage accounts for the recovery of crushed concrete after compression-tension reversal, whereas compressive damage accounts for the re-closing of microcracks after tension-compression reversal (Alfarah et al, 2016). In the incremental theory of plasticity, the strain tensor ε can be decomposed into its elastic and plastic parts according to Equation 26 (Lee and Fenves, 1998)

$$\varepsilon = \varepsilon^e + \varepsilon^p = E^{-1}\sigma + \varepsilon^p \tag{26}$$

where E is the stiffness tensor, and ε^e and ε^p are the elastic and plastic portions of the strain tensor. Therefore, the stress tensor σ can be defined according to Equation 27.

$$\sigma = E(\varepsilon - \varepsilon^p) \tag{27}$$

The effective stress tensor $\bar{\sigma}$ is defined based on the undamaged elastic stiffness, according to Equation 28 (Lee and Fenves, 1998)

$$\bar{\sigma} = E_0(\varepsilon - \varepsilon^p) \tag{28}$$

where E_0 is the initial elastic stiffness tensor. Therefore, the stress can be related to the effective stress through transforming the initial stiffness tensor to the damaged stiffness tensor through a damage parameter (Equation 29).

$$\sigma = (1 - d)\bar{\sigma} \tag{29}$$

The plastic strain for each increment can be found through the plastic strain rate, which is determined through an associative flow rule (Equation 30) (Lapi et al, 2020).

$$\dot{\varepsilon}^p = \dot{\lambda}\,{}^{\delta G}/_{\delta \bar{\sigma}} \tag{30}$$

In Equation 4, *G* is the plastic potential surface and λ is the plastic loading factor. *G* is chosen to have the same shape as the yield surface. The yield surface evolves with the damage variable and limits the current admissible stresses. Because the model accounts for tensile and compressive damage separately, a yield function in terms of f_t and f_c, representing the uniaxial tensile and compressive strengths, is used as in Equation 31 (Lee and Fenves, 1998).

$$F(\sigma, f_t, f_c) \leq 0 \tag{31}$$

By relating stress to effective stress as in Equation 4, and f_t and f_c to their effective versions according to Equations 32 and 33, the yield function can be expressed as in Equation 34.

$$f_t = (1 - d_t)\bar{f_t} \tag{32}$$

$$f_c = (1 - d_c)\bar{f_c} \tag{33}$$

$$F\left(\bar{\sigma}, \bar{f_t}, \bar{f_c}\right) \leq 0 \tag{34}$$

By introducing a vector function for the cohesion $c = c(\bar{f_t}(d_t), \bar{f_c}(d_c))$, the yield function can be written in the following form (Equation 35) for frictional materials such as concrete (Lee and Fenves, 1998).

$$F(\bar{\sigma}) - c = 0 \tag{35}$$

The rate equation for the cohesion is presented in Equation 36 (Lapi et al, 2020)

$$\dot{c} = c\left[\frac{r(\sigma)}{f_t(d_t)}\bar{f_t}(d_t) - \frac{1-r(\sigma)}{f_c(d_c)}\bar{f_c}(d_c)\right]\dot{d} \tag{36}$$

where *r(σ)* is a weight factor defined in Equation 37, and the rate of damage is defined in Equation 38.

$$r(\sigma) = {\sum_{i=1}^{3}\langle\sigma_i\rangle}\Big/{\sum_{i=1}^{3}|\sigma_i|}, \langle\sigma_i\rangle = {1}/{2}\,(I\sigma_i I + \sigma_i) \tag{37}$$

$$\dot{d} = \frac{r(\sigma)}{g_t} f_t(d_t)\dot{\varepsilon}_1^p - \frac{1-r(\sigma)}{g_c} f_c(d_c)\dot{\varepsilon}_3^p \tag{38}$$

In Equation 38, g_t and g_c are the areas under the stress-plastic strain diagrams for uniaxial tension and compression respectively. The yield function *F* used is derived from the yield function for the Lubliner model, presented in Equation 39.

$$F = \frac{1}{1-\alpha}\left(\alpha I_1 + \sqrt{3J_2} + \beta\langle\hat{\sigma}_{max}\rangle - \gamma\langle-\hat{\sigma}_{max}\rangle\right) \tag{39}$$

In Equation 39 α, β, and γ are dimensionless constants defined in Equations 40, 41, and 42, and $\hat{\sigma}_{max}$ is the maximum principal stress.

$$\alpha = {(f_{b0}/f_{c0}) - 1}\Big/{2(f_{b0}/f_{c0}) - 1} \tag{40}$$

$$\beta = \frac{c_c(d_c)}{c_t(d_t)}(1-\alpha) - (1-\alpha) \tag{41}$$

$$\gamma = {3(1-K_c)}\Big/{2K_c - 1} \tag{42}$$

In these equations, f_{b0}/f_{c0} is the ratio of biaxial compressive yield stress to initial uniaxial compressive yield stress and K_c is the ratio of the square root of the second stress invariant on the tensile meridian to that on the compressive meridian (Lapi et al, 2020), as described in Equation 43.

$$K_c = {(\sqrt{J_2})_{TM}}\Big/{(\sqrt{J_2})_{CM}} \tag{43}$$

Since two different damage parameters, resulting in both tensile and compressive cohesion, are considered in the model, the equation for the yield surface becomes that in Equation 44 (Lapi et al, 2020).

$$F = \frac{1}{1-\alpha}\left(\alpha I_1 + \sqrt{3J_2} + \beta(d)\langle\hat{\sigma}_{max}\rangle - \gamma\langle-\hat{\sigma}_{max}\rangle\right) - c_c(d_d) \tag{44}$$

This yield surface takes the form of two combined Drucker-Prager type functions. Since this is the case, a Drucker-Prager type function must be chosen as the plastic potential function in the flow rule (Lee and Fenves, 1998). The plastic potential function chosen is shown in Equation 45.

$$G(\sigma,\psi) = \sqrt{(\epsilon f_{t0} tan\psi)^2 + q^2} - ptan\psi \tag{45}$$

In Equation 45 ψ is the dilation angle, or the angle that sets the slope of the function in the p-q plane, and ϵ is the eccentricity of the flow potential function, which defines the rate at which the function approaches its asymptote (Wosatko et al, 2019). The result of this model is that the evolution of the failure surface is dictated by the post-cracking behaviour of the concrete in tension and the plastic behaviour of the concrete in compression. The softening behaviour of the tension and compression response are determined according to the fracture energy (G_f) and crushing energy (G_c) respectively. However, the crushing energy is not usually considered a property of the material, and its determination is affected by many external factors such as the specimen slenderness and boundary conditions (Lapi et al, 2020). For these reasons, the model does not take into account softening behaviour with respect to the crushing energy and instead only references the fracture energy, which is related to tensile damage through the closing of microcracks.

3.3 Test Specimens

The finite element model was calibrated using two series of slab-column connections, the SB series and the SX series. The SB series was used to initially calibrate the CDP parameters and mesh characteristics, and then the model was applied to the SX series which is a more realistic representation of real-world loading conditions.

The SB series consists of six interior slab-column connections tested in concentric punching by Adetifa and Polak (2005). The specimens (SB1, SB2, SB3, SB4, SB5, and SB6) were 1800mm wide and were supported on neoprene pads during testing in a 1500mm square. Each specimen was 120mm thick and had two flexural reinforcing grids that were centered at 30mm from the top and bottom of the slab respectively. The tensile reinforcing grid had an average reinforcement ratio of 1.2%, whereas the compressive reinforcing grid had an average reinforcement ratio of 0.6%. An increasing displacement was applied on a 150mm square column stub in the center of the specimens. The properties of the concrete and steel used in the specimens is provided in Table 1. The specimens were supported along all four edges on neoprene pads to simulate simple supports, and the corners were prevented from lifting during the tests. SB1 contained no shear reinforcement, whereas SB2, SB3, and SB4/5/6 contained two, three, and four peripheral rows of shear bolts respectively in a double cruciform arrangement. The stem-stem spacing of the peripheral rows of shear bolts was 80mm. Specimens SB5 and SB6 contained four and two openings adjacent to the column stub that were half the width of the column stub. A conceptual loading diagram for the SB series specimens is presented in Figure 5. Plan and profile detail drawings of an SB series specimen are shown in Figure 6.

Series SX consists of eight exterior slab-column connections (XXX, SF0, SX-1SR, SX-2SR, SX-2SB, SH-2SR, HXXX, and HSF0) tested by El-Salakawy et al (1998, 2000) in concentric punching and unbalanced moment. The specimens were 1540x1020mm with a 250mm square column located in the center of the 1540mm width. The slabs were 120mm thick and the column stubs were 1520mm tall. Specimens contained two reinforcing grids. The tension layers had a reinforcement ratio of 0.75% in both directions while the compression layers had a reinforcement ratio of 0.45% in both directions. Columns were sufficiently reinforced to prevent failure prior to the failure of the slabs. Specimens XXX, SF0, HXXX, and HSF0 contained no shear reinforcement, while the remaining specimens were reinforced with one or two peripheral rows of 13mm rods (or 12.7mm bolts in the case of specimen SX-2SB) in a radial arrangement. The specimens were loaded both with a downwards vertical load on the column and a moment applied to the column stub applied via an inwards (towards the slab) load at the top of the column stub and an outwards (away from the slab) load at the bottom of the column stub. The ratio of the moment to the vertical load was kept constant at 0.3m throughout the tests, except in specimens HXXX and HSF0, where the ratio was kept constant at 0.67m. Specimens SF0, HSF0, and SH-2SR contained one 150mm square opening adjacent to the front edge of the column stub. The properties of the concrete and steel used in the samples are provided in Table 1. A conceptual loading diagram for the SX series specimens is presented in Figure 5. Plan and profile detail drawings of an SX series specimen are shown in Figure 6.

Table 1: SB and SX Series Slab and Reinforcement Properties

Series		**SB Series**						**SX Series**					
Specimen		**SB1**	**SB2**	**SB3**	**SB4**	**SB5**	**SB6**	**(H) XXX**	**(H) SF0**	**SX-1SR**	**SX-2SR**	**SX-2SB**	**SH-2SR**
Concrete Strengths (MPa)	f'_t	2.19	2.07	2.07	2.07	2.19	2.19	3.38	2.85	3.66	3.66	3.61	3.66
	f'_c	44.1	40.9	40.9	40.9	44.1	44.1	33.0	31.5	40.2	40.2	40.0	40.2
Flexural Steel Yield Strengths (MPa)	$F_{y,t}$	455	455	455	455	455	455	545	545	545	545	545	545
	$F_{y,c}$	455	455	455	455	455	455	430	430	430	410	410	410
Shear Reinforcement Yield Strength (MPa)	F_y	N/A	381	381	381	381	381	N/A	N/A	340	340	345	340

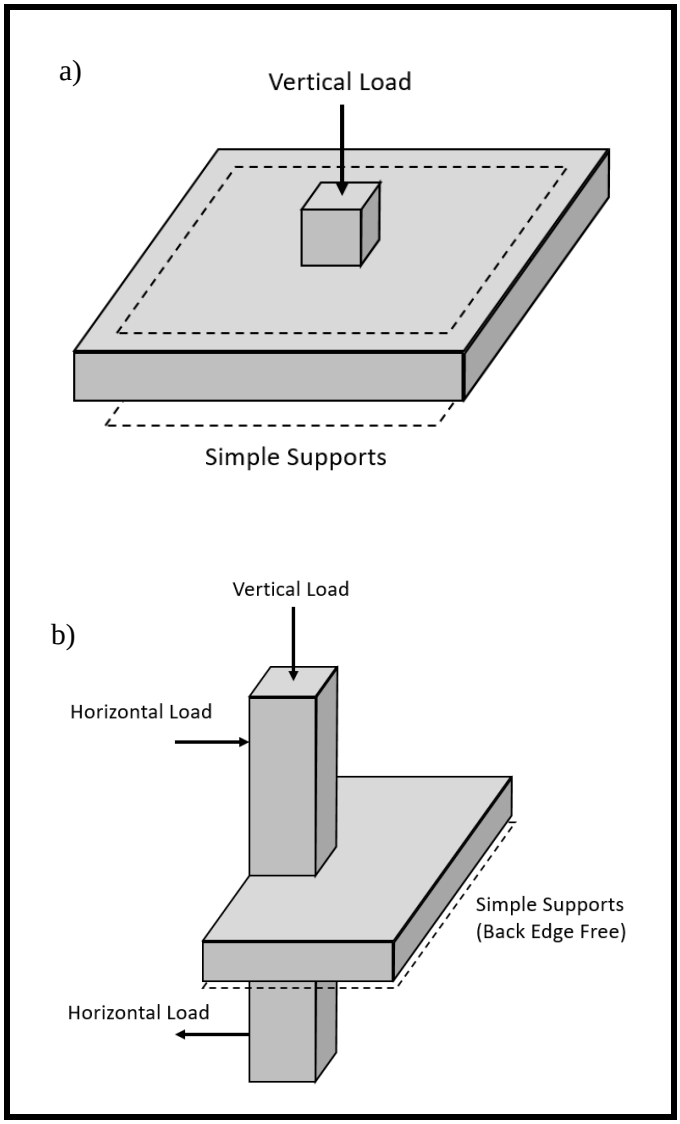

Figure 5: a) SB Series and b) SX Series Conceptual Loading Diagrams

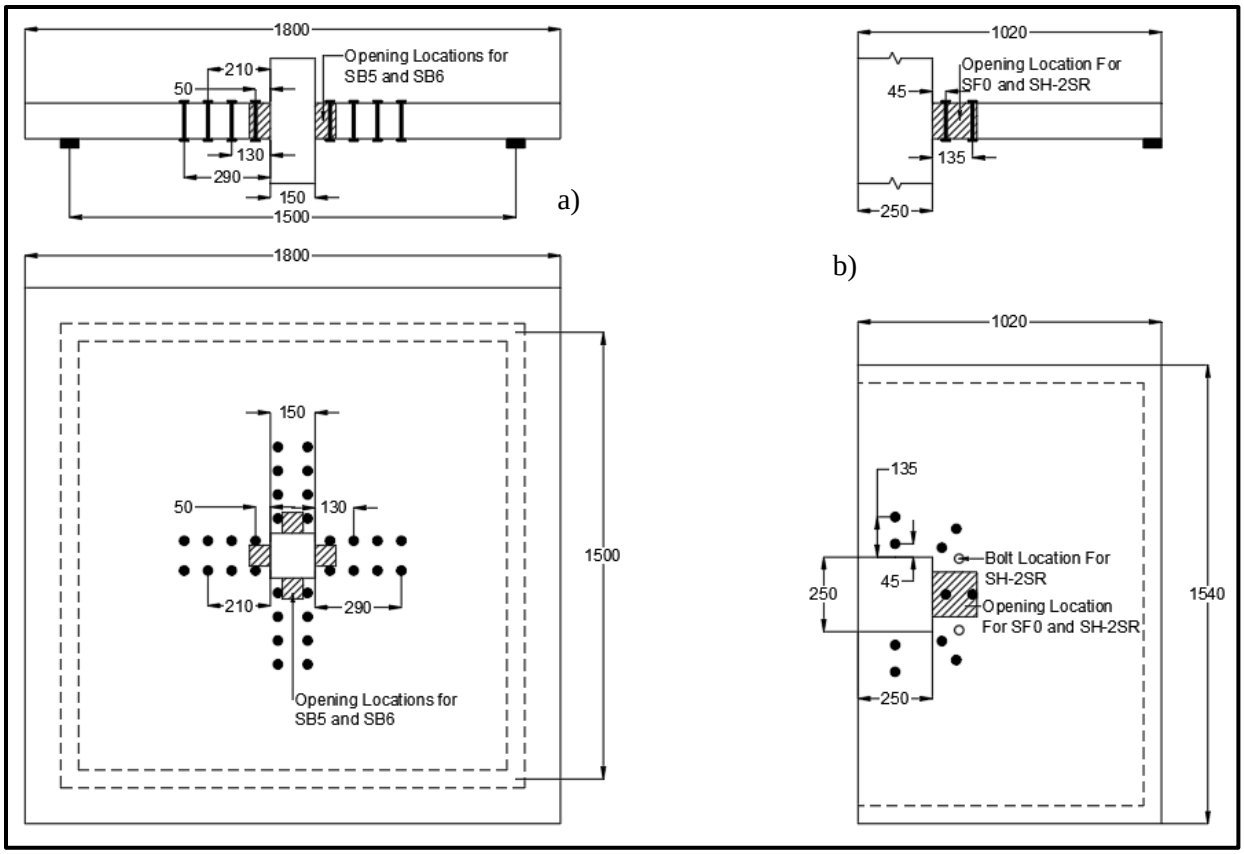

Figure 6: a) SB Series and b) SX Series Plan and Profile Diagrams

4.0 NLFEA Model Calibration

4.1 Introduction to Model Calibration

In this section, calibration of the modelling parameters important for NLFEA using the CDP model is discussed. Several studies which were conducted to determine optimal values of these parameters are presented. In these studies, all parameters were kept constant except for the parameter being studied, which was varied between several values near a base value taken from literature. The calibration was first performed on the SB series specimens due to the more straightforward loading they were subjected to, and the calibrated model was subsequently adjusted and applied to the SX series specimens to determine the model capability for more realistic loads. Final model parameters used for the SB series and SX series models can be found in Table 4 and Table 5 at the end of this Chapter.

4.2 Material Model Calibration

As discussed in Chapter 3, the CDP model is dependent on the post-cracking behaviour of the concrete in tension and the plastic behaviour of the concrete in compression. Therefore the choice of tensile and compressive material parameters and the models chosen for the material's uniaxial responses is important. In the calibrated models, the concrete in uniaxial compression is modelled using a modified Hognestad parabola approximated at 40 points and inputted as tabular data in ABAQUS with linear interpolation between points. In ABAQUS the final data point inputted is continued indefinitely in a horizontal line for values beyond the ultimate strain (Figure 7). Therefore the behaviour of the model near failure could depend on which stress value the parabola is terminated at.

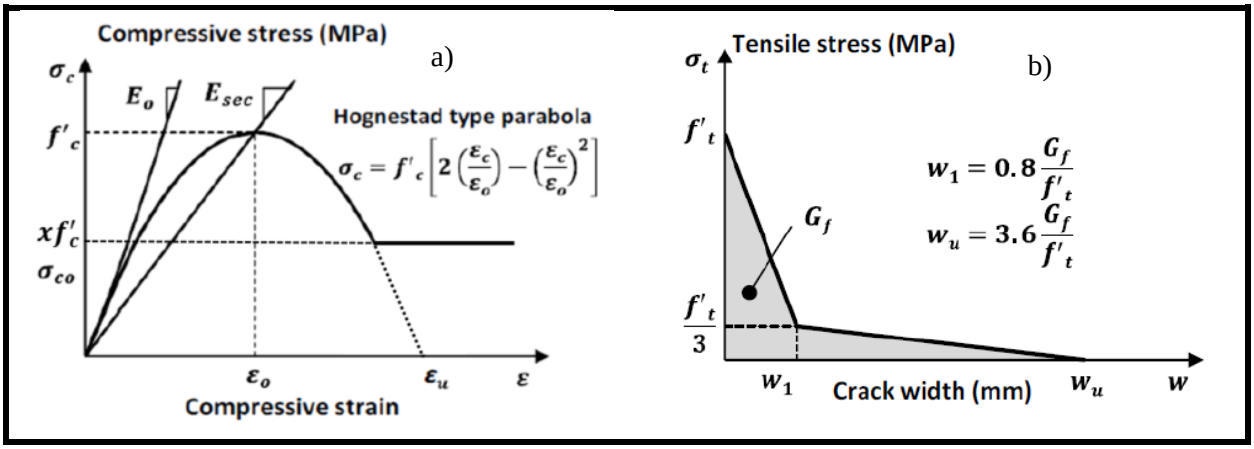

Figure 7: Model for a) Uniaxial Compressive and b) Uniaxial Tensile (Petersson, 1981) Behaviour of Concrete Models

A study was conducted on several of the SB series specimens to determine the optimal termination point considering several different termination points as a function of the concrete compressive strength (f_c'). The base value for the study was a value of 40% of f_c', which was used by Milligan (2018). The results of this study are shown in Figure 8. The results of the study show that variations of the compression curve termination point near the base value had a negligible effect on the overall specimen behaviour, and as such the value of 40% of f_c', which was used by Milligan (2018), was maintained in all future models.

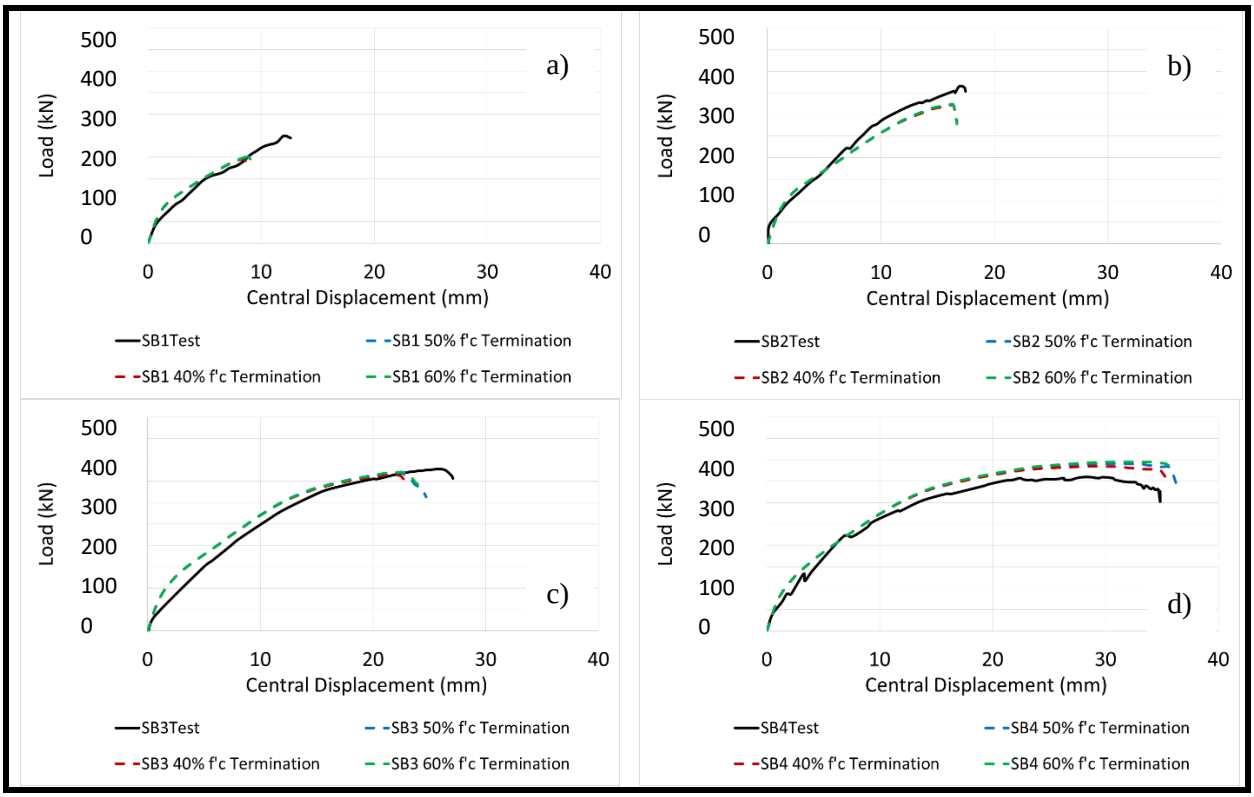

Figure 8: SB Series Compression Curve Termination Point Study a) SB1, b) SB2, c) SB3, and d) SB4

The uniaxial tensile behaviour of the concrete is modelled as linear until the tensile strength of the concrete (f_t') is reached. The subsequent softening behaviour is modelled using a bi-linear stress-crack width relationship from Petersson (1981) (Figure 7). The tensile strength of the concrete is approximated according to Equation 46. Several different equations can be used to calculated the fracture energy (G_f), which influences the post-peak uniaxial tensile behaviour of the concrete, and therefore the stiffness of the cracked concrete overall. In a previous study conducted by Genikomsou and Polak (2015), it was determined that G_f should be calculated according to CEB-FIP Model Code 1990 (Comité Euro-International du Béton, 1993) (Equation 47) for SB series specimen SB1.

$$f_t' = 0.33\sqrt{f_c'} \tag{46}$$

$$G_f = G_{fo}\left({f_{cm}}/{f_{cmo}}\right)^{0.7} \tag{47}$$

In Equation 47 G_{fo} is the base fracture energy value calculated from the maximum aggregate size according to Table 2, f_{cm} is calculated according to Equation 48, and f_{cmo} is equal to 10MPa.

$$f_{cm} = f_{ck} + \Delta f \tag{48}$$

Table 2: Base Values of Fracture Energy (Comité Euro-International du Béton, 1993)

Maximum Aggregate Size d_{max} (mm)	G_{fo} (Nmm/mm^2)
8	0.025
16	0.030
32	0.058

In Equation 48, f_{ck} is related to f_c' by Equation 49, and Δf is equal to 8MPa.

$$f_{ck} = f_c' - 1.6MPa \tag{49}$$

In order to choose the optimal fracture energy when considering more of the SB Series specimens, a study was conducted considering fracture energies near the values calculated from Model Code 1990 for SB series specimens SB1, SB2, SB3, and SB4. The base fracture energy values for the study were those calculated from Model Code 1990 (0.082N/mm for SB1 and 0.078N/mm for the other specimens using a maximum aggregate size of 10mm). The results of the fracture energy study are presented in Figure 9.

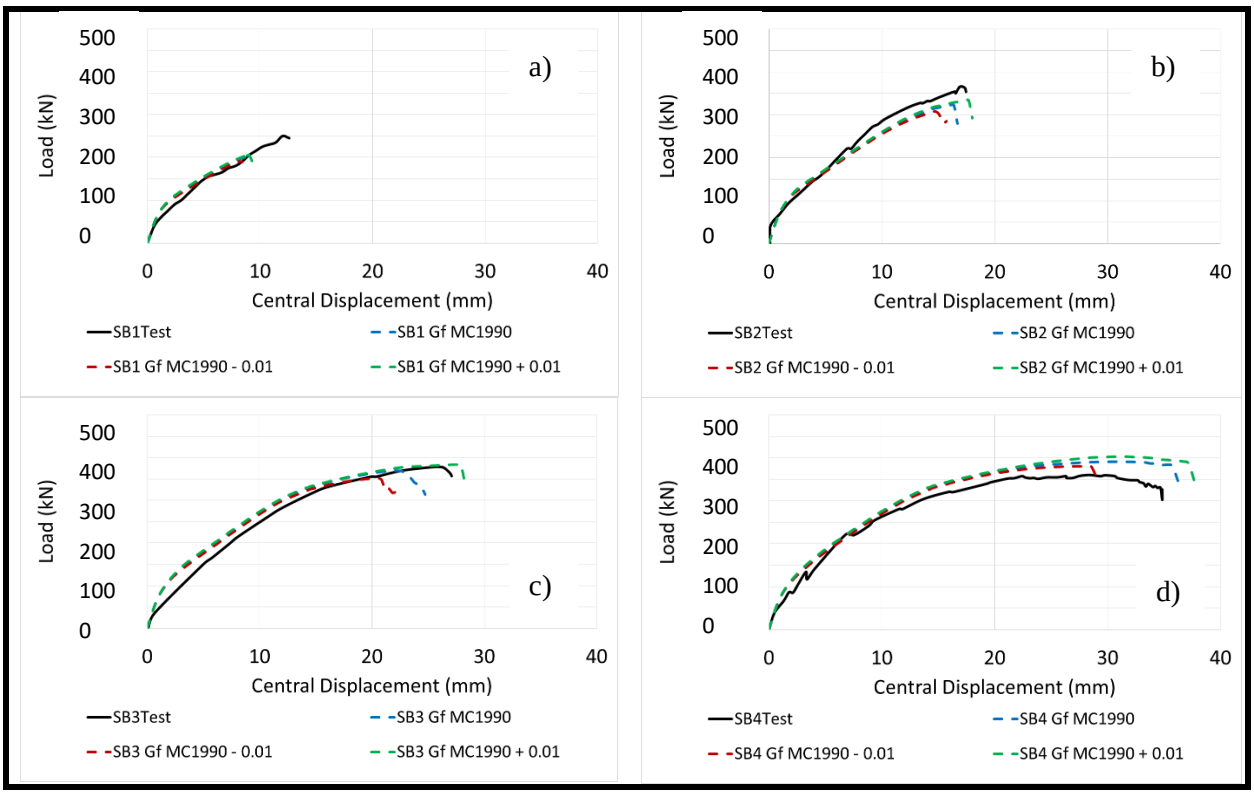

Figure 9: SB Series Fracture Energy Study a) SB1, b) SB2, c) SB3, and d) SB4

As shown in Figure 9 a variation of the fracture energy by 0.01N/mm changes the model capacity by less than 5%, but can change the failure displacement by up to 25%. Based on this study combined with studies on other parameters, the fracture energy chosen for all future SB series models is 0.092 and 0.088 which is 0.01N/mm greater than the value calculated from Model code 1990 and results in more accurately modelled post-peak displacements.

In order to eliminate the possibility of failure occurring in the column stubs of the specimens the column concrete was modelled as linear elastic with a modulus of elasticity five times greater than that of the slab concrete.

The flexural reinforcement and shear bolts/studs were both modelled using a bi-linear elastic-plastic stress strain relationship with the first segment reaching the yield stress and the second segment reaching the ultimate strength of the steel. The yield strengths of the tensile and shear reinforcement for the SB and SX series specimens is provided in Table 1. For the SB series the ultimate strength of the flexural reinforcement was found by Adetifa and Polak (2005) to be 610MPa, and the ultimate strength of the shear studs to be 455MPa. For the SX series, the ultimate strength of the tensile reinforcement was found by El-Salakawy et al (1998) to be 900MPa, the compression reinforcement to be 612MPa, and the shear reinforcement to be 414MPa. A Poisson's ratio of 0.3 was assumed for the reinforcement modelling.

4.3 CDP Model Calibration

The performance of CDP model is dependent on several parameters that define the failure surface and the plastic flow rule. Within ABAQUS, several of these parameters have default values that can be assumed for the modelling of most specimens. The eccentricity of the flow potential function (ϵ) can be set to 0.1, the ratio of biaxial compressive yield stress to initial uniaxial yield stress (f_{b0}/f_{c0}) can be set to 1.16 according to Kupfer et al (1969), and the ratio of the square root of the second stress invariant on the tensile/compressive meridians (K_c) can be set to 0.667.

The CDP model permits the use of a viscosity parameter (μ) which permits stresses to be slightly outside of the yield surface, contributing to better convergence of many models (Demir et al, 2018). For static analysis in ABAQUS standard, a value of 0.0005 is recommended to be used for convergence purposes (Demir et al, 2018), however, if a quasi-static analysis is being performed in ABAQUS Explicit the viscosity parameter can be omitted from the model. As discussed later in this section, the models in this study were ran using a quasi-static procedure, and as such no viscosity parameter was used in the SB or SX series models. Damage parameters can be specified in ABAQUS to determine the stiffness degradation of the concrete under cyclic behaviour. The default values for the damage parameters are 0 for both tension and compressive damage. For tension stiffness recovery and compressive stiffness recovern, the ABAQUS default values are 0 and 1 respectively. These values correspond to compressive stiffness being fully recovered upon crack closure and no tensile stiffness being recovered once cracking has begun, and is valid for most quasi-brittle materials (Dassault Simulia, 2020). Since no cyclic analysis was being conducted in this research, these values were maintained in all SB and SX series models.

An important parameter for the CDP model that doesn't have a default value for a wide range of specimens is the dilation angle (ψ). The dilation angle is used in the CDP model to represent the volume change in the concrete caused by inelastic strains (dilatancy). Lubliner et al (1989) suggested that the dilation angle be equal to 30° when used in the CDP model, however some researchers have found that values of the dilation angle between 35°-45° are more suitable. Genikomsou and Polak (2015) conducted a study on SB series specimen SB1 considering a wide range of dilation angles and found that a dilation angle of 40° was appropriate for that specimen. An additional study was conducted for this calibration considering dilation angles near the base value of 40° for SB specimens SB1, SB2, SB3, and SB4. The results of this study are shown in Figure 10.

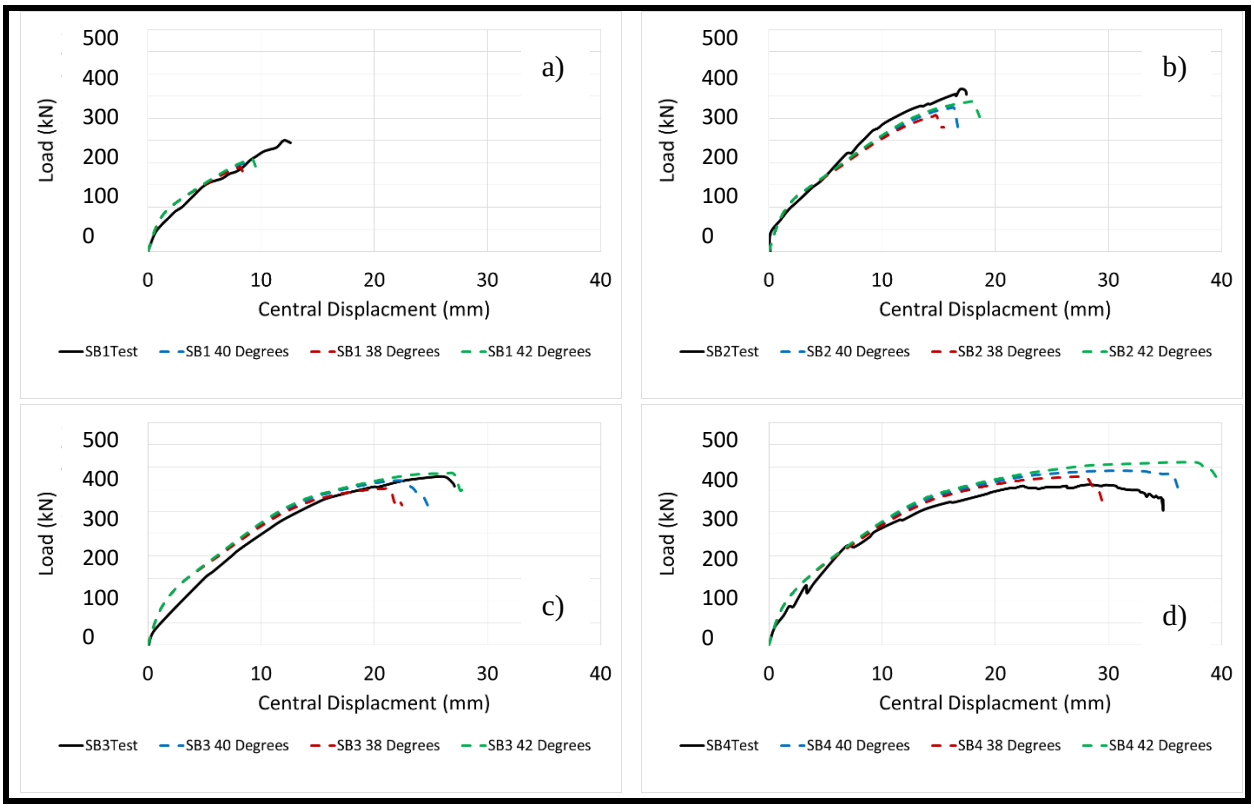

Figure 10: SB Series Dilation Angle Study a) SB1, b) SB2, c) SB3, and d) SB4

As shown in Figure 10, a change of 2° in the dilation angle changes the capacity of the models by less than 5% in all cases, but can change the failure displacement by up to 2%. Based on the results of this and other studies, a dilation angle of 40° was chosen for all future SB and SX series models.

4.4 Mesh Calibration

ABAQUS utilizes a smeared crack approach within the CDP model. In a smeared crack model, the stiffness of the concrete is decreased in the direction of the principal stresses to simulate cracking while maintaining a continuum mesh (Milligan, 2018). This results in behaviour that is mesh dependent, as if the mesh is too fine, the cracking behaviour can localize into a single row of elements giving inaccurate results. Genikomsou and Polak (2015) stated that the mesh size should be greater than the maximum aggregate size, and it is stated in the ABAQUS benchmarks guide (Dassault Simulia, 2016) that at least four elements should be provided through the depth of a specimen to avoid numerical effects such as hourglassing in the elements.

Additionally, the size of the mesh determines the depth at which the reinforcement is located, as the reinforcement elements are mapped to the edge of the solid concrete elements. Considering this, it may be desirable to structure the mesh so that the tensile reinforcing grid is in the same position as the tests, which would result in a mesh size of 15 or 30mm for the SB series specimens and a mesh size of 10 or 20mm for the SX series specimens. A mesh convergence study was conducted on specimen SB4, the results of which are shown in Figure 11.

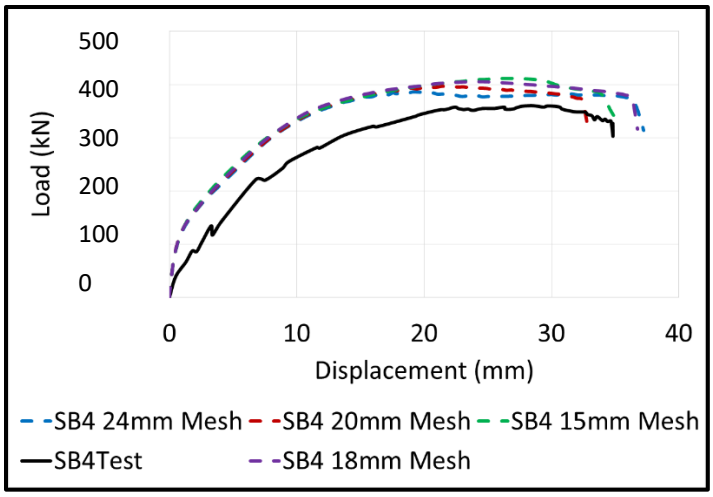

Figure 11: SB4 Mesh Convergence Study

While the size of the mesh had little effect on the model capacity, the failure displacement was best predicted by the 15mm mesh size for SB series specimen SB4. Therefore, structuring the mesh to prevent shifting of the flexural reinforcing grids may play a role in increasing the accuracy of the model. Based on these results a mesh size of 15mm was chosen for all future SB series models, and a mesh size of 20mm was chosen for all future SX series models. Meshed models for an SB series and an SX series model are presented in Figure 12.

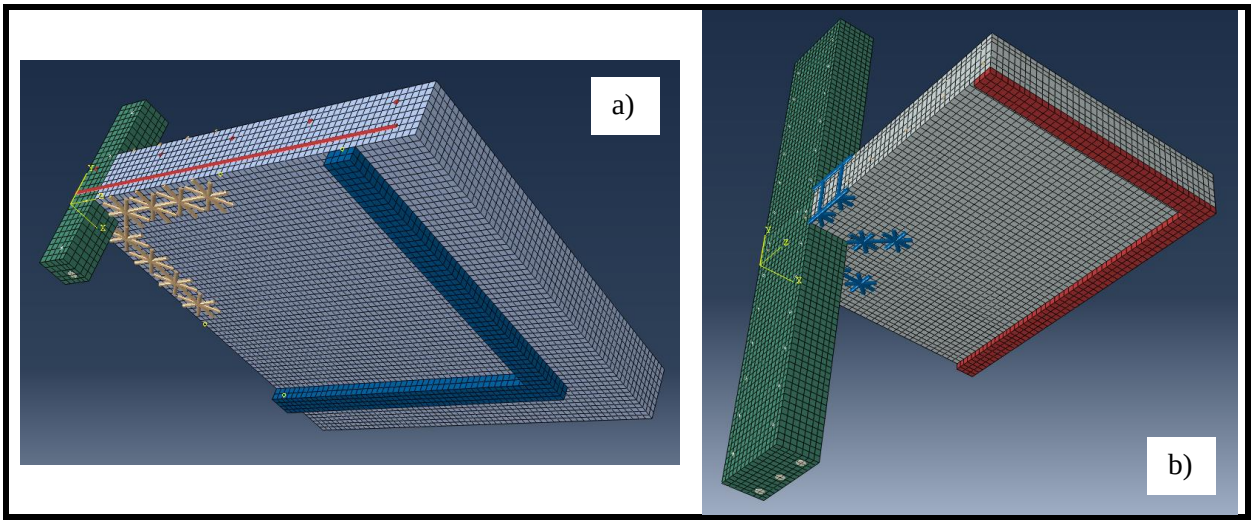

Figure 12: a) SB Series and b) SX series Meshed Models

The element type chosen for the modelling of the slab and column concrete was three-dimensional linear eight node hexahedral reduced integration elements (C3D8R). This was based on a mesh type study conducted on SB specimen SB1 by Genikomsou and Polak (2015) which investigated the performance of the C3D8R element along with three-dimensional linear eight node tetrahedral elements (C3D4) and three-dimensional ten node quadratic tetrahedral modified elements (C3D10M). As linear solid elements were selected for the modelling of the concrete, linear two node truss elements were selected to model the longitudinal reinforcement to provide nodal agreement in the model.

4.5 Loading and Boundary Condition Calibration

Boundary conditions can have a significant impact on the behaviour of a slab-column connection in punching, and a variety of different boundary conditions have been used in different tests by different researchers. For many tests conducted at the University of Waterloo, including those by Adetifa and Polak (2005), the slabs were supported on neoprene supports in an effort to mimic the behaviour of a simple support and allow for rotation of the slab edges. Modelling the boundary conditions of the slab as simple supports along one element edge can lead to stress concentrations in the model, while distributing the simple supports over several rows of elements prevents the rotation of the edges. A more optimal method of modelling this support condition is to model the neoprene pad attached to the slab and support the bottom of the neoprene pad. Genikomsou and Polak (2015) conducted uniaxial tests on the neoprene material used in the tests and determined that the neoprene had an elastic modulus of 8.31MPa and a Poisson's ratio of 0.5. It was also determined that the load levels in the neoprene were very low during testing and that the neoprene would not reach its phase of non-linear response. For this reason the neoprene pad was modelled as linear-elastic in ABAQUS.

Another boundary condition in the models is the loading. The way the load is applied in ABAQUS depends on whether the test was load controlled, where the load increases incrementally and the displacement is dependent on the slab stiffness, or displacement controlled, where the displacement increases incrementally and the load required depends on the slab stiffness. For the test specimens considered, the SB Series specimens were tested and modelled in displacement control and the SX series specimens were tested and modelled in load control.

The method of applying the load in ABAQUS also depends on whether the models are created as static procedures in ABAQUS standard or as quasi-static procedures in ABAQUS explicit. The advantage of running the static analysis using the dynamic version of the program (ABAQUS Explicit) is that the runtime of the models is significantly reduced when ran in this way. Use of a quasi-static procedure also helps identify failure in load-controlled simulations (Milligan, 2018). Researchers such as Genikomsou and Polak (2015), Milligan (2018), and Navarro et al (2018) have successfully used a quasi-static analysis procedure for NLFEA of slabs subjected to punching shear in ABAQUS, however it is important when doing so to verify that the model is not experiencing inertial effects prior to failure that could influence the behaviour of the model. A study was conducted on several SX series specimens to verify the applicability of the quasi-static procedure. First, the kinetic energy and net energy were tracked during a run of the model for specimen SH-2SR, the results of which are shown in Figure 13 and Figure 14.

No significant kinetic energy was present in the model prior to failure, suggesting that the model was in a static state. Also, the energy balance was satisfied up until failure, suggesting that the quasi-static procedure was not negatively influencing the model. Another factor that was checked in this study was whether the length of the timestep for applying load increments was having an effect on the model. If the timestep is too short loads can be applied too suddenly leading to dynamic effects in the models, however using a shorter timestep significantly reduces the runtime of the model. A study was conducted on SX series specimen SX-1SR with several timestep lengths, as well as a static model created in ABSQUS Standard. The results of the study are shown in Figure 15.

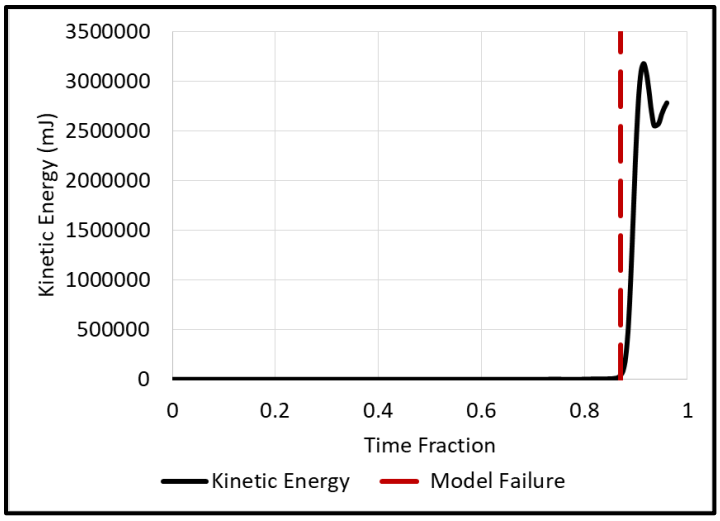

Figure 13: Specimen SH-2SR Kinetic Energy

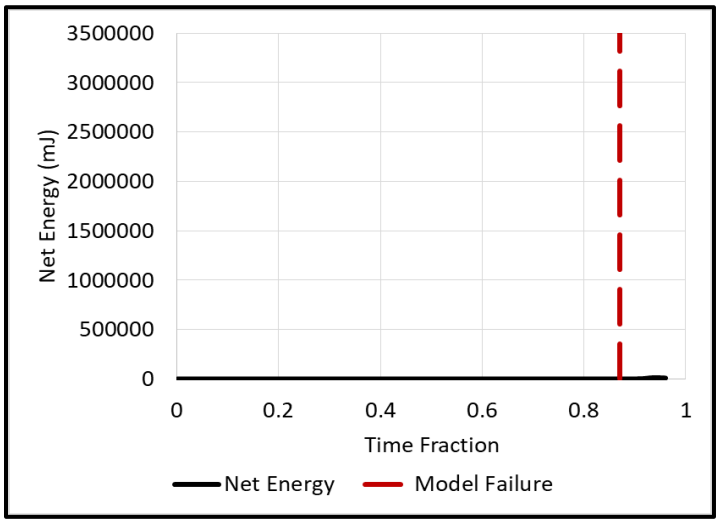

Figure 14: Specimen SH-2SR Net Energy Balance

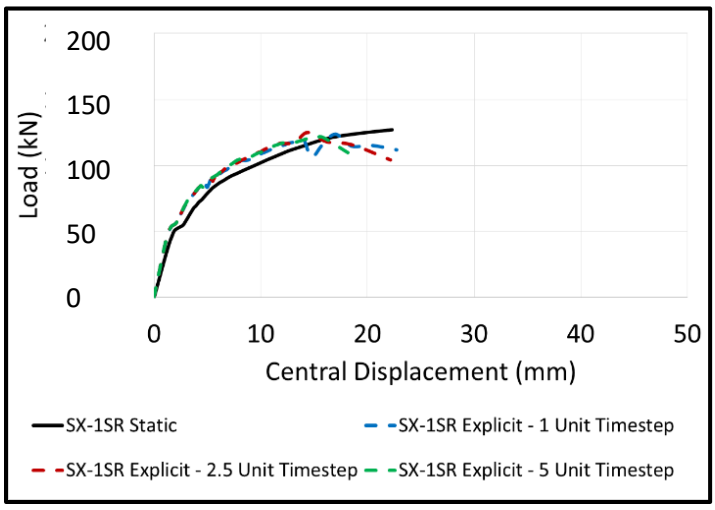

Figure 15: Specimen SX-1SR Timestep Study

When the timestep is set to the shorter values, a disturbance in the load-deflection curve is seen at around 15mm of central displacement. This disturbance is not seen in the static model or the dynamic models with larger timesteps, suggesting that it is a result of the shorter timestep inducing dynamic effects in the model. Other than this disturbance the behaviour of the models in ABAQUS explicit are very similar and accurate to the static model, so the models were created using quasi-static analysis procedures in ABAQUS explicit to save time and the disturbances in the SX series models were treated as outliers and removed in future models.

Based on these criteria the central load for the SB Series specimens was applied as a displacement velocity (mm/time) which increased to a value beyond the failure displacement of the tests by the final timestep. The central load and the loads which made the moment couple for the SX Series specimens were applied as pressure loads multiplied by a linear amplitude which resulted in the correct loads at each timestep as they were applied in the tests.

Finally, in order to reduce runtime, the symmetry of the specimens was utilized so that only one quarter of each SB Series specimen and one half of each SX Series specimen were modelled. All boundary conditions for an SB series model and an SX series model are presented in Figure 16 and Figure 17 respectively.

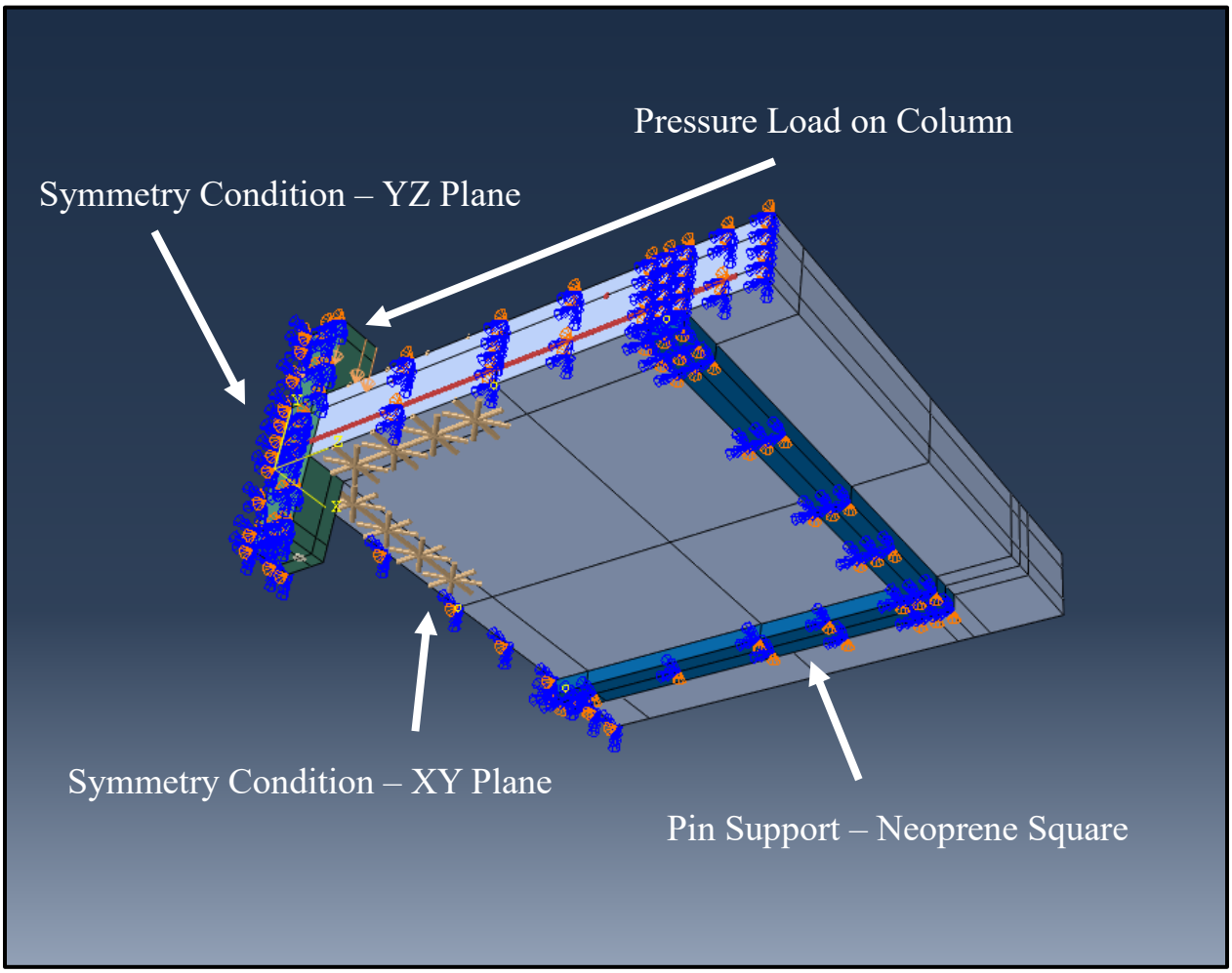

Figure 16: SB Series Model Boundary Conditions

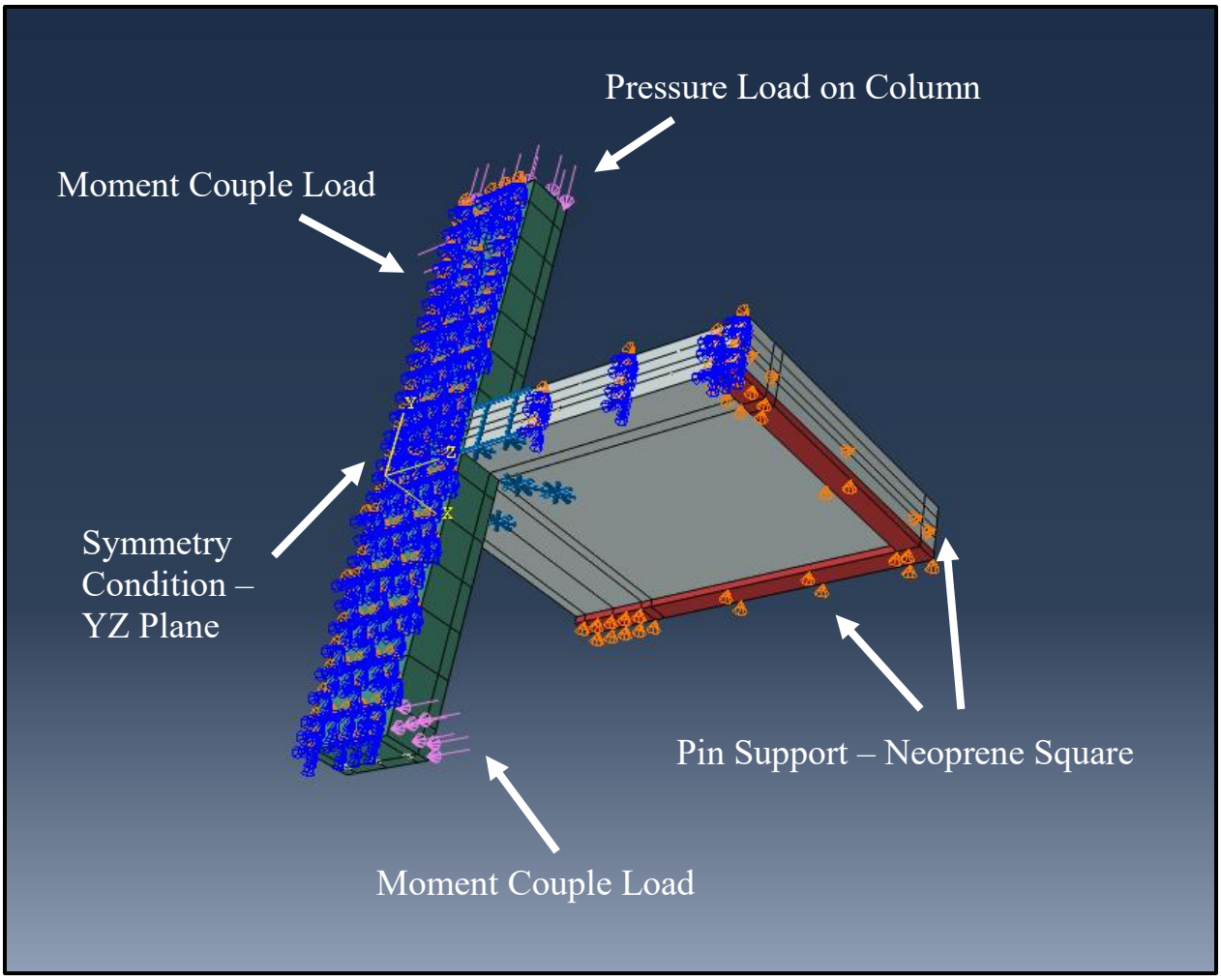

Figure 17: SX Series Model Boundary Conditions

4.6 Shear Reinforcement Model Calibration

The modelling of shear reinforcement is the primary consideration in this work. It should be noted that shear bolts and studs have been found to be identical mechanically and are modelled in the same manner in this research. The method for modelling the shear reinforcement in the SB and SX series models is based on work done by Genikomsou and Polak (2016), who conducted a study on shear bolt modelling in ABAQUS where the shear bolts were modelled as a "stem-star" wire mesh, an I-beam comprised of shell elements, or using solid elements. The study showed that the optimal way of modelling the shear reinforcement was using a wire "stem-star" mesh using quadratic three node beam elements (B32). The shear bolt modelling method is illustrated in Figure 18. This method allowed for the anchorage of the stems to the concrete using the "stars" which transferred the stem load to the concrete surface without inducing a load concentration at the tip of the stem leading to crushing of the adjacent concrete nodes.

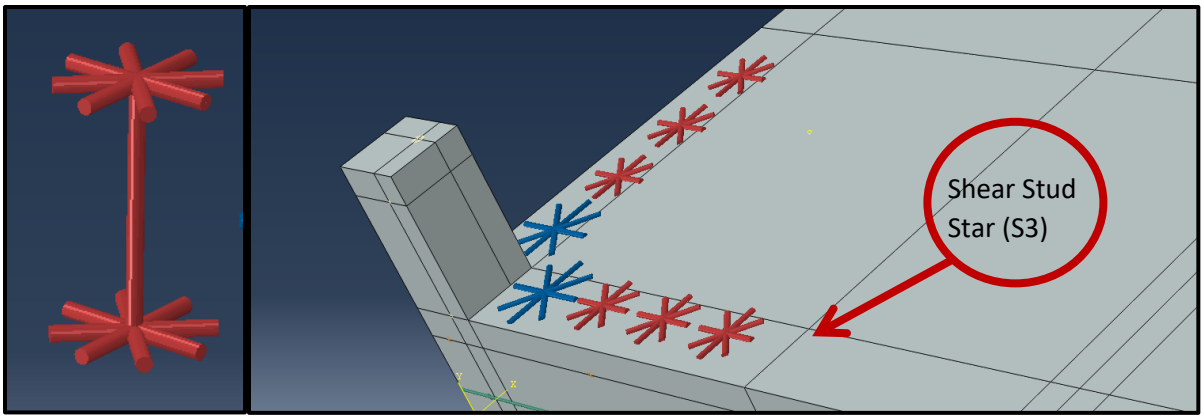

Figure 18: Shear Stud/Bolt Modelling Method

In the models by Genikomsou and Polak (2016) the shear bolt/stud stars (S3s) have a diameter equal to twice the distance between the column face and the first shear bolt (column-stem spacing). When investigating the rotational behaviour of the SX series models, the models for specimens SX-2SR and SX-2SB showed overly stiff moment-rotation behaviour using S3s of this size. The deformed shape of the models revealed rigid movement of the slab next to the column as a result of the overlapping S3s.

In order to investigate the effect of changing the S3 diameter, a study was conducted considering 20 models of the SX series specimen SX-2SR with S3 diameters varying between 24% and 100% of the spacing between adjacent shear studs (stem-stem spacing). The strain in the shear studs was investigated first, and three distinct "zones" of behaviour were identified in the studs depending on the S3 diameter as shown in Figure 19 for the second edge bolt. Bolt strain diagrams for all of the S3 study specimens are provided in Appendix A.

The first zone (type 1) occurs when the S3 diameter is less than 60% of the stem-stem spacing, and results in many of the bolts developing small strains meaning that their influence in shear carrying capacity is underestimated. This is because the S3 diameter is too small to properly confine the surrounding concrete, and cracking can be seen between and around the studs, specifically between the first stud and the column perpendicular to the moment. This can be seen by observing the model crack patterns (eg. Figure 20).

The second zone (type 2) occurs when the S3 diameter is between 60-80% of the stem-stem spacing. It can be shown through an analysis of the model crack patterns that this type shows significantly less strain between the column and first row of shear studs, however significant strain is still present within the column and first shear stud to prevent it from behaving rigidly (eg, Figure 21).

Finally the third zone (type 3) occurs when the S3 diameter is greater than 80% of the stem-stem spacing, and shows very little strain between the column and first shear stud (eg Figure 22). This means the specimen is behaving rigidly at its connection point, preventing the correct rotational behaviour from occurring. All S3 study crack patterns are provided in Appendix A.

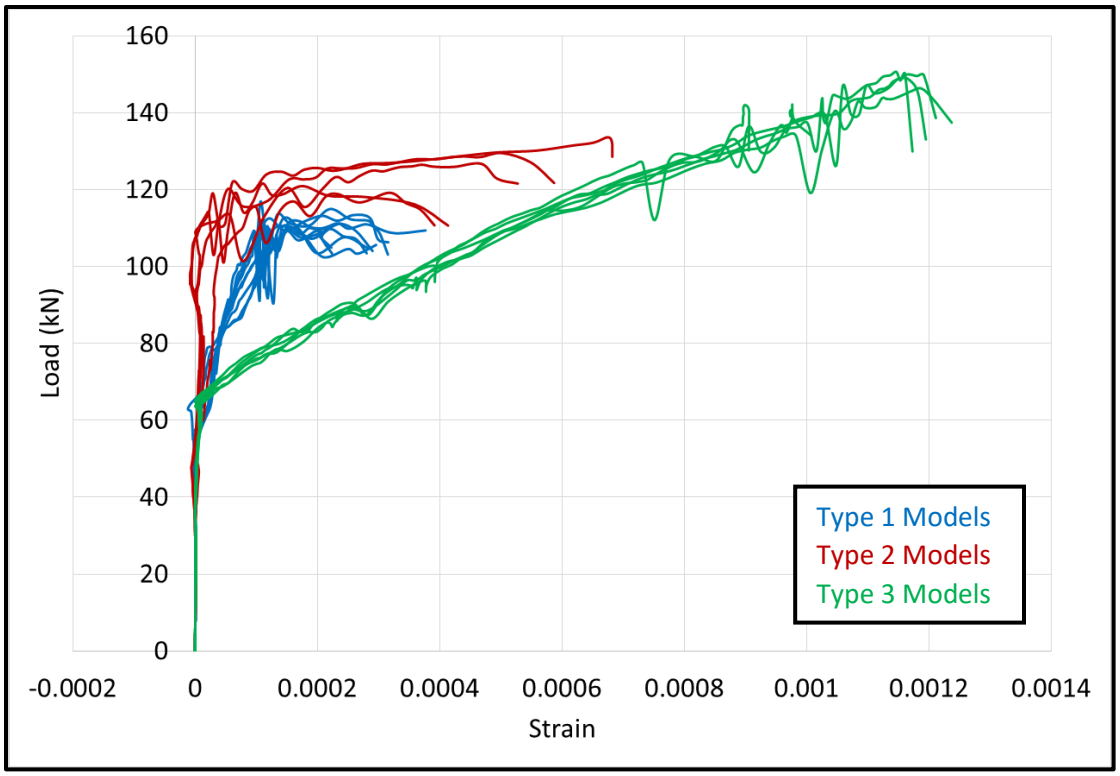

Figure 19: S3 Study SX-2SR Specimen Edge Bolt 2 Strains

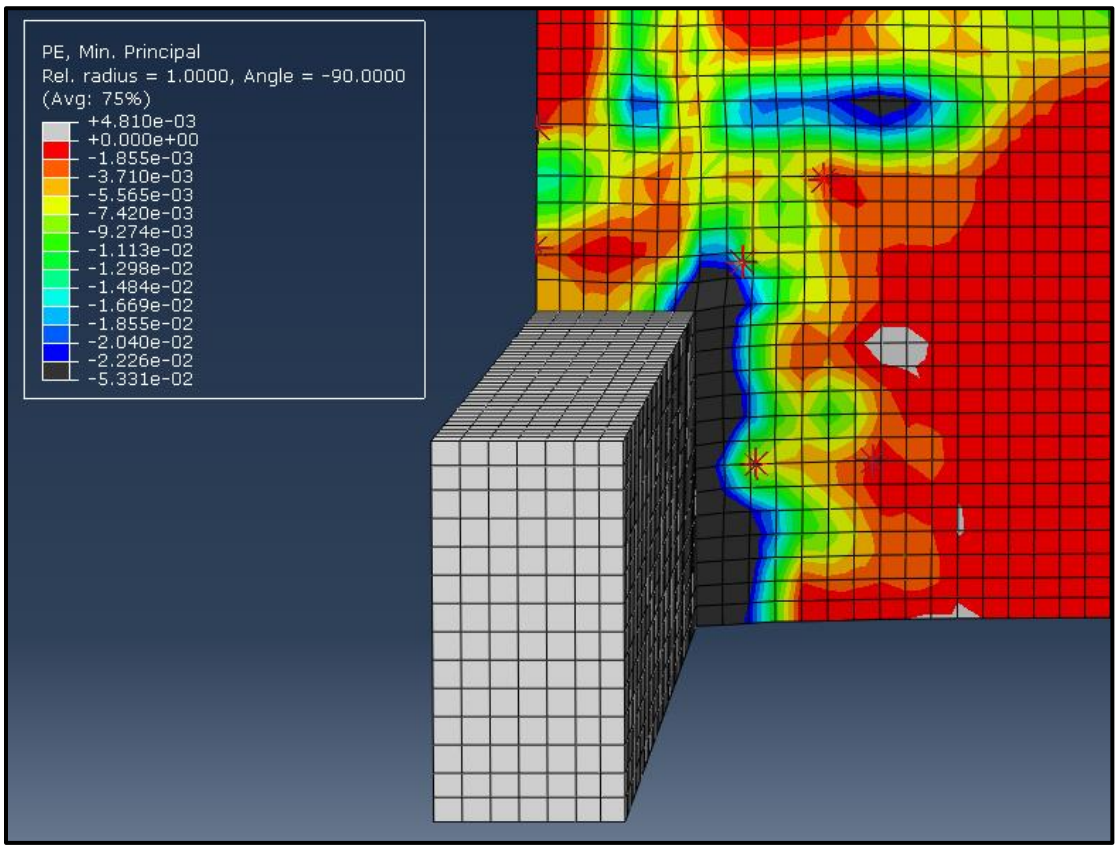

Figure 20: S3 Study SX-2SR Type 1 Crack Pattern

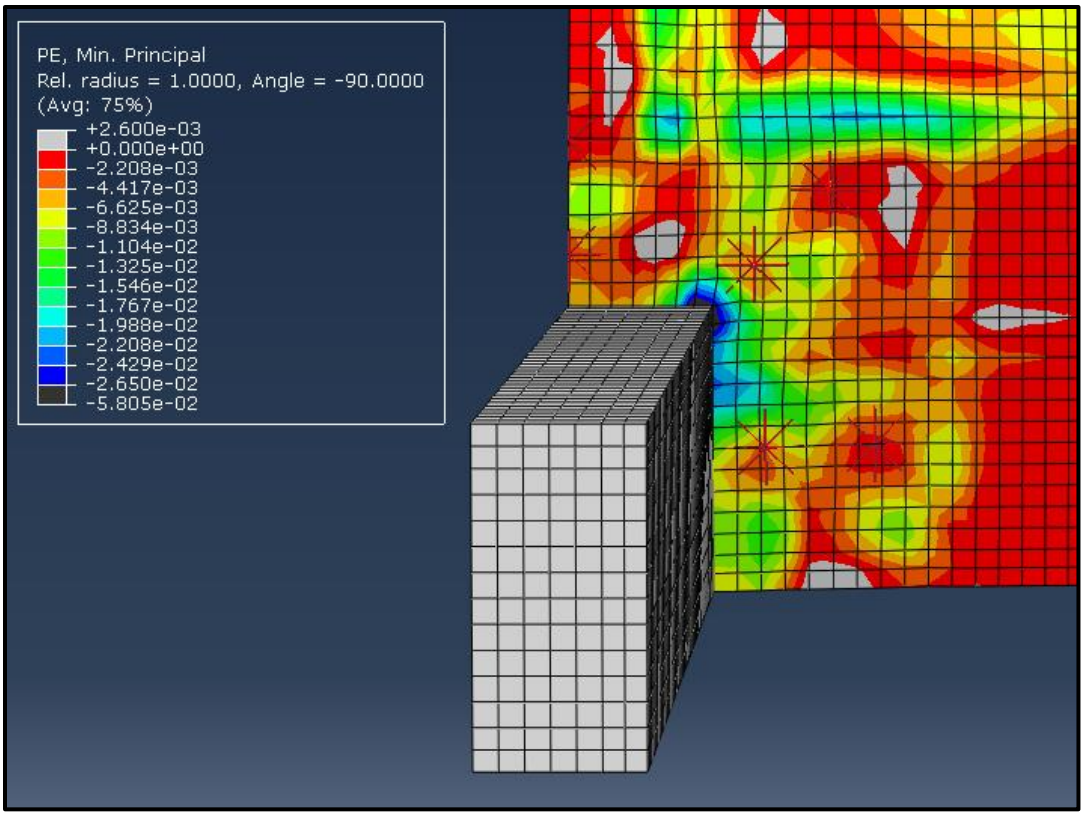

Figure 21: S3 Study SX-2SR Type 2 Crack Pattern

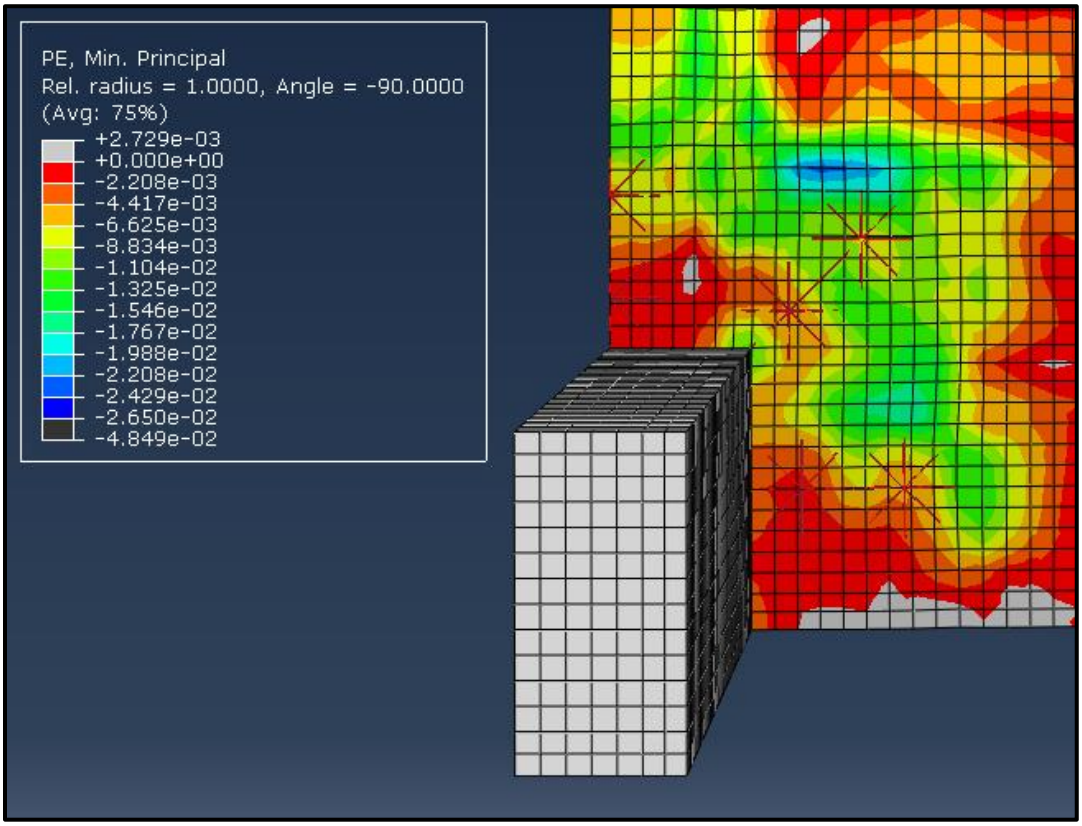

Figure 22: S3 Study SX-2SR Type 3 Crack Pattern

Moment-curvature and load-deflection behaviour for selected S3 study SX-2SR curves and the test data for specimen SX-2SR are presented in Figure 23. Based on the moment-curvature data, the models that are accurate within 10% of the test results are type 2 models with S3 diameters of 69%, 73%, and 77% of the stem-stem spacing and type 3 models with S3 diameters of 82% and 86% of the stem-stem spacing. Based on the load-deflection behaviour, the models that show the same level of accuracy are all of the type 3 models. This suggests that the optimal models are the type three models with lower S3 diameters, which experience flexural failure outside of the shear reinforced zone consistent with the failure behaviour of the test specimen SX-2SR.

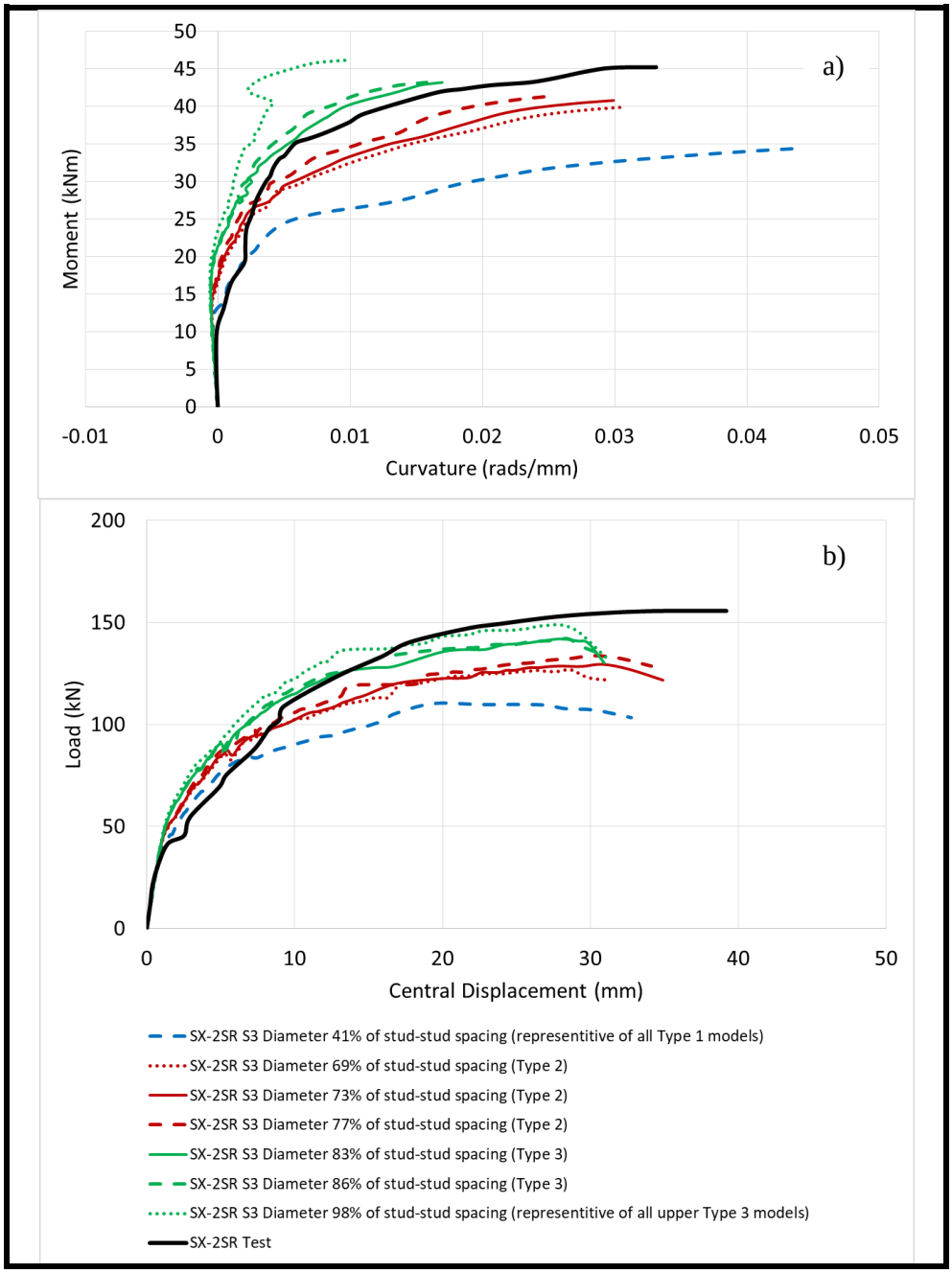

Figure 23: S3 Study SX-2SR a) Moment-Curvature Behaviour and b) Load-Deflection Behaviour

To verify the results of this study, models with S3 diameters that fell within the lower stem-stem spacing range of the type 3 zone for specimen SX-2SR were created for SB series specimen SB4 to determine if the resulting behaviour was still reasonable. Load-deflection behaviour for these models is shown in Figure 24. Figure 24 shows that these models have significantly decreased capacity and stiffness when compared to the original model with S3 diameters (125% of the stem-stem spacing) used by Genikomsou and Polak (2016). Interestingly the models, which have S3 diameters of 80% and 84% of the stem-stem spacing, behave very similarly to a model with a S3 diameter of 23% (type 1). This suggests that the S3 diameter cannot be set as a percentage of the stem-stem spacing across different specimens.

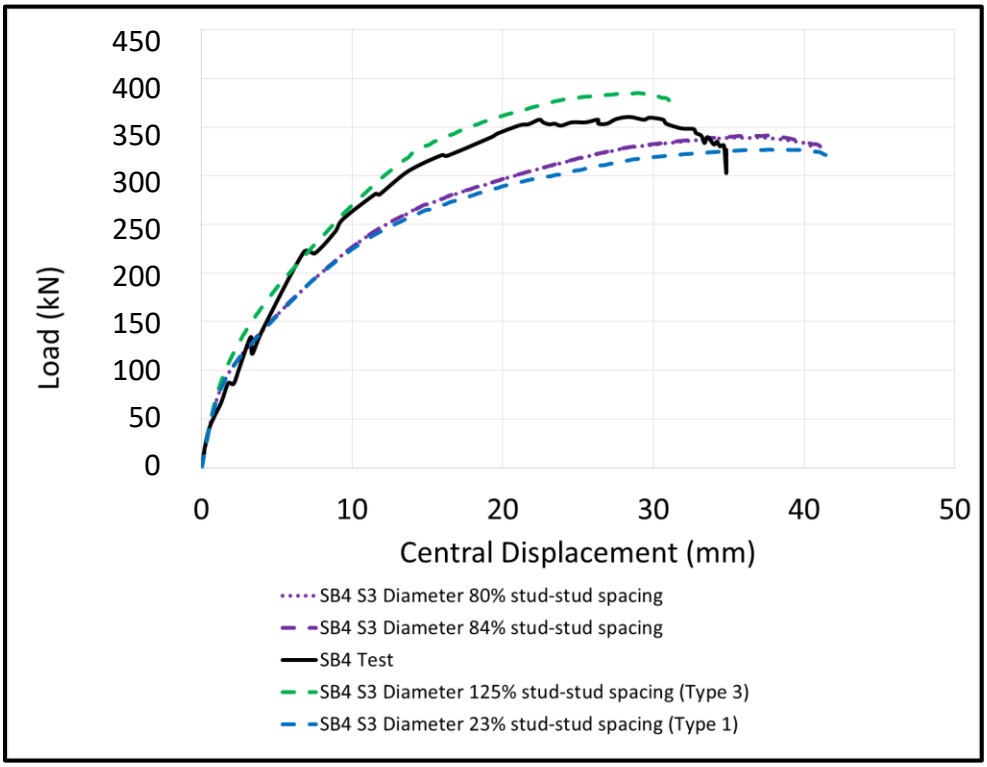

Figure 24: S3 Study SB4 Models with S3 Diameters Comparable to Successful SX-2SR Models' Stem-Stem Spacing Percentage

The main difference between the model "zones" is the presence of large strains between the column and the first shear stud (Figure 20, Figure 21, and Figure 22), therefore the problem was next investigated in terms of the distance between the column and the edge of the first S3 (column-first S3 gap). The first row of shear reinforcement has been shown to be the most critical in determining the punching behaviour of slab-column connections (Lips et al, 2012), and has stricter code requirements (for example, CSA A23.3-10 Cl 13.3.8.6).

This would explain why the SB4 models displayed a type 1 behaviour when the same SX-2SR models did not, as the column-stem spacing was larger for the SB series specimens when compared to the subsequent stem-stem spacing (50mm, 80mm, 80mm, 80mm). The column-stem spacing was exactly half of the stem-stem spacing for the SX series specimens (45mm, 90mm). This concept is illustrated in Figure 25. If the gap between the column-stem is the determining factor in the model behaviour, the S3 diameter of the subsequent studs/bolts would have little effect on the overall behaviour. To investigate this, several "hybrid" models were created for SB specimen SB4, with S3 diameter configurations according to Table 3. The load-deflection behaviour of these specimens is shown in Figure 26.

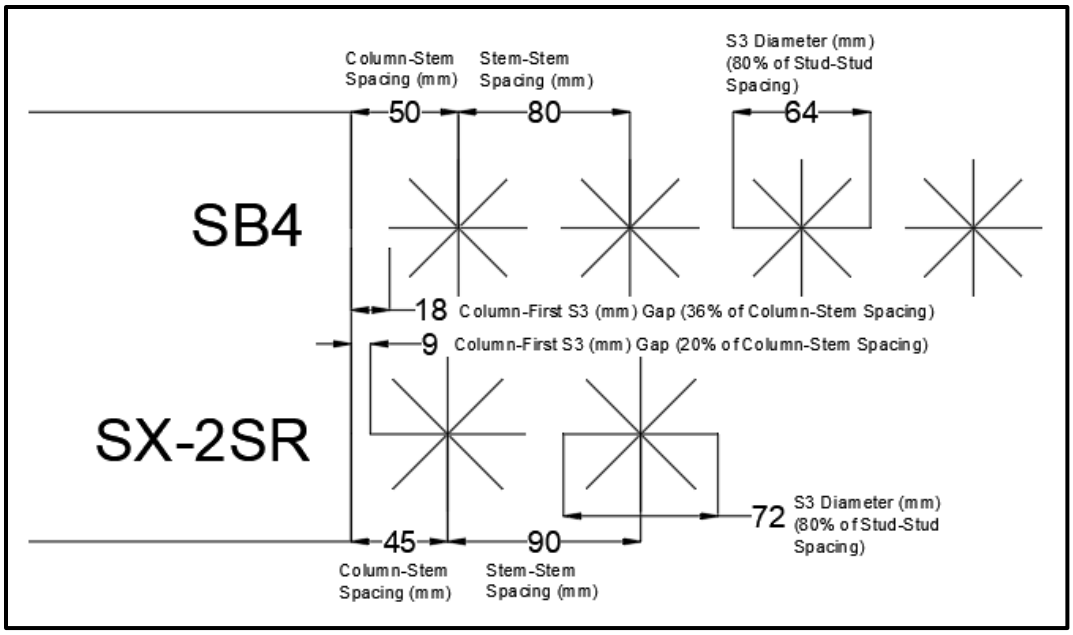

Figure 25: S3 Study Conceptual Plan Drawing

Table 3: S3 Study SB4 Hybrid Models S3 Diameter Configuration

Model	Bolt 1 S3 Diameter (% stem-stem spacing)	Bolt 2 S3 Diameter (% stem-stem spacing)	Bolt 2 S3 Diameter (% stem-stem spacing)	Bolt 2 S3 Diameter (% stem-stem spacing)
SB4a	80	80	80	80
SB4b	125	80	80	80
SB4c	125	125	80	80
SB4d	125	125	125	80
SB4e	125	125	125	125

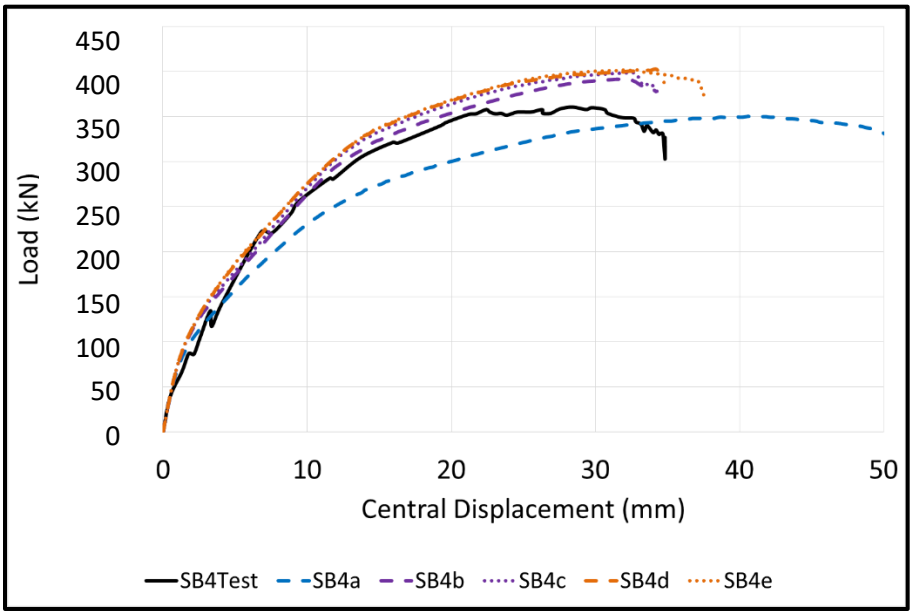

Figure 26: S3 Study SB4 Hybrid Models Load-Deflection Behaviour

As shown in Figure 26, while little difference in the behaviour of the models was observed when the S3 diameter of the second, third, or fourth row of bolts was changed, a large difference in the behaviour was shown when the S3 diameter of the first row of bolts was changed. This behaviour can also be shown for the SX-2SR models. Re-framing the lower type 3 models from the SX-2SR portion of the study in the new context of the column-first S3 gap, the acceptable models are now those with a column-to-first-S3 gap of between 6.5mm and 10.2mm (resulting in a S3 diameter of between 77% and 85% of the column-stem spacing). To confirm this behaviour is consistent for specimens SX-2SR and SB4, a model with a S3 diameter resulting in a 7.2mm column-first S3 gap for specimen SB4 was created. 7.2 mm was chosen as it was suspected that this would be close to the optimal value for specimen SX-2SR based on Figure 23, and results in a S3 diameter of 85% of the column-stem spacing for SB4. The remaining S3 diameters in the model were kept at 80% of the stem-stem spacing to allow for gaps between all S3s. Load-deflection data for this model is shown in Figure 27.

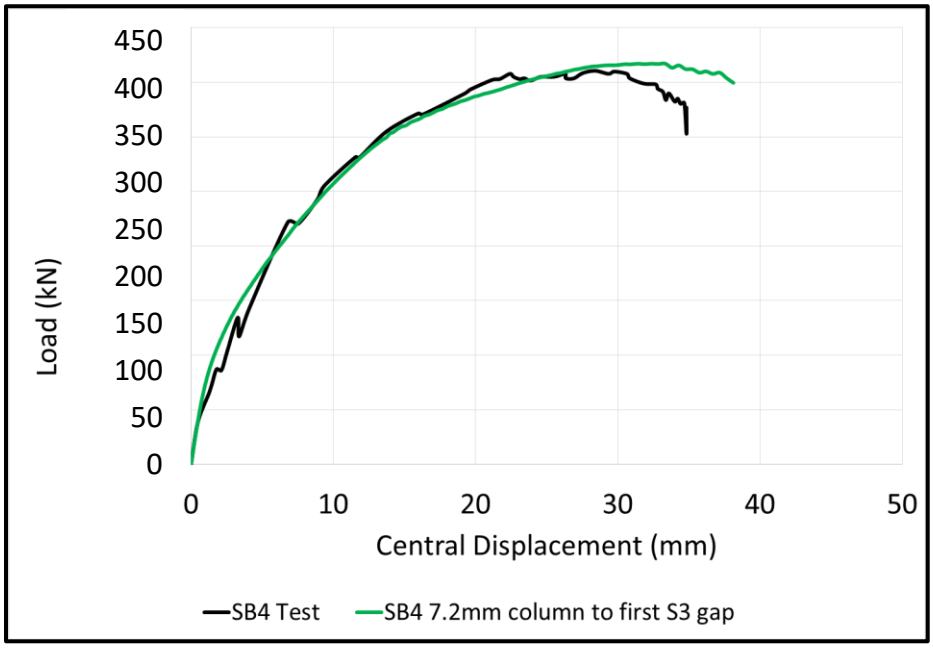

Figure 27: S3 Study SB4 7.2mm Column-to-First-S3 Model Load-Deflection Behaviour

This model predicts the test data very well, with the difference in the capacity being 2% and the difference in the failure displacement being 14%. Based on these results it can be said that when modelling the shear reinforcement of a slab-column connection in punching shear using a star method, it must be ensured that the first S3 is proportioned so that the column-first S3 gap is between 6-10mm in order for correct rotational behaviour and reasonable capacity estimates to be maintained. This value however, is based on a calibration using 120mm thick slabs, and optimal values for the column-first S3 gap are expected to be larger for thicker slabs. For thicker slabs a gap between the column face and the edge of the first S3 equal to between 80% and 85% of the column-stem spacing may be applicable.

While the size of the S3's after the first reinforcement row were shown to have a negligible effect when varied between 80% and 125% of the stem-stem spacing in Figure 26, an additional study was conducted to determine the impact of varying the 2nd to 4th S3 diameter in specimen SB4 between 0% and 100% of the stem-stem spacing. The results of this study are shown in Figure 28.

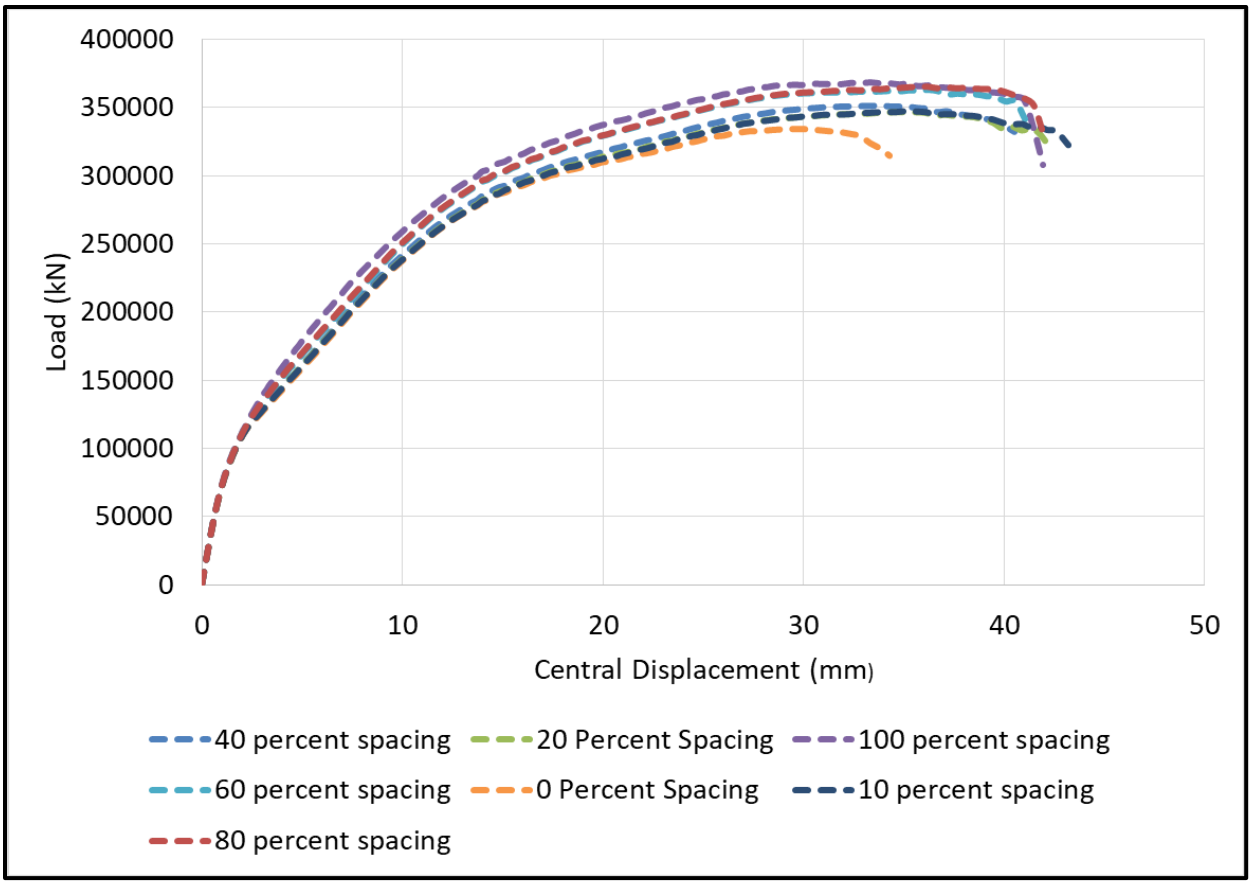

Figure 28: S3 Study SB4 Subsequent S3 Study Load Deflection Behaviour

As shown in Figure 28 the S3 diameters for the remaining peripheral rows of shear reinforcement can do not significantly affect the behaviour of the connection as long as some star (and therefore some confinement) is provided. Some gap between stars is recommended to allow for potential rotation of specimen between studs which could occur in a real-world test. A value of 80% of the stem-stem spacing was chosen for the models in this research.

4.7 Final Model Parameters

Table 4: SB Series Calibrated Model Parameters

Concrete Parameters	
ABAQUS Material Model	Concrete Damaged Plasticity
Density (tonne/m^3)	2.4E-9
Modulus of Elasticity (MPa)	36483 (SB1,5-6), 35217 (SB2-4), (=5500$\sqrt{f_c'}$)
Poisson's Ratio	0.2
Compression Model	Hognestad Parabola
Compression Parabola Termination Point (MPa)	17.6 (SB1,5-6), 16.4 (SB2-4), (=0.4f_c')
Tension Model	Bilinear Tensile Stress-Crack Width (Petersson)
Fracture Energy (N/mm)	0.092 (SB1,5-6), 0.087 (SB2-4)
Dilation Angle	40
Eccentricity	0.1, (ABAQUS Default)
Ratio of Biaxial to Uniaxial Compressive Strength	1.16, (ABAQUS Default)
Yield Surface Parameter K_c	2/3, (ABAQUS Default)
Viscosity	0, (Not Used in ABAQUS Explicit)
Tensile Damage Parameter	0, (No Recovery)
Compressive Damage Parameter	1, (Full Recovery)
Element Type	C3D8R
Approximate Element Size (mm)	15
Flexural Steel Parameters	
ABAQUS Material Model	Linear Elastic, Plastic with Tension Stiffening
Density (tonne/m^3)	7.8E-9
Modulus of Elasticity (MPa)	200000
Poisson's Ratio	0.3
Yield Strength (MPa)	455
Element Type	T3D2
Approximate Element Size (mm)	15
Shear Stud Parameters	
ABAQUS Material Model	Linear Elastic, Plastic with Tension Stiffening
Density (tonne/m^3)	7.8E-9
Modulus of Elasticity (MPa)	200000
Poisson's Ratio	0.3
Yield Strength	381
Element Type	B32
Approximate Element Size (mm)	15
First S3 Diameter (mm)	85.5
Subsequent S3 Diameters (mm)	64

Table 5: SX Series Calibrated Model Parameters

Concrete Parameters	
ABAQUS Material Model	Concrete Damaged Plasticity
Density (tonne/m^3)	2.4E-9
Modulus of Elasticity (MPa)	31595 ((H)XXX), 30869 ((H)SF0), 34872 (SX-1SR - SH-2SR), (=5500$\sqrt{f_c'}$)
Poisson's Ratio	0.2
Compression Model	Hognestad Parabola
Compression Parabola Termination Point (MPa)	13.2 ((H)XXX), 12.6 ((H)SF0), 16.1 (SX-1SR - SH-2SR), (=0.4f_c')
Tension Model	Bilinear Tensile Stress-Crack Width (Petersson)
Fracture Energy (N/mm)	0.077 ((H)XXX), 0.066 ((H)SF0), 0.087 (SX-1SR - SH-2SR)
Dilation Angle	40
Eccentricity	0.1, (ABAQUS Default)
Ratio of Biaxial to Uniaxial Compressive Strength	1.16, (ABAQUS Default)
Yield Surface Parameter K_c	2/3, (ABAQUS Default)
Viscosity	0, (Not Used in ABAQUS Explicit)
Tensile Damage Parameter	0, (No Recovery)
Compressive Damage Parameter	1, (Full Recovery)
Element Type	C3D8R
Approximate Element Size (mm)	20
Flexural Steel Parameters	
ABAQUS Material Model	Linear Elastic, Plastic with Tension Stiffening
Density (tonne/m^3)	7.8E-9
Modulus of Elasticity (MPa)	200000
Poisson's Ratio	0.3
Yield Strength (MPa)	545 (430)
Element Type	T3D2
Approximate Element Size (mm)	20
Shear Stud Parameters	
ABAQUS Material Model	Linear Elastic, Plastic with Tension Stiffening
Density (tonne/m^3)	7.8E-9
Modulus of Elasticity (MPa)	200000
Poisson's Ratio	0.3
Yield Strength	340
Element Type	B32
Approximate Element Size (mm)	20
First S3 Diameter (mm)	75.6
Subsequent S3 Diameters (mm)	75.6

5.0 Verification of NLFEA Model Capability

5.1 Introduction to Model Verification

In this Chapter several techniques are presented through which the capability of the models to correctly predict the behaviour of the test specimens was assessed. While the performance of the models was good in many aspects, the accuracy in several aspects of the verification process could be improved through further calibration of the model and additional specified research into those areas. Several methods were used to verify the performance of the models relative to the test results, including analysis of the load-deflection behaviour, moment-curvature behaviour for the SX series, strains in the shear reinforcement, strains in the flexural reinforcing grids, analysis of the tensile crack patterns, and analysis of the side crack profiles.

5.2 SB Series Model Verification

Load-deflection response of the first four SB series specimens (SB1, SB2, SB3, and SB4) models, along with the load-deflection response of the test specimens, is presented in Figure 29.

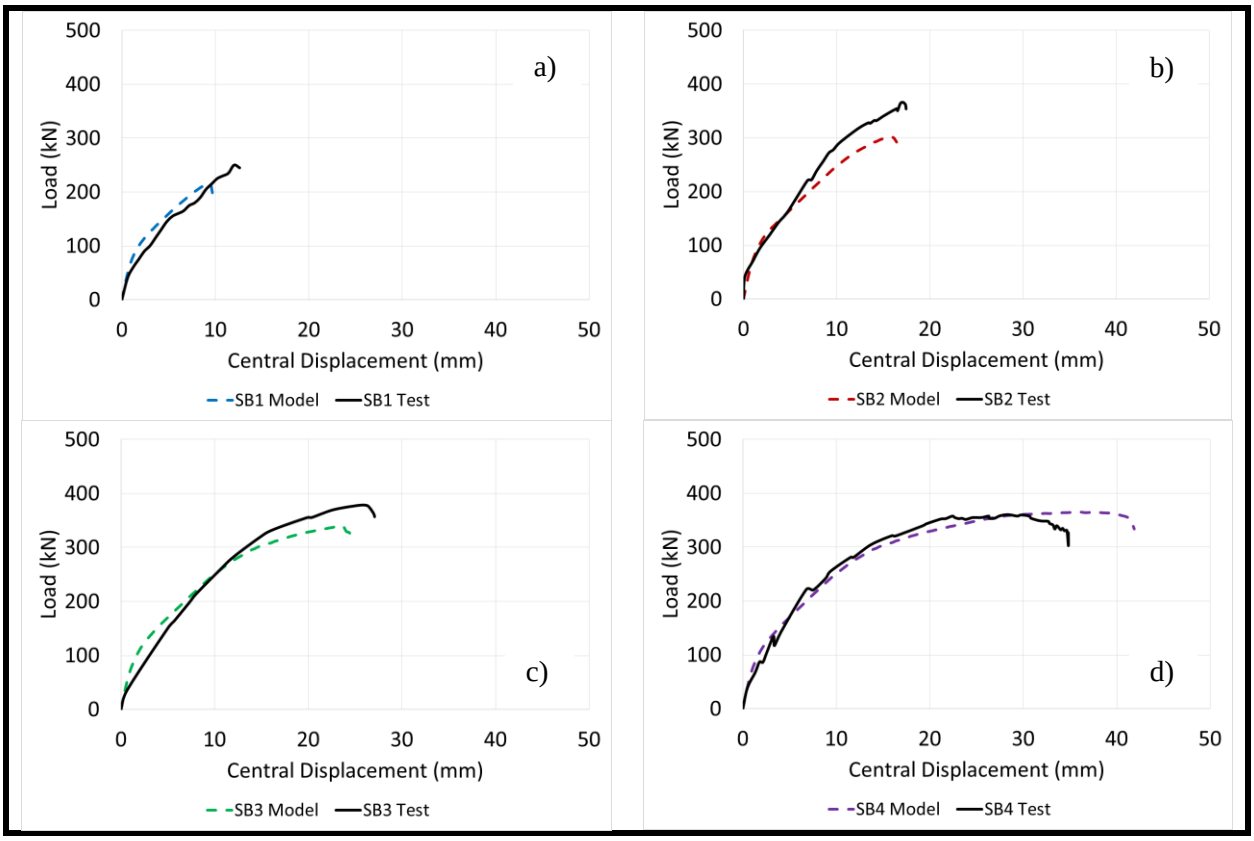

Figure 29: a) SB1, b) SB2, c) SB3, and d) SB4 Load-Deflection Behaviour

As shown in Figure 29, the model is fairly accurate for all four of the specimens. The largest capacity difference is 17% (SB2) and the largest difference in failure displacement is 27% (SB4). It is noted that the test capacity of specimen SB1 is slightly higher than predicted by design codes, which predict a capacity more akin to the SB1 model. Load deflection behaviour for the test and models of SB series specimens SB5 and SB6 are presented in Figure 30.

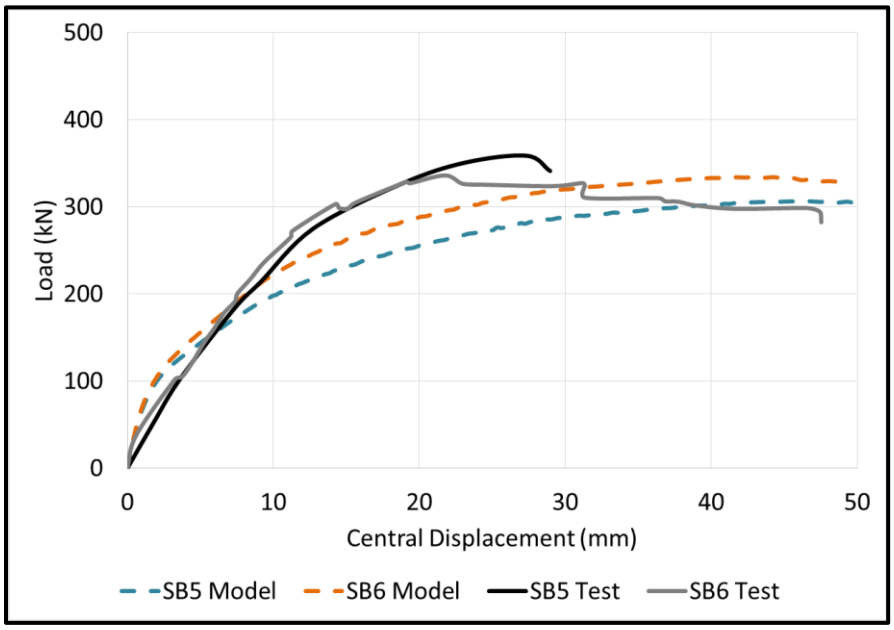

Figure 30: SB5 and SB6 Load-Deflection Behaviour

The model also accurately predicts the capacity of the two SB series specimens with openings. The maximum discrepancy in the capacity is 13% (SB5). It is also noted that the test data predicts a higher capacity for specimen SB5 than SB6, despite specimen SB5 having more openings near the column and the openings being of equal size. A more expected behaviour would be that specimen SB6 has a slightly higher capacity than specimen SB5, which is what the model predicts.

Adetifa (2003) recorded the strains in one shear bolt in each peripheral row at 25%, 50%, 75%, and 95% of the maximum load. This data was also recorded in the models and compared to the test data. This comparison is provided for specimen SB4 in Figure 31. All SB series bolt strain diagrams can be found in Appendix B. Figure 31 shows that the bolts in the model activate earlier and more uniformly than in the tests. This behaviour is similar for all of the SB series specimens. One possible reason for this behaviour is that the method with which cracking is handled in the CDP model results in a shallower shear failure surface than is present during the tests, and that this failure surface passes through all of the bolts activating them more evenly. This theory is supported by the pre-failure side crack profile, which shows a shear crack passing through all of the bolts (Figure 32). However the model does correctly predict the lowest activation in the bolt furthest from the column. It should also be noted that both the model and test show failure outside of the shear reinforced zone in all of the SB series specimens. This is supported by the presence of significant strains on the flexural reinforcing grids in the models outside of the shear reinforced zone as shown in the post-failure side crack profile (Figure 33). The models correctly predict that the yield strain was not reached for any of the bolts prior to failure, and in general the magnitudes of the strains in the shear bolts predicted by the model are reasonable.

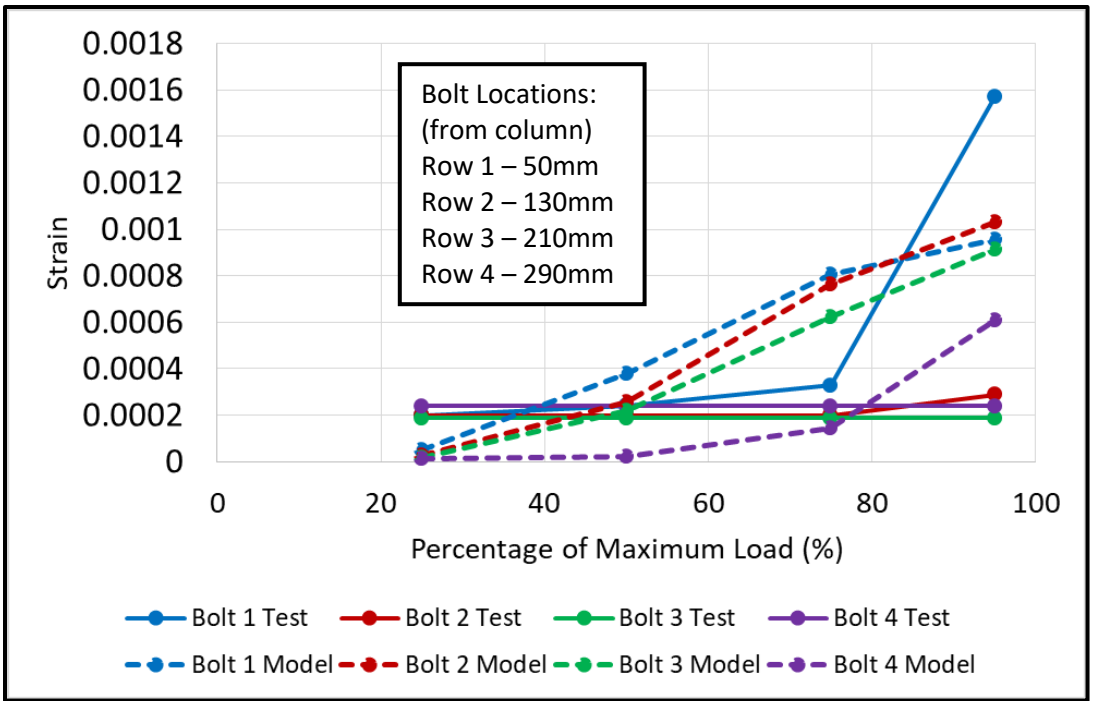

Figure 31: SB4 Shear Bolt Strain Behaviour

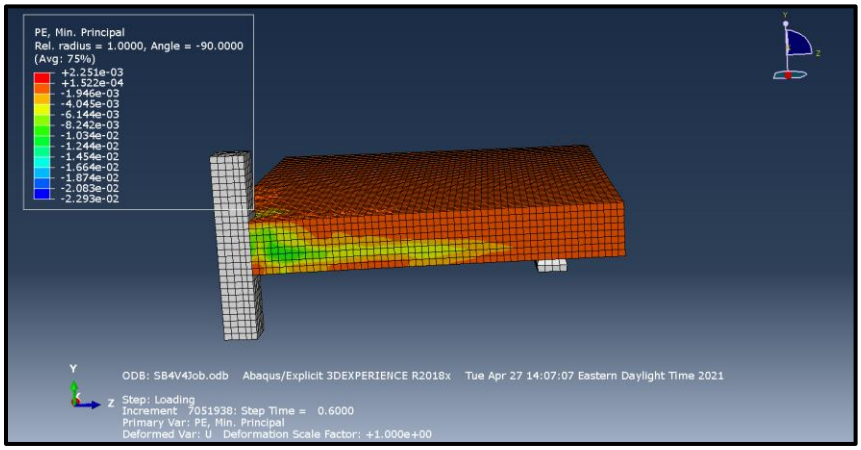

Figure 32: SB4 Model Shear Crack

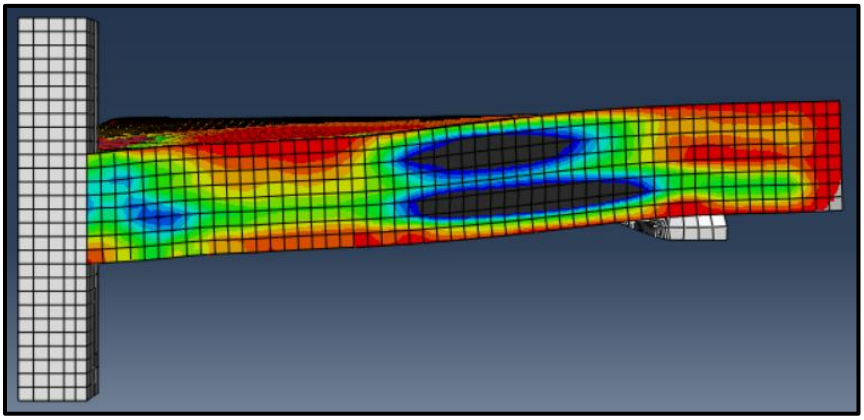

Figure 33: SB4 Post-Failure Side Crack Profile

Another metric that was tracked during the tests of the SB series specimens was the load corresponding to the first yielding of the longitudinal reinforcing grids, and the location of first yielding of the longitudinal reinforcing grids. This data was also tracked in the models and is compared to test data for all of the SB series specimens in Table 6. As shown in Table 6, the model predicts the load at first yield fairly accurately, with a maximum discrepancy of 22% (SB5). Possible factors that would cause discrepancy in this comparison include that strains were only measured at several discrete locations in the test, while they were measured at all points in the model. The location of first yield was also predicted fairly accurately for all specimens.

Table 6: SB Series Load at First Yield of Longitudinal Reinforcement

Test Specimen	Load at First Yielding During Test (kN)	Load at First Yielding From Model (kN)
SB1	240	187
SB2	224	266
SB3	260	269
SB4	240	269
SB5	250	194
SB6	250	206

Experimental and model-generated crack patterns for the tensile span face were also compared for all SB series specimens. An example comparison is provided in Figure 34 for specimen SB4. In general, the crack patterns showed more flexural cracking away from the column as more shear reinforcement was added, suggesting that the shear reinforcement is successful in transition the failure mode from punching to flexure in the models. All crack patterns and side crack profiles for the SB series specimens can be found in Appendix B.

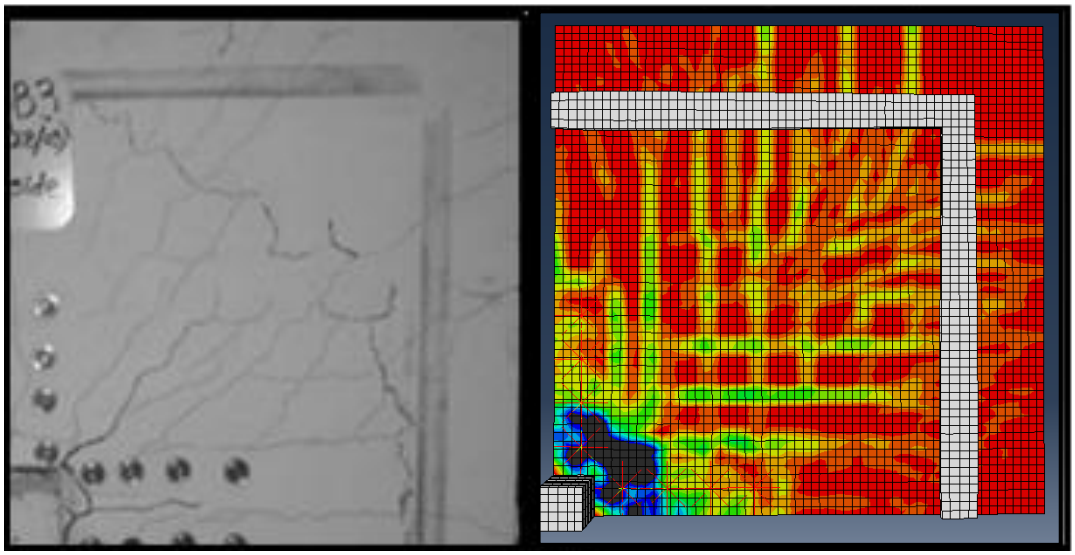

Figure 34: SB4 Experimental and Model-Generated Crack Patterns (Tensile Slab Face)

5.3 SX Series Model Verification

Load-deflection behaviour for the SX series specimens is provided in Figure 35 and Figure 36. The SX specimens were tested in load control, and therefore often didn't display a distinct point of failure during the tests. In the models, failure was defined as the point at which the error in the vertical force equilibrium of the specimen reached 5%. The value of 5% was selected as it was large enough to discount numerical outliers that could result from the quasi-static analysis procedure.

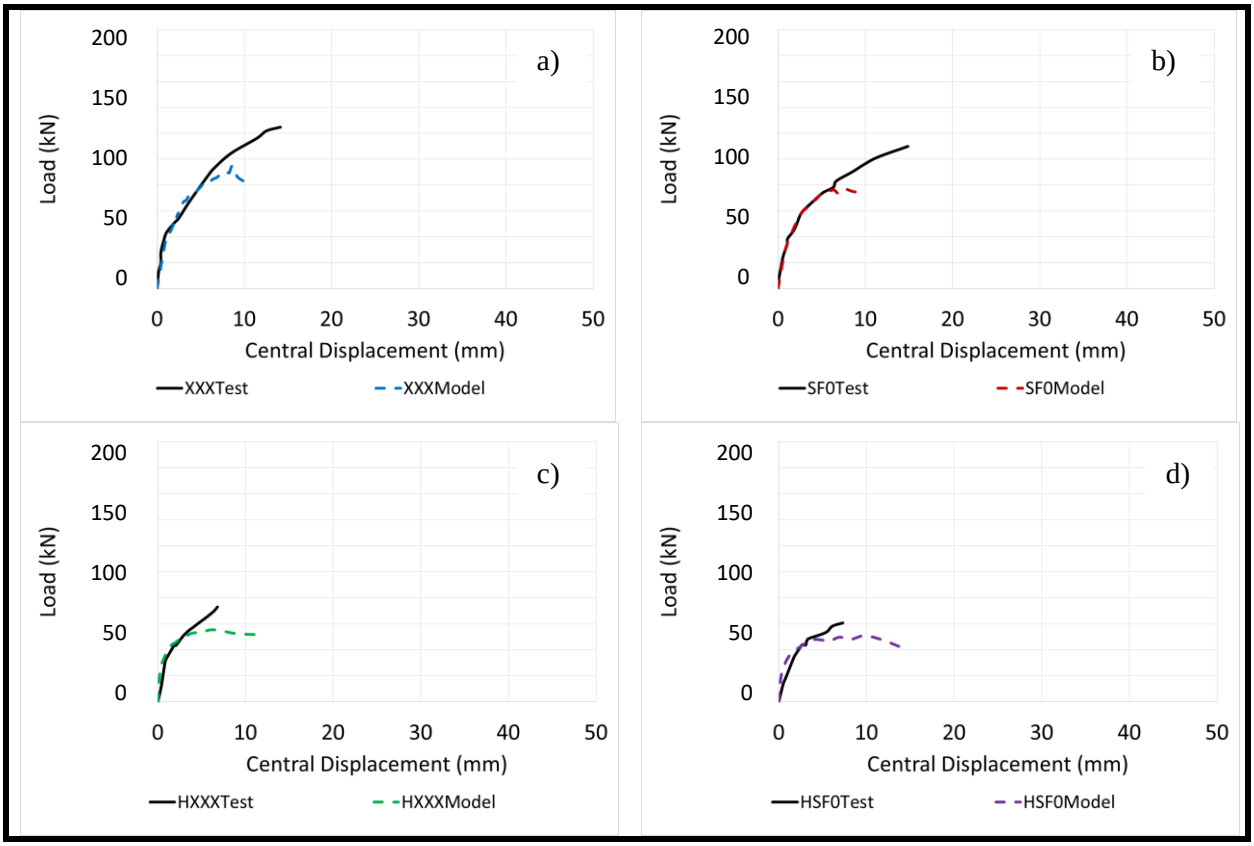

Figure 35: a) XXX, b) SF0, c) HXXX, and d) HSF0 Load-Deflection Behaviour

The load-deflection response of the SX specimens without shear reinforcement (Figure 35), tend to tail off in the models between 70% and 80% of the test capacity. This could possibly be due to the load controlled nature of the tests and a slight misidentification of the point of failure. The largest discrepancy in the capacities is 30% (SF0) and the largest error in the failure displacements is 25% (HSF0). This behaviour can also be seen to a lesser extent in specimen SX-1SR (Figure 36a), which has the lowest amount of shear reinforcement.

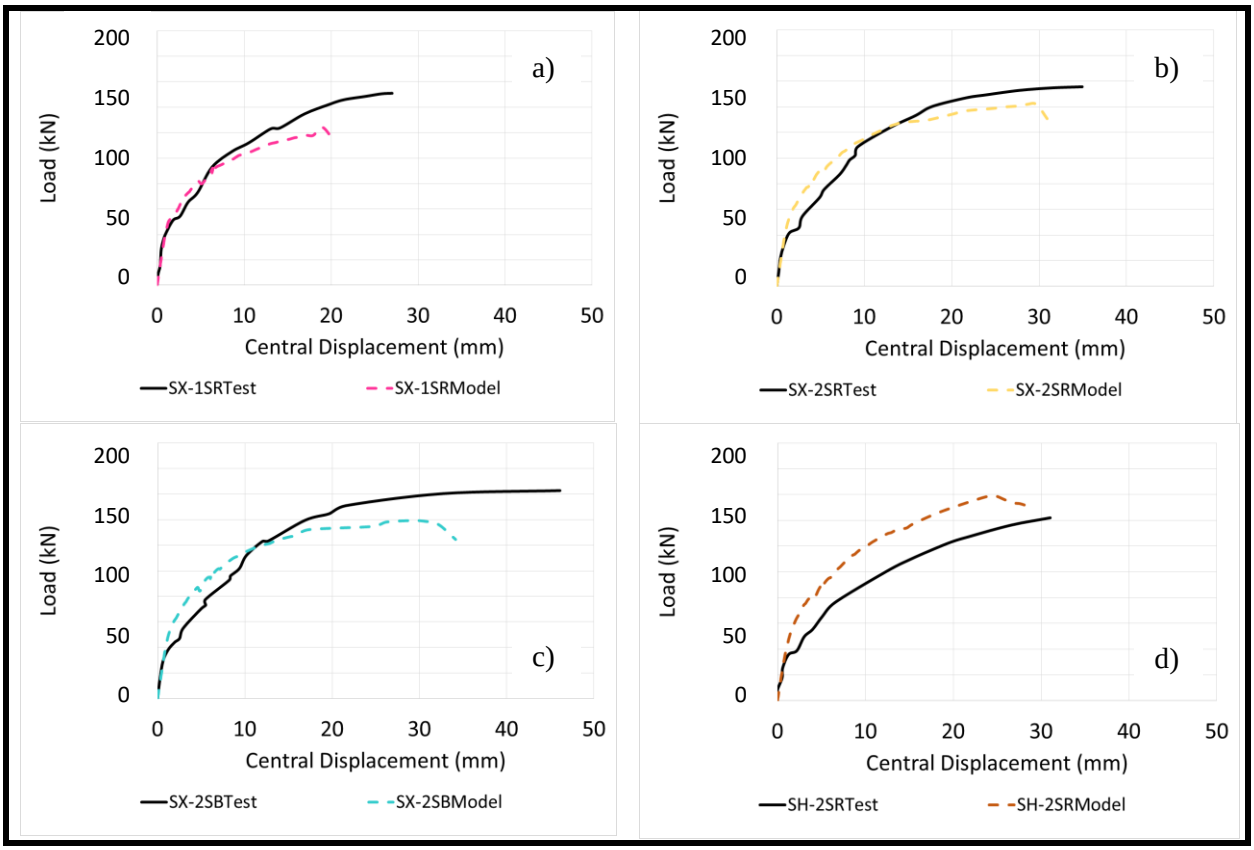

Figure 36: a) SX-1SR, b) SX-2SR, c) SX-2SB, and d) SH-2SR Load-Deflection Behaviour

The specimens with shear reinforcement (Figure 36) however, are modelled very well. The largest discrepancy in the capacities for the three models with two rows of shear reinforcement is 14% (SX-2SB). The largest failure displacement in these three models is 37% (SX-2SB), however the test results for this specimen show suspicious ductility when compared to specimen SX-2SR, potentially due to the load controlled nature of the tests. If the ductility of SX-2SB was more similar to that of SX-2SR the model would be much more accurate. Finally, specimen SH-2SR is much stiffer in the model than in the test. The model does not provide the expected drop in stiffness from the addition of the opening which was experienced in the SF0 model or the SB5/6 models.

Moment-rotation behaviour was also considered for verification of the SX series specimens. Moment-curvature behaviour for the SX series models is provided in Figure 37 and Figure 38.

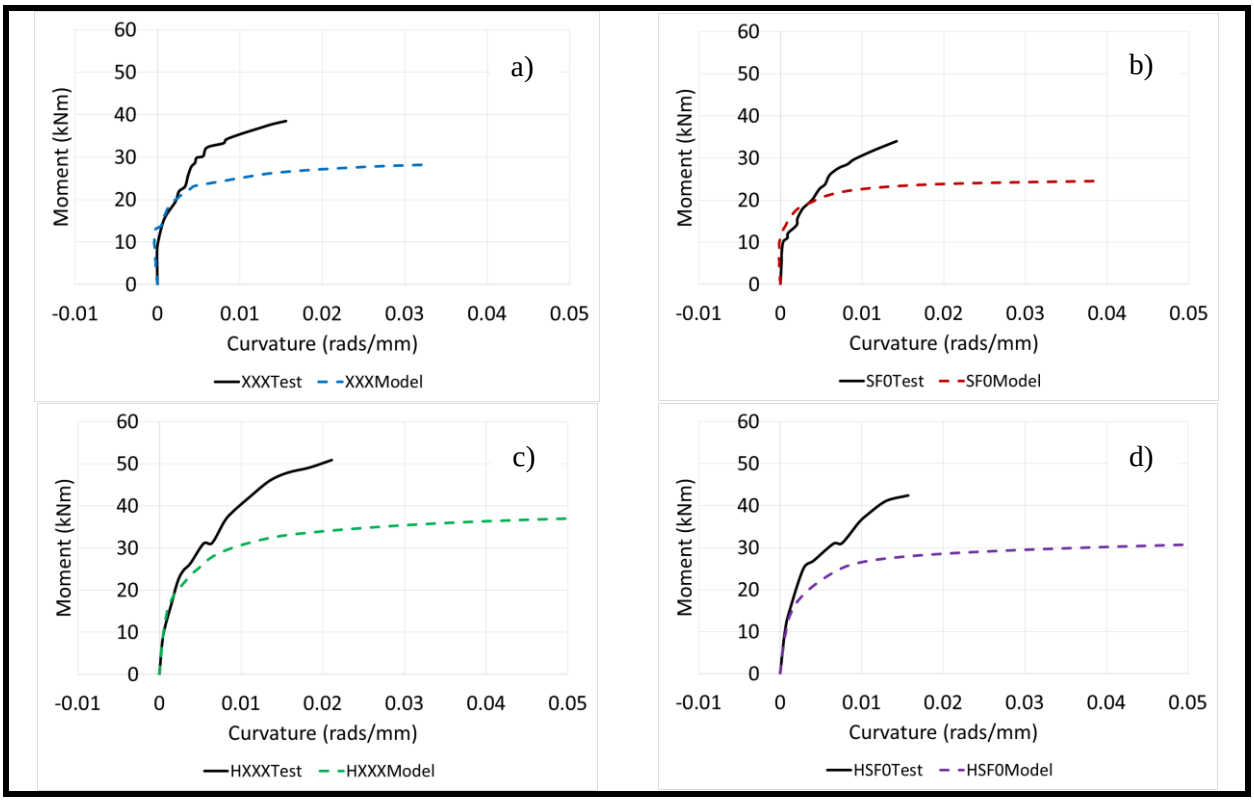

Figure 37: a) XXX, b) SF0, c) HXXX, and d) HSF0 Moment-Curvature Behaviour

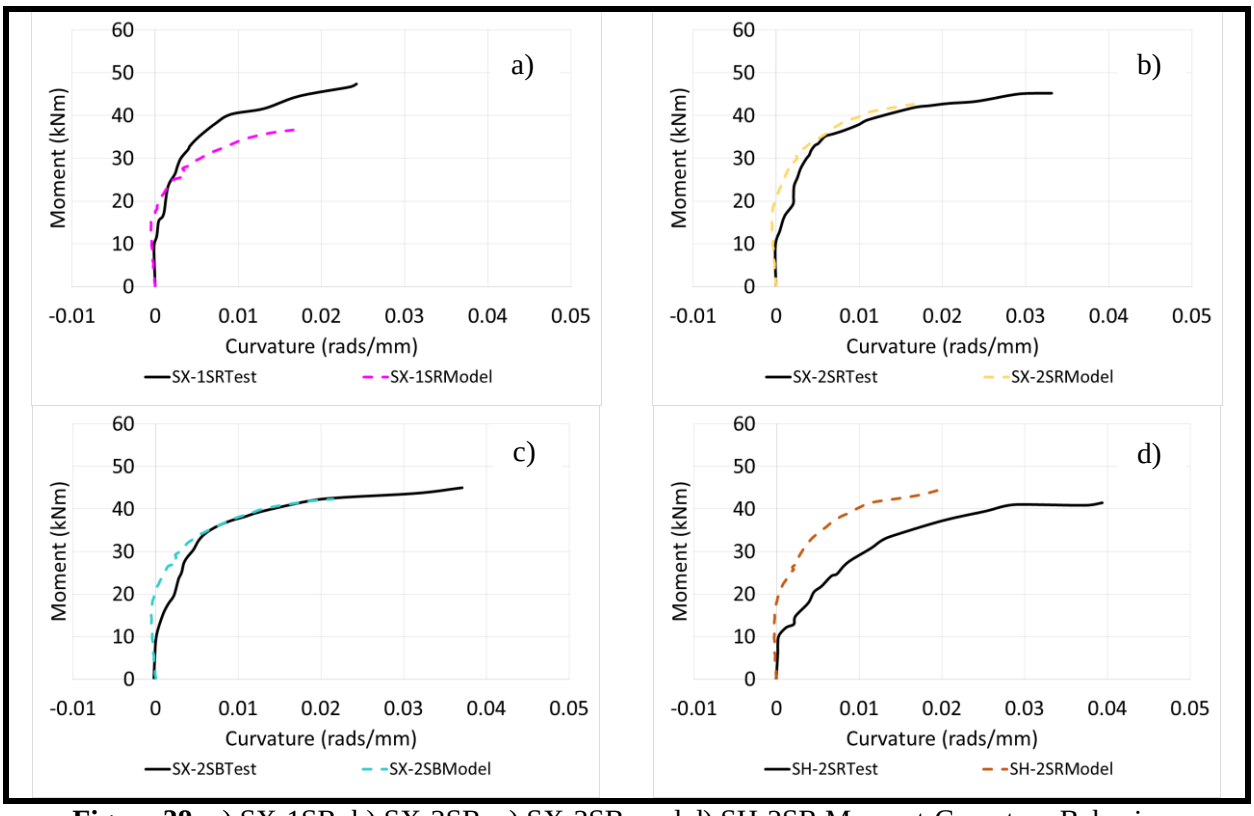

Figure 38: a) SX-1SR, b) SX-2SR, c) SX-2SB, and d) SH-2SR Moment-Curvature Behaviour

The rotational behaviour of the specimens shows a greater error between the tests and the models. This is most obviously seen in the large over-rotations in the two specimens with the larger moment-shear ratio (HXXX and HFS0). This is probably due to a misidentification of the exact point of failure in the models, as curvature values increase rapidly in the models around failure, especially in the specimens with high moment. However, it could also be useful to investigate modelling the region near the column in a different manner to mitigate this problem. For example, Silva Mamede et al (2013) used a finer mesh to model the region near the column. This could improve the accuracy of the rotational behaviour that the model provides. When the correct S3 sizes are used, the moment-curvature behaviour of the specimens with shear reinforcement are modelled fairly well, especially specimens SX-2SR and SX-2SB, however there is still some error in the maximum curvature at failure. It is also observed that the test data for specimen SX-1SR suggests that it rotates almost equally to the specimens with two rows of shear studs/bolts, despite in theory having less of a stiff region near the support. If the test data showed slightly more rotation than it would be represented well by the model. Similar to what was shown in the analysis of the load-deflection diagrams, the model does not predict enough rotation for specimen SH-2SR. Regardless of the absolute rotational behaviour for each specimen, trends in the specimen behaviour were predicted well as parameters in the models were varied.

Figure 39 shows the strains in the first row of shear studs for the test and model for specimen SX-2SR. Figure 40 shows the strains in all shear studs for the model for specimen SX-2SR. The shear stud strain diagrams show a similar behaviour to those for the SB series specimens, in that the shear reinforcement tends to activate fairly evenly in the models. In general the models show that more strains are developed in the second row of shear reinforcement and that the least strain is developed in the shear reinforcement located at the column center. None of the reinforcement was found to yield in any of the models, which is consistent with test behaviour. All bolt strain diagrams for the SX series specimens can be found in Appendix B.

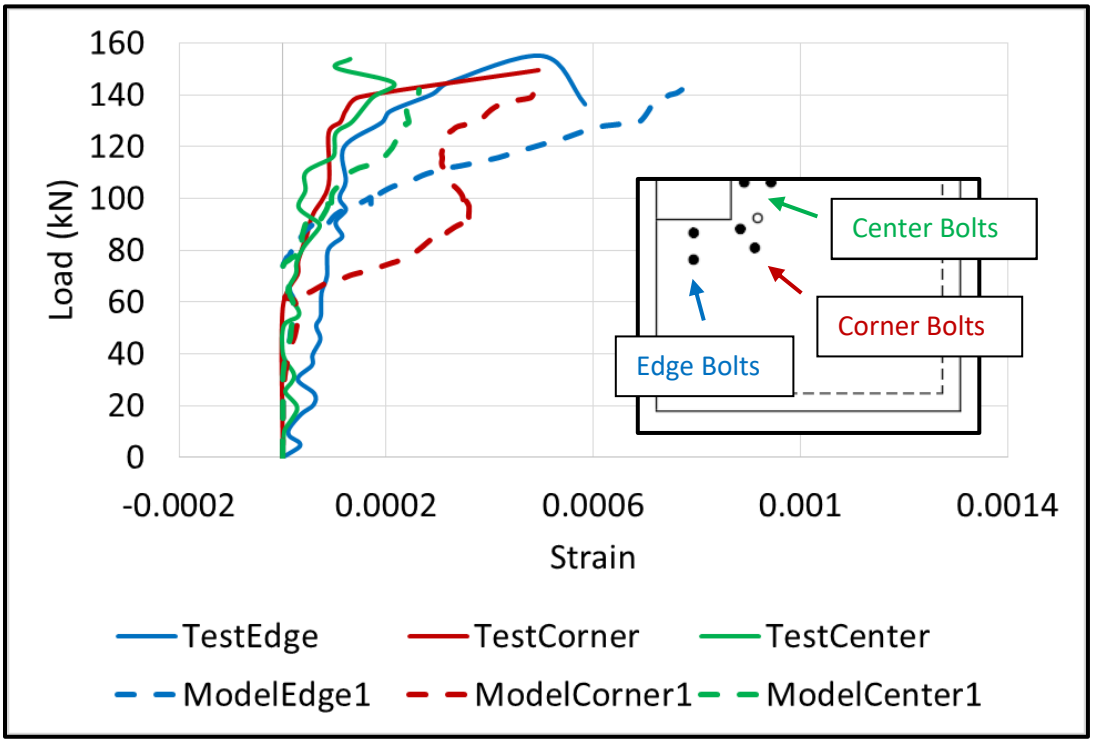

Figure 39: SX-2SR Row 1 Shear Stud Strain Behaviour

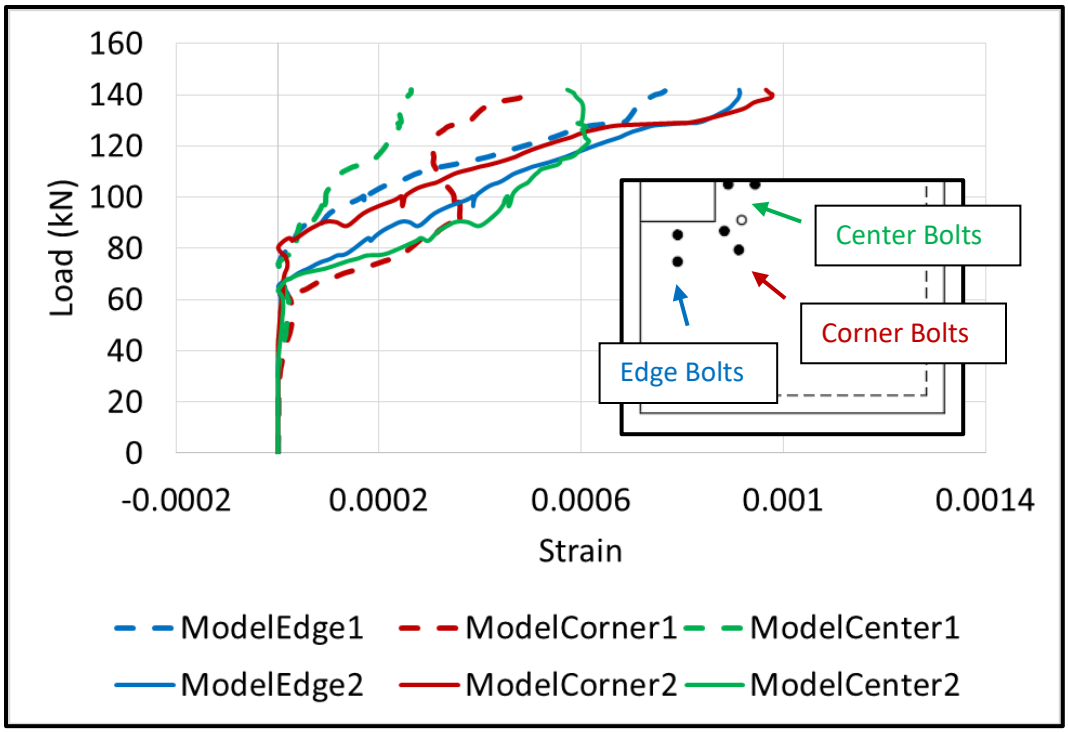

Figure 40: SX-2SR Shear Stud Strain Behaviour

By observing the post-failure side crack profiles for the SX specimens (for example, for SX-2SR shown in Figure 41), it is shown that the failure strains occur outside of the shear reinforcement when provided. However, the strains in these specimens are concentrated closer to the middle of the specimen cross-section, suggesting that strains caused by shear are more dominant in these specimens than in the SB series specimens. Thusly a combined flexural-punching failure mode would be predicted by the models. This was the failure mode shown in the test for specimen SX-1SR, however the specimens with two rows of shear reinforcement experienced fully flexural failure in the tests.

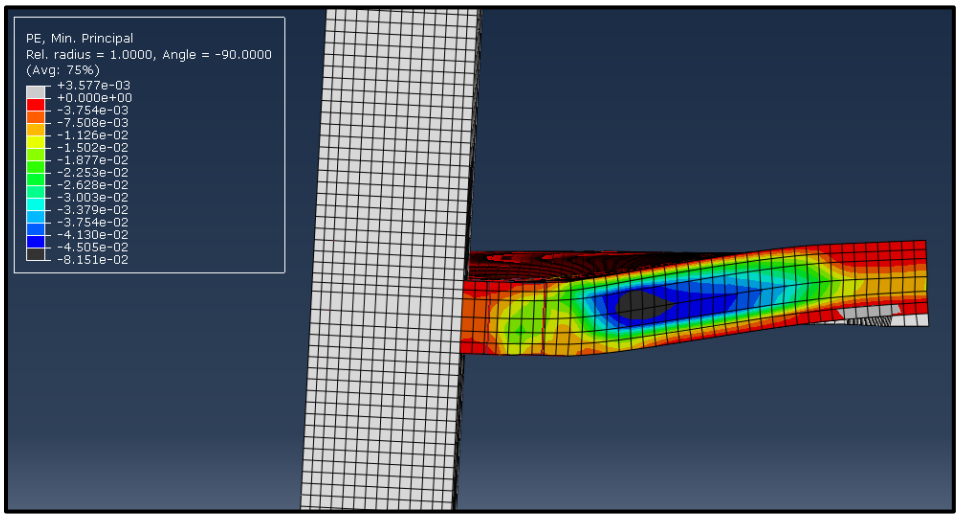

Figure 41: SX-2SR Post-Failure Side Crack Profile

Two metrics for the strain in the longitudinal reinforcing grids were tracked for the SX series specimens. Table 7 shows the load corresponding to the first yielding of the longitudinal reinforcement, as was

tracked for the SB series specimens. Table 8 shows the maximum strain in the longitudinal reinforcing grids at the point of slab failure.

Table 7: SX Series Load at First Yield of Longitudinal Reinforcement

Specimen	Load at First Yielding During Test (kN)	Load at First Yielding From Model (kN)
XXX	88	68
SF0	68	63
SX-1SR	109	117
SX-2SR	69	136
SX-2SB	79	137
SH-2SR	75	157
HXXX	48	44
HSF0	44	39

Table 8: SX Series Maximum Longitudinal Strain at Failure

Specimen	Maximum Strain at Failure During Test	Maximum Strain at Failure From Model
XXX	0.0126	0.0325
SF0	0.0159	0.0244
SX-1SR	0.0131	0.0173
SX-2SR	0.0149	0.0271
SX-2SB	0.0142	0.0243
SH-2SR	0.0221	0.0249
HXXX	0.0119	0.0297
HSF0	0.0114	0.0282

The models predict the strains in the longitudinal reinforcement fairly well in some cases (for example SH-2SR), but is inconsistent. The maximum discrepancy in the load corresponding to first yielding of the longitudinal reinforcement being 46% (SX-2SR) and the maximum error in the maximum strain at failure being 61% (XXX). Possible factors that would cause discrepancy in this comparison again include that strains were only measured at several discrete locations in the test, while they were measured at all points in the model. The locations of first yield and maximum strain were predicted fairly accurately for all specimens.

Experimental and model-generated crack patterns for the tensile face were also compared for all SB series specimens. An example comparison is provided in Figure 42 for specimen SX-2SR. The model crack patterns showed less cracking outside of the shear reinforced zone than in the experimental crack patterns and more strains near the shear reinforcement, suggesting that the failure mode may be flexural punching in the models, rather than the flexural failure mode seen in the test. The crack patterns also show that the unbalanced moment has the effect of confining the area adjacent to the column parallel to the moment on the tensile side, which is the reason that the center bolts developed less strains in the model. All crack patterns and side crack profiles for the SX series specimens are provided in Appendix B.

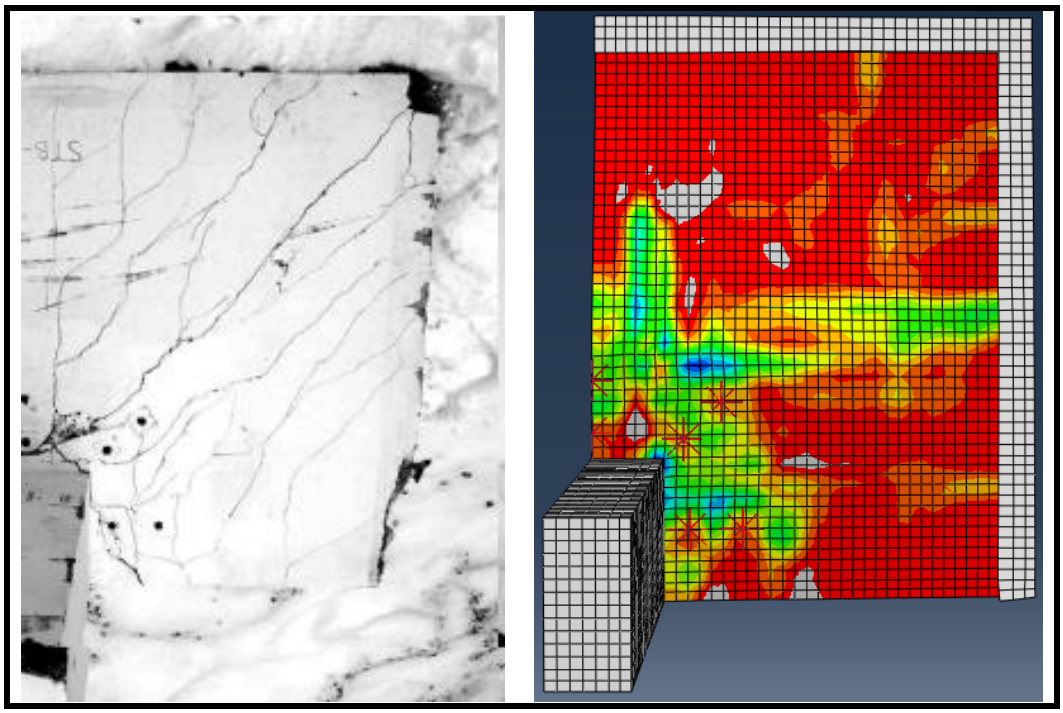

Figure 42: SX-2SR Experimental and Model-Generated Crack Patterns (Tensile Slab Face)

6.0 Parametric Studies

6.1 Introduction to Parametric Studies

In this Chapter, several parametric studies are presented using versions of the calibrated SB and SX series models with one parameter varied between the models. The intention of these parametric studies are to supplement existing experimental programs with NLFEA analysis to determine the effect of changing a parameter which hasn't been investigated experimentally. Three parametric studies are presented:

1. The first study investigates the effect of changing the number of shear reinforcement rows and the spacing between adjacent rows of shear reinforcement.

2. The second study investigates the effect of changing the size and number of openings adjacent to the column, and the change in placement of shear reinforcement which must occur as a result of the opening changes.

3. The third study investigates the impact of anchorage-controlled reinforcement, which was proposed by Topuzi et al (2017) to increase the ductility of slab-column connections under cyclic loading without inducing higher lateral stresses in the connection, on the overall capacity of the connections.

For each study, specific study objectives are described, the models created to conduct the study are presented, the results of the study are discussed, and conclusions are drawn based on the study results.

6.2 Shear Reinforcement Spacing Study

6.2.1 Shear Reinforcement Spacing Study Objectives

The first parametric study that was run on the calibrated models was an investigation of the effect of changing the number of peripheral rows of shear studs/bolts and their distance away from the column through changing the stem-stem spacing. Specific objectives of the study are as follows:

1. For each peripheral row of shear reinforcement determine whether the addition of the row provides a capacity/ductility benefit to the connection at various distances from the column.

2. Determine if two specimens with the same shear reinforced area but a different number of shear reinforcement rows (a different number of shear reinforcement rows are provided within the same distance from the column face) would behave similarly or more like other specimens with the same number of reinforcement rows.

3. Determine whether the behaviour of a connection is significantly affected by changing the stem-stem spacing of the farther reinforcement rows between 0.75 and 1.5 times the effective depth of the slab. Determine whether a stem-stem spacing of 1.5d prevents inter-stud punching from occurring between different reinforcement rows.

6.2.2 Shear Reinforcement Spacing Study Models

In order to achieve the objectives of the spacing parametric study, 36 models were created based on the calibrated SB and SX series models with varying numbers of shear reinforcement rows up to six rows. The column-first-stem and stem-stem spacing for the first two rows were kept constant at their original values in the SB and SX series models, and subsequent rows were modified by between 75%-150% of their original spacing. The models were separated into the SBS series and SXS series depending on which series of specimen models the study models were based on.

The models were named according to the following convention. SB# or SX-#SR indicates whether the specimen is part of the SBS or SXS series and denotes the SB or SX series specimen which the model was based on (and shares properties with). The next number indicates the total number of reinforcement rows in the model between 1 and 6. The spacing of the first two rows were always maintained at their original spacing, which for the SBS series specimens was 0.55d for the first row and 0.89d for the remaining rows, and for the SXS series was 0.5d for the first row and d for the remaining rows. The spacing of the reinforcement rows beyond those in the original SB or SX series model are denoted by the letters at the end of the model names. The letters A, B, C, and D denote that a reinforcement row is at 1x, 1.25x, 1.5x, and 0.75x the original spacing for the SB or SX series model respectively. For example SB2-3-B would have 3 reinforcement rows with the spacing of the third row being 1.11d, and would have the properties of SB series specimen SB2. The SBS and SXS series models, including the number and position of their shear reinforcement rows, are summarized in Table 9 and Table 10.

Table 9: Shear Reinforcement Spacing Study SBS Series Models and Bolt Locations (From Column)

Specimen	Number of Rows	Bolt 1 Location (mm)	Bolt 2 Location (mm)	Bolt 3 Location (mm)	Bolt 4 Location (mm)	Bolt 5 Location (mm)	Bolt 6 Location (mm)
SB2-2	2	50	130				
SB3-3	3	50	130	210			
SB2-3-B	3	50	130	230			
SB2-3-C	3	50	130	250			
SB4-4	4	50	130	210	290		
SB2-4-BB	4	50	130	230	330		
SB2-4-CC	4	50	130	250	370		
SB4-5-A	5	50	130	210	290	370	
SB3-5-BB	5	50	130	210	310	410	
SB3-5-CC	5	50	130	210	330	450	
SB2-5-BBB	5	50	130	230	330	430	
SB2-5-CCC	5	50	130	250	370	490	
SB4-6-AA	6	50	130	210	290	370	450
SB4-6-BB	6	50	130	210	290	390	490
SB4-6-CC	6	50	130	210	290	410	530
SB3-6-BBB	6	50	130	210	310	410	510
SB3-6-CCC	6	50	130	210	330	450	570
SB2-6-BBBB	6	50	130	230	330	430	530
SB2-6-BBCC	6	50	130	230	330	450	570
SB2-6-CCBB	6	50	130	250	370	470	570

Table 10: Shear Reinforcement Spacing Study SXS Series Models and Bolt Locations (From Column)

Specimen	Number of Rows	Bolt 1 Location (mm)	Bolt 2 Location (mm)	Bolt 3 Location (mm)	Bolt 4 Location (mm)	Bolt 5 Location (mm)	Bolt 6 Location (mm)
SX-1SR-1	1	45					
SX-2SR-2	2	45	135				
SX-2SR-3-A	3	45	135	225			
SX-2SR-3-B	3	45	135	247.5			
SX-2SR-3-C	3	45	135	270			
SX-2SR-4-AA	4	45	135	225	315		
SX-2SR-4-BB	4	45	135	247.5	360		
SX-2SR-4-CC	4	45	135	270	405		
SX-2SR-5-AAA	5	45	135	225	315	405	
SX-2SR-5-ABB	5	45	135	225	237.5	450	
SX-2SR-5-ACC	5	45	135	225	360	495	
SX-2SR-5-BBB	5	45	135	247.5	360	472.5	
SX-2SR-5-CCC	5	45	135	270	405	540	
SX-2SR-6-AAAA	6	45	135	225	315	405	495
SX-2SR-6-AABB	6	45	135	225	315	427.5	540
SX-2SR-4-DD	4	45	135	202.5	270		

6.2.3 Shear Reinforcement Spacing Study Results and Discussion

All of the models in the study were run and post-processed through the use of a custom Python script. The script outputted several metrics of results from the models, including load-deflection behaviour, strains in the shear reinforcement, and crack patterns. Moment-curvature behaviour was also produced for the eccentric specimens.

Load-deflection behaviour for the SBS series models is shown in Figure 43. In Figure 43, the model curves are colour-coded based on the number of shear reinforcement rows present in the models. Due to the method of displacement-controlled loading present in the models all of the models were terminated when the central displacement reached 56mm, resulting in the descending branch of several models getting cut off. However, these models are expected to experience a flexural failure mode and would likely show very similar load-deflection behaviour to each other. Load-deflection behaviour and moment-curvature behaviour for the SXS series models are shown in Figure 44 and Figure 45 respectively. Models are again colour-coded based on the number of shear reinforcement rows present in the models. Two SXS series showed unexpected load-deflection behaviour when compared to similar models. SX-2SR-4-BB (four rows of shear reinforcement with rows 3 and 4 at 1.25d stem-stem spacing) showed uncharacteristically low capacity and ductility, and SX-2SR-6-AABB (six rows of shear reinforcement with rows 5 and 6 at 1.25d stem-stem spacing) showed uncharacteristically high ductility.

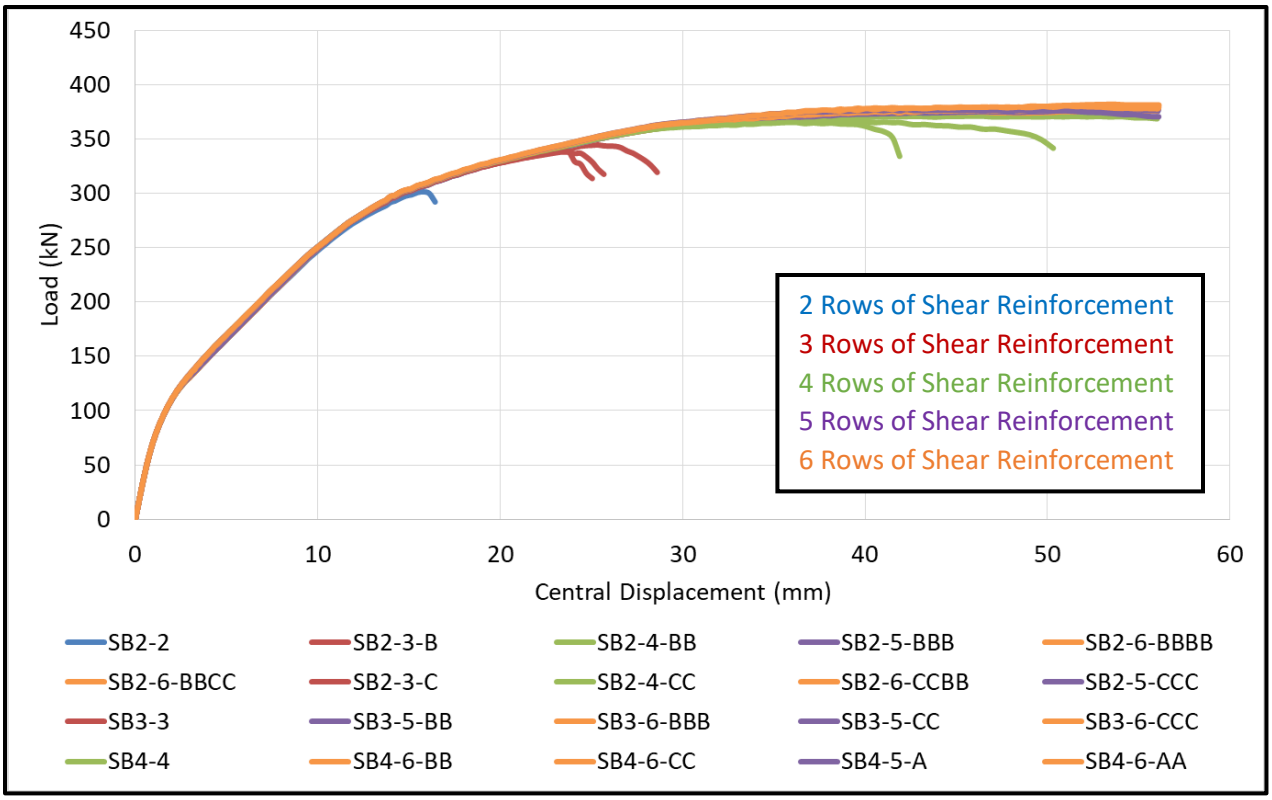

Figure 43: Shear Reinforcement Spacing Study SBS Series Load-Deflection Behaviour

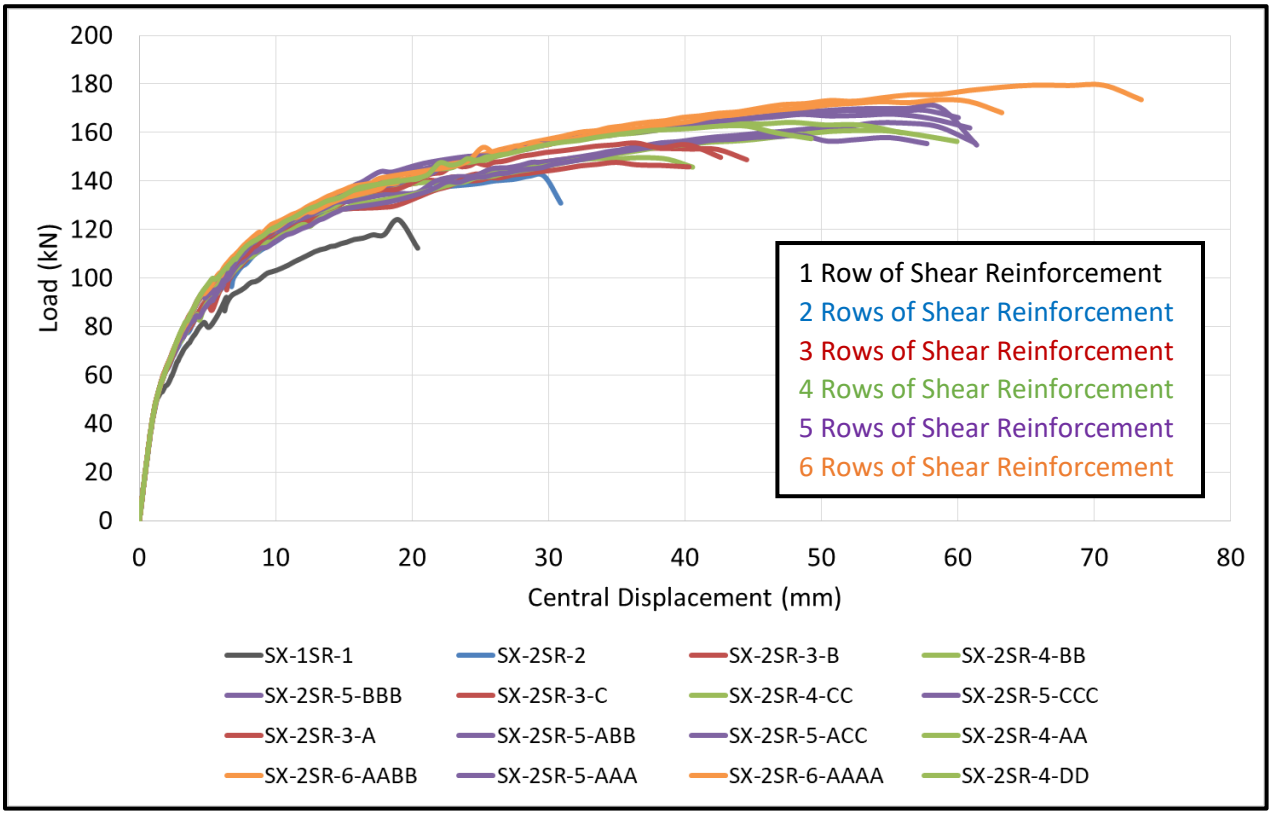

Figure 44: Shear Reinforcement Spacing Study SXS Series Load-Deflection Behaviour

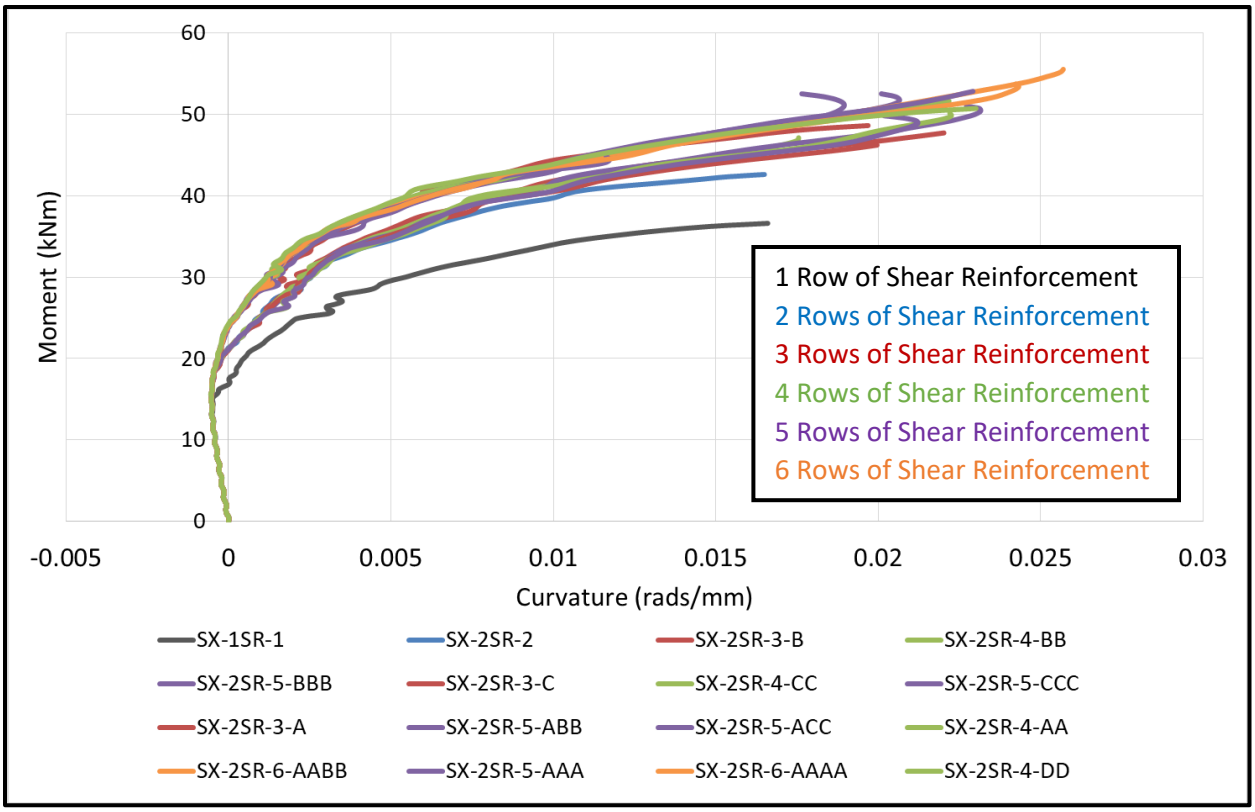

Figure 45: Shear Reinforcement Spacing Study SXS Series Moment-Curvature Behaviour

The presence of the first two peripheral rows of shear reinforcement clearly provide a significant capacity and ductility benefit to the connections considered. This can be seen by comparing the SXS series models with one (SX-1SR-1) and two (SX-2SR-2) rows of shear reinforcement to a model with no shear reinforcement (XXX from the SX series) which is shown in Figure 46. By adding 1 row of shear reinforcement the capacity is increased by 31% and the failure displacement is increased by 120%. By adding 2 rows of shear reinforcement the capacity is increased by 50% and the failure displacement is increased by 243%.

The presence of the third and fourth rows of shear reinforcement also have a significant impact on the ductility of the connection, but have less of an impact on the connection capacity as the failure mode of the connection is more flexural when a greater amount of shear reinforcement rows are provided. This can be seen by comparing models with 2-4 rows of shear reinforcement for the SBS series (Figure 47) and SXS series (Figure 48). For the SBS series on average, the addition of the third row of shear reinforcement increases the capacity by 13% and increases the failure displacement by 53%, and the addition of the third and fourth rows of shear reinforcement increases the capacity by 22% and increases the failure displacement by 153%. For the SXS series on average, the addition of the third row of shear reinforcement increases the capacity by 7% and increases the failure displacement by 24%, and the addition of the third and fourth rows of shear reinforcement increases the capacity by 14% and increases the failure displacement by 61%.

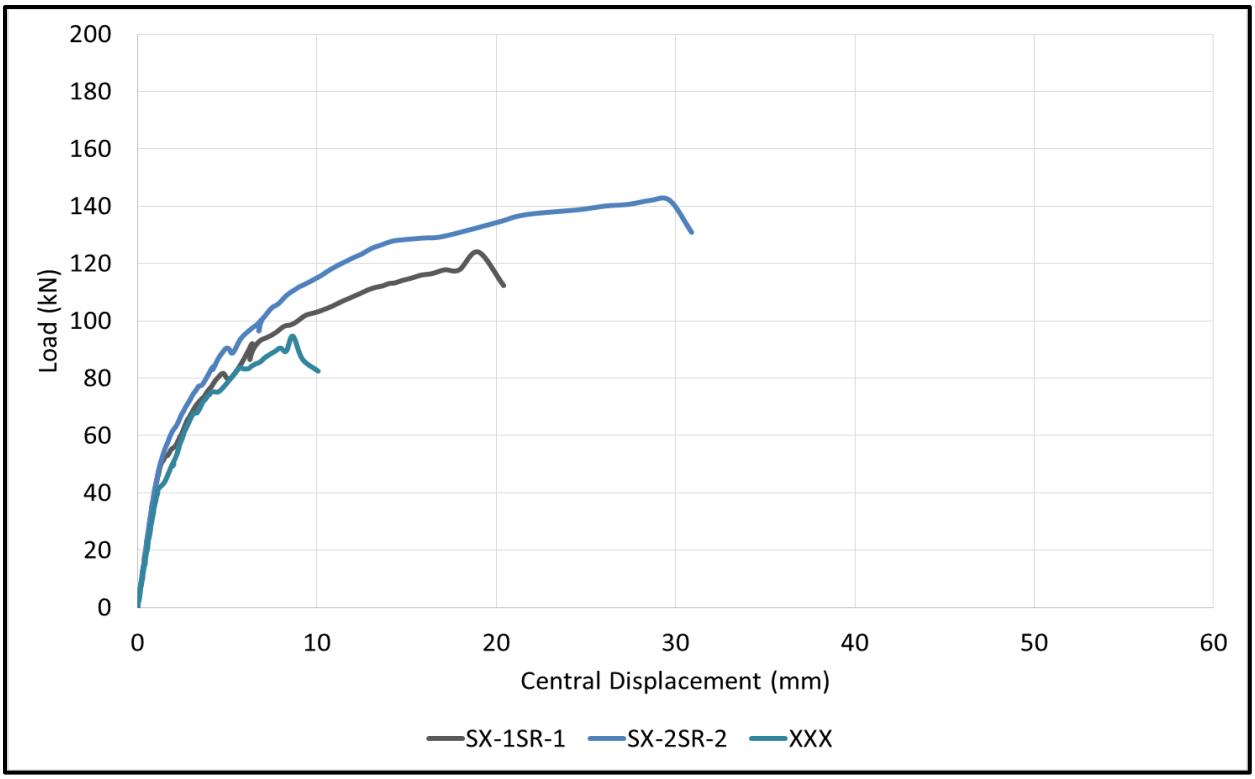

Figure 46: Shear Reinforcement Spacing Study SXS Models with 0-2 Reinforcement Rows Load-Deflection Behaviour

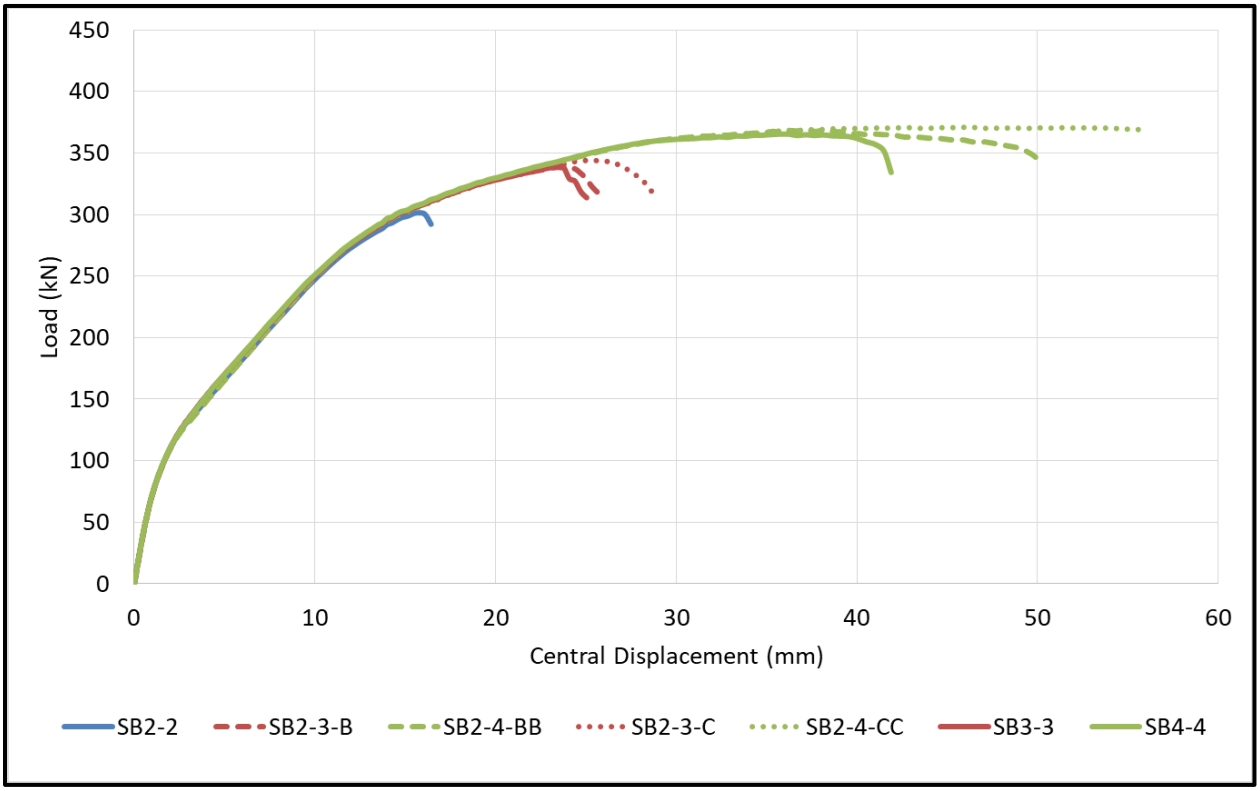

Figure 47: Shear Reinforcement Spacing Study SBS Models with 2-4 Reinforcement Rows Load-Deflection Behaviour

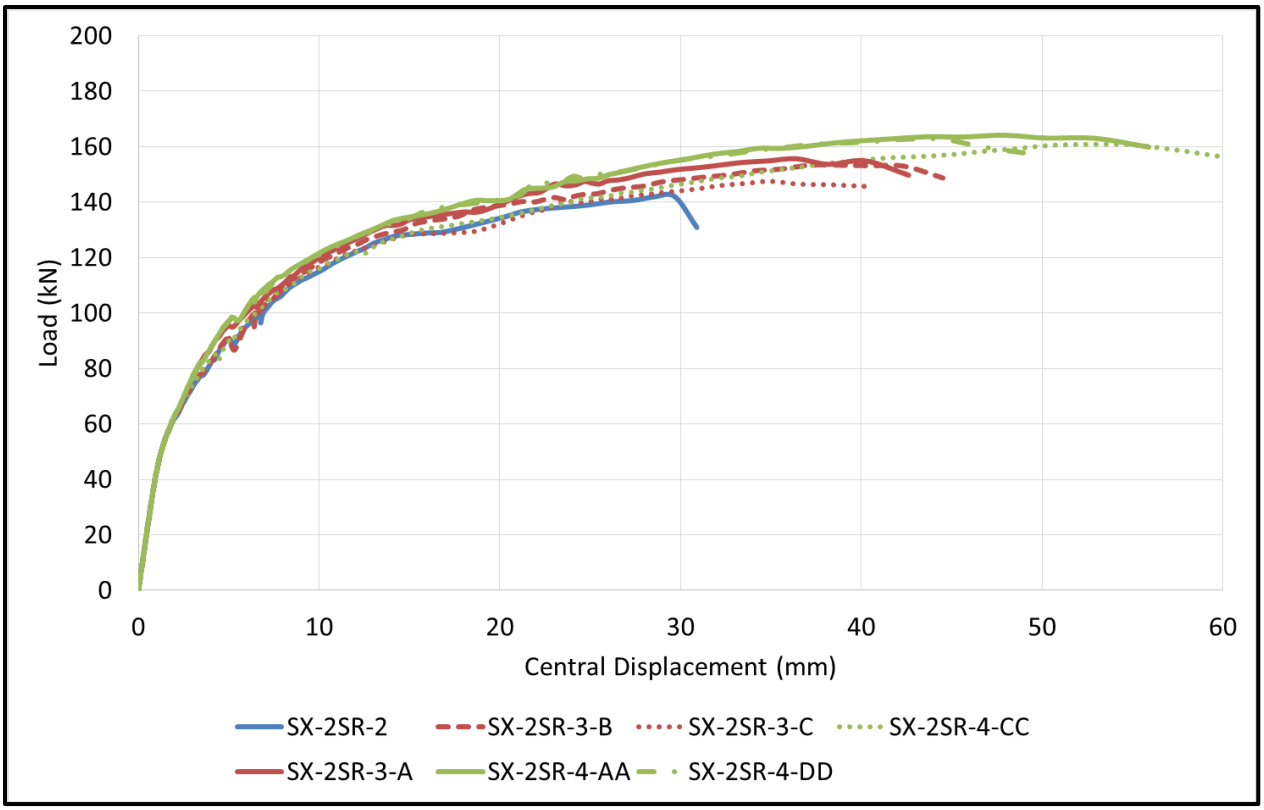

Figure 48: Shear Reinforcement Spacing Study SXS Models with 2-4 Reinforcement Rows Load-Deflection Behaviour

It can be seen from Figure 47 and Figure 48 that the change in stem-stem spacing of the rows results in a more drastic change in failure displacement when more rows or shear reinforcement are provided. A larger shear reinforced area (resulting from larger stem-stem spacing) results in more specimen ductility in most cases, however does not necessarily equate to a greater capacity (for example model SX-2SR-4-CC vs model SX-2SR-4-AA in Figure 48). The impact of the third and fourth rows of shear reinforcement can be further analysed through the bolt strain diagrams for the shear reinforcement spacing study models. Bolt strain diagrams for models SB2-6-BBBB (six rows of shear reinforcement with rows three to six at 1.11d stem-stem spacing) and SB3-6-BBB (six rows of shear reinforcement with rows four to six at 1.11d stem-stem spacing) are shown in Figure 49 and Figure 50 respectively. These two specimens are different in that the stem-stem spacing between the second and third rows of shear reinforcement is 1.11d for specimen SB2-6-BBBB and is 0.89d for specimen SB3-6-BBB.

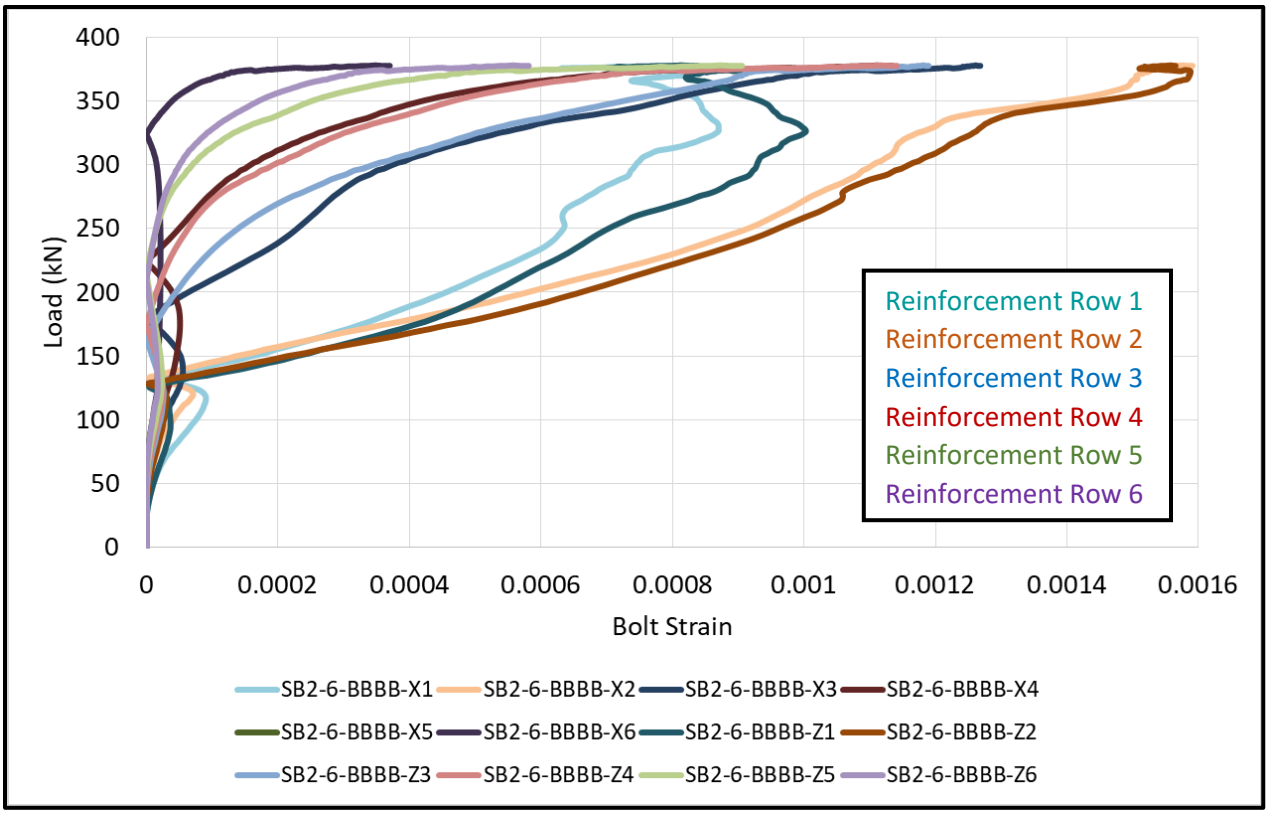

Figure 49: Shear Reinforcement Spacing Study SB2-6-BBBB Bolt Strain Diagram

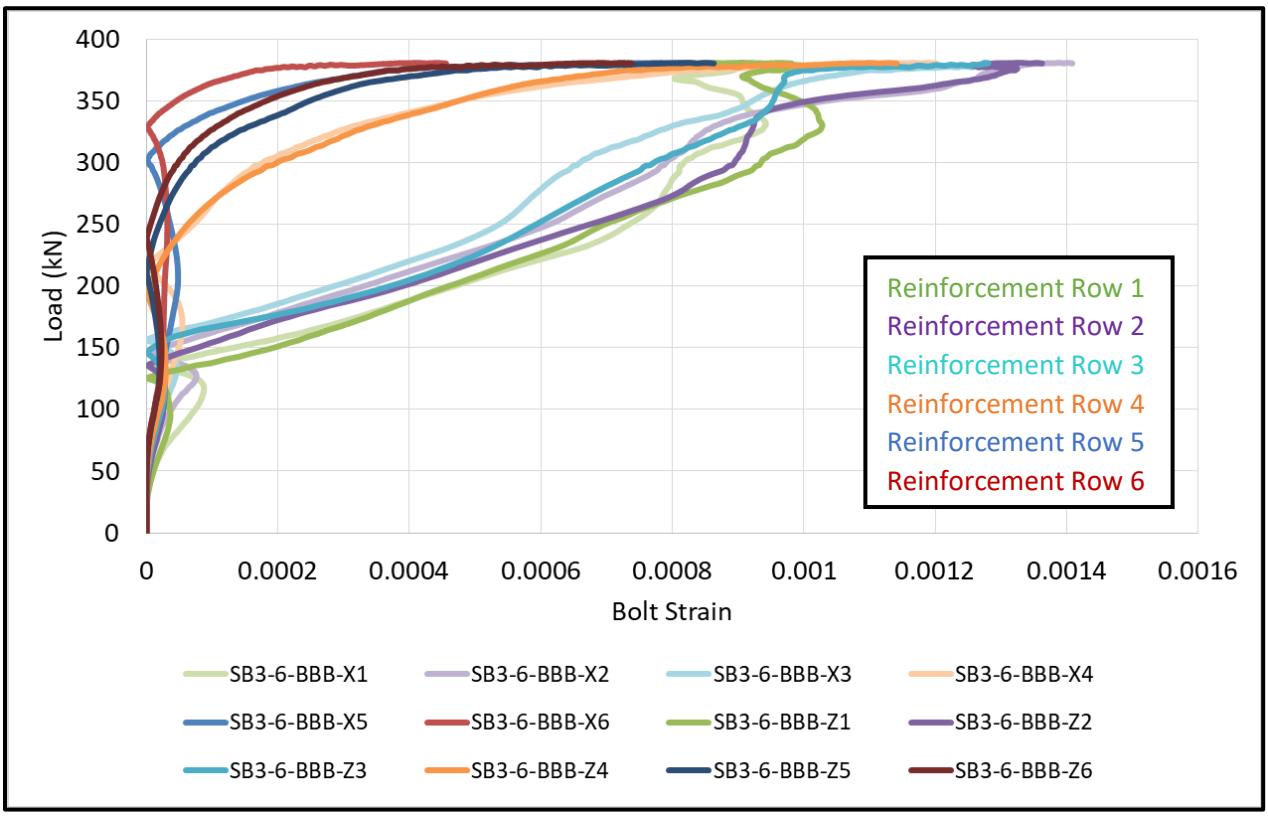

Figure 50: Shear Reinforcement Spacing Study SB3-6-BBB Bolt Strain Diagram

As shown in Figure 49 and Figure 50, while the behaviour of the fourth row of shear reinforcement is very similar regardless of its position within the slab (activating at around 200kN and developing around 0.00115 strain units at failure) the behaviour of the second and third rows or shear reinforcement behave differently depending on the position of the third reinforcement row. When the third reinforcement row is 2.33d from the column (Figure 50) this row activates at around 150kN and develops strains at a similar pace to the second reinforcement row up until failure where both rows have developed approximately 0.0013 units of strain. When the third reinforcement row is greater than 2.33d from the column (Figure 49) it activates later (at around 175kN) and develops strains much slower than the second row of shear reinforcement, which develops strains quicker to compensate and as a result develops around 20% more strain at failure. This response can be explained by analyzing the pre-failure side crack profile of specimen SB2-6-BBBB (Figure 51). All shear reinforcement spacing study bolt strain diagrams are provided in Appendix C.

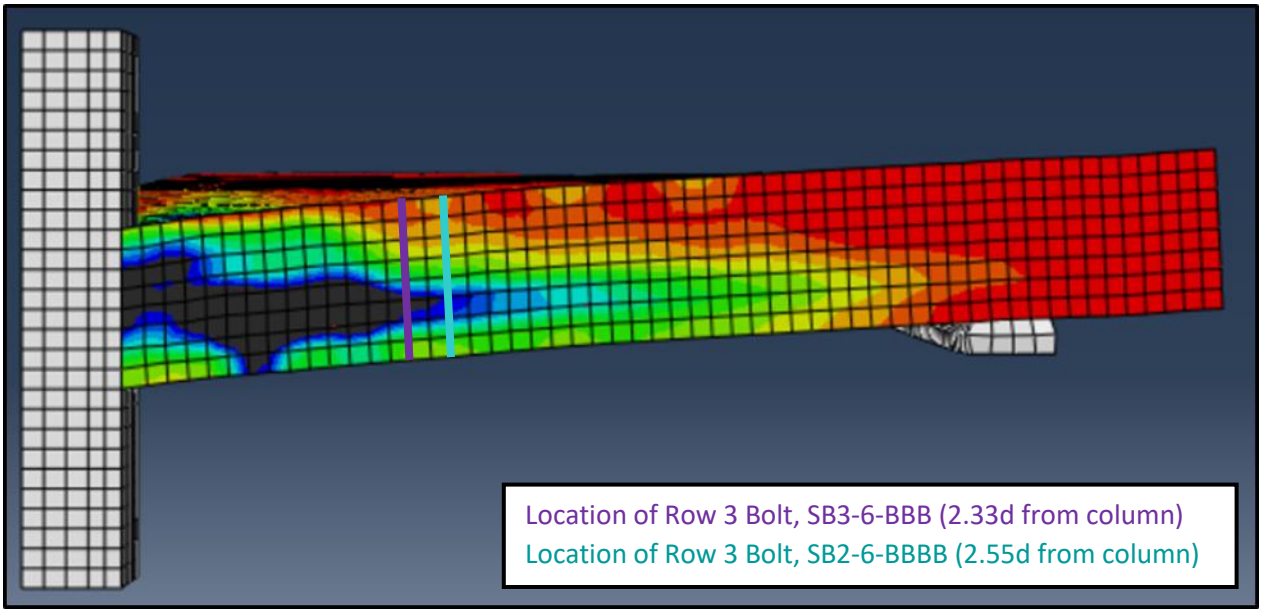

Figure 51: Shear Reinforcement Spacing Study SB2-6-BBBB Pre-Failure Side Crack Profile

The location of the third bolt row is approximately at the tip of the shear crack which develops prior to failure of the specimen, and the position of the bolt within the crack or outside the crack significantly impacts its behaviour. This also suggests that the location of this bolt row would have a larger impact on the behaviour of the specimen than the subsequent bolt rows. The position of the third reinforcement row can also be shown to have an impact on the moment-curvature behaviour of the connection when models are grouped into those with the third row of shear reinforcement at 2.33d and those with the third row of shear reinforcement beyond 2.33d as in Figure 52.

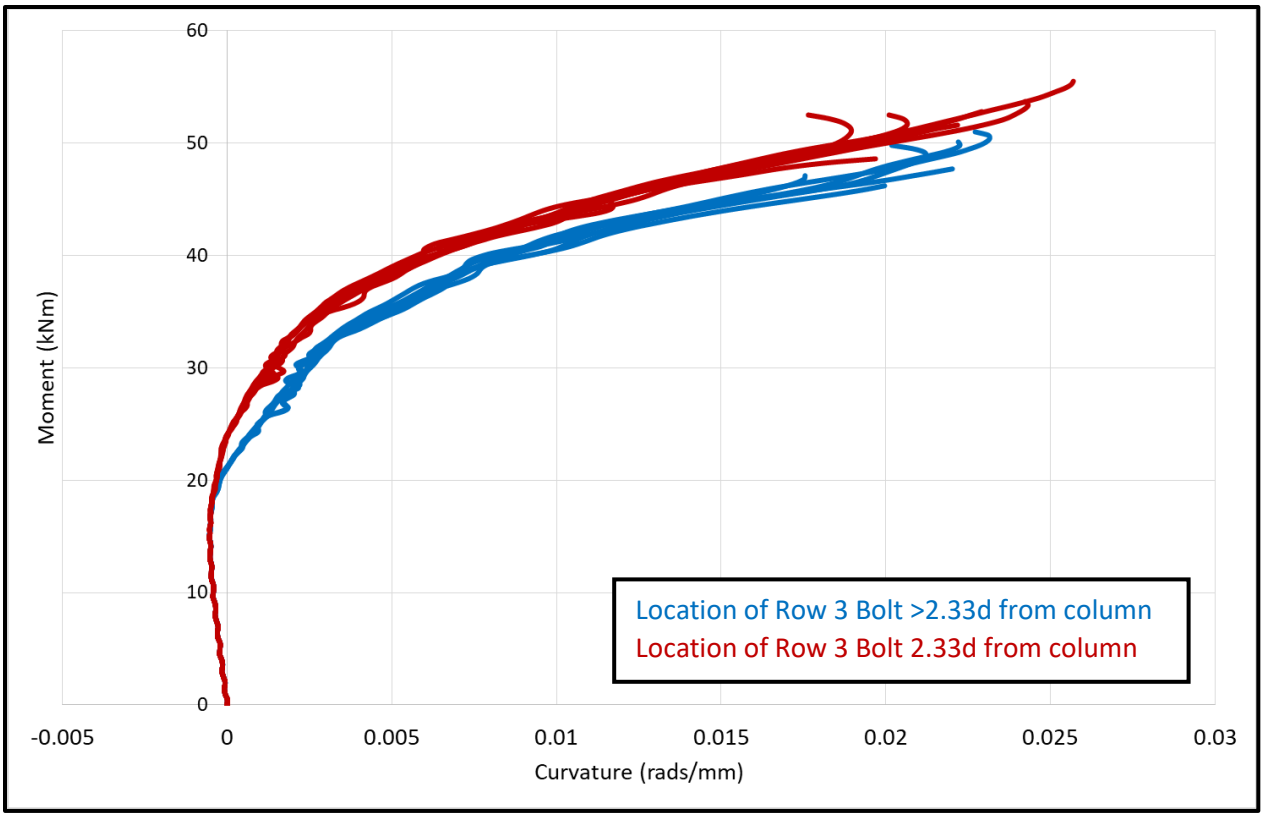

Figure 52: Shear Reinforcement Spacing Study SXS Series Moment-Curvature Behaviour by Row 3 Location

As shown in Figure 52, two separate rotational stiffnesses are shown for models depending on the location of the third row of shear reinforcement, further highlighting its importance in determining connection behaviour.

The presence of the fifth and sixth shear reinforcement rows have negligible impact on the behaviour of the models. This can be seen by analyzing the load-deflection behaviour of the SXS series specimens with five and six shear reinforcement rows (Figure 53). When compared to a specimen with four shear reinforcement rows at their original spacing, the addition of the fifth shear reinforcement row on average increases the capacity by 2% and increases the failure displacement by 15%. The addition of the fifth and sixth shear reinforcement rows on average increases the capacity by 6% and the failure displacement by 21%. This is because when more than four shear reinforcement rows are provided the failure mode of the connection is entirely flexural, and the addition of more shear reinforcement will not significantly impact the point at which the flexural reinforcement will yield.

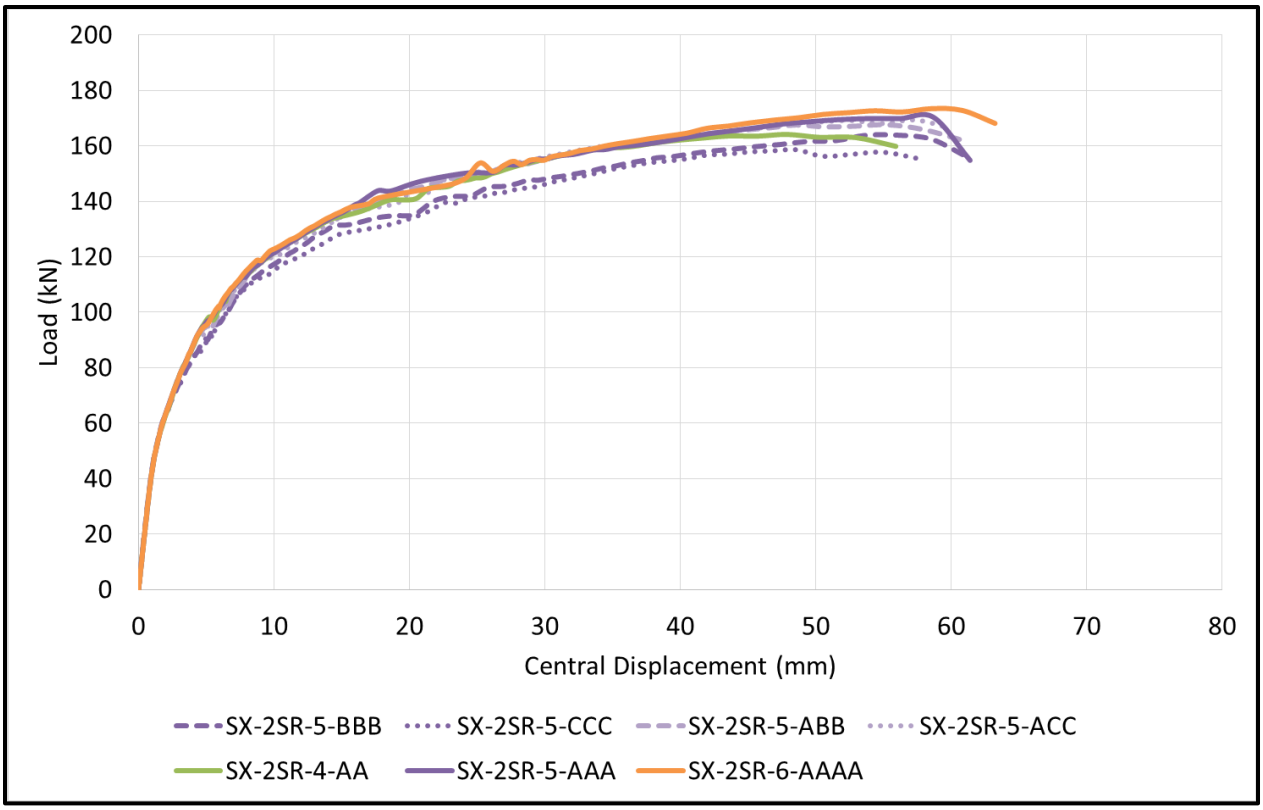

Figure 53: Shear Reinforcement Spacing Study SXS Models with 5-6 Reinforcement Rows Load-Deflection Behaviour

The behaviour of two different models with the same shear reinforced area and different number of shear reinforcement rows can be assessed through models SX-2SR-3-C (three shear reinforcement rows with row three at 1.5d stem-stem spacing) and SX-2SR-4-DD (four shear reinforcement rows with rows three and four at 0.75d stem-stem spacing), which both have a shear reinforced area with the diameter 3d. Load-deflection behaviour for these two specimens, as well as similar specimens with 3 and 4 rows of shear reinforcement, are presented in Figure 54.

Figure 54 shows that the models with equal shear reinforced areas behave more similarly to the models with the same number of shear reinforcement rows than to each other. However, the capacity and failure displacement of model SX-2SR-3-C is lower than expected when compared with model SX-2SR-3-A, which has the same number of shear reinforcement rows and a smaller shear reinforced area. If the behaviour of model SX-2SR-3-C was to SX-2SR-3-A what model SX-2SR-4-AA is to model SX-2SR-4-DD (which also has the same number of shear reinforcement rows and a smaller shear reinforced area) then the behaviour of the two models with equal shear reinforced areas would be very similar. This suggests that while the number of shear reinforcement rows does still play a role in the connection behaviour, if the shear reinforcement rows are provided over the same area and no inter-stud punching occurs in the connection the behaviour these connections would be very similar.

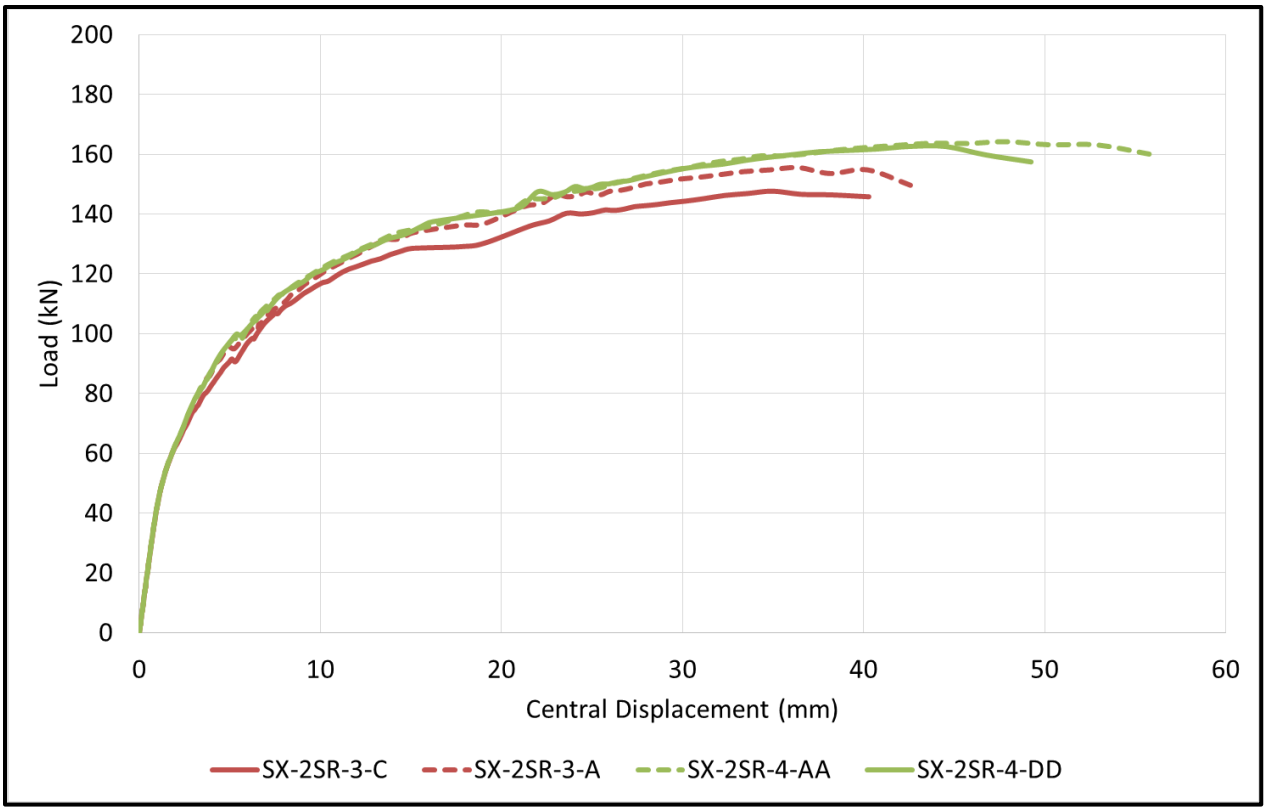

Figure 54: Shear Reinforcement Spacing Study SXS Series Load-Deflection Behaviour for Models with Equal Shear Reinforced Areas

Finally, as shown in Figure 43, Figure 44, Figure 45 no model behaved in a way which would suggest that inter-stud punching occurred as the failure mode. Additionally, no yielding was seen in any of the shear studs/bolts presented in Figure 49, Figure 50, or found in Appendix C. To determine the failure mode of the models the post-failure side crack profiles were also analyzed for each model. Post-failure crack profiles for SBS series specimen SB2-3-C (three shear reinforcement rows with the third row at 1.33d stem-stem spacing) and SXS Series Specimen SX-2SR-3-B (three shear reinforcement rows with the third row at 1.25d stem-stem spacing) are presented in Figure 55 and Figure 56 respectively.

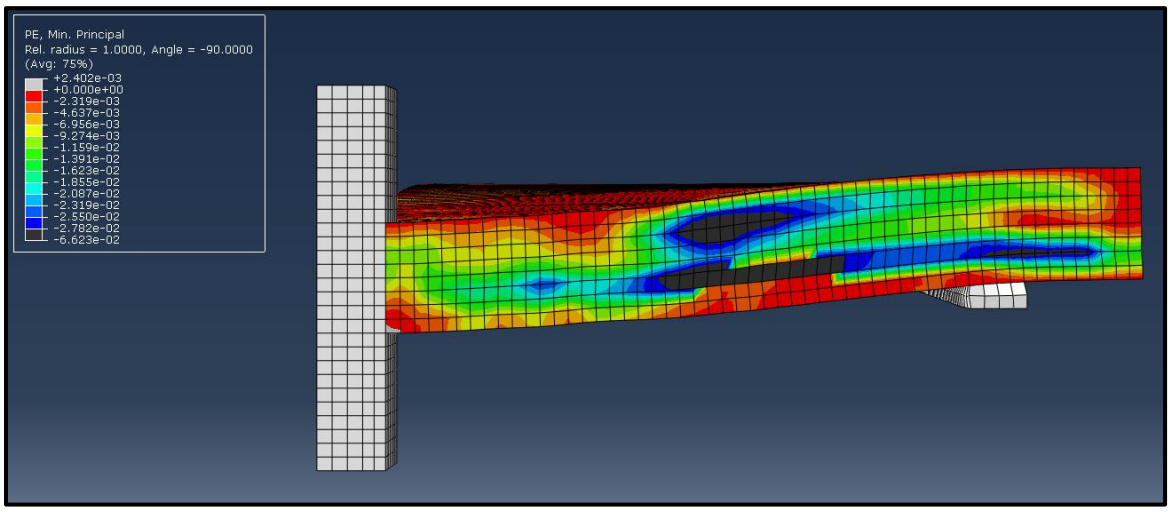

Figure 55: Shear Reinforcement Spacing Study SB2-3-B Post-Failure Side Crack Profile

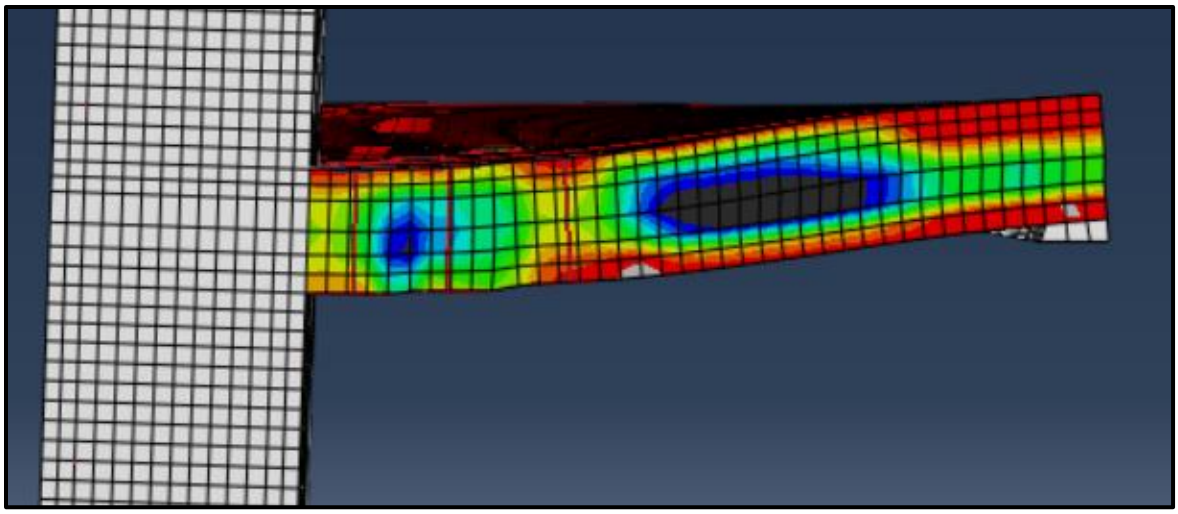

Figure 56: Shear Reinforcement Spacing Study SX-2SR-3-B Post-Failure Side-Crack Profile

As shown in Figure 55, the model shows the strains on the longitudinal reinforcement outside of the shear reinforced zone associated with flexural failure of the model. This is consistent with the failure modes shown buy the SB series models and test specimens. As shown in Figure 56, the model shows strains outside of the shear reinforced zone and a curvature which would suggest a combined shear and punching failure mode. This is consistent with the SX series models. No specimen shows a post-failure crack pattern which has the characteristics of a punching failure occurring between rows of shear reinforcement. This suggests that a stem-stem spacing of up to 1.5d is valid for preventing inter-stud punching from occurring in a slab-column connection. All post-failure side crack profiles for the shear reinforcement spacing study are provided in Appendix C.

Crack patterns showing the tension side of the models were also produced by the script for all of the models. The crack pattern for model SB2-3-C (three rows of shear reinforcement with row three at 1.5d spacing) is shown in Figure 57. The crack pattern for model SX-2SR-4-CC (four rows of shear reinforcement with rows three and four at 1.5d spacing) is shown in Figure 58. By comparing the crack patterns for similar models, it can be determined whether changing a parameter has a significant effect on the failure behaviour of the model. Crack patterns for all of the shear reinforcement spacing study models can be found in Appendix C.

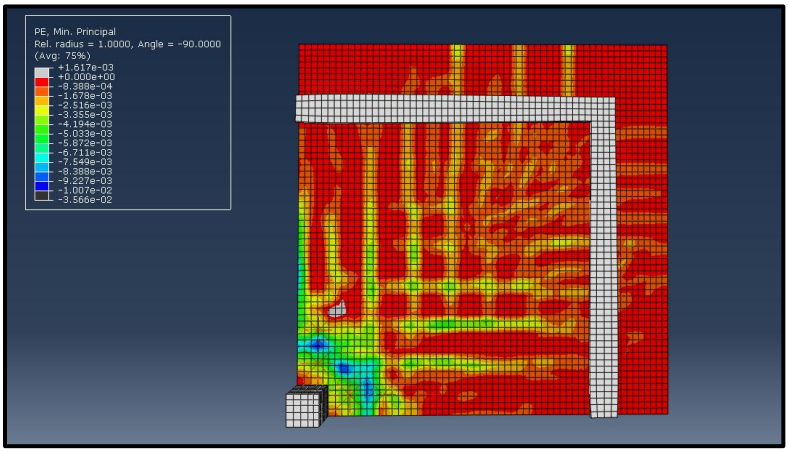

Figure 57: Shear Reinforcement Spacing Study SB2-3-C Tensile Slab Face Crack Pattern

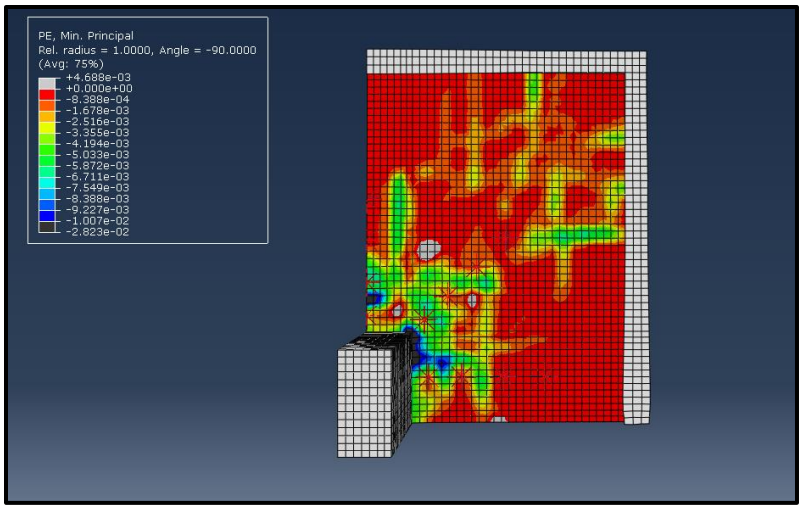

Figure 58: Shear Reinforcement Spacing Study SX-2SR-4-CC Tensile Slab Face Crack Pattern

6.2.4 Shear Reinforcement Spacing Study Conclusions

Based on these results, the conclusions of the shear reinforcement spacing study are as follows:

1. The presence of the first four rows of shear reinforcement have a significant impact on the behaviour of a slab-column connection when the stem-stem spacing of the rows is between 0.75d-1.5d. The spacing of the first three rows of shear reinforcement have the most impact on the connection behaviour because they are located within the major shear crack which develops before the specimen failure. The presence of the a fifth or sixth row of shear reinforcement has a negligible effect on the overall connection behaviour as the failure mode of the connection is mostly flexural after four shear reinforcement rows are provided.

2. Two specimens with equal shear reinforced areas and different numbers of shear reinforcement rows will display very similar behaviour to each other. The additional reinforcement row will provide only a minor increase in capacity and ductility.

3. A stem-stem spacing of up to 1.5d successfully prevents inter-stud punching from occurring in the connections considered. Current code provisions which require smaller stem-stem spacing (for example CSA A23.3-19 Cl 13.3.8.6) could be raised to this limit based on these tests, however connections with different reinforcement ratios and thicknesses should also be considered.

6.3 Openings Study

6.3.1 Openings Study Objectives

The second parametric study investigated the effect of changing the size and number of openings adjacent to the column on the failure mode and failure behaviour of the model. Openings are important to include in a slab-column connection to allow for the routing of utilities and vents through a building, and adjacent to a column is usually the most convenient place to locate these utilities. Openings have a significant effect on the shear resistance of a connection, as they reduce the amount of concrete present to resist the shear demand. The presence of openings also influences the position of the shear reinforcement in a slab column connection, as enough cover must be provided between the reinforcement and the edge of the

openings in order for the reinforcement to be effective. Since shear reinforcement is often provided in the form of stud rails, all peripheral rows of shear reinforcement often have to be moved further from the column centerline as a result of the inclusion of an opening near the column. This is illustrated in Figure 59.

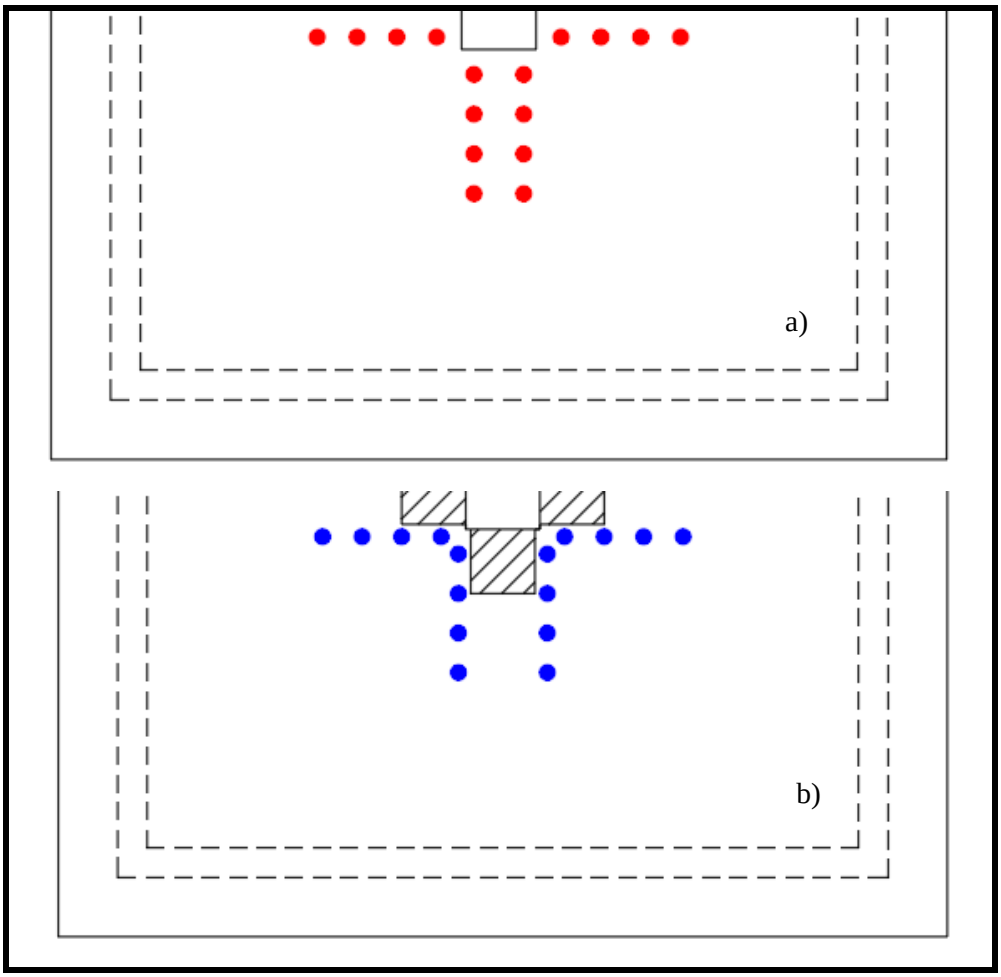

Figure 59: Openings Study a) Double Cruciform Bolt Locations and b) Double Cruciform Bolt Locations with 130mm Opening

The objectives of this study are to:

1. Determine what is the maximum size an opening can be adjacent to a column without having too detrimental of an impact on the connection behaviour, and

2. Determine whether moving the peripheral rows of shear reinforcement outside of an opening (farther from the column centerline) have an effect on the behaviour of the shear reinforcement for different opening sizes.

6.3.2 Openings Study Models

Fourteen models were created in this study (SBO series models). The control model for the study was that for specimen SB4. The other models were separated into those with four openings around the column stub, similar to specimen SB5, and those with two openings around the column stub, similar to specimen SB6. All models had four rows of shear bolts with a stem-stem spacing of 80mm (50mm for the first row). The openings were all square, and the opening widths were varied between 30mm (20% of the column stub width), and 150mm (equal to the column width) in increments of 20mm. No specimen was created with four openings of 150mm width as that would completely disconnect the column stub from the slab. Shear bolts were located so that 10mm of cover is provided between the opening and the bolt washer as used in the original SB series specimens tested by Adetifa and Polak (2005).

Models for this study are named according to the following naming convention. All models were based on specimen SB4 and begin with SB4. The following number denotes the number of openings in the model (0, 2, or 4). Finally the number at the end of the model name denotes the width of the opening in mm. For example SB4-2-50 would have 2 50mm openings adjacent to its column stub. The opening study specimens, including their opening sizes and shear reinforcement locations relative to the column center are provided in Table 11.

Table 11: Opening Study (SBO Series) Models

Specimen	Number of Openings	Opening Width (mm / Ratio to Column Width)	X Bolt Offset from Column Centerline (mm)	Z Bolt Offset from Column Centerline (mm)
SB4-0			50	50
SB4-4-30	4	30 / 0.2	50	50
SB4-4-50	4	50 / 0.33	57	57
SB4-4-70	4	70 / 0.46	67	67
SB4-4-90	4	90 / 0.6	77	77
SB4-4-110	4	110 / 0.73	87	87
SB4-4-130	4	130 / 0.86	97	97
SB4-2-30	2	30 / 0.2	50	50
SB4-2-50	2	50 / 0.33	57	50
SB4-2-70	2	70 / 0.46	67	50
SB4-2-90	2	90 / 0.6	77	50
SB4-2-110	2	110 / 0.73	87	50
SB4-2-130	2	130 / 0.86	97	50
SB4-2-150	2	150 / 1	107	50

6.3.3 Openings Study Results and Discussion

Results for the opening study were obtained through the use of a custom Python script which outputted load-deflection behaviour, bolt strain behaviour, and tensile crack patterns for all of the SBO series models. Load-deflection behaviour for the SBO series models with four and two openings are provided in Figure 60 and Figure 61 respectively.

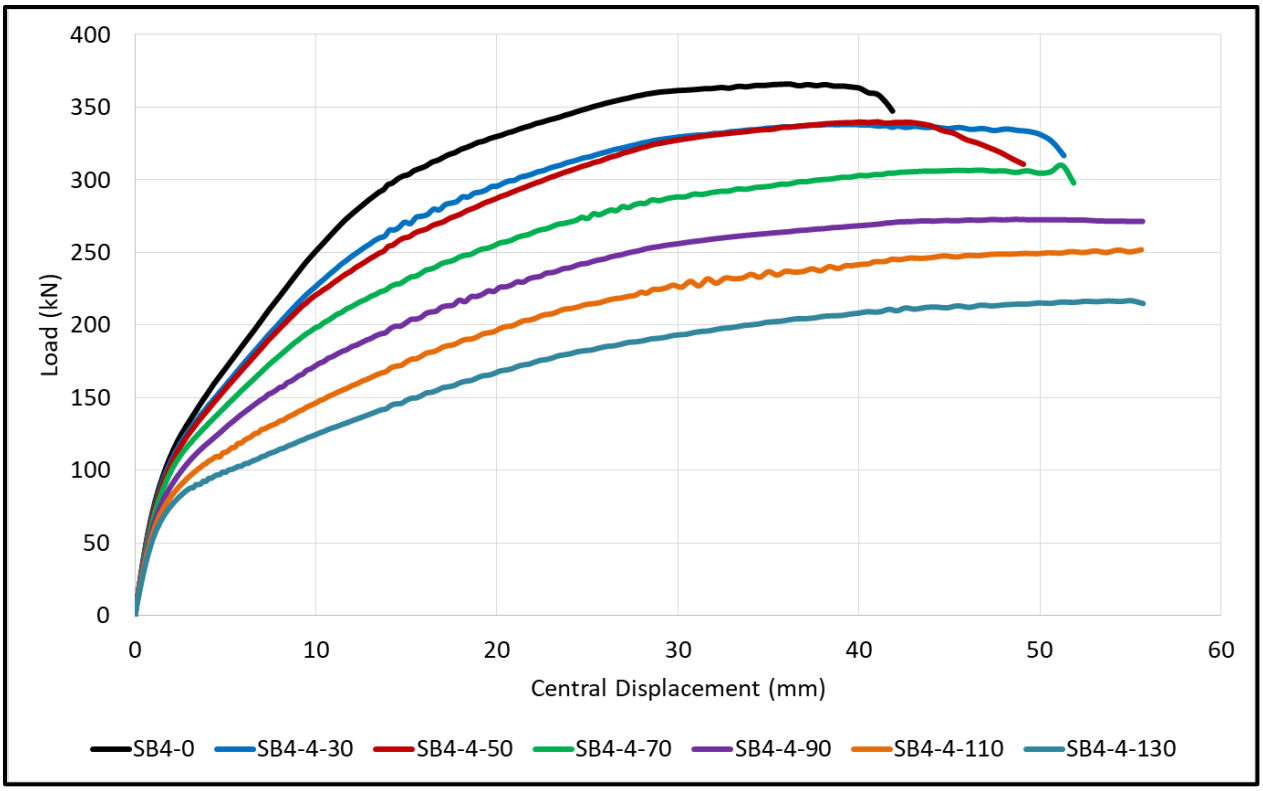

Figure 60: Openings Study SBO Series Load-Deflection Behaviour (4 Openings)

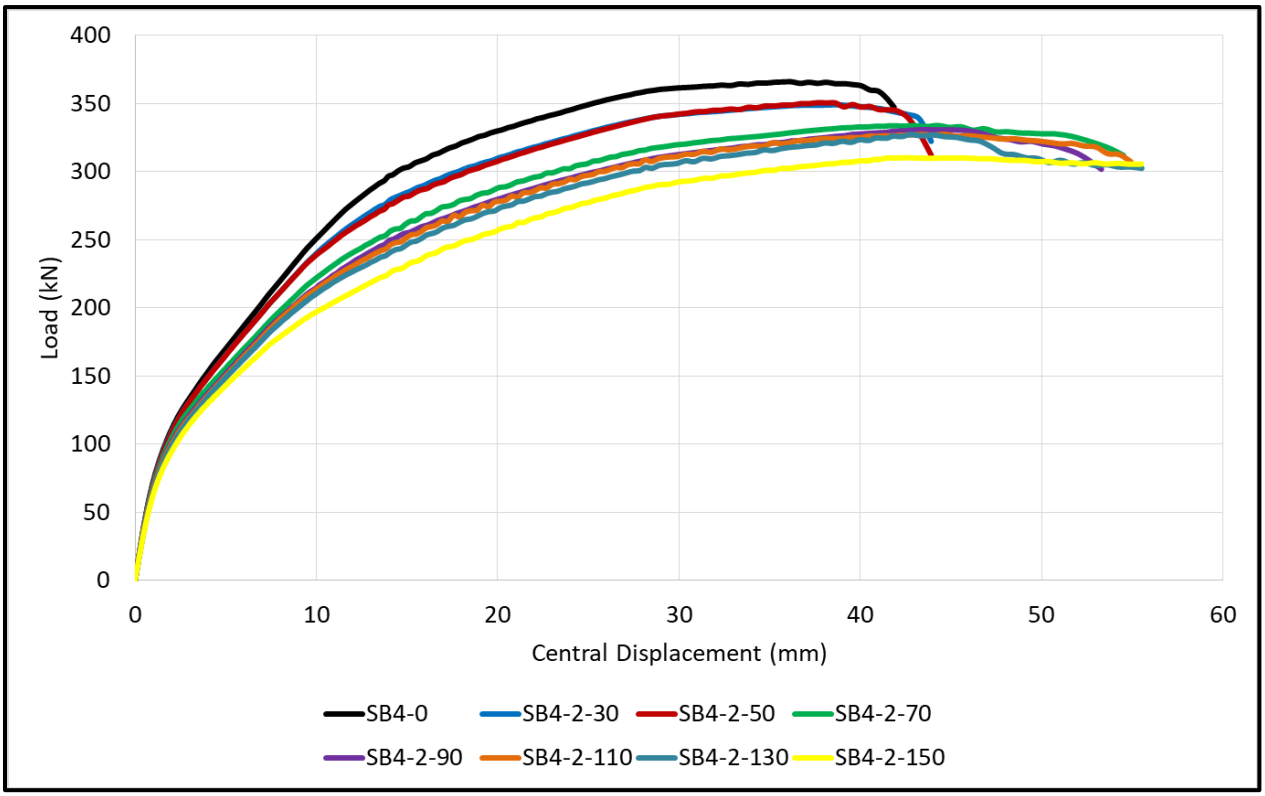

Figure 61: Openings Study SBO Series Load-Deflection Behaviour (2 Openings)

As shown in Figure 60 and Figure 61, as the size of the openings in the models are increased the capacity and stiffness of the model decreases. In addition, it can be seen that this effect is much more extreme for the models with four openings near the column than for those with two openings near the column. For discussion purposes, based on Figure 60 and Figure 61, the percentage of the capacity of the SB4-0 model is recorded in Table 12.

Table 12: Openings Study Models Percentage of SB4 Capacity

Percentage of SB4 Capacity Reached c = column width		
Opening Width	**Number of Openings**	
	2	**4**
0.2c	95.4%	92.4%
0.33c	95.8%	92.9%
0.46c	91.2%	83.8%
0.6c	90.4%	74.6%
0.73c	89.5%	68.8%
0.86c	89.4%	59.2%
c	84.7%	

Table 12 shows that when you have four openings, you maintain at least 90% of the opening-less capacity if the openings provided are less than a third of the column width, and that when you have two openings 90% of the opening-less capacity is maintained when the opening width is less than 60% of the column width (and is still close to 90% of the opening-less capacity when the opening width is 86% of the column width).

However, as shown in Figure 61, two different stiffness are shown for specimens with two openings less than 33% of the column width and greater than 46% of the column width. The approximate failure displacement of SB4-0 is only maintained for opening study models SB4-2-30 (two openings of 30mm width) and SB4-2-50 (two openings of 50mm width). In order to investigate this, the failure behaviour of the opening study models was observed through the post-failure side crack profiles. This profile for opening study model SB4-2-50 (two openings of 50mm width) is shown in Figure 62, for opening study model SB4-2-50 (four openings of 50mm width) is shown in Figure 63, and for opening study model SB4-4-90 (four openings of 90mm width) is shown in Figure 64. All post-failure side crack profiles can be found in Appendix D.

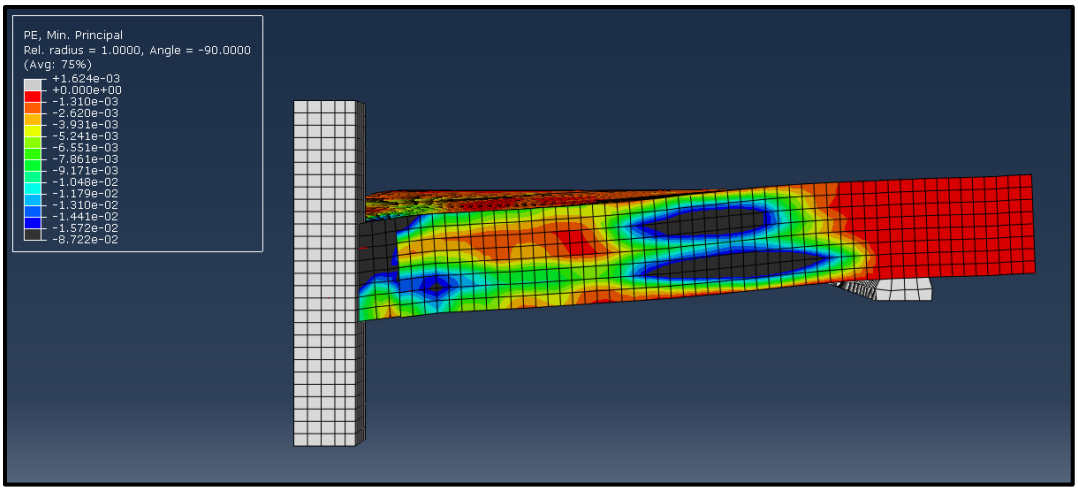

Figure 62: Openings Study SB4-2-50 Post-Failure Crack Profile

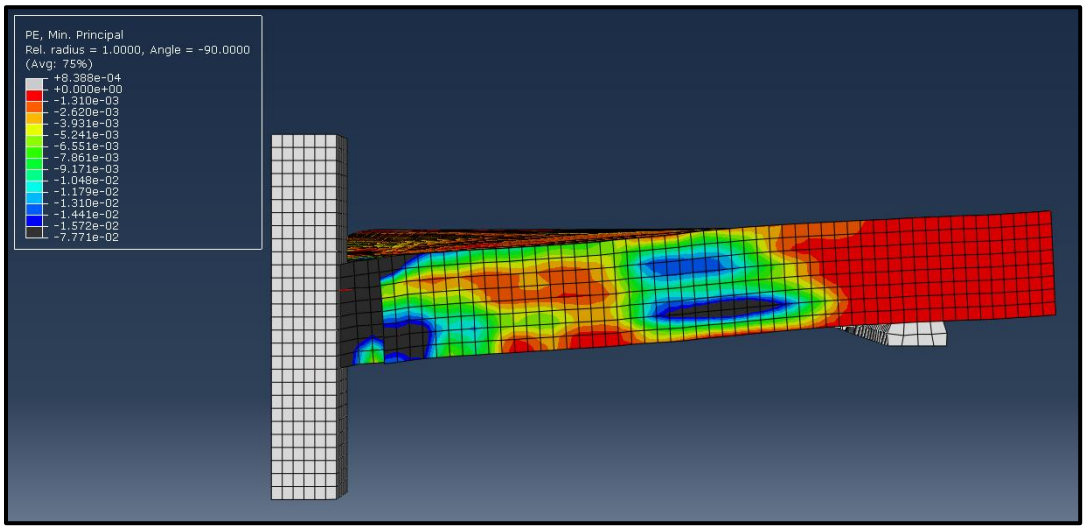

Figure 63: Openings Study SB4-2-50 Post-Failure Crack Profile

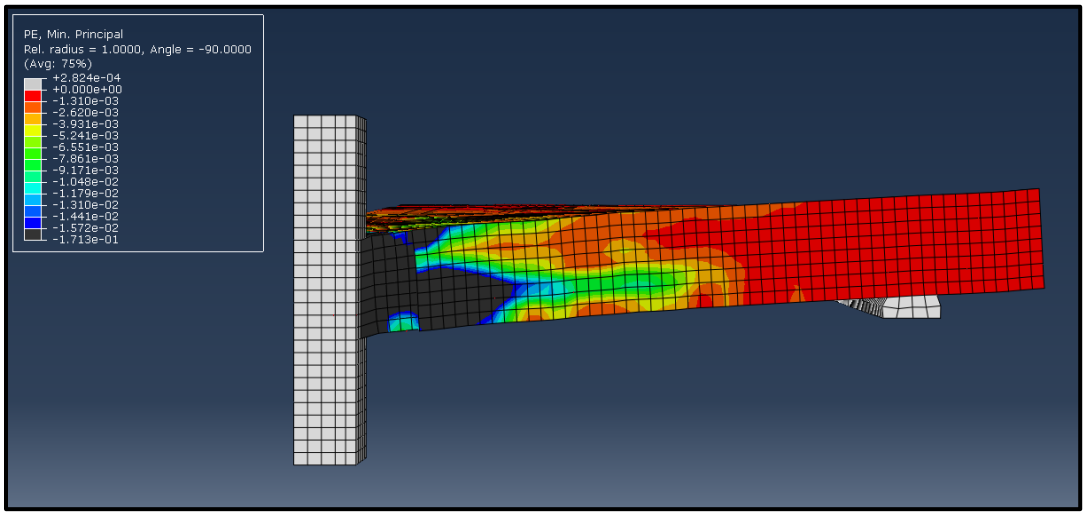

Figure 64: Openings Study SB4-4-90 Post-Failure Crack Profile

The post-failure crack profiles show that for the models with two openings and an opening width less than 33% of the column width, the failure mode is still mostly flexural as evidenced by the longitudinal strains and curvature outside the shear reinforced zone as in SB4-0. As the opening size increases, or more openings are added, the failure mode becomes more of a combined flexural and punching mode, as the longitudinal strains are still present but lessened, and more strain is seen in the area near the openings/column stub. As the size of the openings is increased more, the longitudinal strains disappear, the strain field near the column dominates, and the curvature of the specimen is seen only near the column, suggesting punching failure within the shear reinforced zone. This explains the difference in stiffness behaviour in Figure 61, and suggests that for a flexural failure mode to be maintained two openings with widths less than 33% of the column width should be provided.

To determine if the shear bolts behave differently in the models, bolt strain diagrams were analyzed for all of the SBO series models. Bolt strain diagrams for specimens SB4-2-30 (two openings of 30mm width), which has the same bolt locations as in the control specimen SB4, and SB4-4-130 (four openings 130mm width, bolts offset 97mm from the column centerline) are provided in Figure 65,and Figure 66 respectively. Figure 65 shows that for a model with the original bolt locations the bolts activate at between 100kN and 160kN and all four rows of shear reinforcement develop around 0.0014 units of strain at failure. Figure 66 shows that for a specimen with large openings the bolts activate at between 60kN and 130kN and only the first three rows of bolts reach a strain of 0.0013 at failure.

The earlier activation could be a result of having less concrete within the shear reinforced area to resist shear forces, which would mean the shear reinforcement is needed earlier to supplement the concrete's shear capacity. Additionally, as shown in Figure 64, the specimens with larger openings show the majority of their cracking close to the column near failure, which would explain why the shear bolts farther from the column show reduced strains at failure. Beyond these observations, there was little variation in any of the analyzed bolt strain diagrams which would suggest that position the bolts farther from the column centerline has a significant effect on their behaviour. No bolts experienced yielding in any of the models. All opening study bolt strain diagrams can be found in Appendix D.

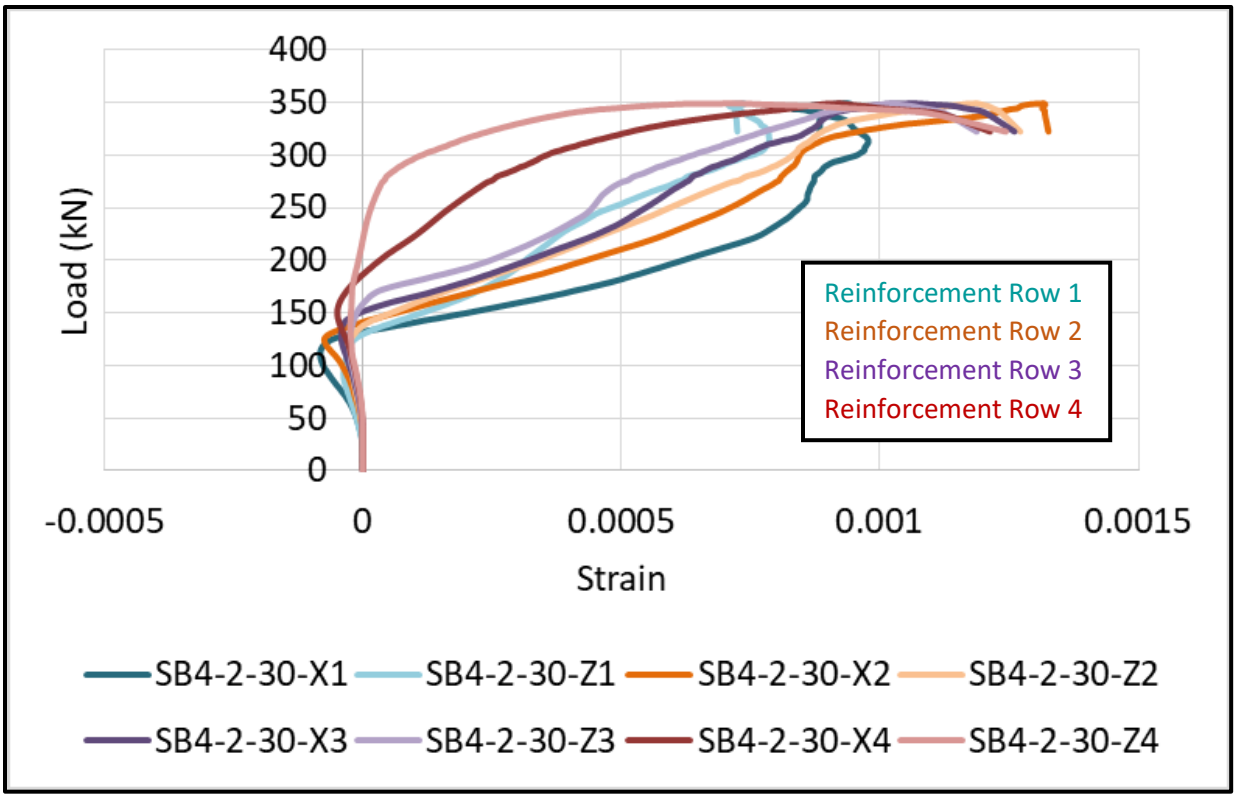

Figure 65: Openings Study SB4-2-30 Bolt Strain Diagram

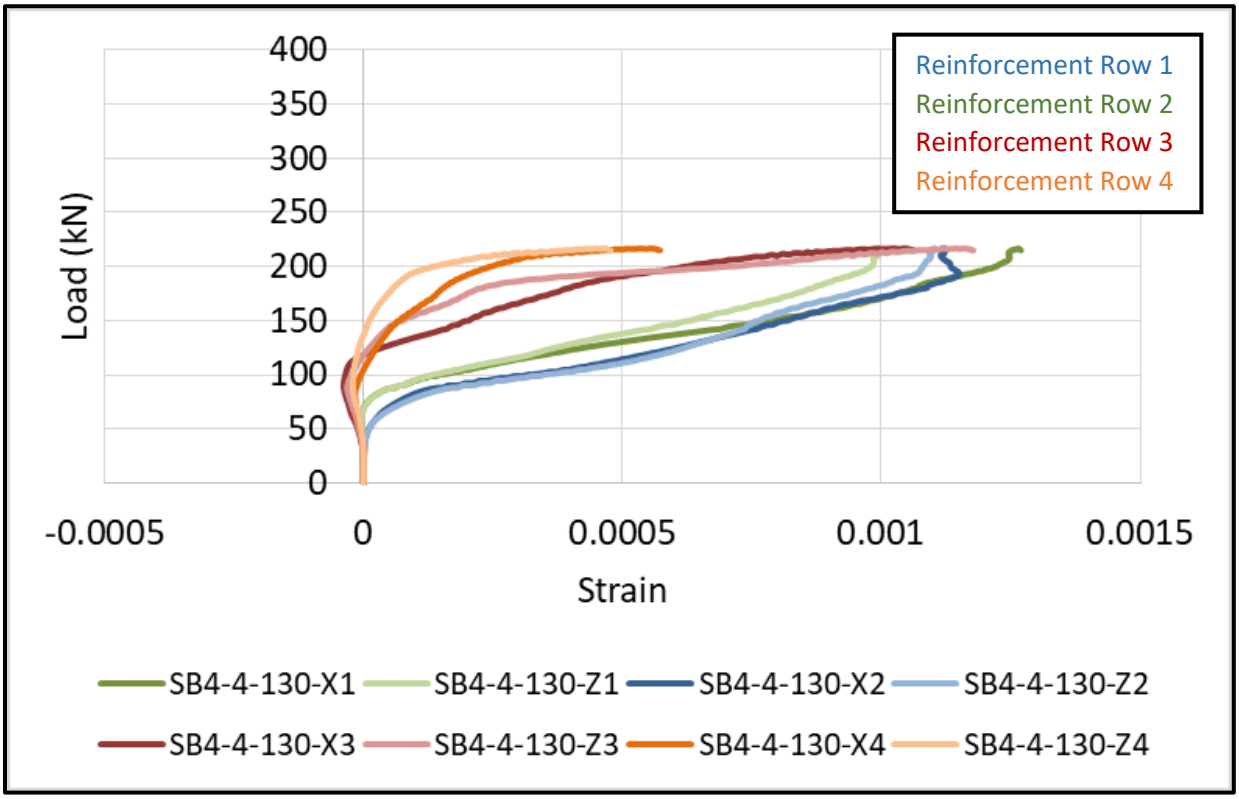

Figure 66: Openings Study SB4-4-130 Bolt Strain Diagram

Crack patterns showing the tension side of the specimens were also produced by the script for all of the models. The crack pattern for specimen SB4-2-130 (two openings of 130mm width) is shown in Figure 67. Comparison of crack patterns between models was also used to determine if the change of opening size had an effect on the model behaviour. Crack patterns for all of the opening study models can be found in Appendix D.

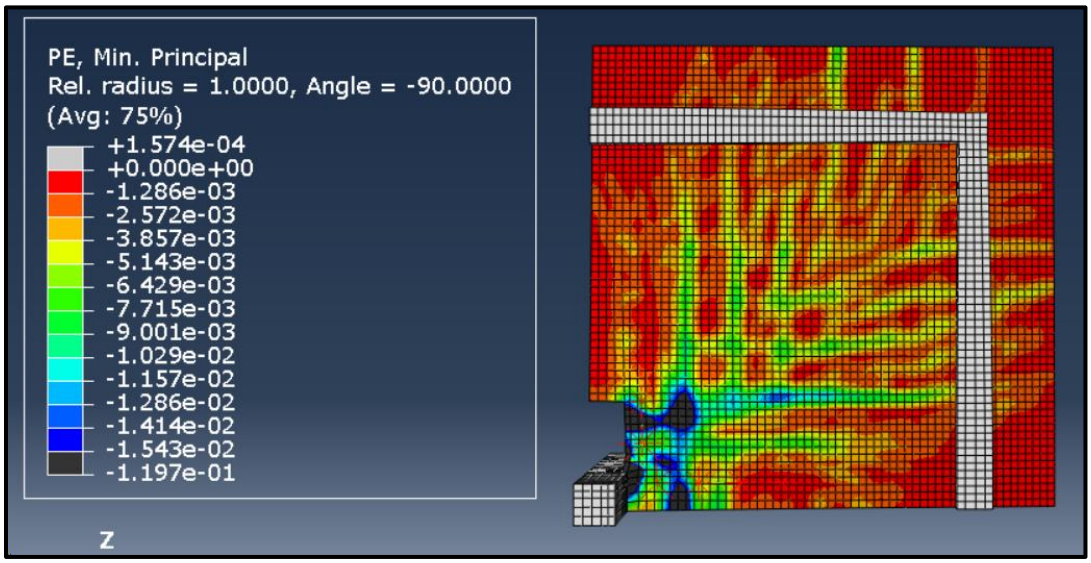

Figure 67: Openings Study SB4-2-130 Crack Pattern

6.3.4 Openings Study Conclusions

Based on all of these results, the conclusions to the opening study are as follows:

1. It is recommended that the width of an opening adjacent to the column in a slab-column connection be less than 60% of the column width if two openings are provided adjacent to the column, and less than one third of the column width if four openings are provided adjacent to the column. However, it must be noted that the stiffness of the opening-less specimen is only maintained if two openings with widths less than one third of the column width are provided.

2. No adverse effects are experienced in the shear bolts if they are provided farther from the column centerline to accommodate the openings. It is therefore recommended that the shear stud rails simply be moved outside of the openings by a distance necessary to provide proper anchorage and cover when openings are provided in a slab-column connection.

6.4 Anchorage-Controlled Shear Reinforcement Study

6.4.1 Anchorage-Controlled Shear Reinforcement Study Objectives

Anchorage-controlled shear reinforcement, or retrofitted shear bolts with flexible nylon washers, was proposed by Topuzi et al (2017) as a method of increasing the ductility of a reinforced concrete slab-column connection during cyclic lateral loading while limiting the overall stiffness of the connection. Ductility is necessary when a connection is under cyclic lateral loading because, while slab-column connections are typically not a part of a structure's lateral force resisting system, they must be able to

withstand the lateral drift of the structure. This can be achieved through conventional shear studs/bolts, however when conventional reinforcement is used the stiffness of the connection attracts more load to the connection and away from the lateral force resisting system. This was shown by Topuzi et al (2017) in Figure 68.

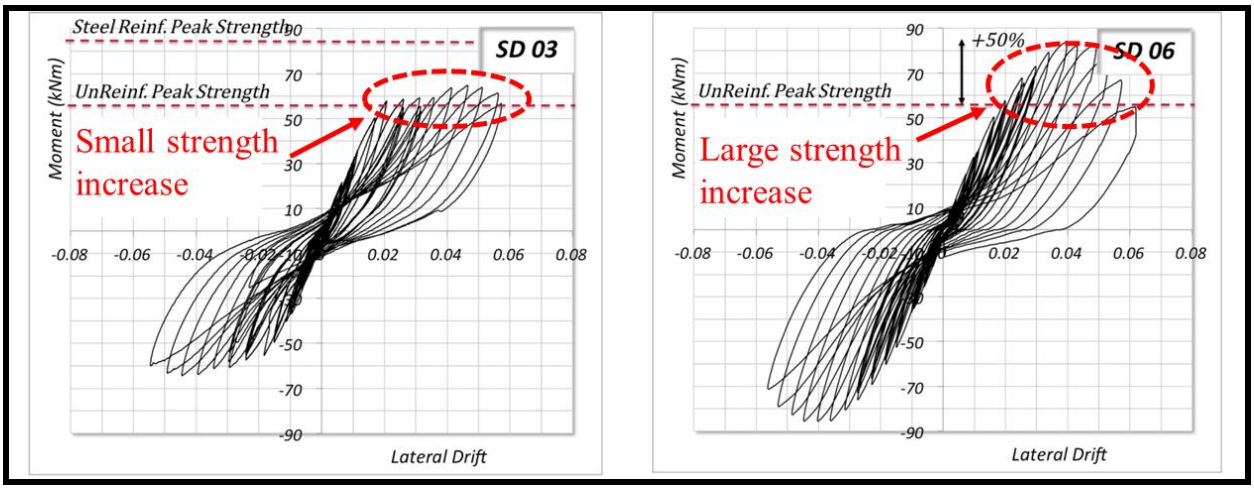

Figure 68: Anchorage-Controlled Shear Reinforcement Study Lateral Drift Response of Anchorage-Controlled (Left) vs Conventional (Right) Shear Reinforcement (Topuzi et al, 2017)

By including a flexible washer when installing the shear bolts, a limited amount of crack opening is allowed prior to the activation of the shear bolts, thereby decreasing the stiffness of the connection. A conceptual diagram of an anchorage-controlled bolt and the finite element model for an anchorage-controlled bolt is presented in Figure 69.

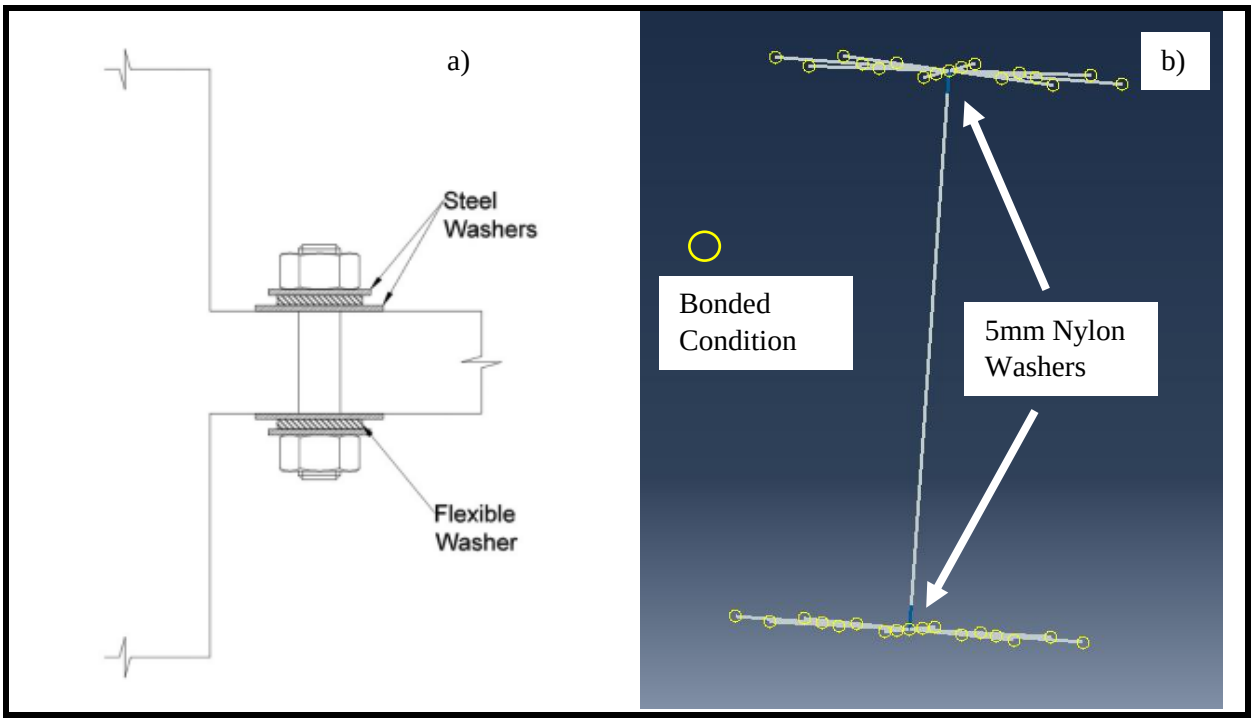

Figure 69: Anchorage-Controlled Reinforcement Study a) Conceptual Diagram (Topuzi et al, 2017) and b) Model of Reinforcement

The objectives of the anchorage-controlled shear reinforcement study are as follows:

1. Confirm that the use of anchorage-controlled shear reinforcement would not significantly affect the shear capacity of the slab-column connection or the failure mode of the connection for both the concentric punching and punching with unbalanced moment cases.

2. Confirm that the addition of a flexible washer to a shear stud/bolt would not significantly impact the behaviour of the stud/bolt after it is activated.

6.4.2 Anchorage-Controlled Shear Reinforcement Study Models

In order to investigate the effect of anchorage-controlled reinforcement for both loading scenarios, twenty models were created for this study. The specimens considered were SB Series specimens SB2, SB3, and SB4 (SBF series models), and SX Series specimens SX-1SR and SX-2SR (SXF series models). In order for the modelled nylon washers to be able to expand freely, the stems of the shear reinforcement must be modelled as unbonded from the concrete rather than embedded in the concrete as they were in all previous models. To ensure this would not significantly affect the model behaviour unbonded models without any flexible washers were created for all control specimens. Additionally, models with one and two flexible washers (5mm thick) were created for each specimen.

Models were named according to the following convention. SB# or SX-#SR denotes the SB or SX series model (including number of shear bolts) the model takes the properties from. The boundary condition of the stem (unbonded or bonded) is then denoted by the letter b (bonded) or u (unbonded). Finally, at the end of the specimen name the number of 5mm washers provided (0-2) is denoted. The flexible washer study models are presented in Table 13.

Table 13: Anchorage-Controlled Shear Reinforcement Study Models

Specimen	Shear Reinforcement Model	Number of Flexible Washers
SB2-b-0	Bonded	0
SB2-u-0	Unbonded	0
SB2-u-1	Unbonded	1
SB2-u-2	Unbonded	2
SB3-b-0	Bonded	0
SB3-u-0	Unbonded	0
SB3-u-1	Unbonded	1
SB3-u-2	Unbonded	2
SB4-b-0	Bonded	0
SB4-u-0	Unbonded	0
SB4-u-1	Unbonded	1
SB4-u-2	Unbonded	2
SX-1SR-b-0	Bonded	0
SX-1SR-u-0	Unbonded	0
SX-1SR-u-1	Unbonded	1
SX-1SR-u-2	Unbonded	2
SX-2SR-b-0	Bonded	0
SX-2SR-u-0	Unbonded	0
SX-2SR-u-1	Unbonded	1
SX-2SR-u-2	Unbonded	2

6.4.3 Anchorage-Controlled Shear Reinforcement Study Results and Discussion

Results for the anchorage-controlled shear reinforcement study were also obtained through the use of two custom Python scripts which outputted load-deflection behaviour, bolt strain behaviour, and post-failure side crack profiles for the SBF series models and load-deflection behaviour, moment-curvature behaviour, bolt strain behaviour, and post-failure side crack profiles for the SXF series models. Load-deflection behaviour for the SBF series models is presented in Figure 70.

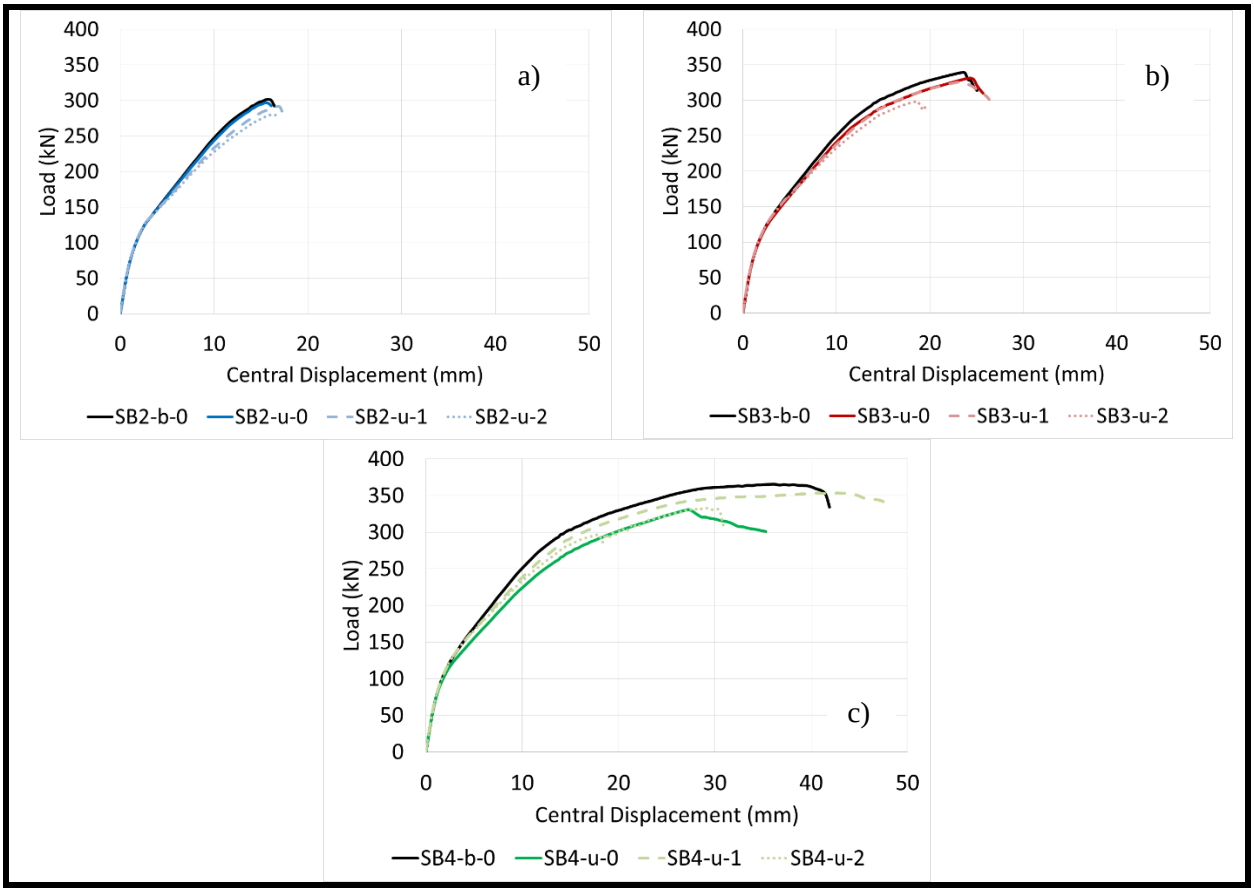

Figure 70: Anchorage-Controlled Shear Reinforcement Study SBF Series Load-Deflection Behaviour a) SB2+Washer Models, b) SB3+Washer Models, c) SB4+Washer Models

As shown in Figure 70 the difference between the bonded and unbonded models is minuscule for models based on SB2 and SB3, however there is a large difference between the bonded and unbonded models for specimen SB4. It would not be reasonable for this effect to occur only when four reinforcement rows are present so it is expected that an error occurred during the analysis of this model. It is also shown that for most of the models the addition of a flexible washer has very limited effect on the capacity of the connection, with the exception of the models for specimens SB3-u-2 and SB4-u-2, which seem to undergo similar modelling errors to that of specimen SB4-u-0. This is expected because of the similarity of the responses for models SB4-u-0 and SB4-u-2. The addition of the flexible washers also results in a slight ductility increase for specimen SB4-u-1. Load-deflection behaviour for the SXF series models is shown in Figure 71, and moment-curvature behaviour for the same specimens is shown in Figure 72.

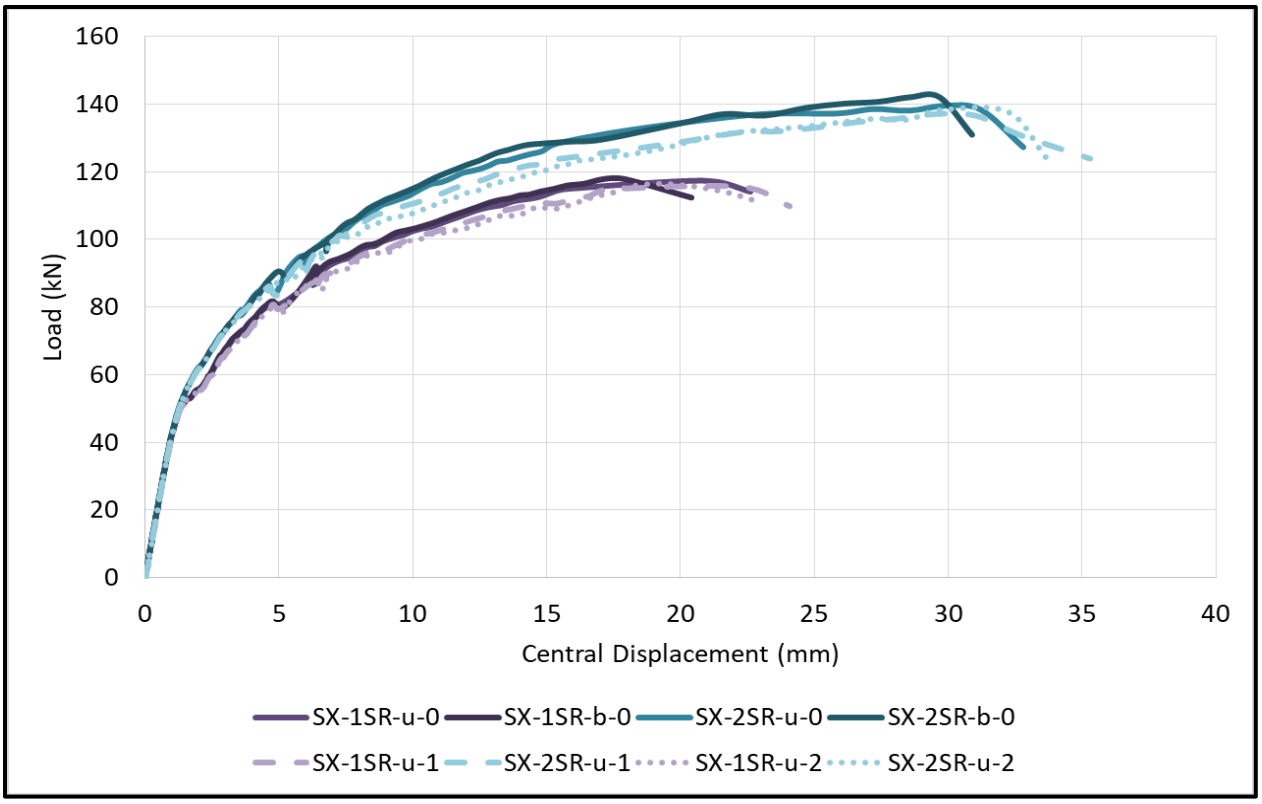

Figure 71: Anchorage-Controlled Shear Reinforcement Study SXF Series Load-Deflection Behaviour

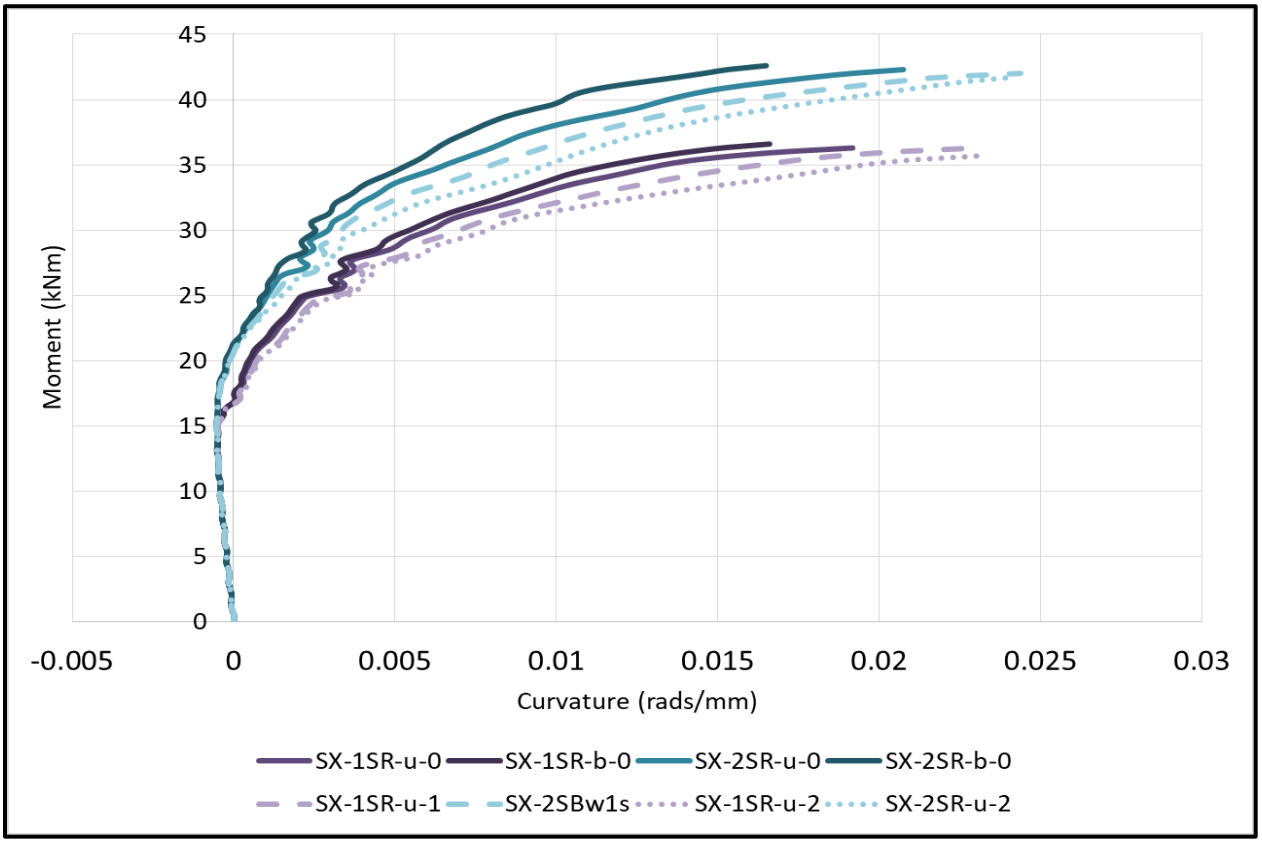

Figure 72: Anchorage-Controlled Shear Reinforcement Study SX Series Moment-Curvature Behaviour

Figure 71 and Figure 72 also show minimal change when a flexible washer is added to the unbonded model for the unbalanced moment loading condition other than a slight stiffness reduction and slight overall rotation increase. This would suggest that the presence of unbalanced moment at the connection has little impact on the effectiveness of the anchorage-controlled reinforcement. The maximum difference in the capacity between models with and without flexible washers for each specimen is presented in Table 14. Specimens which are expected to have encountered modelling errors which impacted their capacities have been neglected in this analysis.

Table 14: Anchorage-Controlled Shear Reinforcement Study Maximum Drops in Capacity

Specimen	Maximum Difference in Capacity (%)
SB2	7.1
SB3	4.2
SB4	3.2
SX-1SR	3.0
SX-2SR	3.4

As shown in Table 14, the loss in capacity as a result of the inclusion of the flexible washers is minimal for all specimens including those subjected to unbalanced moment. This shows that using anchorage-controlled reinforcement to provide ductility to a specimen without increasing its overall stiffness does not have any significant negative impact on the existing capacity of the connection or shear reinforcement. The impact of including anchorage-controlled shear reinforcement on the failure behavior of the connection is analyzed through the post-failure side crack profiles. The post-failure side crack profiles for SBF models SB4-u-0 and SB4-u-1 are presented in Figure 73 and Figure 74.

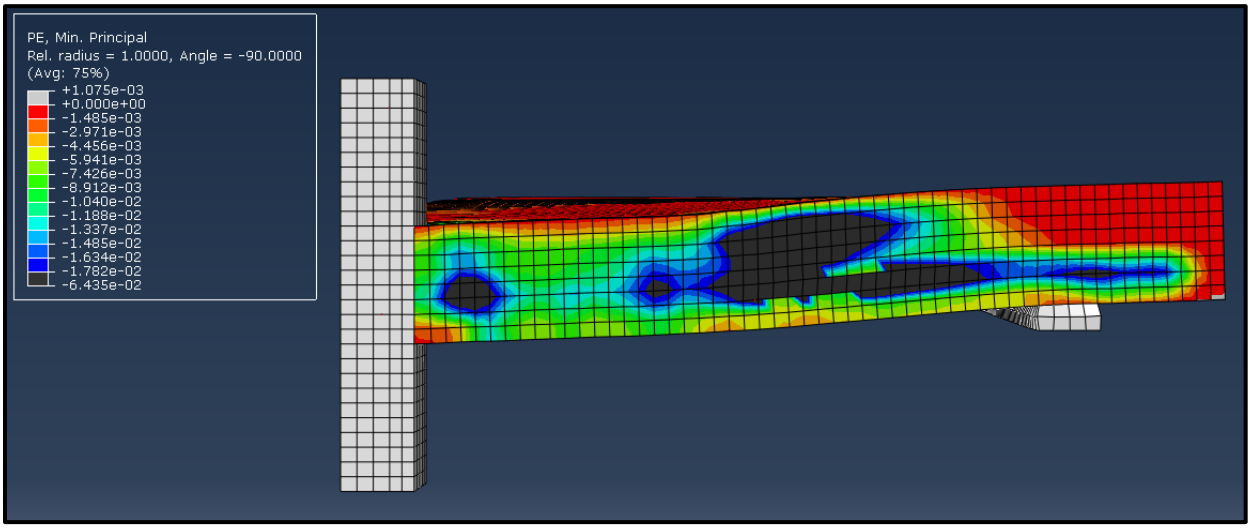

Figure 73: Anchorage-Controlled Shear Reinforcement Study SB4-u-0 Post-Failure Side Crack Profile

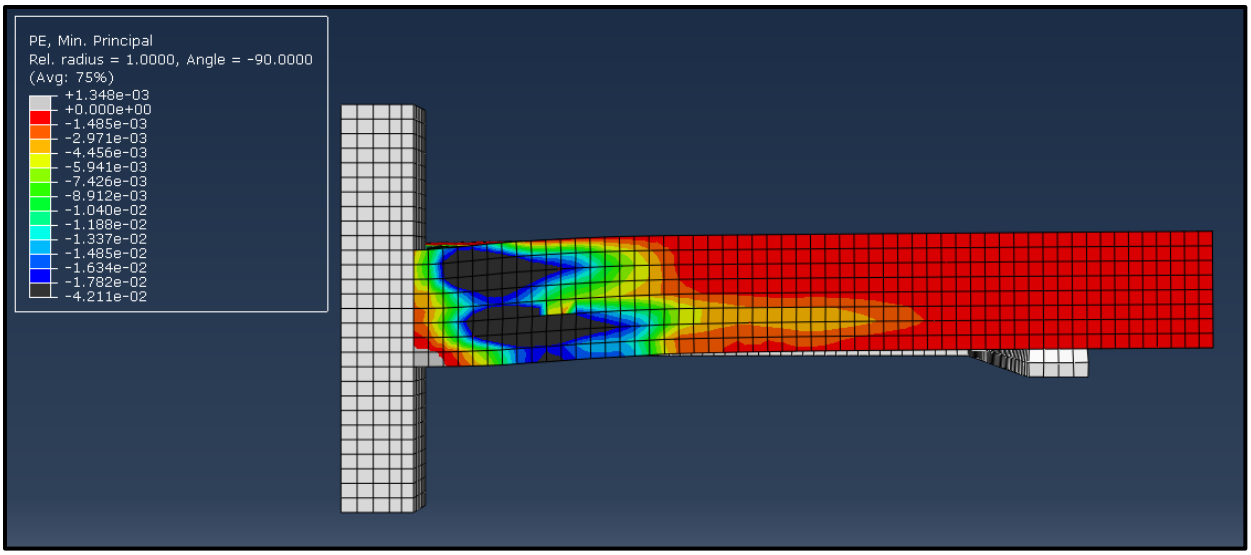

Figure 74: Anchorage-Controlled Shear Reinforcement Study SB4-u-1 Post-Failure Side Crack Profile

The post-failure side crack profiles for the SBF series models show that as a result of allowing the opening of cracks within the shear reinforced zone the failure of the model moves within the shear reinforced zone as supposed to the failure outside of the shear reinforced zone experienced by the control models. However, the strains are still centered on the flexural reinforcing grids suggesting that the failure mode still mostly flexurally controlled. This suggests that more combined flexure and punching governed failure modes could be expected using this type of reinforcement. Post-failure side crack profiles for anchorage-controlled shear reinforcement study models SX-2SR-b-0 and SX-2SR-u-1 are presented in Figure 75 and Figure 76.

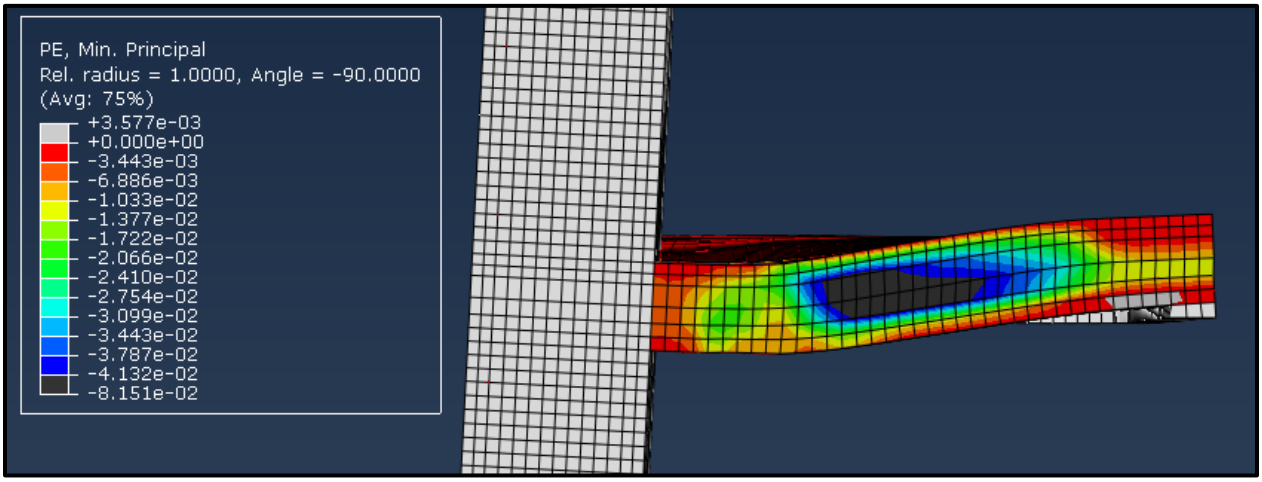

Figure 75: Anchorage-Controlled Shear Reinforcement Study SX-2SR-b-0 Post-Failure Side Crack Profile

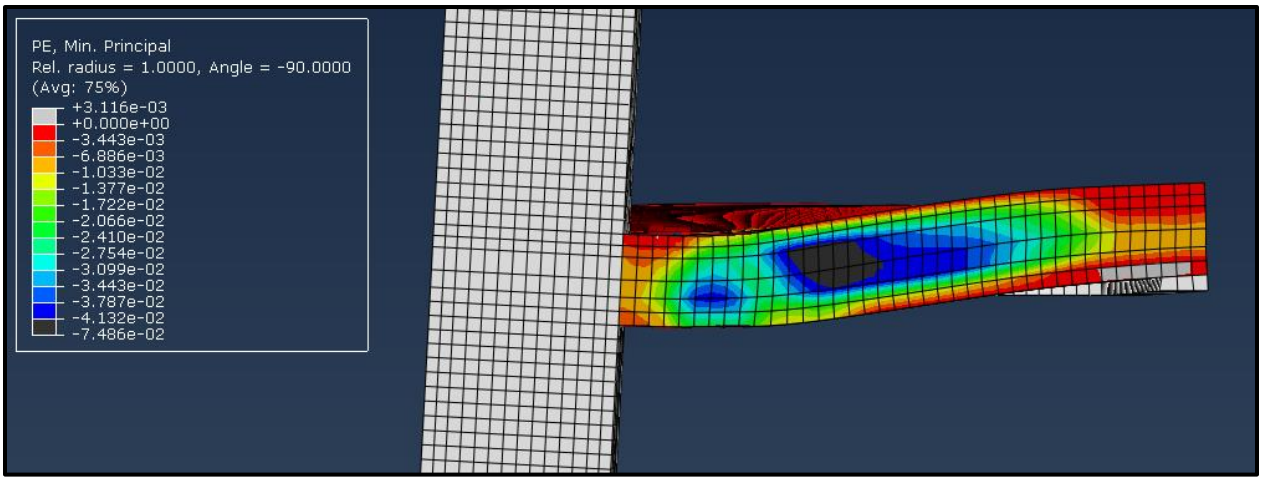

Figure 76: Anchorage-Controlled Shear Reinforcement Study SX-2SR-u-1 Post-Failure Side Crack Profile

Less of a change is seen in these post-failure crack profiles than was seen in those for the SBF series model specimens, however the failure mode for the original SX series models was already expected to be combined shear and punching, so less of a change would be expected overall. The amount of strain seen within the shear reinforced area increases for the SXF series models as it did for the SBF series models. All post-failure side crack profiles for the anchorage-controlled shear reinforcement study can be found in Appendix E.

The performance of the shear reinforcement after activation can be assessed through the analysis of bolt/stud strain diagrams for the study models. Bolt strain diagrams for the SBF series models SB3-b-0, SB3-u-0 and SB3-u-1 are provided in Figure 77, Figure 78, and Figure 79. All anchorage-controlled shear reinforcement study bolt/stud strain diagrams can be found in Appendix E.

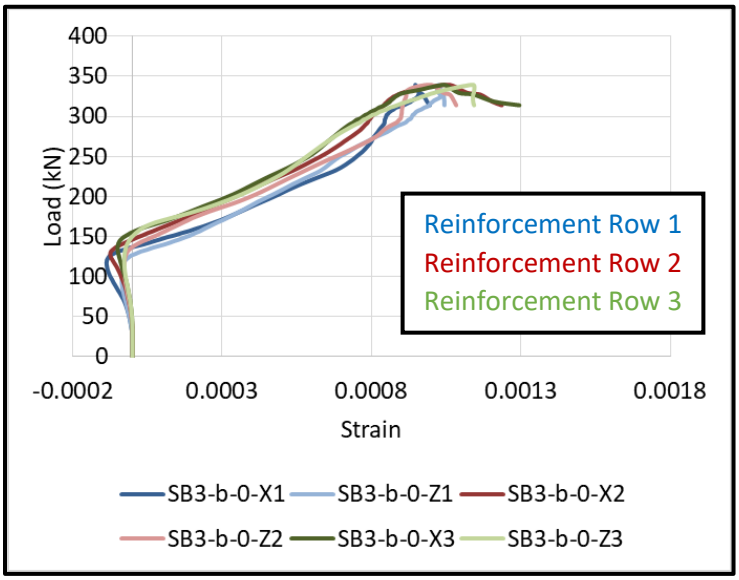

Figure 77: Anchorage-Controlled Shear Reinforcement Study SB3-b-0 Bolt Strain Diagram

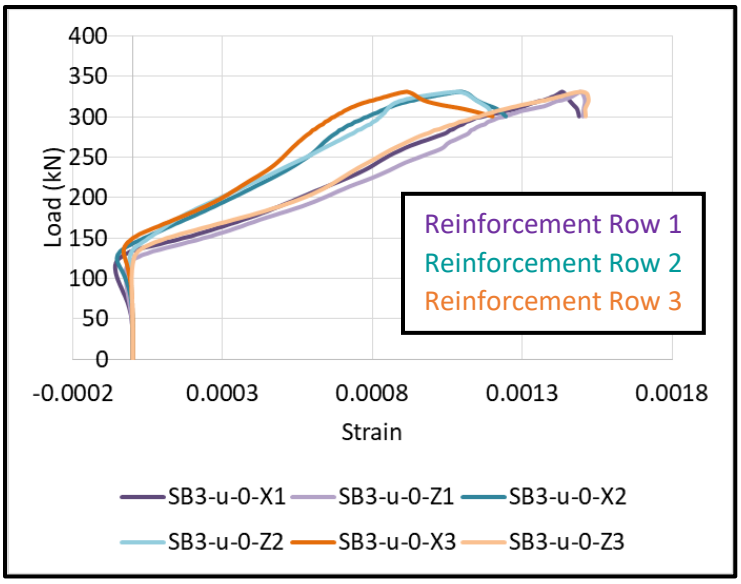

Figure 78: Anchorage-Controlled Shear Reinforcement Study SB3-u-0 Bolt Strain Diagram

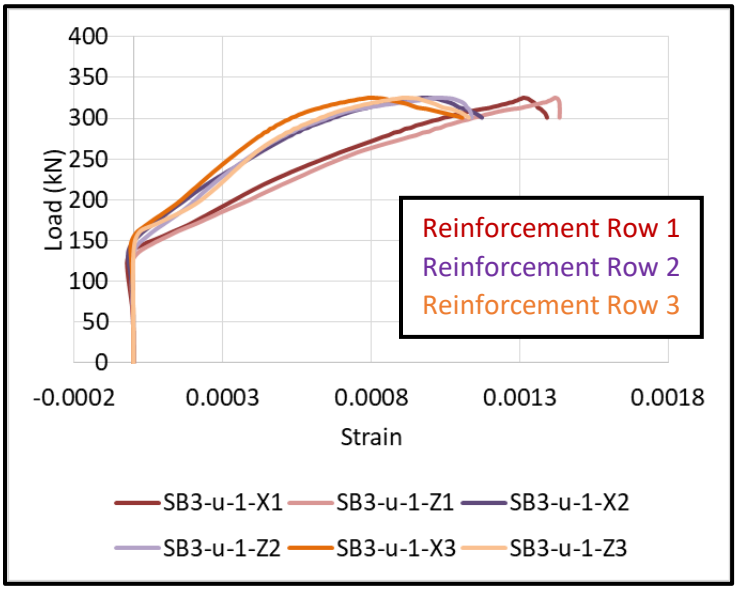

Figure 79: Anchorage-Controlled Shear Reinforcement Study SB3-u-1 Bolt Strain Diagram

In the models without flexible washers presented the bolts activate at almost the same point (at about 130kN), and a slightly later activation (at around 140kN) is shown for the SB3-u-1 model. This gap make sense as the flexible washer must extend prior to the activation of the shear bolt in this model. As a result of modelling the bolts as unbonded (in SB3-u-0 relative to SB3-b-0) more strain is developed in the first row of shear reinforcement and less strain is developed in the subsequent rows. This behaviour is also seen in the bolt strain diagram for model SB3-u-1, which is very similar to that of SB3-u-0 in both strain rate and strain developed at failure.

Finally, tensile face crack patterns were also produced for the anchorage-controlled shear reinforcement study models. These crack patterns were also compared to determine if the model behaviour changed significantly as a result of the addition of flexible washers. All tensile face crack patterns are provided in Appendix E.

6.4.4 Anchorage-Controlled Shear Reinforcement Study Conclusions

The conclusions to the anchorage-controlled shear reinforcement study are as follows:

1. The inclusion of anchorage-controlled shear reinforcement in a slab-column connections does not result in a significant drop in the shear capacity of the connection. However, the failure mode of the connection may move inside of the shear reinforced area when anchorage-controlled shear reinforcement is included because of the additional allowance for cracks to open within the shear reinforced area. The failure mode did however remain mostly flexural in nature.

2. Once activated the shear reinforcement behaves quite similarly regardless of the presence of the flexible washer.

7.0 Conclusions and Recommendations for Future Work

7.1 Summary of Work Presented

While many experimental tests have been conducted by various researchers on the punching behaviour of reinforced concrete flat slabs supported on columns with shear reinforcement, there are still many parameters which have not been adequately studied in the laboratory due to cost or time constraints. Researchers such as Genikomsou and Polak (2015), Navarro et al (2018), and Lapi et al (2020) have proven that these experimental tests can be supplemented using properly calibrated NLFEA models in the commercial software ABAQUS. The work presented in this thesis aimed to calibrate models using the CDP material model in ABAQUS based on concentric punching and punching with unbalanced moment tests on slab-column specimens with headed stud/bolt shear reinforcement. The main consideration during the calibration was effectively modelling the shear reinforcement and shear reinforced area based on the method used by Genikomsou and Polak (2016). This included a detailed analysis of the modelling of the S3 parameter to ensure enough rotational capability was provided in the shear reinforced region of the slab without significantly reducing the predicted capacity of the model. Additional effects such as changing the moment-shear ratio and the effect of adding openings near the column were also considered during calibration.

These calibrated models were then used to conduct several parametric studies on parameters related to the shear reinforcement in the specimens. Three parametric studies were presented in this thesis. The first study investigated the effect of changing the number of shear reinforcement rows and the spacing between adjacent rows of shear reinforcement. The second study investigated the effect of changing the size and number of openings adjacent to the column, and the change in placement of shear reinforcement which must occur as a result of the opening changes. Finally the third study investigated the impact of anchorage-controlled reinforcement, which was proposed by Topuzi et al (2017) to increase the ductility of slab-column connections under cyclic loading without inducing higher lateral stresses in the connection, on the overall capacity of the connections. The capability of the calibrated model and the results of the parametric studies were measured using a variety of metrics, including load-deflection behaviour, moment-curvature behaviour, strain behaviour of the shear reinforcement, strain behaviour of the flexural reinforcing grids, tensile slab face crack patterns, and side (shear) crack profiles.

7.2 NLFEA Model Calibration Conclusions

Chapter 4 and Chapter 5 presented the methodology used to calibrate the NLFEA model based on experimental specimens tested by Adetifa and Polak (2005) (SB series) and El Salakawy et al (1998, 2000) (SX series). Based on this calibration process, the following conclusions can be made:

1. The model predicts the behvaiour of the SB series specimens very well, predicting the capacity of the test specimens within 20% in all cases. The behaviour of the SX series specimens is predicted well when shear reinforcement is present in the specimens (predicting the capacity within 15% in all cases), however a loss of stiffness is experienced in the SX series specimens with no shear reinforcement prior to when it was shown to occur in the tests.

2. Strains in the shear reinforcement were shown to develop more evenly across the peripheral rows of shear reinforcement in the models than in the tests. The shear cracks which propagate in the models show a much shallower angle than in the tests, which would explain why all rows of shear reinforcement develop strains.

3. Through the analysis of the post-failure side crack profiles, it can be determined that the SB series models fail due to the yielding of the flexural reinforcement outside of the shear reinforced area, which is consistent with the test specimens. This is supported by the shear bolts, of which none experienced yielding in any of the models. This same analysis predicts a combined shear and flexural punching failure mode for the SX series models, which was experienced for the test specimen SX-1SR but is inconsistent with the failure mode for the other test specimens.

4. The termination point of the model for the uniaxial compressive behaviour of the slab concrete had minimal effect on the overall slab behaviour. A dilation angle of 40° and a fracture energy of 0.01N/mm greater than the value predicted by CEB-FIP Model Code 1990 (Comité Euro-International du Béton, 1993) were optimal for the considered test specimens. Default values for the eccentricity, ratio of biaxial compressive stress to initial uniaxial yield stress, ratio of the second stress invariant on the tensile/compressive meridians, and damage parameters can be used for the modelling of punching tests of slab-column specimens.

5. The quasi-static analysis procedure used in ABAQUS was found to have some effect on the analysis results when the timestep was low, but overall had little effect on the behaviour of the slab-column connection. Changing the mesh size had little effect on the model behaviour within the bounds set by Genikomsou and Polak (2015) and Dassault Simulia (2016). It is possible that structuring the mesh to place the flexural reinforcing grids in the same position as in the test specimens influences the behavior of the specimens.

6. Three different slab-column behaviours were found to occur when the S3 parameter of the shear reinforcement was varied. The main factor which drove this change in behaviour was found to be the variation of the gap between the column and the edge of the first S3 which allowed a certain amount of cracking or deformation to occur in the slab immediately adjacent to the column. For the considered test specimens, which all had 120mm thick slabs, it was found that the best results for moment-curvature and load-deflection behaviour occurred when the gap between the column and the first S3 was between 6-10mm. The size of the subsequent S3s had a minimal effect on the overall behaviour of the slab, however some gap is still recommended between these S3s to allow for the potential rotation of the slab between rows of shear reinforcement if the area around the first row is stiffened for some reason.

7.3 Parametric Studies Conclusions

Chapter 6 presented the three parametric studies outlined previously in this Chapter. Based on these studies the following conclusions can be made:

1. A stem-stem spacing of up to 1.5d successfully prevents inter-stud punching from occurring in the connections. Current code provisions which require smaller stem-stem spacing (for example CSA A23.3-19 Cl 13.3.8.6) could be raised to this limit based on these tests, however additional connections with thicker slabs or differing reinforcement ratios should also be considered.

2. Two specimens with equal shear reinforced areas and different numbers of shear reinforcement rows will display very similar behaviour to each other. The additional reinforcement row will provide only a minor increase in capacity and ductility.

3. The presence of the first four rows of shear reinforcement have a significant impact on the behaviour of a slab-column connection when the stem-stem spacing of the rows is between 0.75d-1.5d. The spacing of the first three rows of shear reinforcement have the most impact on the connection behaviour because they are located within the major shear crack which develops before the specimen failure. The presence of the a fifth or sixth row of shear reinforcement has a negligible effect on the overall connection behaviour as the failure mode of the connection is mostly flexural after four shear reinforcement rows are provided.

4. When two openings were provided adjacent to the column stub, 90% of the connection's capacity was maintained when the opening width was 60% of the column width or less. When four openings were provided adjacent to the column stub, 90% of the connection's capacity was maintained when the opening width was 33% of the column width or less. To maintain the stiffness of the opening-less model two openings with an opening width of 33% of the column width of less should be provided.

5. When openings were provided, moving the shear reinforcement rows horizontally outside the openings appeared to have little effect on their ability to develop strains and resist the shear stresses in the connection. When providing stud rails as reinforcement to slab-column connections with openings it is ok to install the stud rails outside the openings in a double-cruciform formation.

6. The inclusion of anchorage-controlled reinforcement in the connection to increase the ductility of the connection during cyclic lateral loading while limiting its overall stiffness to not induce additional stresses in the connection had little effect on the overall capacity of the connection. Capacity drops of less than 10% were experienced in all connections considered as a result of including the anchorage-controlled reinforcement.

7. Once activated, the shear bolts/studs behaved very similarly with or without the addition of the flexible washer in the anchorage-controlled reinforcement. However, by allowing cracks to open more within the shear reinforced area of the slab, the governing failure mode of the models with anchorage-controlled reinforcement was mostly some combination of flexural and punching and in some cases occurred within the shear reinforced area.

7.4 Recommendations for Future Work

Recommendations for areas in which the work presented in this thesis could be extended are as follows:

1. Further investigation of the parameters which influence cracking in the model could be done to more accurately predict the shear failure surface, and thereby more accurately predict the strains developed in the shear bolts/studs in the models.

2. The calibration of the S3 parameter could be extended to specimens with thicker slabs. The size effect of the slab could be considered when recommending a S3 size or column to first S3 gap across all slab specimens.

3. To more optimally model the test specimens considered in this thesis, a recalibration of the CDP and mesh parameters could be undertaken considering the adjusted S3 sizes determined based on the S3 calibration study.

4. An investigation of using finer meshes in critical areas of the connection such as the area adjacent to the column, similar to the process used by Silva Mamede et al (2013), could be done to more accurately model the test specimens. A mesh study would have to be undertaken to determine the correct area and mesh size to use to optimally model the test specimens.

5. The shear reinforcement spacing study could be extended to include a variation of the spacing until the spacing becomes large enough where inter-stem punching occurs in the models. The stem-stem and column-to-first-stem spacing of the first two rows of shear reinforcement could be considered in the study, as they would have the largest impact on the behaviour of the model. Additionally, different reinforcement layouts could be considered and the effect of changing the spacing in these arrangements could be compared to that of the double-cruciform case.

6. The openings study could be extended to include investigating the effect of adding openings of different sizes/arrangements to specimens with unbalanced moment or edge specimens. The reinforcement layout could also be changed in specimens with openings to observe the effect of openings with different shear reinforcement arrangements.

7. The anchorage-controlled shear reinforcement study could be extended to include cyclic analysis in the models. This would be useful as the anchorage-controlled reinforcement is intended to provide benefit to slab-column connections subjected to cyclic lateral loads. If this study were to be undertaken, a calibration of the damage parameters would be necessary as they have an impact on the behaviour of the slab concrete when loaded cyclically.

8. Unbalanced moment could be added to the SB series specimens and the moment/shear ratio of the specimens could be varied in both the SX series and adjusted SB series specimens to assess the effect of different moment-shear ratios.

9. Finally, slab continuity could be added to the considered test specimens by mimicking the associated compressive membrane forces in the calibrated models.

References

Adetifa, B., and Polak, M.A. (2005). “Retrofit of interior slab-column connections for punching using shear bolts.” ACI Structural Journal, 102(2), 268–274.

Adetifa, B. (2003). "A New Punching Shear Strengthening Technique for Reinforced Concrete Slabs at Interior Slab-Column Connections." Masters Thesis, University of Waterloo, Waterloo, Ontario, Canada.

Alam, A. J., Amanat, K., & Seraj, S. M. (2009). "An Experimental Study on Punching Shear Behavior of Concrete Slabs." Advances in Structural Engineering, 12(2), 257-265.

Alexander, S.D.B., and Simmonds, S.H. (1992). “Tests of column-flat plate connections.” ACI Structural Journal 1; 89:495-502.

Alfarah, B., Lopéz-Almansa, F., and Oller, S. (2016). "New Methodology for Calculating Damage Variables Evolution in Plastic Damage Model for RC Structures." Engineering Structures, 132, 70-86.

ACI Committee 318. (2019). "Building Code Requirements for Structural Concrete (ACI 318M-19) and Commentary (ACI 318RM-19)." Farmington Hills, MI: American Concrete Institute.

Barrage, R. (2017). "Finite Element Modelling of FRP Reinforced Concrete Beams and Comparative Analysis of Current Strength Prediction Models." Masters Thesis, University of Waterloo, Waterloo, Ontario, Canada.

Birkle, G., and Dilger, W. (2008). “Influence of Slab Thickness on Punching Shear Strength.” ACI Structural Journal, 105(2):180-188.

Borges, L.L.J., Melo, G. S., and Gomes, R.B. (2013). “Punching shear of reinforced concrete flat plates with openings.” ACI Structural Journal, 110(4):547-556.

Broms, C. E. (2000). “Elimination of flat plate punching failure mode.” ACI Structural Journal, 97(1), 94-101.

Broms, C. E. (2007). “Flat plates in seismic areas: Comparison of shear reinforcement systems.” ACI Structural Journal, 104(6), 712-721.

Bu, W., and Polak, M.A. (2009). “Seismic Retrofit of Reinforced Concrete Slab - Column Connections using Shear Bolts.” ACI Structural Journal, 106(4):514-522.

Comité Euro-International du Béton, CEB-FIP-model Code 1990: Design code, Thomas Telford, London, 1993.

Corley, W.G., and Hawkins, N.M. (1968). “Shearhead reinforcement for slabs.” ACI Structural Journal, 65(10), 811-824.

Dassault Systemes Simulia Corp., (2016) "ABAQUS Benchmarks Guide 6.14." Providence, RI, USA.

Dassault Systemes Simulia Corp., (2020). "ABAQUS Analysis User's Manual 6.14." Providence, RI, USA.

Demir, A., Ozturk, H., Edip, K., Stojmanovska, M., and Bogdanovic, A. (2018). "Effect of Viscosity Parameter on the Numerical Simulation of Reinforced Concrete Deep Beam Behaviour." Online Journal of Science and Technology, 8(3):50-56.

Eder, M.A., Vollum, R.L., ELghazouli, A.Y., and Abdel-Fattah, T. (2010). "Modelling and experimental assessment of punching shear in flat slabs with shearheads." Engineering Structures, 32 (12):3911-3924.

Einpaul, J., Fernandez Ruiz, M., and Muttoni, A. (2015). "Influence of moment redistribution and compressive membrane action on punching shear strength of flat slabs." Engineering Structures, 86(4):33-42.

Elgabry, A.A., and Ghali, A. (1987). "Tests on Concrete Slab-Column Connections with Stud-Shear Reinforcement Subjected to Shear-Moment Transfer." ACI Structural Journal, 86:433-442.

El-Salakawy, E.F., Polak, M.A., and Soliman, M.H. (1998). "Reinforced Concrete Slab-Column Edge Connections subjected to High moments." Canadian Journal of Civil Engineering, 25(3):526-538.

El-Salakawy, E.F., Polak, M.A. and Soliman, M.H. (2000). "Reinforced Concrete Slab-Column Edge Connections with Shear Studs." Canadian Journal of Civil Engineering, 27(2):338-348.

Elstner, R.C. and Hognestad, E. (1956). "Shearing strength of reinforced concrete slabs." ACI Structural Journal, 53(2):29–58.

Fick, D.R., Sozen, M.A., and Kreger, M.E. (2017). "Response of Full-Scale Three-Story Flat-Plate Test Structure to Cycles of Increasing Lateral Load." ACI Structural Journal, 114:1507-1518.

Gardner, N. J., & Shao, X.-y. (1996). "Punching Shear of Continuous Flat Reinforced Concrete Slabs." ACI Structural Journal, 96(2), 218-228.

Gasparini, D. A. (2002). "Contributions of C.A.P. Turner to development of reinforced concrete flat slabs 1905-1909." Journal of Structural Engineering, 128(10), 1243-1252.

Genikomsou, A.S., and Polak, M.A. (2015). "Finite element analysis of punching shear of concrete slabs using damaged plasticity model in ABAQUS." Engineering Structures, 98(4):38-48.

Genikomsou, A. S., & Polak, M. (2016). "Finite-element analysis of reinforced concrete slabs with punching shear reinforcement." Journal of Structural Engineering, 142(12), 04016129.

Genikomsou, A. (2015). "Nonlinear finite element analysis of punching shear of reinforced concrete slab-column connections." PhD Thesis, University of Waterloo, Waterloo, Ontario, Canada.

González-Vidosa, F., Kotsovos, M. D., & Pavlovic, M. N. (1988). "Symmetrical Punching of Reinforced Concrete Slabs: An Analytical Investigation Based on Nonlinear Finite Element Modeling." ACI Structural Journal, 85(3), 241-250.

Graf, O. (1933). “Versuche über die Widerstandsfähigkeit von Eisenbetonplatten unter konsentrierten Last nahe einem Auflager.” Deutscher Ausschuss fürEisenbeton, 73, 1-16.

Guan, H., and Polak, M.A. (2007). “Finite element studies of reinforced concrete slab-edge column connections with opening.” Canadian Journal of Civil Engineering, 34(8), 952-965.

Guandalini, S., Burdet, O. L., & Muttoni, A. (2009). "Punching Tests of Slabs with Low Reinforcement Ratios." ACI Structural Journal, 106(1), 87-95.

Hallgren, M. (1996). "Punching Shear Capacity of Reinforced High Strength Concrete Slabs." PhD Thesis, Royal Institute of Technology, Stockholm, Sweden.

Hanson, N.W., and Hanson, J.M. (1968). “Shear and Moment Transfer between Concrete Slabs and Columns.” Journal of the PCA Research and Development Laboratory, 2-16.

Hawkins, N.M., Criswell, M.E., and Roll, F. (1974). "Shear Strength of Slabs without Shear Reinforcement." ACI SP-42, 677-704.

Hawkins, N.M. (1974). “Shear Strength of Slabs with Shear Reinforcement.” ACI SP-42, 785-816.

Hussein, A.H., and El-Salakawy, E.F. (2018). "Punching Shear Behaviour of Glass Fiber-Reinforced Polymer-Reinforced Concrete Slab-Column Interior Connections." ACI Structural Journal, 115:1075-1088.

Inácio, M. M., Almeida, A. F., Faria, D. M., Lúcio, V. J., & Ramos, A. P. (2015). "Punching of high strength concrete flat slabs without shear reinforcement." Engineering Structures, 103, 275-284.

Jiang, L., Orabi, M.A., Jiang, J., and Usmani, A. (2021). "Modelling Concrete Slabs Subjected to Fires Using Nonlinear Layered Shell Elements and Concrete Damaged Plasticity Model." Engineering Structures, 234:1-15.

Johnson, R. P. (2009). "Eurocodes, 1970-2010: why 40 years?" Proceedings of the Institution of Civil Engineers-Structures and Buildings, 162(6), 371-379.

Kang, T.H.-K., and Wallace, J.W. (2005). “Dynamic responses of flat plate systems with shear reinforcement.” ACI Structural Journal, 102(5):763-773.

Kinnunen, S., and Nylander, H. (1960) “Punching of concrete slabs without shear reinforcement.” Transactions 158, Royal Institute of Technology, Stockholm, Sweden.

Kupfer, H., Hilsdorf, H.K., and Rusch, H. (1969). “Behavior or concrete under biaxial stresses.” ACI Structural Journal, 66(8):656-666.

Lapi, M., Secci, L., Ramos, A.P., and Orlando, M. (2020). "A Hybrid Method for the Calibration of Finite Element Models of Punching-Shear in R/C Flat Slabs." Computers and Structures, 238:1-14.

Lee, J., and Fenves, G.L. (1998). “Plastic-Damage Model for Cyclic Loading of Concrete Structures.” Journal of Engineering Mechanics, 124(8):892-900.

Lips, S., Fernández Ruiz, M., & Muttoni, A. (2012). "Experimental investigation on punching strength and deformation capacity of shear-reinforced slabs." ACI Structural Journal, 109(6), 889-900.

Long, A.E., and Masterson, D.M. (1974). "Improved Experimental Procedure for Determining the Punching Strength of Reinforced Concrete Flat Slab Structures." ACI SP-42, 921-943.

Lubliner, J., Oliver, J., Oller, S., and Oñate, E. (1989). "A plastic-damage model for concrete." International Journal Solids Structures, 25(3):299-326.

MacGregor, G.J., and Bartlett, M.F. (2000). "Reinforced Concrete: Mechanics and Design." Pearson Canada.

Mahmoud, A. M. (2015). "Finite element implementation of punching shear behaviours in shear reinforced flat slabs." Ain Shams Engineering Journal, 6(3), 735-75

Marques, M.G., Liberati, E.A.P., Gomes, R.B., Almeida, L.C., and Trautwein, L.M. (2020). "Study of Failure Mode of Reinforced Concrete Flat Slabs with Openings and Studs." ACI Structural Journal, 117:39-48.

Marzouk, H., & Hussein, A. (1991). "Punching shear analysis of reinforced high-strength concrete slabs." Canadian Journal of Civil Engineering, 18(6), 594-963.

Masterson, D.M., and Long, A.E. (1974). "The punching strength of slabs, a flexural approach using finite elements." ACI Special Publication S-42, 2(4):747-68.

Megally, S., and Ghali, A. (2000). "Seismic Behaviour of Edge Slab-Column Connections with Stud Shear Reinforcement." ACI Structural Journal, 97(1):53-60.

Menétrey, P., Walther, R., Zimmermann, T., Willam, K. J., & Regan, P. E. (1997). "Simulation of punching failure in reinforced-concrete structures." Journal of Structural Engineering, 123(5), 652-659.

Milligan, G. (2018). "Nonlinear Finite Element Analysis of Punching Shear of Reinforced Concrete Slabs Supported on Rectangular Columns." Masters Thesis, University of Waterloo, Waterloo, Ontario, Canada.

Moe, J. (1961). "Shearing strength of reinforced concrete slabs and footings under concentrated loads." Development Department Bulletin D47, Portland Cement Association, Skokie, Illinois.

Mowrer, R. D., & Vanderbilt, M. D. (1967). "Shear strength of lightweight aggregate reinforced concrete flat plates." Journal Proceedings, 64(11), 722-729.

Muttoni, A. (2008). "Punching shear strength of reinforced concrete slabs without transverse reinforcement." ACI Structural Journal, 105(4):440-450.

Naaman, A.E., Likhitruangsilo, V., and Parra-Montesinos, G. (2007). "Punching Shear Response of High Performance Fiber-Reinforced Cementitious Composite Slabs." ACI Structural Journal, 104(2):170-179.

Navarro, M., Ivorra, S., and Varona, F.B. (2018). "Parametric Computational Analysis for Punching Shear in RC Slabs." Engineering Structures, 165:254-263.

Navarro, M., Ivorra, S., and Varona, F.B. (2018). "Parametric Finite Element Analysis of Punching Shear Behaviour of RC Slabs Reinforced with Bolts." Computers and Structures, 228:1-12.

Pan, A., and Moehle, J.P. (1989). "Lateral Displacement Ductility of Reinforced Concrete Flat Plates." ACI Structural Journal, 86:250-258.

Panahi, H., and Genikomsou, A.S. (2021). "Comparative Investigation of Concrete Plasticity Models for Nonlinear Finite-Element Analysis of Reinforced Concrete Specimens." Practice Periodical on Strucral Design and Construction, 27(2).

Petersson, P.E. (1981). “Crack Growth and Development of Fracture Zones in Plain Concrete and Similar Materials.” Lund Institute of Technology, 1-174.

Pillai, S.U., Kirk, W., and Scavuzzo, L. (1982). “Shear Reinforcement at Slab-Column Connections in a Reinforced Concrete Flat Plate Structure.” ACI Structural Journal, 79(1):36-42.

Polak, M. A. (1998). "Modeling Punching Shear of Reinforced Concrete Slabs Using Layered Finite Elements." ACI Structural Journal, 95(1), 71-80.

Polo, G.E., Bayrak, O., and Hrynyk, T.D. (2021). "Shear-Resisting Performance of Reinforced Concrete Flat Plates with Different Headed Stud Layouts." ACI Structural Journal, 118:5-16.

Rankin, G.I.B, and Long, A.E. (1987). “Predicting the enhanced punching shear strength of interior slab-column connections.” Proceedings of the Institute of Civil Engineers; 82(1):1165-86.

Richart, F.E. (1948). "Reinforced concrete walls and column footings, part 1 and 2.” ACI Structural Journal, 20(2): 97-127, 20(3):237-260.

Robertson, I.N., and Durrani, A.J. (1991). "Gravity Load Effect on Seismic Behaviour of Exterior Slab-Column Connections." ACI Structural Journal, 88:255-267.

Robertson, I.N., Kawai, T., Lee, J., and Johnson, G. (2002). “Cyclic Testing of Slab-Column Connections with shear reinforcement.” ACI Structural Journal, 99(5):605-613.

Sagaseta, J., Muttoni, A., Fernández Ruiz, M., & Tassinari, L. (2011). "Non-axis-symmetrical punching shear around internal columns of RC slabs without transverse reinforcement." Magazine of Concrete Research, 63(6), 441-457. doi:10.1680/macr.10.00098

Salama, A.E., Hassan, M., and Benmokrane, B. (2019). "Effectiveness of Glass Fiber-Reinforced Polymer Stirrups as Shear Reinforcement in Glass Fiber-Reinforced Polymer-Reinforced Concrete Edge Slab-Column Connections." ACI Structural Journal, 116:97-112.

Santos, J.B., Souze, R.M., Melo, G.S., and Gomes, R.B. (2022). "Punching Resistance of Flat Slabs with Openings Adjacent to the Columns." ACI Structural Journal, 119:41-53.

Seible, F., Ghali, A., and Dilger, H.W. (1980). “Preassembled shear reinforcing units for flat plates.” ACI Structural Journal, 77(1):28-35.

Shehata, A., & Regan, P. E. (1989). "Punching in R.C. slabs." Journal of Structural Engineering, 115(7), 1726-1740.

Sherif, A. G., & Dilger, W. H. (1996). "Critical review of the CSA A23.3-94 punching shear strength provisions for interior columns." Canadian Journal of Civil Engineering, 23(5), 998-1011.

Silva Mamede, N.F., Ramos, A.P., and Faria, D.M.V. (2013). "Experimental and Parametric 3D Nonlinear Finite Element Analysis of Punching of Flat Slabs with Orthogonal Reinforcement." Engineering Structures, 48:442-457.

Stoner, J. G. (2015). "Finite Element Modelling of GFRP Reinforced Concrete Beams." Masters Thesis, University of Waterloo, Waterloo, Ontario, Canada.

Swamy, R., and Ali, S. (1982). “Punching shear behaviour of reinforced slab-column connections made with steel fiber concrete.” ACI Structural Journal, 79:392-406.

Talbot, A.N. (1913). "Reinforced concrete wall footings and column footings." University of Illinois Engineering Experiment Station, Bulletin No 67, 114.

Tan, Y., and Teng, S. (2005). “Interior Slab-Rectangular Column Connections under Biaxial Lateral Loadings.” Punching Shear in Reinforced Concrete Slabs, ACI SP232-09, 147-174.

Teng, S., Cheong, H.K., Kuang, K.L., and Geng, J.Z. (2004). “Punching shear strength of slabs with openings and supported on rectangular columns.” ACI Structural Journal, 101(5):678- 687.

Topuzi, D., Polak, M.A., and Narasimhan, S. (2017). "A New Technique for the Seismic Retrofit of Slab-Column Connections." ACI Structural Journal, 114:1471-1481.

Winkler, K., & Stangenberg, F. (2008). "Numerical analysis of punching shear failure of reinforced concrete slabs." ABAQUS Users' Conference.

Wosatko, A., Pamin, J., & Polak, M. (2015). "Application of damage-plasticity models in finite element analysis of punching shear." Computers and Structures, 151, 73-85.

Yamada, T., Nanni, A., & Endo, K. (1992). "Punching Shear Resistance of Flat Slabs: Influence of Reinforcement Type and Ratio." ACI Structural Journal, 88(4), 555-563.

Appendices

Appendix A: S3 Study Supplemental Figures

List of Figures

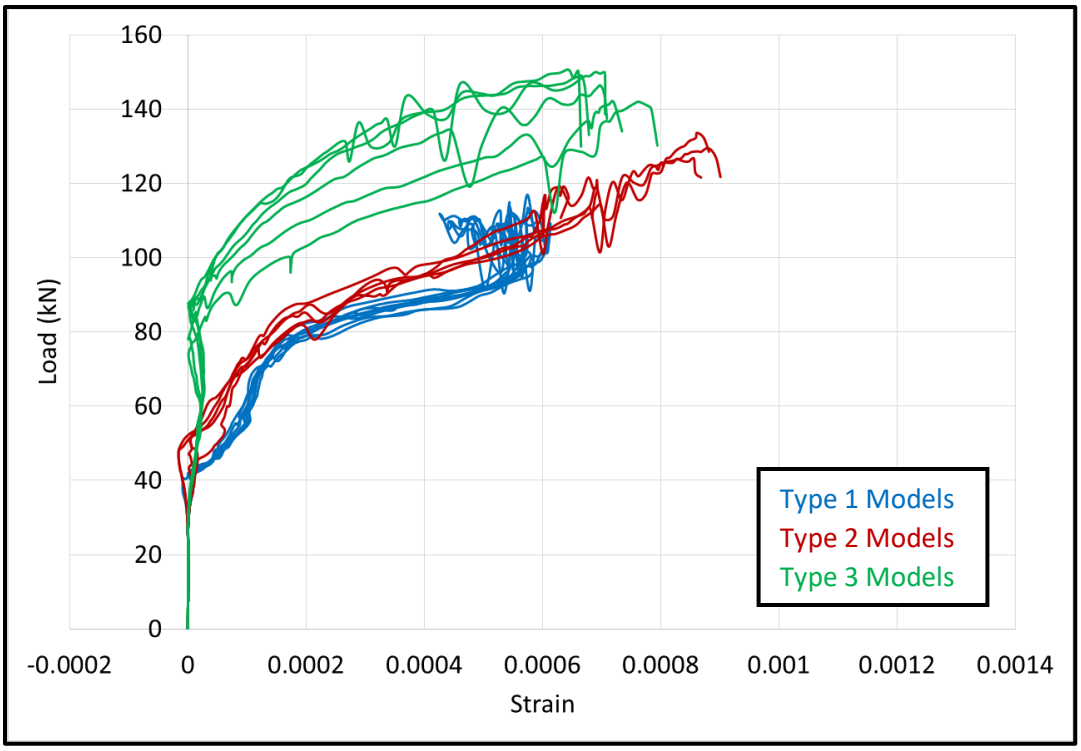

Figure A1: SX-2SR S3 Study Edge Bolt 1 Strains

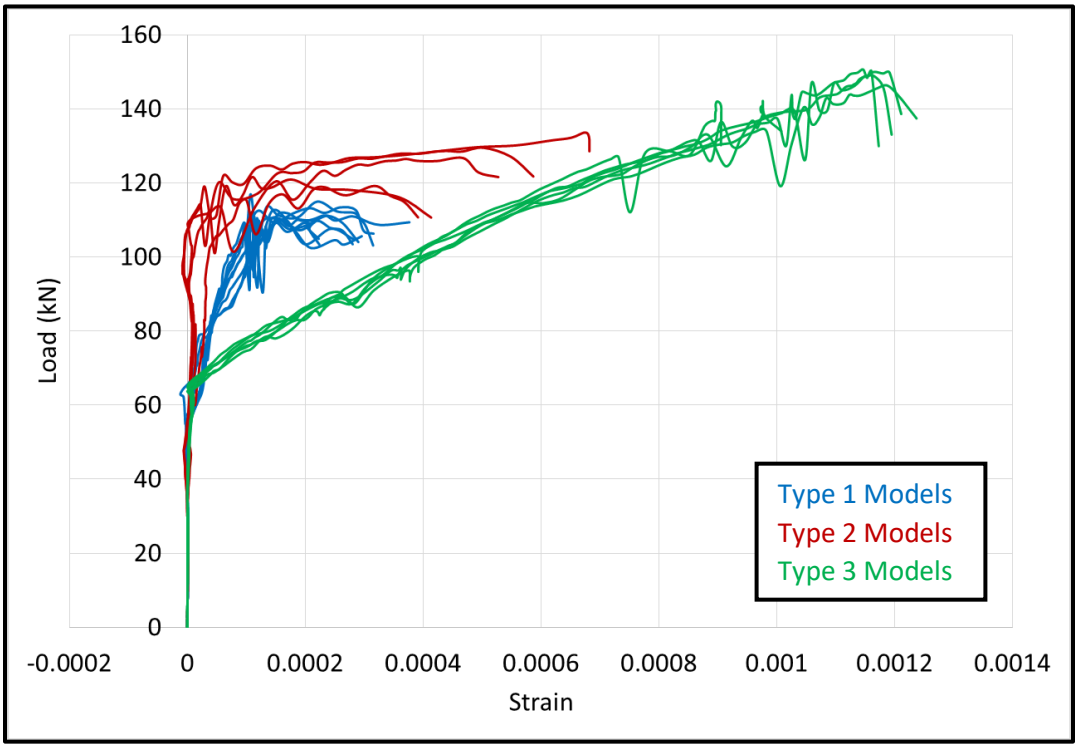

Figure A2: SX-2SR S3 Study Edge Bolt 2 Strains

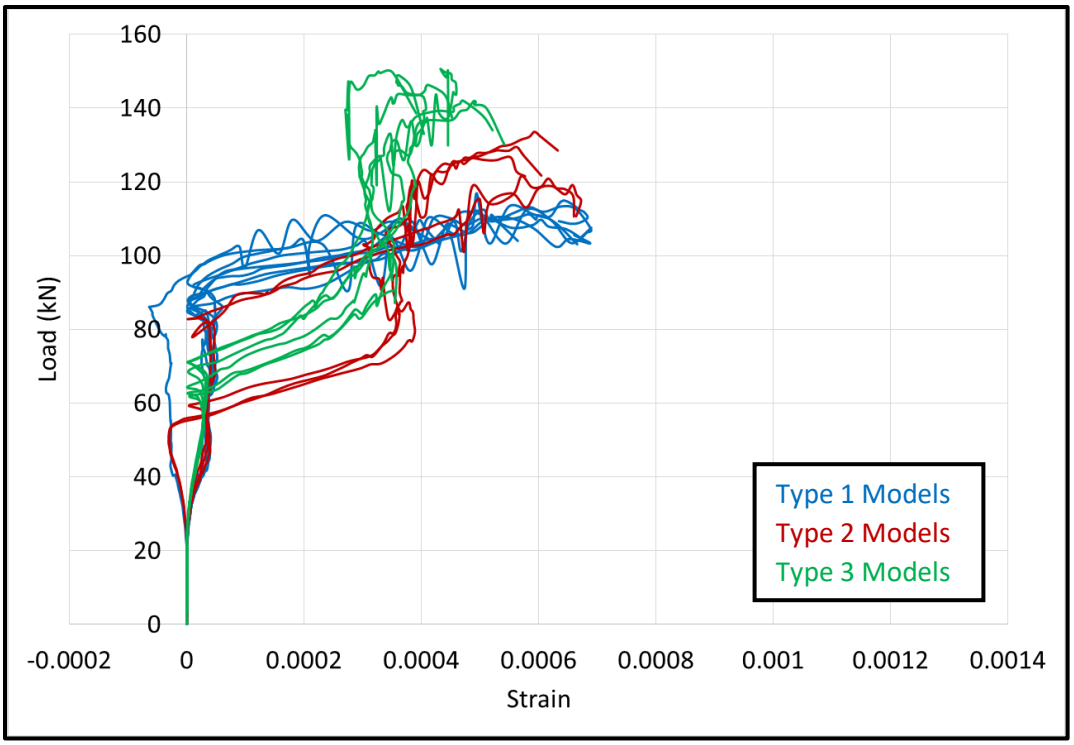

Figure A3: SX-2SR S3 Study Corner Bolt 1 Strains

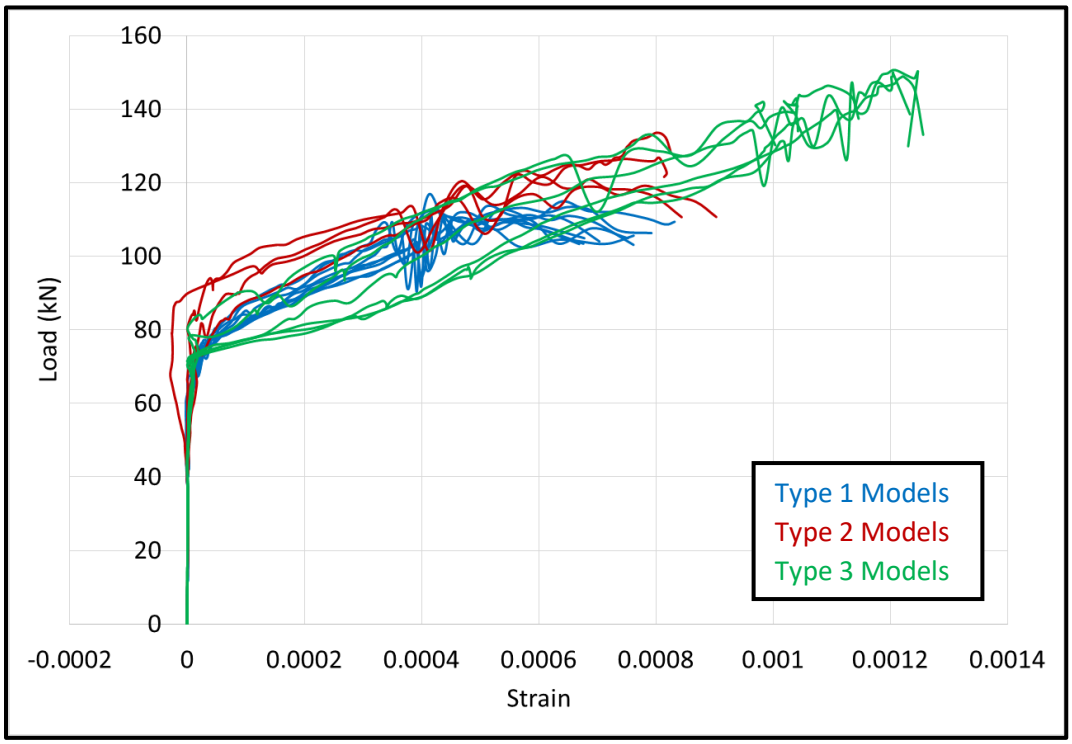

Figure A4: SX-2SR S3 Study Corner Bolt 2 Strains

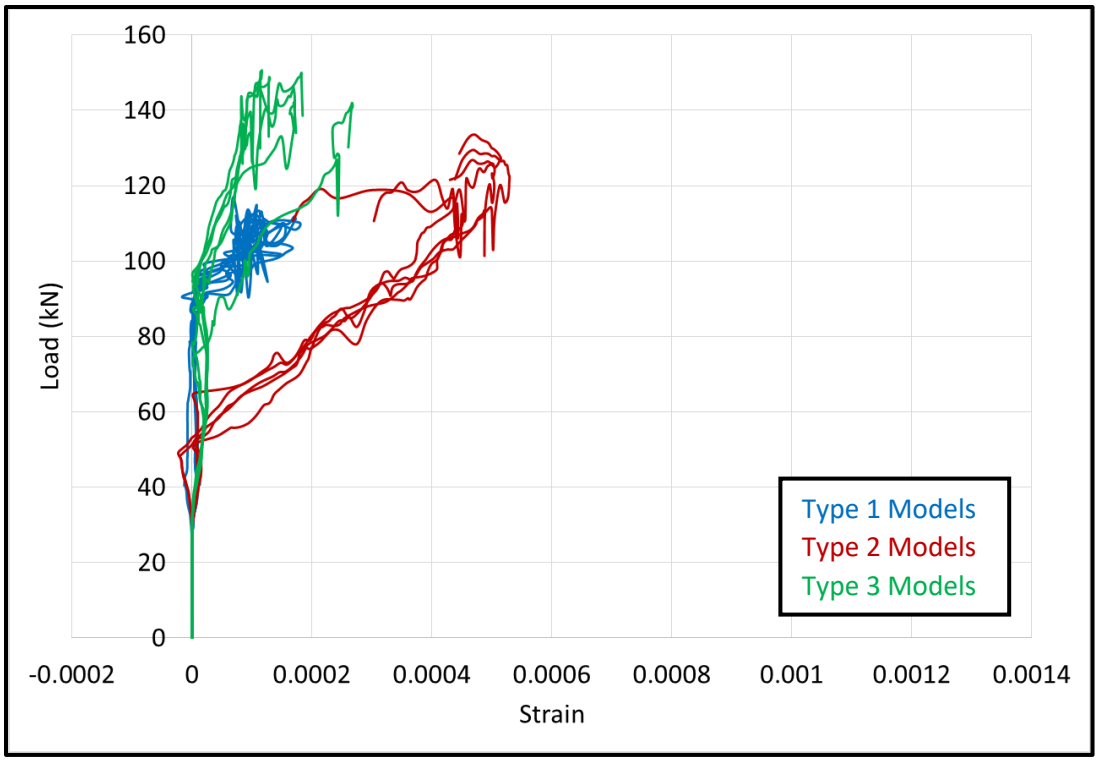

Figure A5: SX-2SR S3 Study Center Bolt 1 Strains

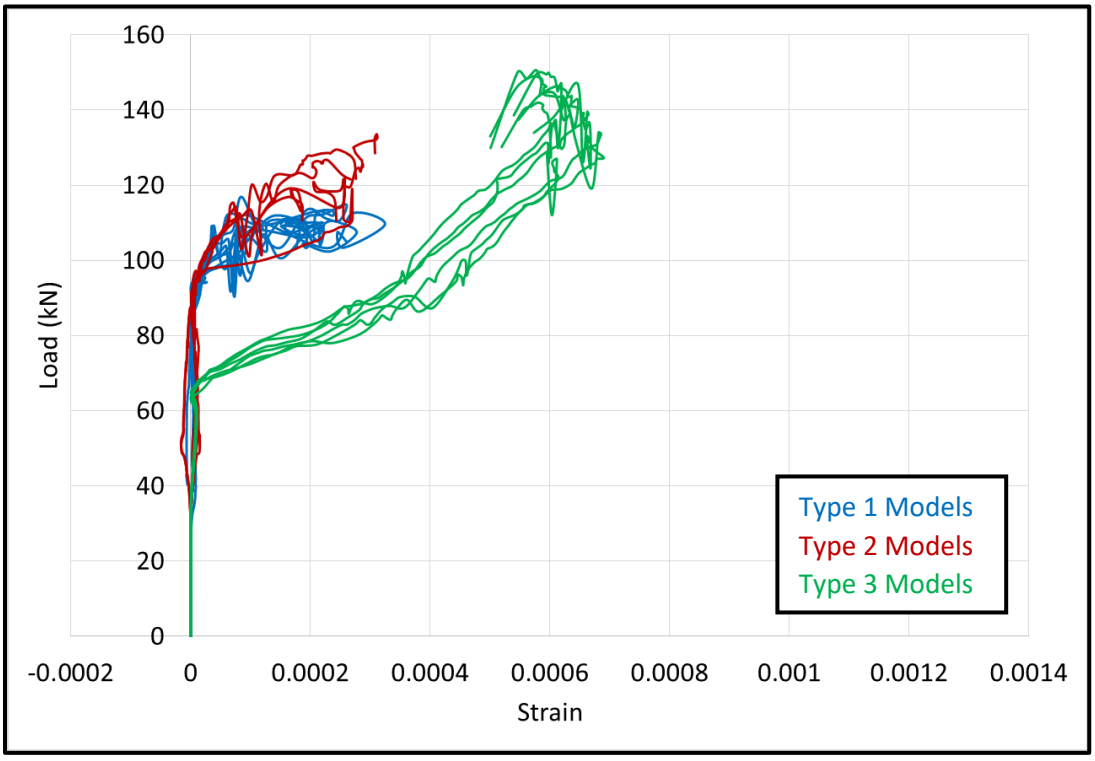

Figure A6: SX-2SR S3 Study Center Bolt 2 Strains

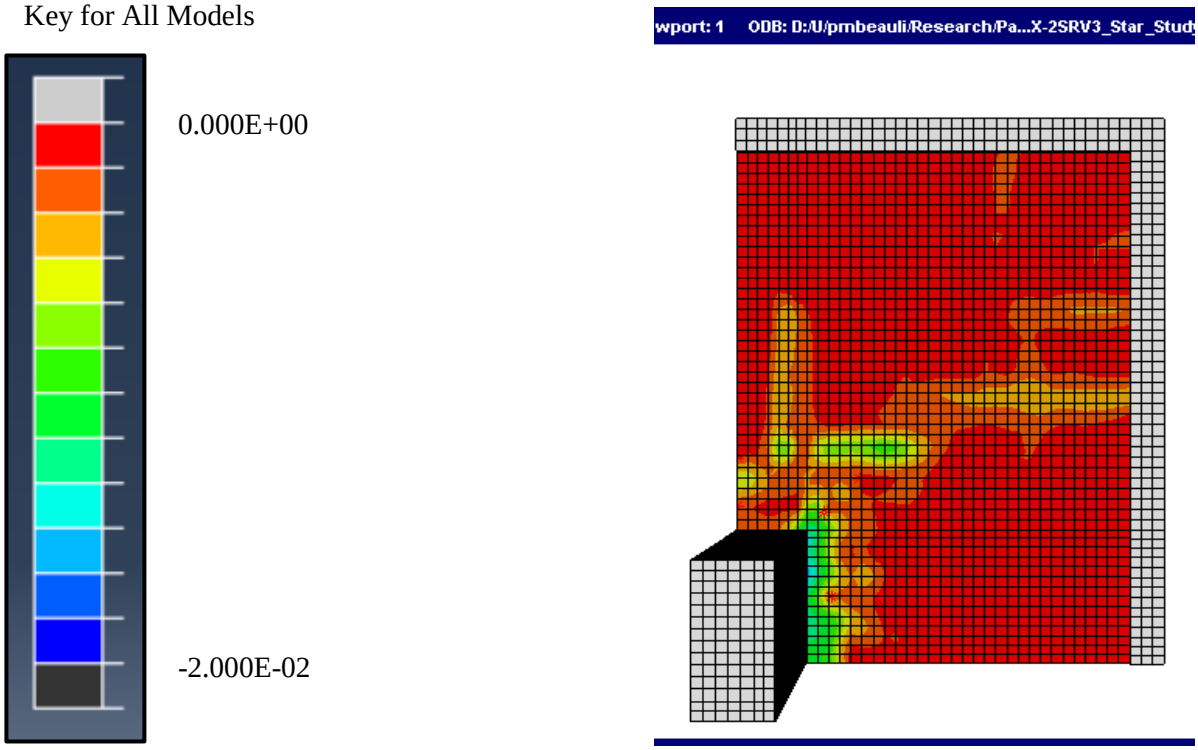

Figure A7: SX-2SR S3 Study 24% Stem-Stem Spacing Tensile Face Crack Pattern

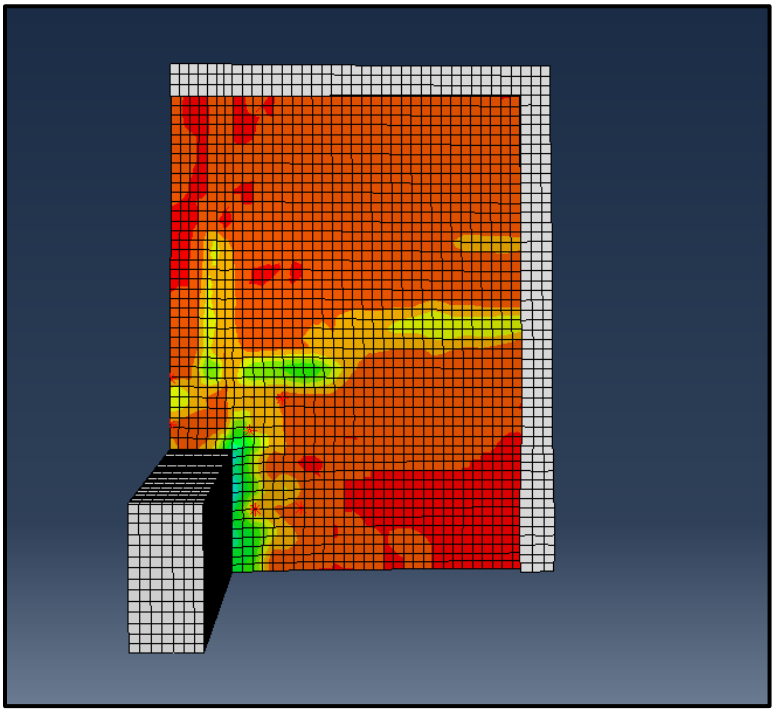

Figure A8: SX-2SR S3 Study 28% Stem-Stem Spacing Tensile Face Crack Pattern

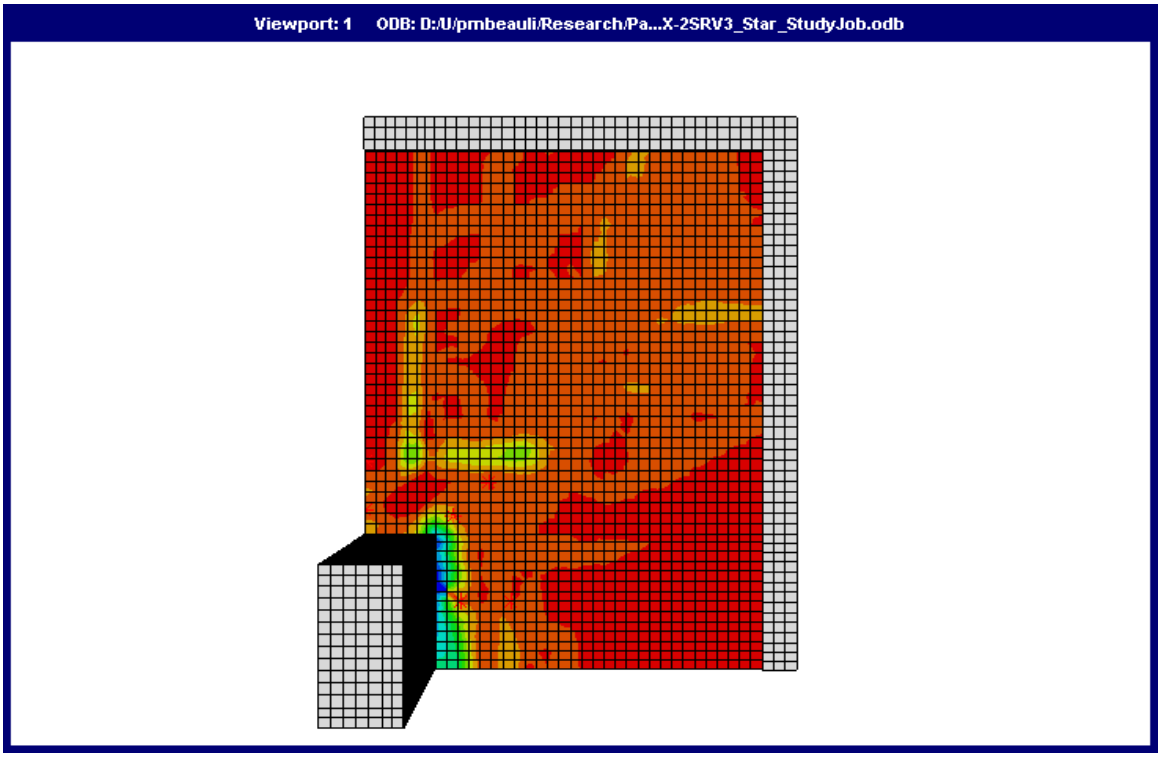

Figure A9: SX-2SR S3 Study 33% Stem-Stem Spacing Tensile Face Crack Pattern

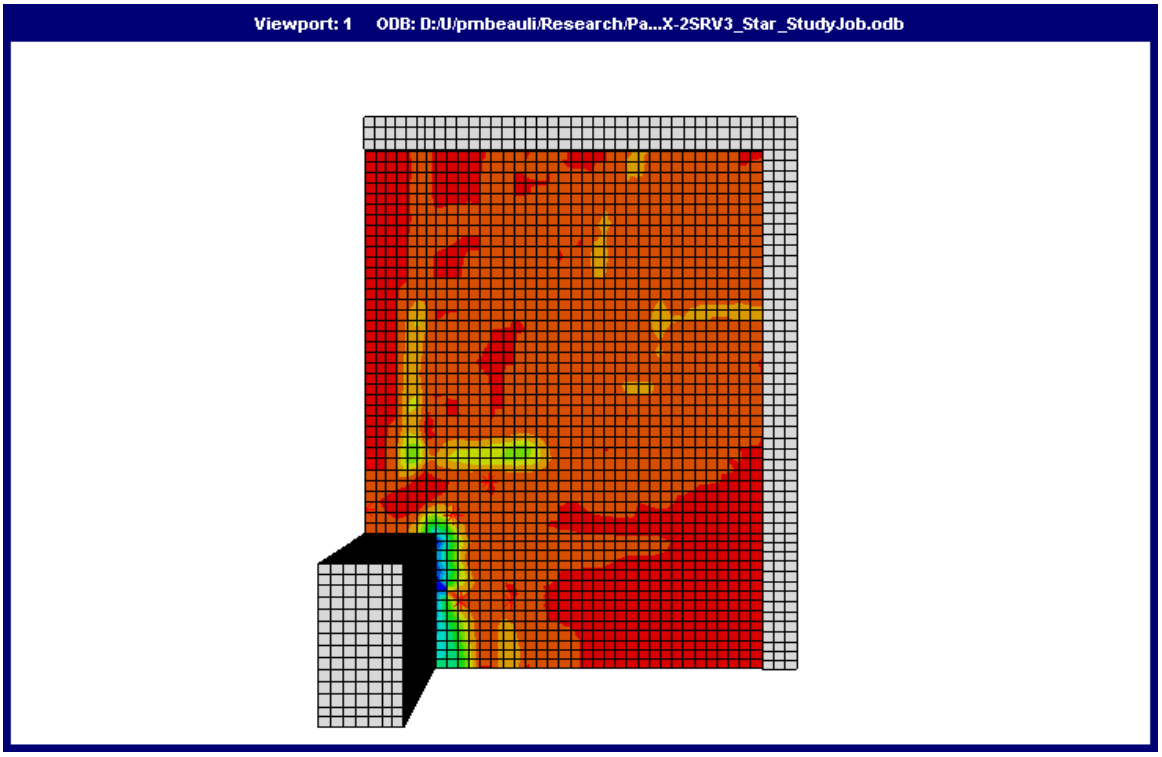

Figure A10: SX-2SR S3 Study 37% Stem-Stem Spacing Tensile Face Crack Pattern

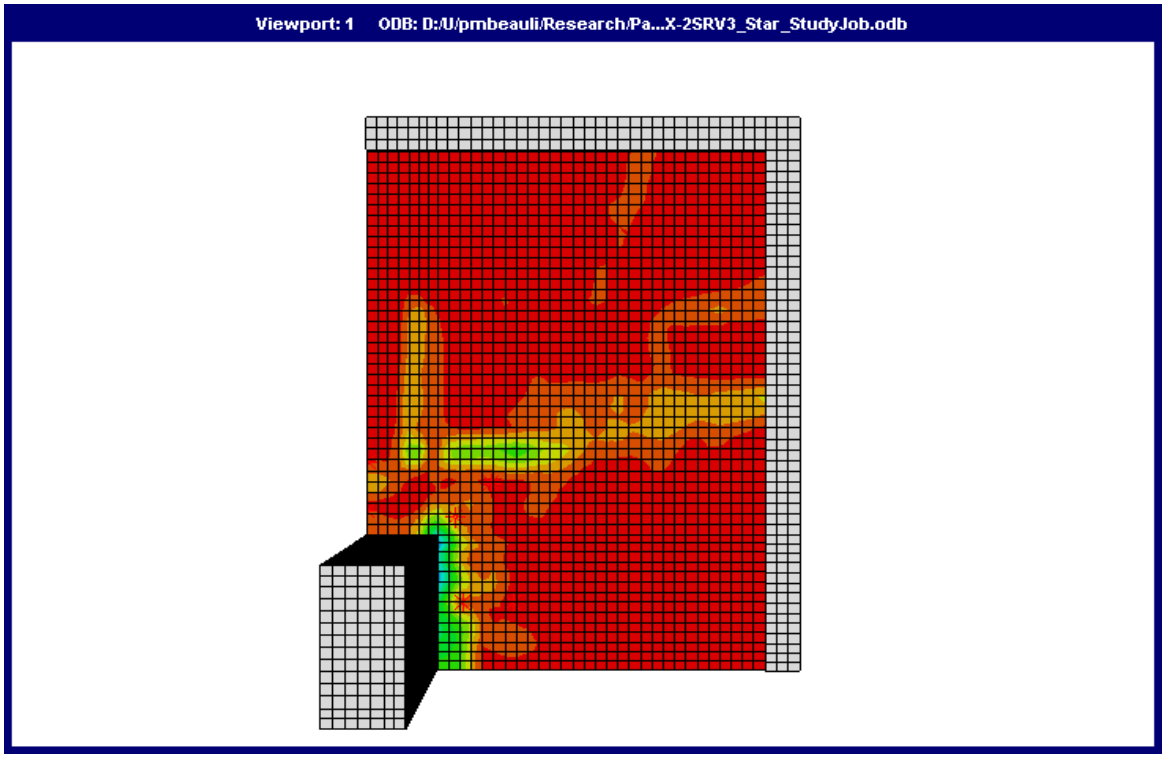

Figure A11: SX-2SR S3 Study 41% Stem-Stem Spacing Tensile Face Crack Pattern

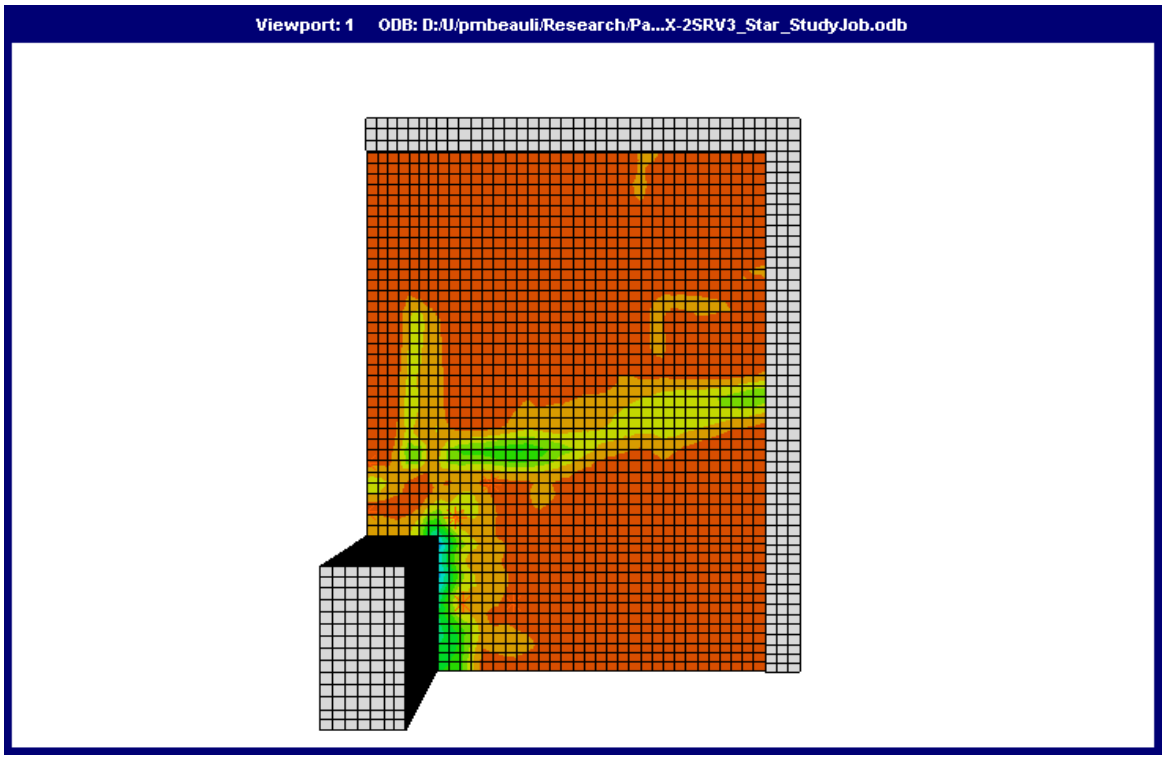

Figure A12: SX-2SR S3 Study 45% Stem-Stem Spacing Tensile Face Crack Pattern

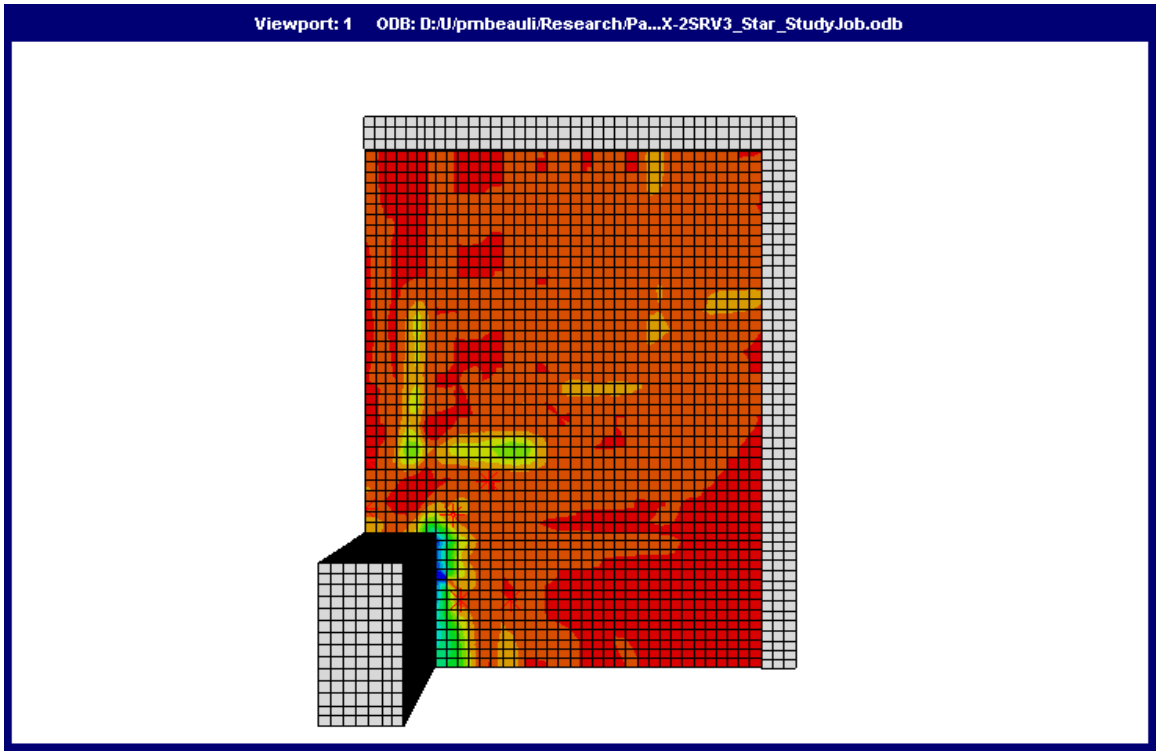

Figure A13: SX-2SR S3 Study 49% Stem-Stem Spacing Tensile Face Crack Pattern

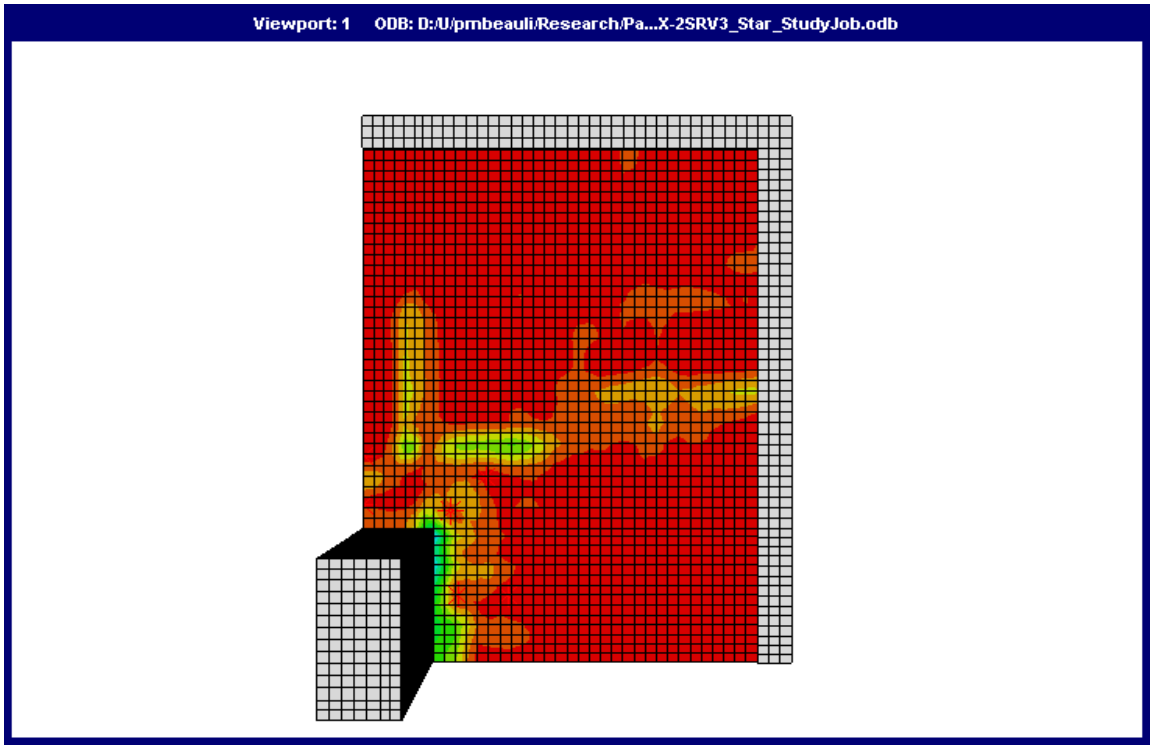

Figure A14: SX-2SR S3 Study 53% Stem-Stem Spacing Tensile Face Crack Pattern

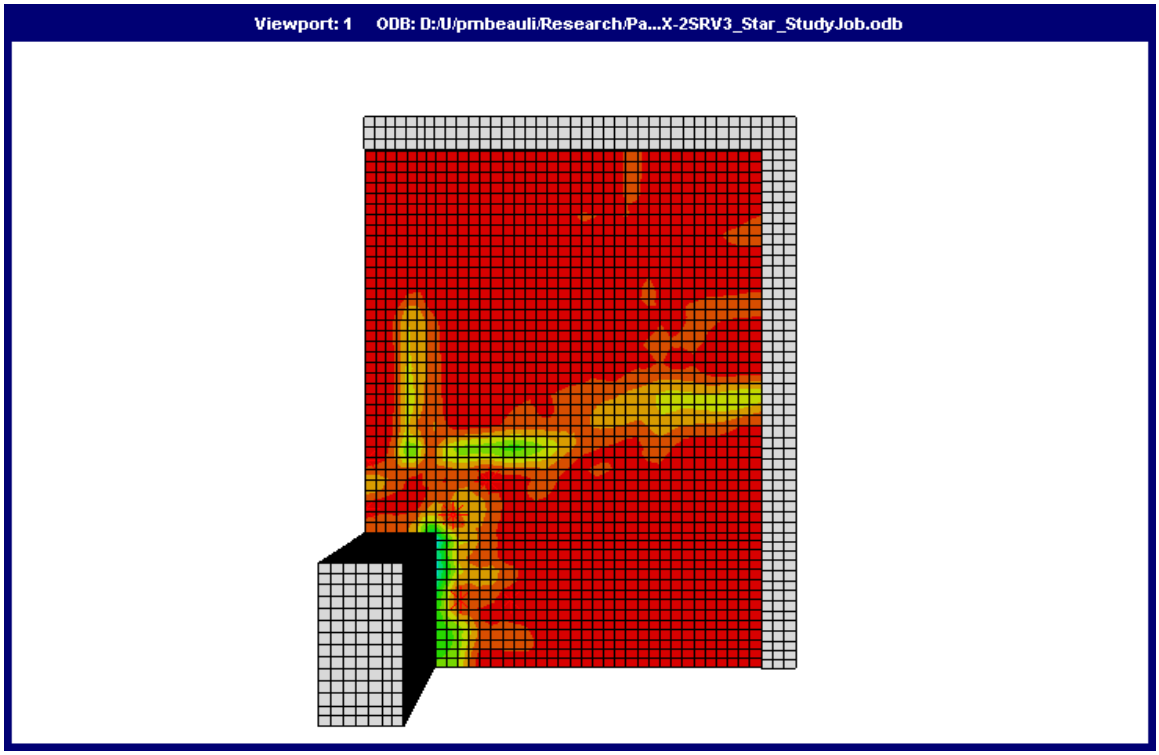

Figure A15: SX-2SR S3 Study 57% Stem-Stem Spacing Tensile Face Crack Pattern

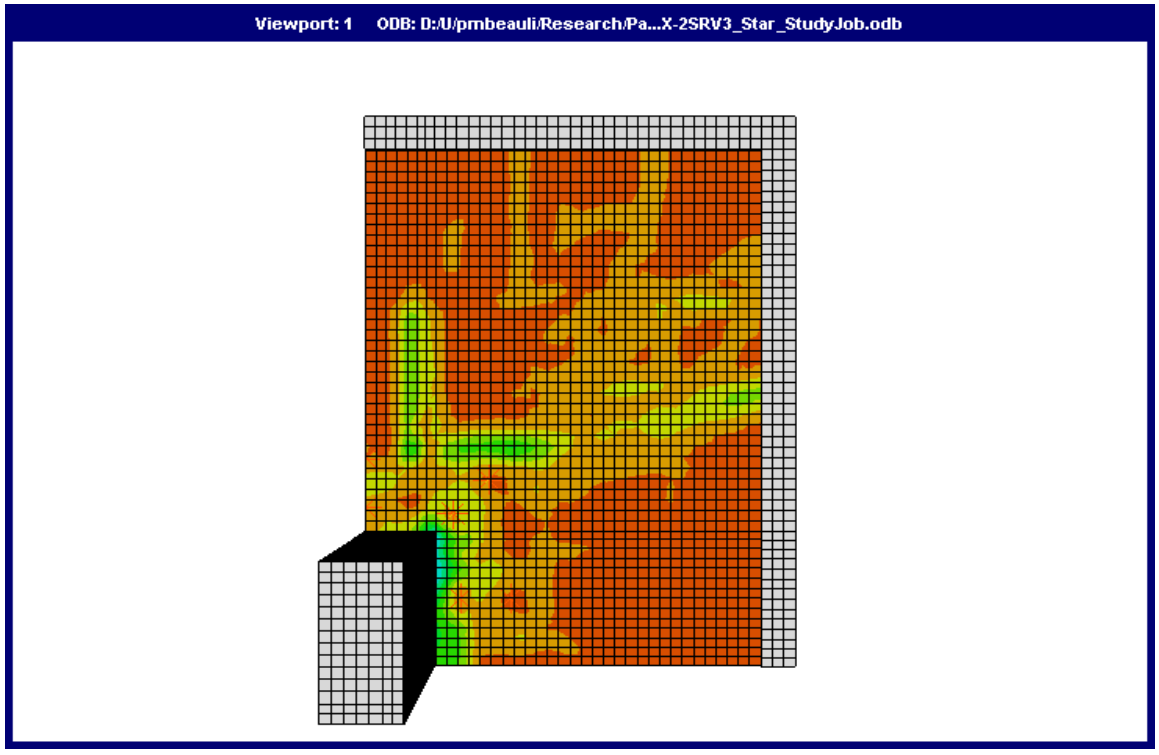

Figure A16: SX-2SR S3 Study 61% Stem-Stem Spacing Tensile Face Crack Pattern

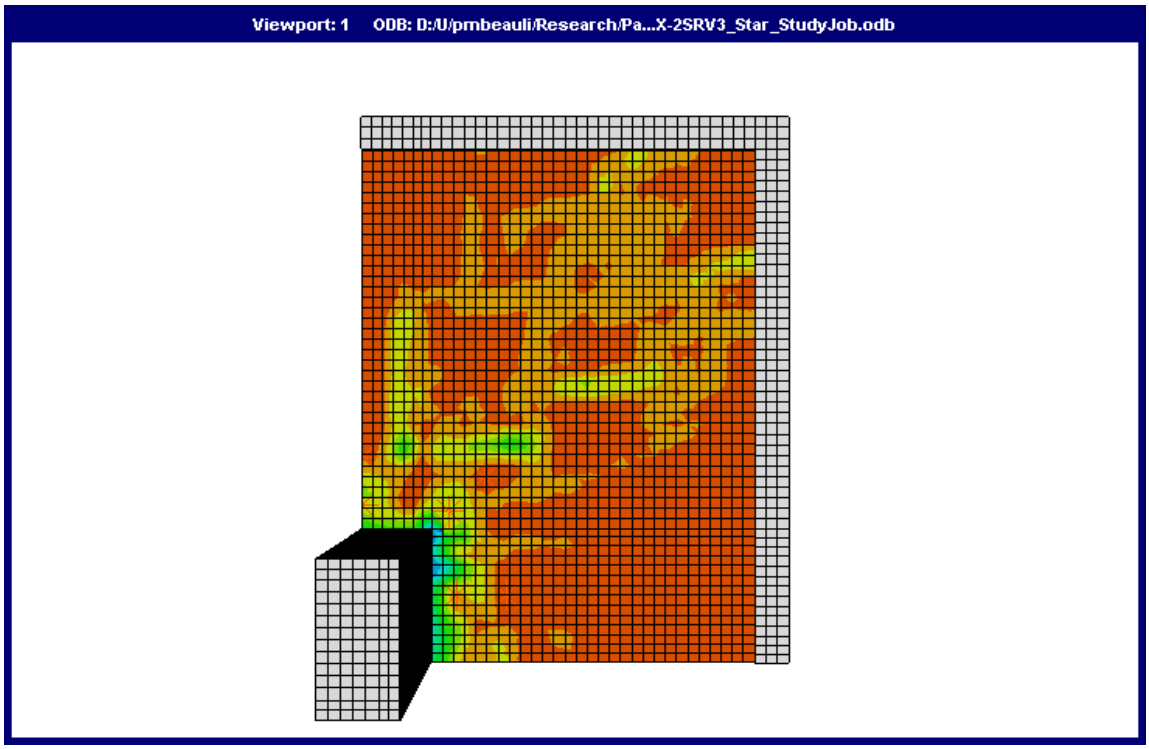

Figure A17: SX-2SR S3 Study 65% Stem-Stem Spacing Tensile Face Crack Pattern

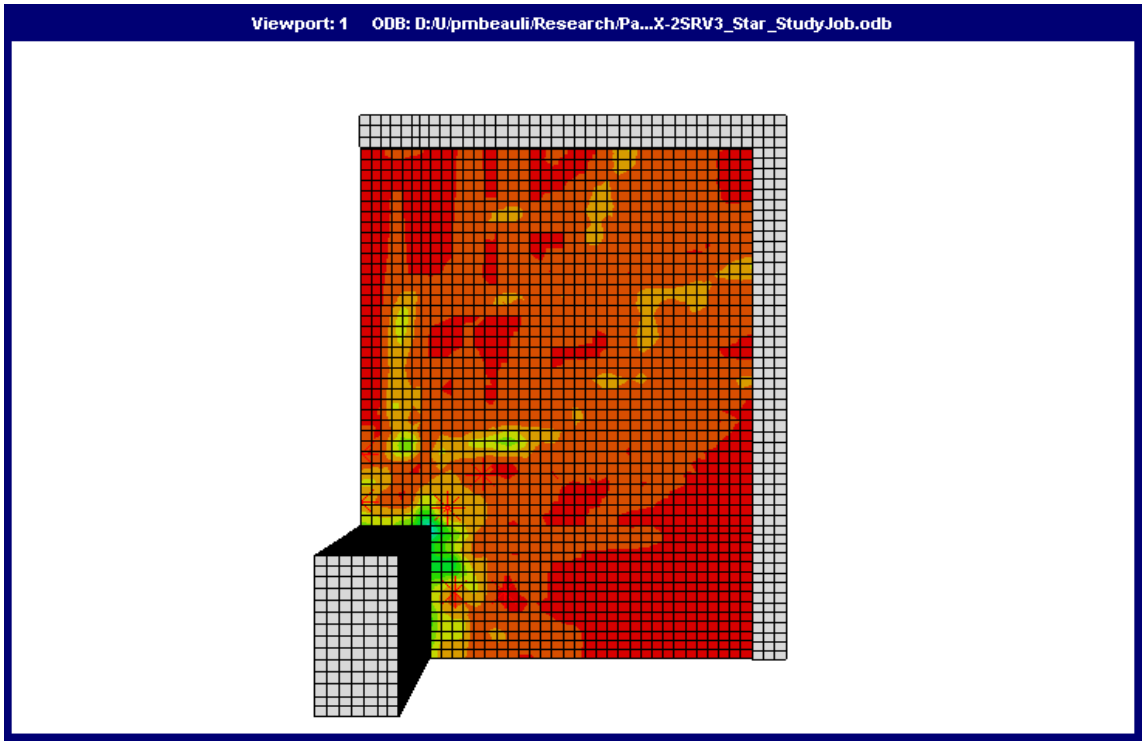

Figure A18: SX-2SR S3 Study 69% Stem-Stem Spacing Tensile Face Crack Pattern

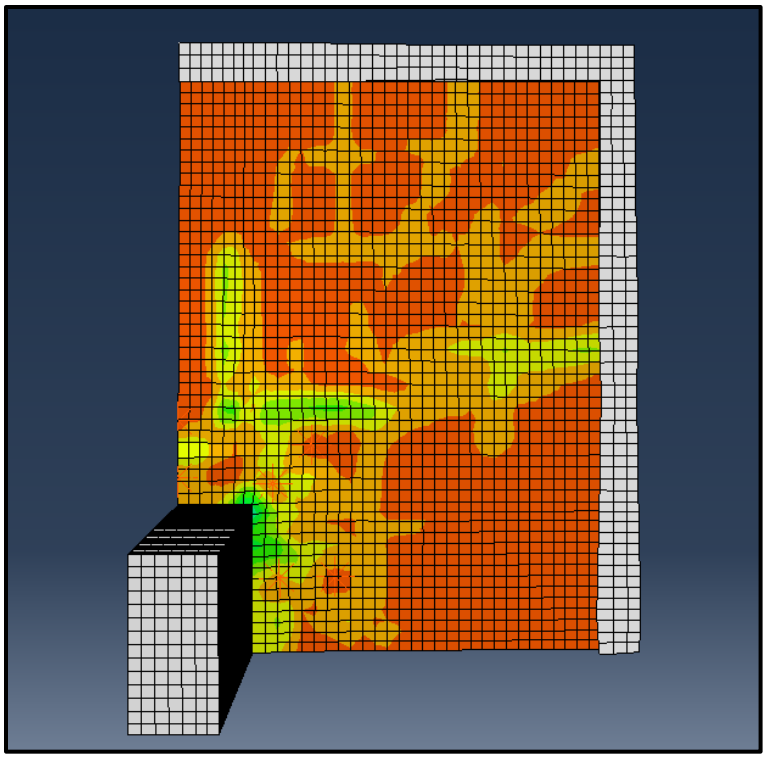

Figure A19: SX-2SR S3 Study 73% Stem-Stem Spacing Tensile Face Crack Pattern

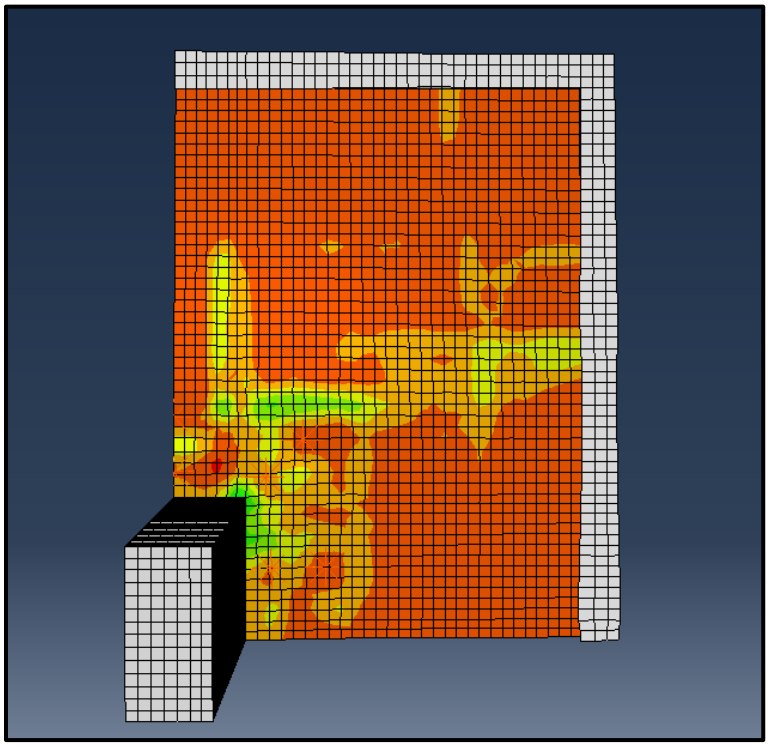

Figure A20: SX-2SR S3 Study 77% Stem-Stem Spacing Tensile Face Crack Pattern

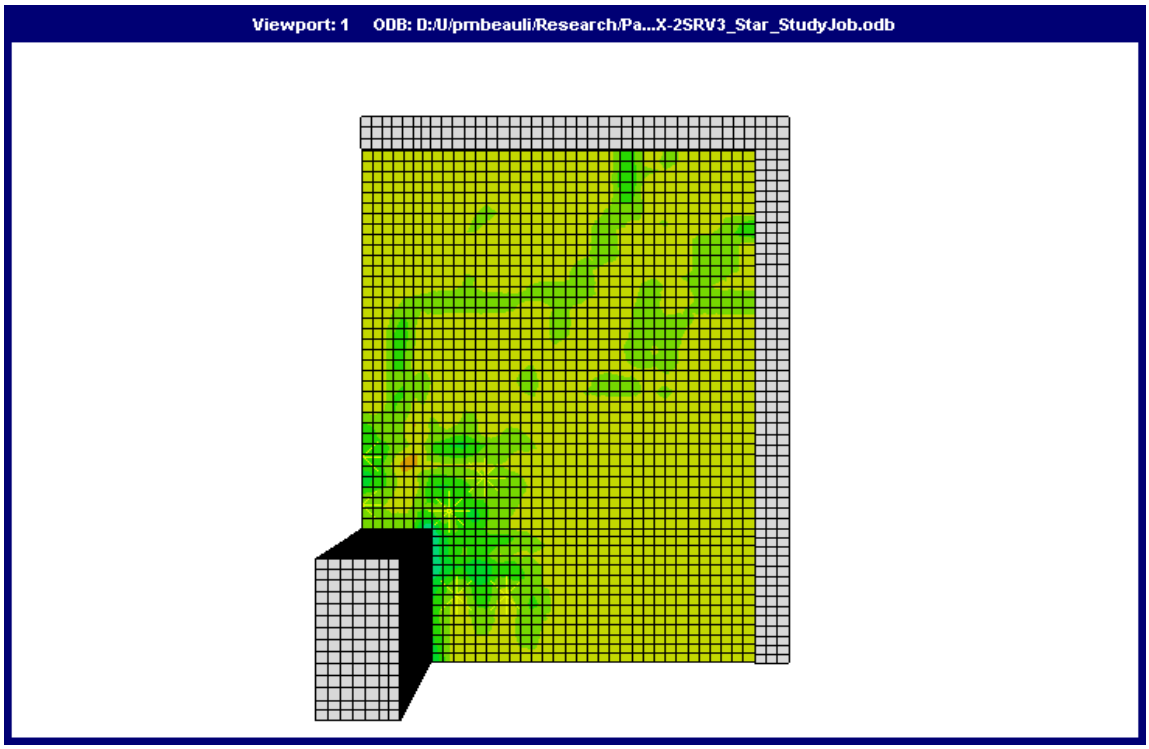

Figure A21: SX-2SR S3 Study 82% Stem-Stem Spacing Tensile Face Crack Pattern

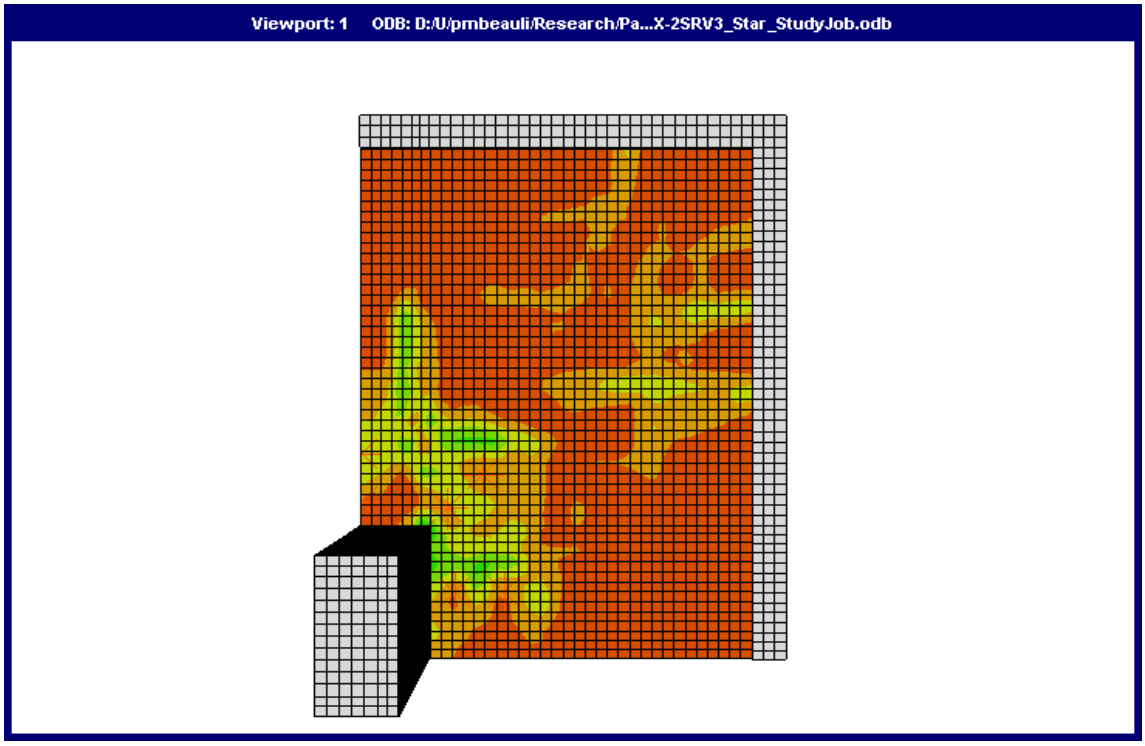

Figure A22: SX-2SR S3 Study 86% Stem-Stem Spacing Tensile Face Crack Pattern

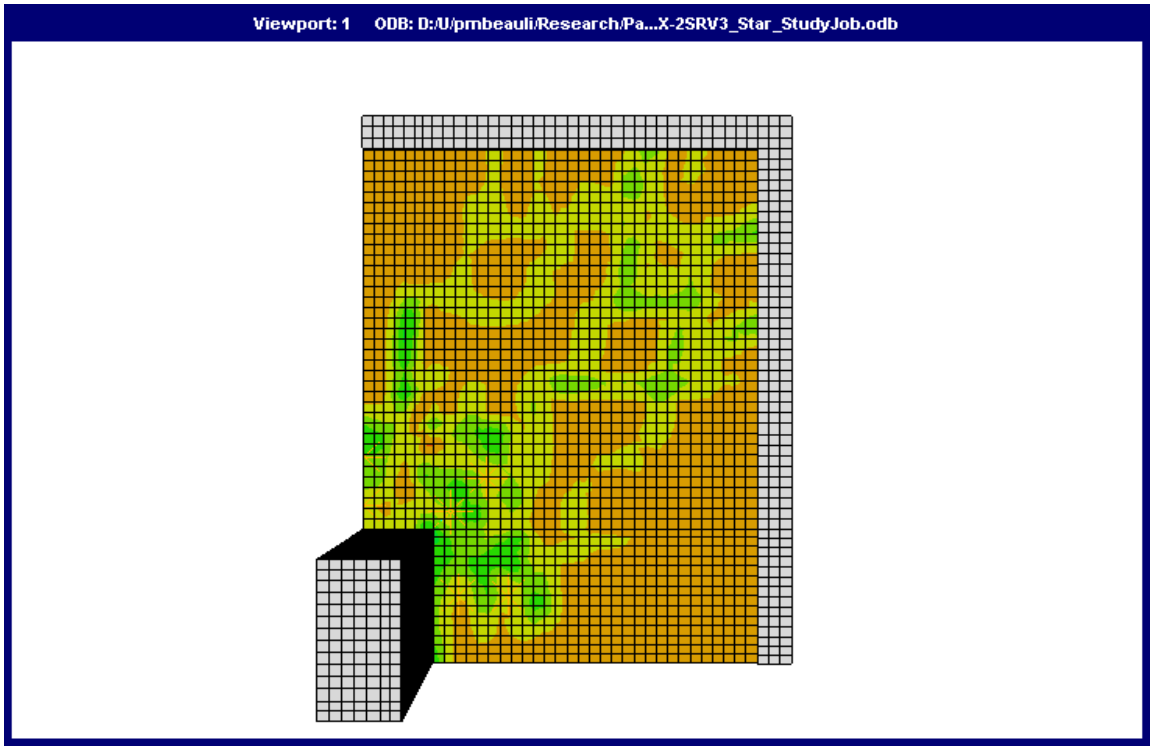

Figure A23: SX-2SR S3 Study 90% Stem-Stem Spacing Tensile Face Crack Pattern

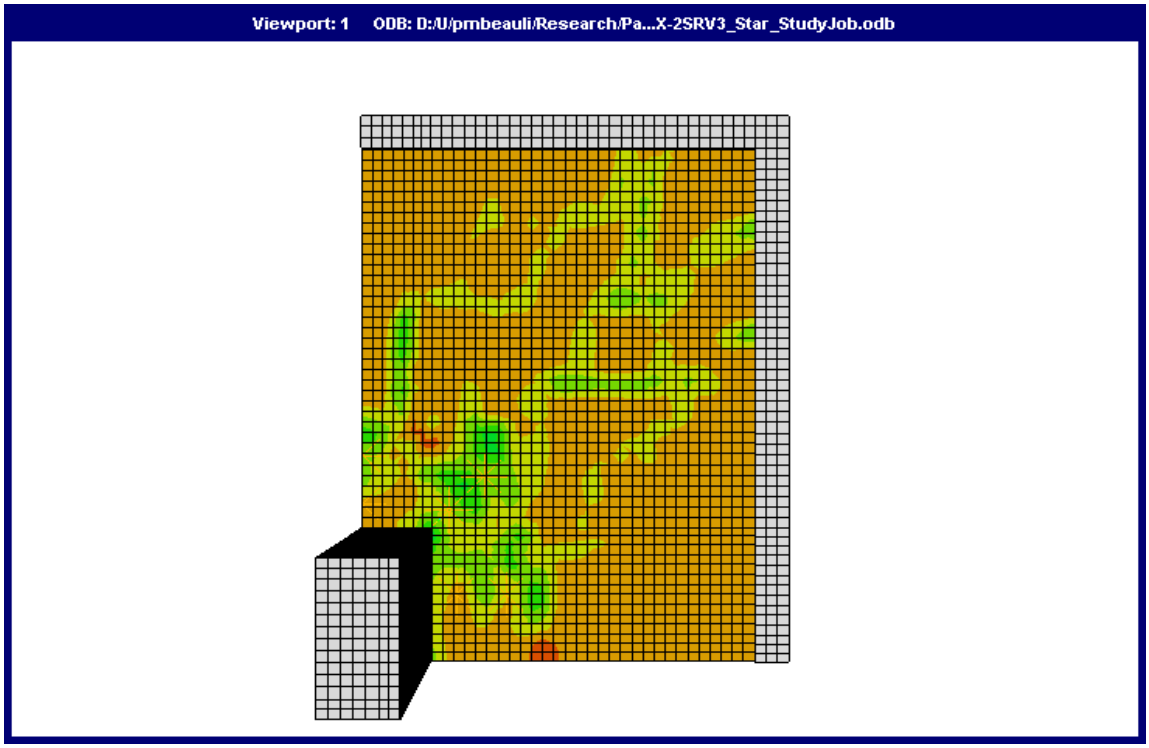

Figure A24: SX-2SR S3 Study 94% Stem-Stem Spacing Tensile Face Crack Pattern

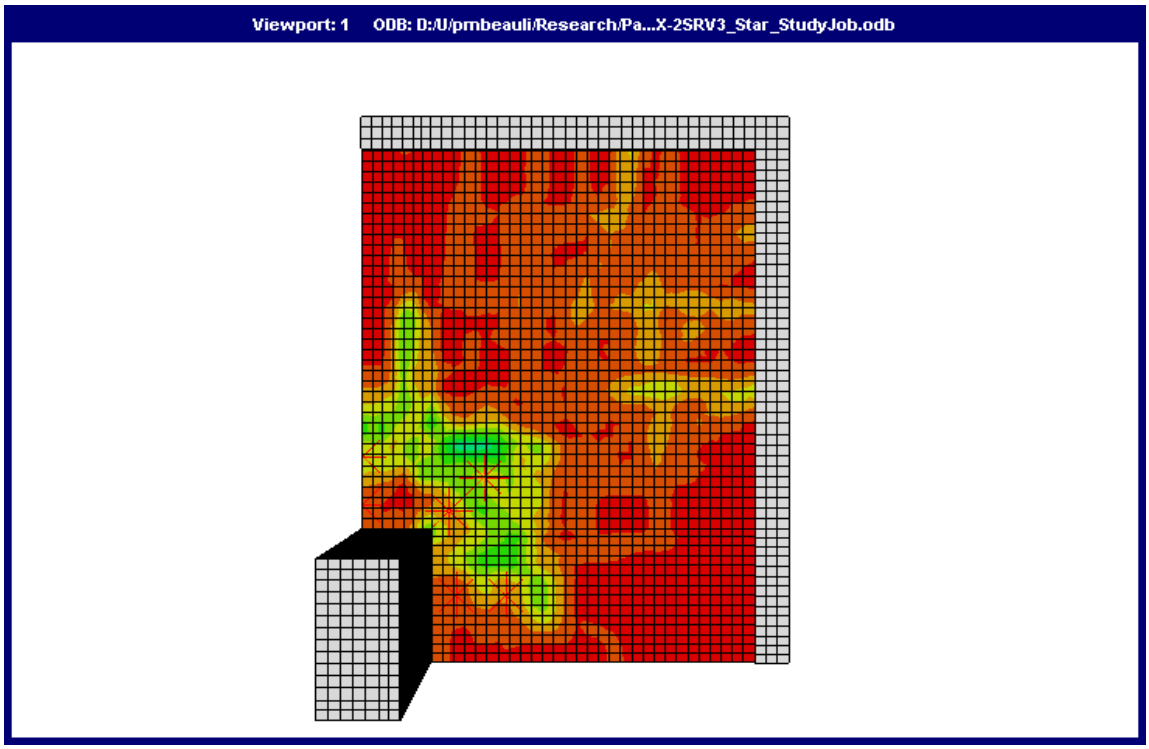

Figure A25: SX-2SR S3 Study 98% Stem-Stem Spacing Tensile Face Crack Pattern

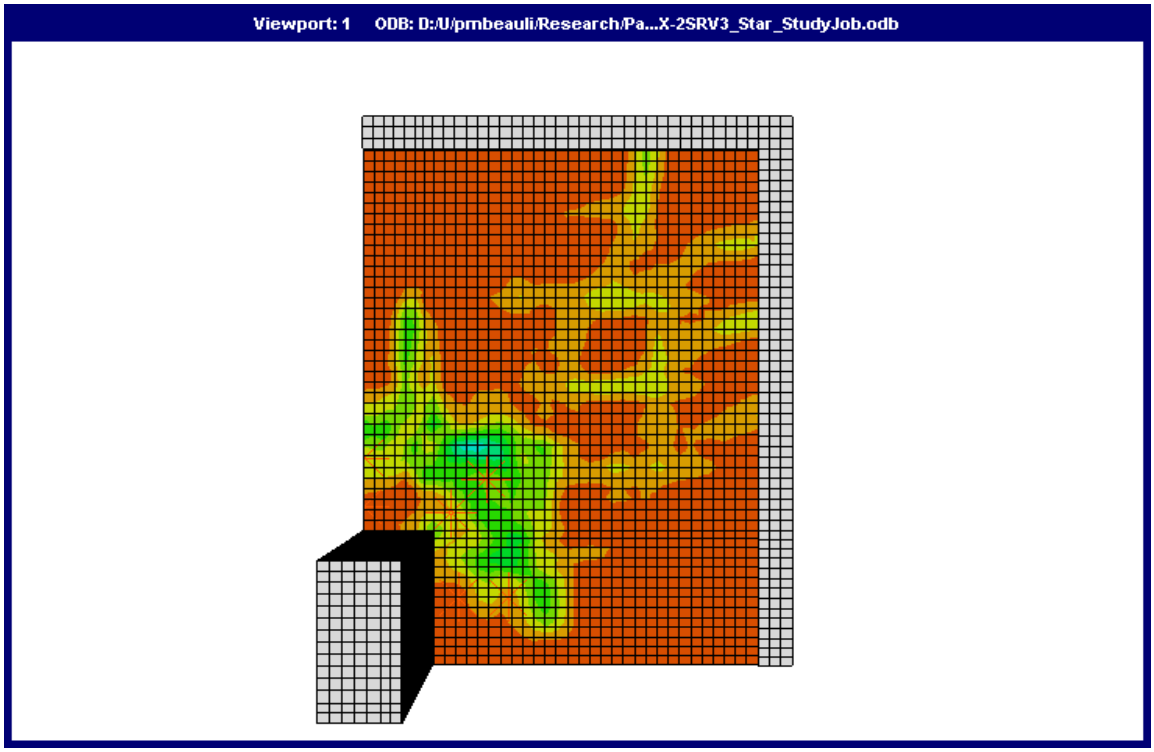

Figure A26: SX-2SR S3 Study 102% Stem-Stem Spacing Tensile Face Crack Pattern

Appendix B: NLFEA Model Calibration Supplemental Figures

List of Figures

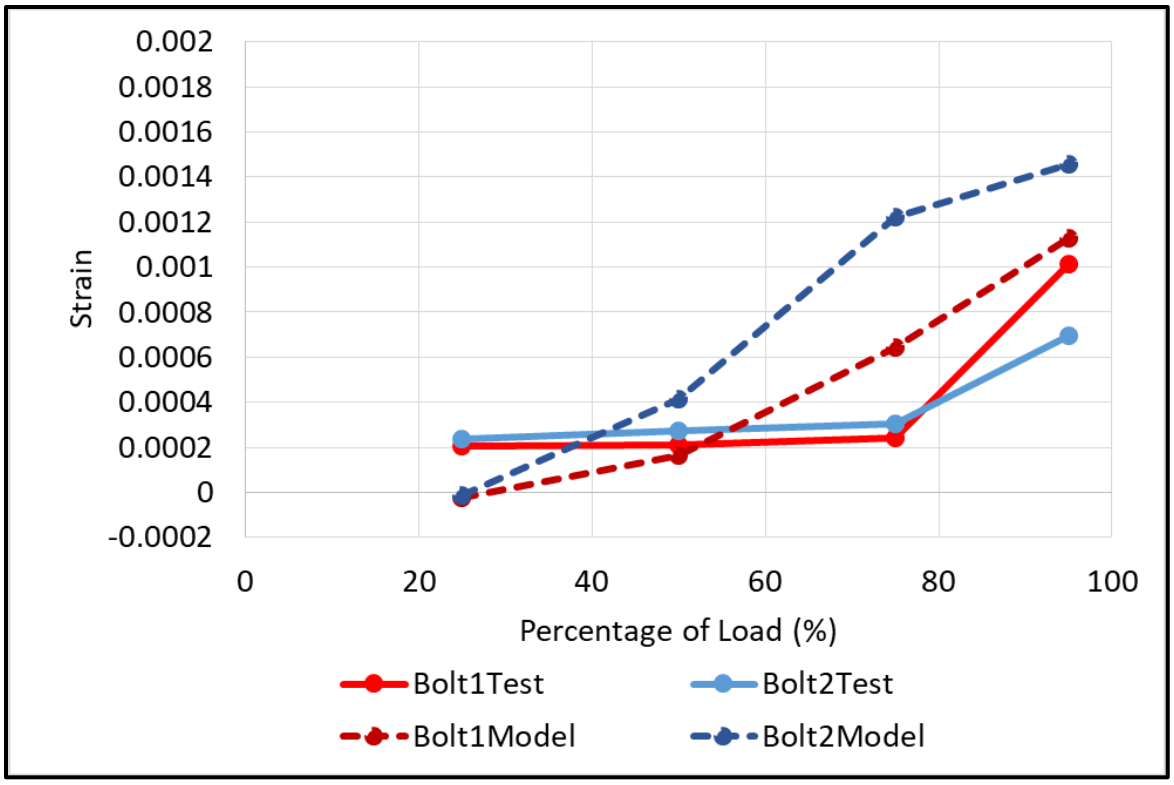

Figure B1: SB2 Bolt Strain Diagram

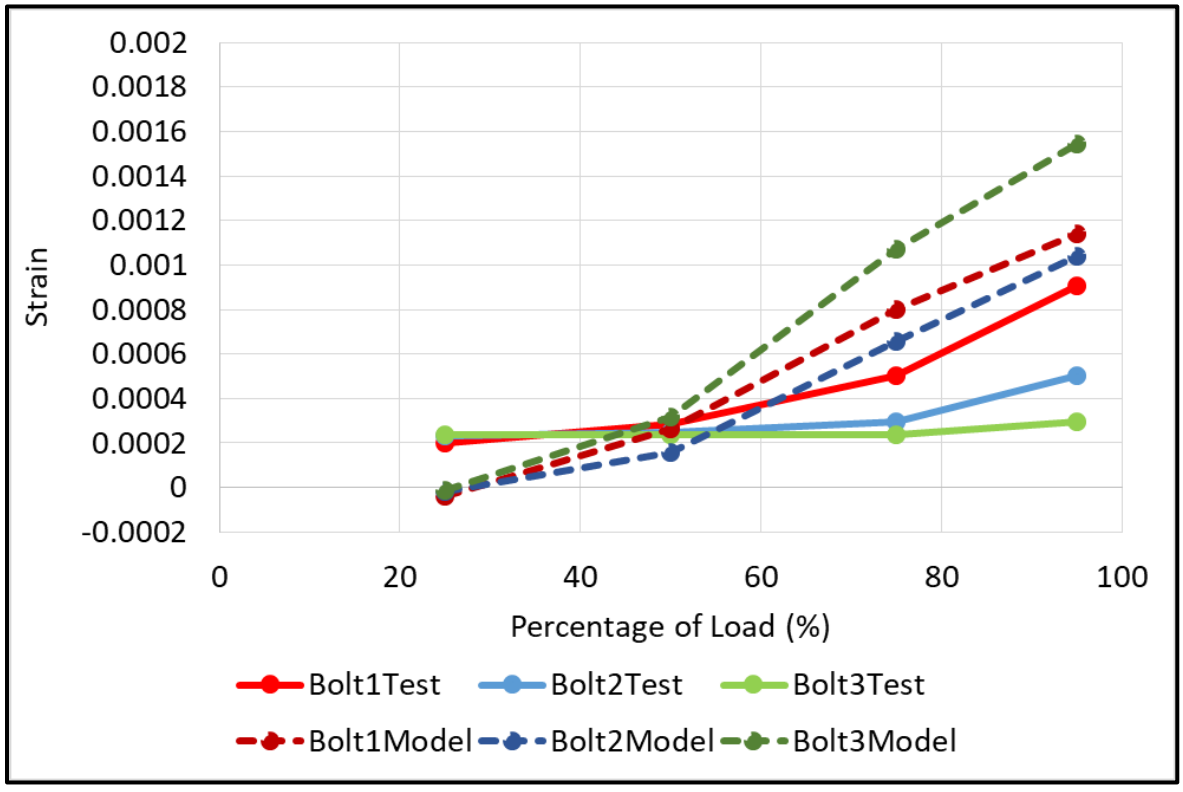

Figure B2: SB3 Bolt Strain Diagram

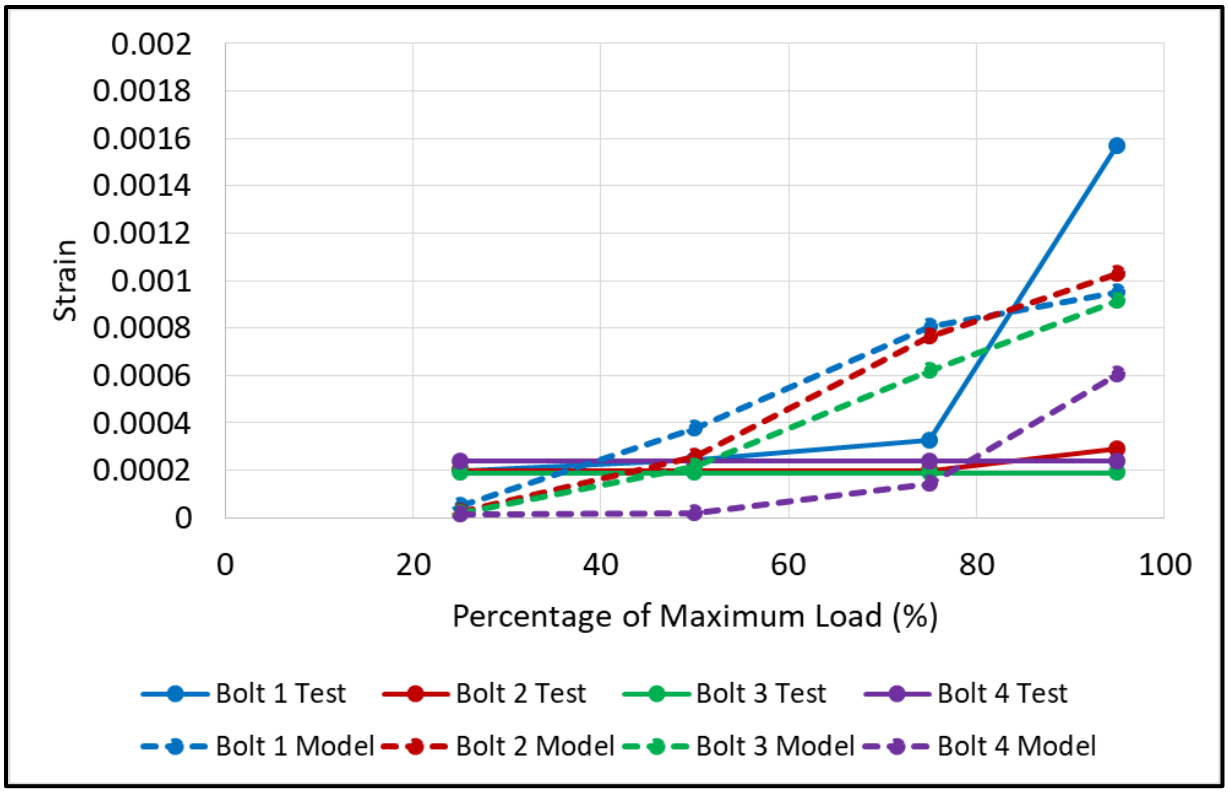

Figure B3: SB4 Bolt Strain Diagram

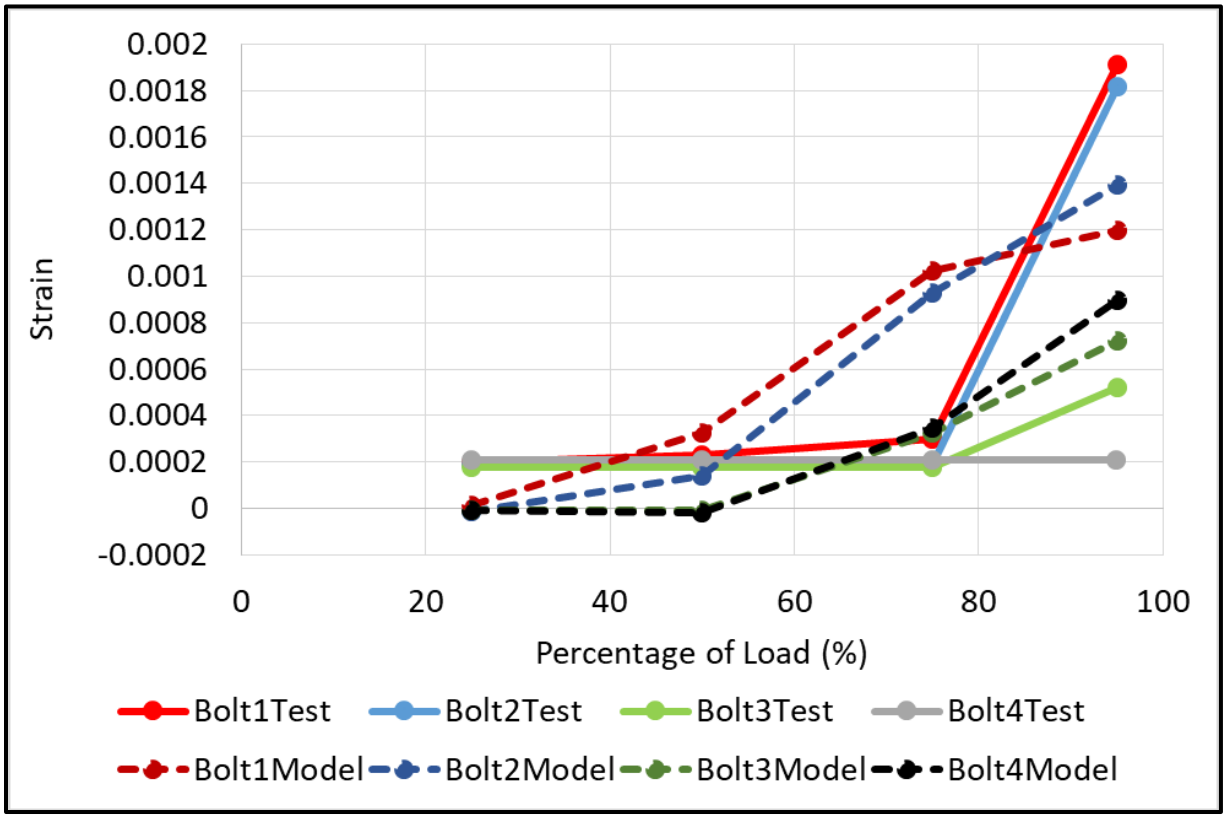

Figure B4: SB5 Bolt Strain Diagram

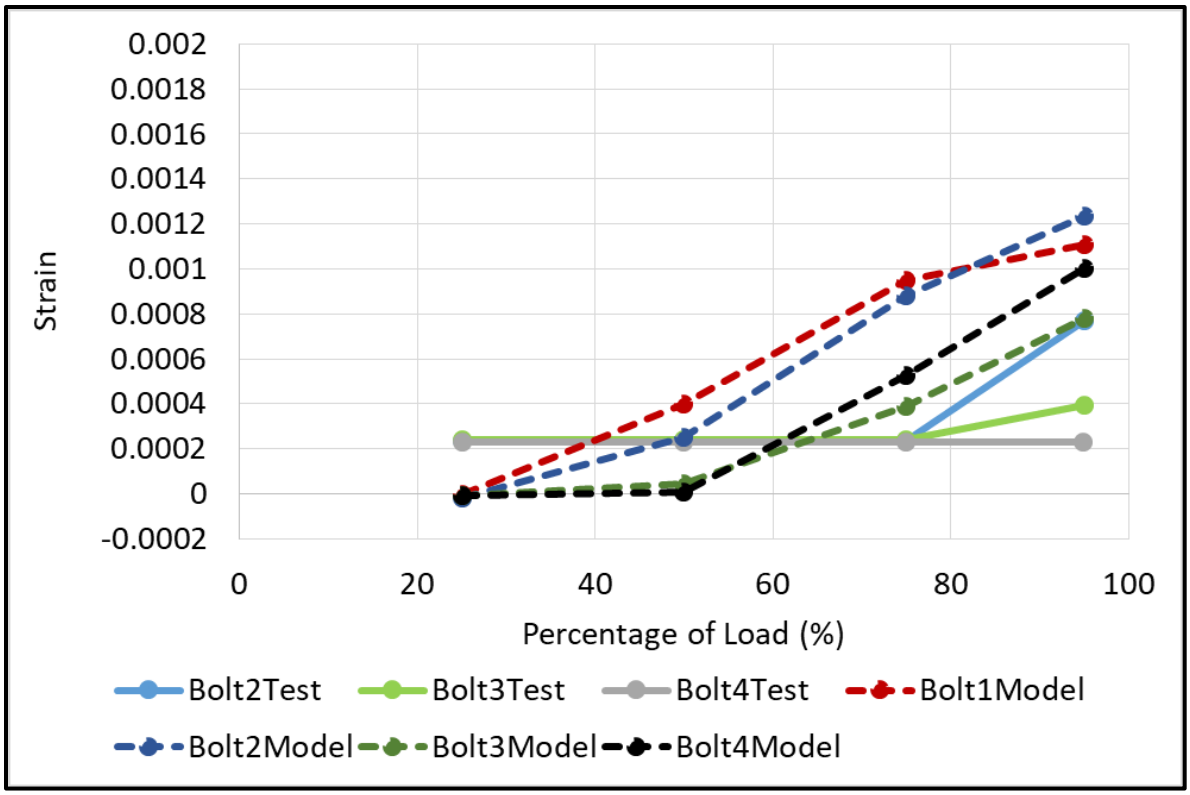

Figure B5: SB6 Bolt Strain Diagram

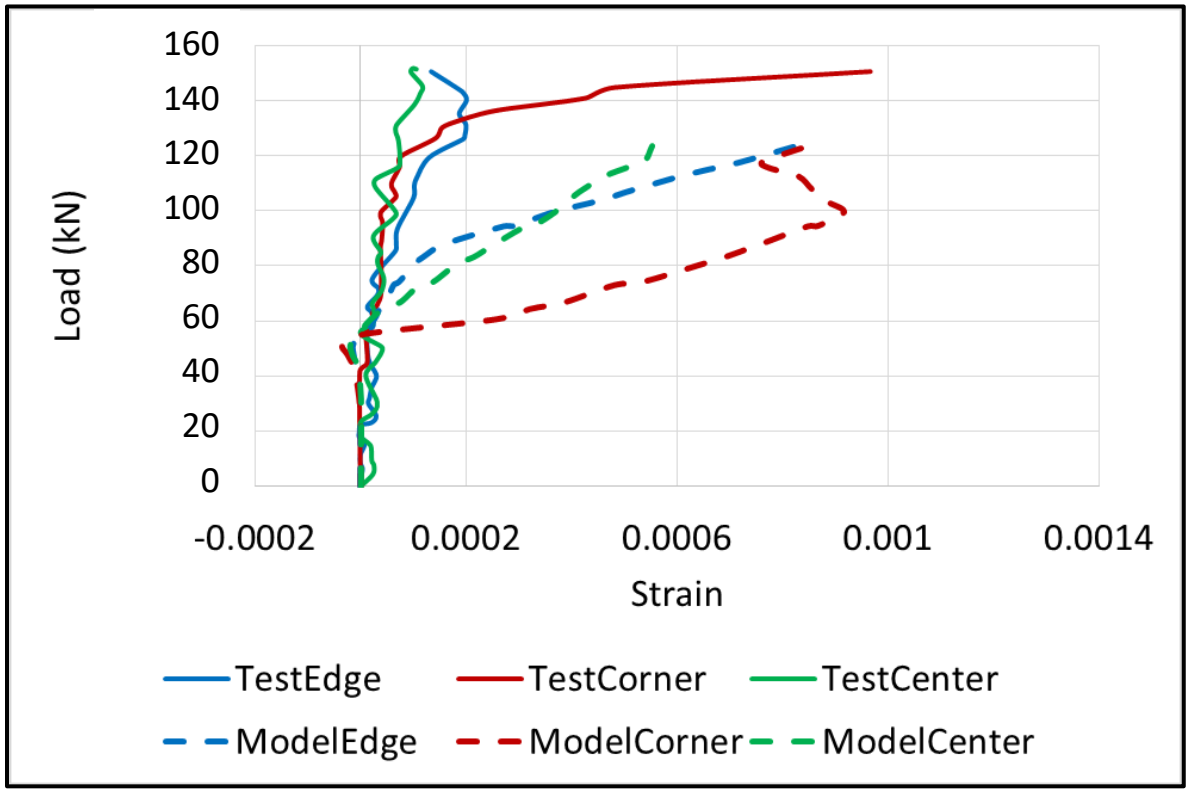

Figure B6: SX-1SR Row 1 Stud Strain Diagram

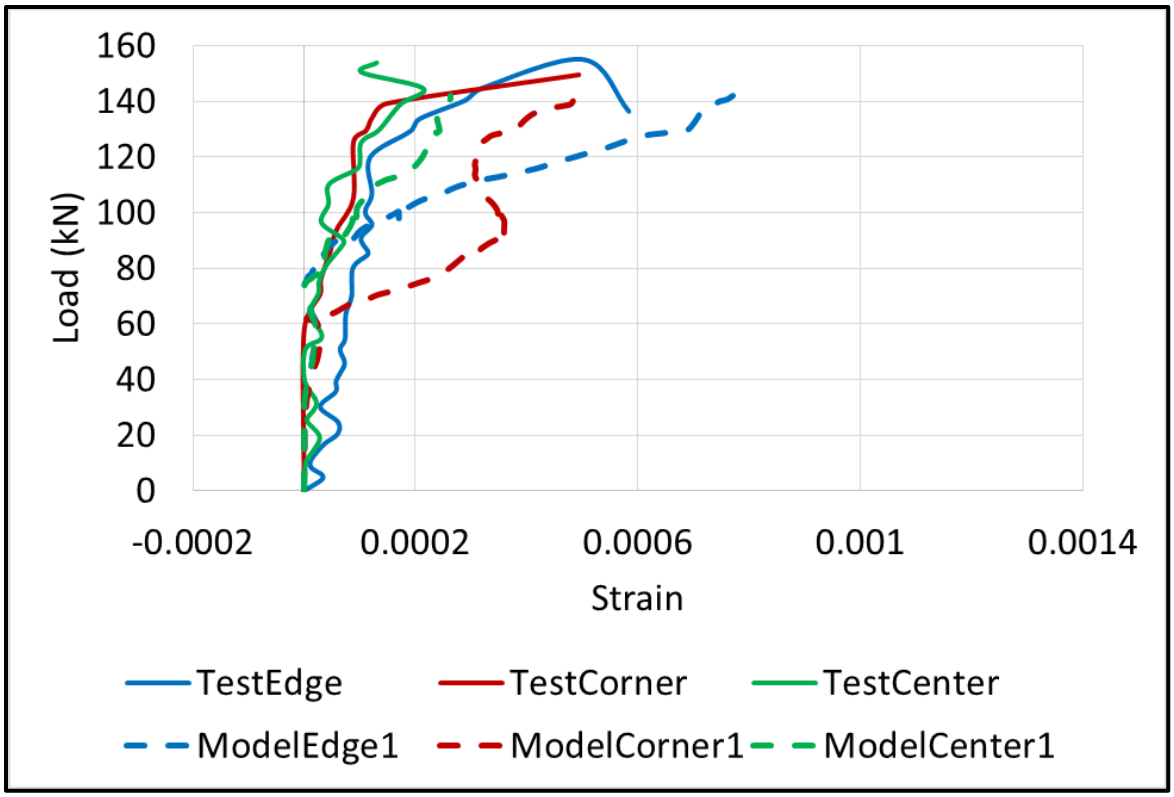

Figure B7: SX-2SR Row 1 Stud Strain Diagram

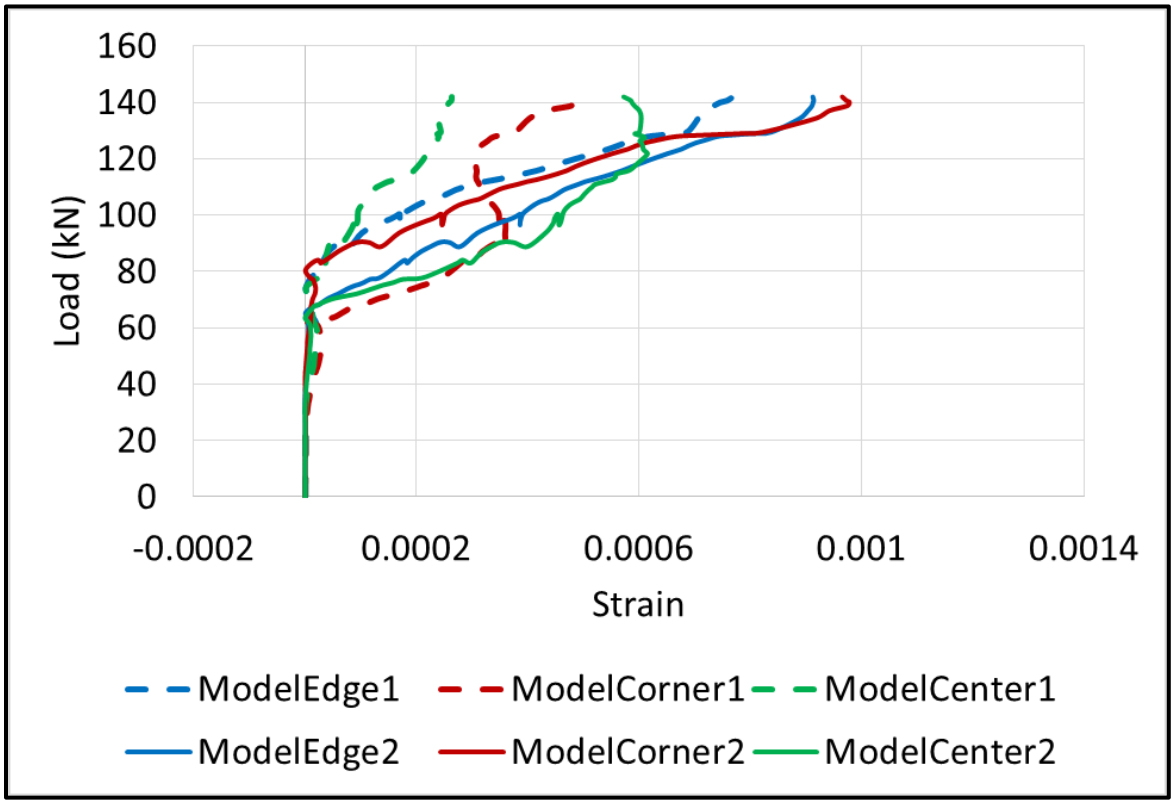

Figure B8: SX-2SR Stud Strain Diagram

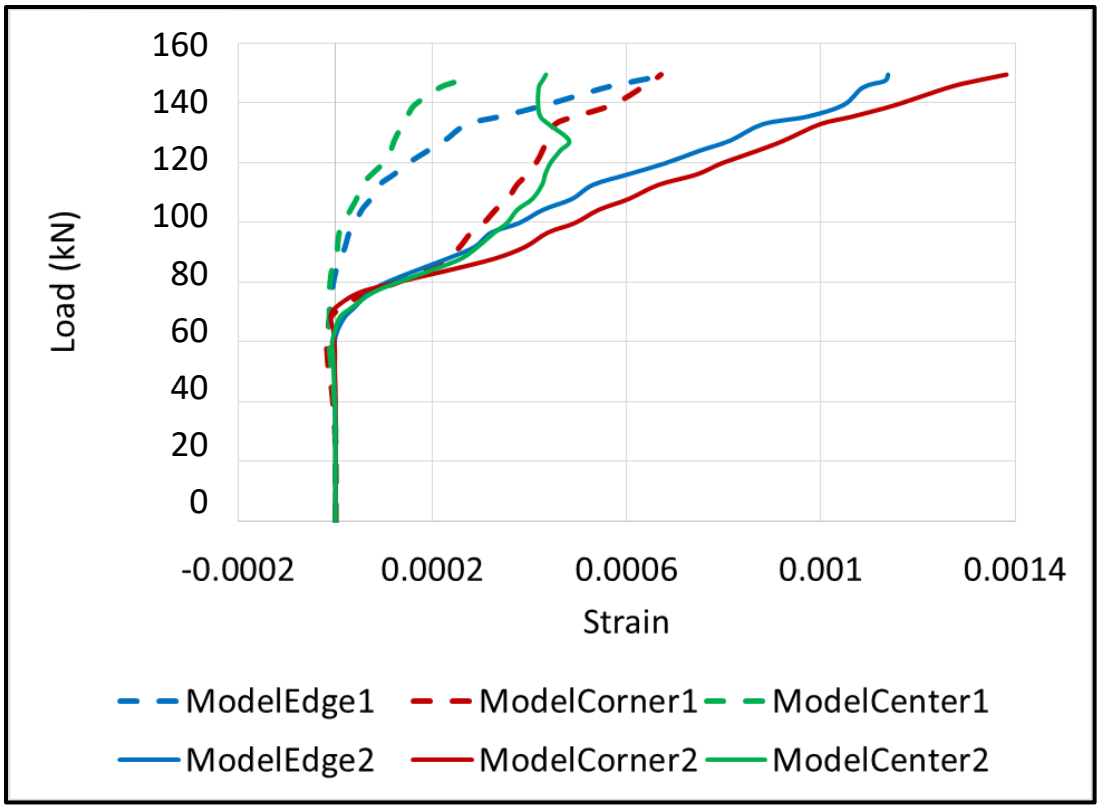

Figure B9: SX-2SB Bolt Strain Diagram

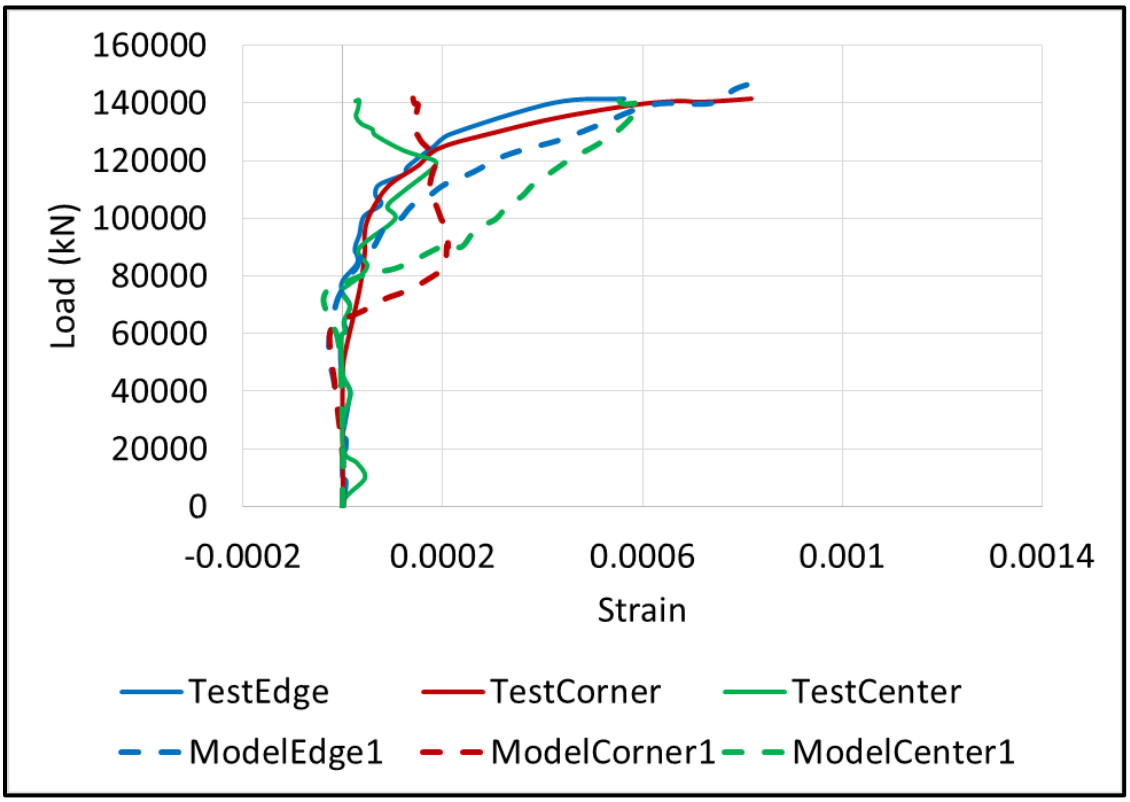

Figure B10: SH-2SR Row 1 Stud Strain Diagram

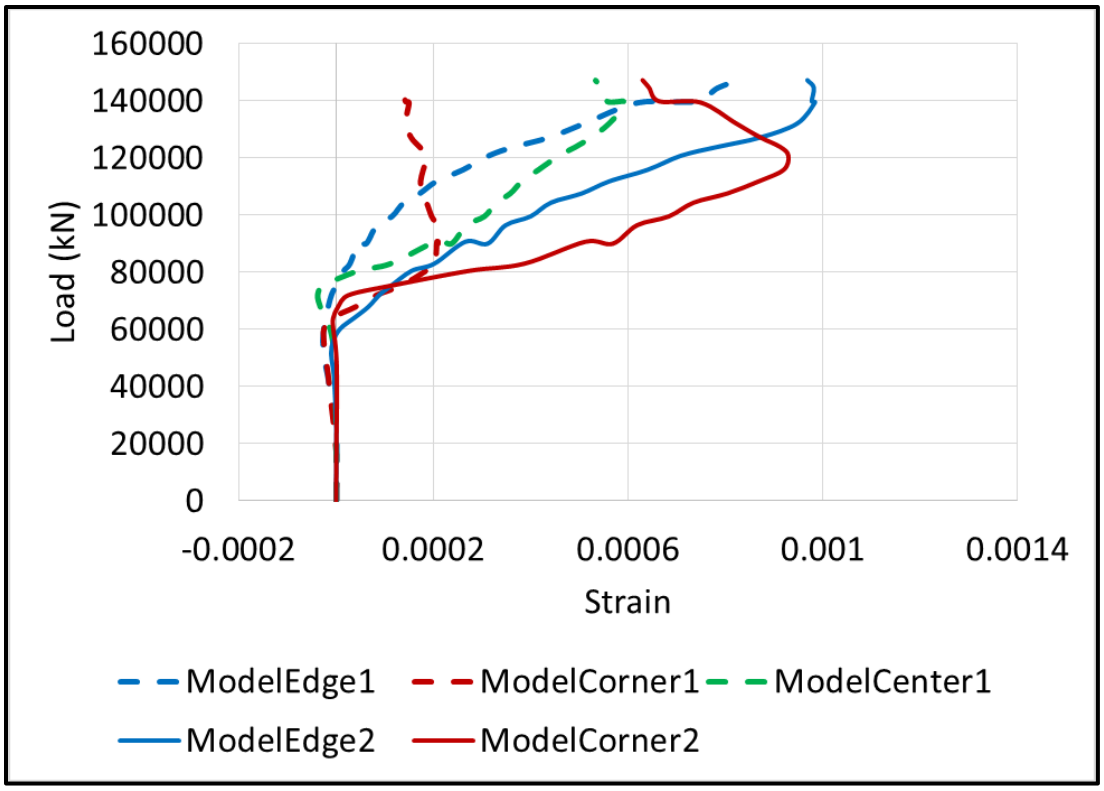

Figure B11: SH-2SR Stud Strain Diagram

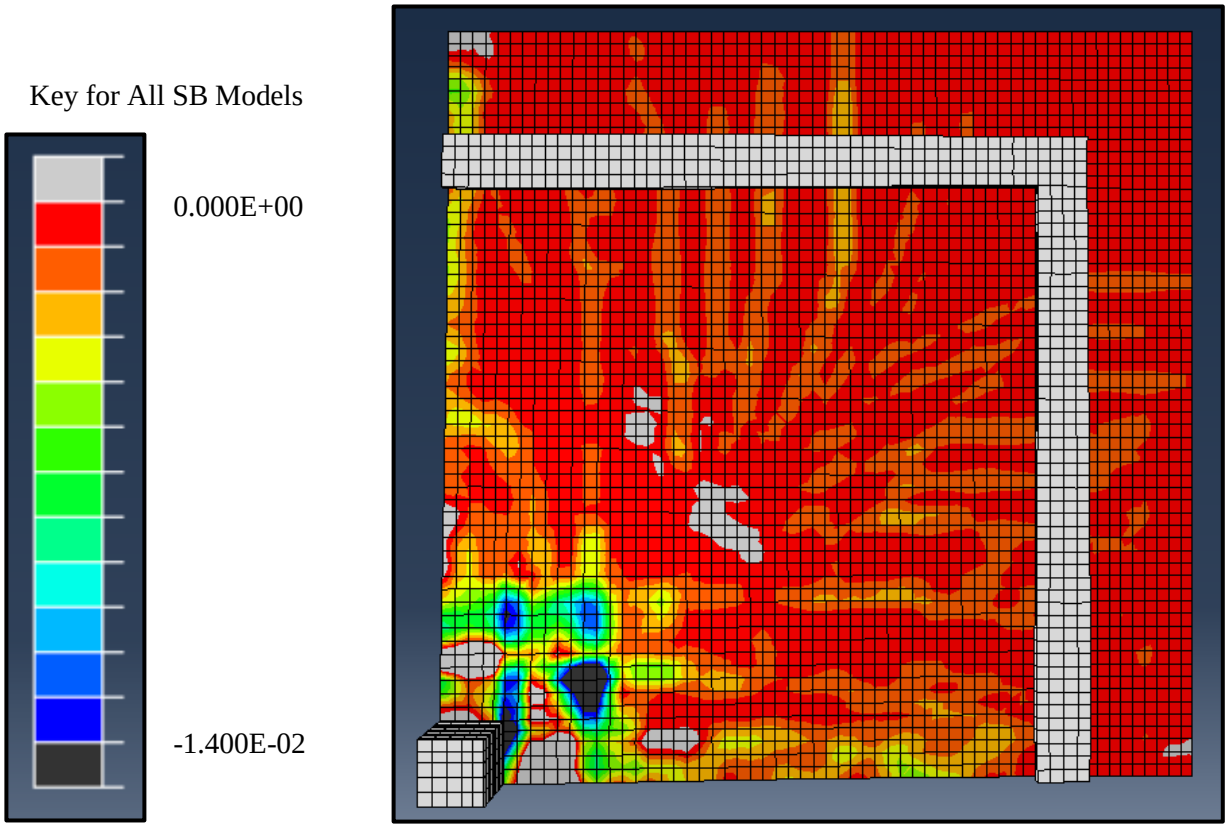

Figure B12: SB1 Tensile Face Crack Pattern

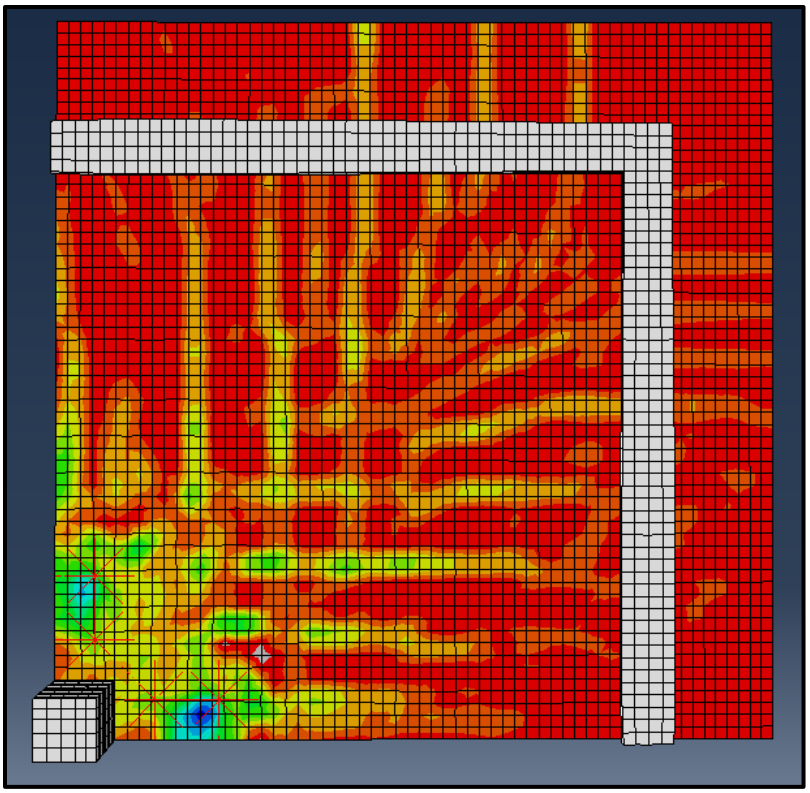

Figure B13: SB2 Tensile Face Crack Pattern

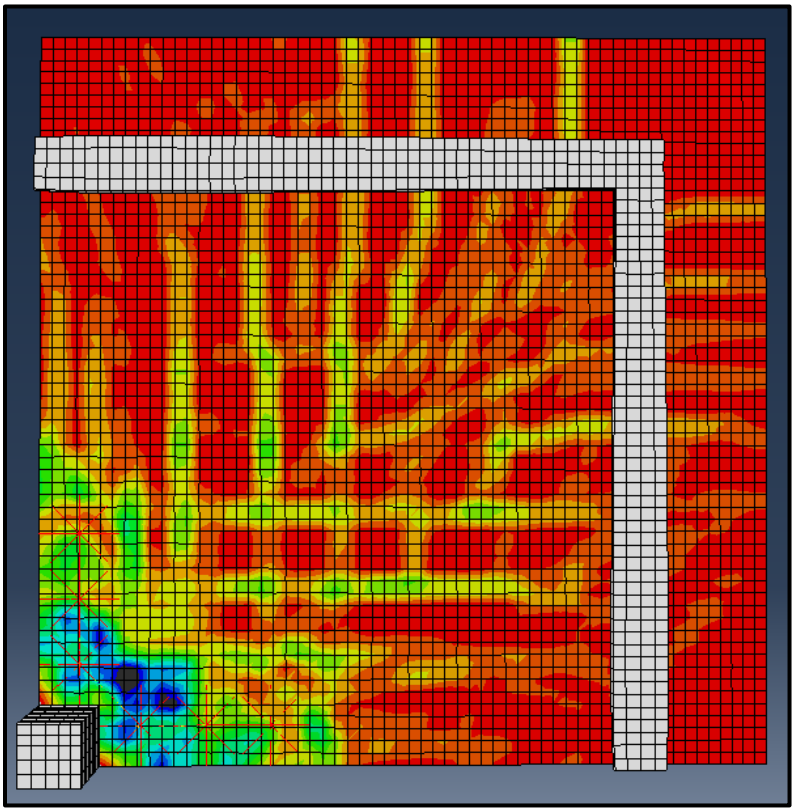

Figure B14: SB3 Tensile Face Crack Pattern

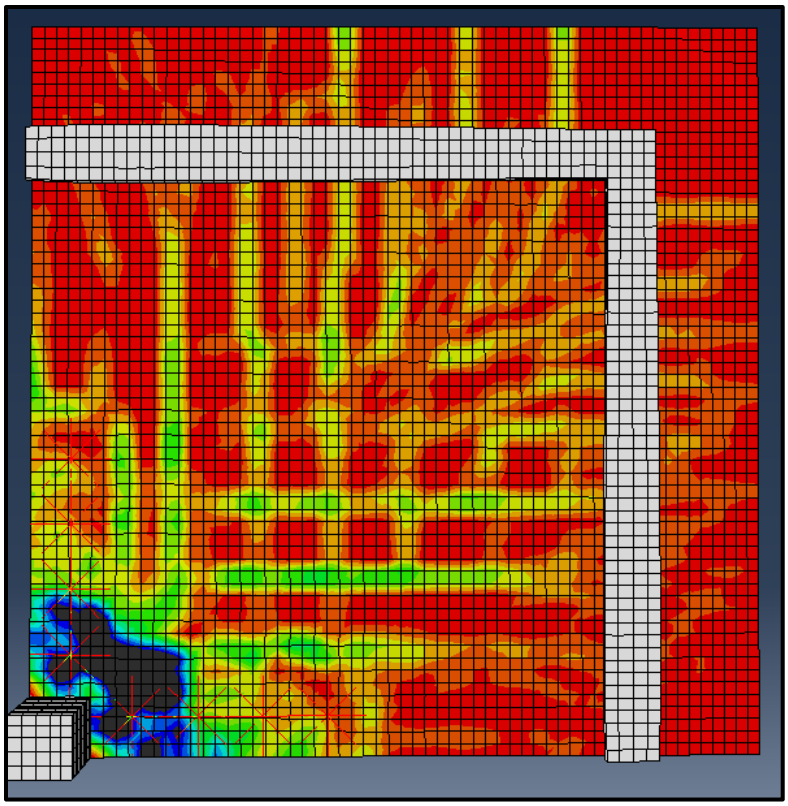

Figure B15: SB4 Tensile Face Crack Pattern

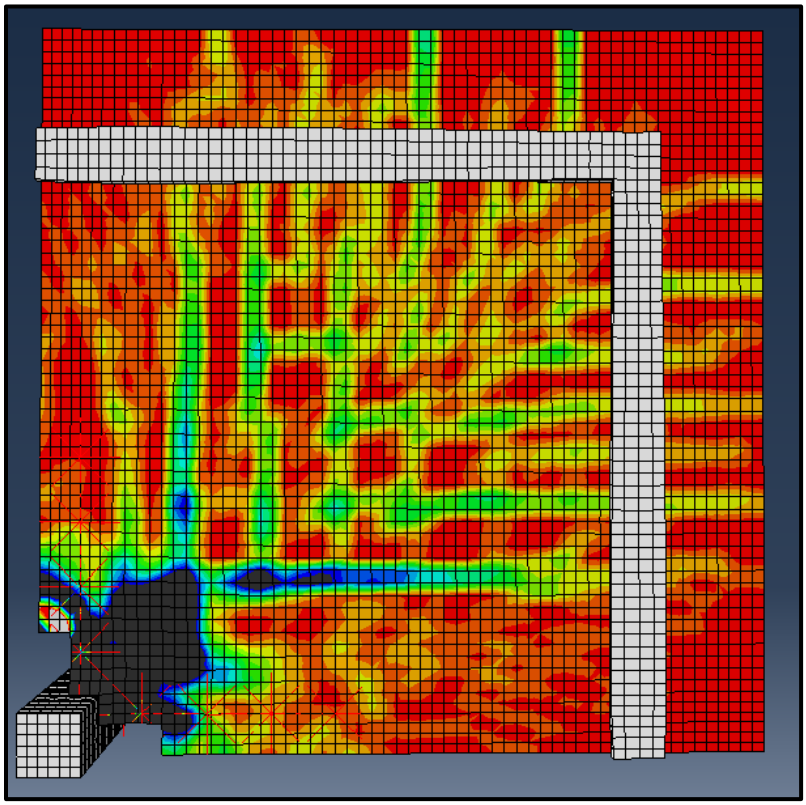

Figure B16: SB5 Tensile Face Crack Pattern

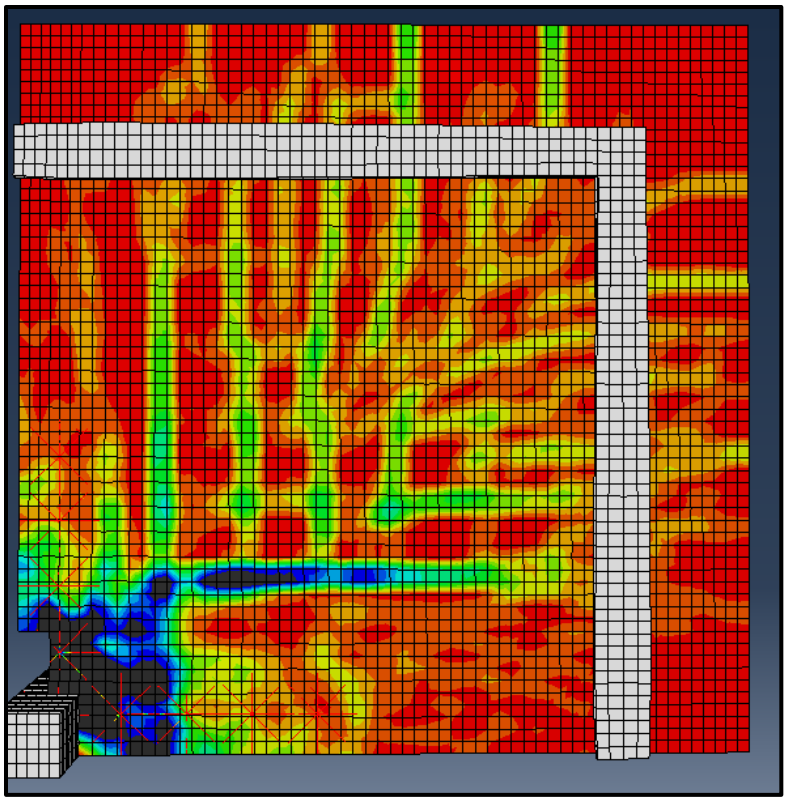

Figure B17: SB6 Tensile Face Crack Pattern

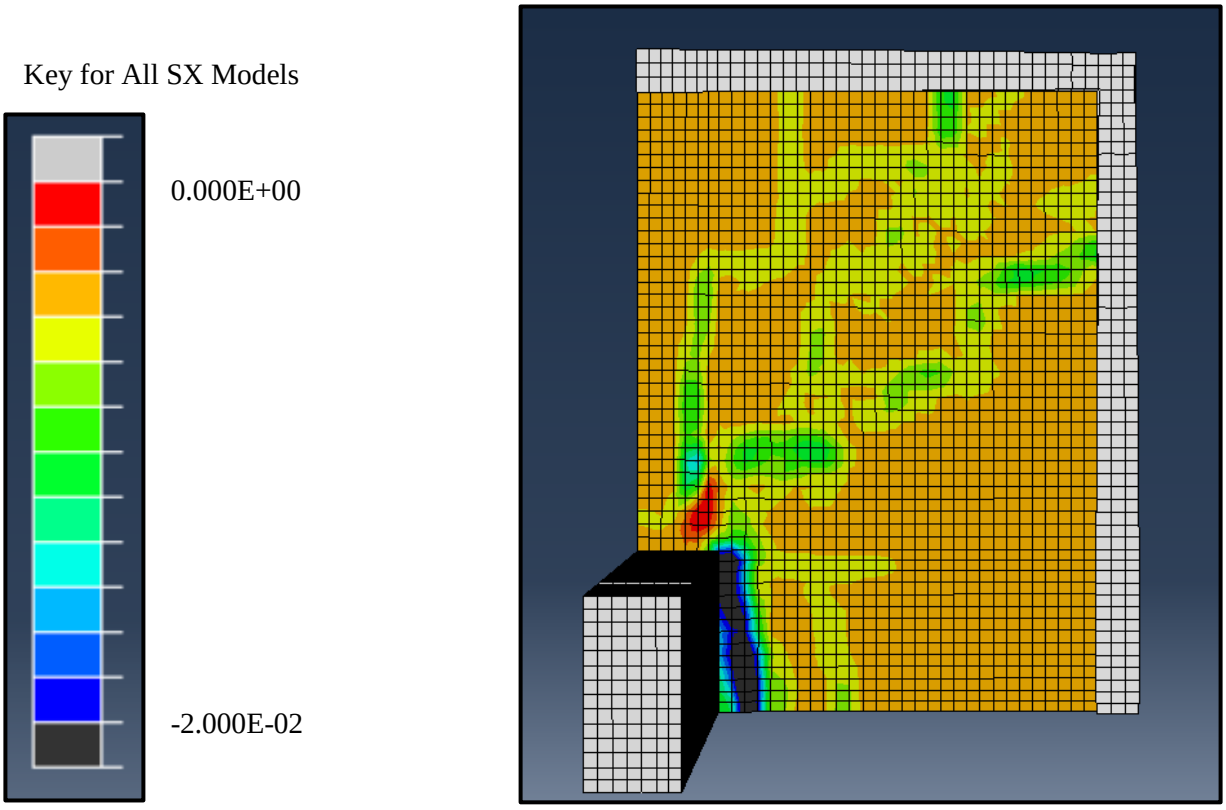

Figure B18: XXX Tensile Face Crack Pattern

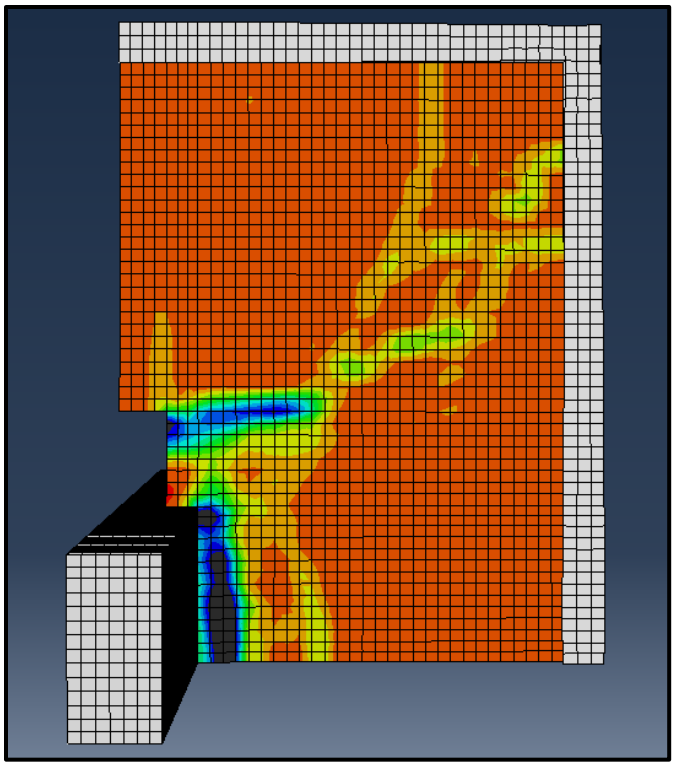

Figure B19: SF0 Tensile Face Crack Pattern

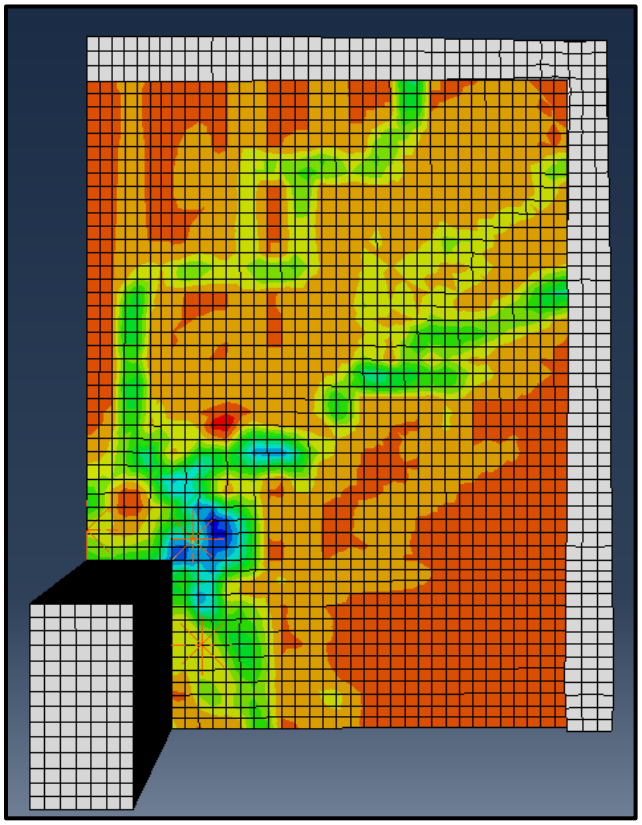

Figure B20: SX-1SR Tensile Face Crack Pattern

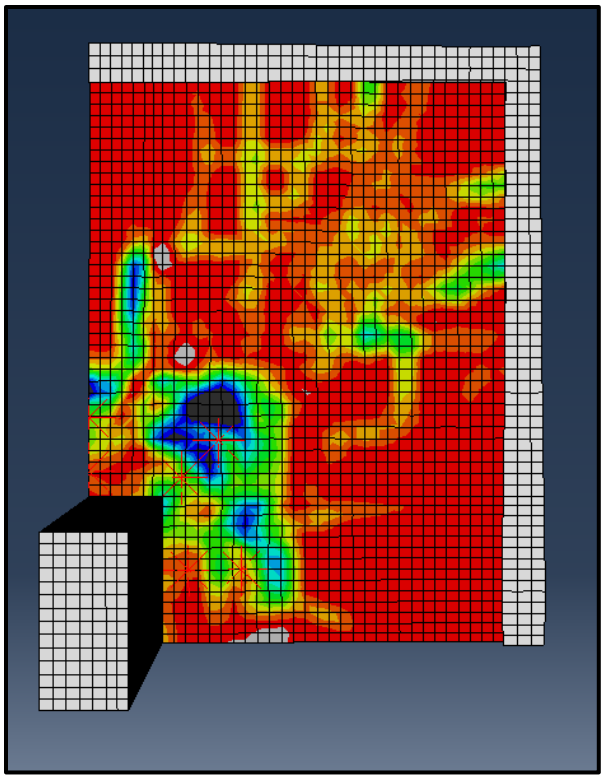

Figure B21: SX-2SR Tensile Face Crack Pattern

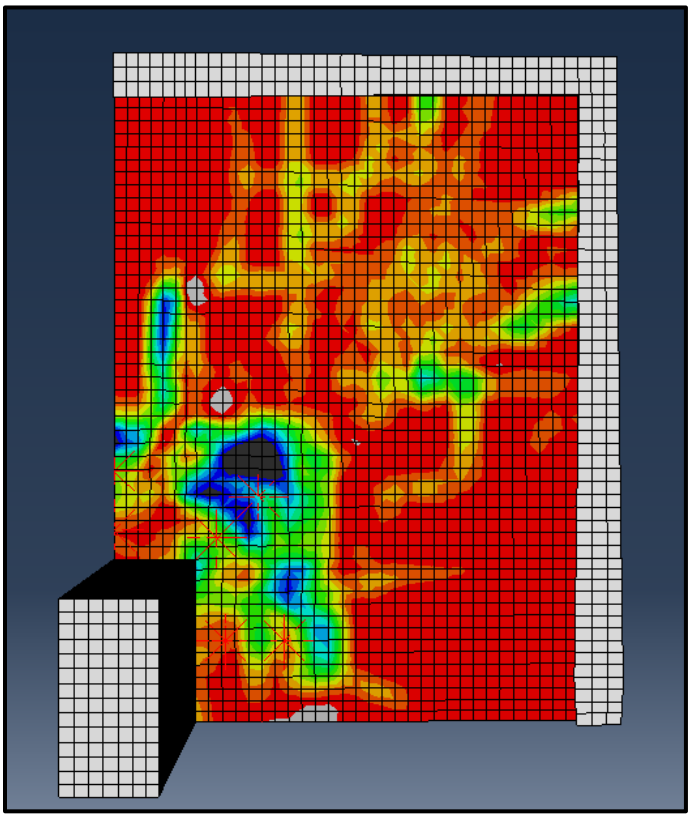

Figure B22: SX-2SB Tensile Face Crack Pattern

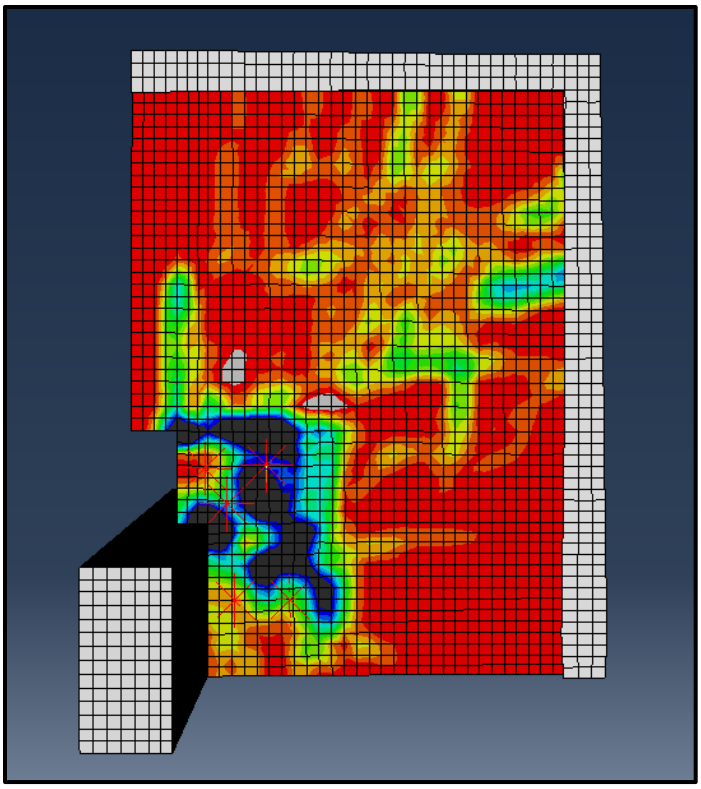

Figure B23: SH-2SR Tensile Face Crack Pattern

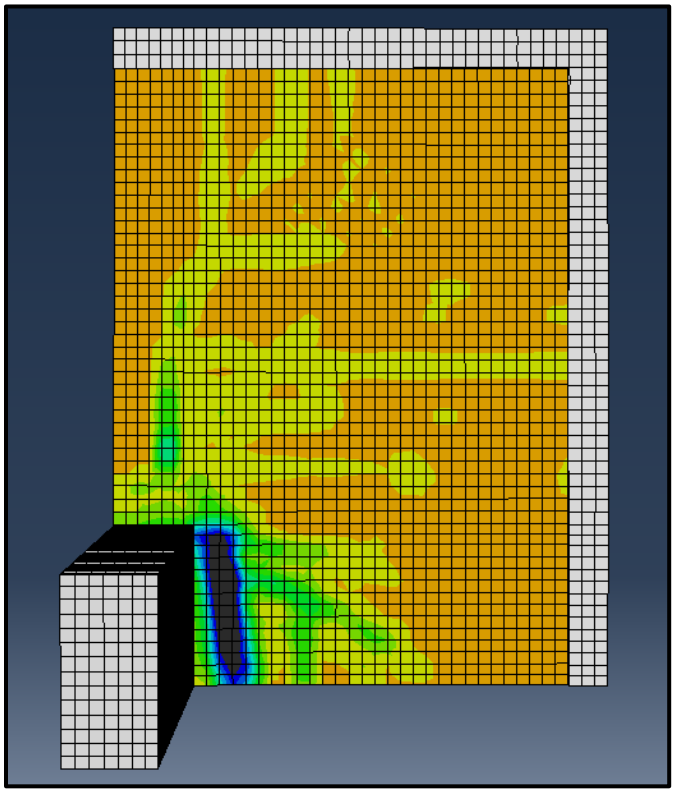

Figure B24: HXXX Tensile Face Crack Pattern

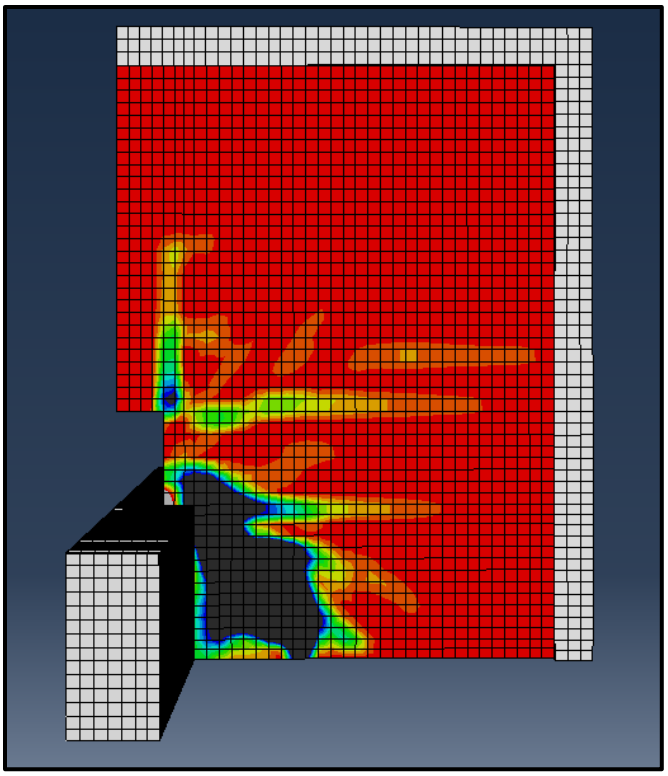

Figure B24: HSF0 Tensile Face Crack Pattern

Key for All SB Models

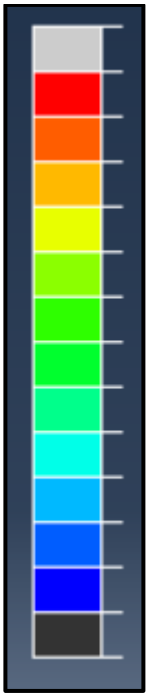

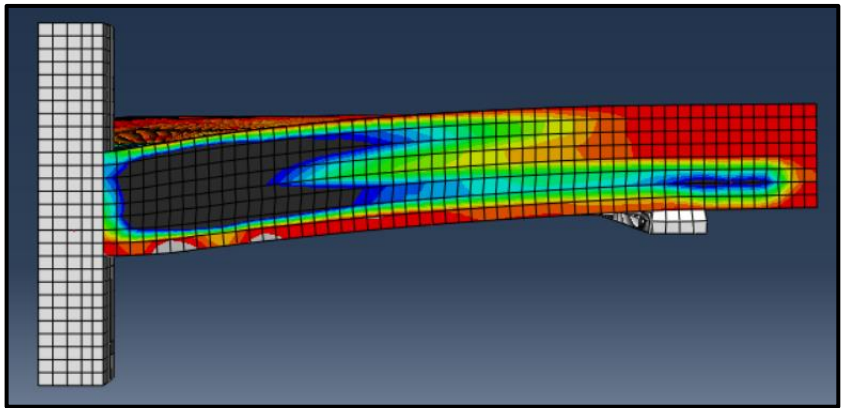

Figure B26: SB1 Post-Failure Side Crack Profile

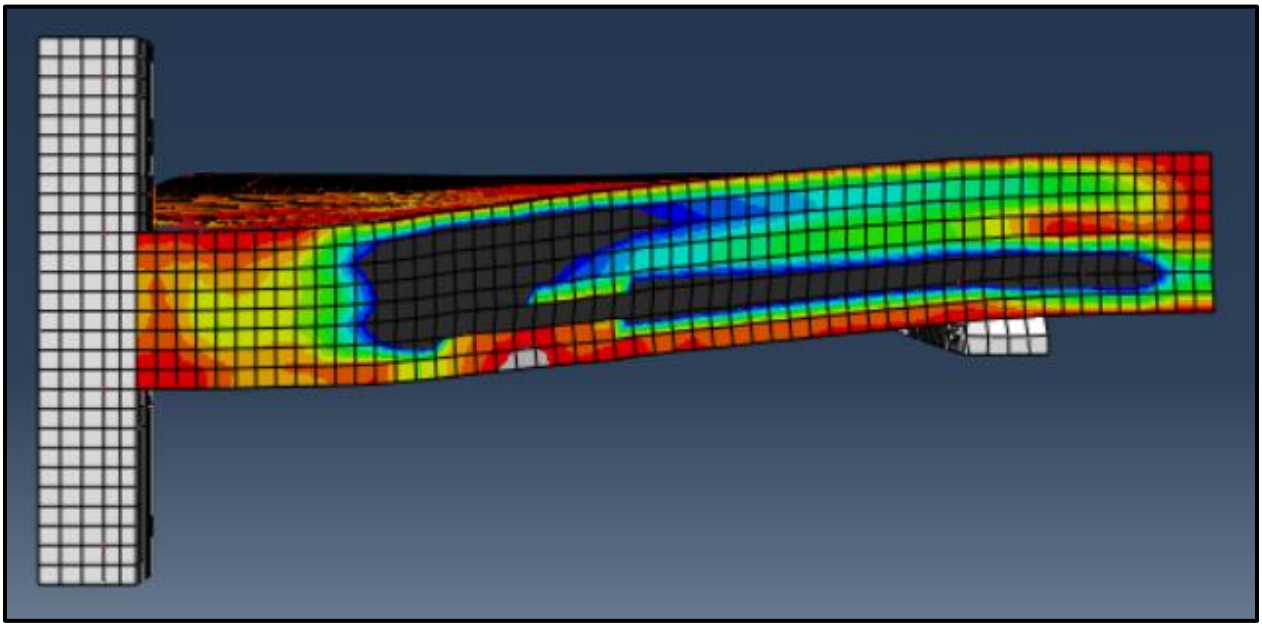

Figure B27: SB2 Post-Failure Side Crack Profile

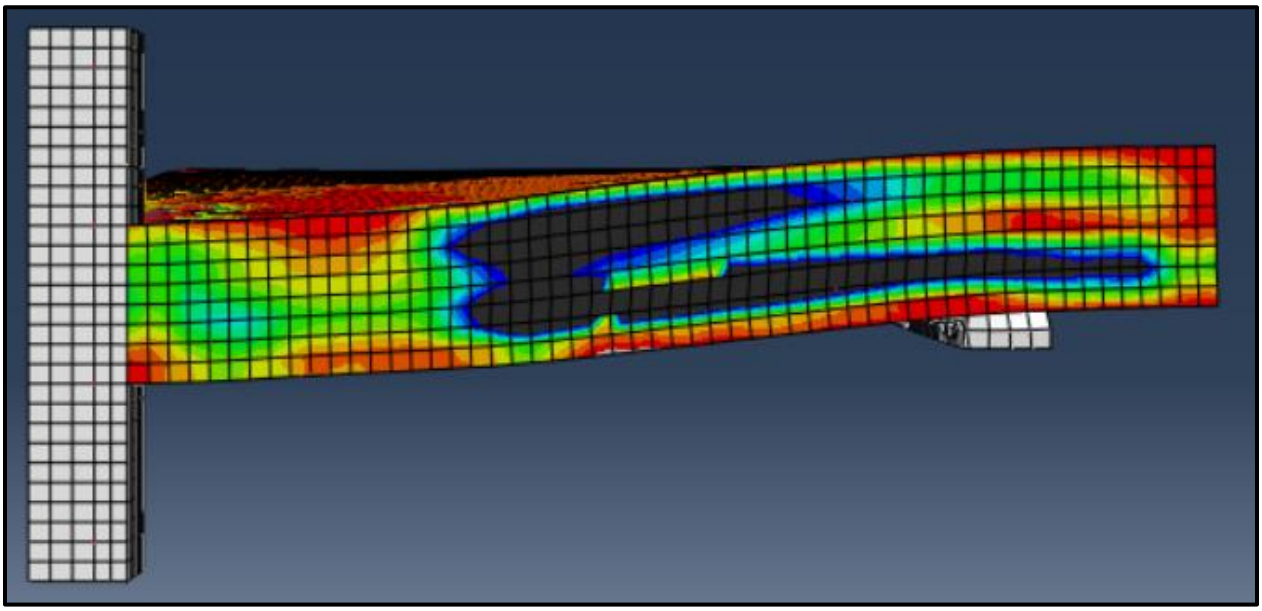

Figure B28: SB3 Post-Failure Side Crack Profile

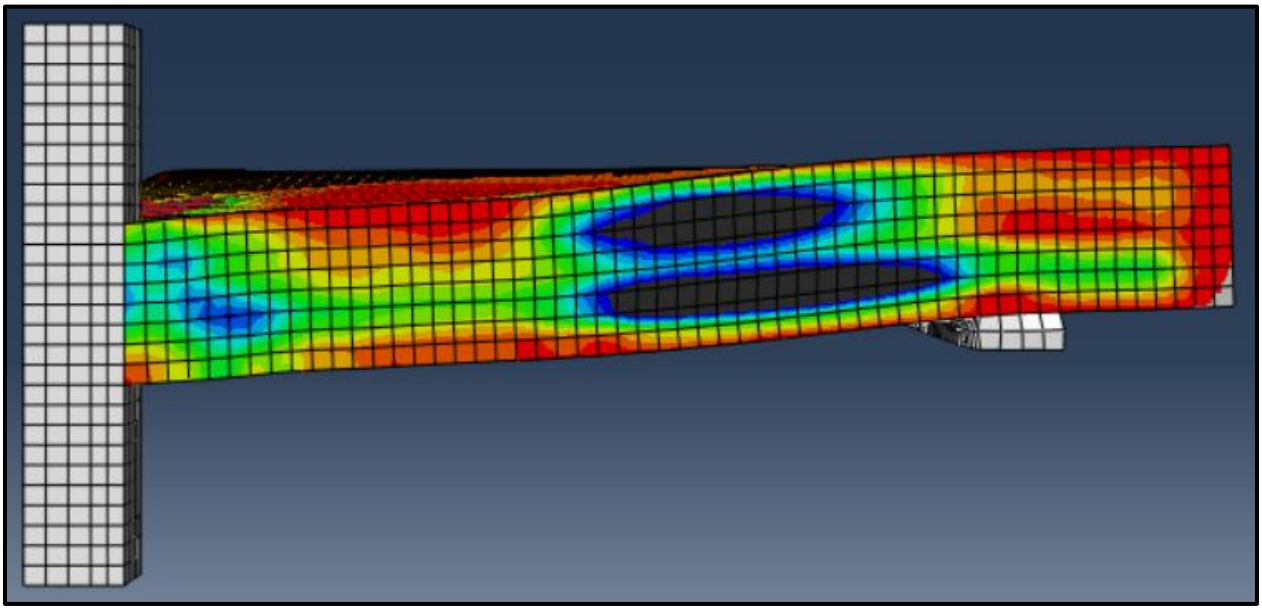

Figure B29: SB4 Post-Failure Side Crack Profile

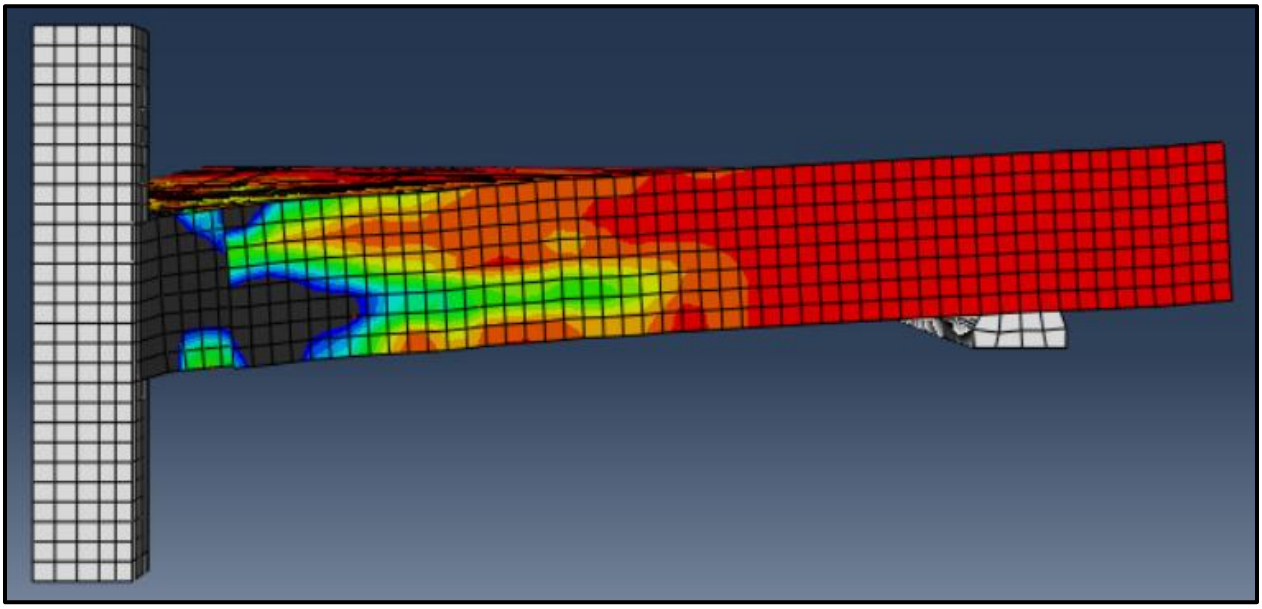

Figure B30: SB4 Post-Failure Side Crack Profile

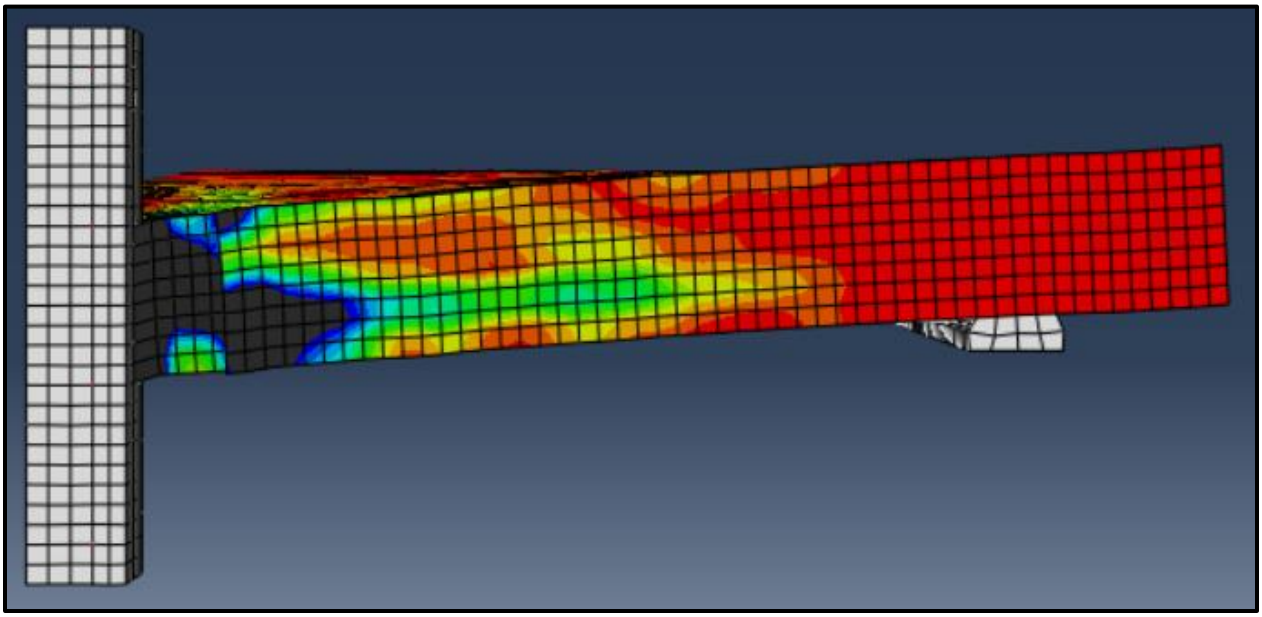

Figure B31: SB6 Post-Failure Side Crack Profile

Key for All SX Models

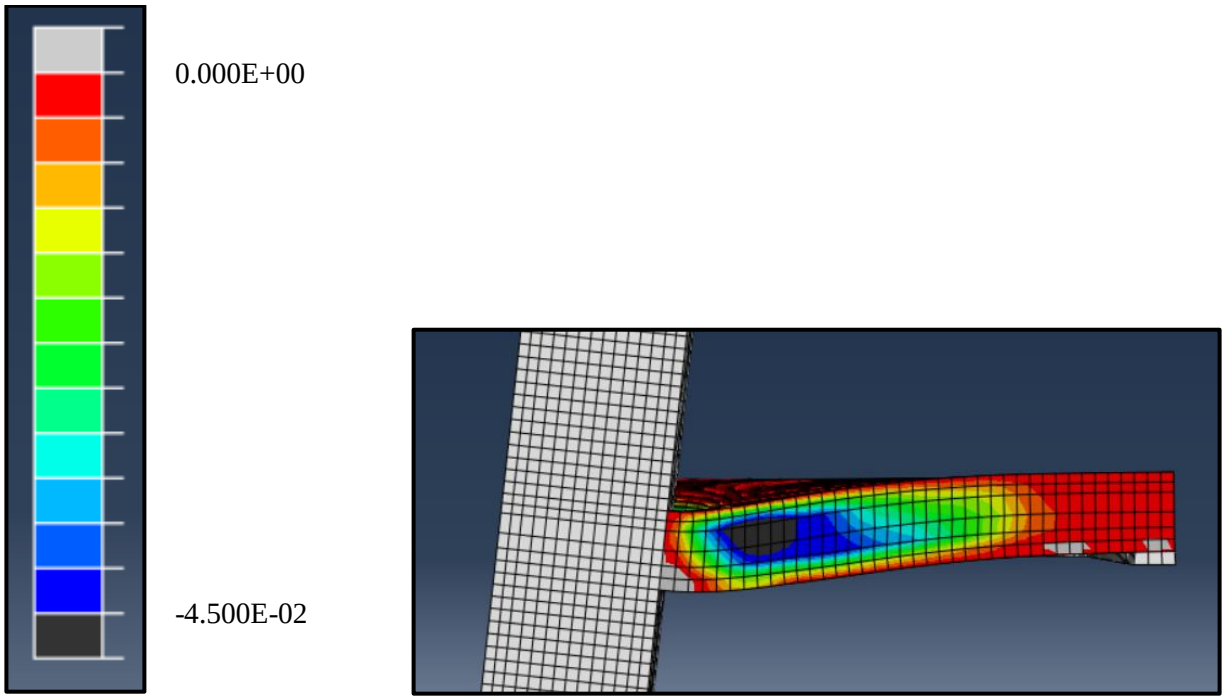

Figure B32: XXX Post-Failure Side Crack Profile

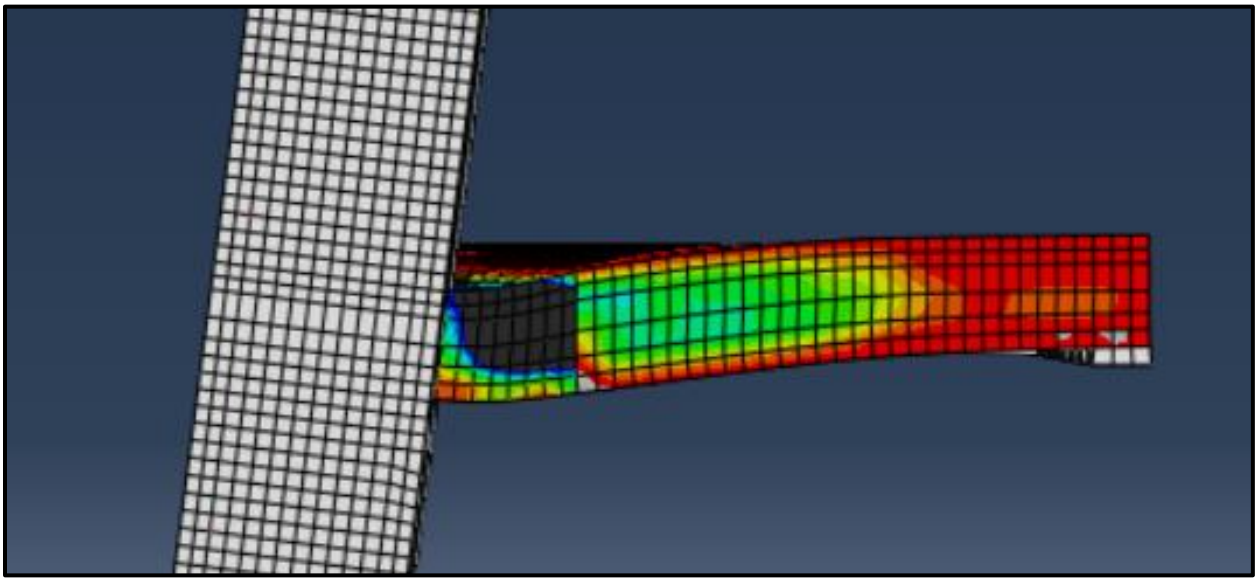

Figure B33: SF0 Post-Failure Side Crack Profile

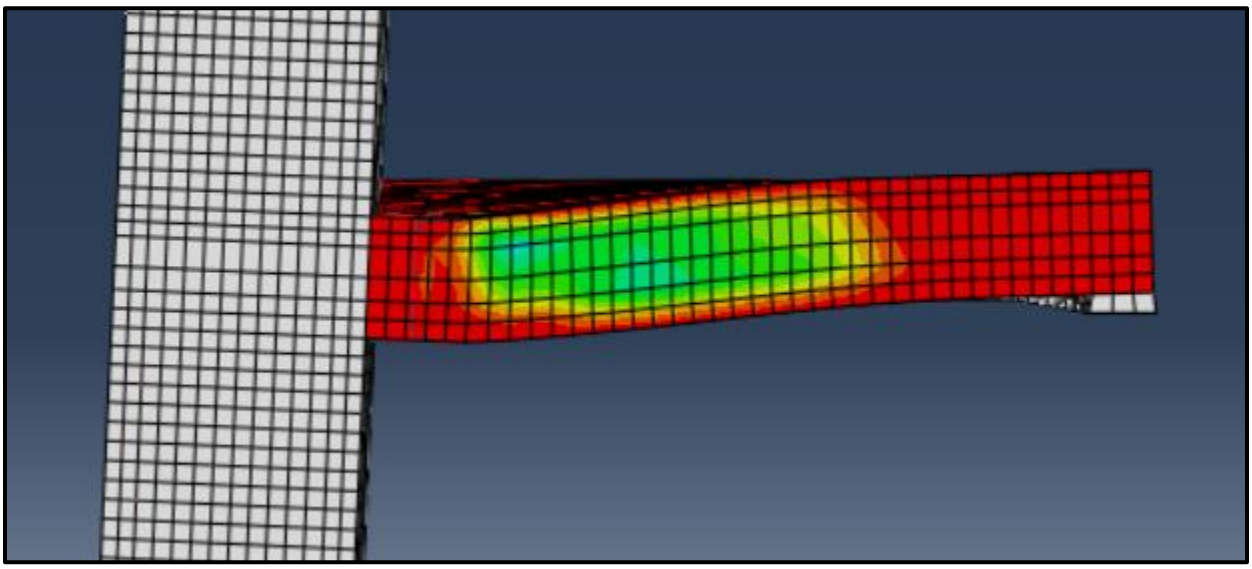

Figure B34: SX-1SR Post-Failure Side Crack Profile

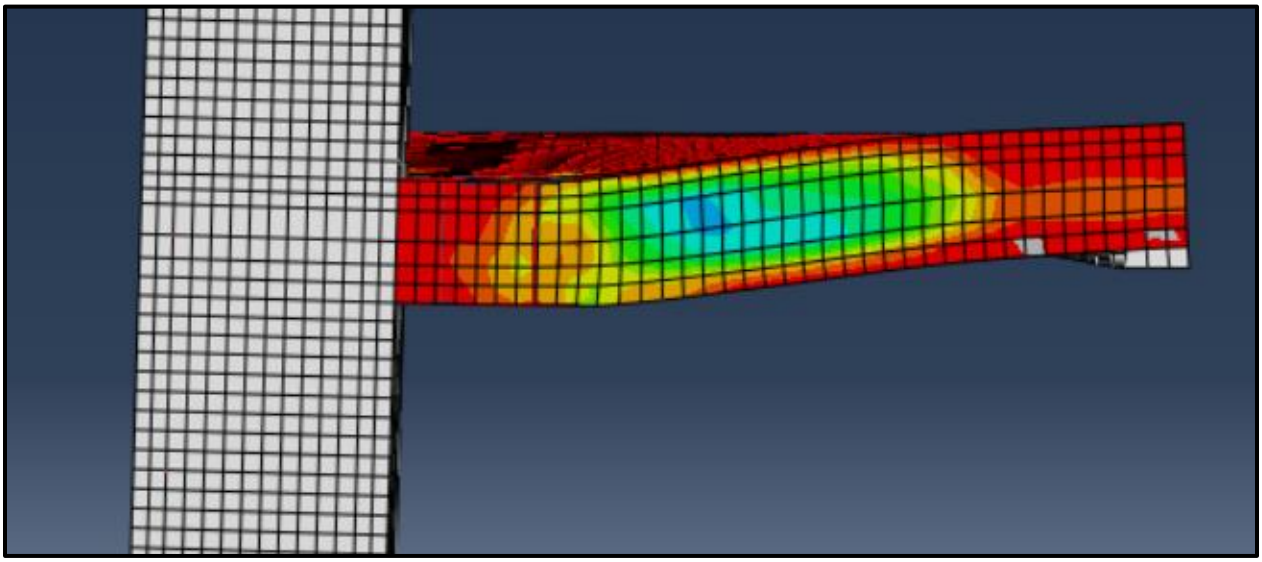

Figure B35: SX-2SR Post-Failure Side Crack Profile

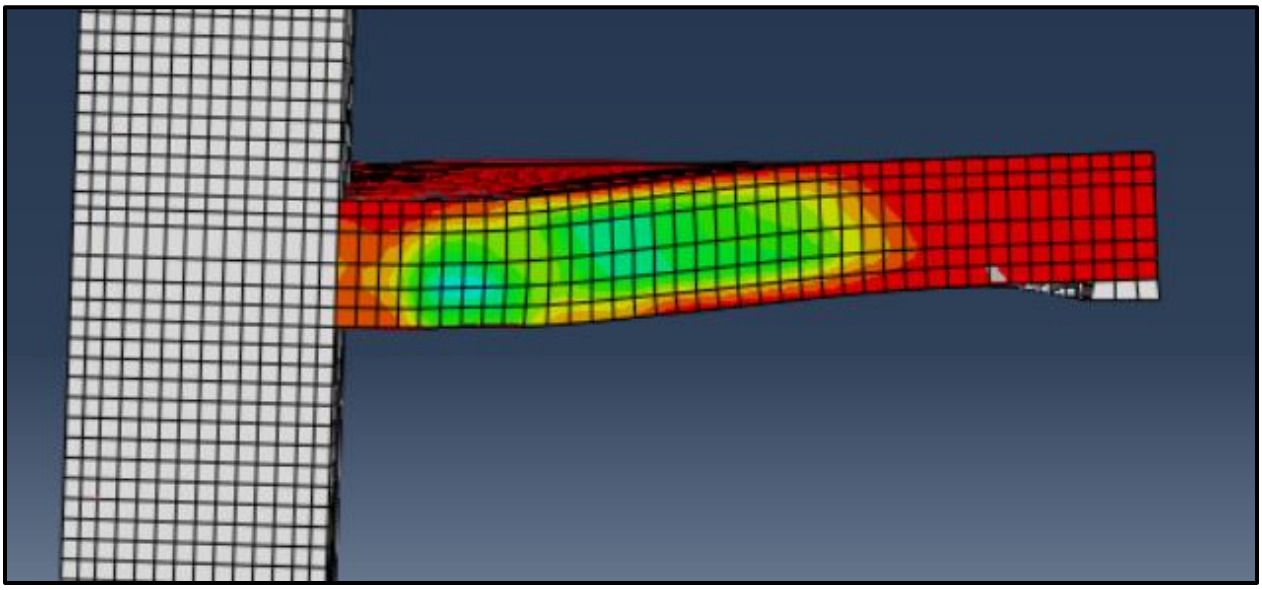

Figure B36: SX-2SB Post-Failure Side Crack Profile

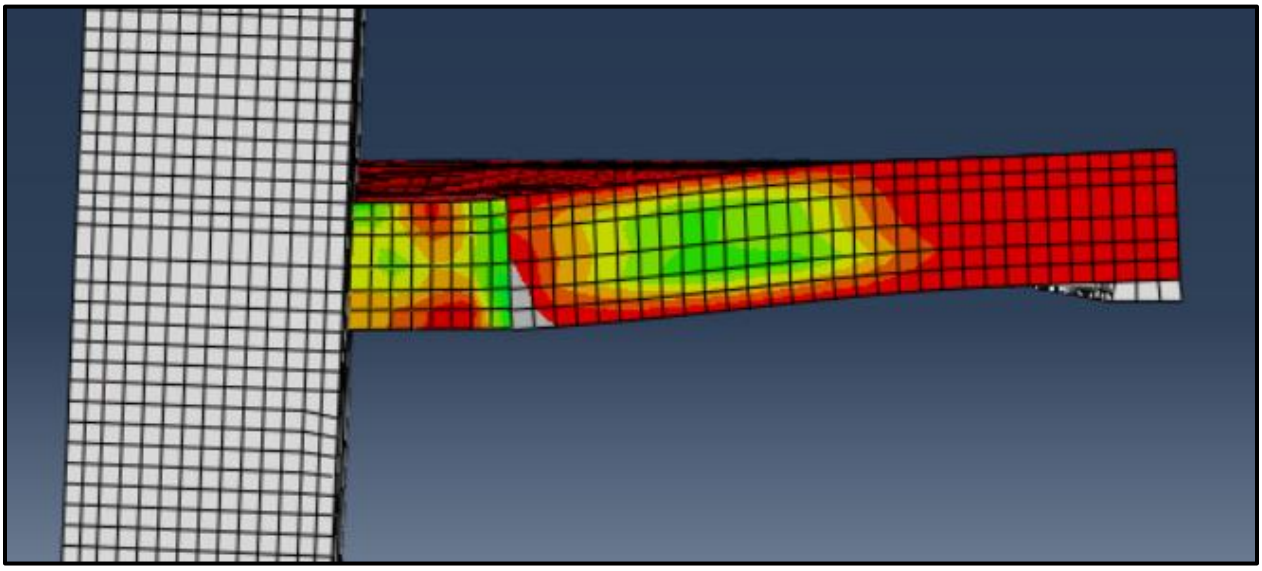

Figure B37: SH-2SR Post-Failure Side Crack Profile

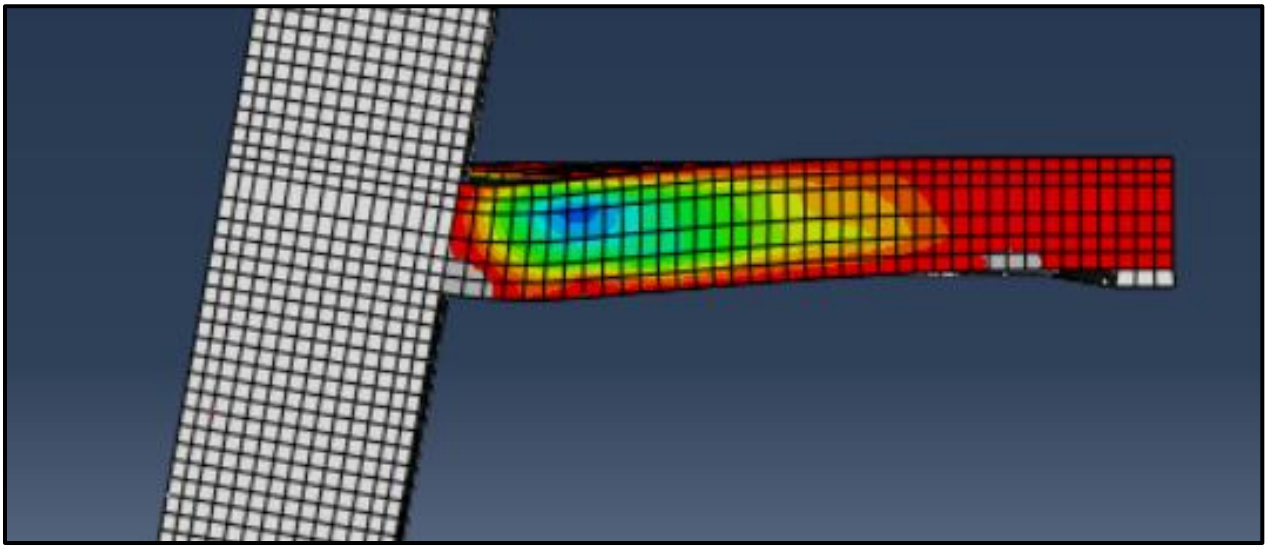

Figure B38: HXXX Post-Failure Side Crack Profile

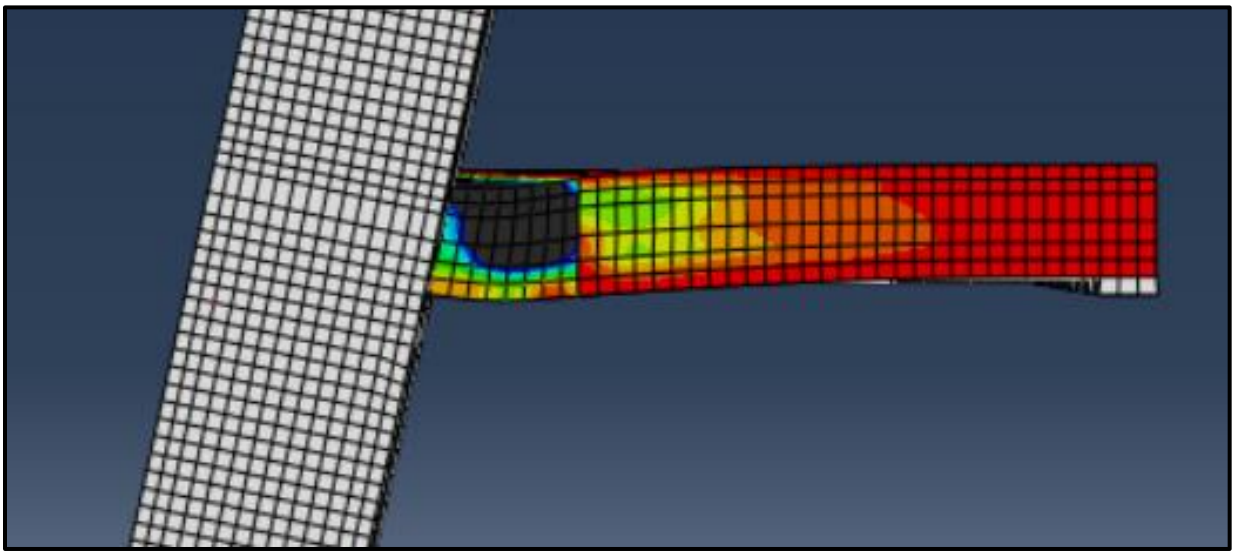

Figure B39: HSF0 Post-Failure Side Crack Profile

Appendix C: Shear Reinforcement Spacing Study Supplemental Figures

List of Figures

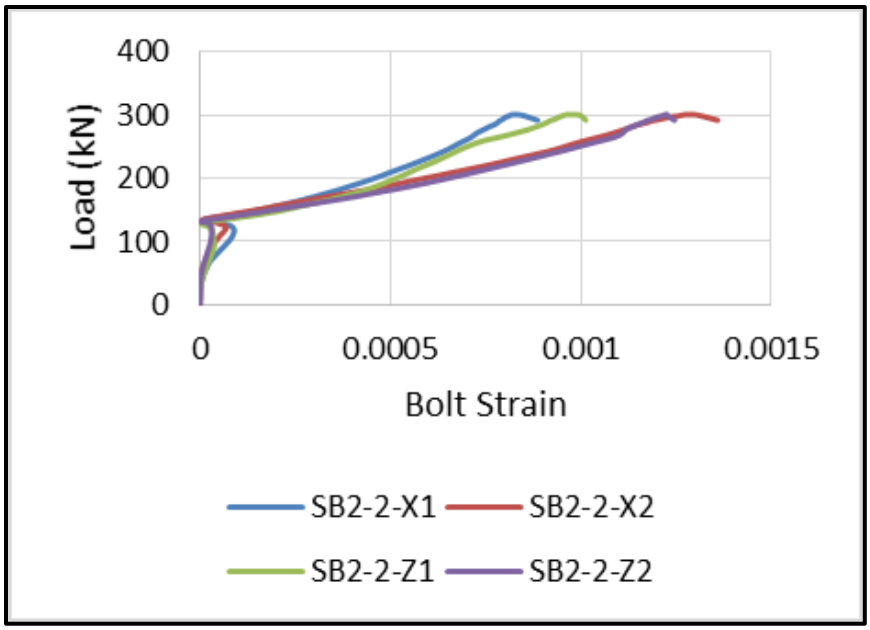

Figure C1: SB2-2 Bolt Strain Diagram

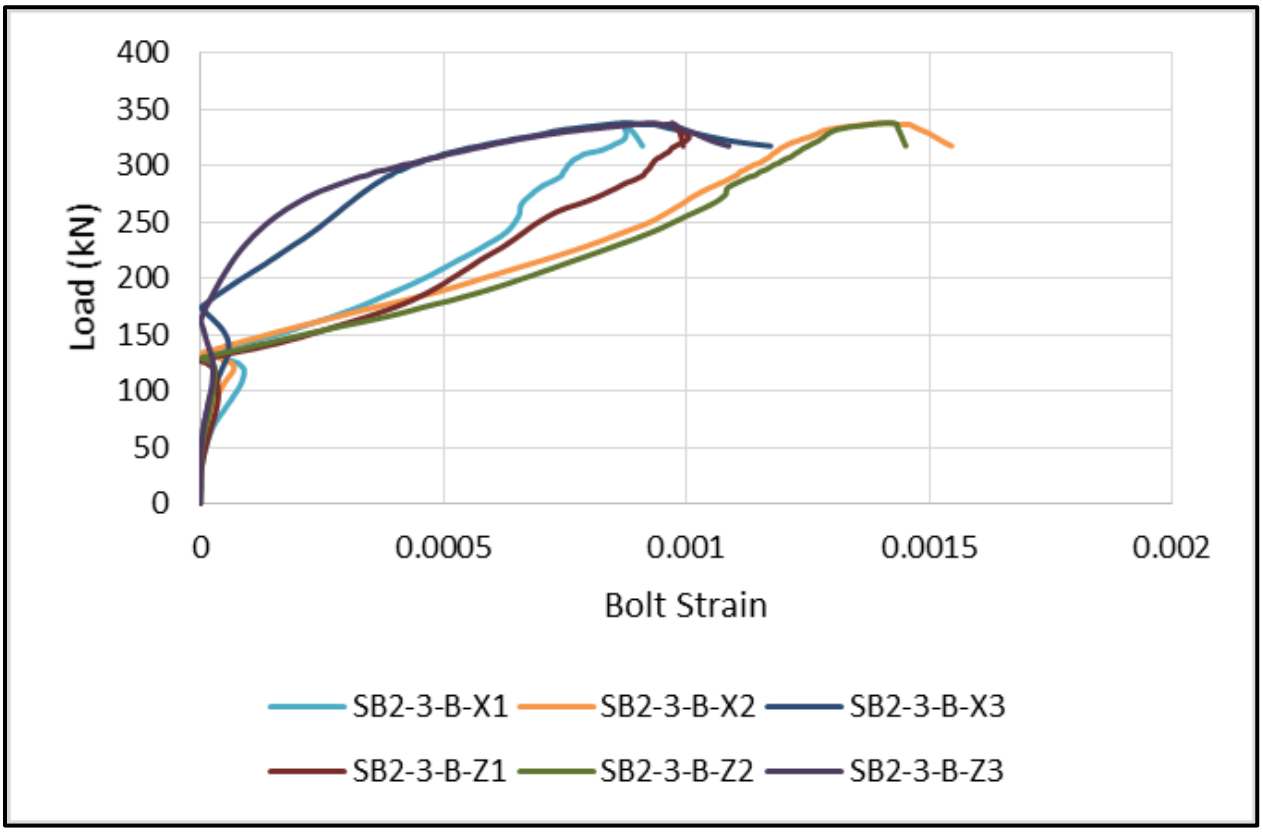

Figure C2: SB2-3-B Bolt Strain Diagram

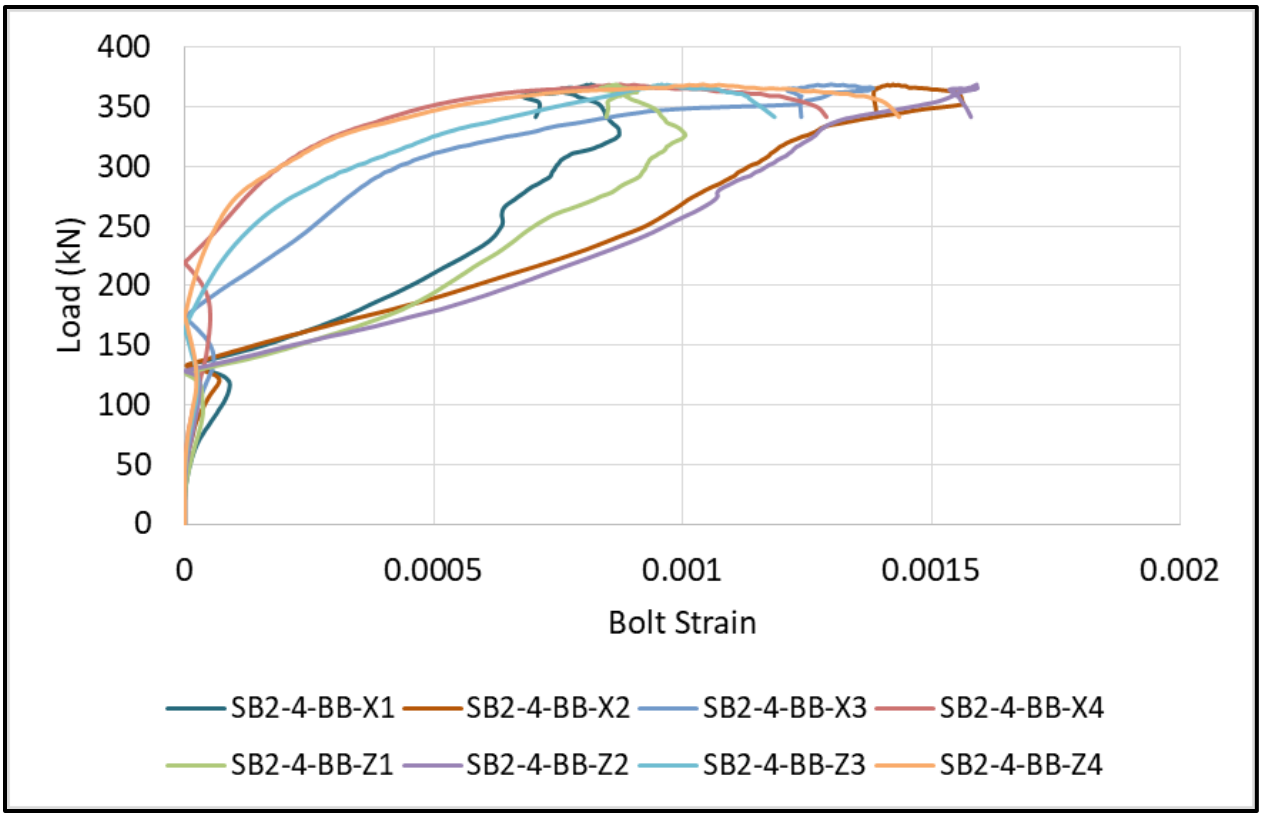

Figure C3: SB2-4-BB Bolt Strain Diagram

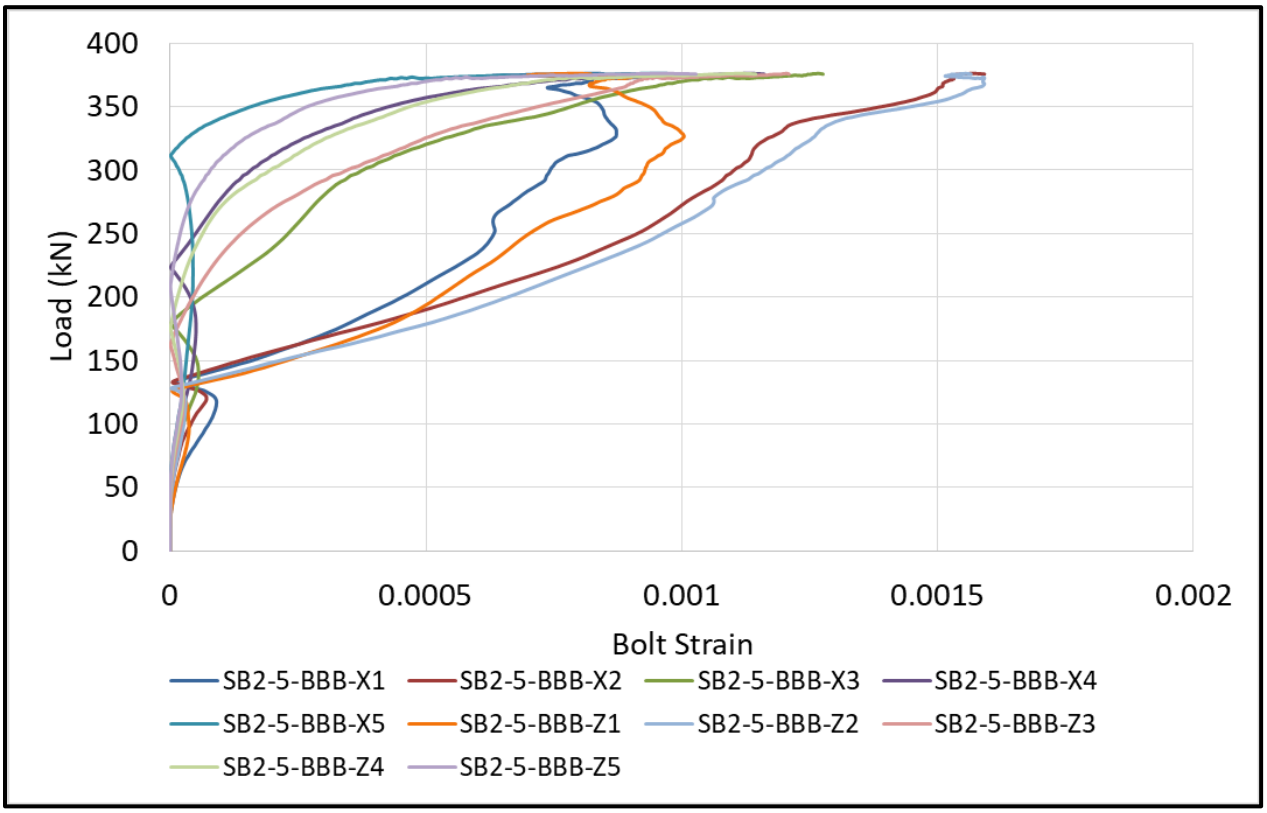

Figure C4: SB2-5-BBB Bolt Strain Diagram

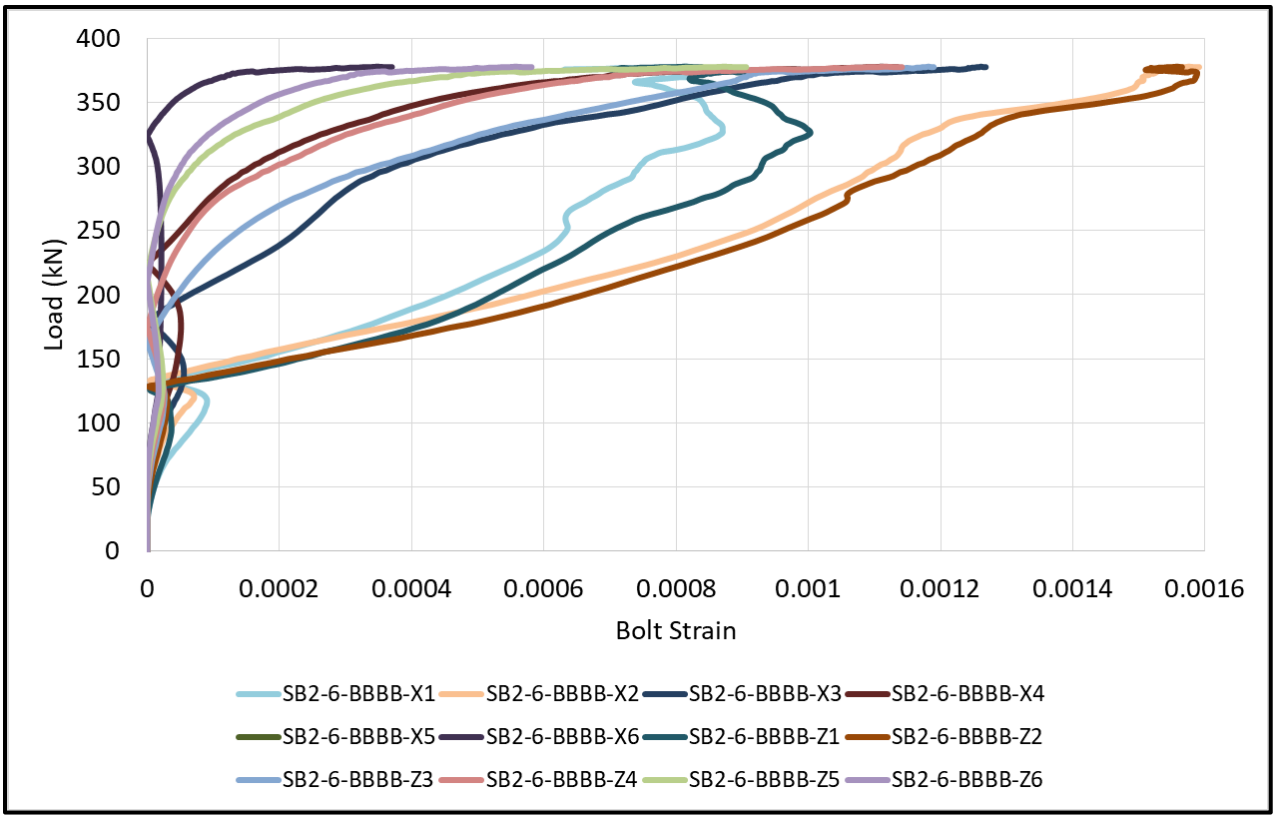

Figure C5: SB2-6-BBBB Bolt Strain Diagram

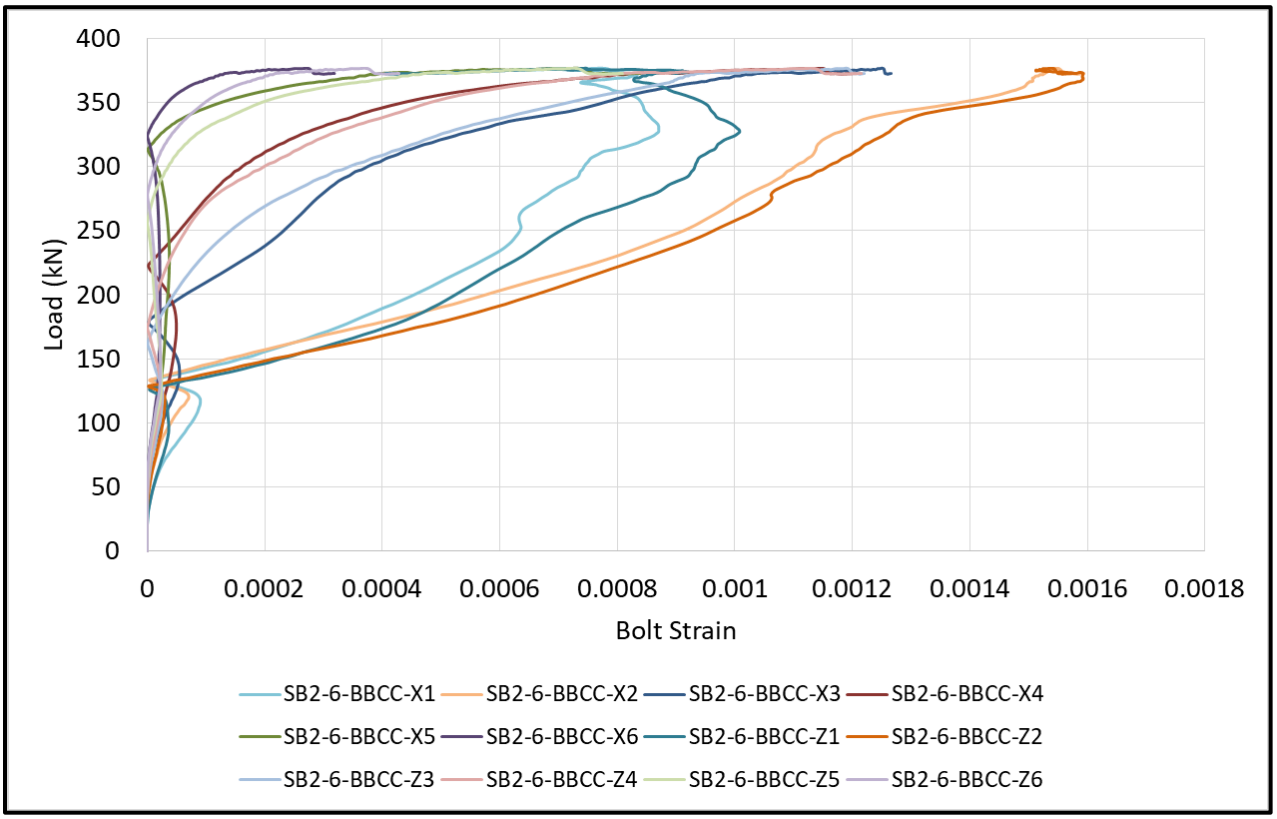

Figure C6: SB2-6-BBCC Bolt Strain Diagram

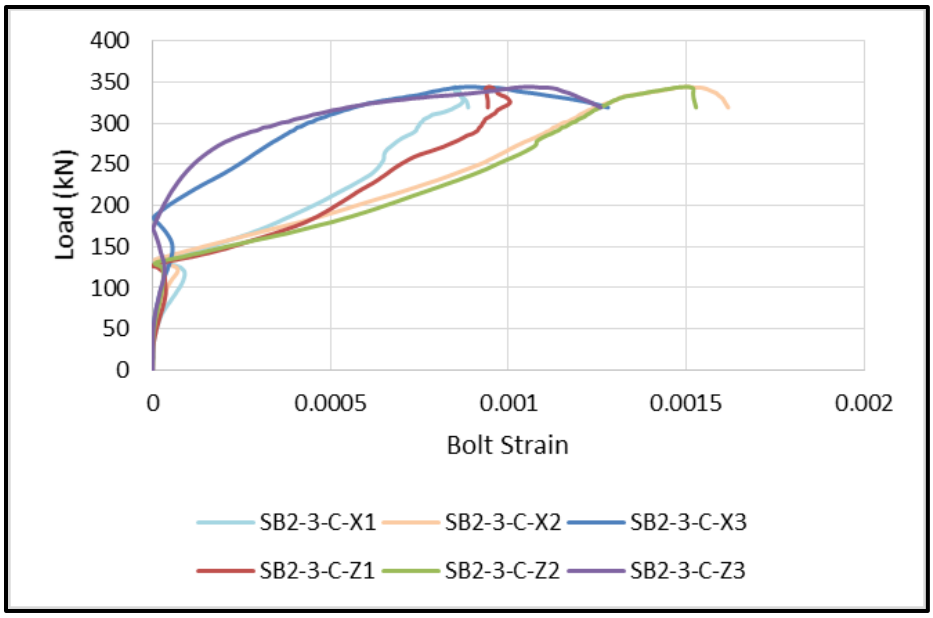

Figure C7: SB2-3-C Bolt Strain Diagram

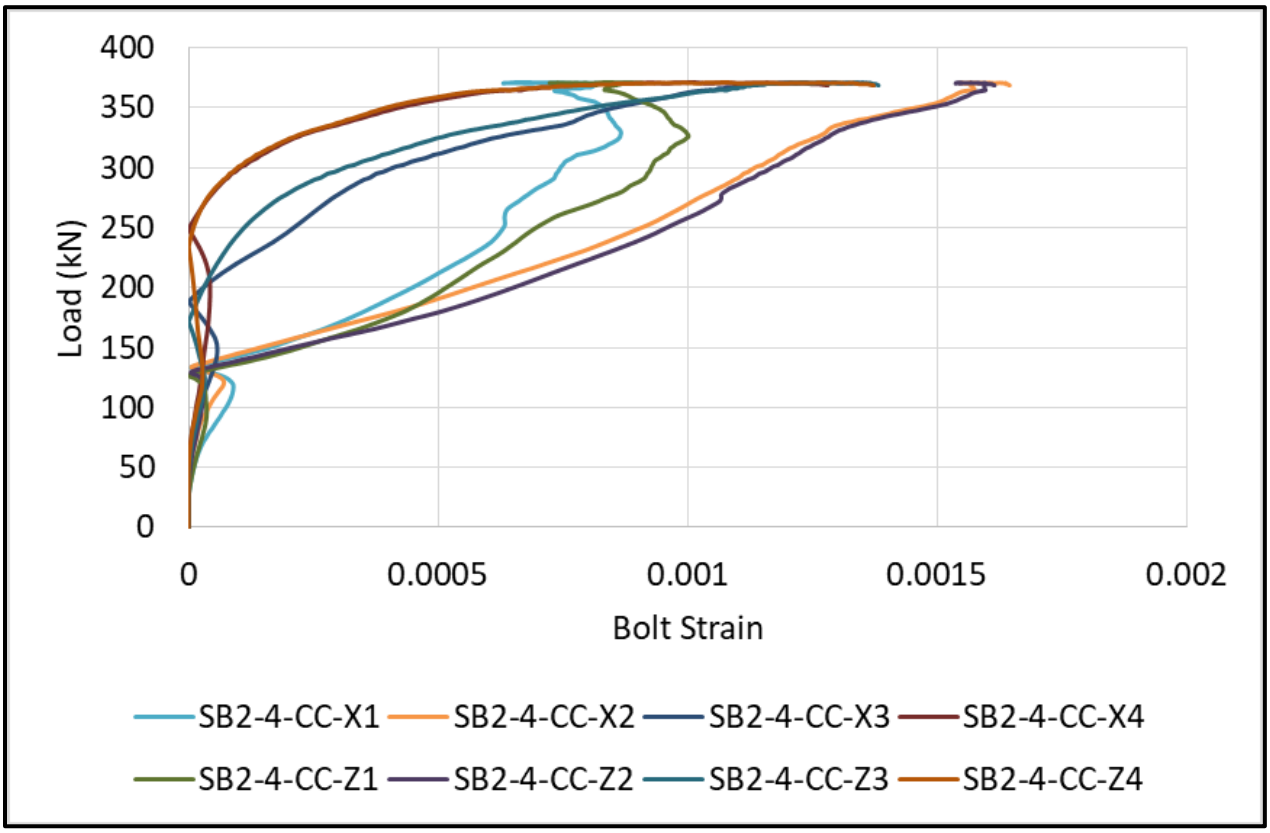

Figure C8: SB2-4-CC Bolt Strain Diagram

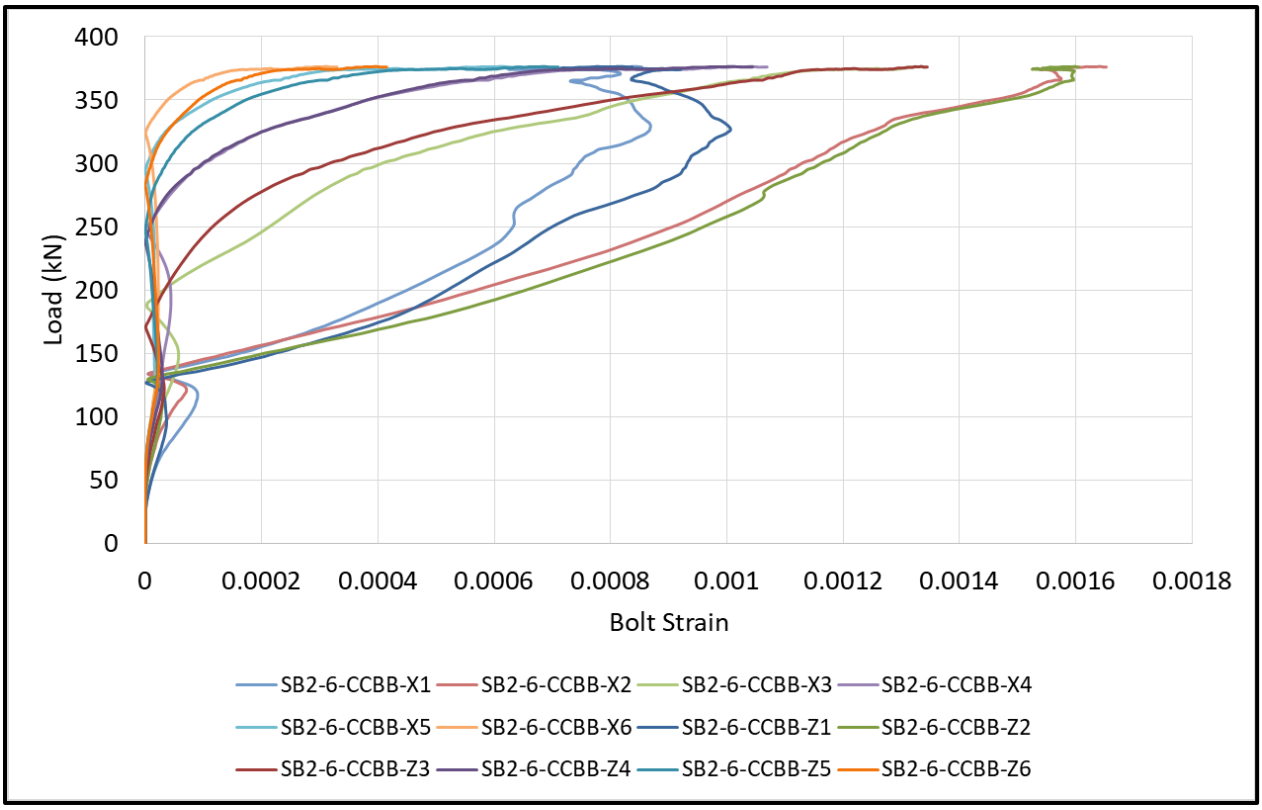

Figure C9: SB2-6-CCBB Bolt Strain Diagram

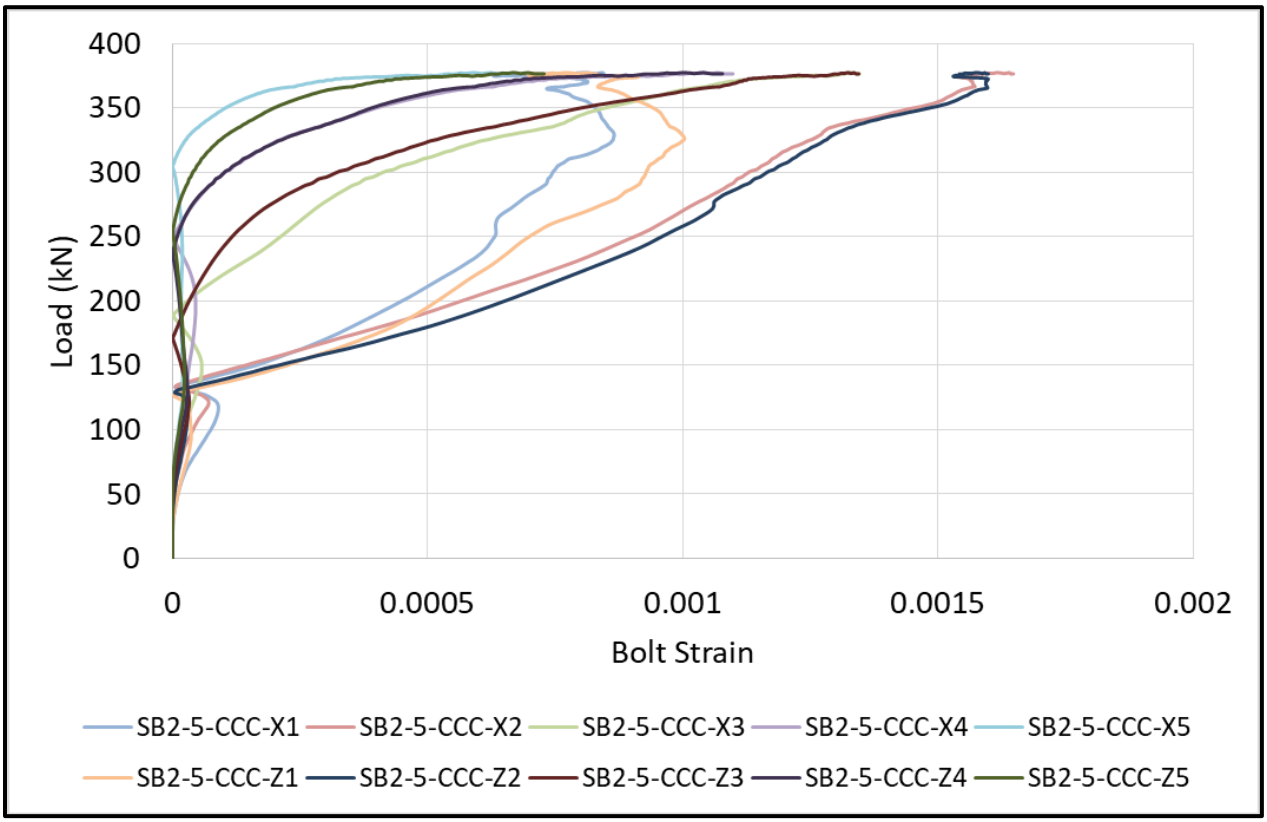

Figure C10: SB2-5-CCC Bolt Strain Diagram

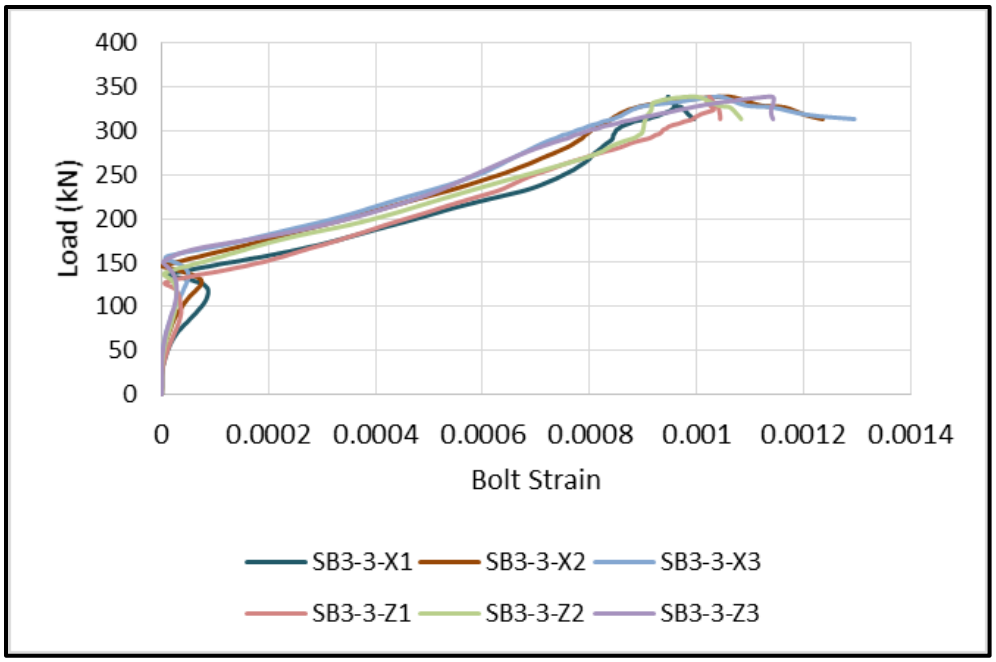

Figure C11: SB3-3 Bolt Strain Diagram

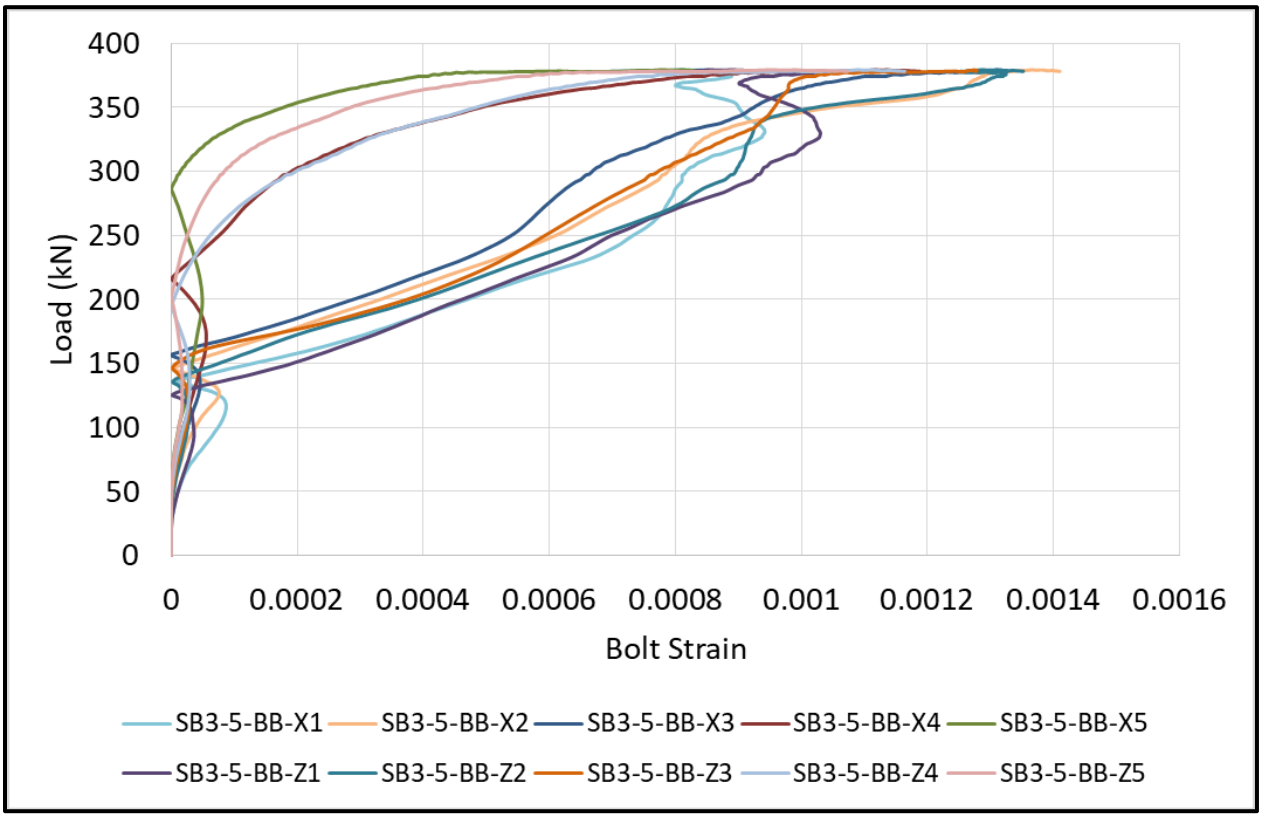

Figure C12: SB3-5-BB Bolt Strain Diagram

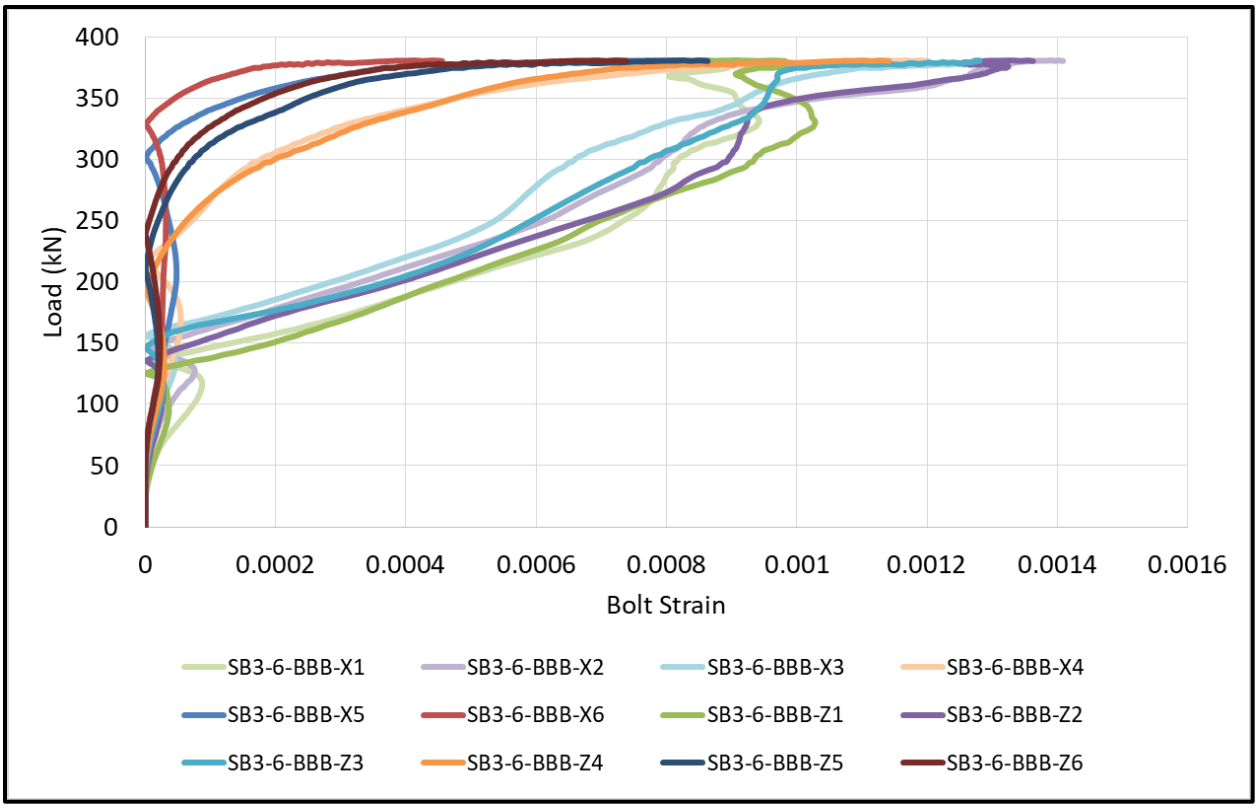

Figure C13: SB3-6-BBB Bolt Strain Diagram

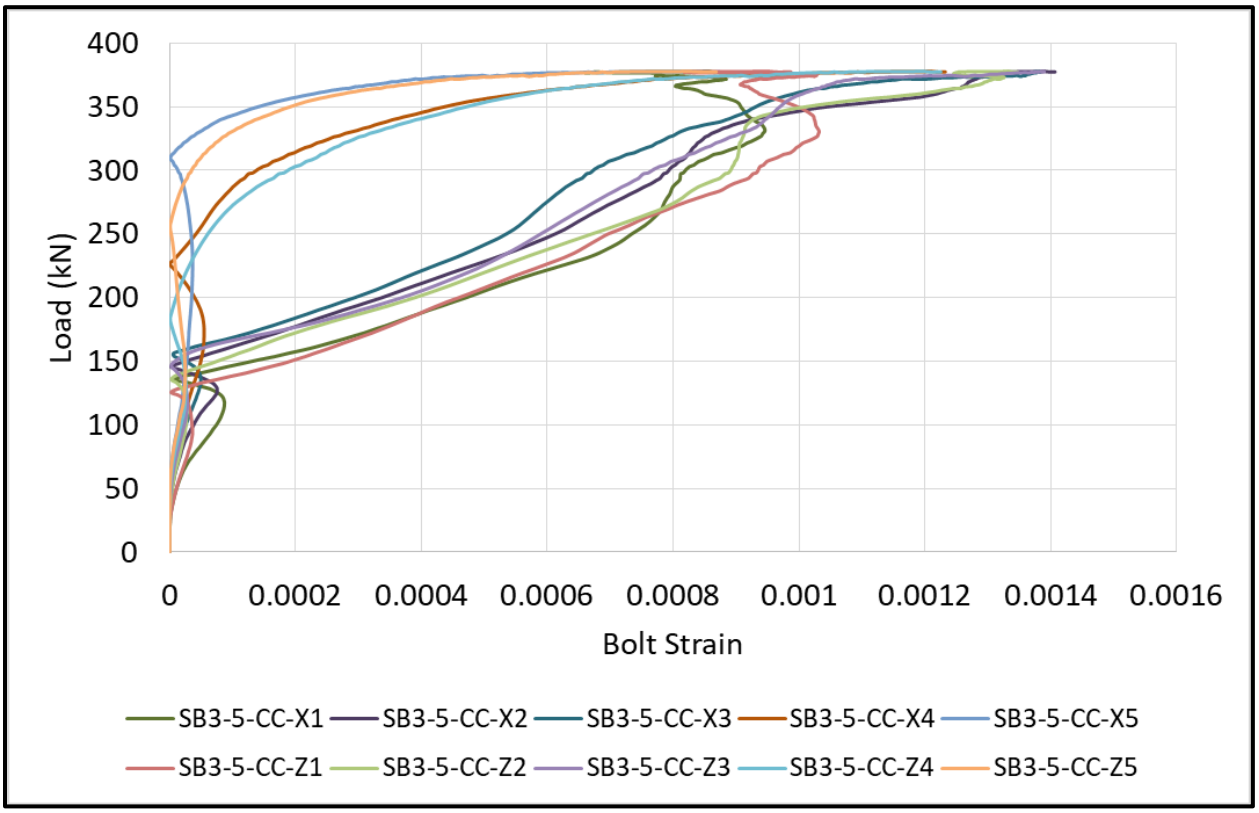

Figure C14: SB3-5-CC Bolt Strain Diagram

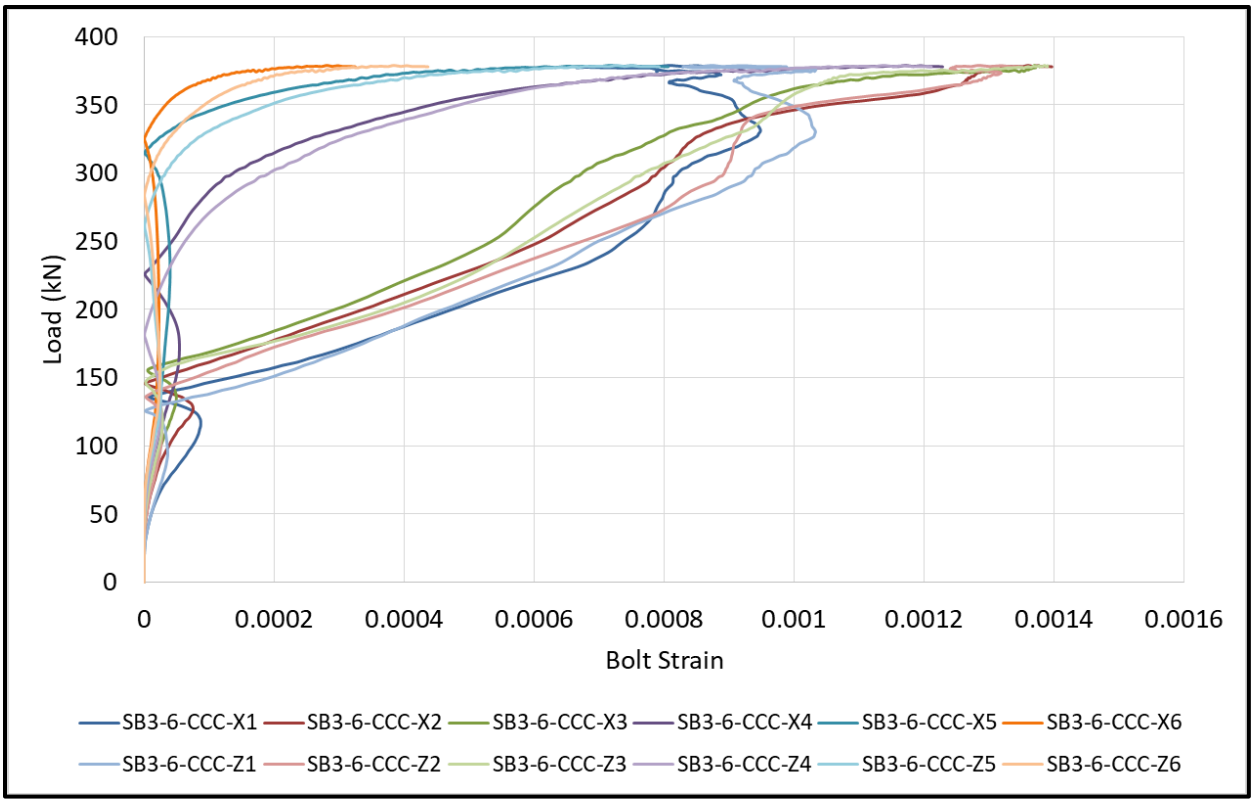

Figure C15: SB3-6-CCC Bolt Strain Diagram

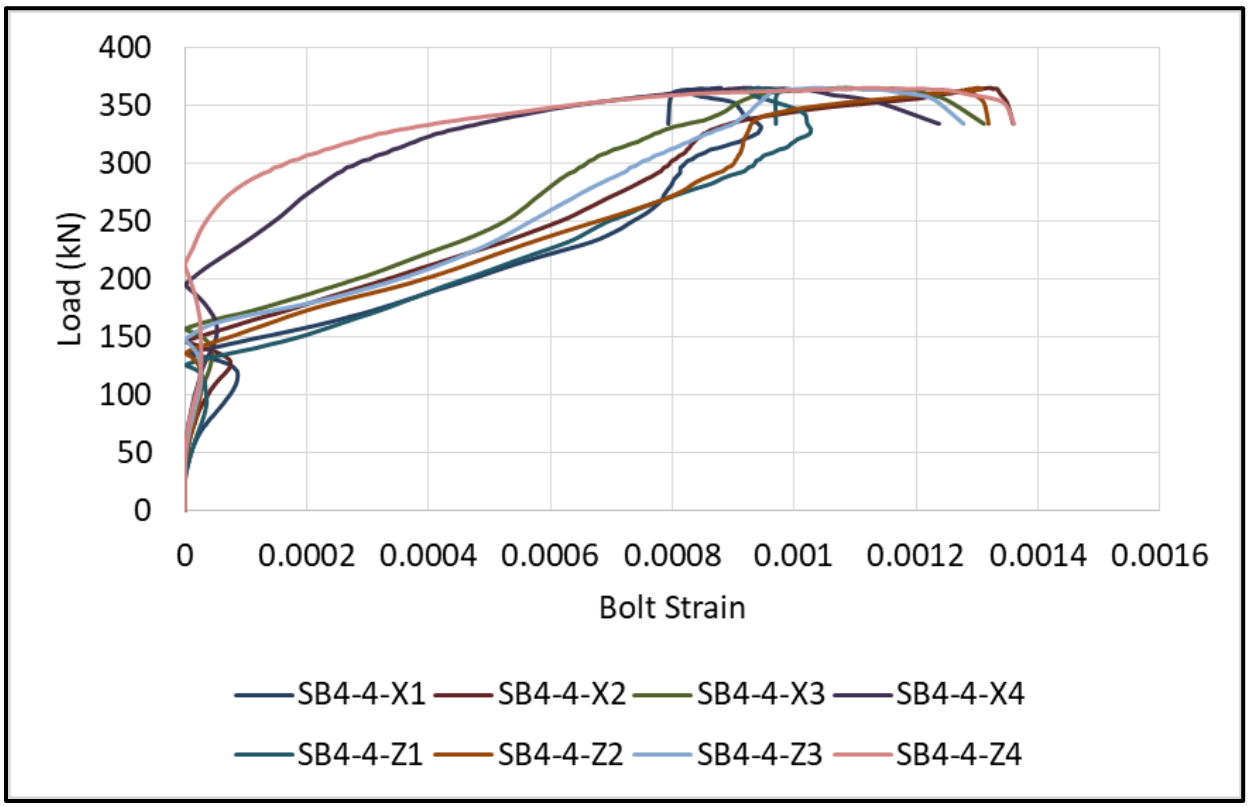

Figure C16: SB4-4 Bolt Strain Diagram

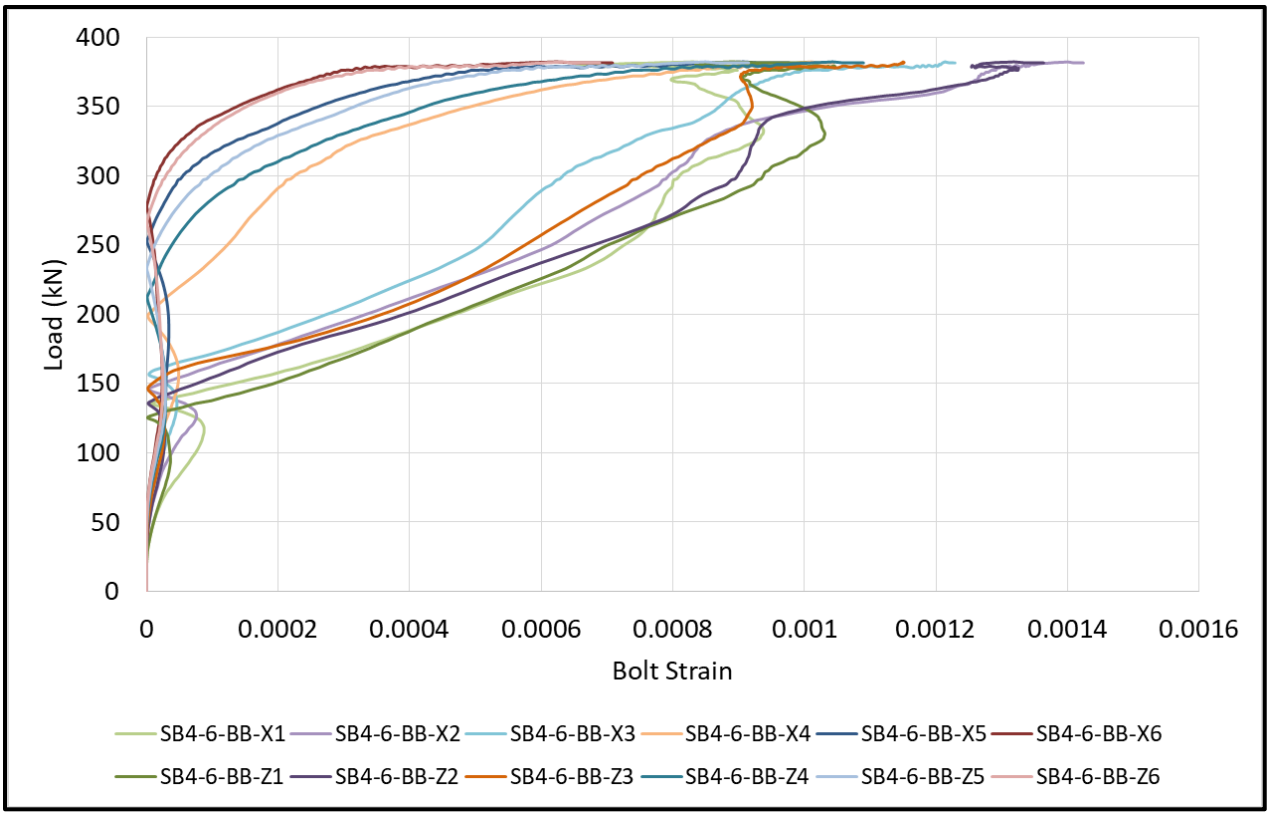

Figure C17: SB4-6-BB Bolt Strain Diagram

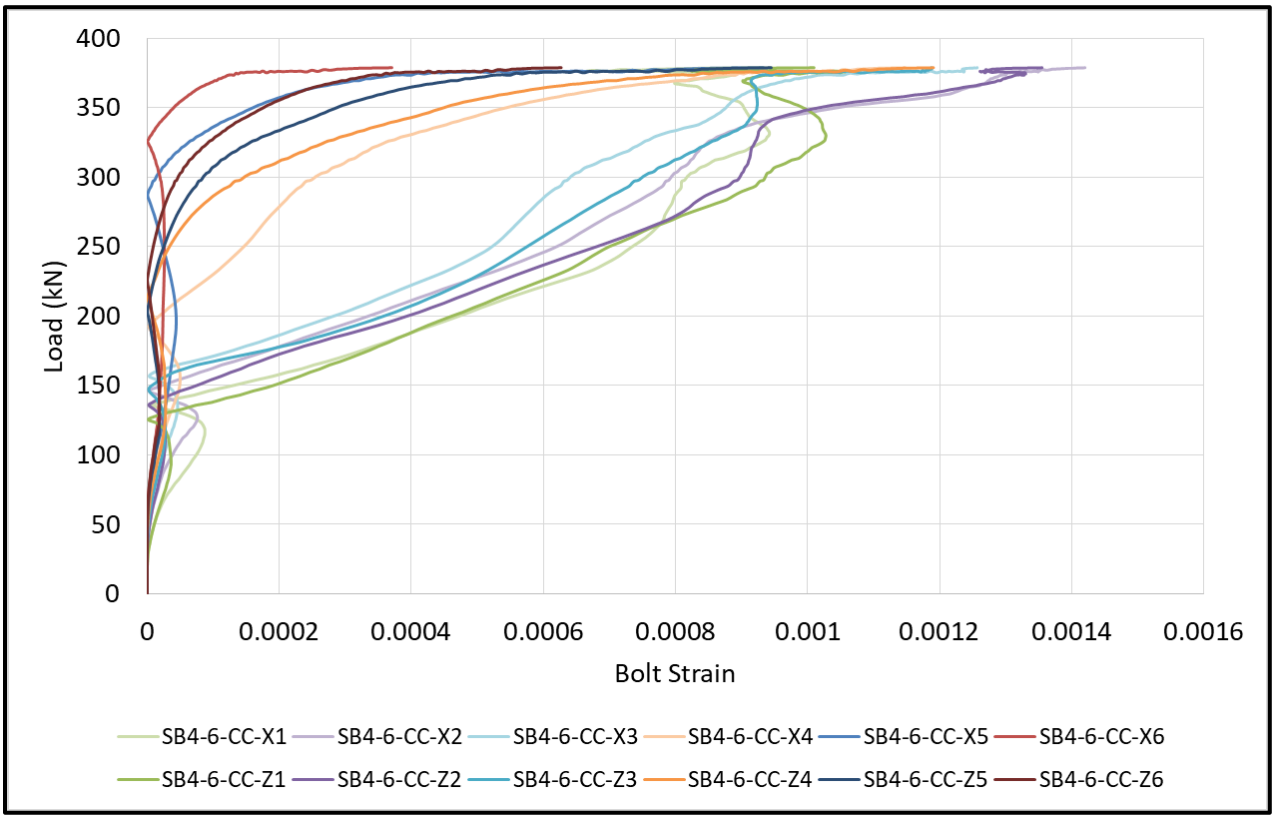

Figure C18: SB4-6-CC Bolt Strain Diagram

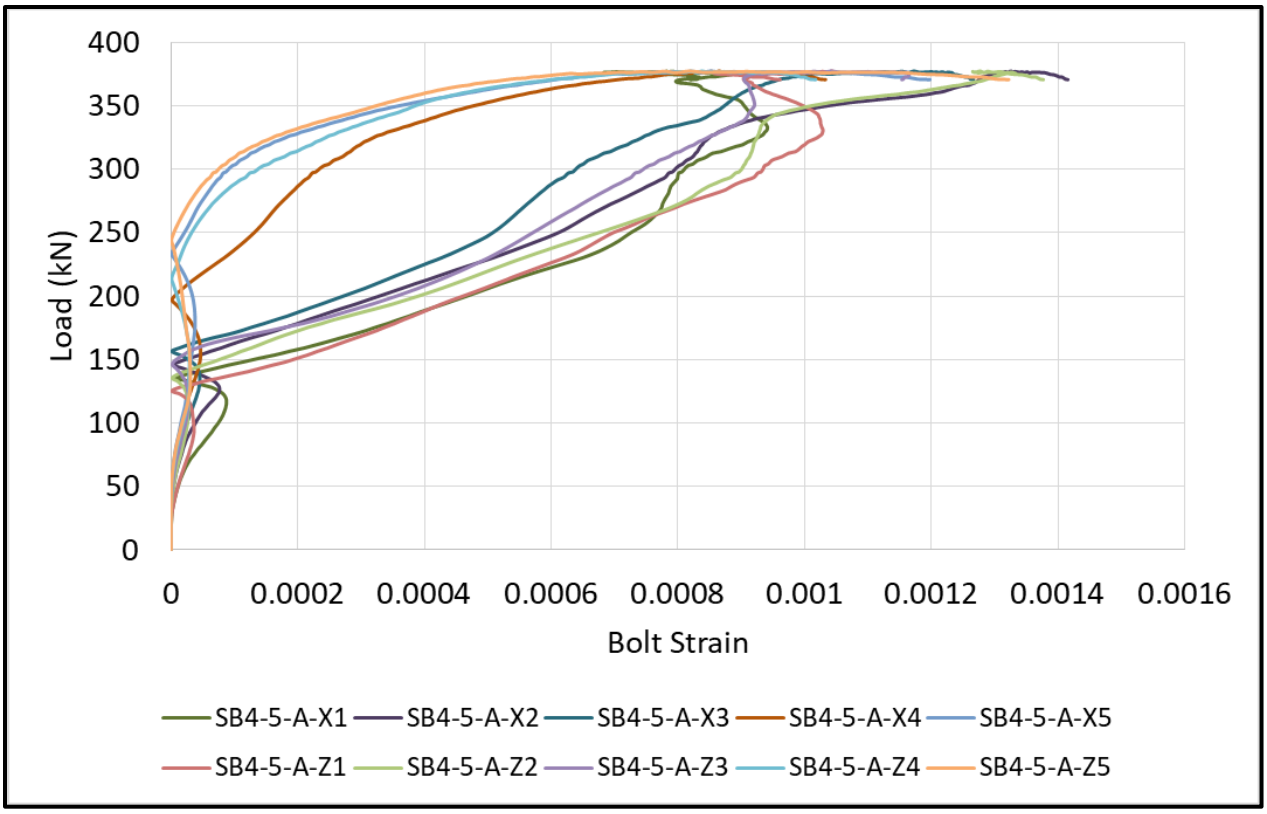

Figure C19: SB4-5-A Bolt Strain Diagram

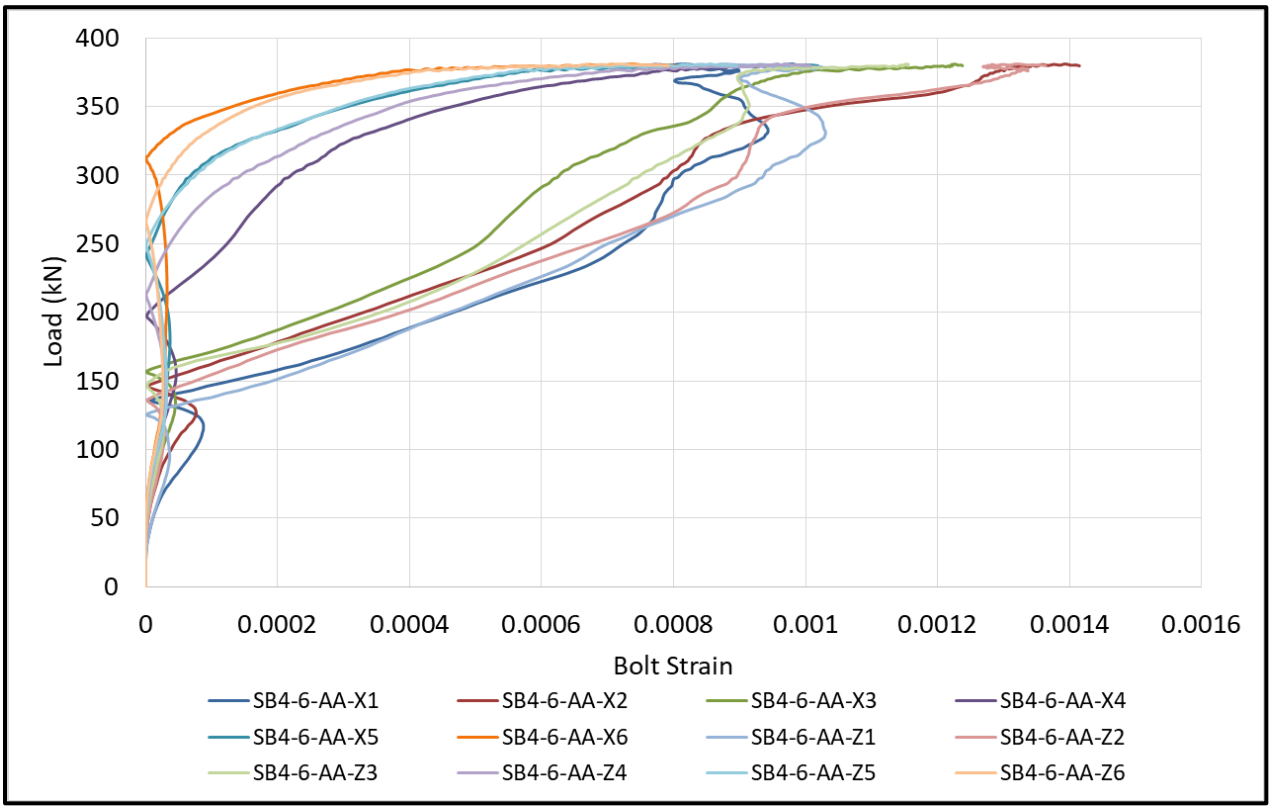

Figure C20: SB4-6-AA Bolt Strain Diagram

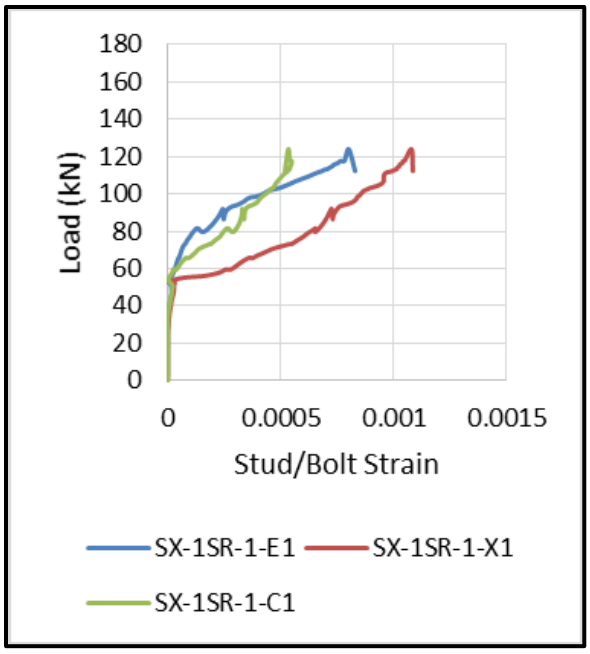

Figure C21: SX-1SR-1 Stud Strain Diagram

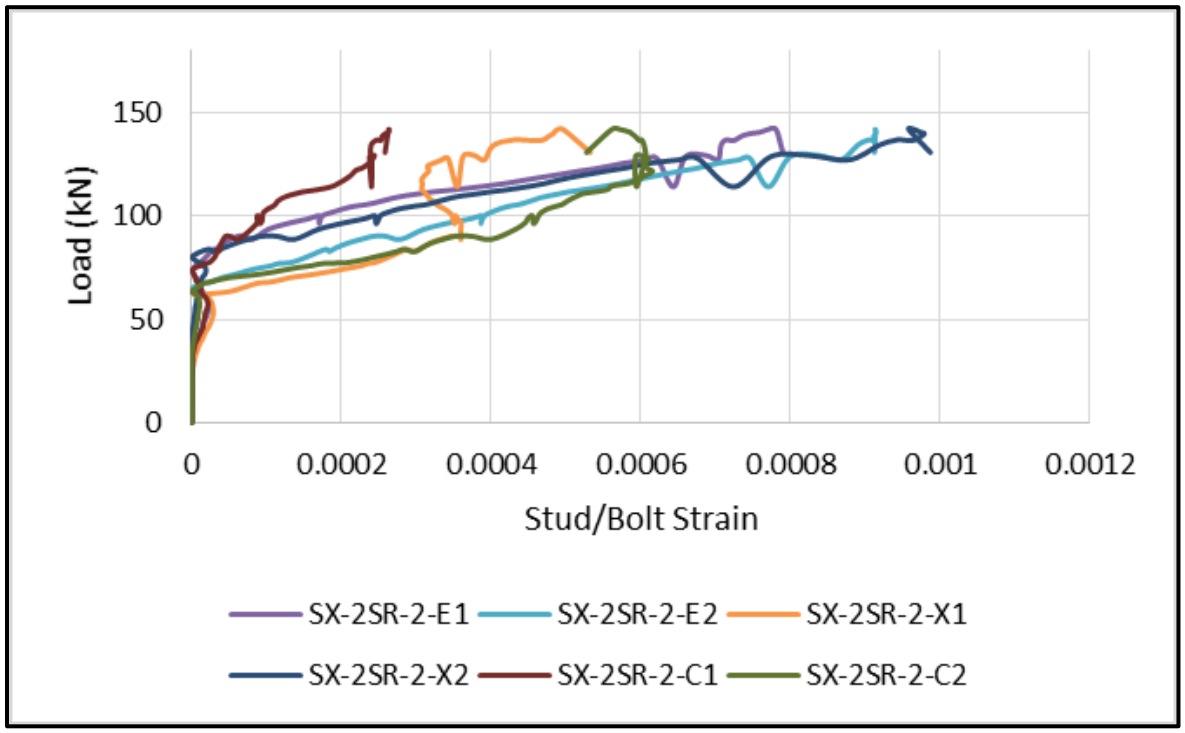

Figure C22: SX-2SR-2 Stud Strain Diagram

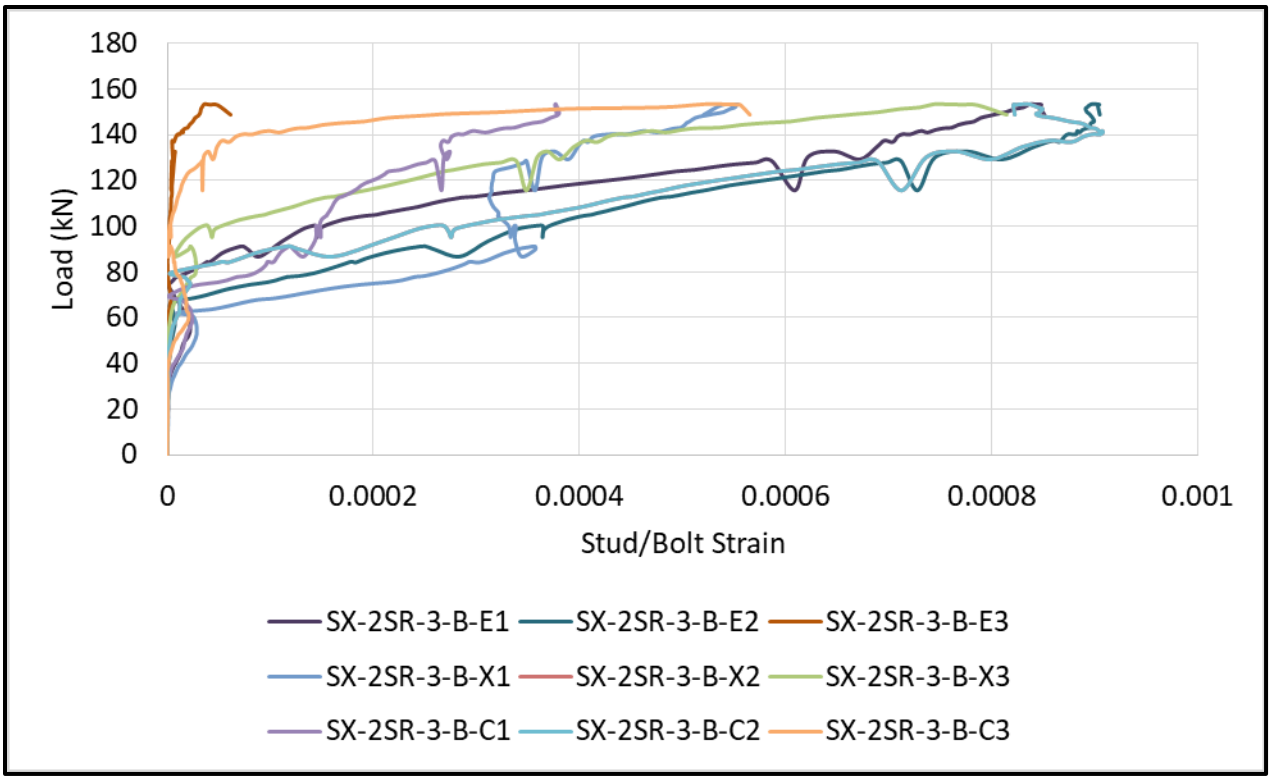

Figure C23: SX-2SR-3-B Stud Strain Diagram

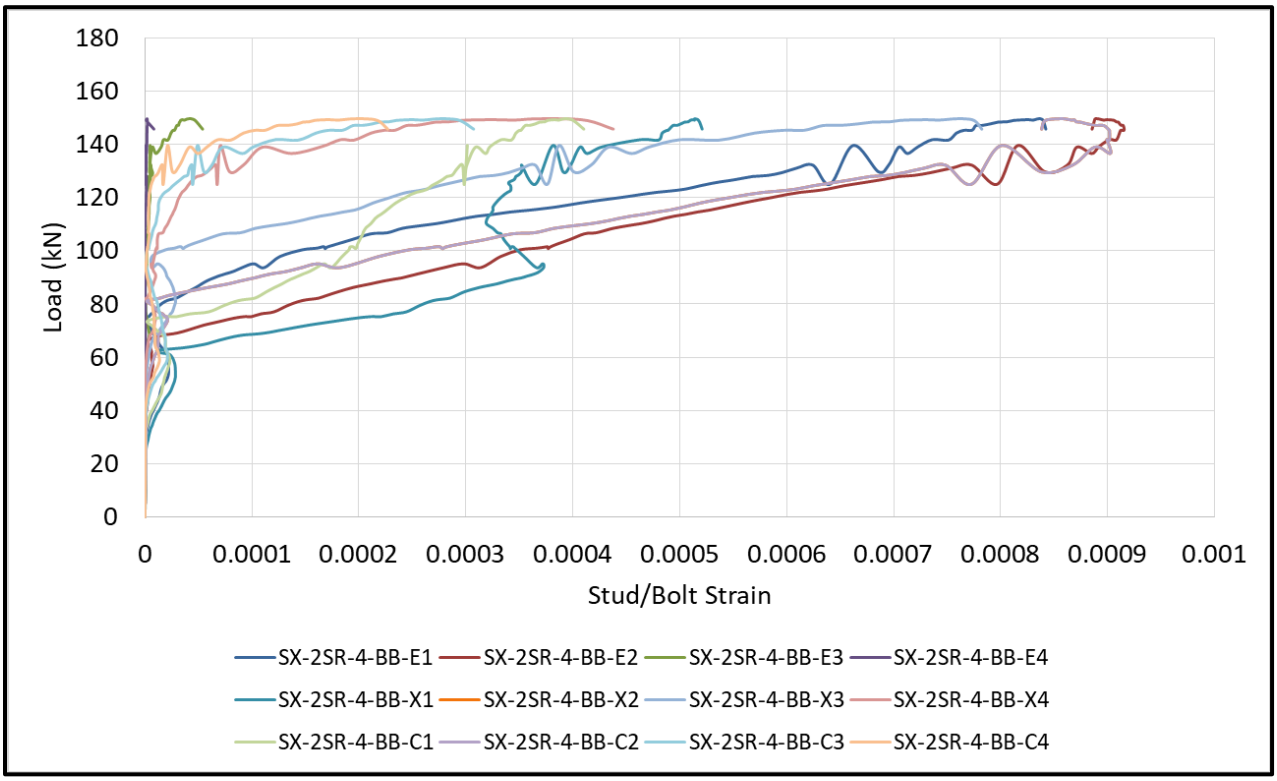

Figure C24: SX-2SR-4-BB Stud Strain Diagram

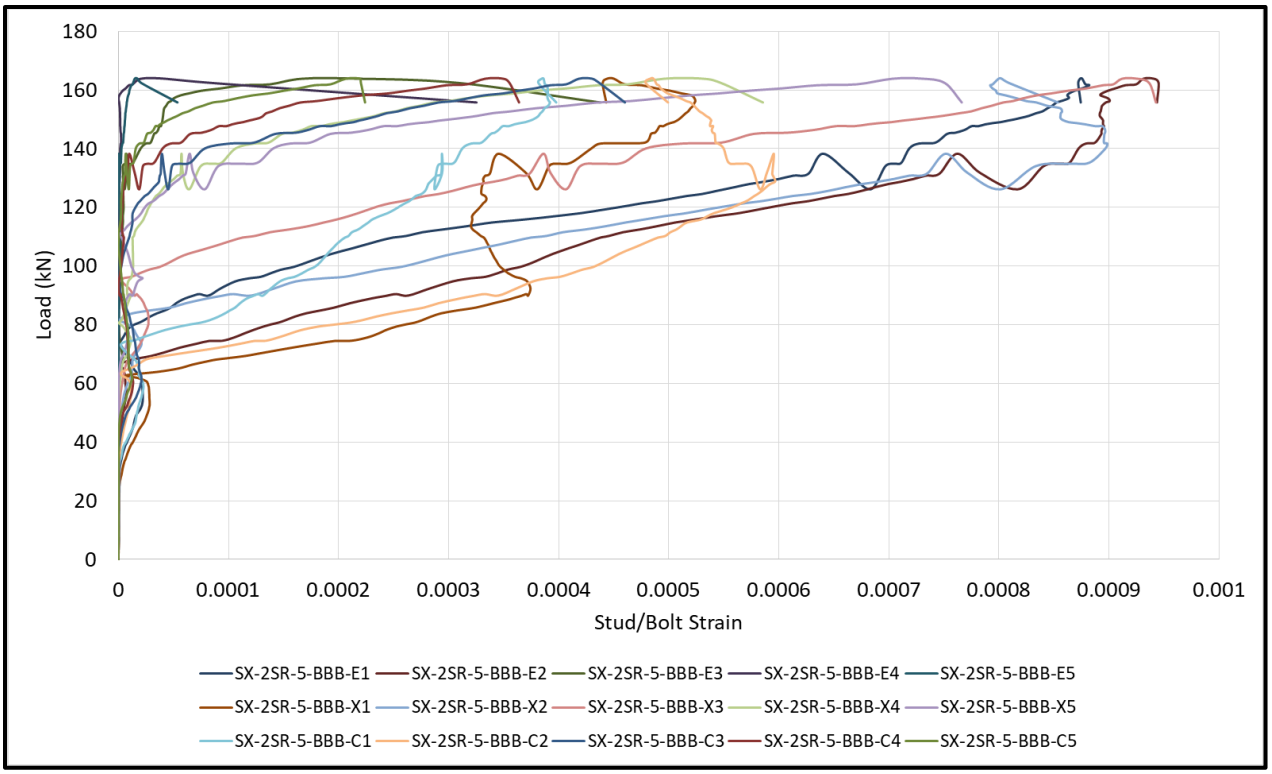

Figure C25: SX-2SR-5-BBB Stud Strain Diagram

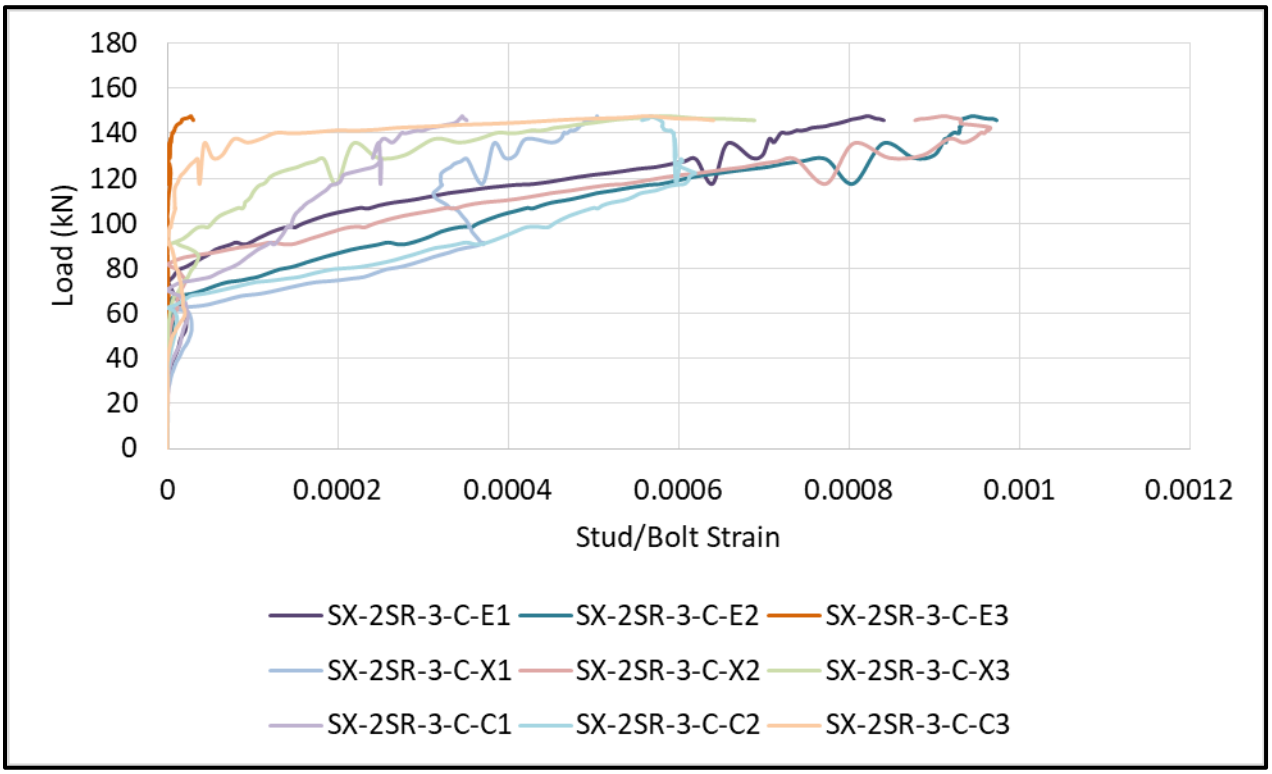

Figure C26: SX-2SR-3-C Stud Strain Diagram

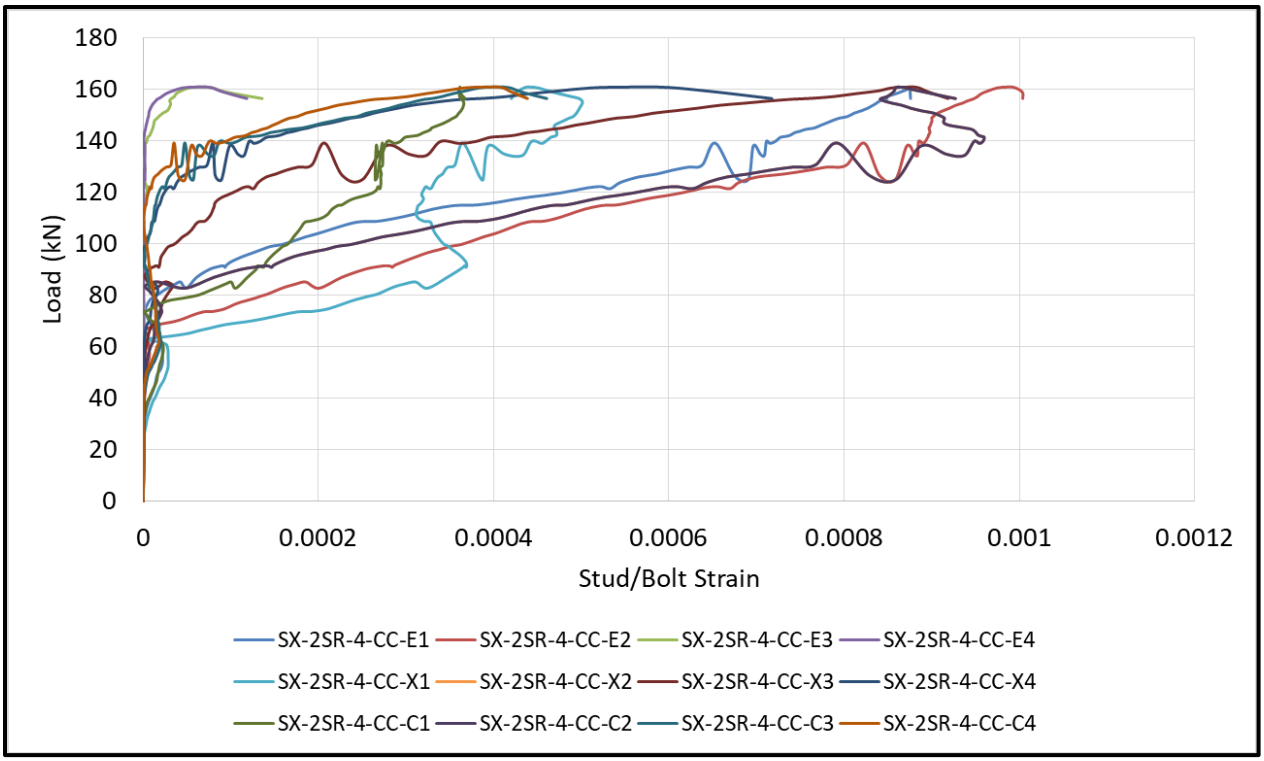

Figure C27: SX-2SR-4-CC Stud Strain Diagram

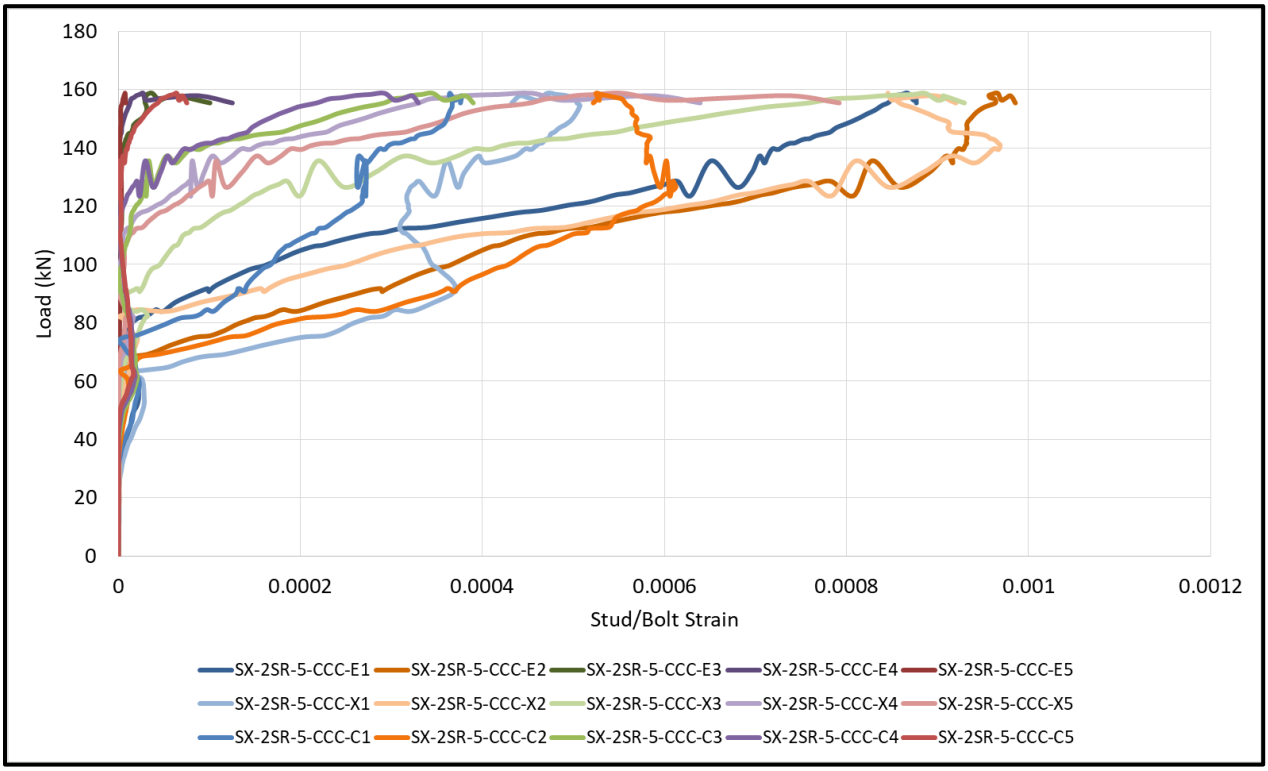

Figure C28: SX-2SR-5-CCC Stud Strain Diagram

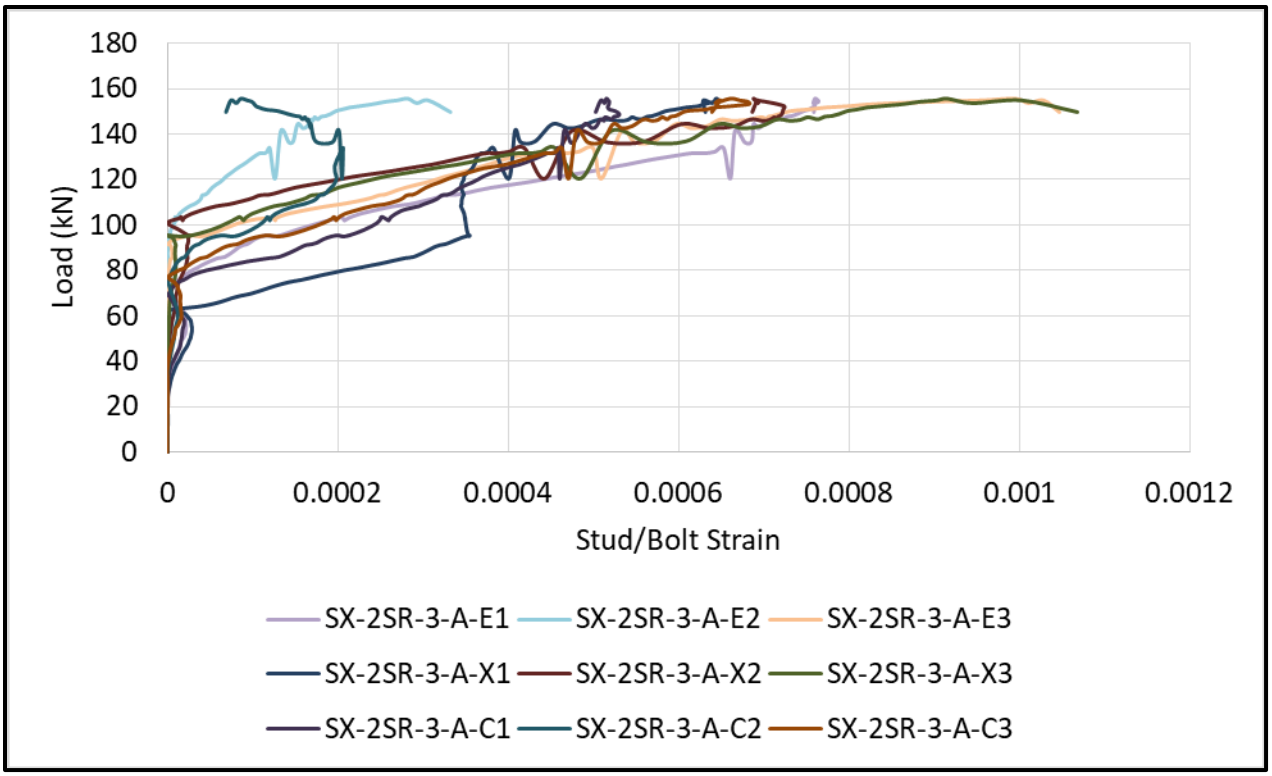

Figure C29: SX-2SR-3-A Stud Strain Diagram

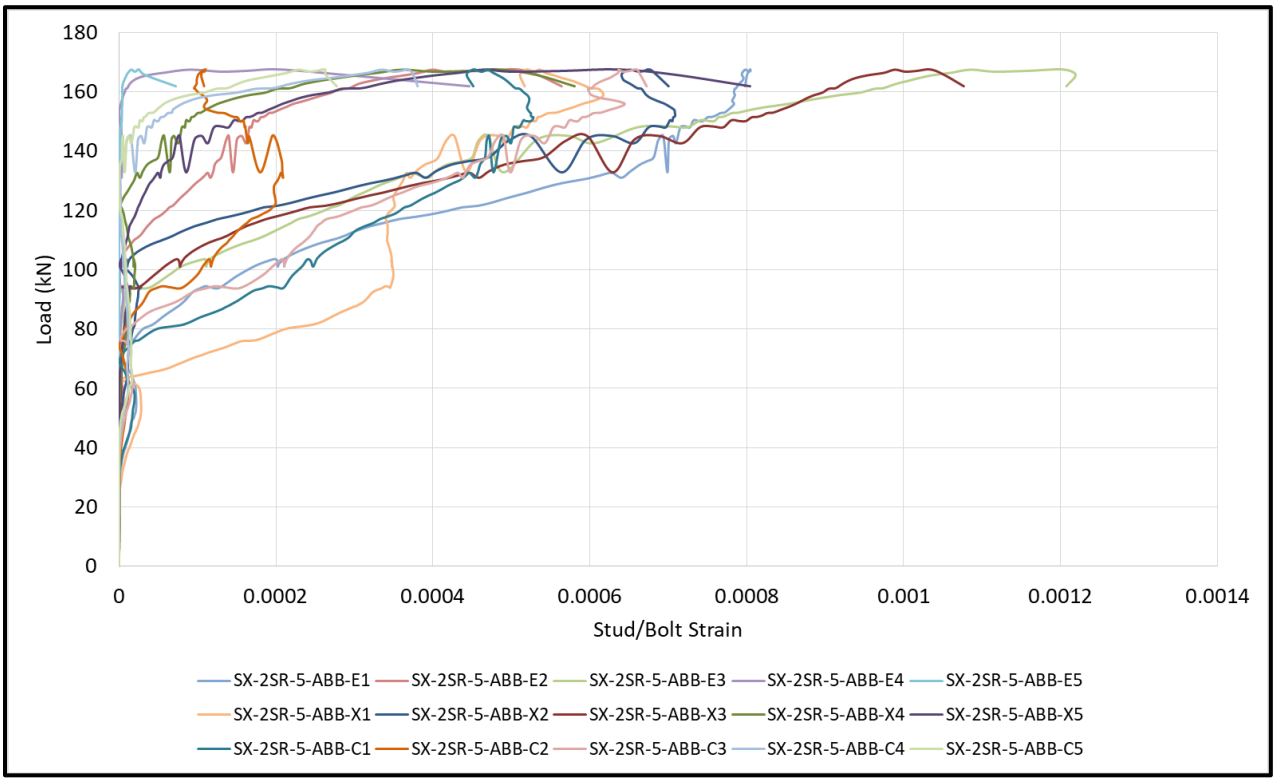

Figure C30: SX-2SR-5-ABB Stud Strain Diagram

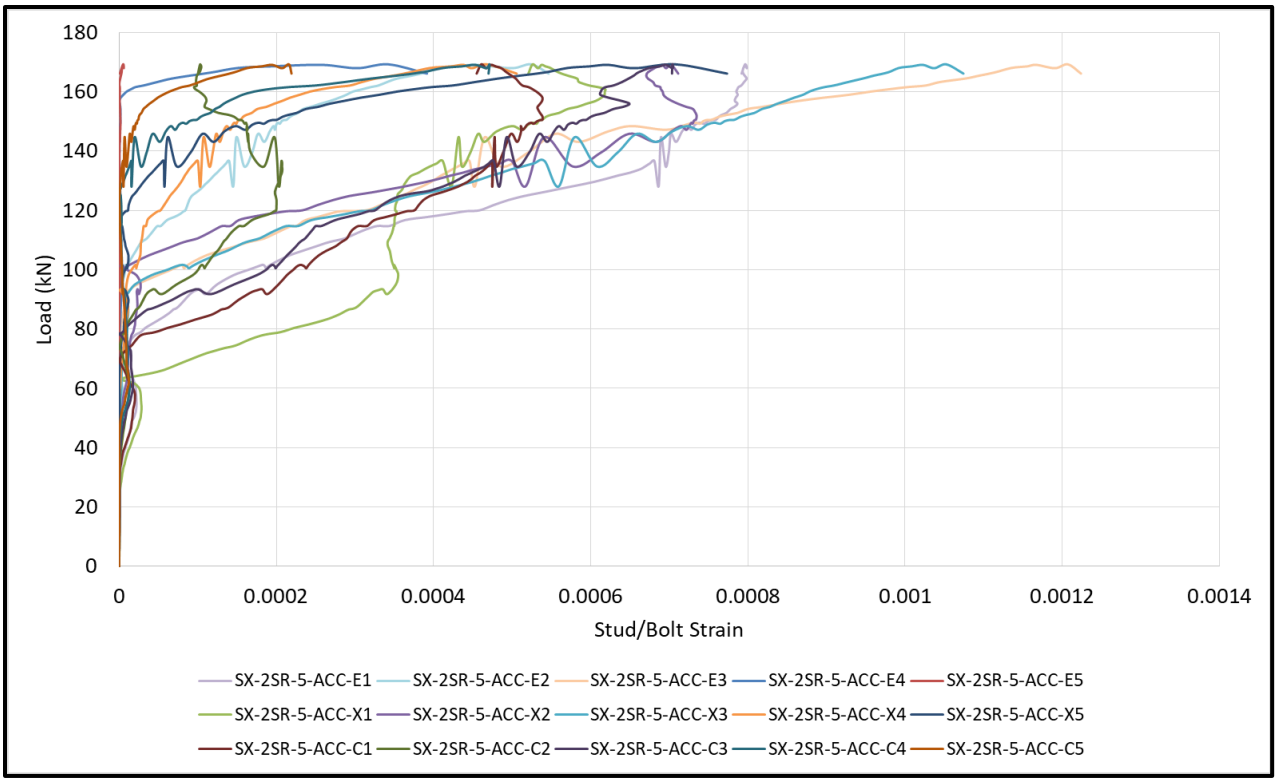

Figure C31: SX-2SR-5-ACC Stud Strain Diagram

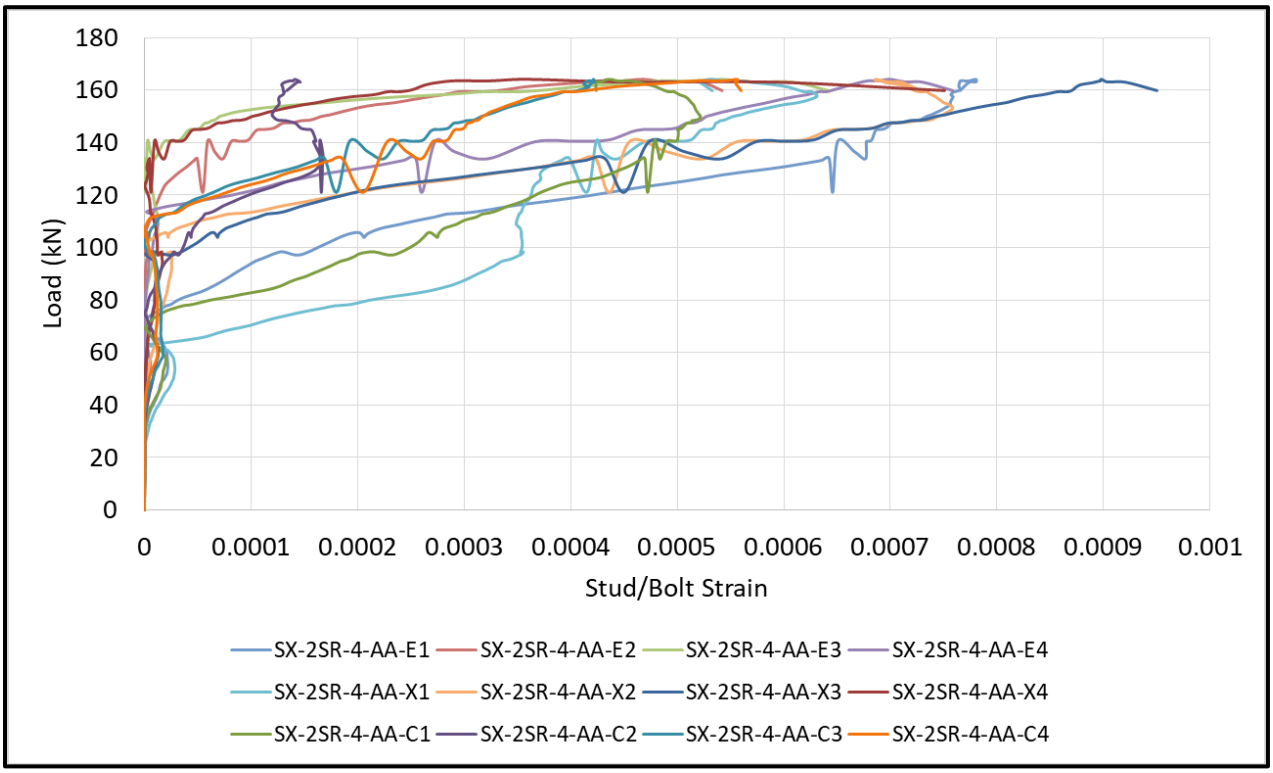

Figure C32: SX-2SR-4-AA Stud Strain Diagram

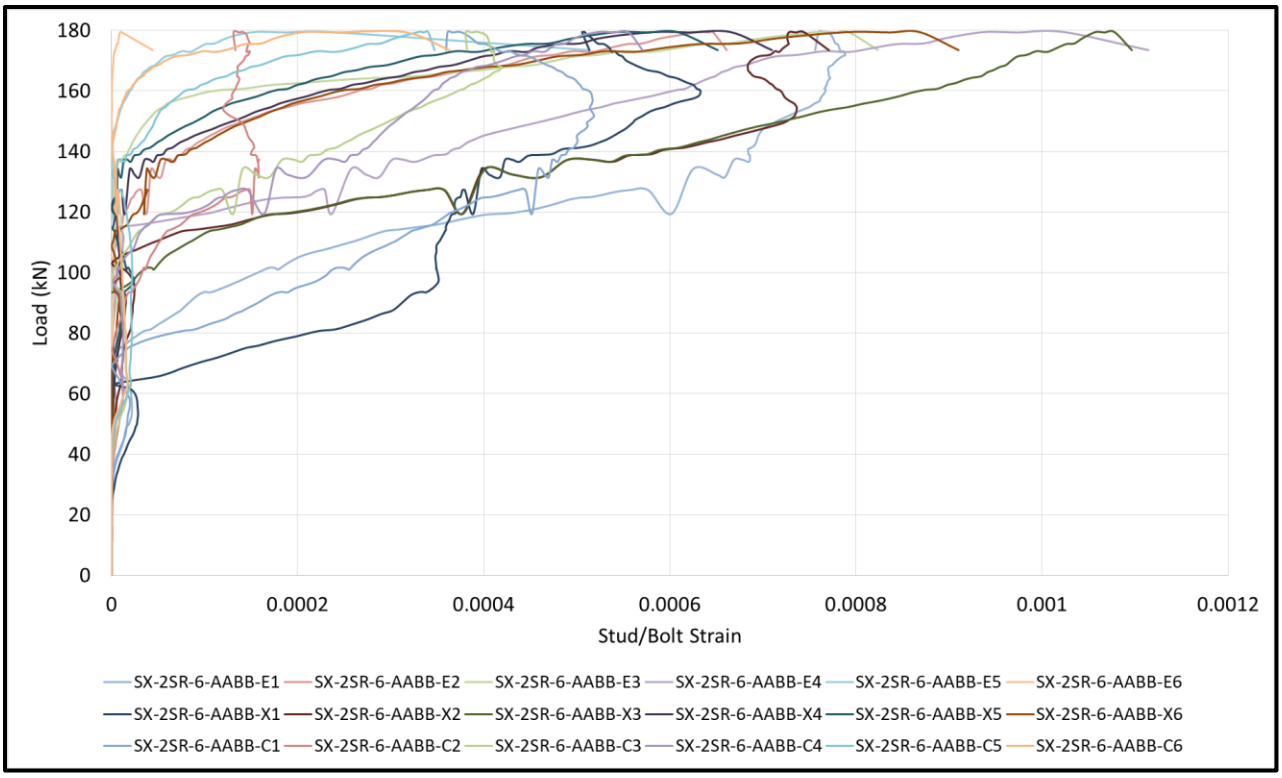

Figure C33: SX-2SR-6-AABB Stud Strain Diagram

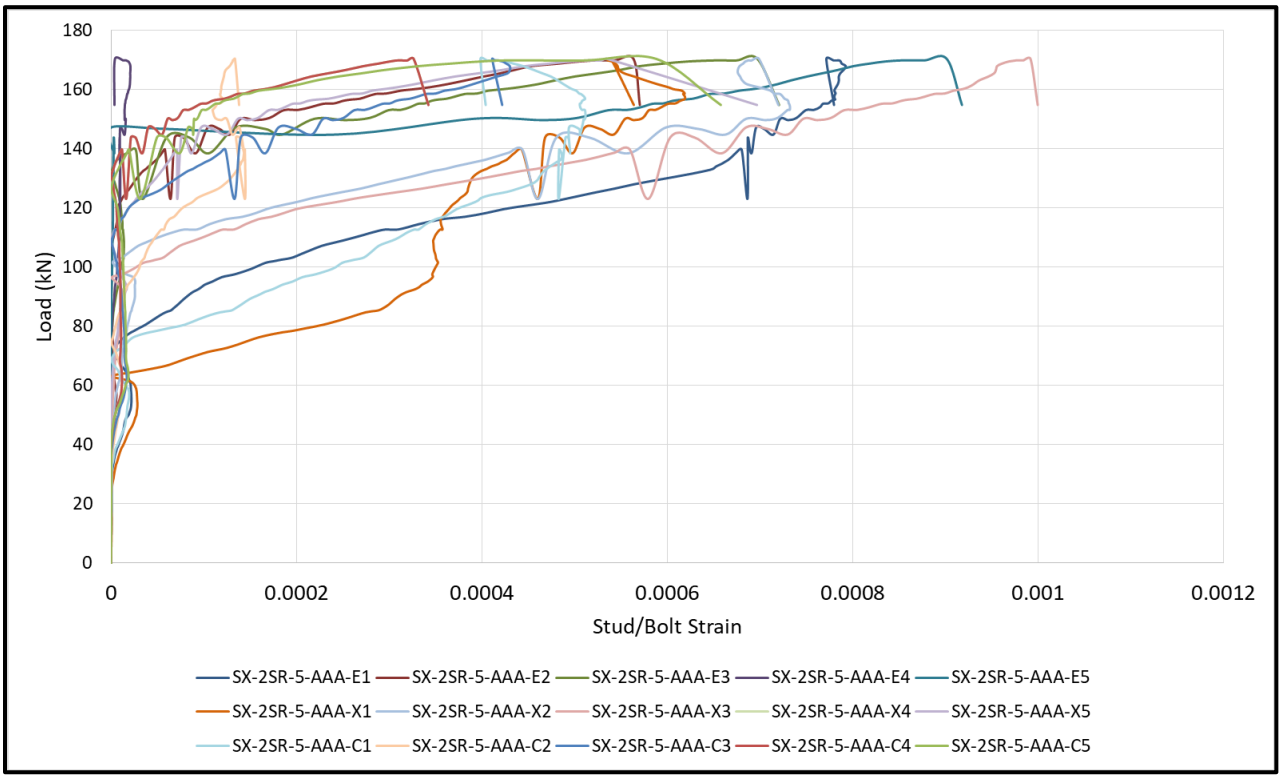

Figure C34: SX-2SR-5-AAA Stud Strain Diagram

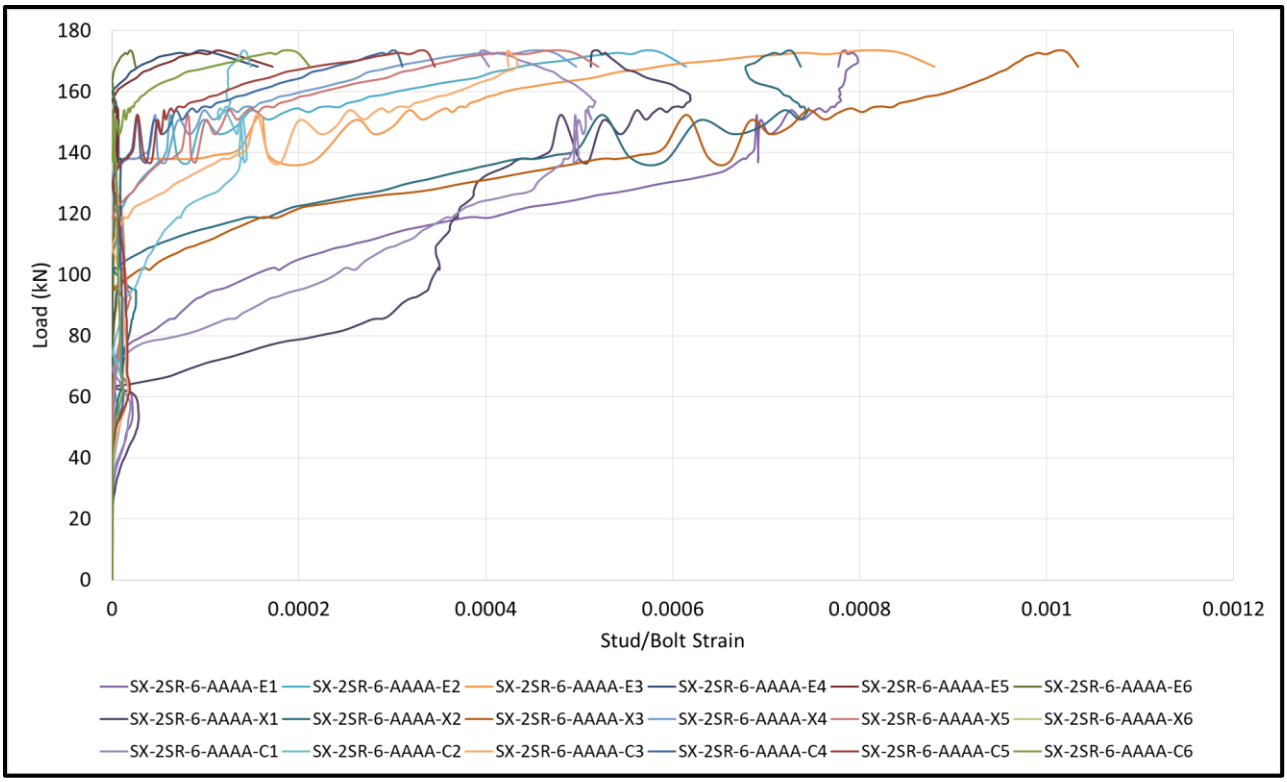

Figure C35: SX-2SR-6-AAAA Stud Strain Diagram

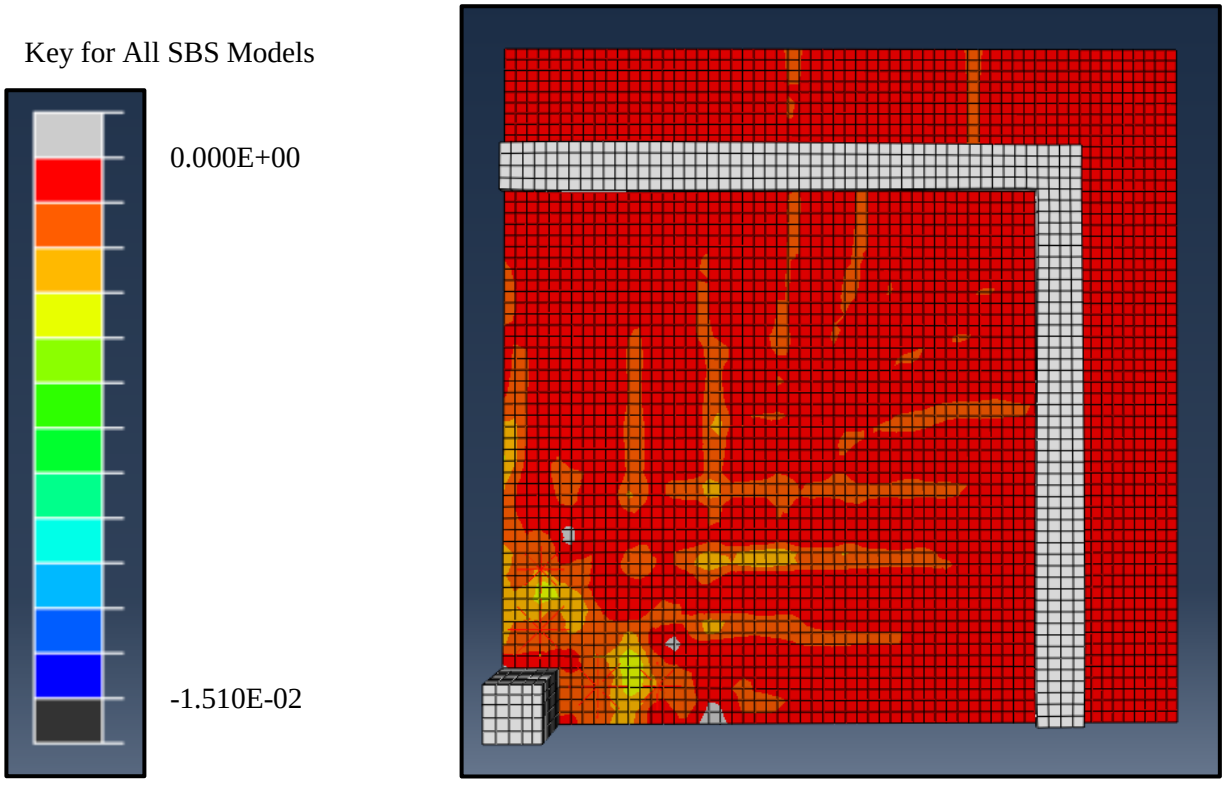

Figure C36: SB2-2 Tensile Face Crack Pattern

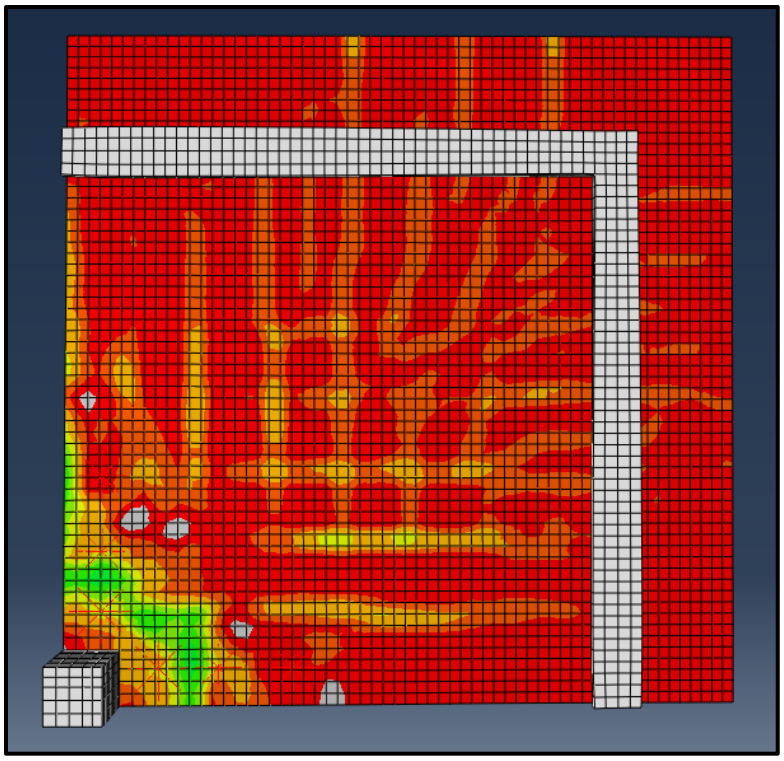

Figure C37: SB2-3-B Tensile Face Crack Pattern

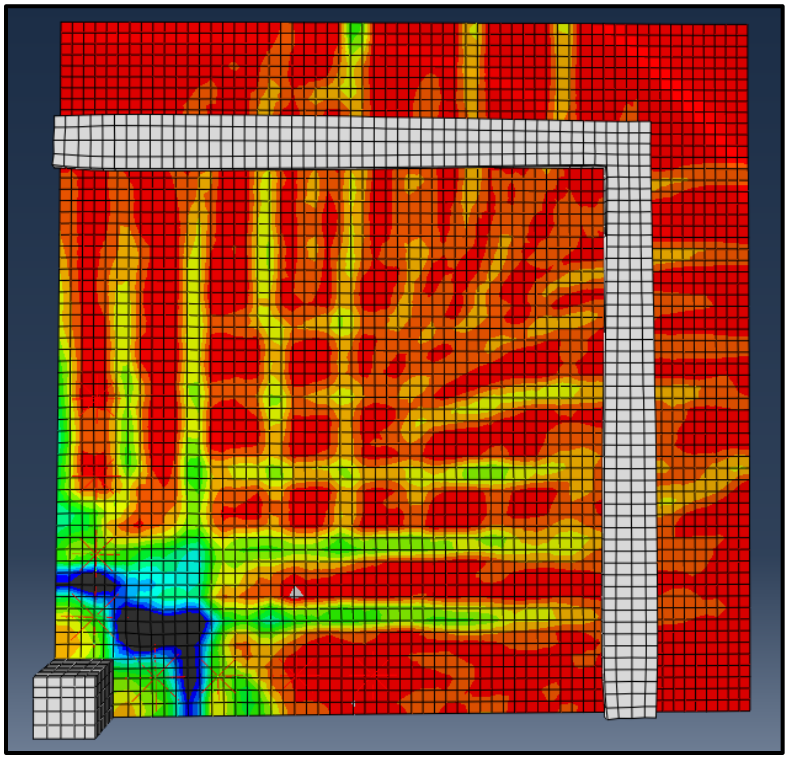

Figure C38: SB2-4-BB Tensile Face Crack Pattern

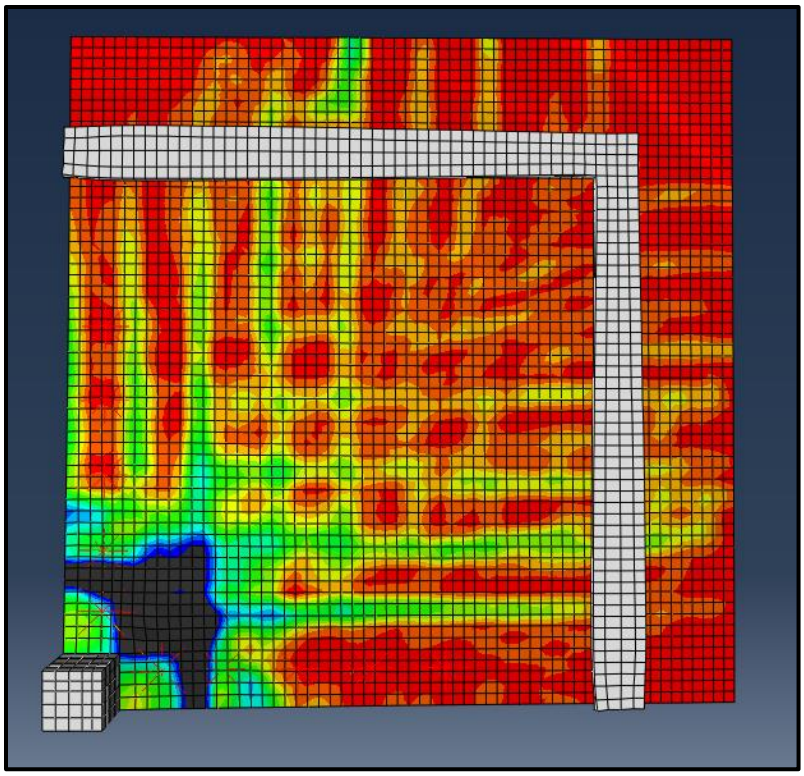

Figure C39: SB2-5-BBB Tensile Face Crack Pattern

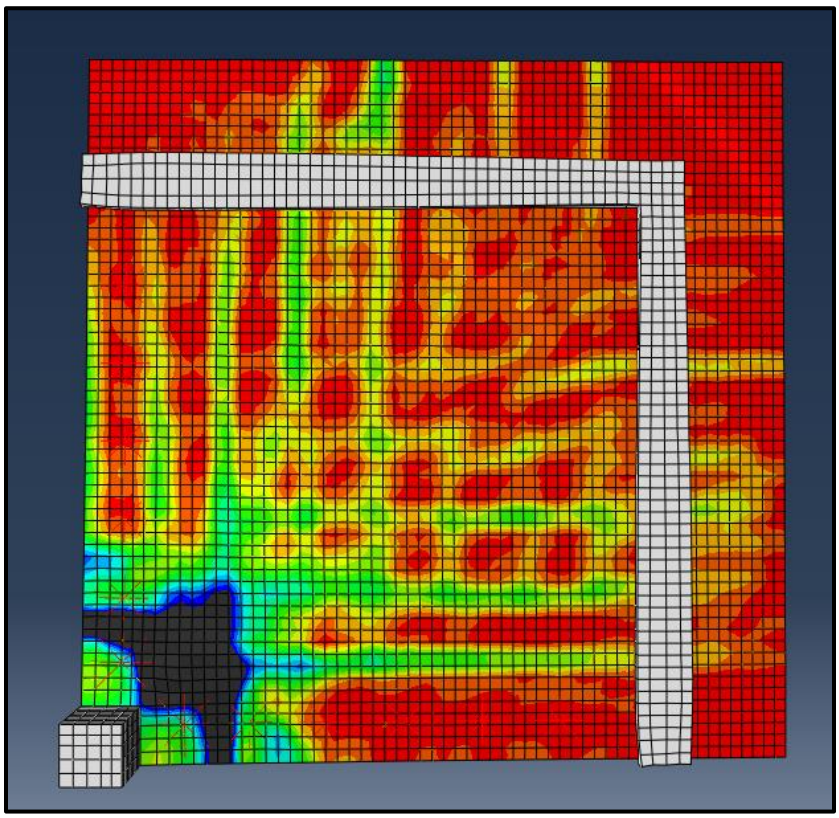

Figure C40: SB2-6-BBBB Tensile Face Crack Pattern

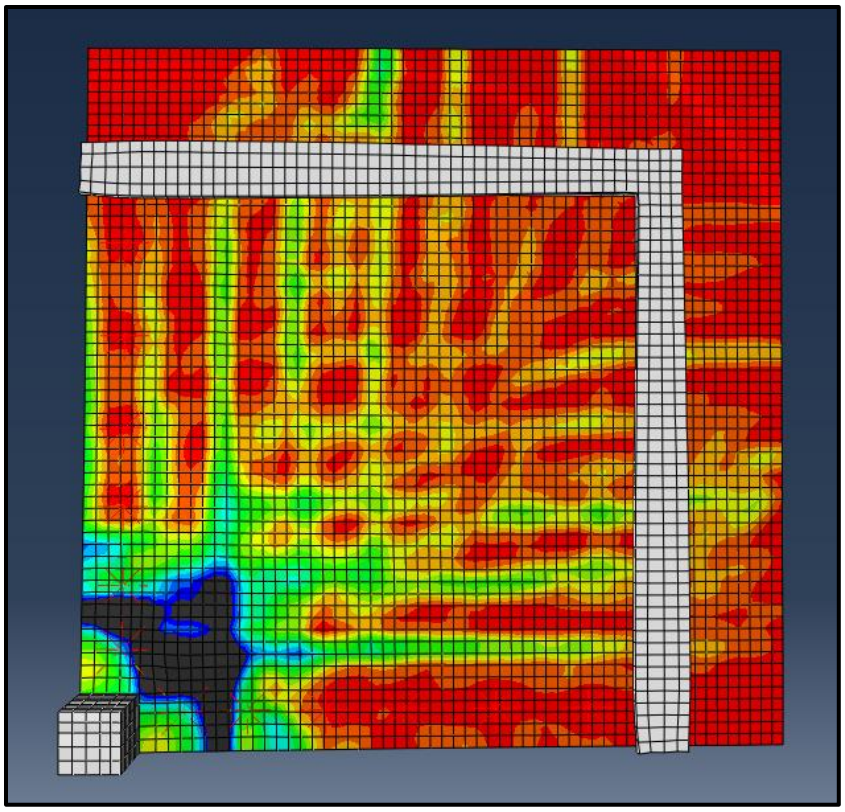

Figure C41: SB2-6-BBCC Tensile Face Crack Pattern

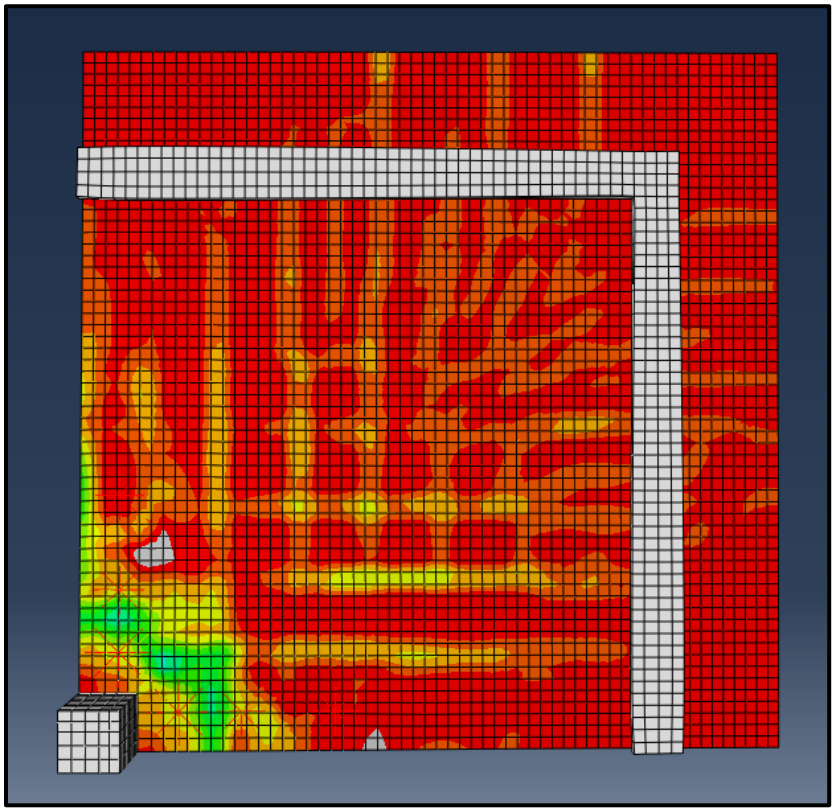

Figure C42: SB2-3-C Tensile Face Crack Pattern

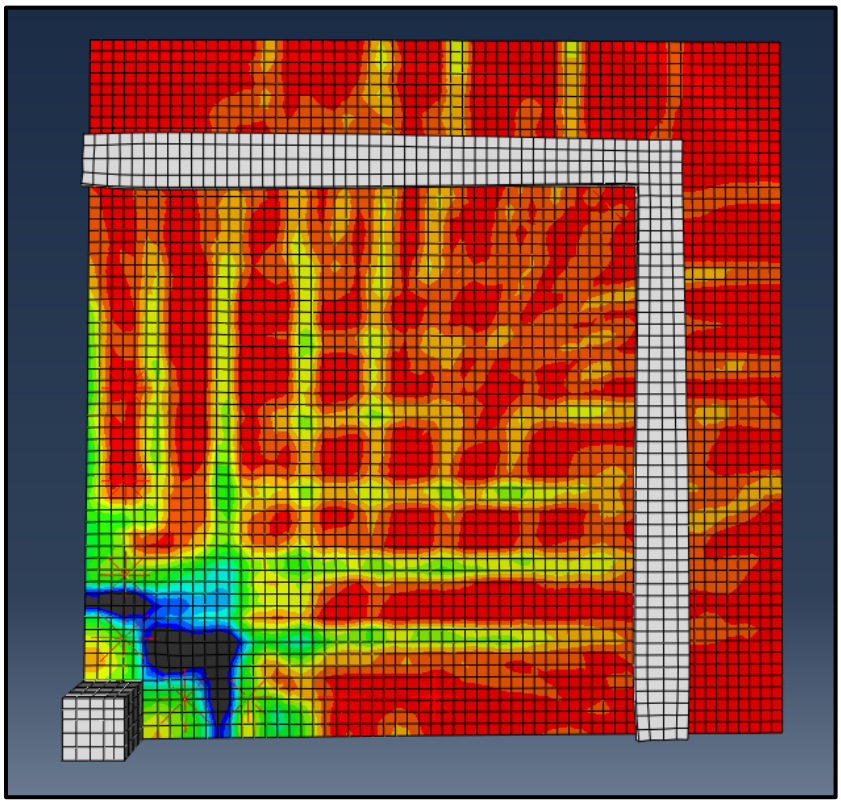

Figure C43: SB2-4-CC Tensile Face Crack Pattern

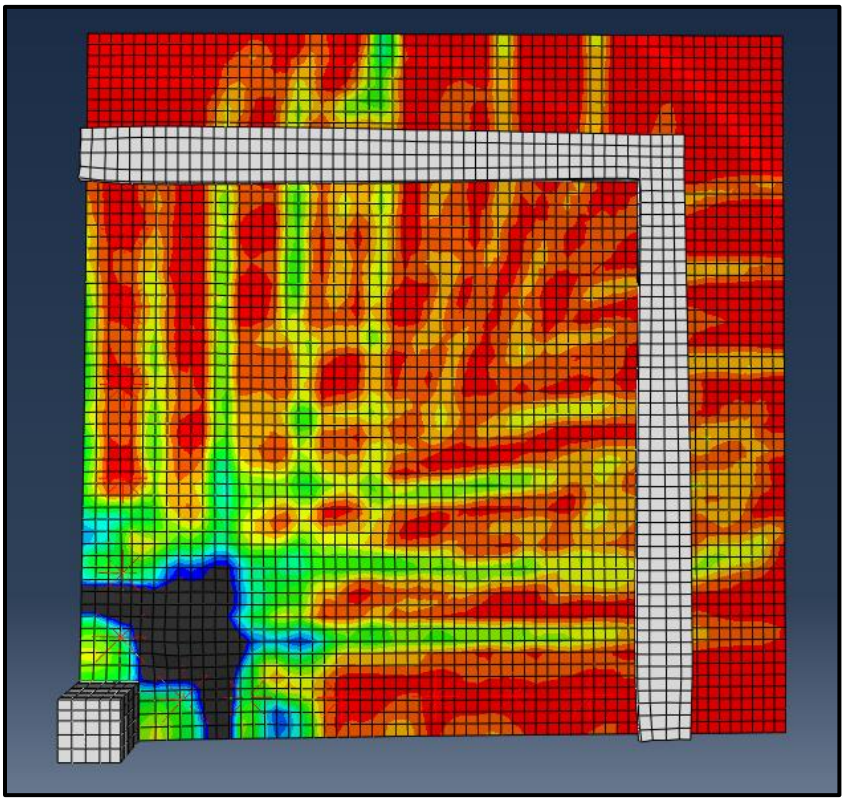

Figure C44: SB2-6-CCBB Tensile Face Crack Pattern

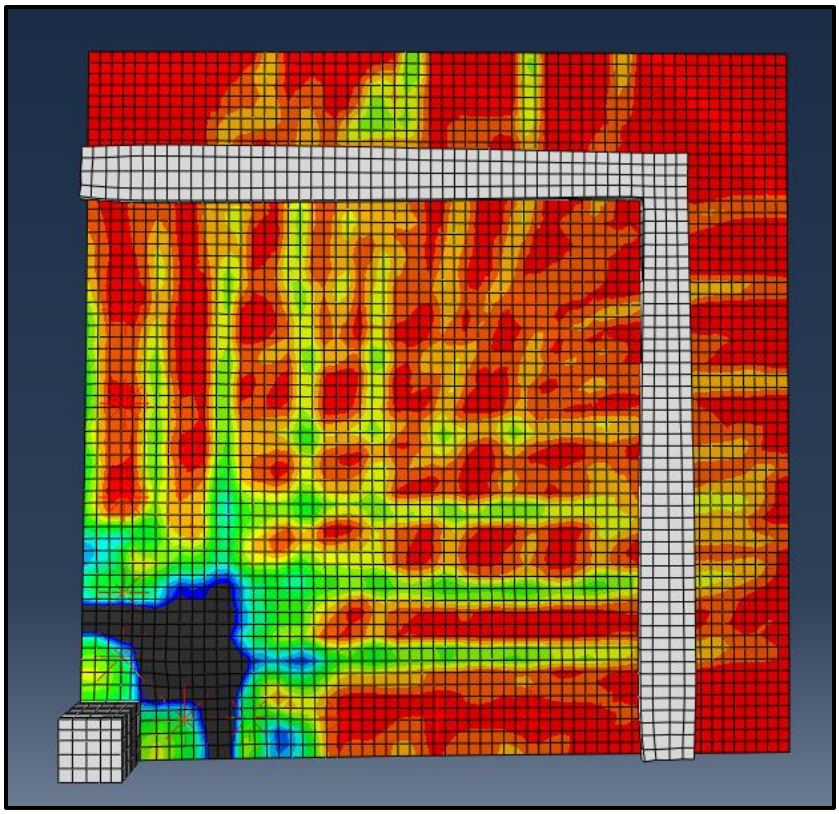

Figure C45: SB2-5-CCC Tensile Face Crack Pattern

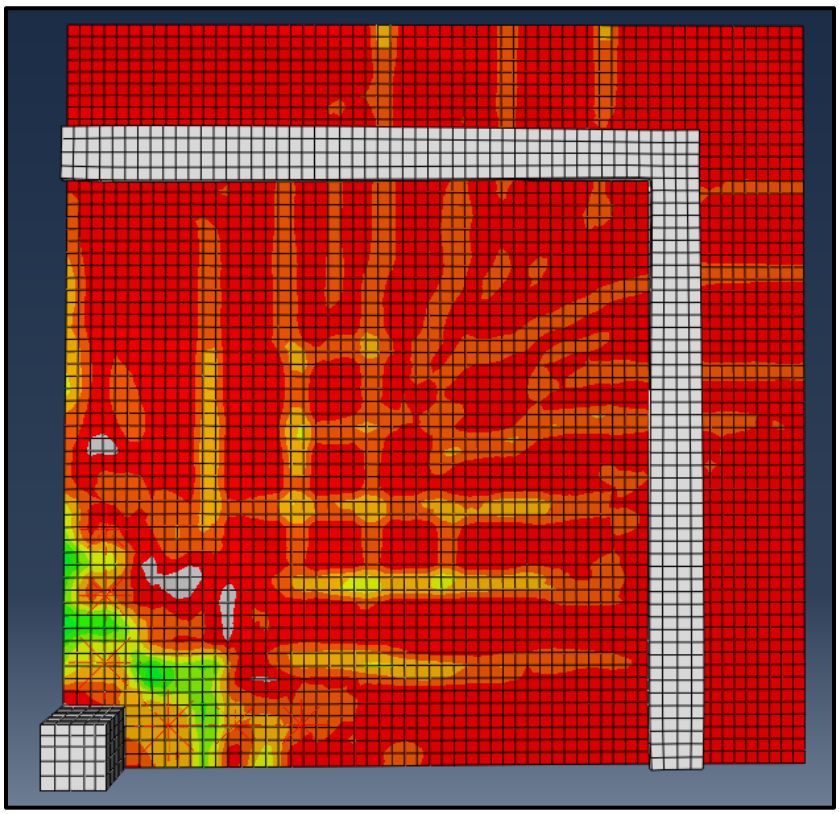

Figure C46: SB3-3 Tensile Face Crack Pattern

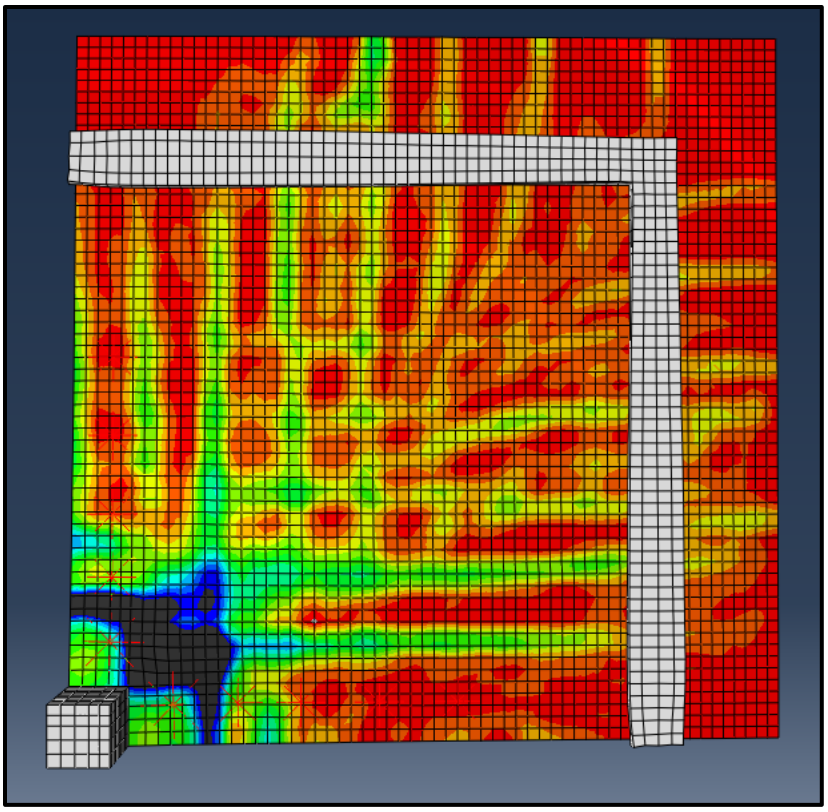

Figure C47: SB3-5-BB Tensile Face Crack Pattern

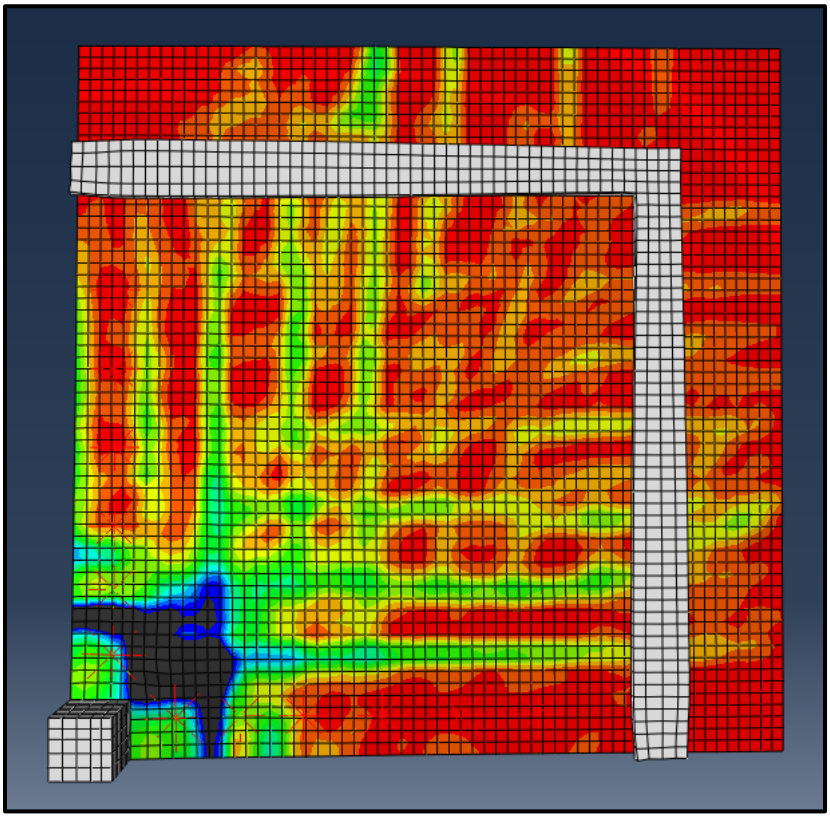

Figure C48: SB3-6-BBB Tensile Face Crack Pattern

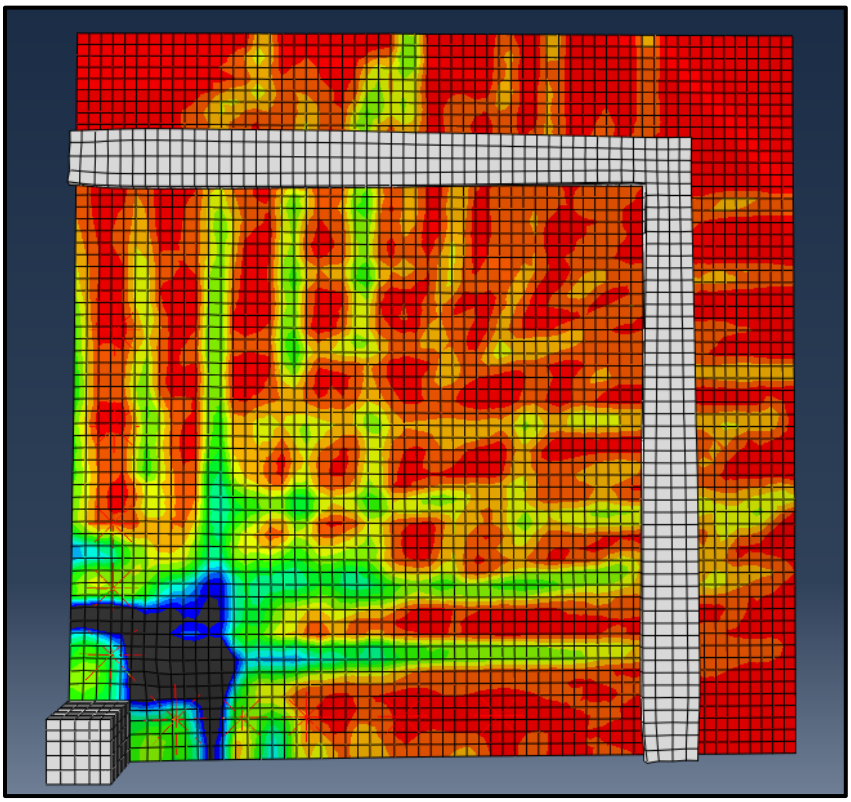

Figure C49: SB3-5-CC Tensile Face Crack Pattern

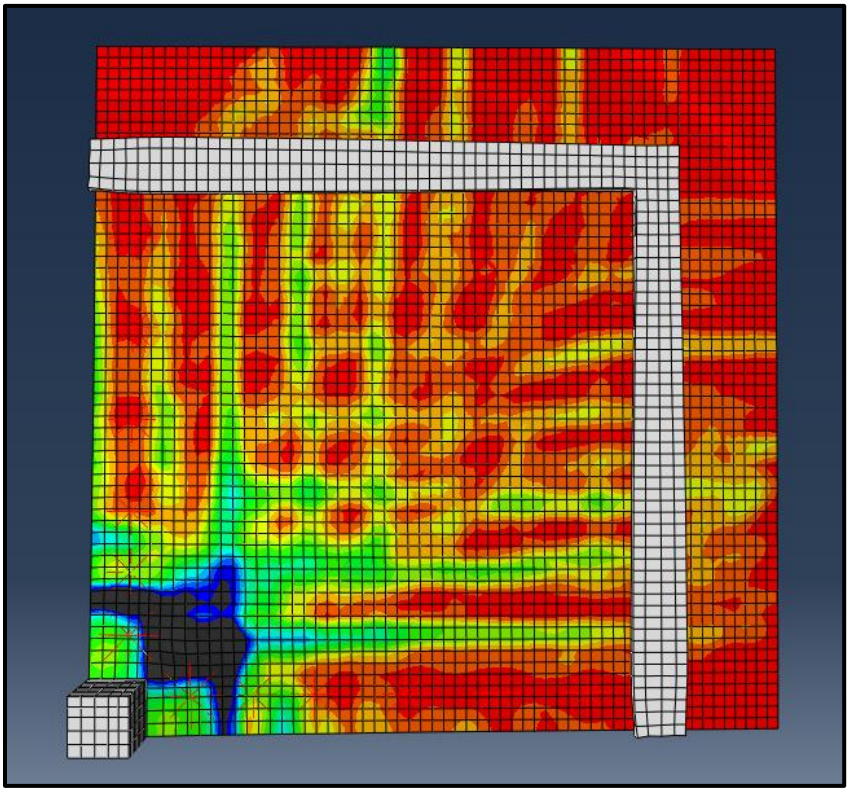

Figure C50: SB3-6-CCC Tensile Face Crack Pattern

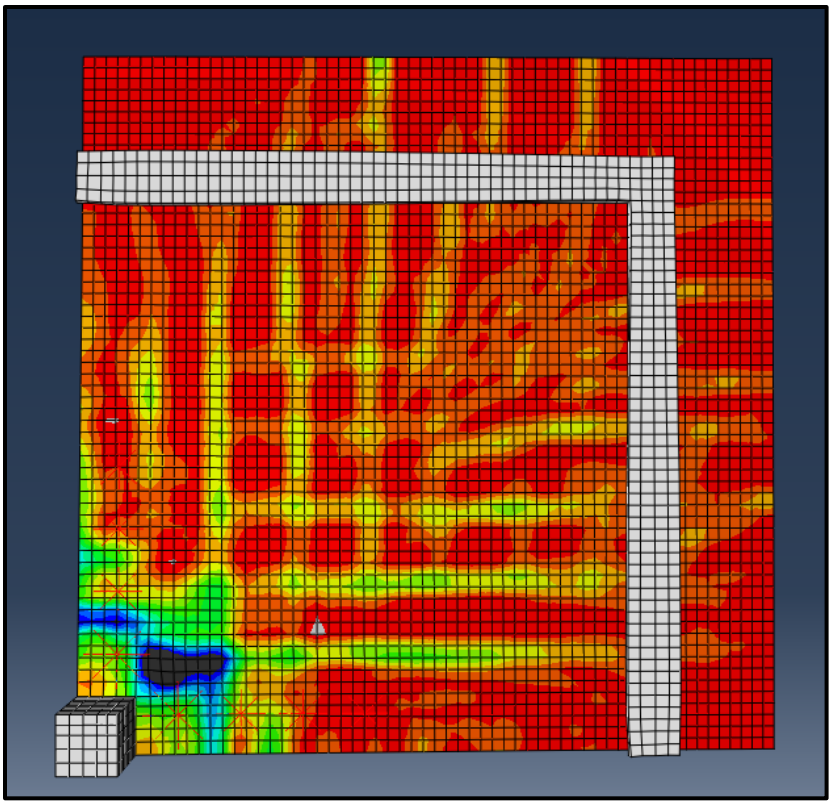

Figure C51: SB4-4 Tensile Face Crack Pattern

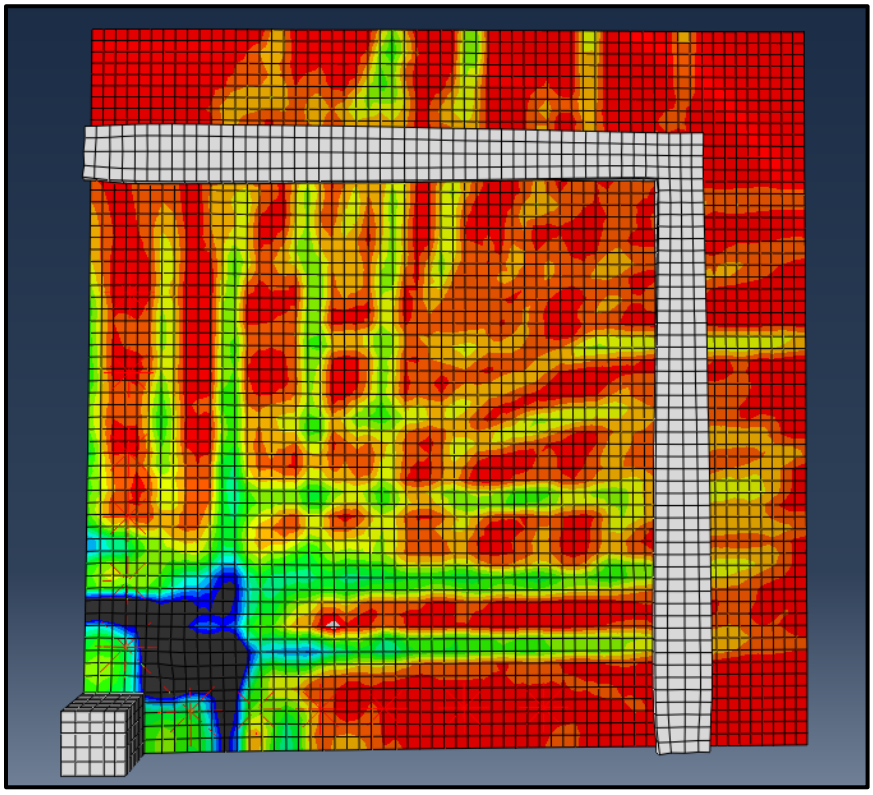

Figure C52: SB4-6-BB Tensile Face Crack Pattern

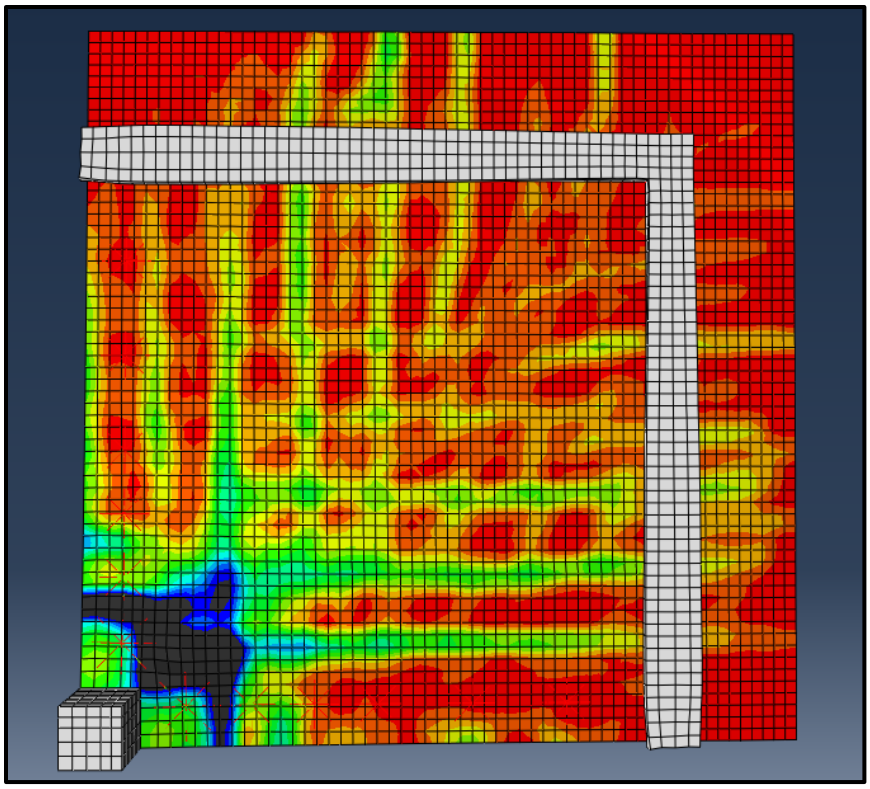

Figure C53: SB4-6-CC Tensile Face Crack Pattern

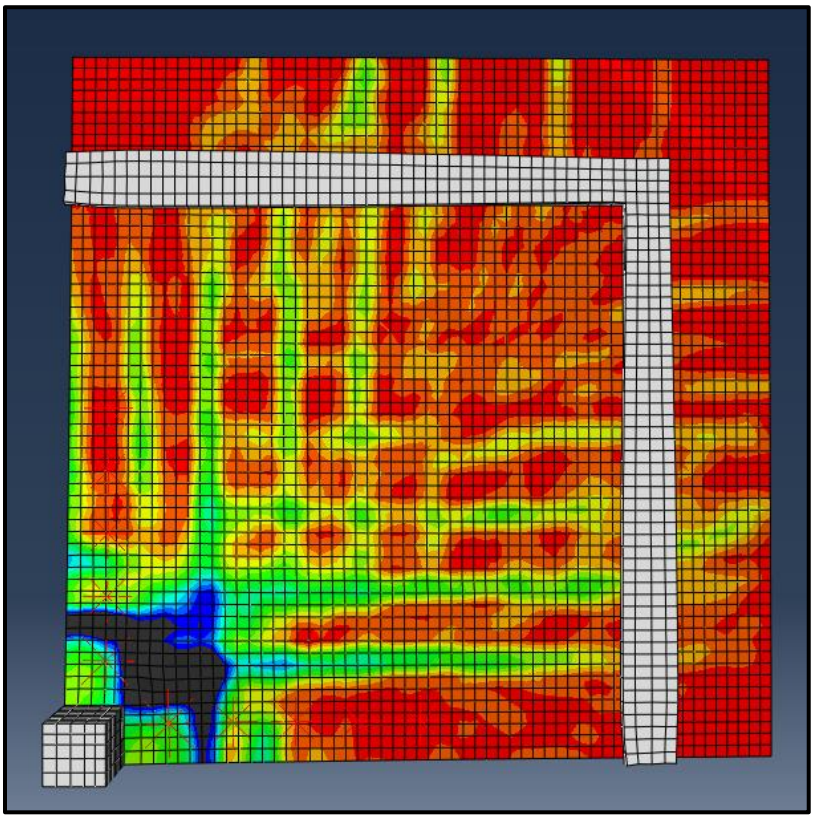

Figure C54: SB4-5-A Tensile Face Crack Pattern

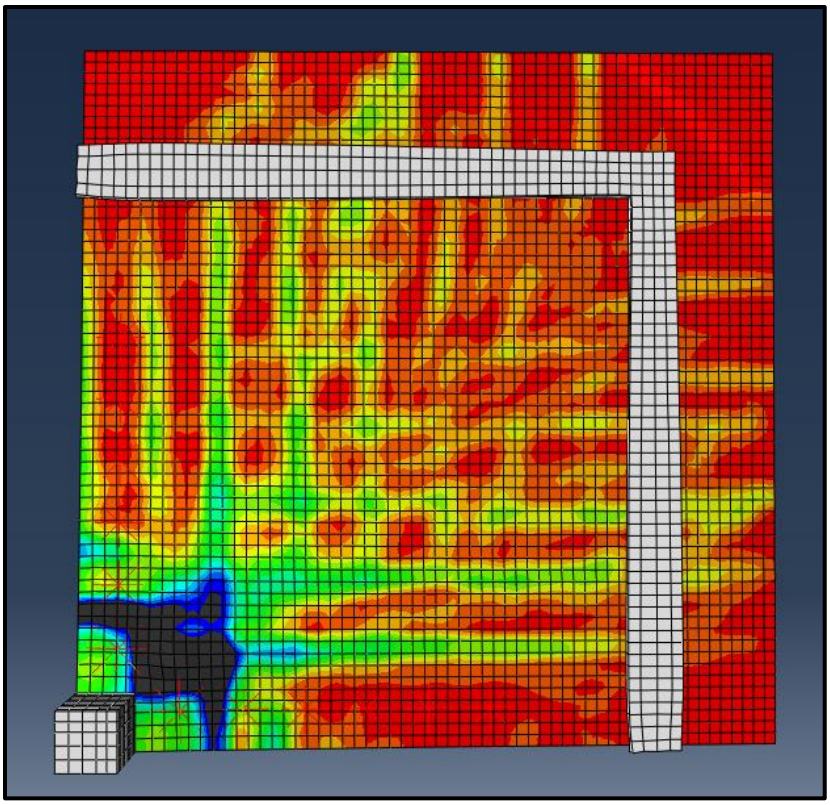

Figure C55: SB4-6-AA Tensile Face Crack Pattern

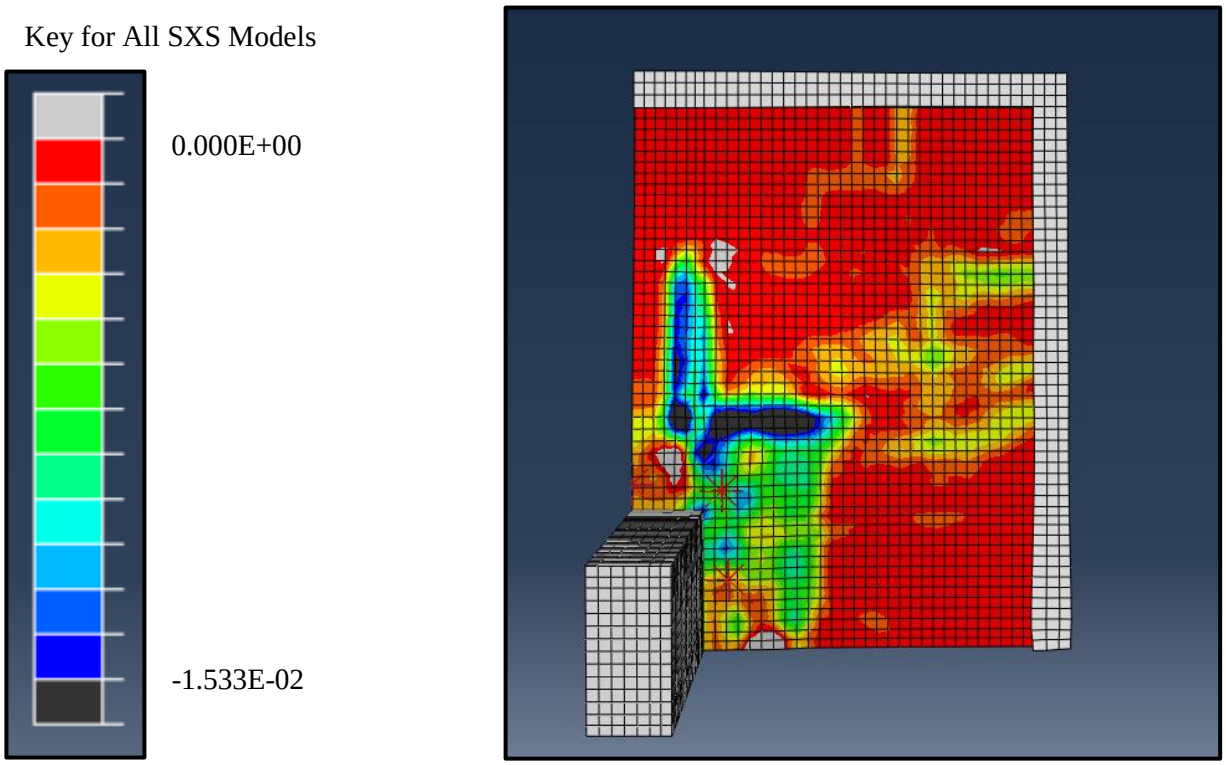

Figure C56: SX-1SR-1 Tensile Face Crack Pattern

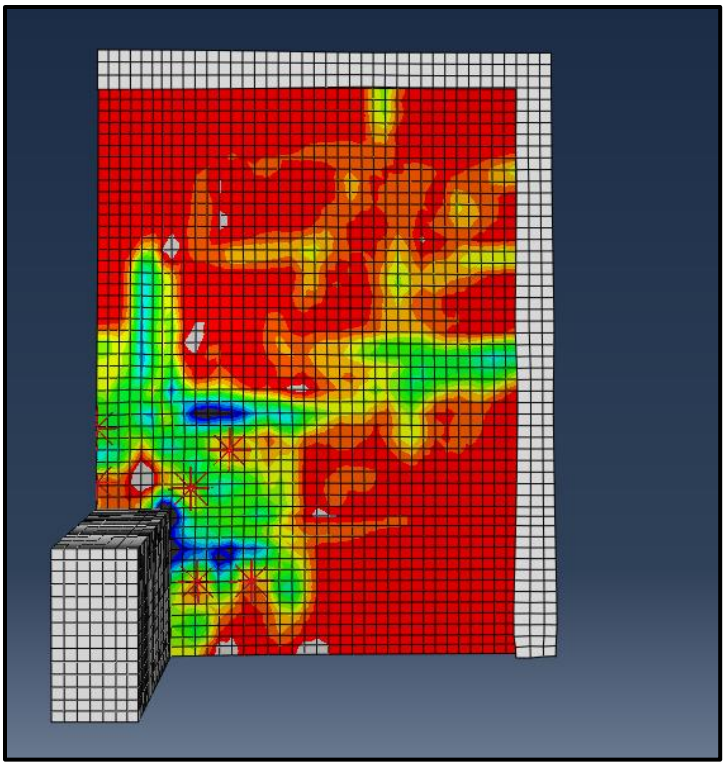

Figure C57: SX-2SR-2 Tensile Face Crack Pattern

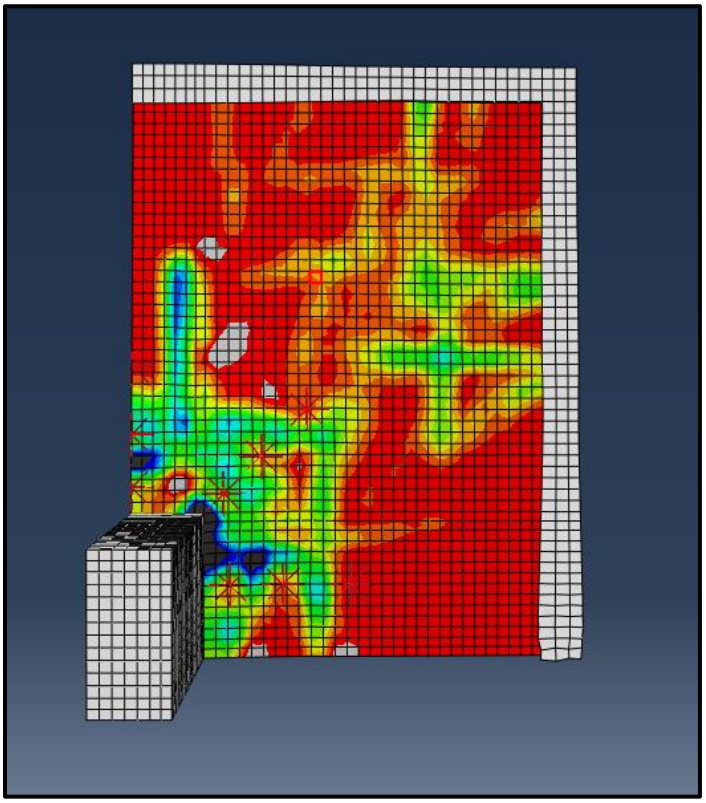

Figure C58: SX-2SR-3-B Tensile Face Crack Pattern

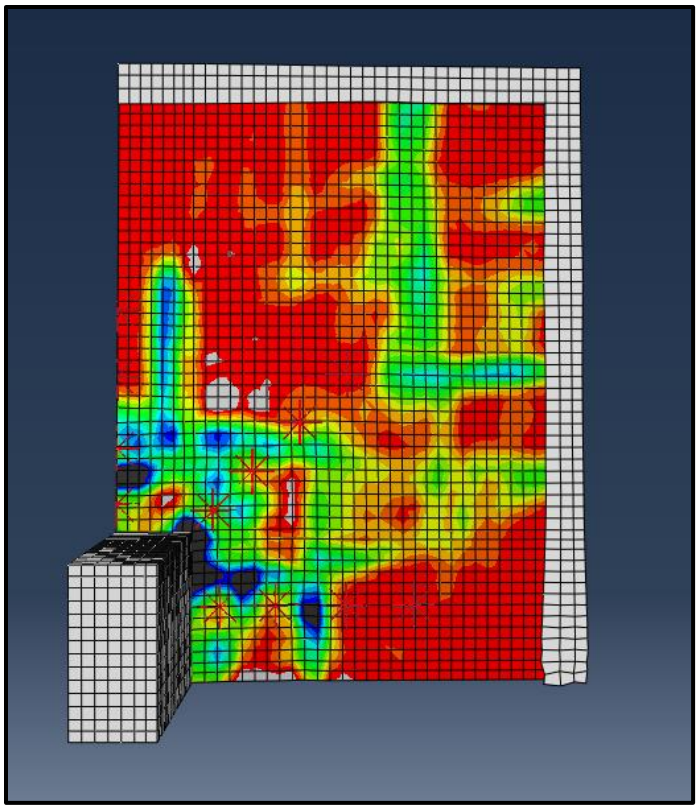

Figure C59: SX-2SR-4-BB Tensile Face Crack Pattern

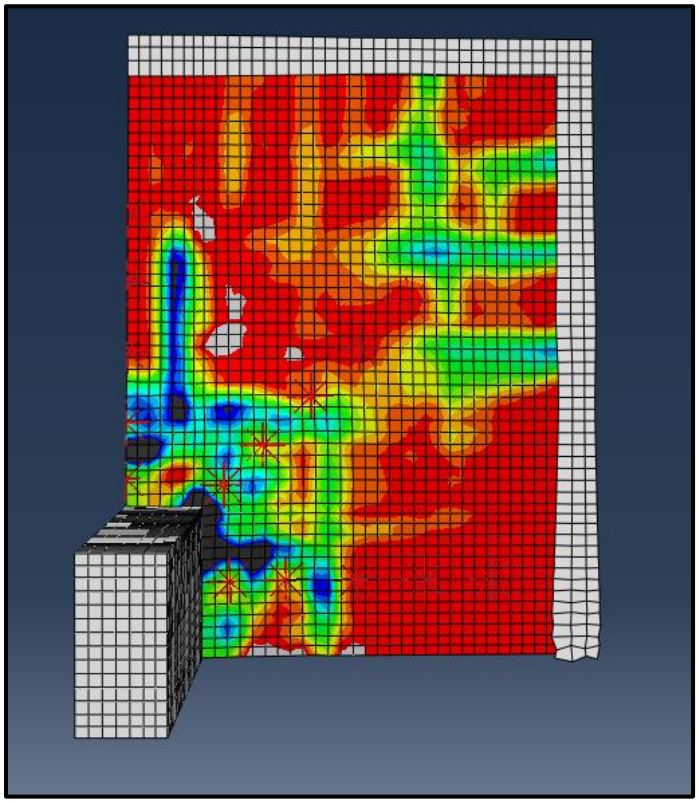

Figure C60: SX-2SR-5-BBB Tensile Face Crack Pattern

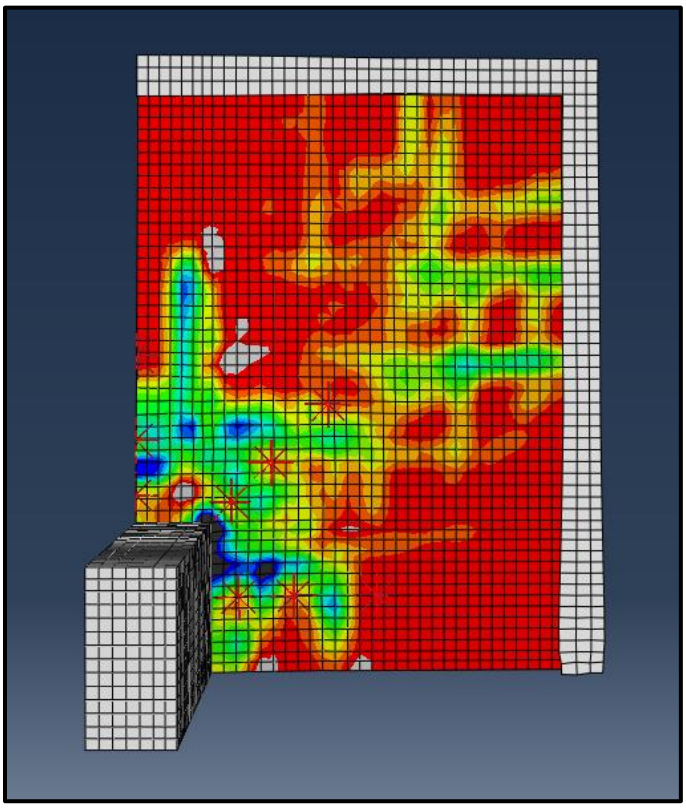

Figure C61: SX-2SR-3-C Tensile Face Crack Pattern

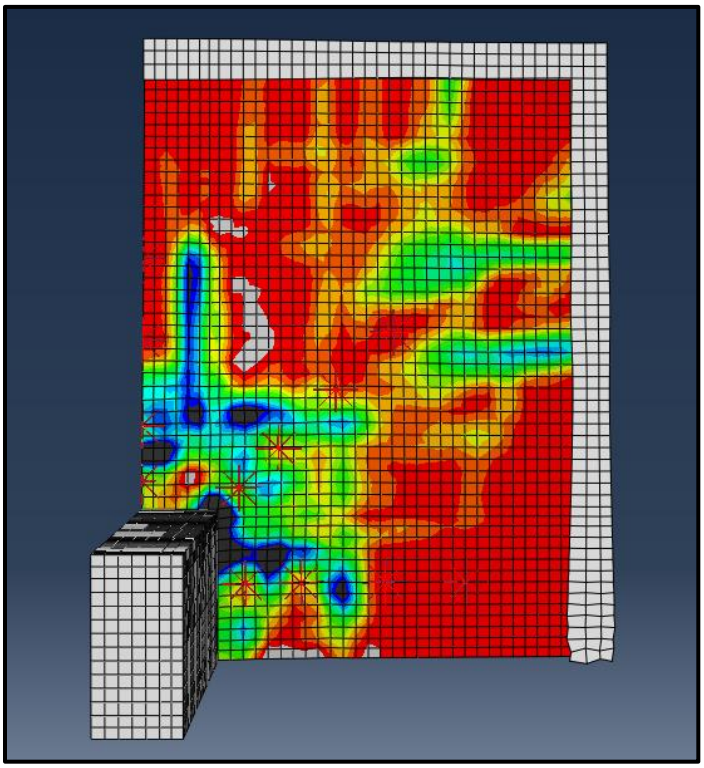

Figure C62: SX-2SR-4-CC Tensile Face Crack Pattern

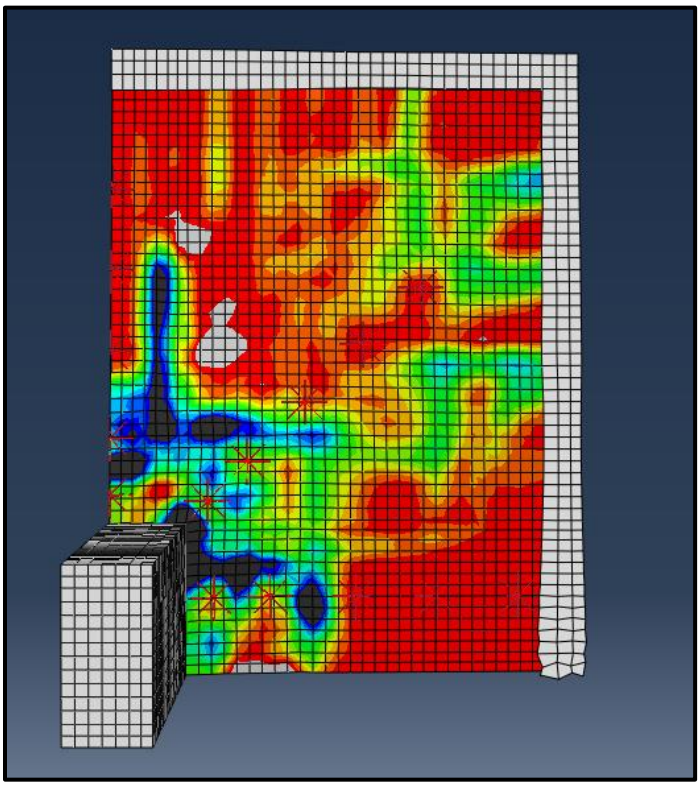

Figure C63: SX-2SR-5-CCC Tensile Face Crack Pattern

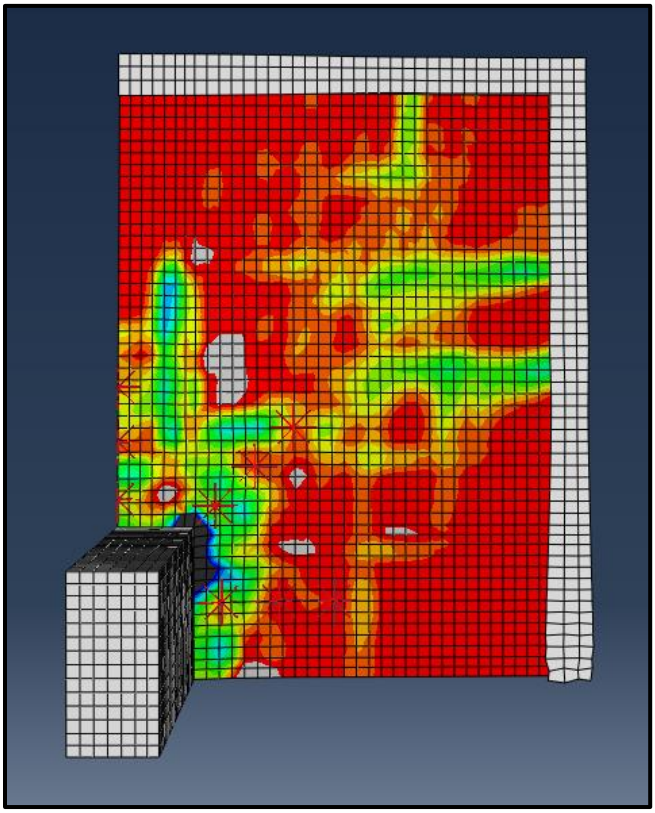

Figure C64: SX-2SR-3-A Tensile Face Crack Pattern

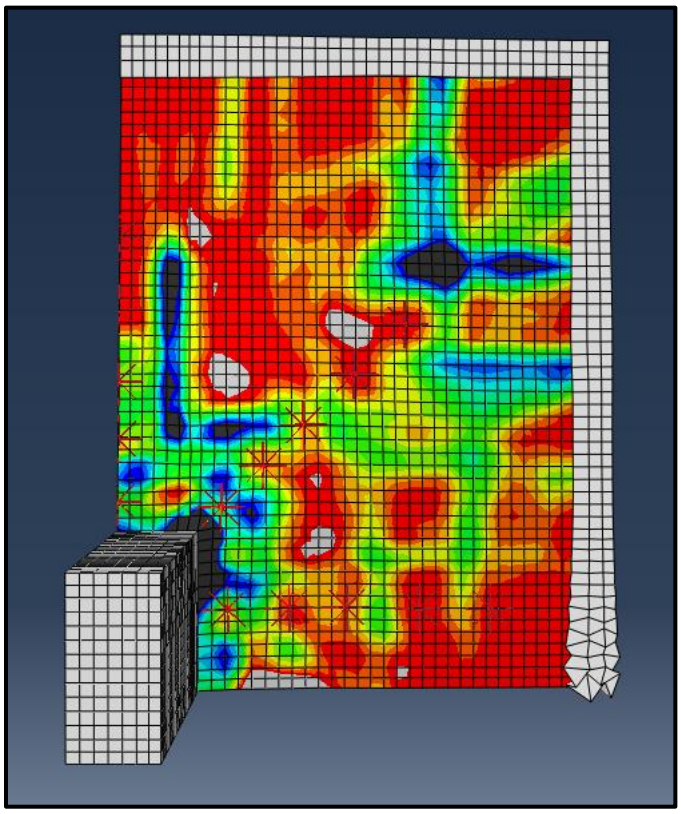

Figure C65: SX-2SR-5-ABB Tensile Face Crack Pattern

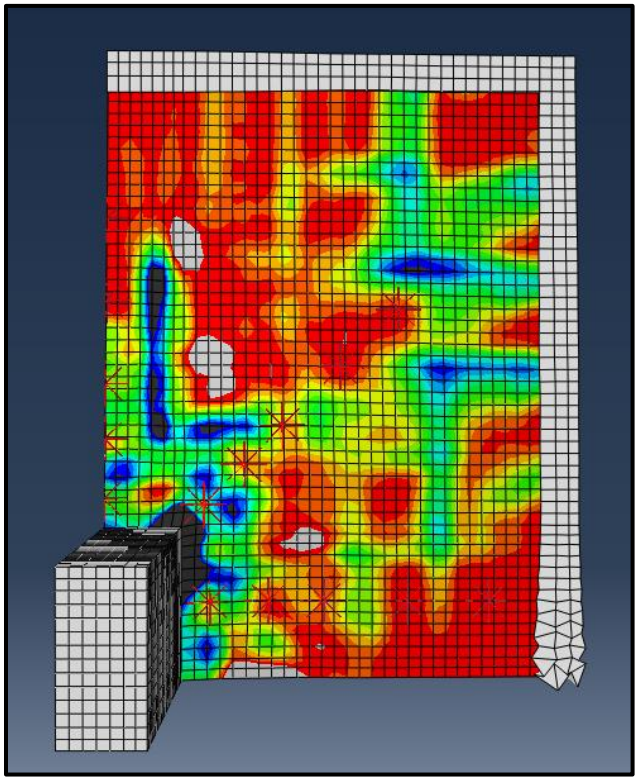

Figure C66: SX-2SR-5-ACC Tensile Face Crack Pattern

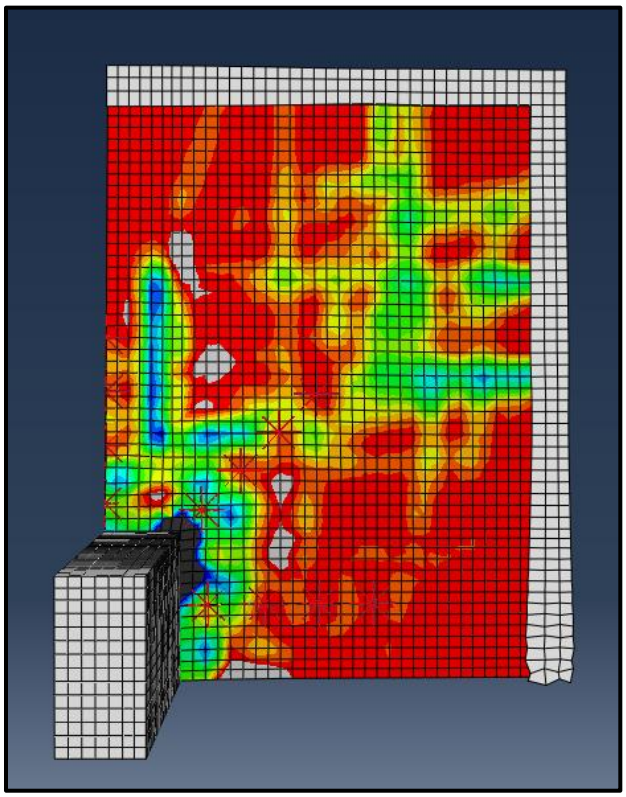

Figure C67: SX-2SR-4-AA Tensile Face Crack Pattern

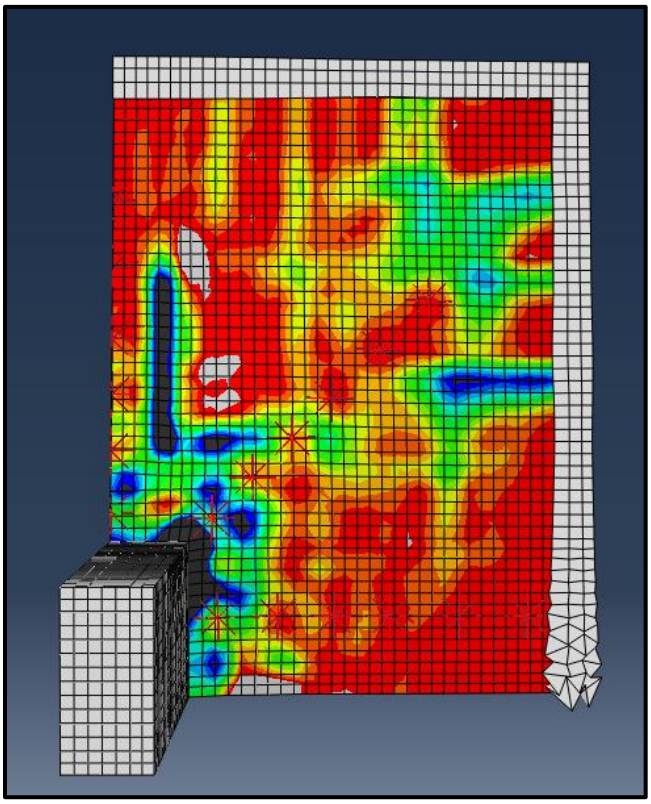

Figure C68: SX-2SR-6-AABB Tensile Face Crack Pattern

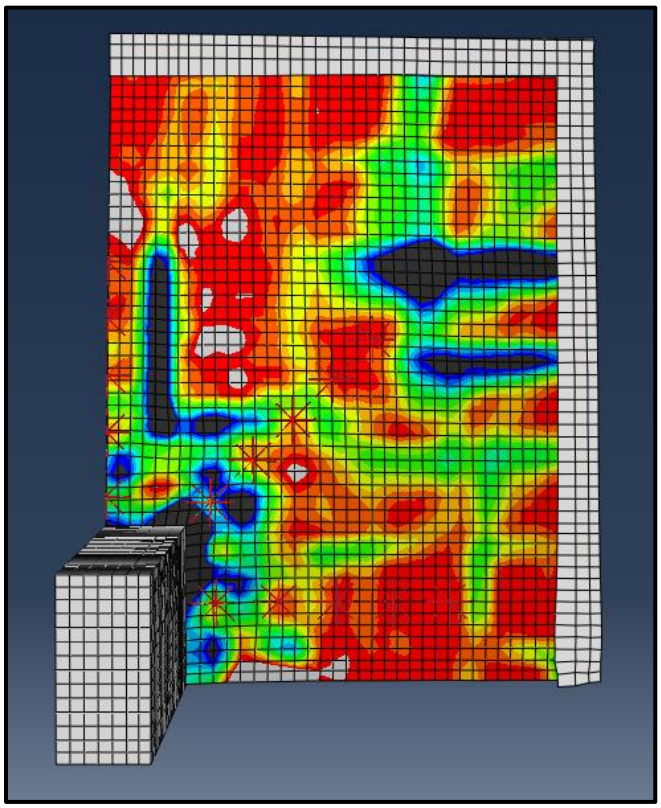

Figure C69: SX-2SR-5-AAA Tensile Face Crack Pattern

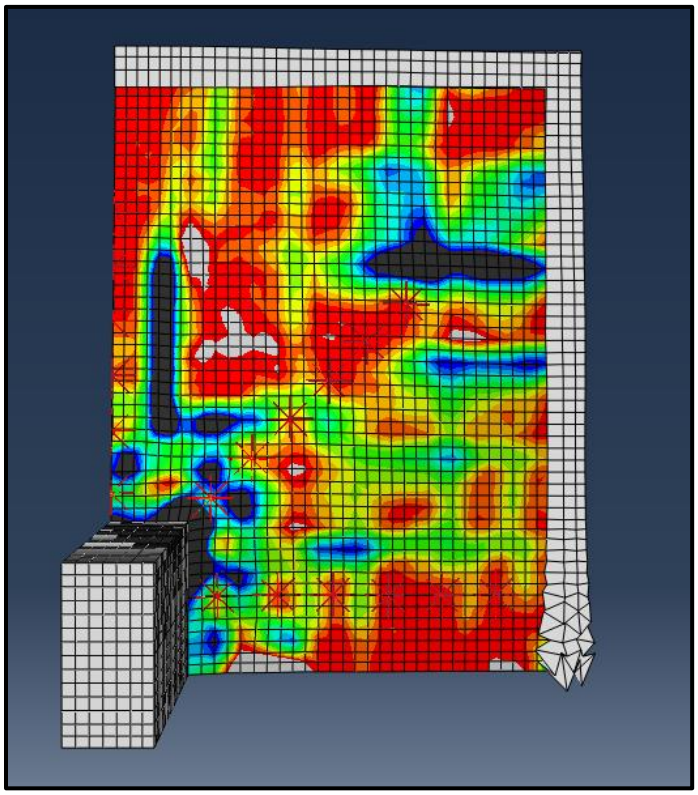

Figure C70: SX-2SR-6-AAAA Tensile Face Crack Pattern

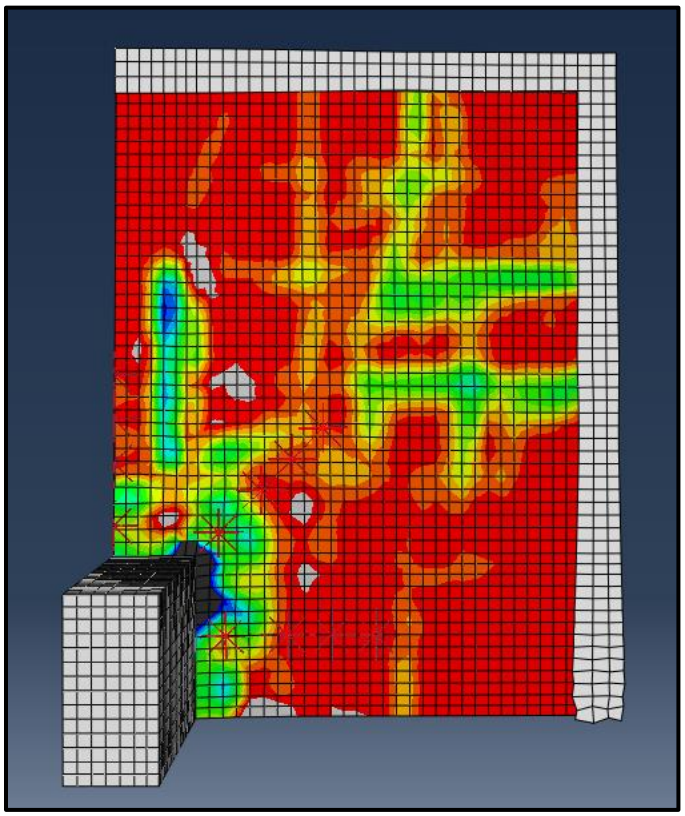

Figure C71: SX-2SR-4-DD Tensile Face Crack Pattern

Key for All SBS Models

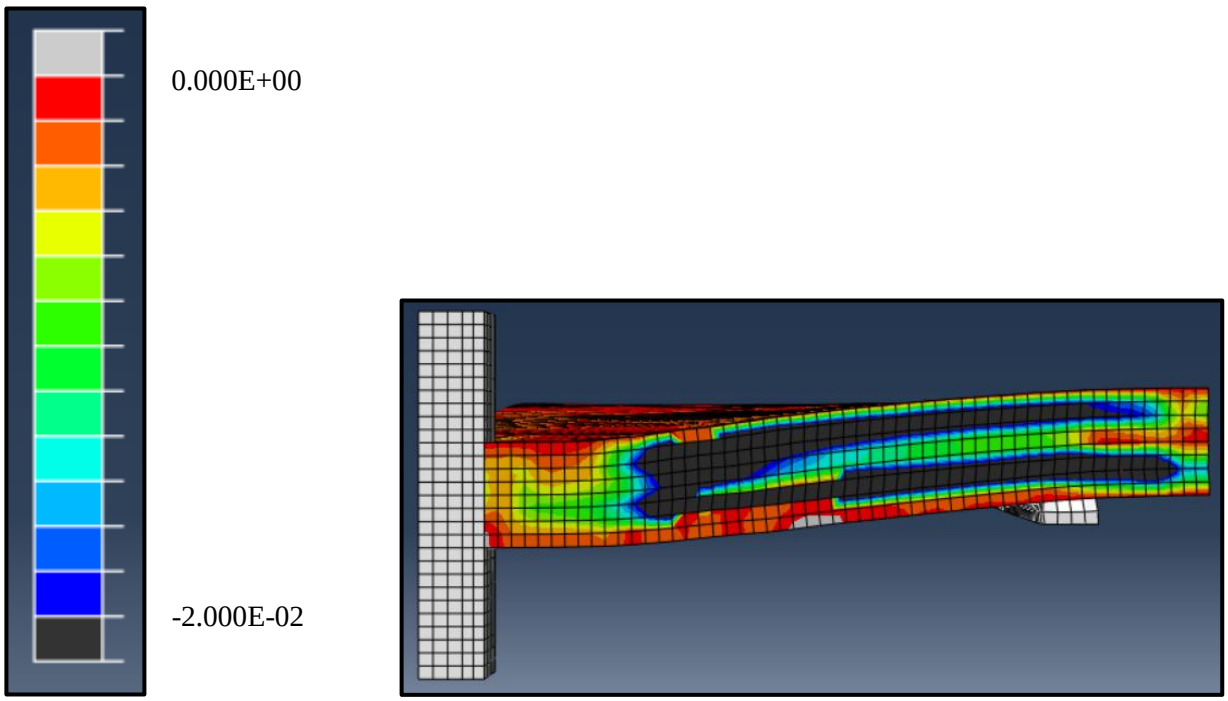

Figure C72: SB2-2 Post-Failure Side Crack Profile

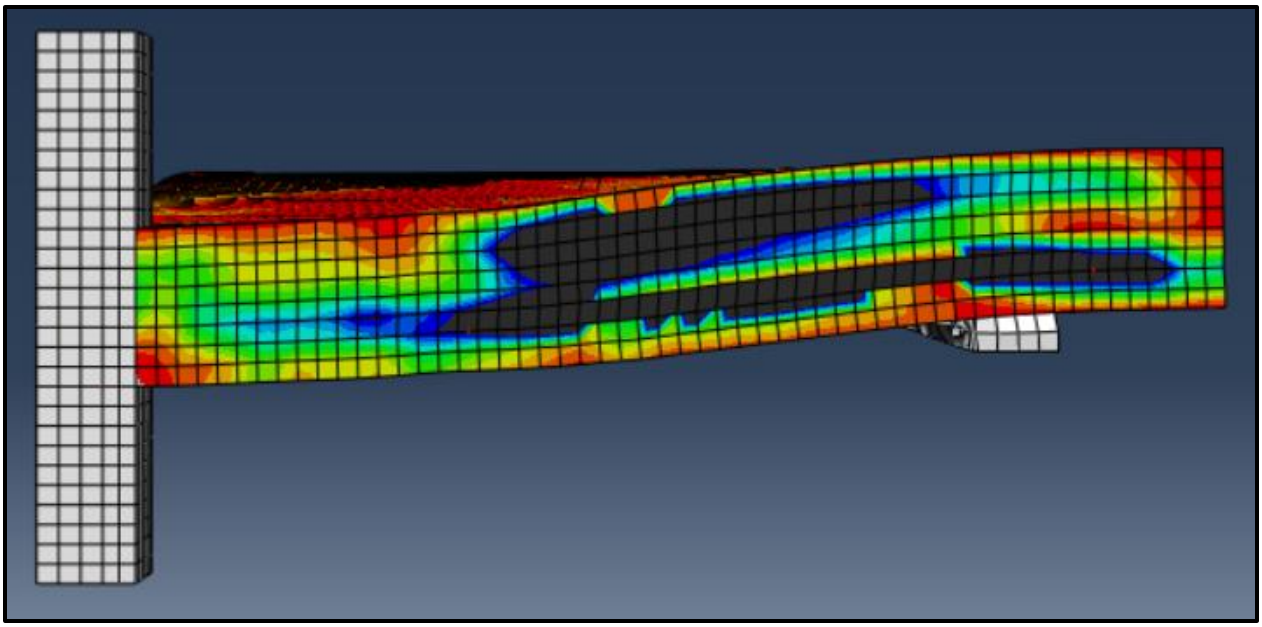

Figure C73: SB2-3-B Post-Failure Side Crack Profile

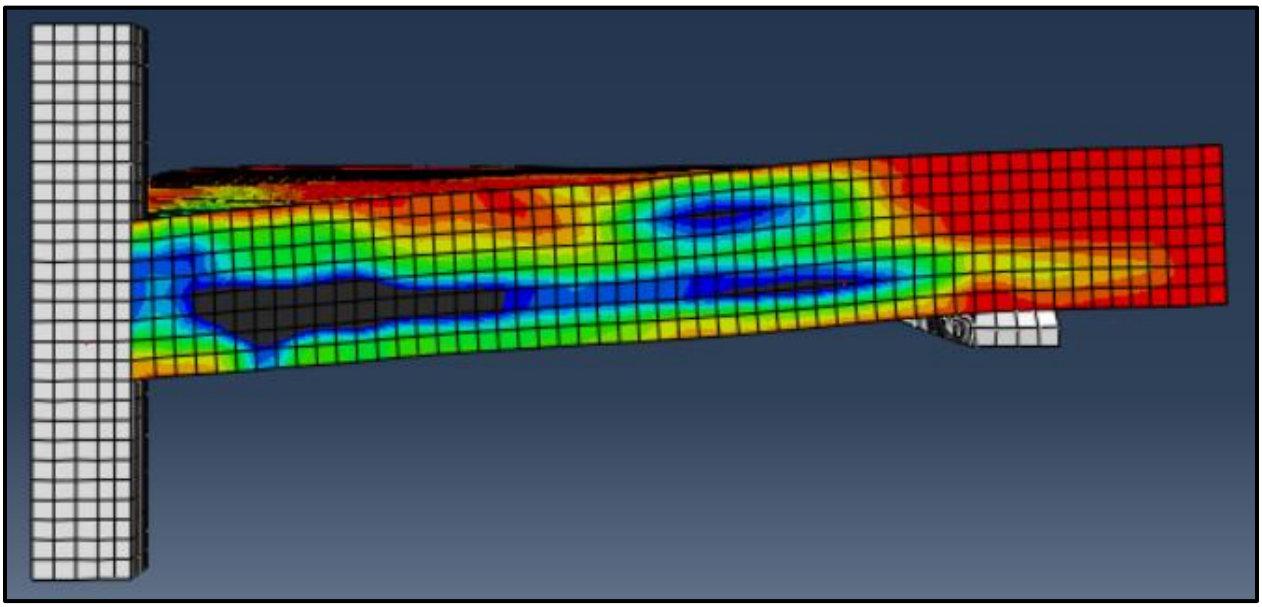

Figure C74: SB2-4-BB Post-Failure Side Crack Profile

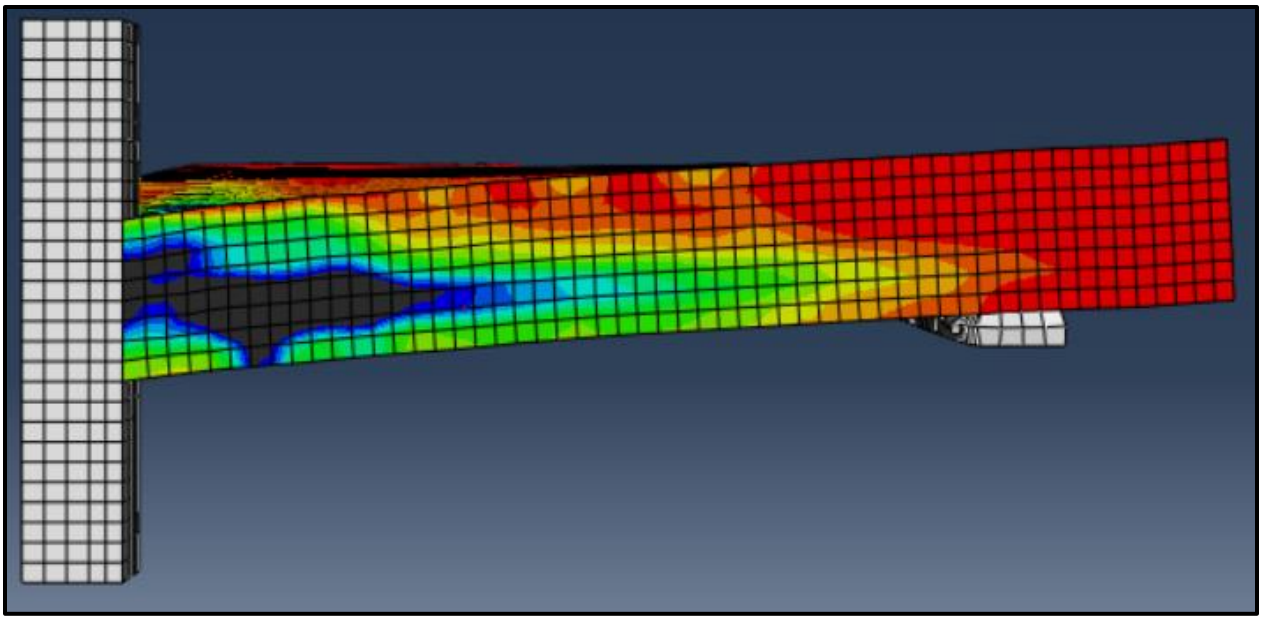

Figure C75: SB2-5-BBB Pre-Failure Side Crack Profile

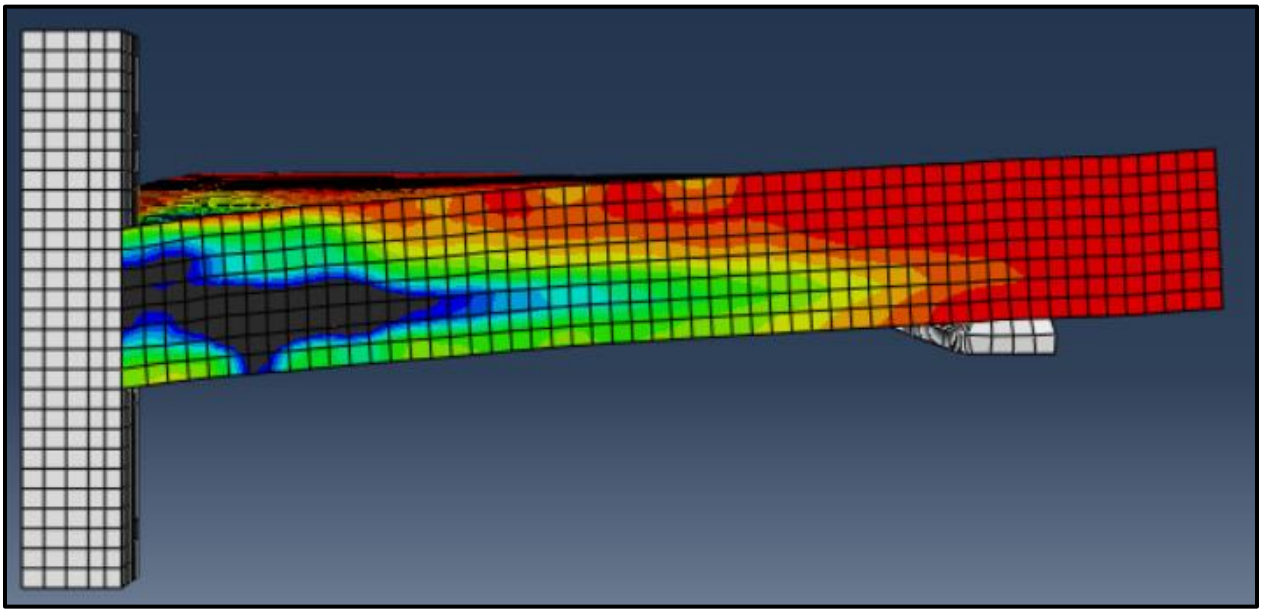

Figure C76: SB2-6-BBBB Pre-Failure Side Crack Profile

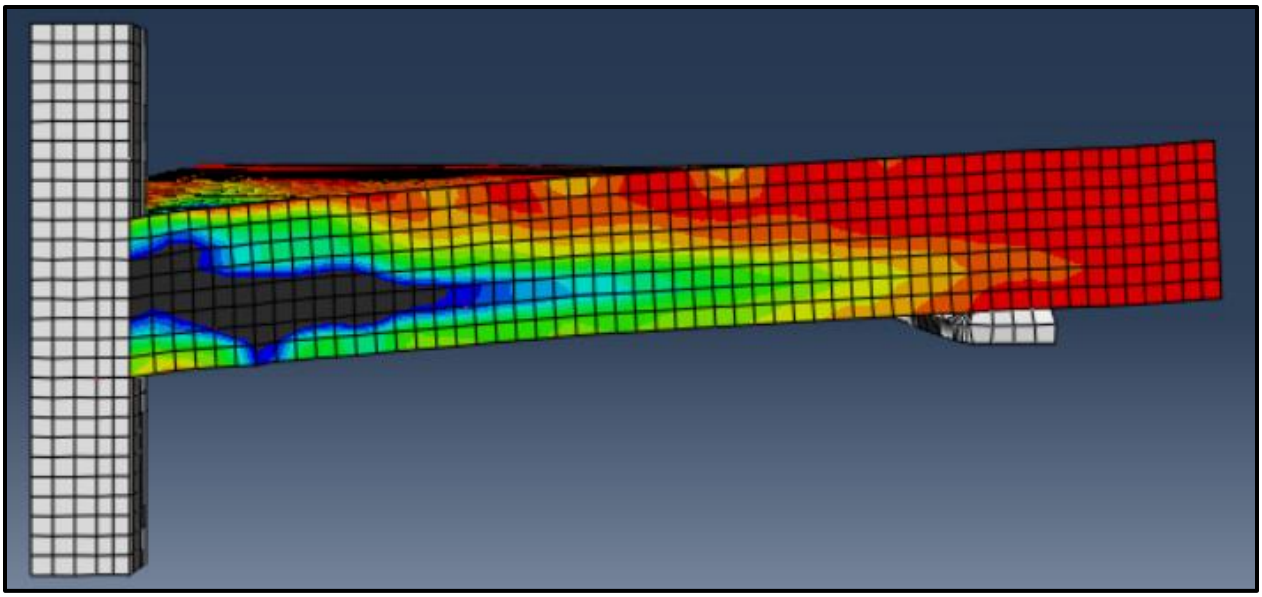

Figure C77: SB2-6-BBCC Pre-Failure Side Crack Profile

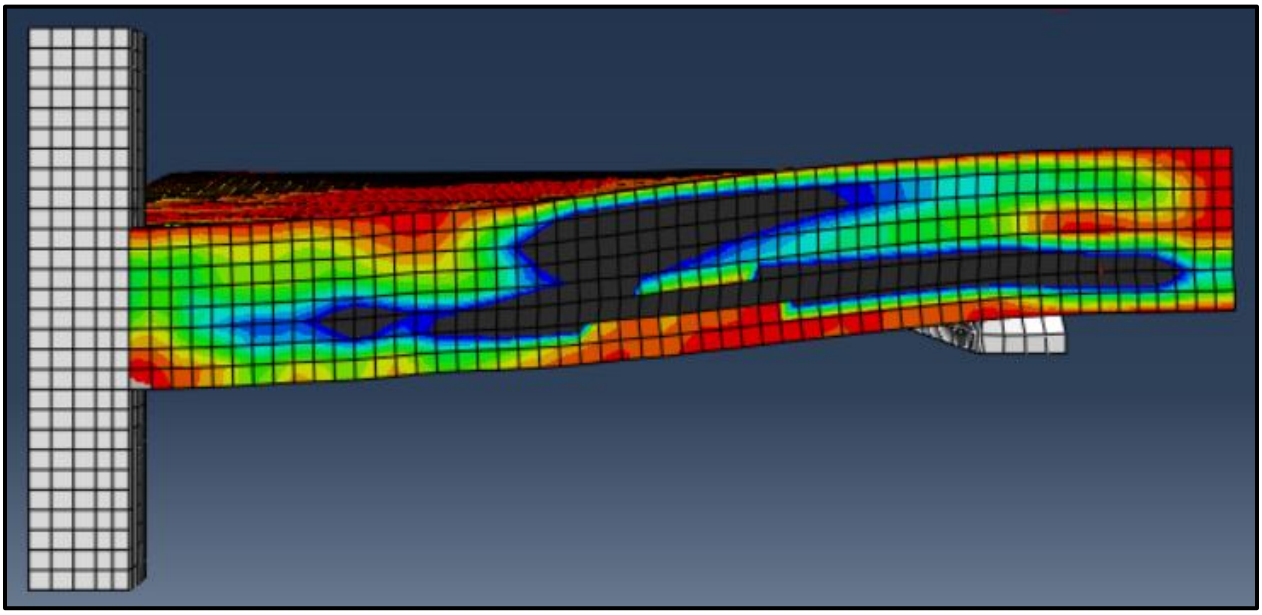

Figure C78: SB2-3-C Post-Failure Side Crack Profile

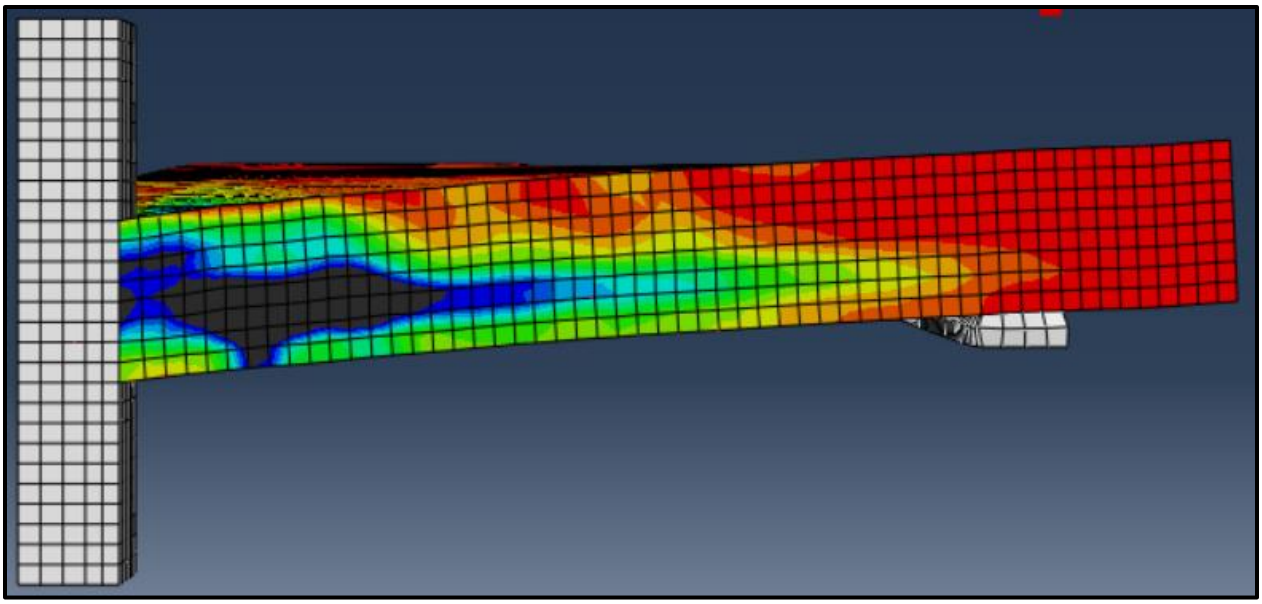

Figure C79: SB2-4-CC Pre-Failure Side Crack Profile

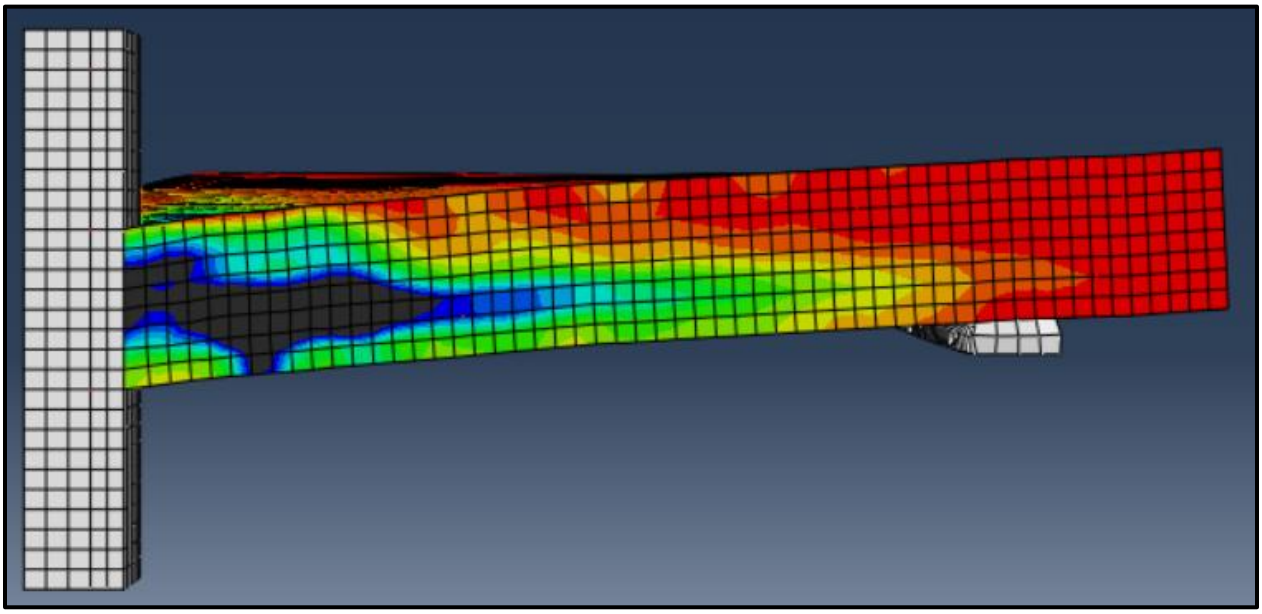

Figure C80: SB2-6-CCBB Pre-Failure Side Crack Profile

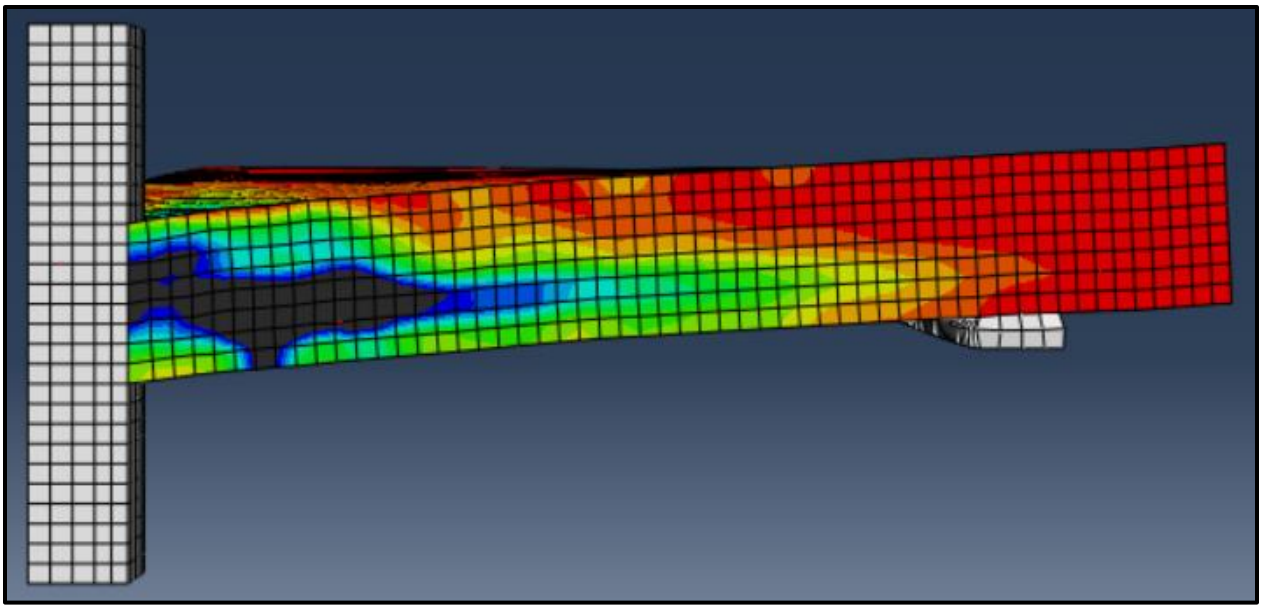

Figure C81: SB2-5-CCC Pre-Failure Side Crack Profile

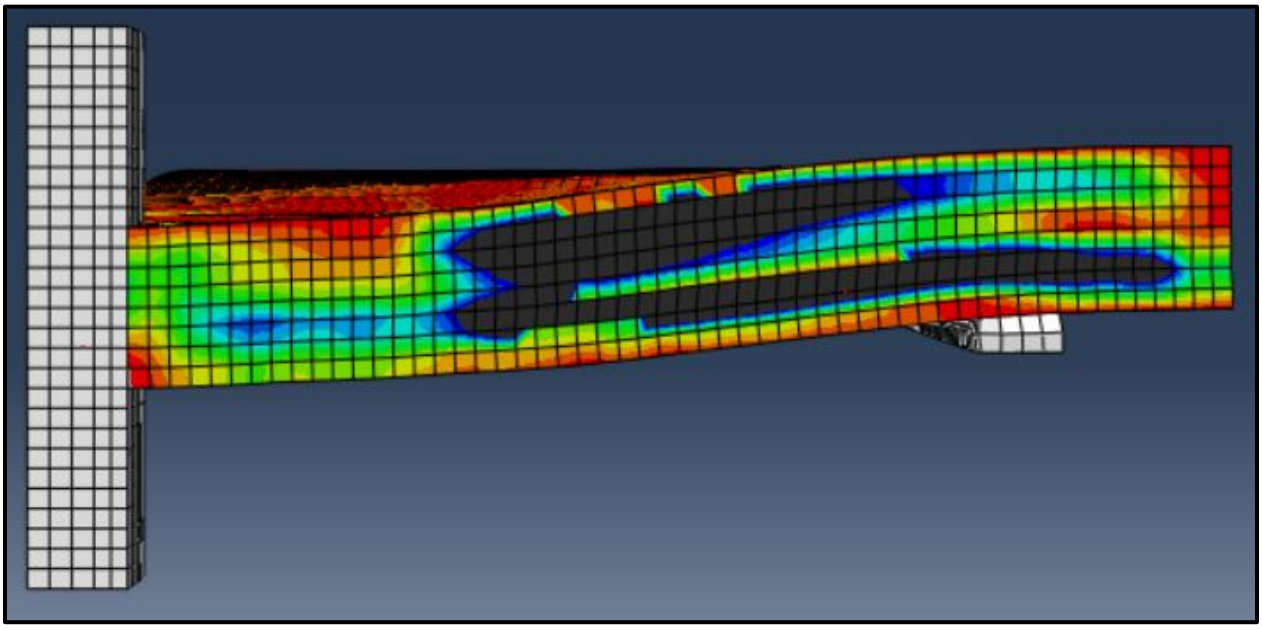

Figure C82: SB3-3 Post-Failure Side Crack Profile

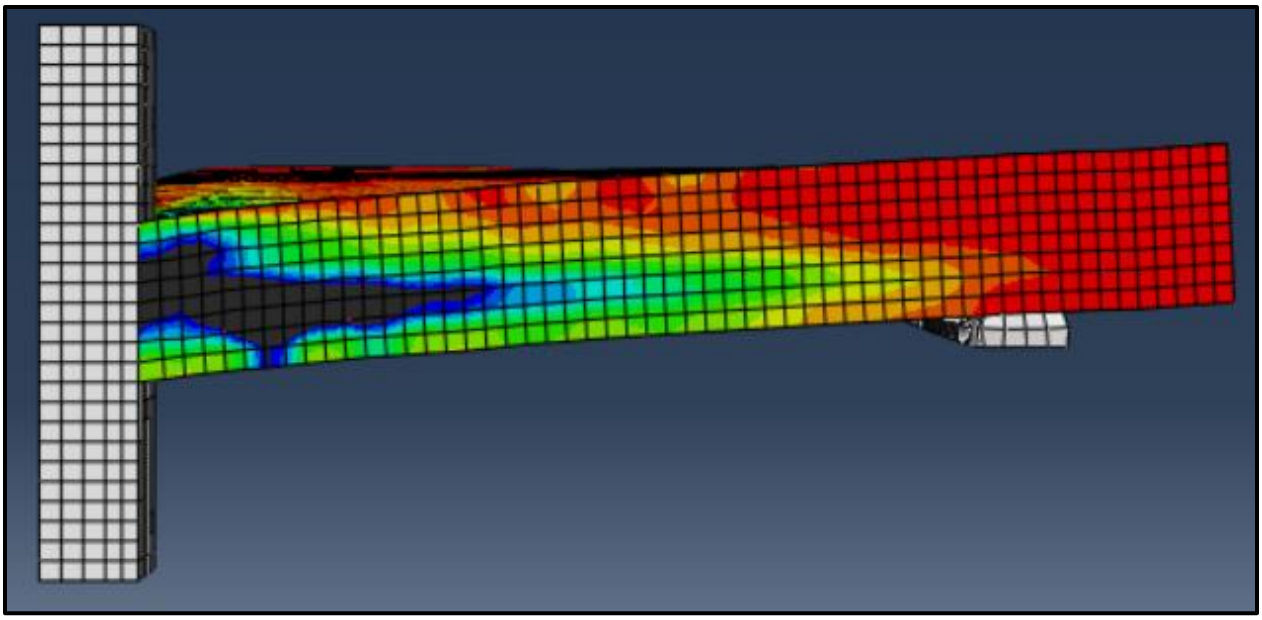

Figure C83: SB3-5-BB Pre-Failure Side Crack Profile

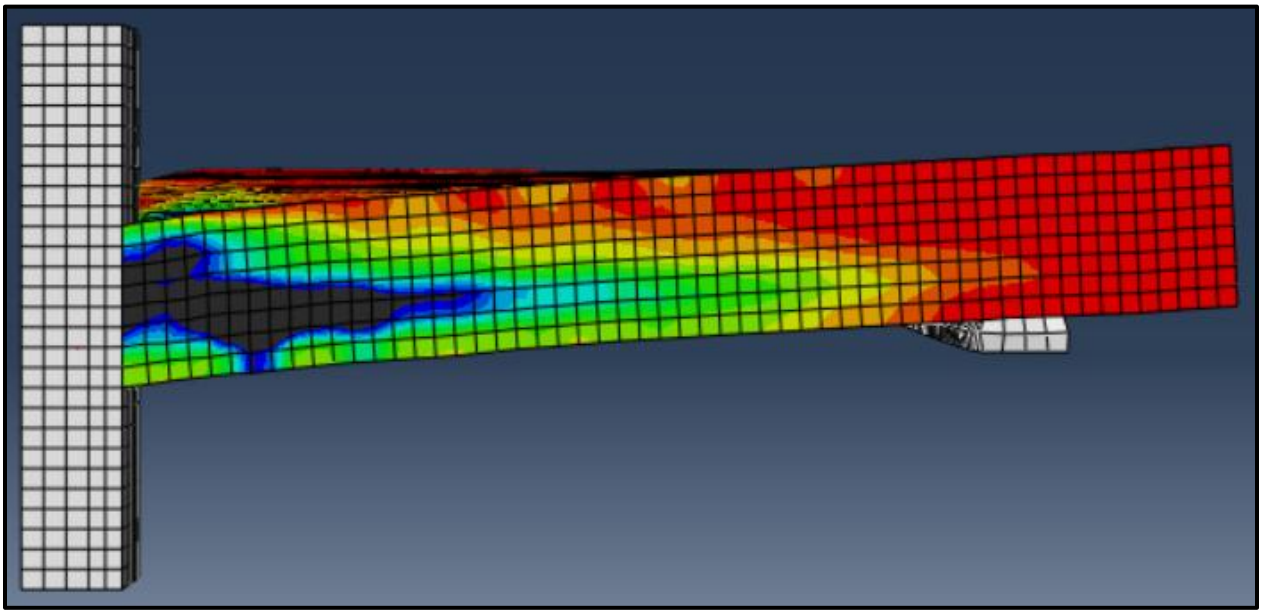

Figure C84: SB3-6-BBB Pre-Failure Side Crack Profile

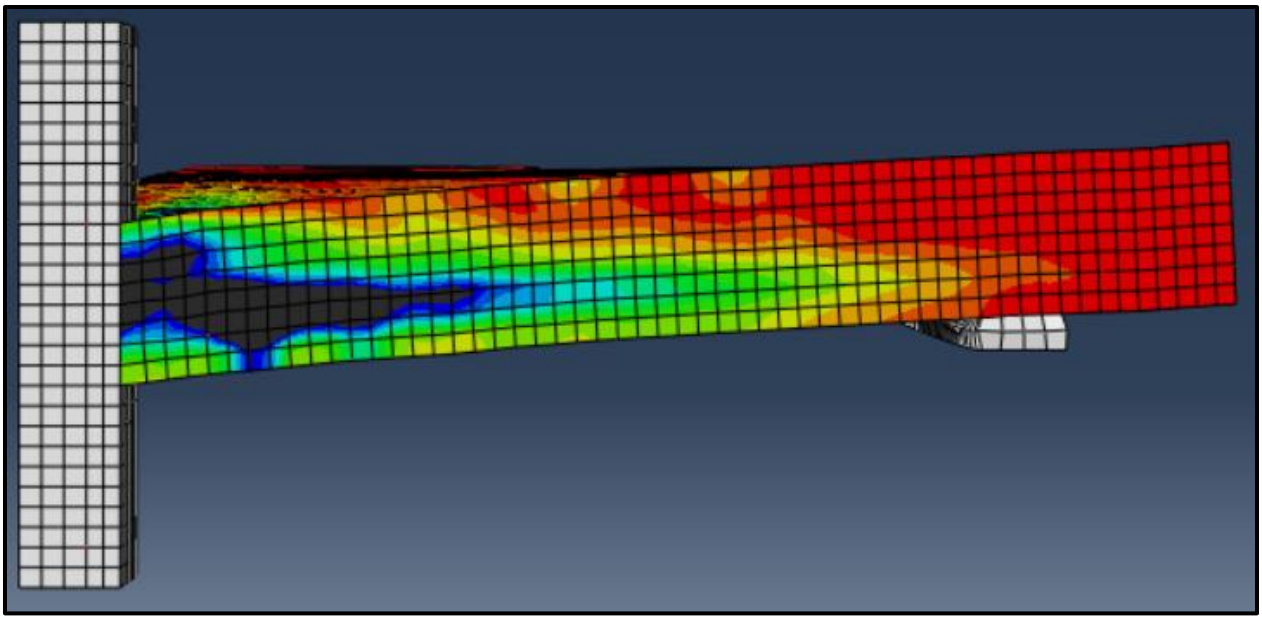

Figure C85: SB3-5-CC Pre-Failure Side Crack Profile

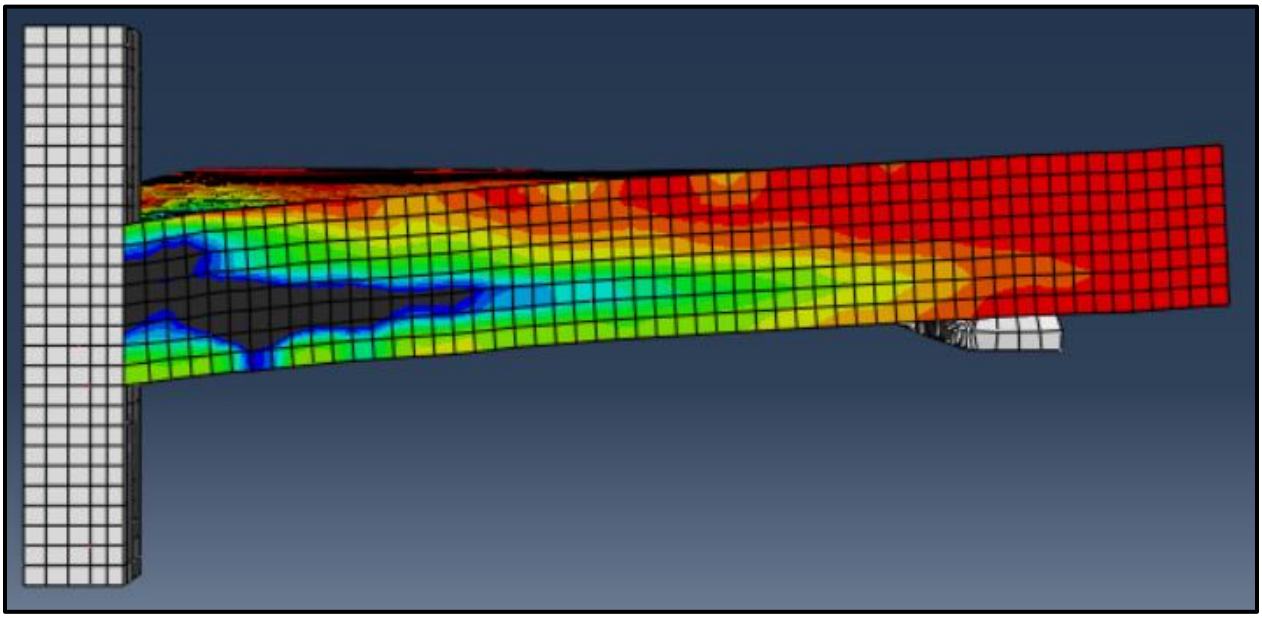

Figure C86: SB3-6-CCC Pre-Failure Side Crack Profile

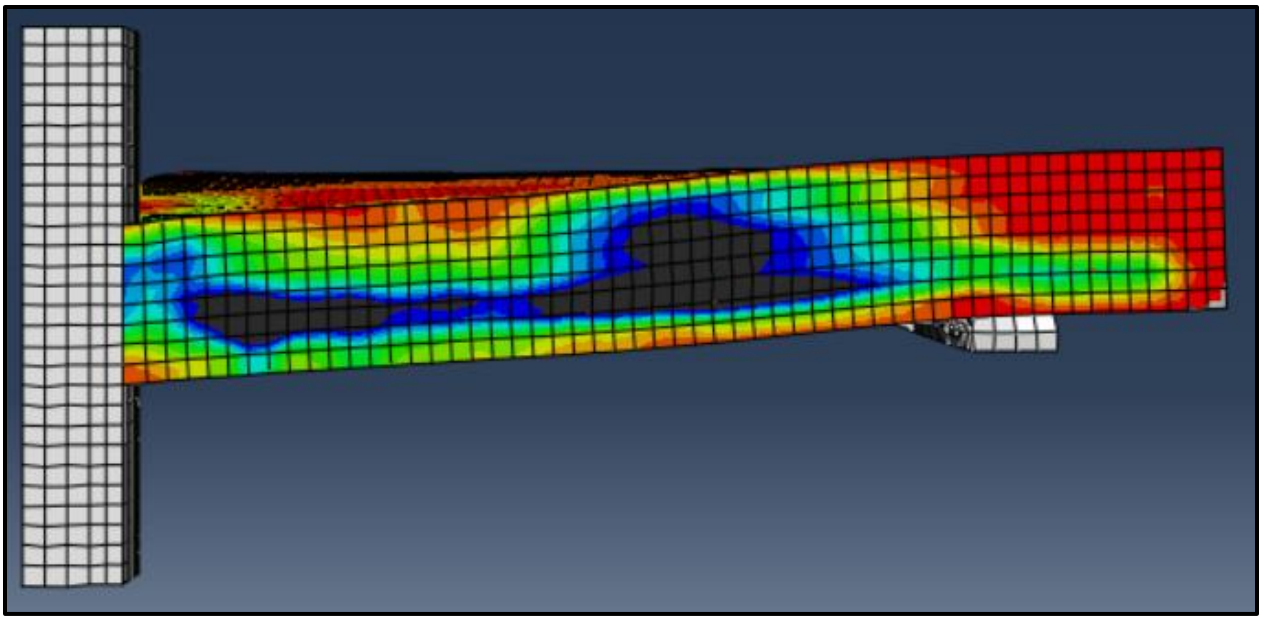

Figure C87: SB4-4 Post-Failure Side Crack Profile

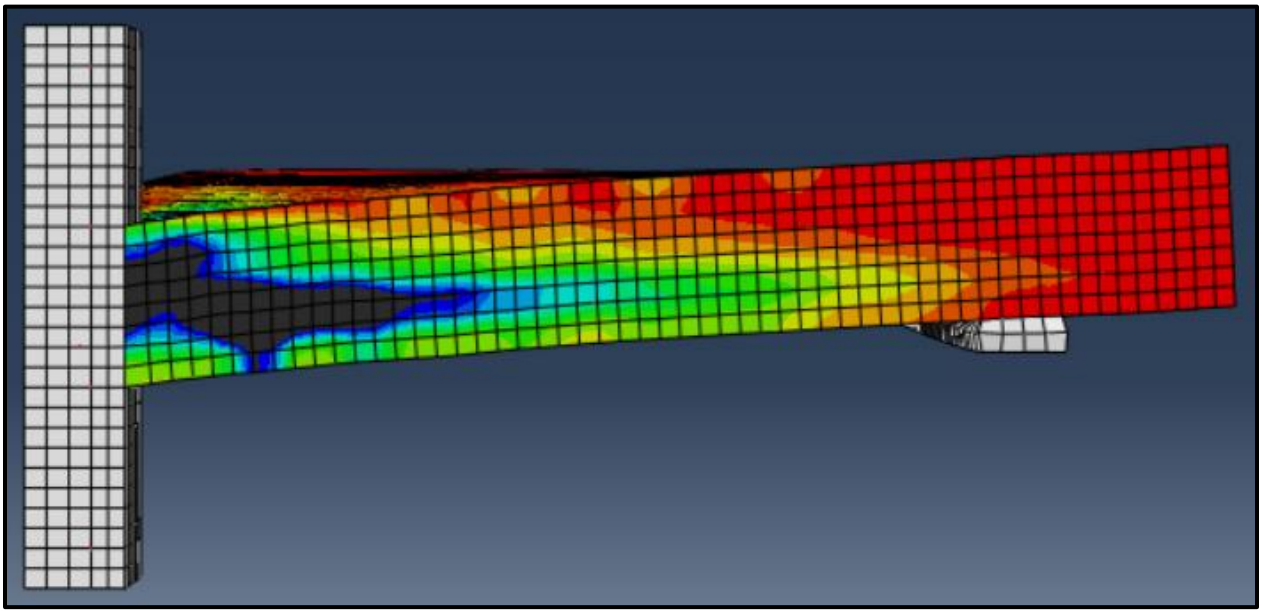

Figure C88: SB4-6-BB Pre-Failure Side Crack Profile

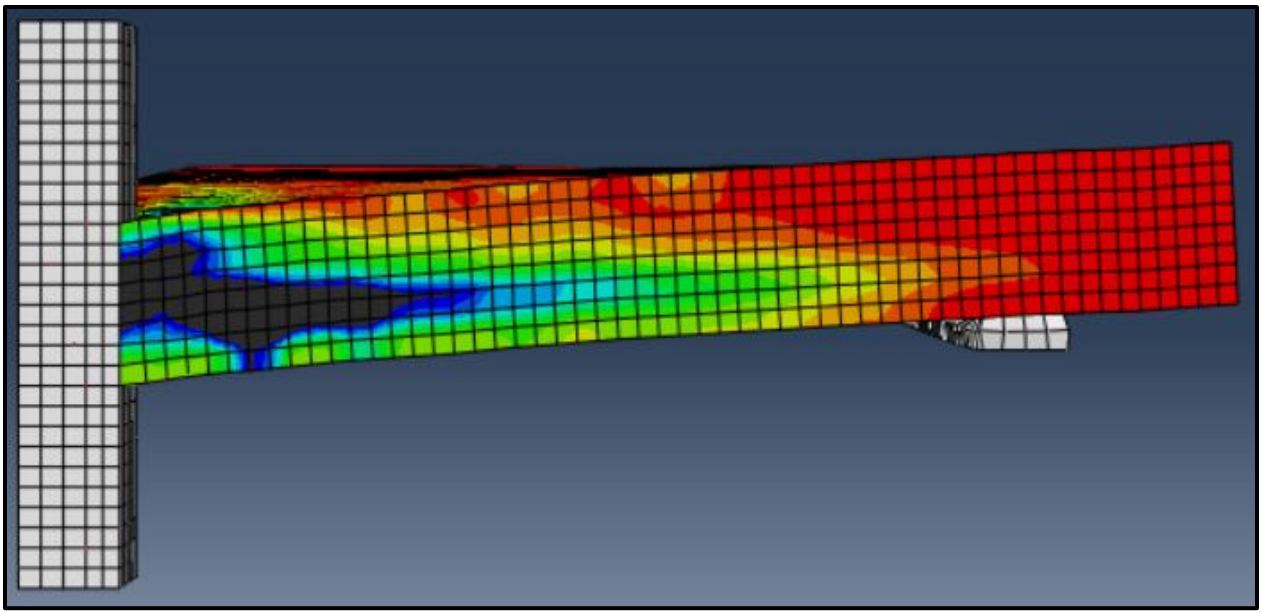

Figure C89: SB4-6-CC Pre-Failure Side Crack Profile

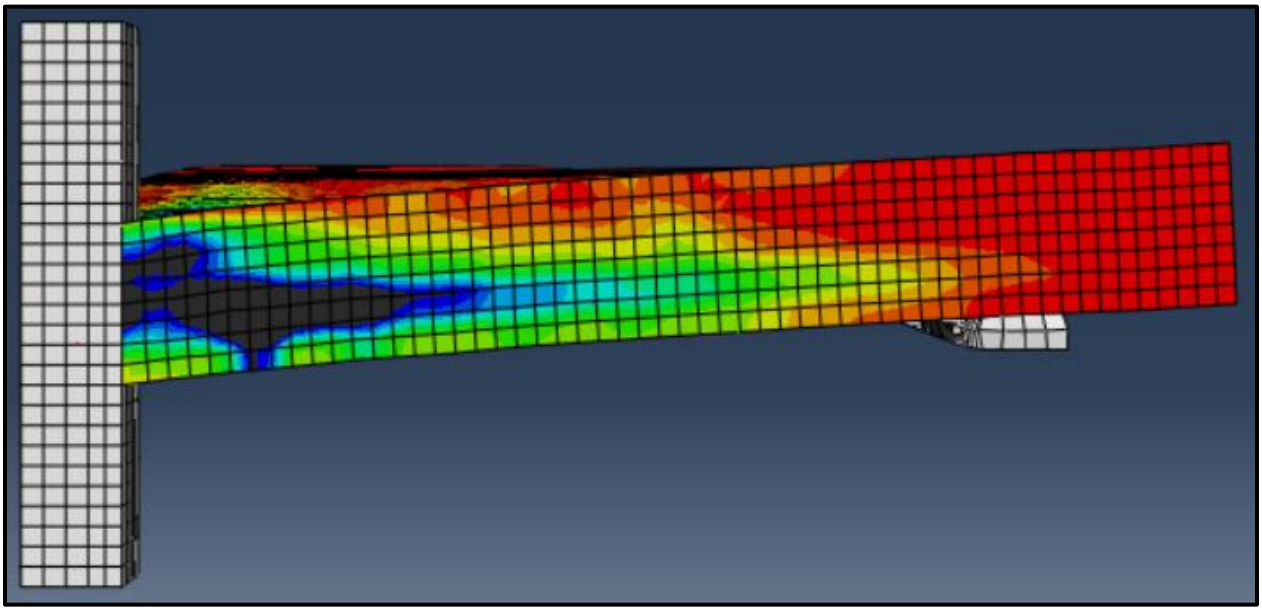

Figure C90: SB4-5-A Pre-Failure Side Crack Profile

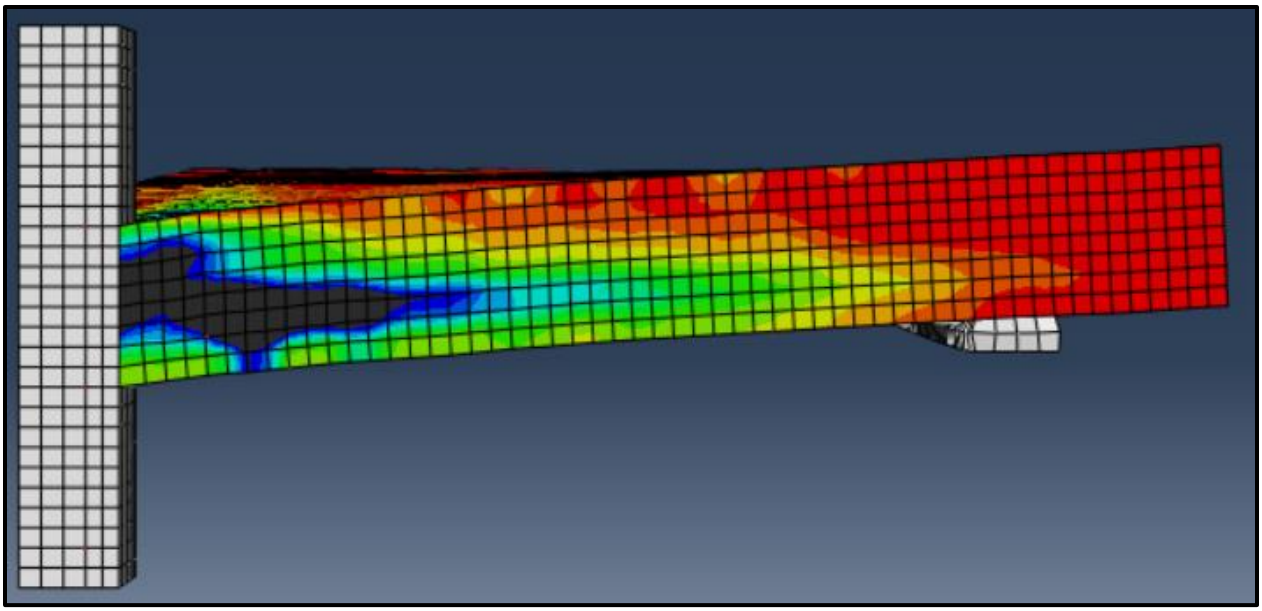

Figure C91: SB4-6-AA Pre-Failure Side Crack Profile

Key for All SXS Models

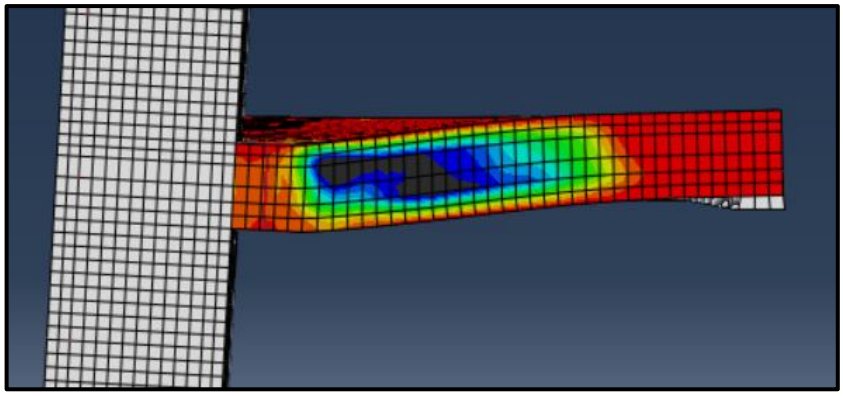

Figure C92: SX-1SR-1 Post-Failure Side Crack Profile

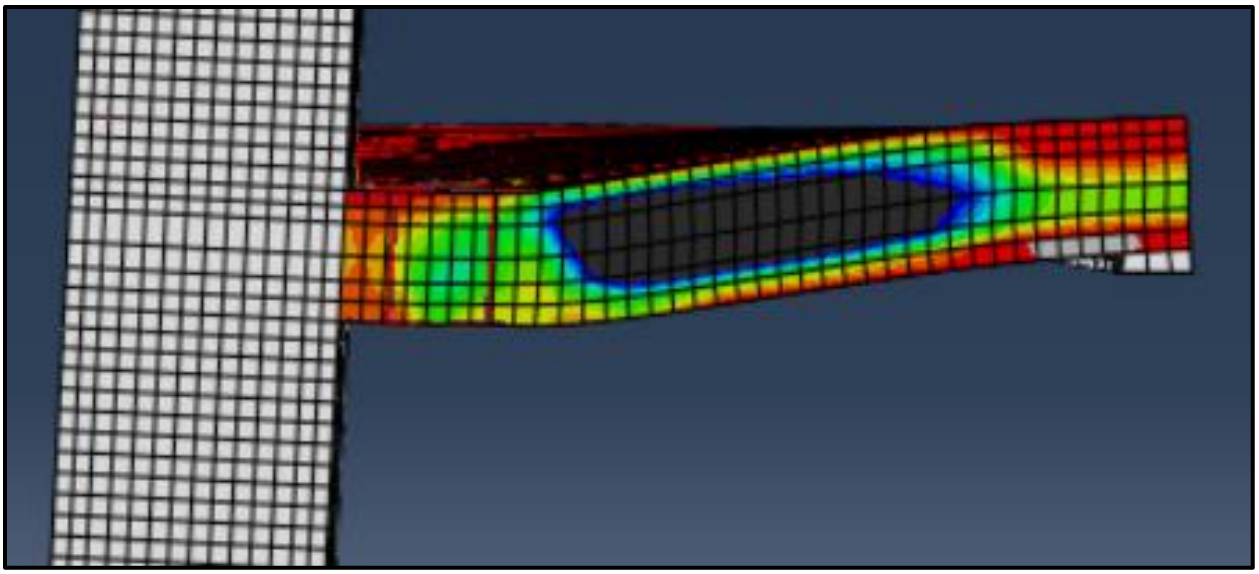

Figure C93: SX-2SR-2 Post-Failure Side Crack Profile

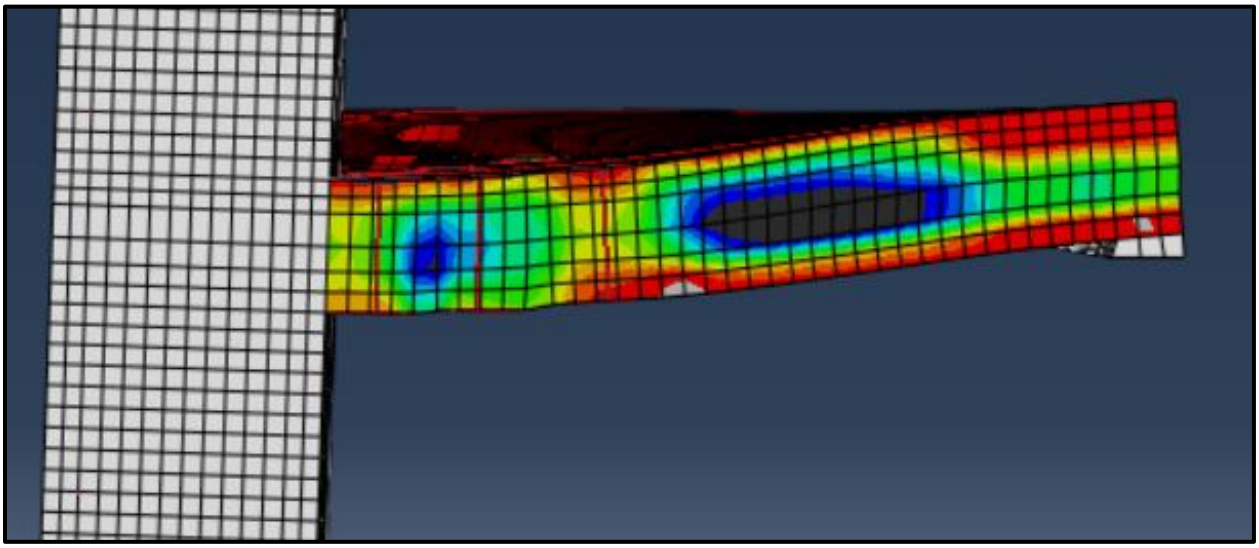

Figure C94: SX-2SR-3-B Post-Failure Side Crack Profile

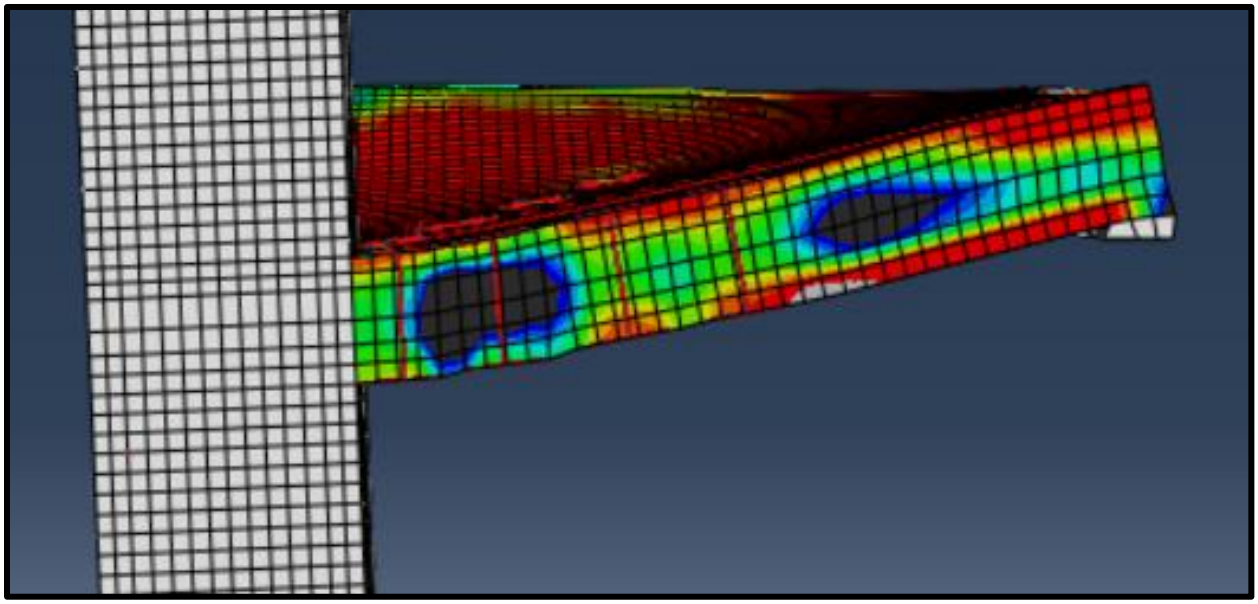

Figure C95: SX-2SR-4-BB Post-Failure Side Crack Profile

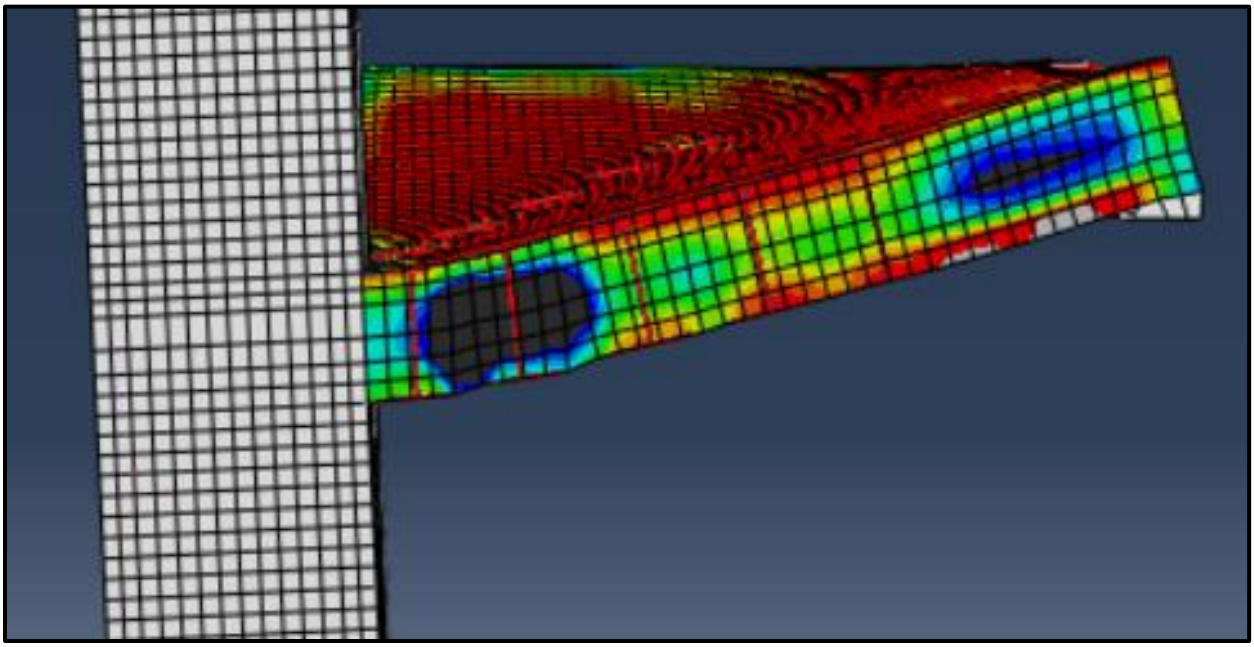

Figure C96: SX-2SR-5-BBB Post-Failure Side Crack Profile

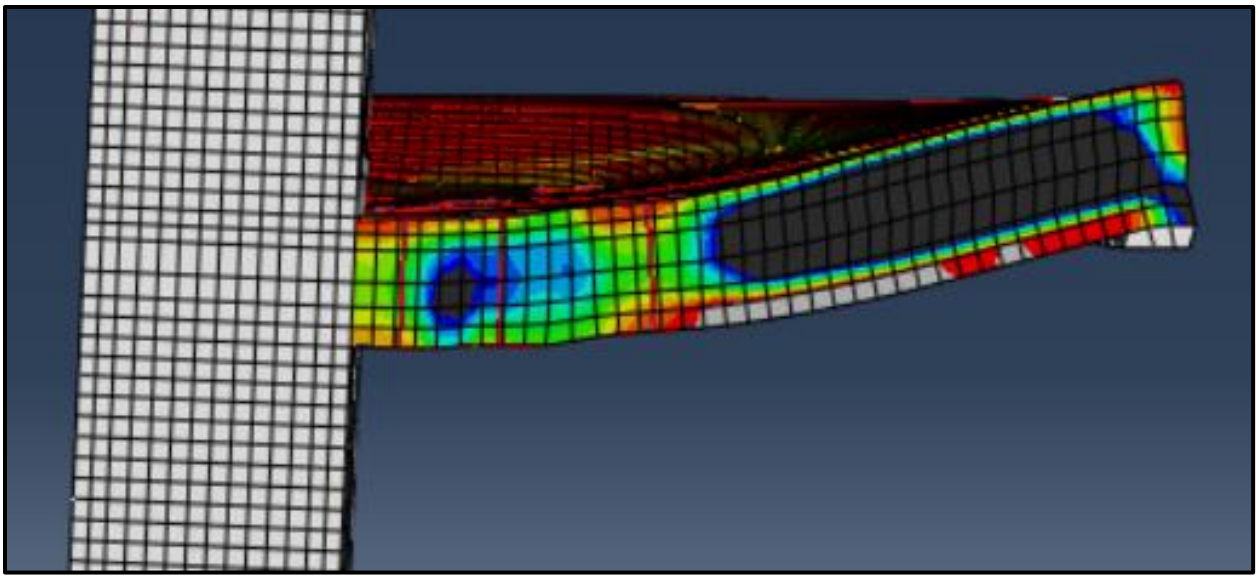

Figure C97: SX-2SR-3-C Post-Failure Side Crack Profile

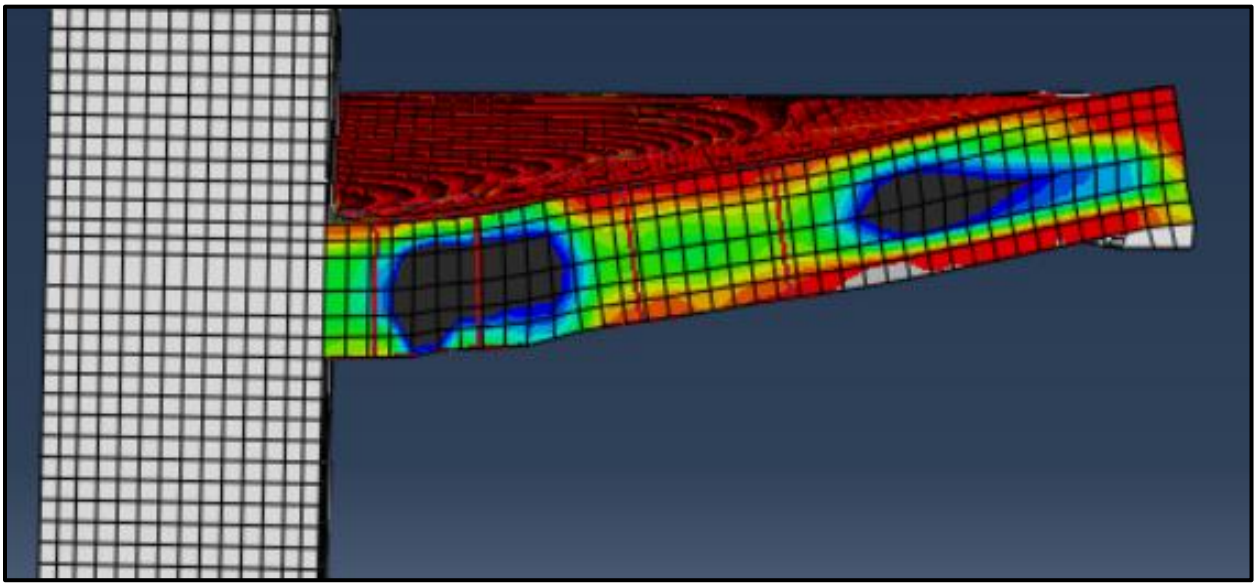

Figure C98: SX-2SR-4-CC Post-Failure Side Crack Profile

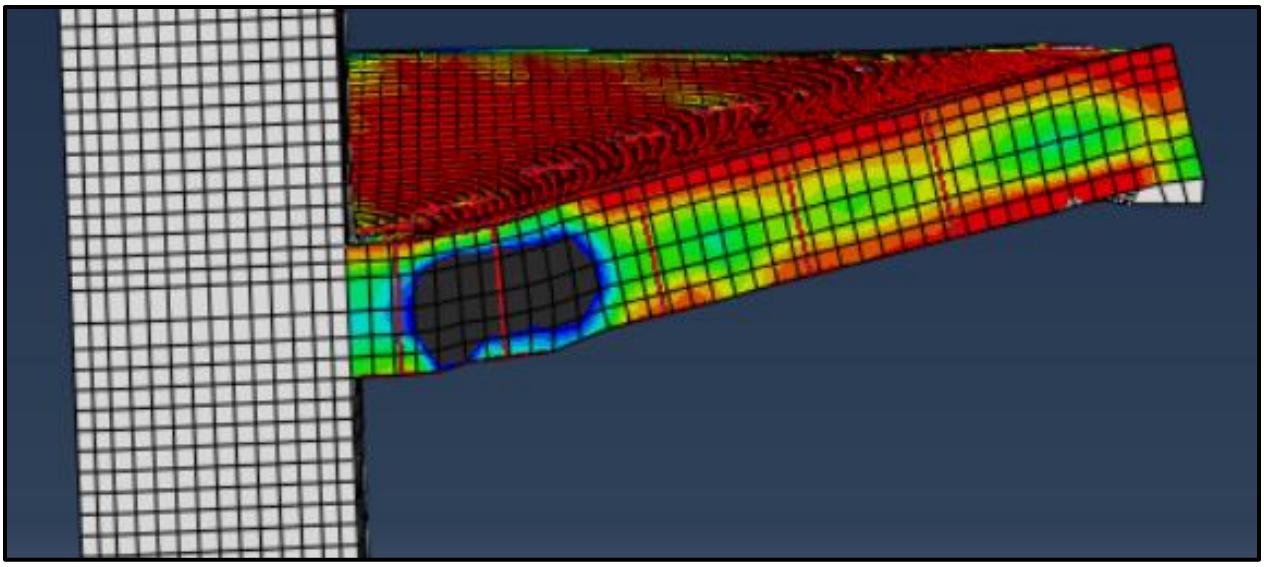

Figure C99: SX-2SR-5-CCC Post-Failure Side Crack Profile

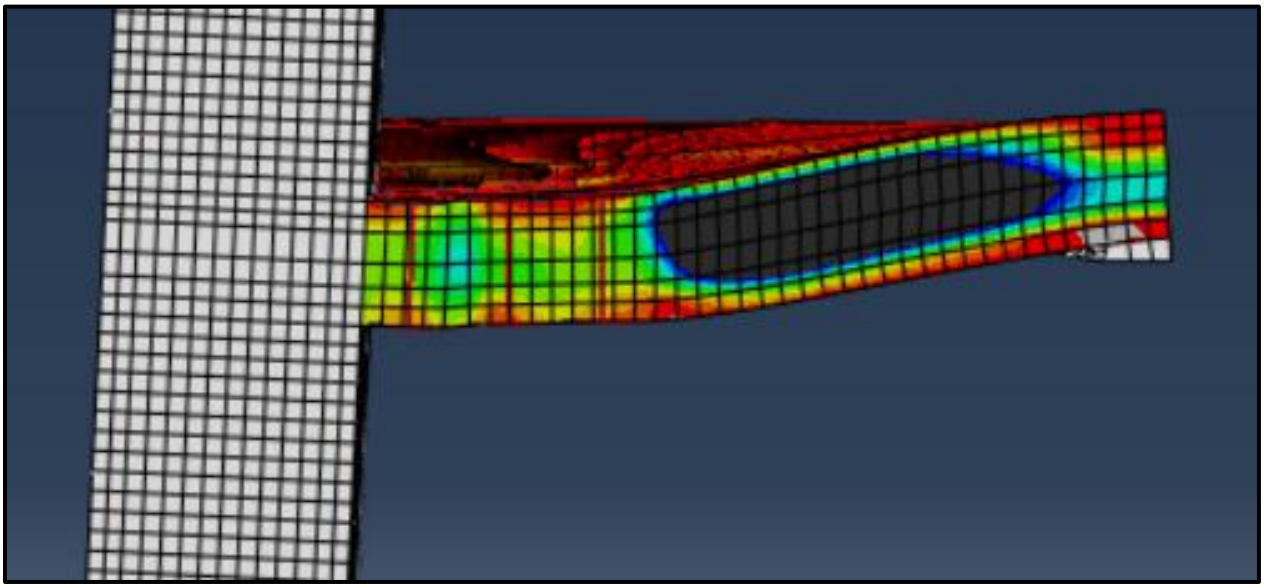

Figure C100: SX-2SR-3-A Post-Failure Side Crack Profile

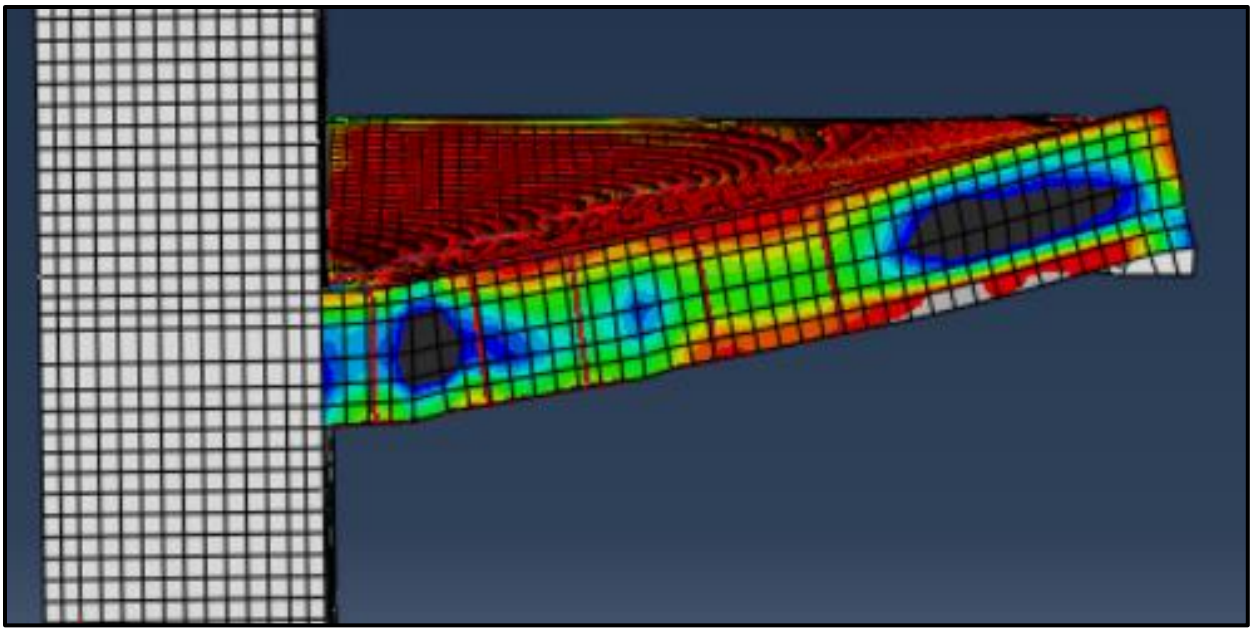

Figure C101: SX-2SR-5-ABB Post-Failure Side Crack Profile

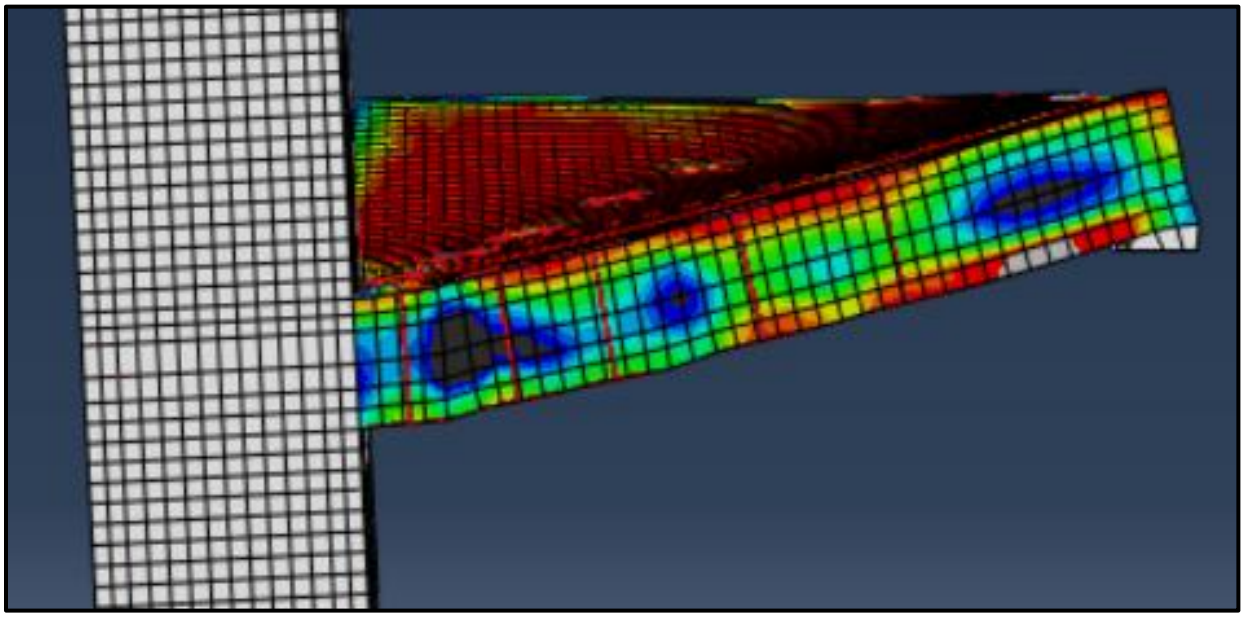

Figure C102: SX-2SR-5-ACC Post-Failure Side Crack Profile

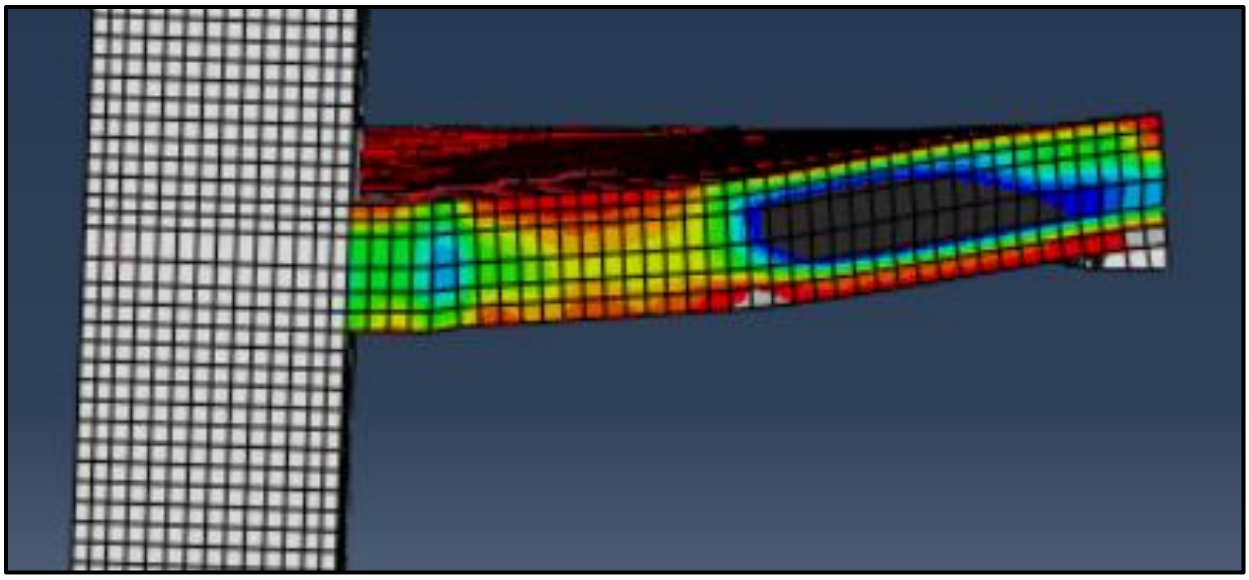

Figure C103: SX-2SR-4-AA Post-Failure Side Crack Profile

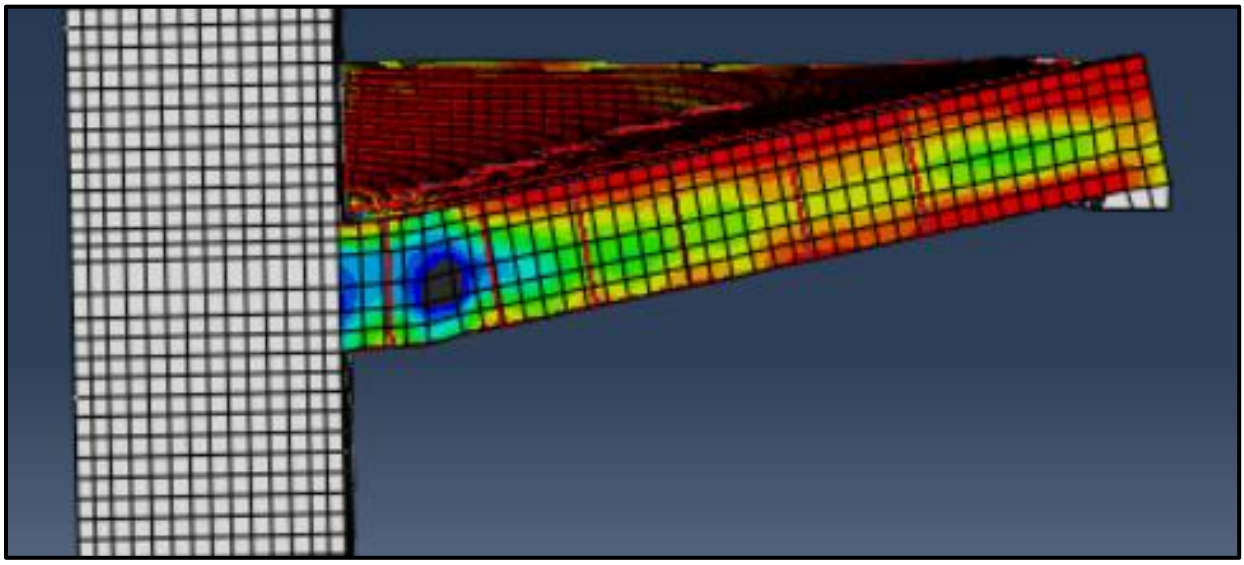

Figure C104: SX-2SR-6-AABB Post-Failure Side Crack Profile

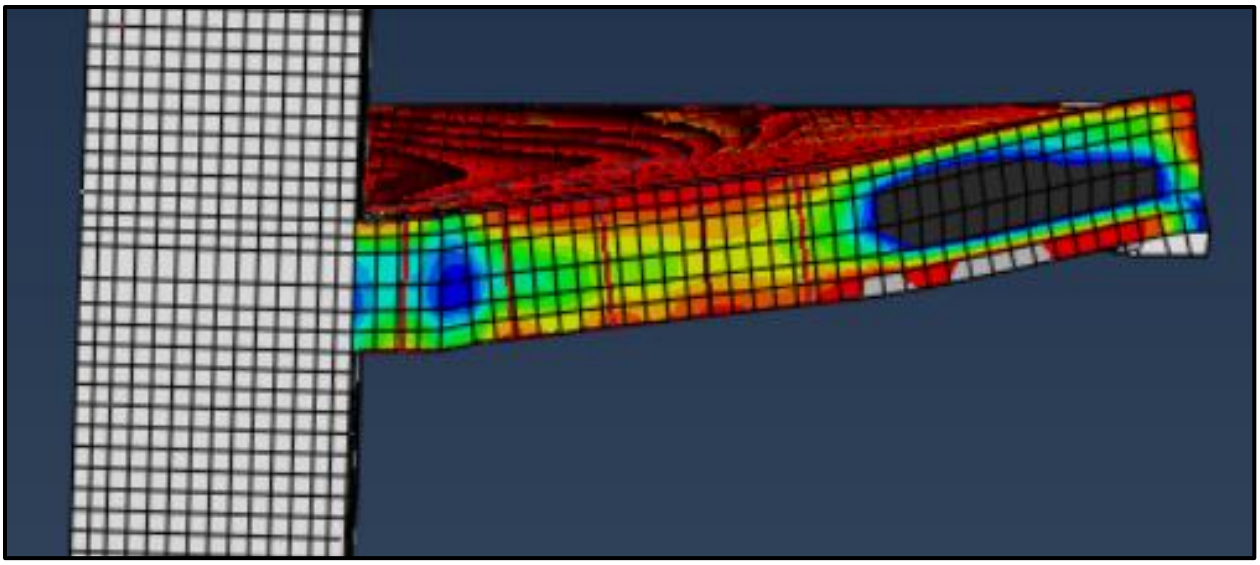

Figure C105: SX-2SR-5-AAA Post-Failure Side Crack Profile

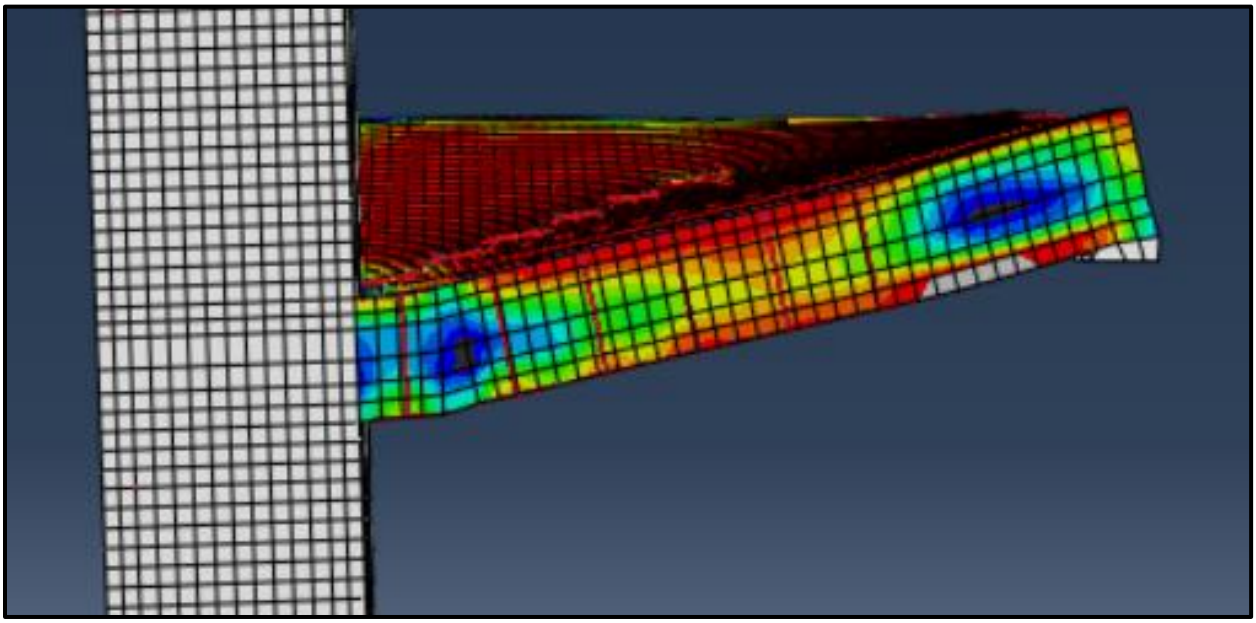

Figure C106: SX-2SR-6-AAAA Post-Failure Side Crack Profile

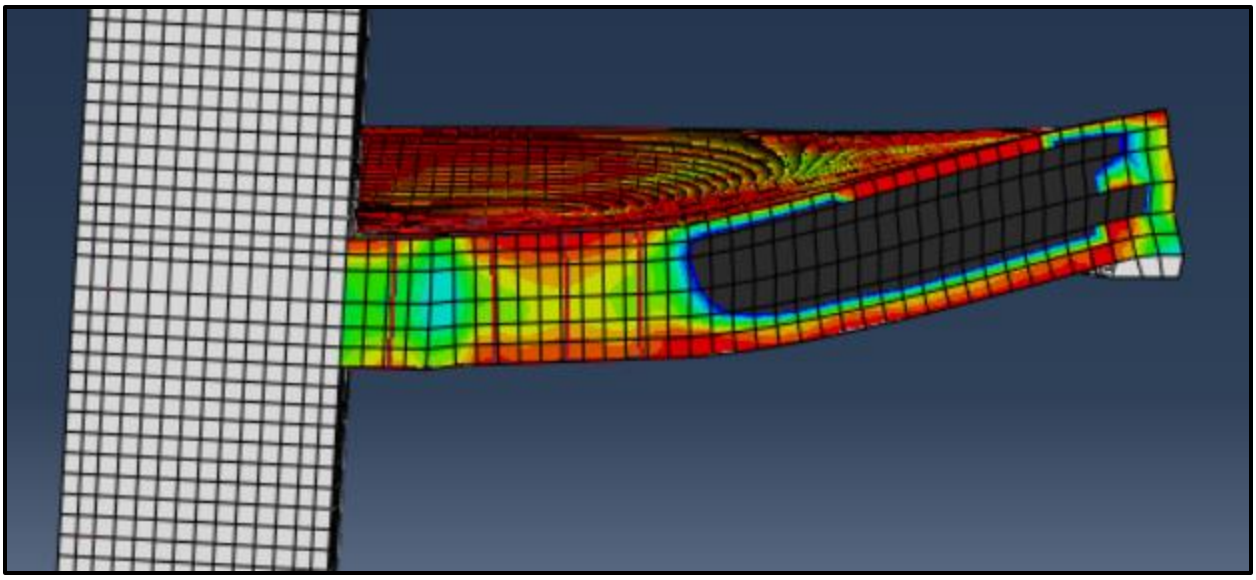

Figure C107: SX-2SR-4-DD Post-Failure Side Crack Profile

Appendix D: Openings Study Supplemental Figures

List of Figures

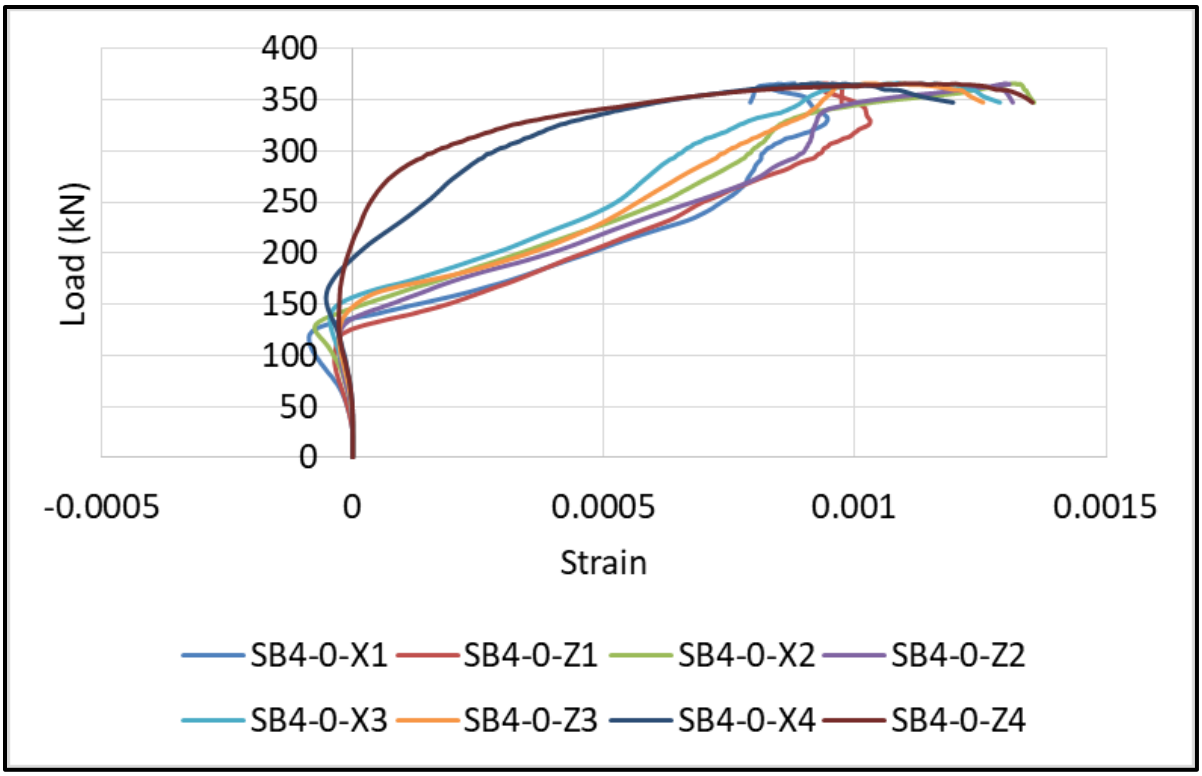

Figure D1: SB4-0 Bolt Strain Diagram

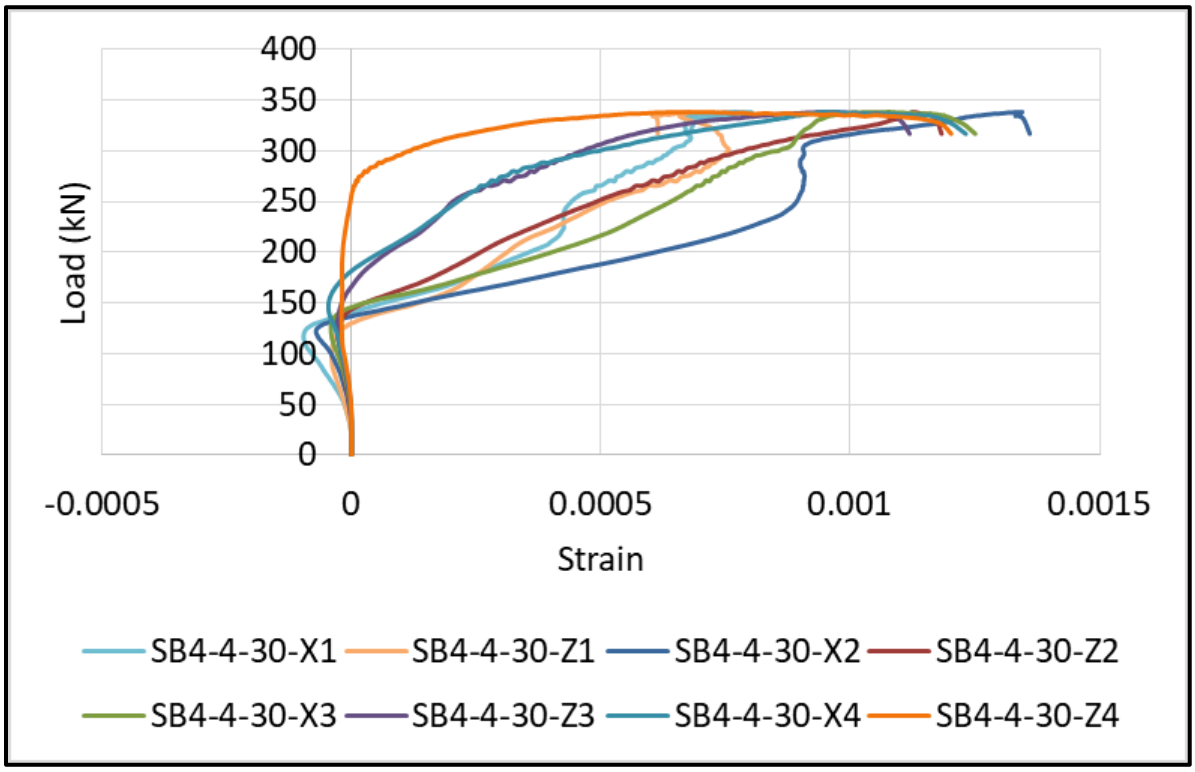

Figure D2: SB4-4-30 Bolt Strain Diagram

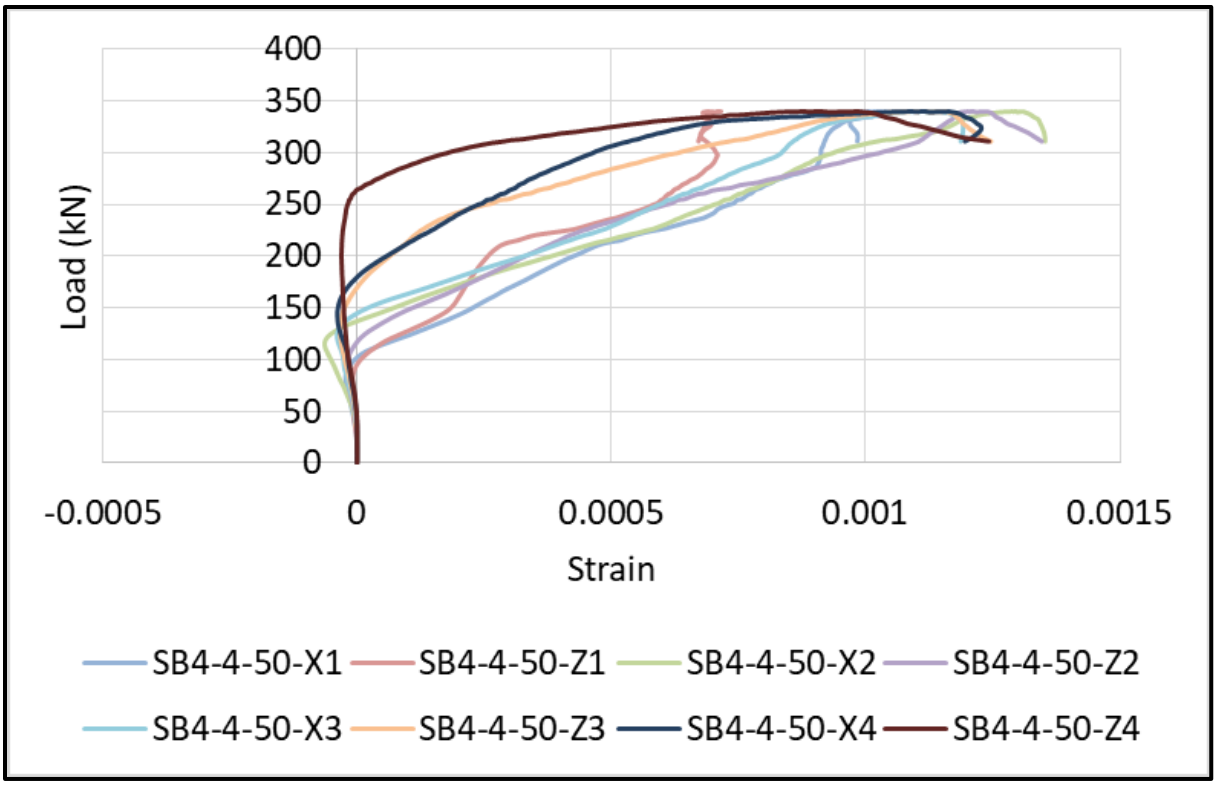

Figure D3: SB4-4-50 Bolt Strain Diagram

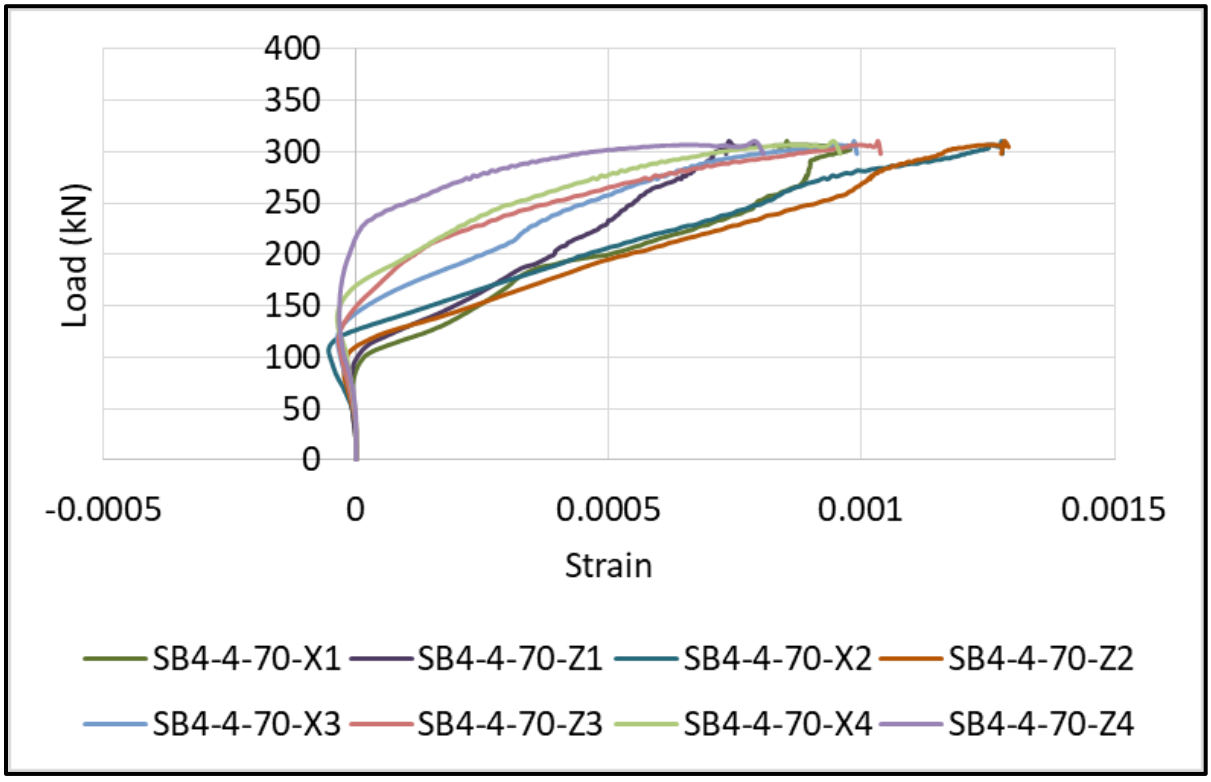

Figure D4: SB4-4-70 Bolt Strain Diagram

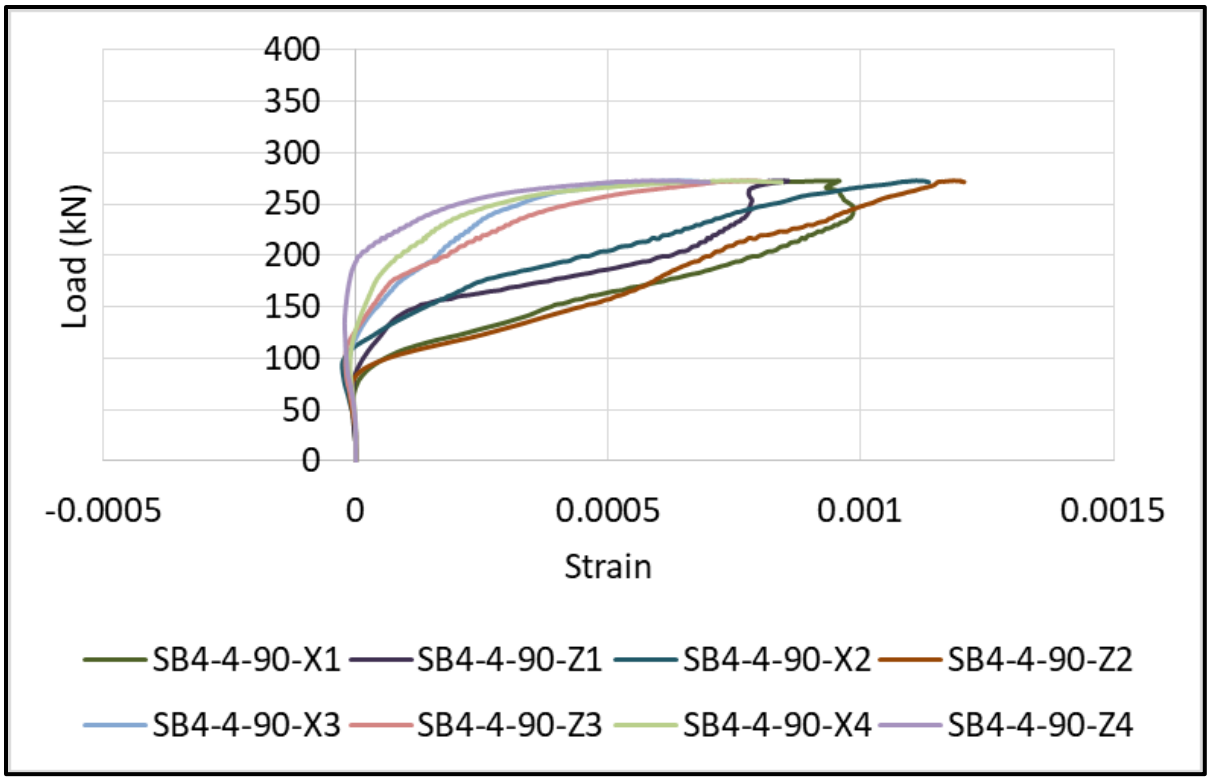

Figure D5: SB4-4-90 Bolt Strain Diagram

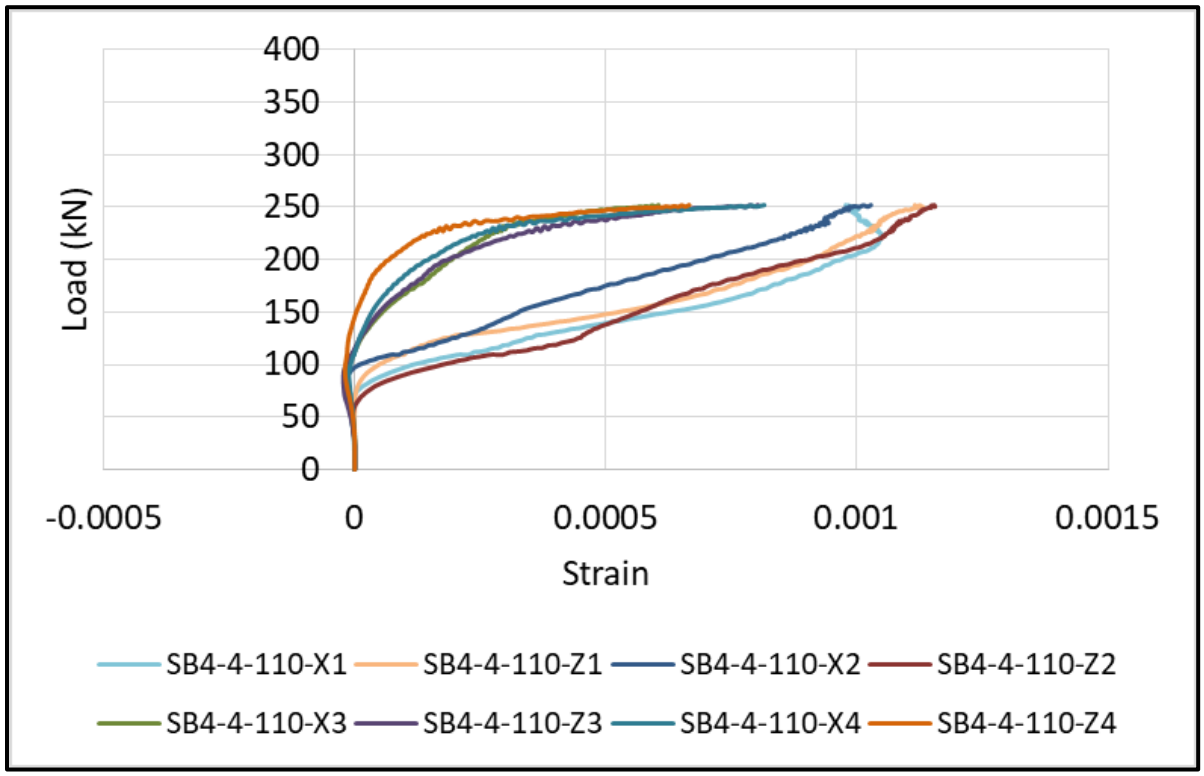

Figure D6: SB4-4-110 Bolt Strain Diagram

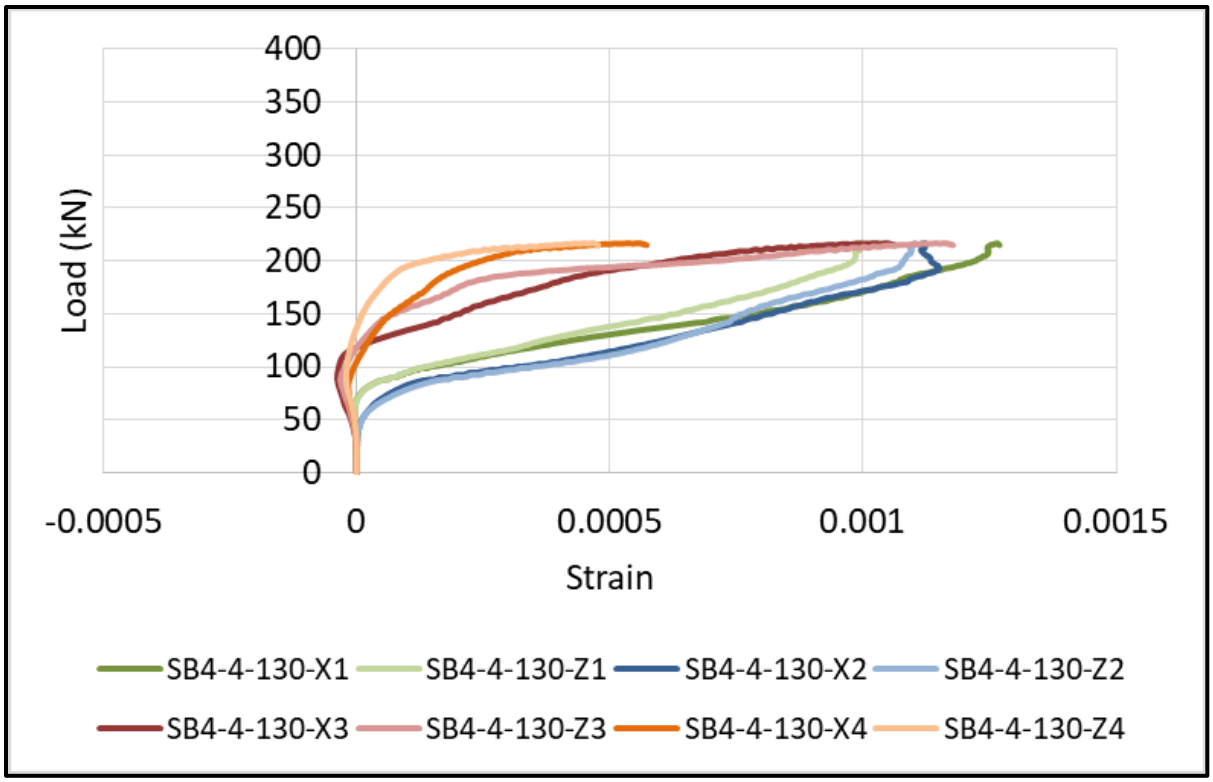

Figure D7: SB4-4-130 Bolt Strain Diagram

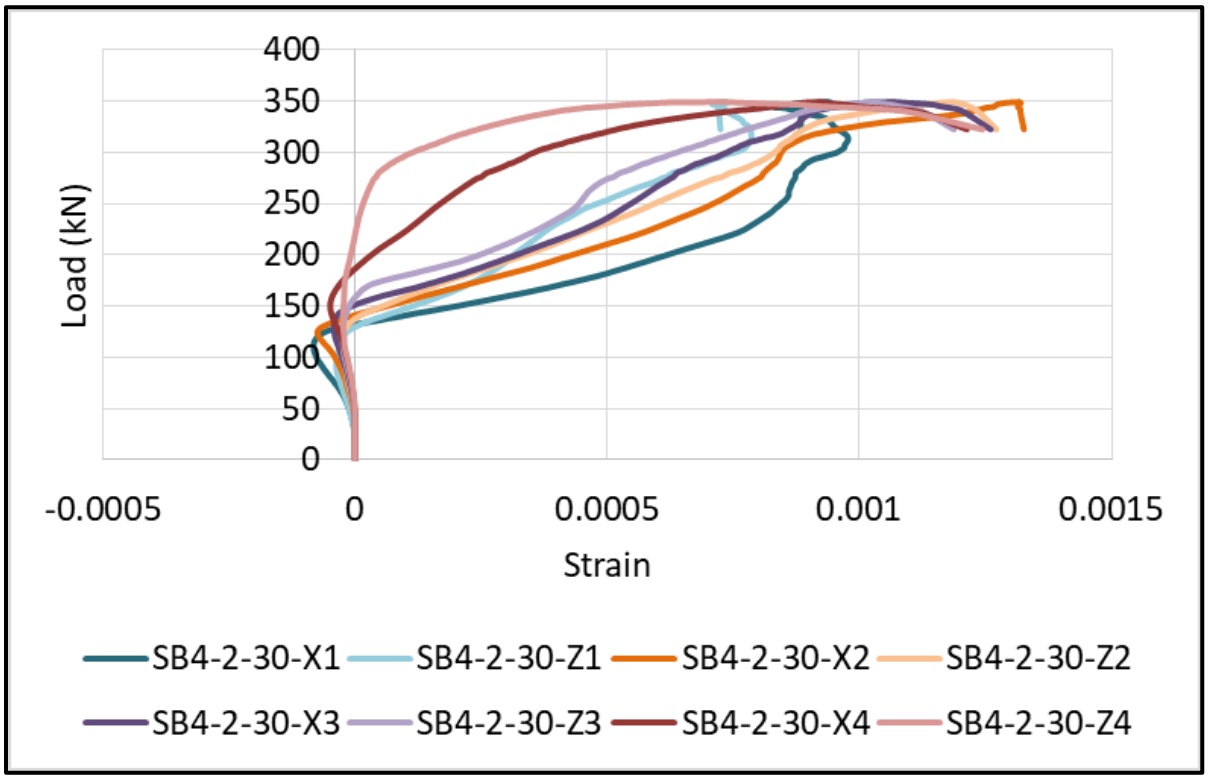

Figure D8: SB4-2-30 Bolt Strain Diagram

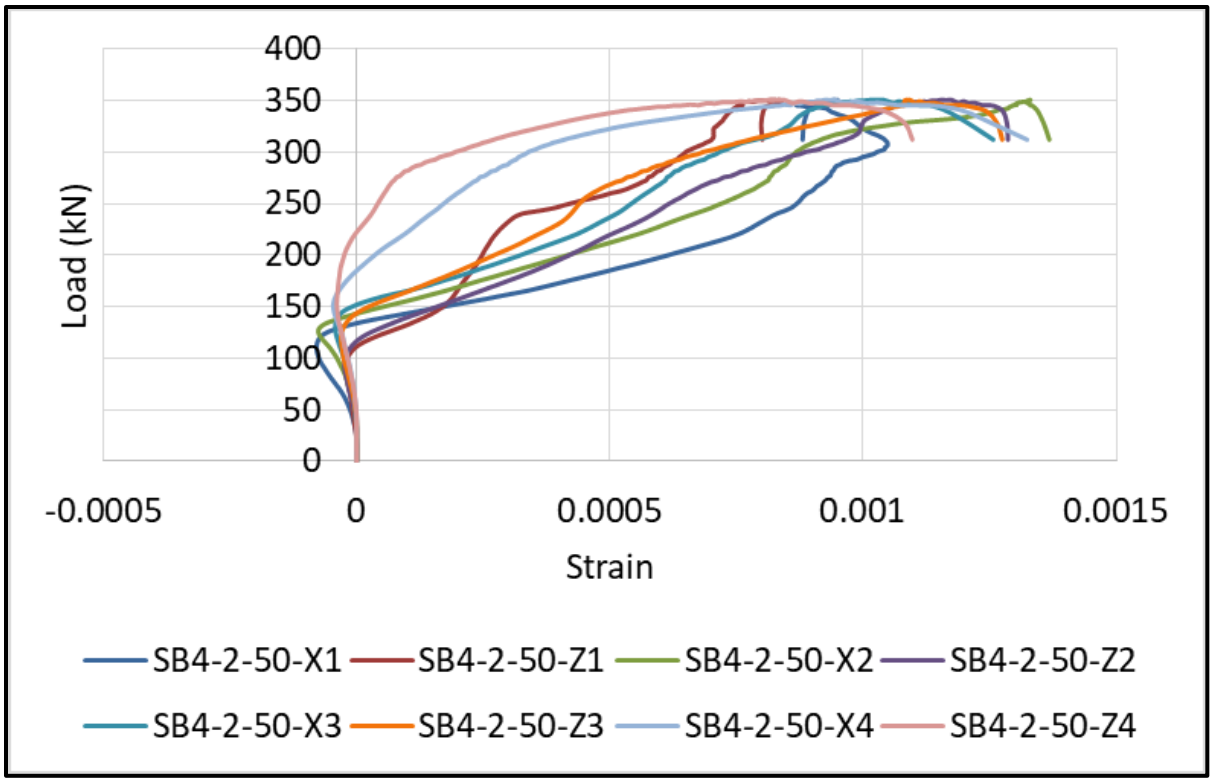

Figure D9: SB4-2-50 Bolt Strain Diagram

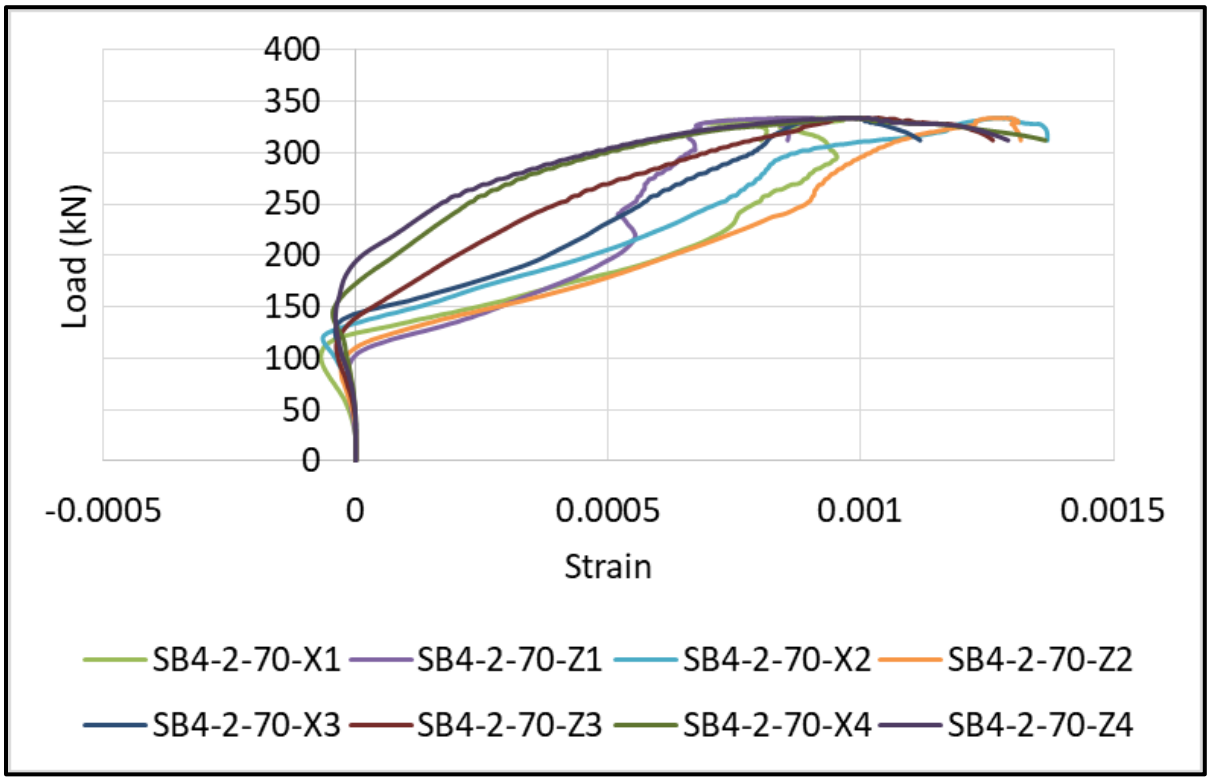

Figure D10: SB4-2-70 Bolt Strain Diagram

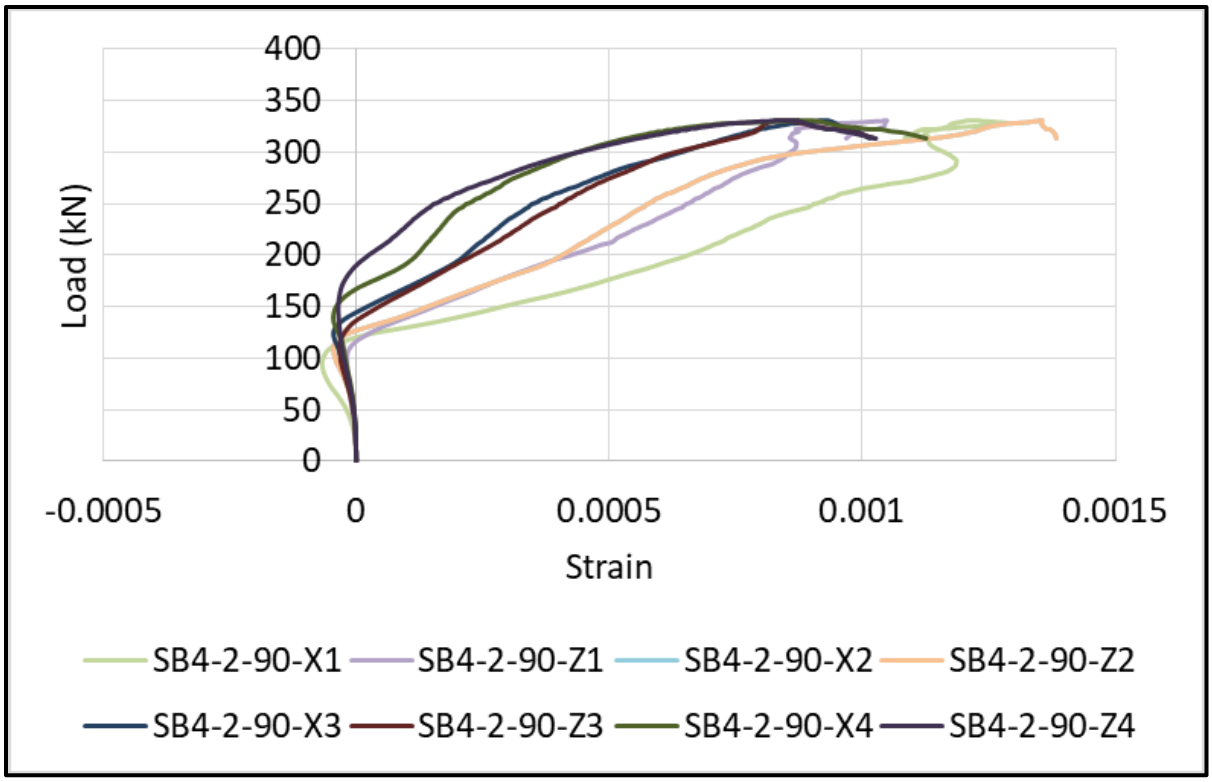

Figure D11: SB4-2-90 Bolt Strain Diagram

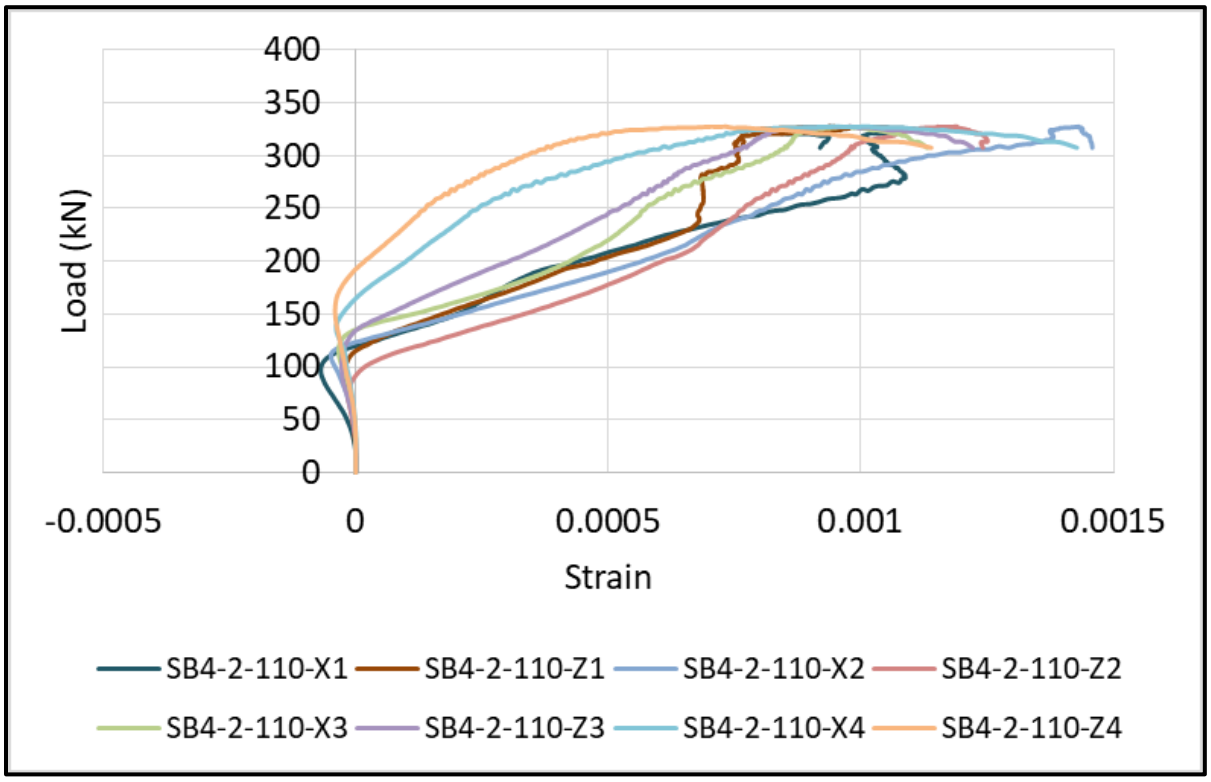

Figure D12: SB4-2-110 Bolt Strain Diagram

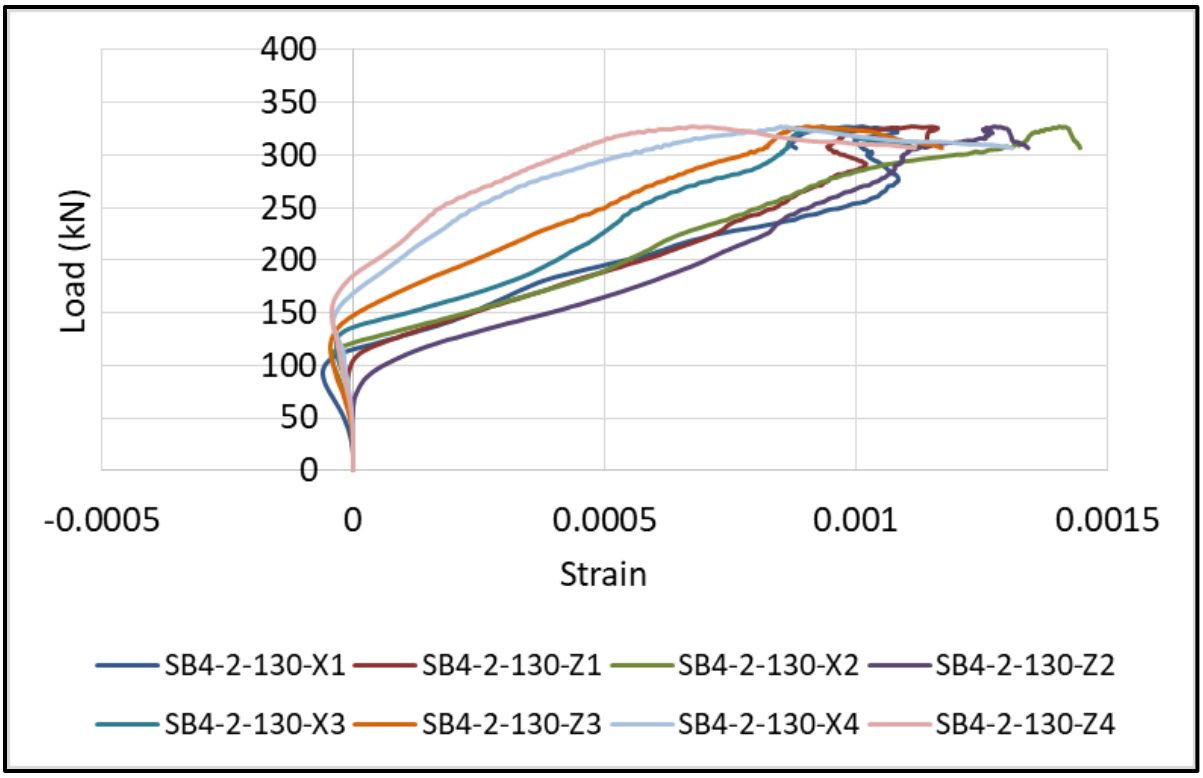

Figure D13: SB4-2-130 Bolt Strain Diagram

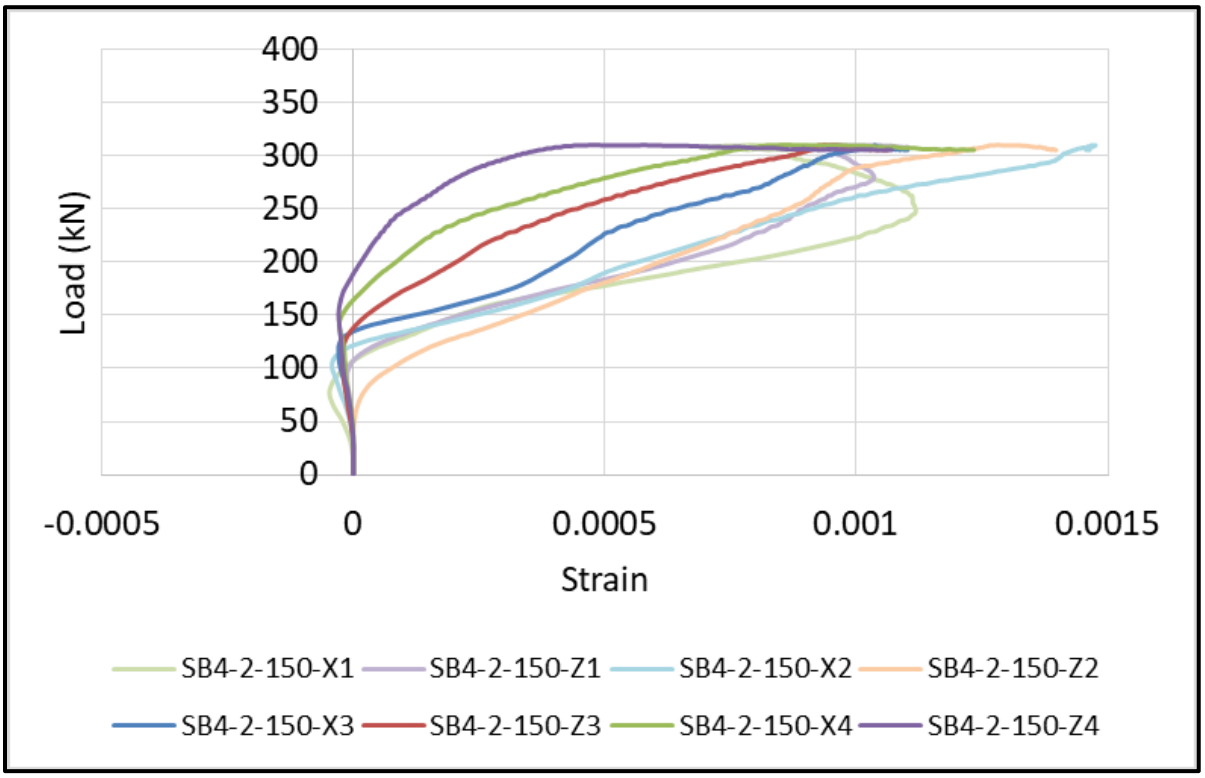

Figure D14: SB4-2-150 Bolt Strain Diagram

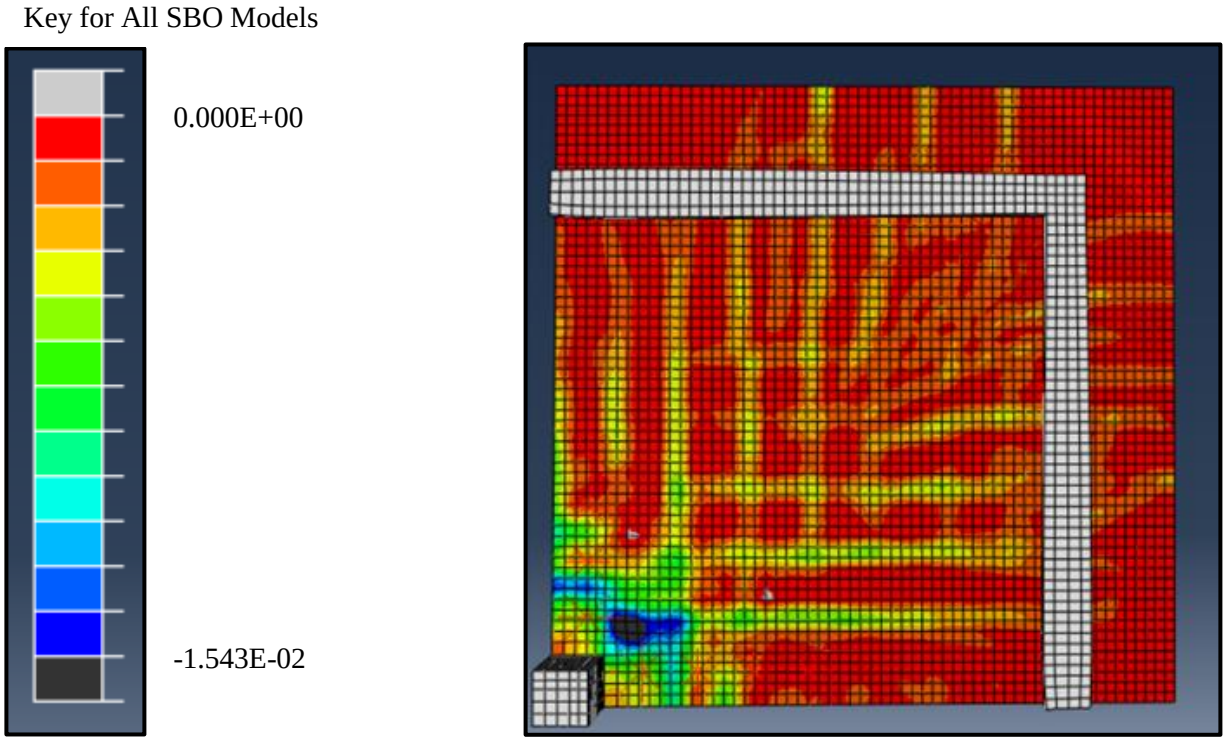

Figure D15: SB4-0 Tensile Face Crack Pattern

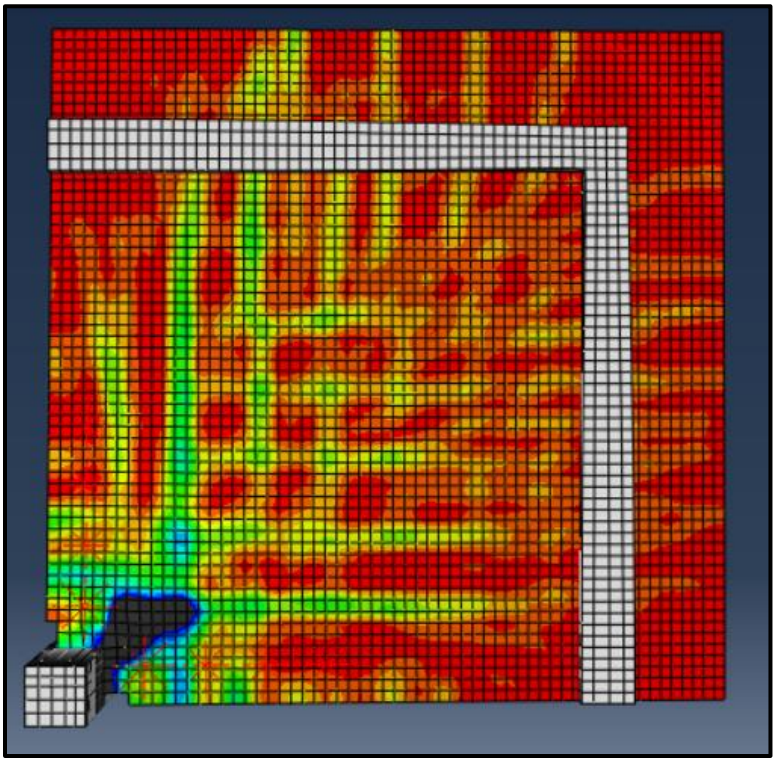

Figure D16: SB4-4-30 Tensile Face Crack Pattern

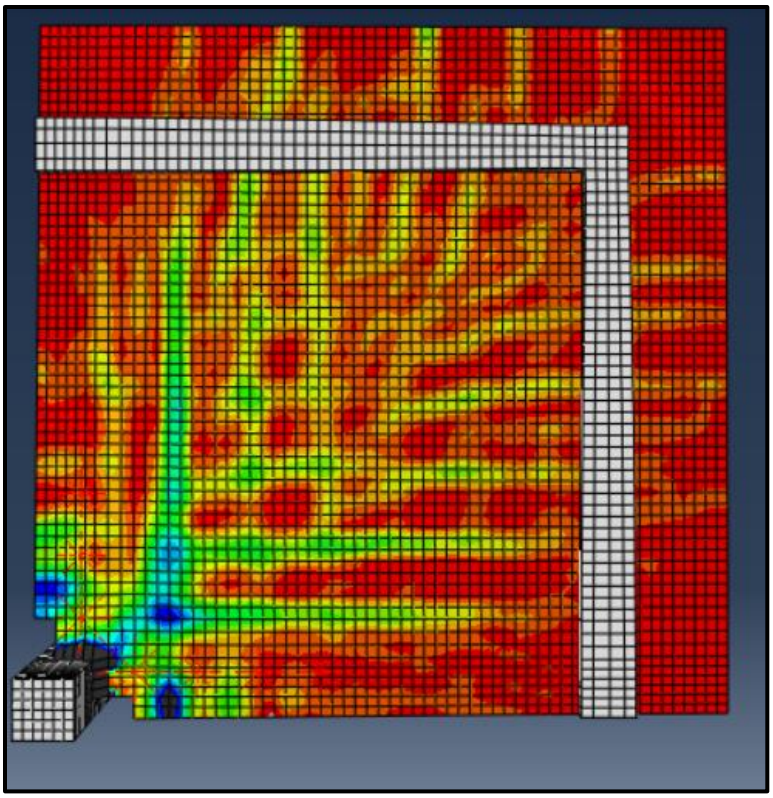

Figure D17: SB4-4-50 Tensile Face Crack Pattern

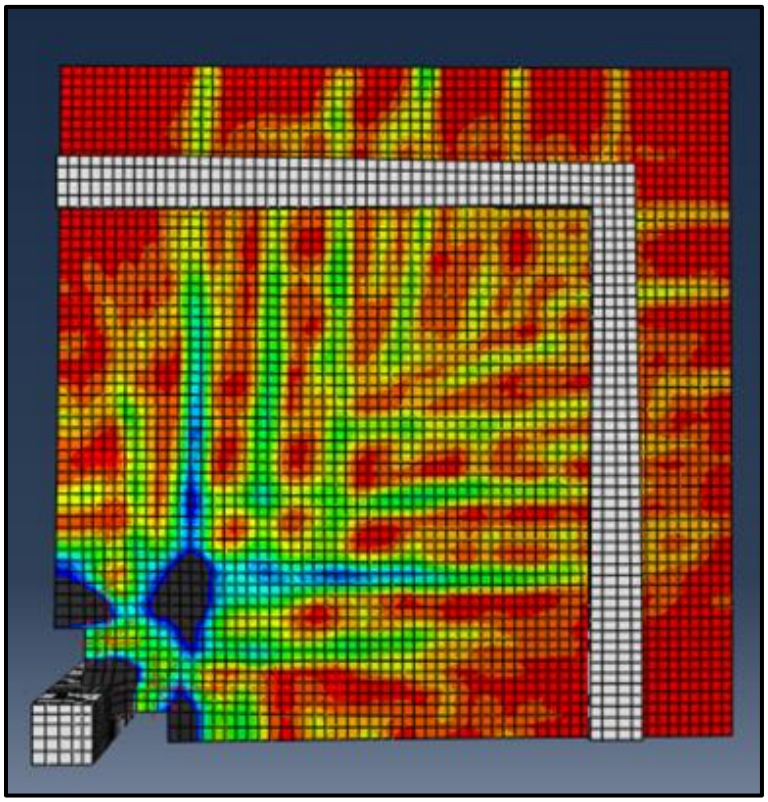

Figure D18: SB4-4-70 Tensile Face Crack Pattern

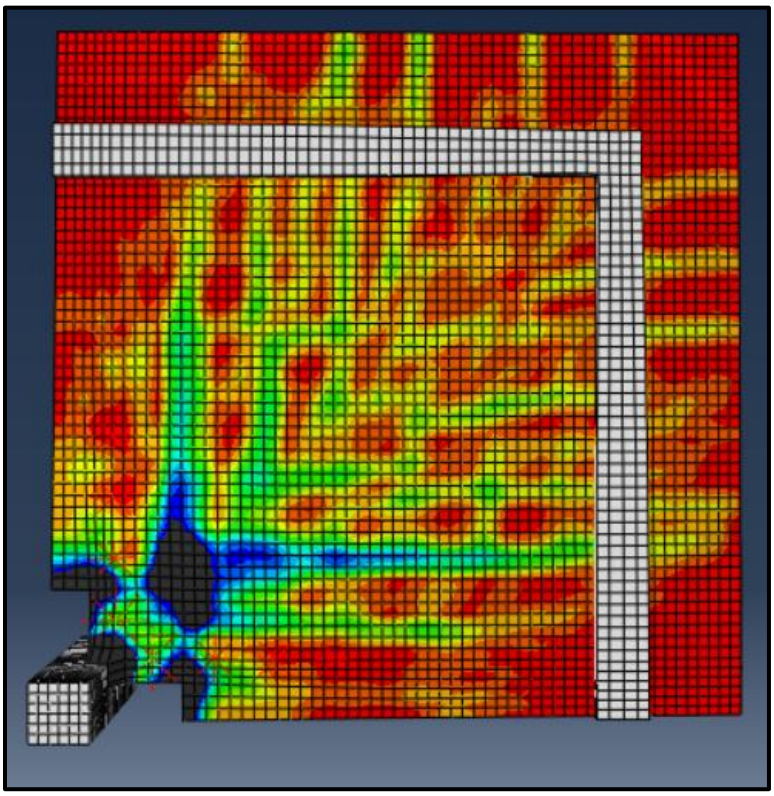

Figure D19: SB4-4-90 Tensile Face Crack Pattern

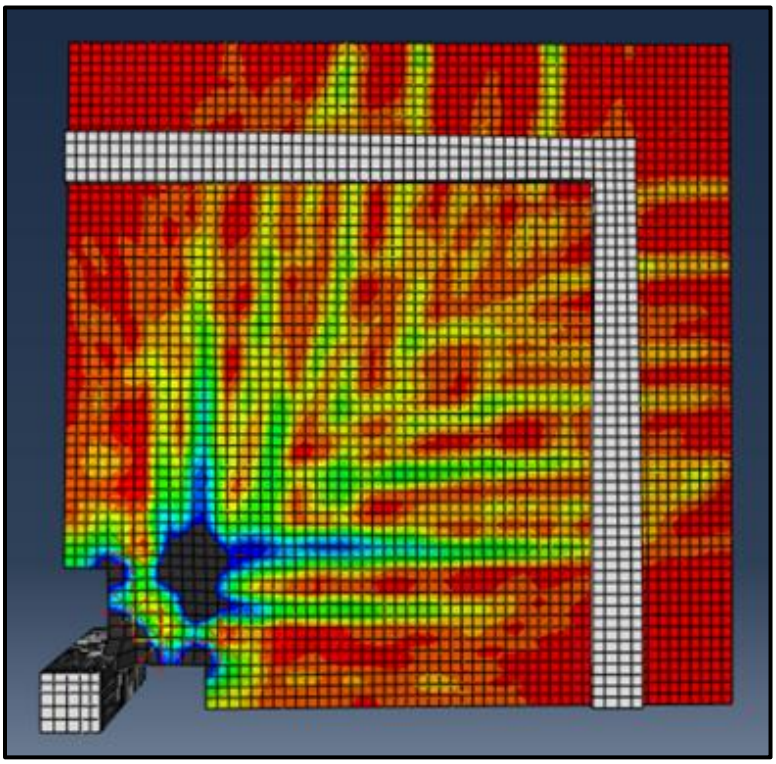

Figure D20: SB4-4-110 Tensile Face Crack Pattern

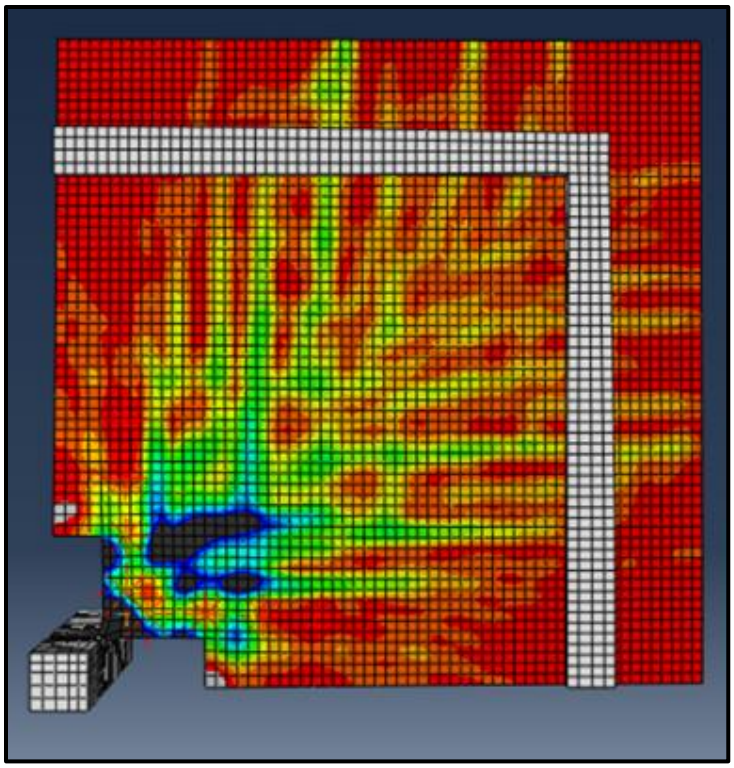

Figure D21: SB4-4-130 Tensile Face Crack Pattern

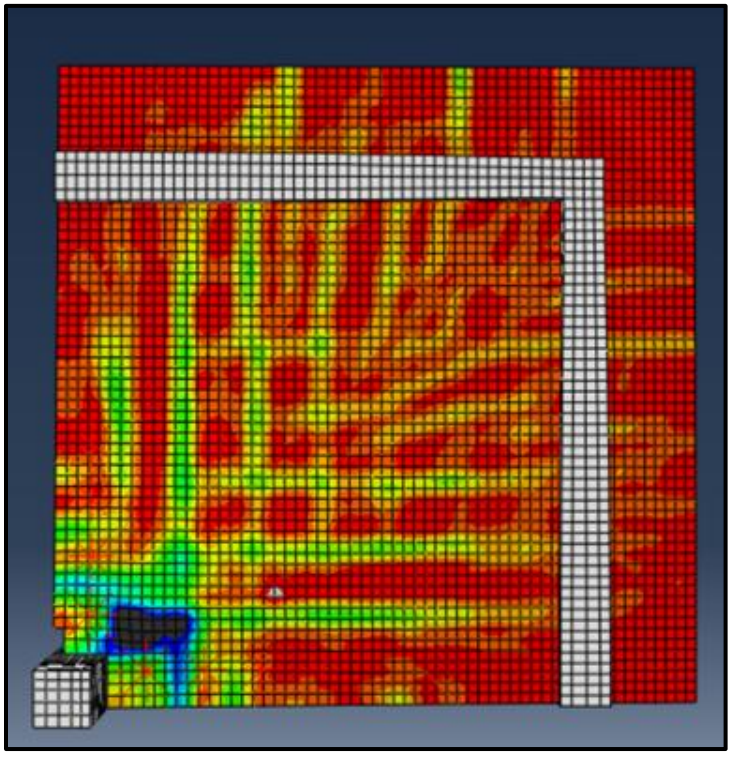

Figure D22: SB4-2-30 Tensile Face Crack Pattern

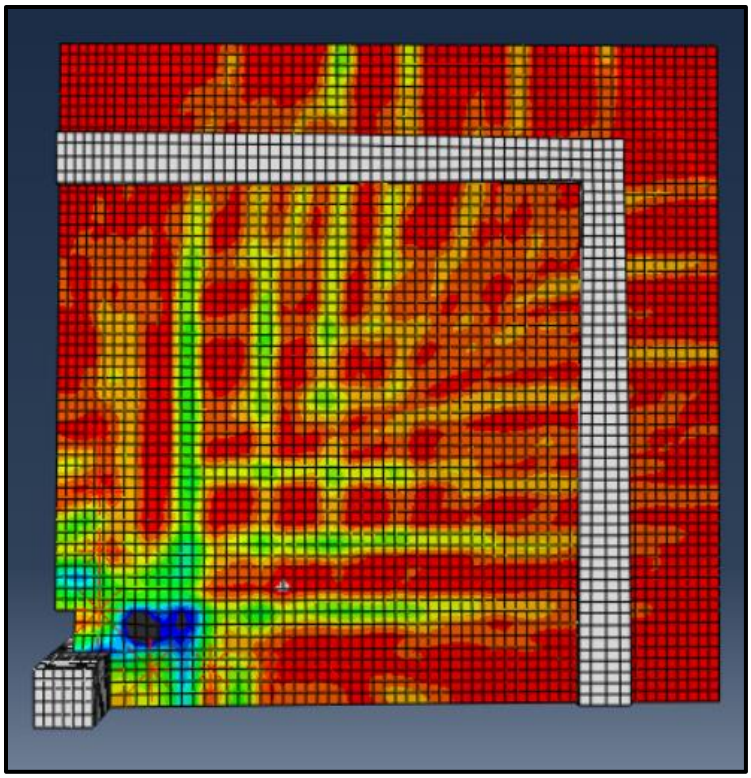

Figure D23: SB4-2-50 Tensile Face Crack Pattern

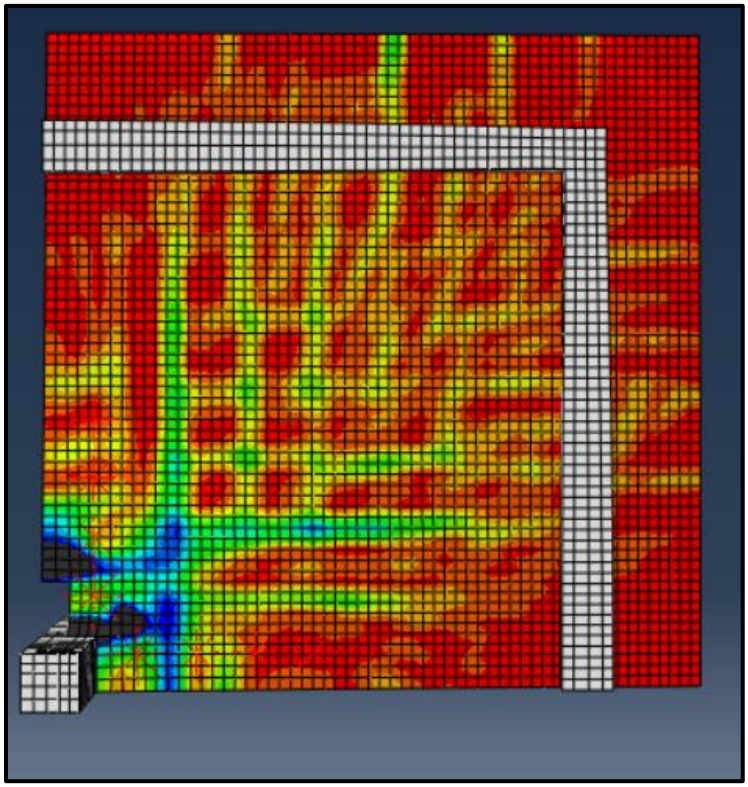

Figure D24: SB4-2-70 Tensile Face Crack Pattern

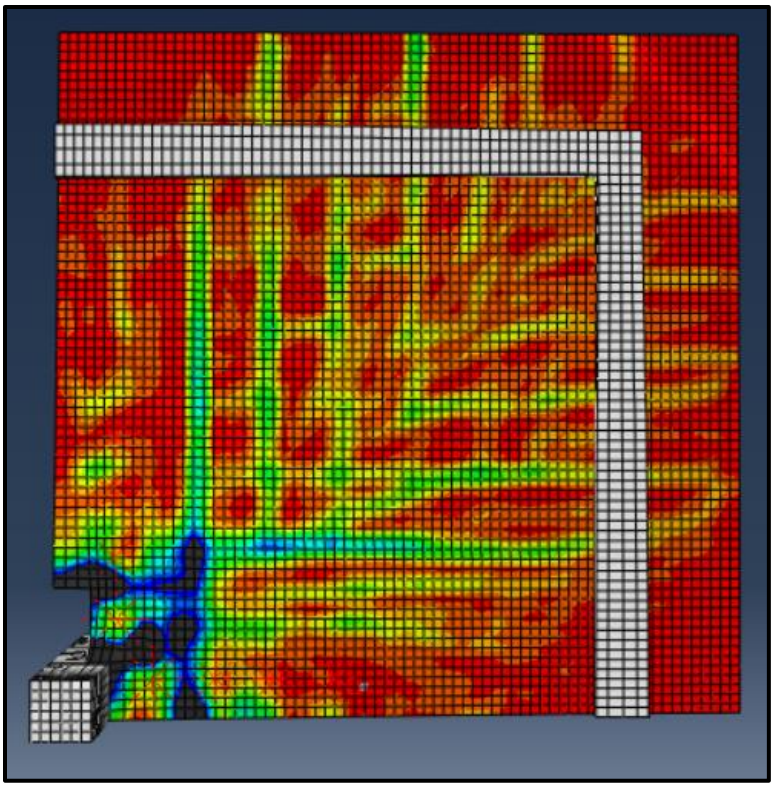

Figure D25: SB4-2-90 Tensile Face Crack Pattern

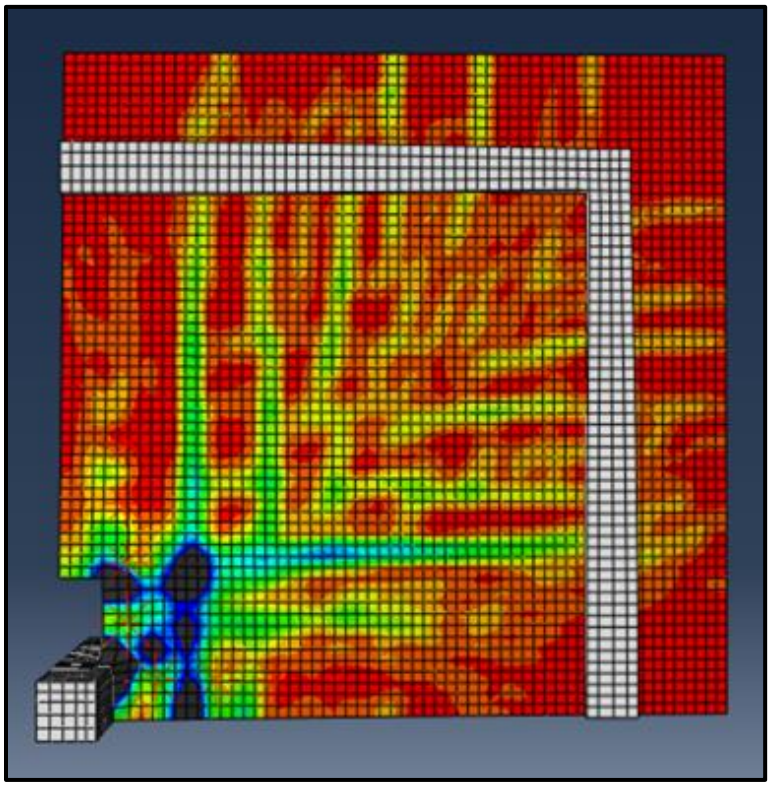

Figure D26: SB4-2-110 Tensile Face Crack Pattern

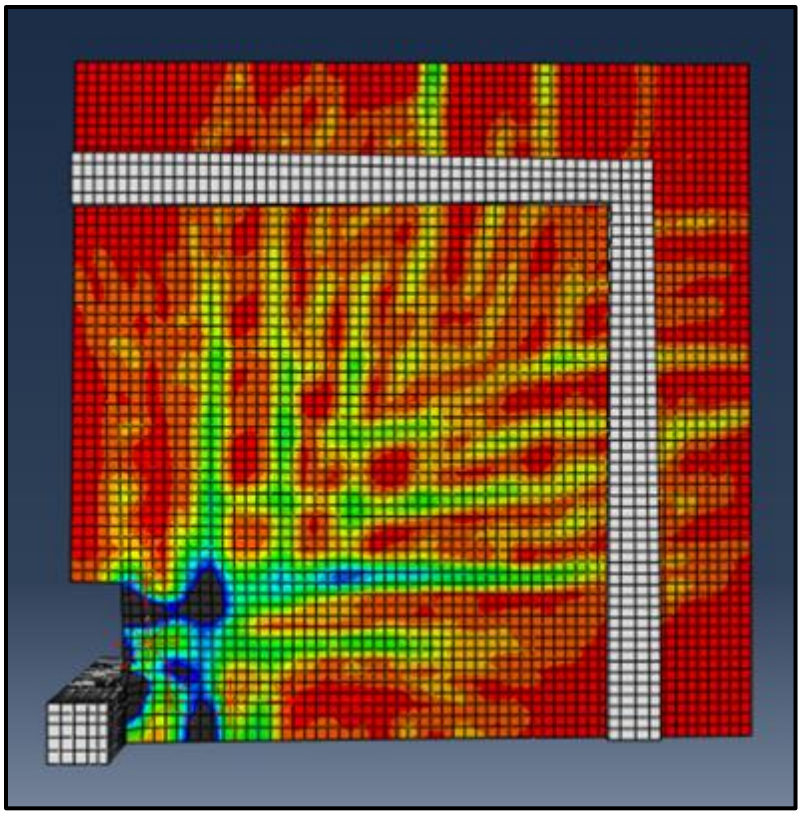

Figure D27: SB4-2-130 Tensile Face Crack Pattern

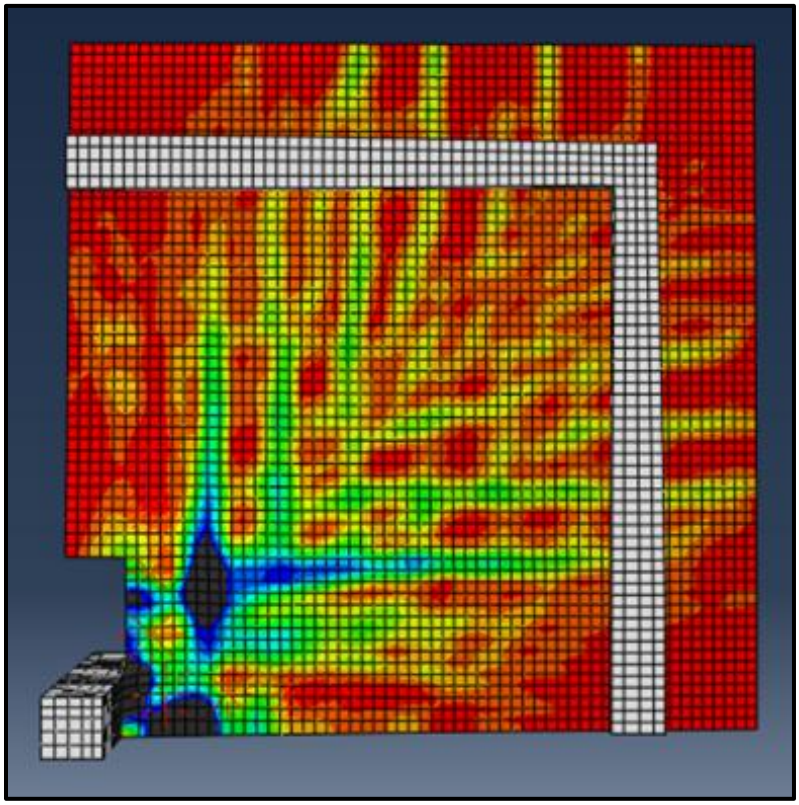

Figure D28: SB4-2-150 Tensile Face Crack Pattern

Key for All SBO Models

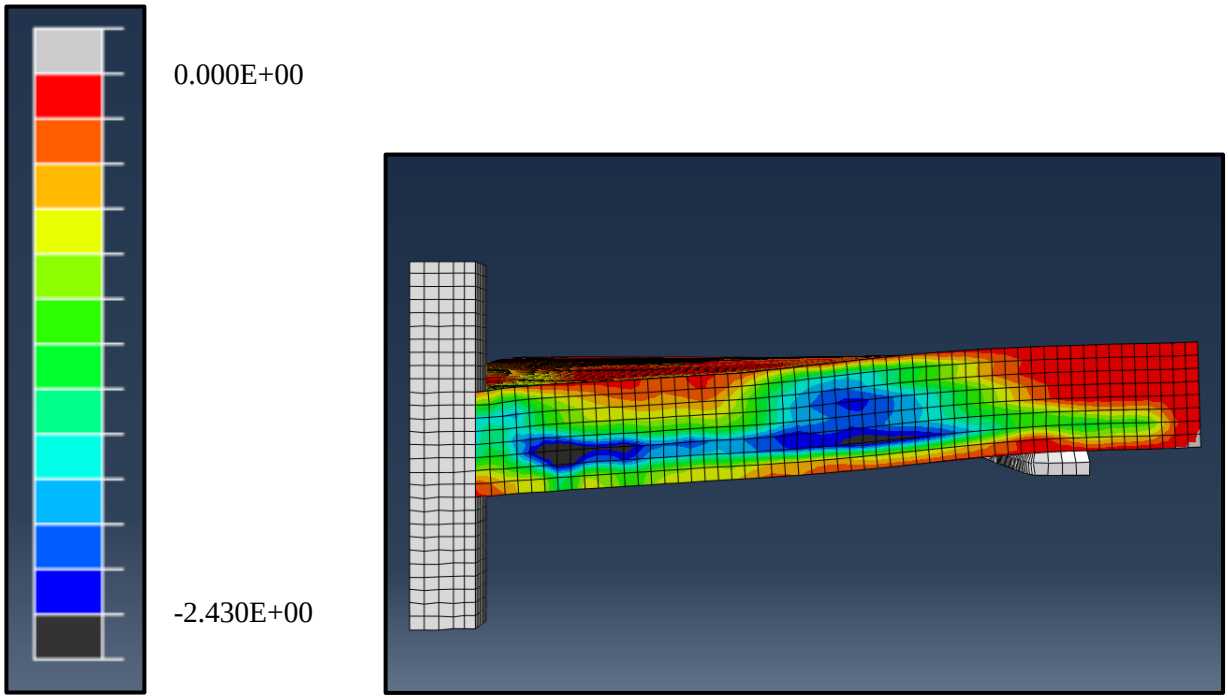

Figure D29: SB4-0 Post-Failure Side Crack Profile

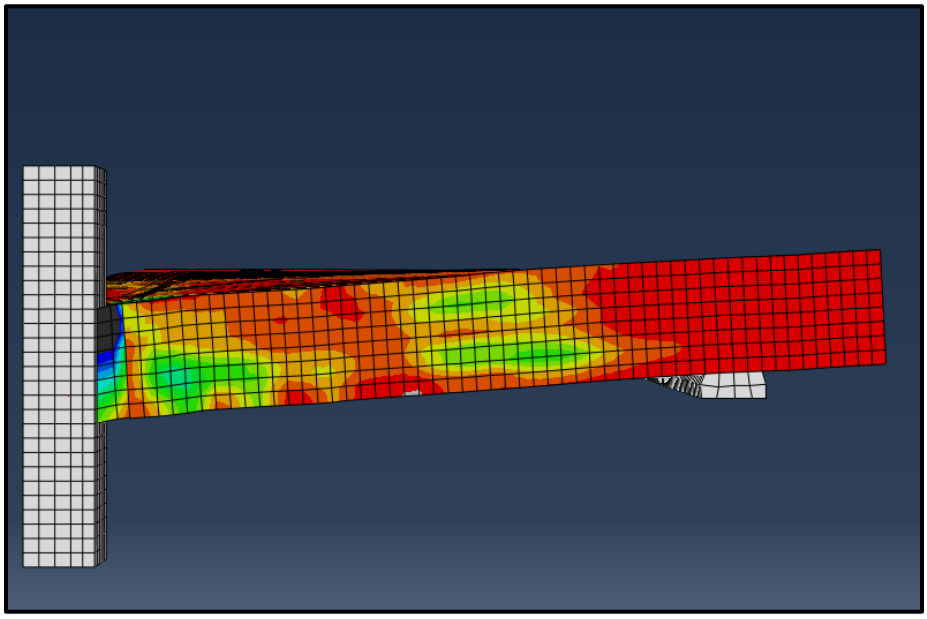

Figure D30: SB4-4-30 Post-Failure Side Crack Profile

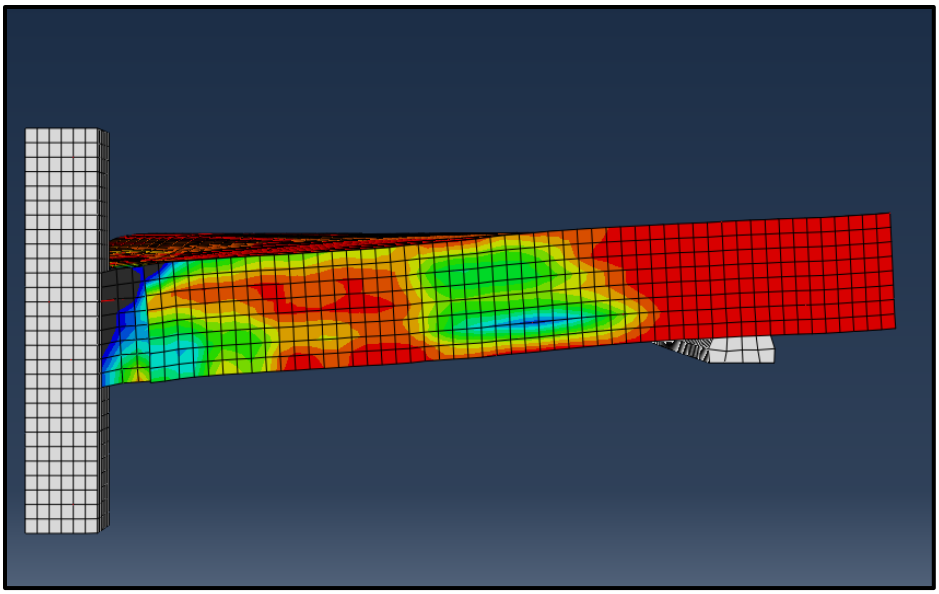

Figure D31: SB4-4-50 Post-Failure Side Crack Profile

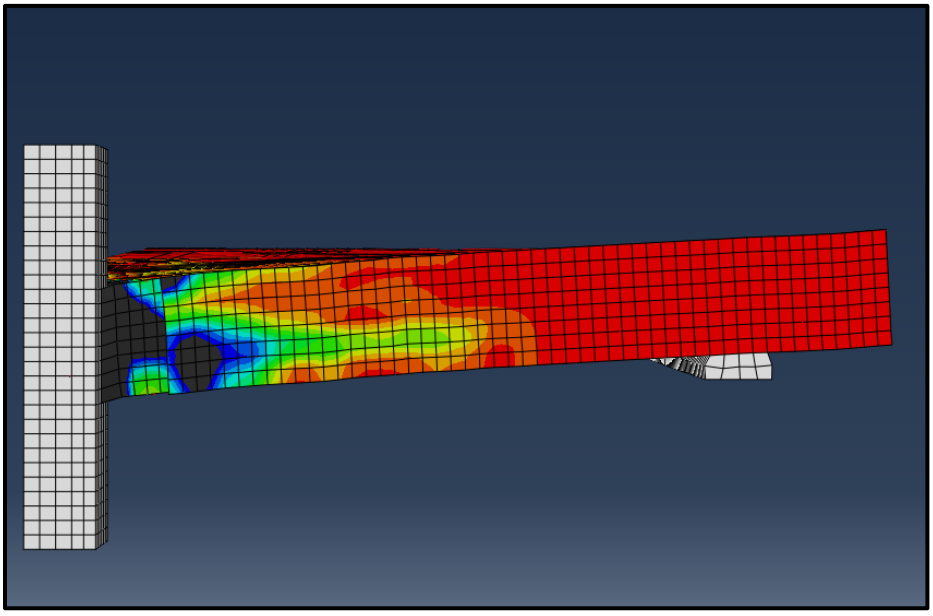

Figure D32: SB4-4-70 Post-Failure Side Crack Profile

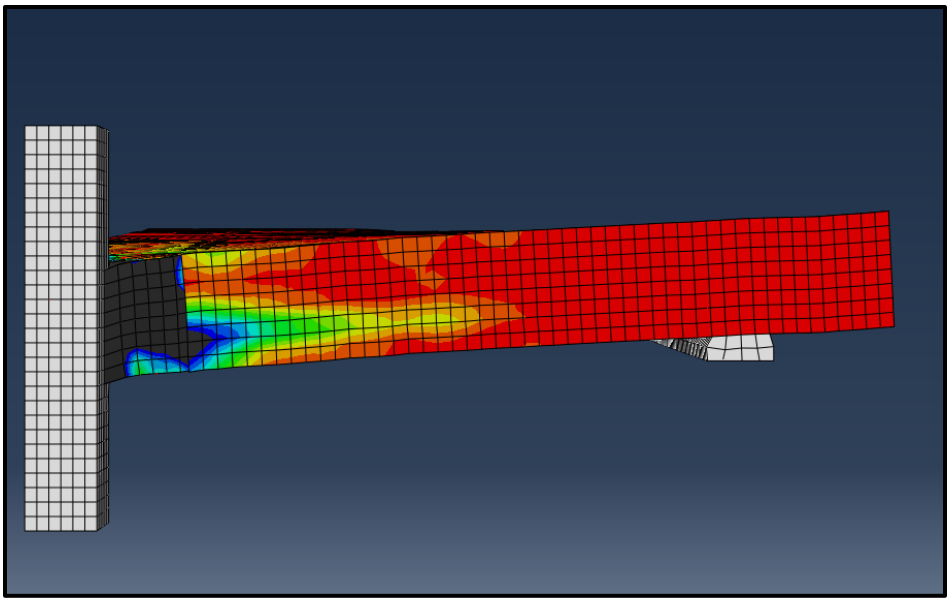

Figure D33: SB4-4-90 Post-Failure Side Crack Profile

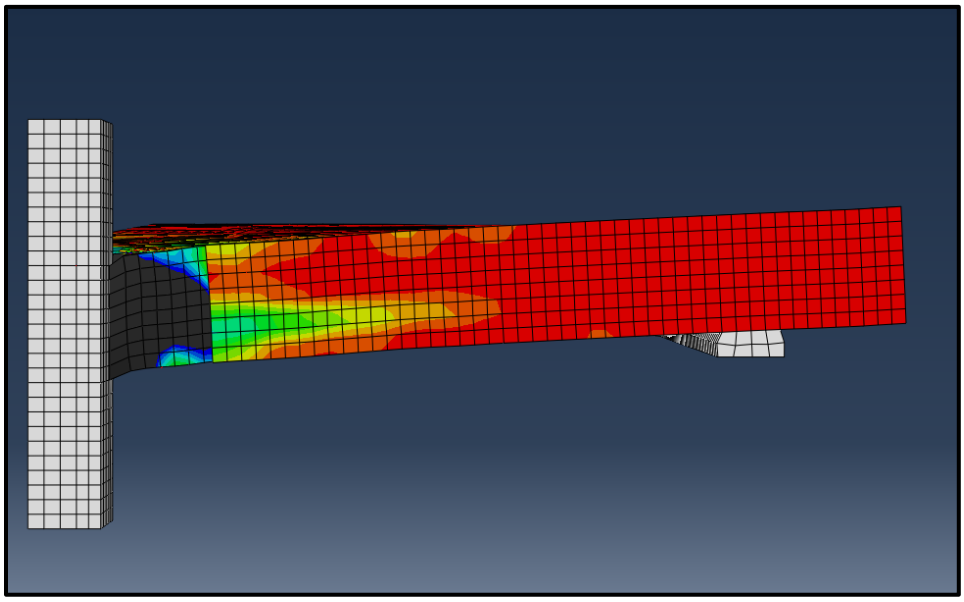

Figure D34: SB4-4-110 Post-Failure Side Crack Profile

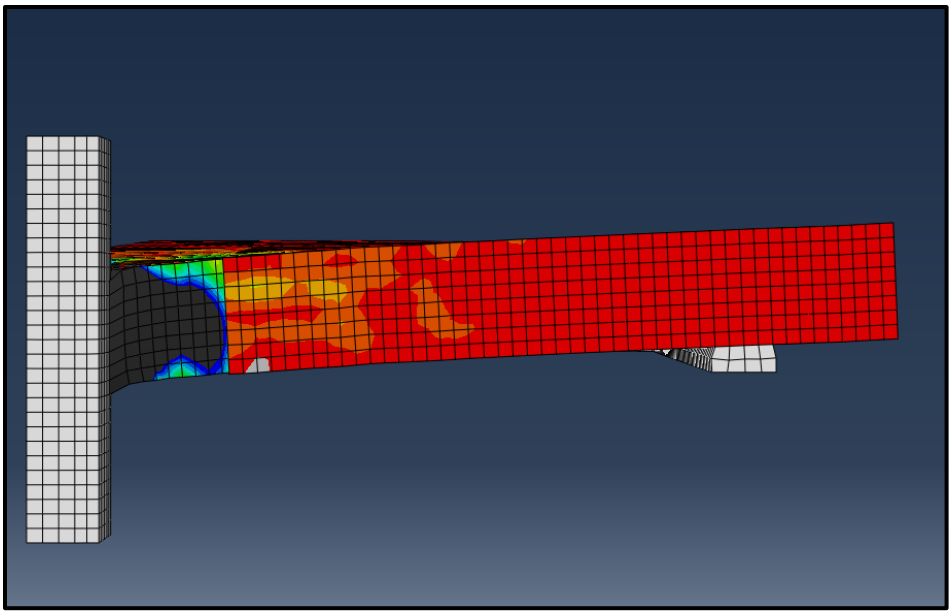

Figure D35: SB4-4-130 Post-Failure Side Crack Profile

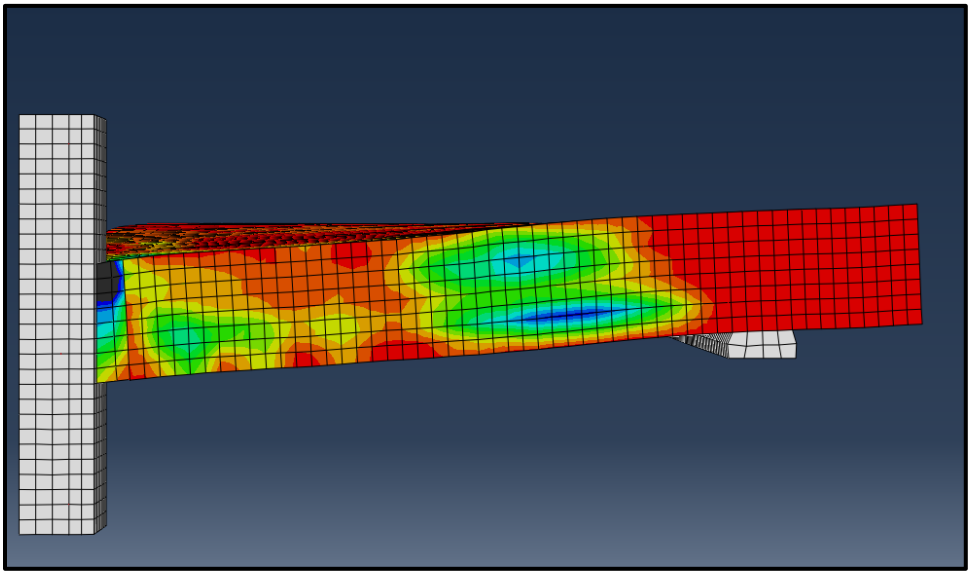

Figure D36: SB4-2-30 Post-Failure Side Crack Profile

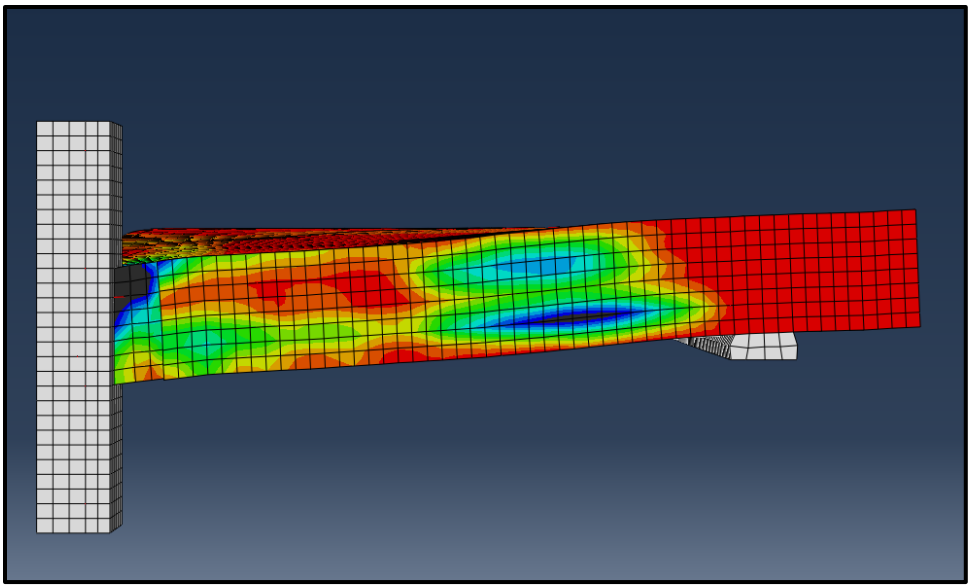

Figure D37: SB4-2-50 Post-Failure Side Crack Profile

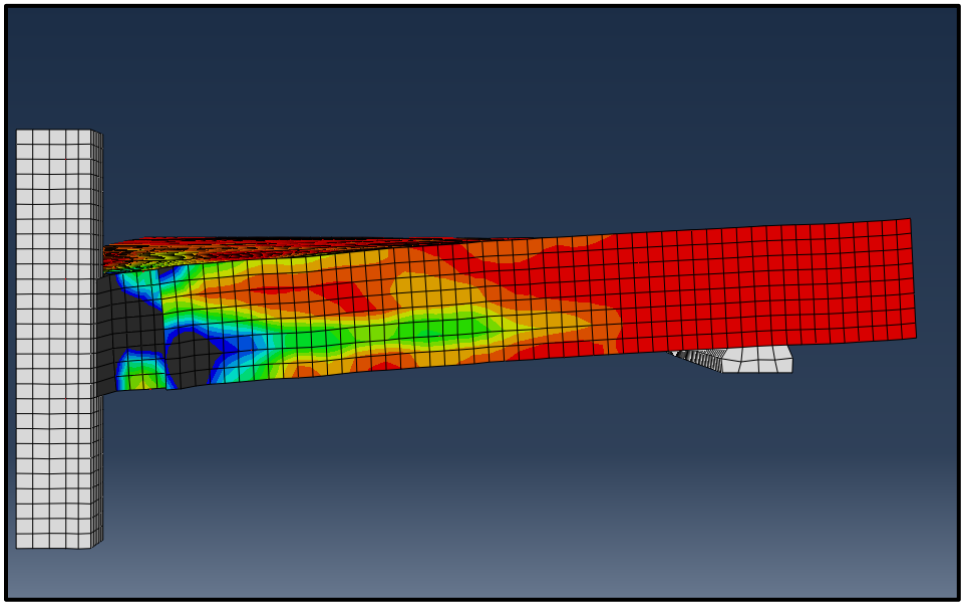

Figure D38: SB4-2-70 Post-Failure Side Crack Profile

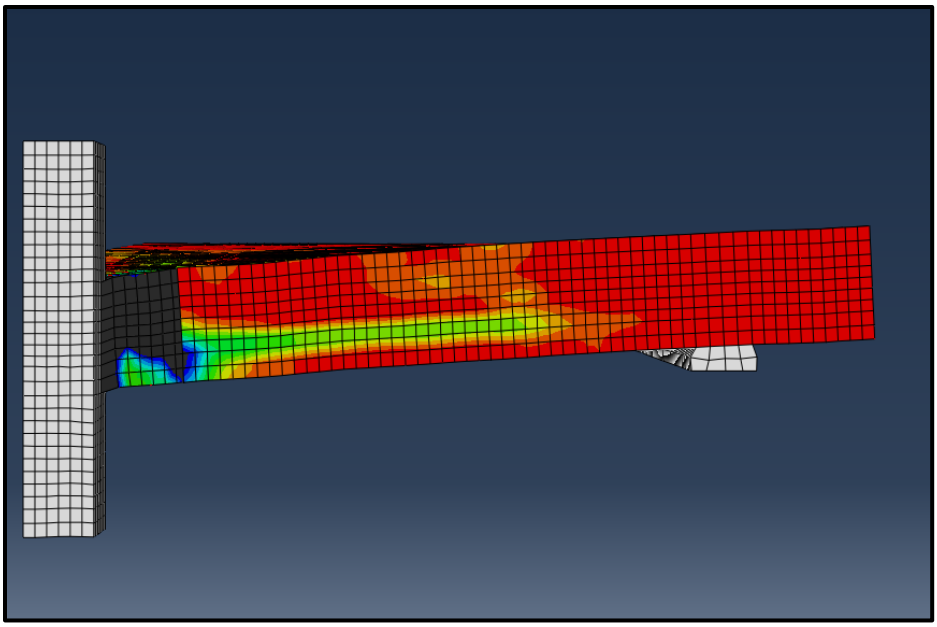

Figure D39: SB4-2-90 Post-Failure Side Crack Profile

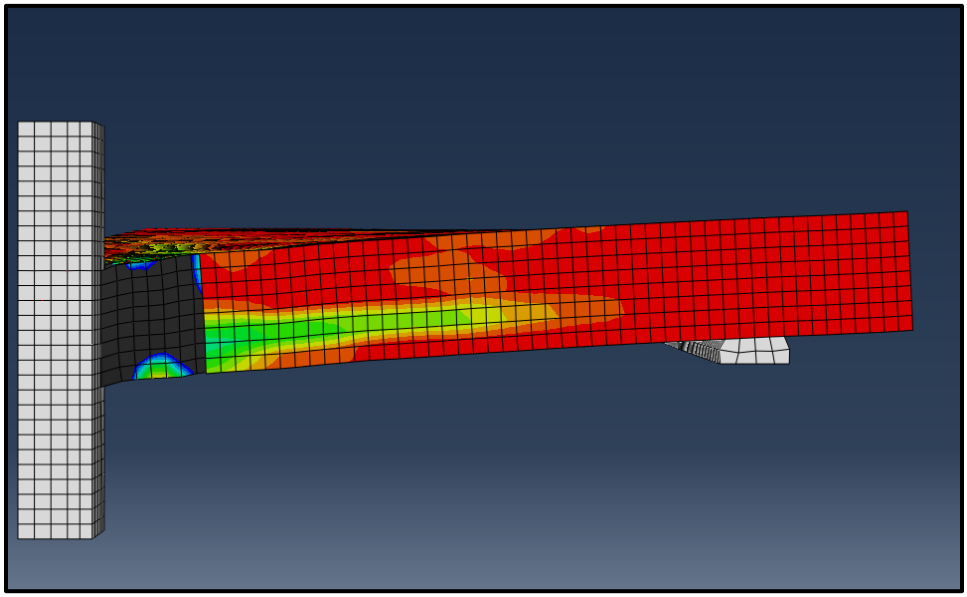

Figure D40: SB4-2-110 Post-Failure Side Crack Profile

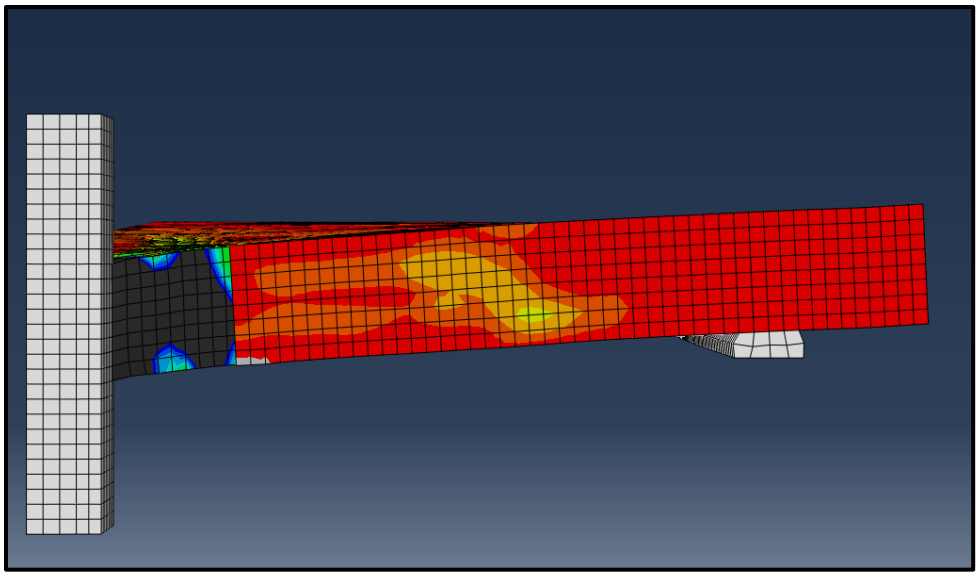

Figure D41: SB4-2-130 Post-Failure Side Crack Profile

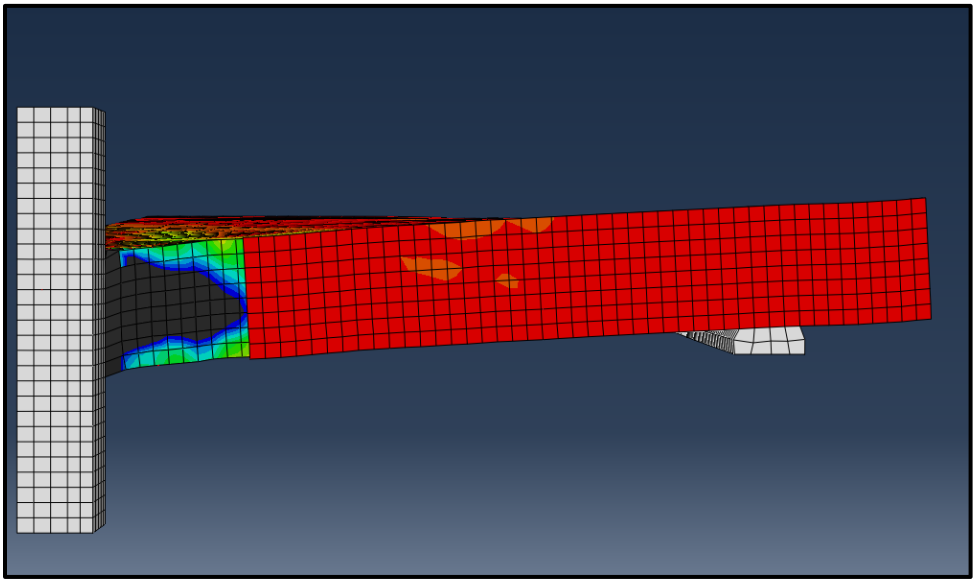

Figure D42: SB4-2-150 Post-Failure Side Crack Profile

Appendix E: Anchorage-Controlled Shear Reinforcement Study Supplemental Figures

List of Figures

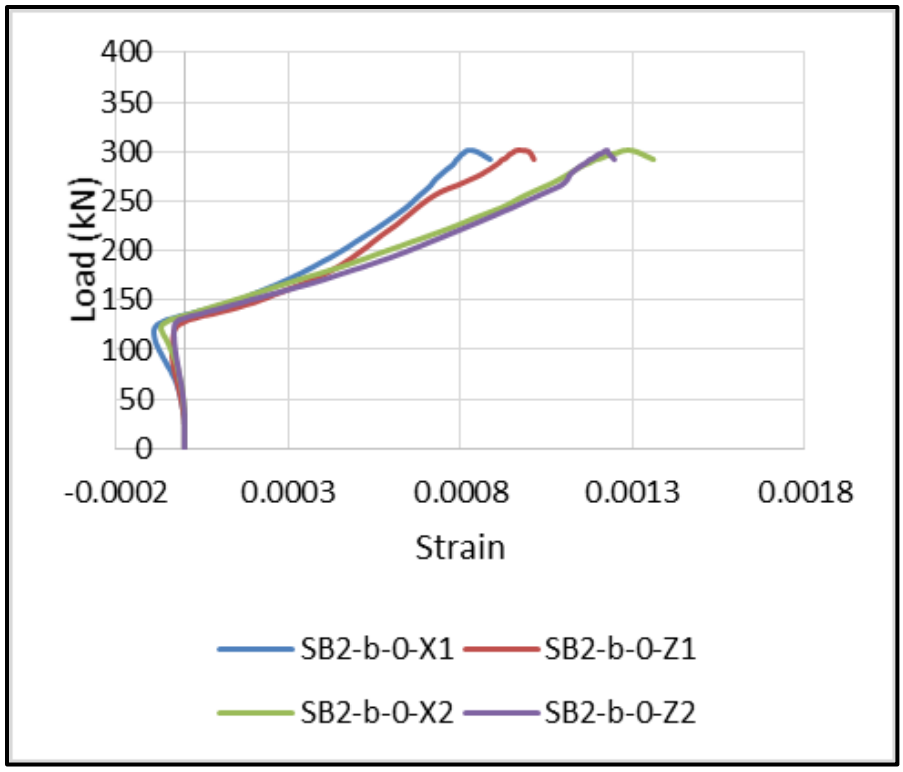

Figure E1: SB2-b-0 Bolt Strain Diagram

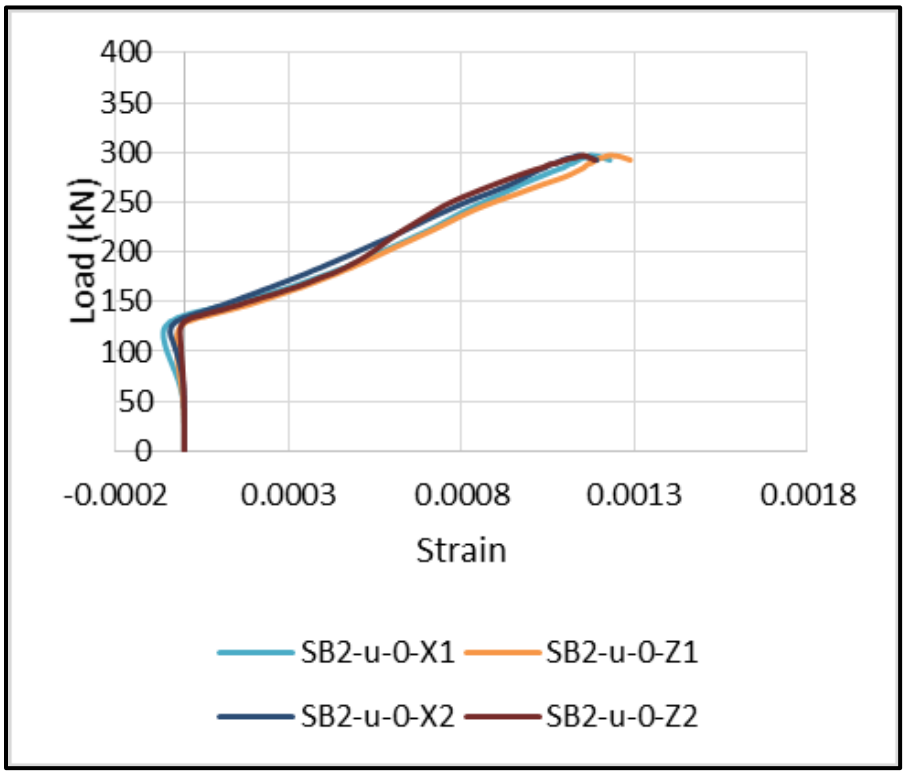

Figure E2: SB2-u-0 Bolt Strain Diagram

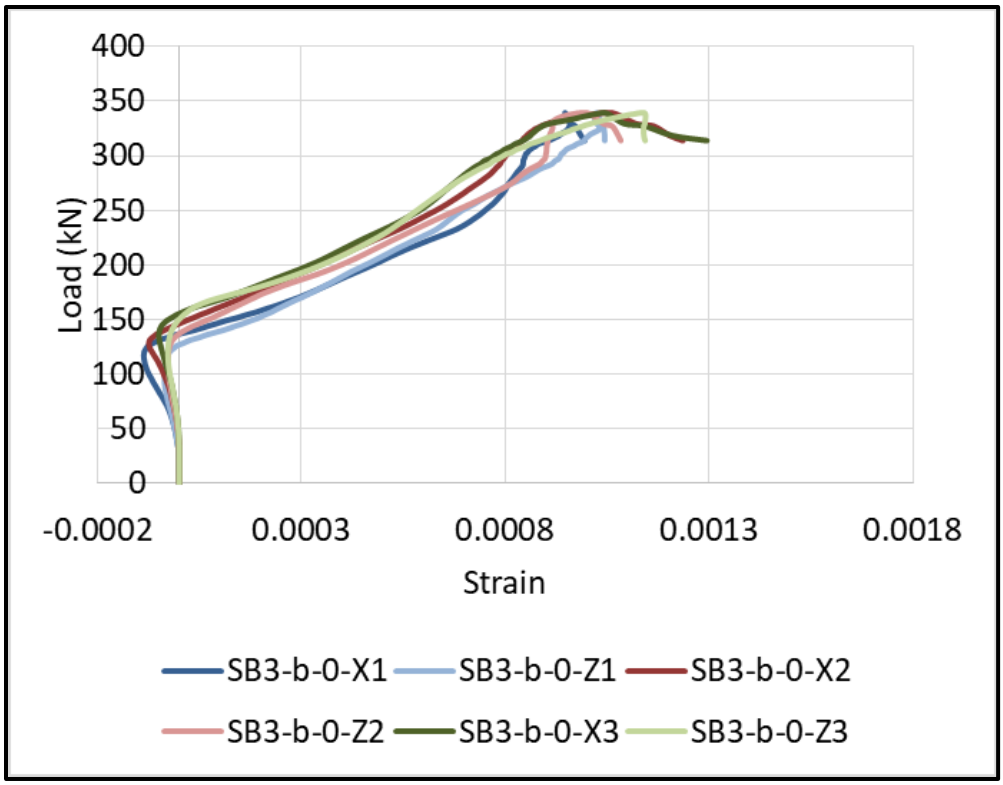

Figure E3: SB3-b-0 Bolt Strain Diagram

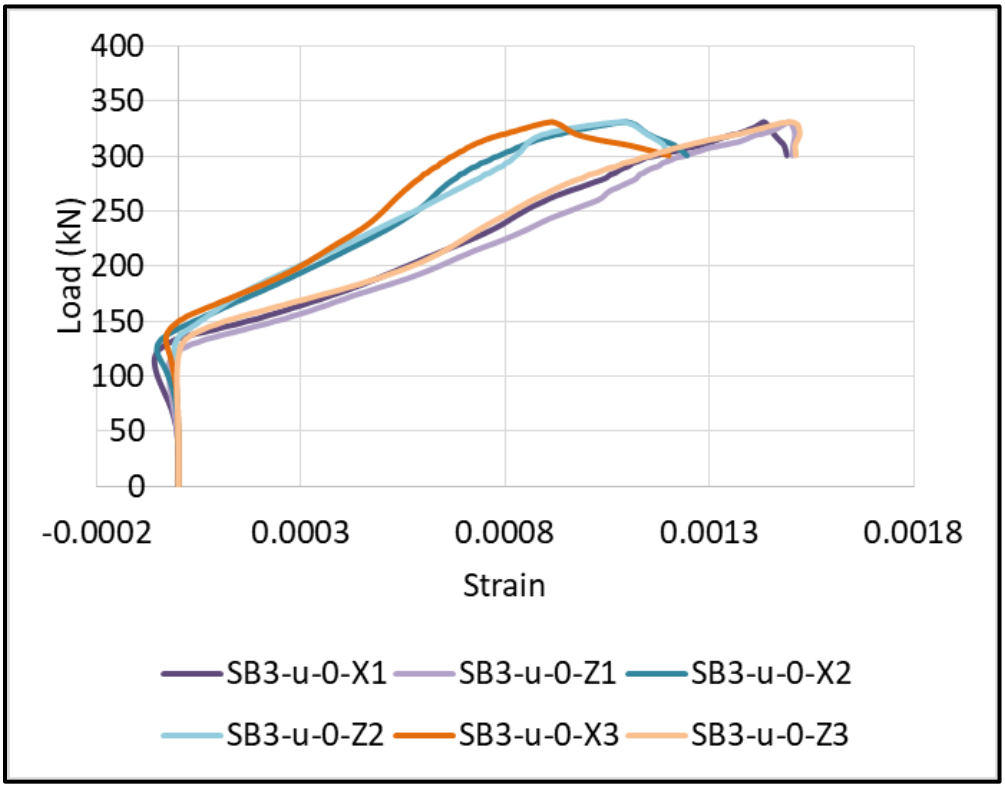

Figure E4: SB3-u-0 Bolt Strain Diagram

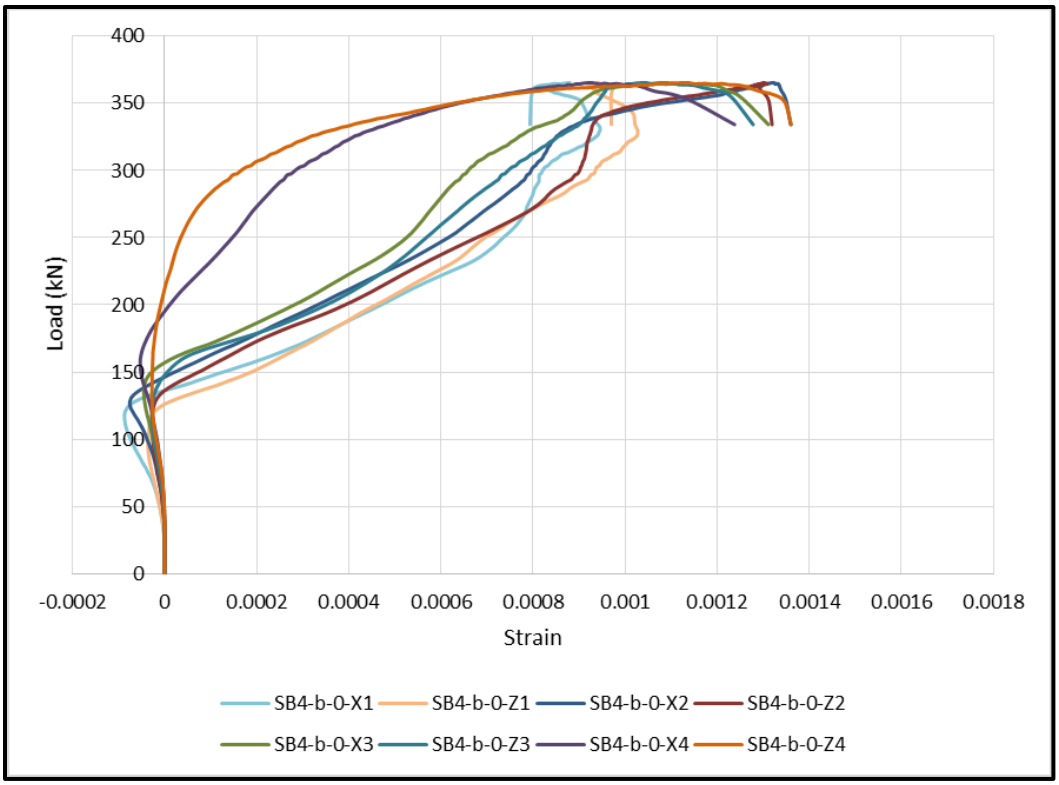

Figure E5: SB4-b-0 Bolt Strain Diagram

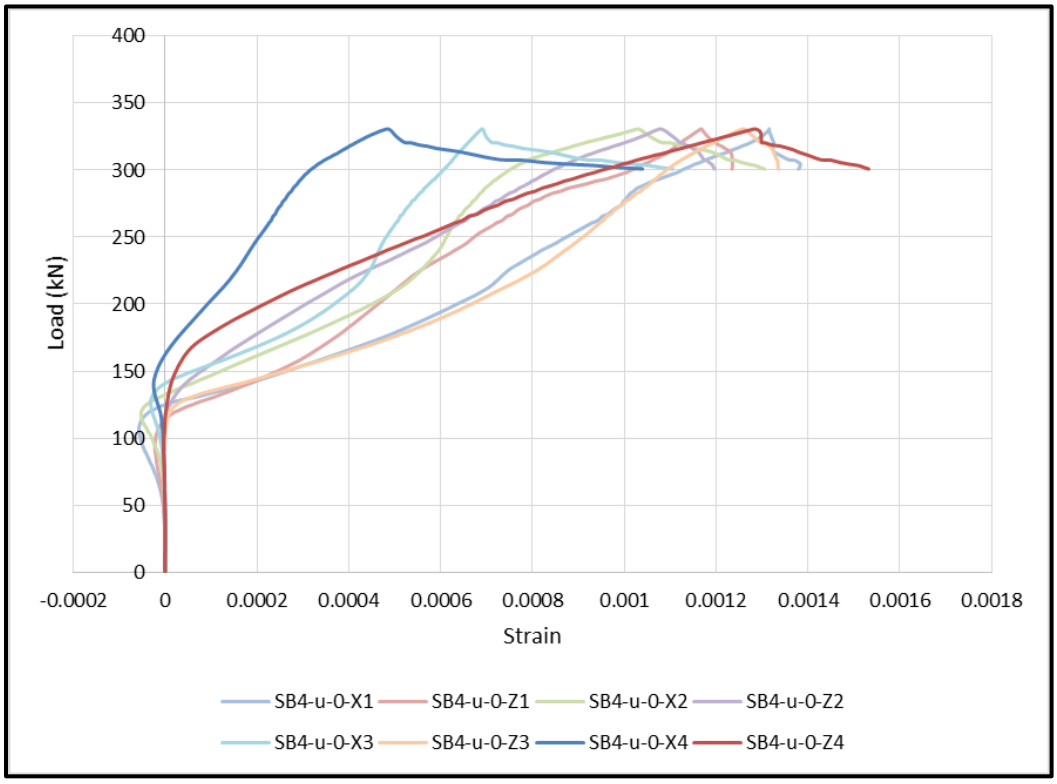

Figure E6: SB4-u-0 Bolt Strain Diagram

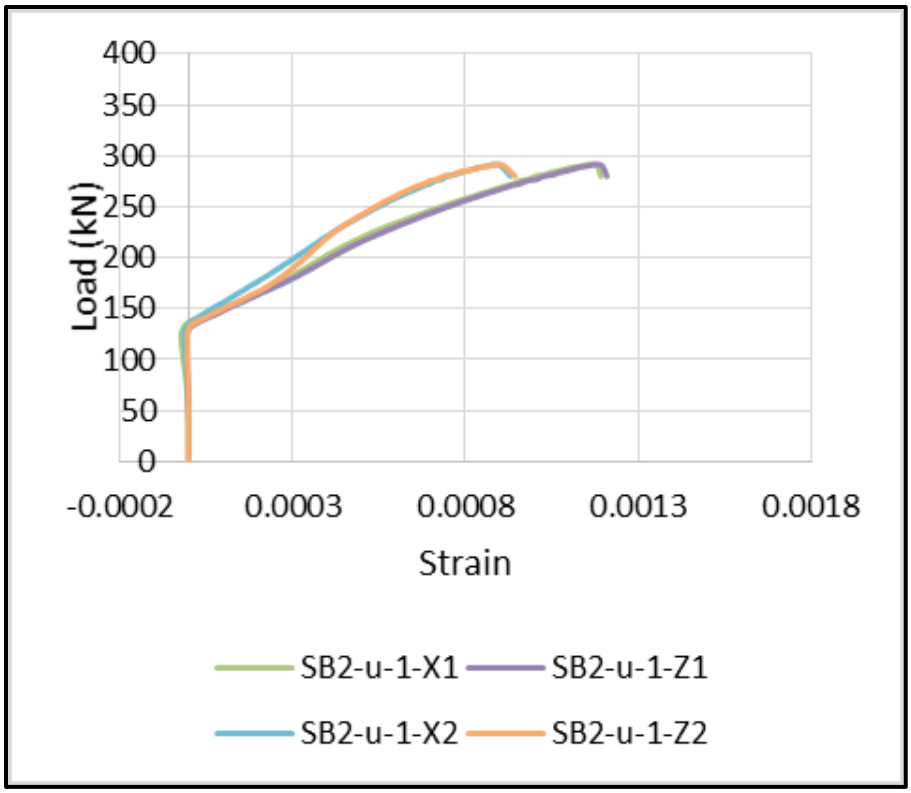

Figure E7: SB2-u-1 Bolt Strain Diagram

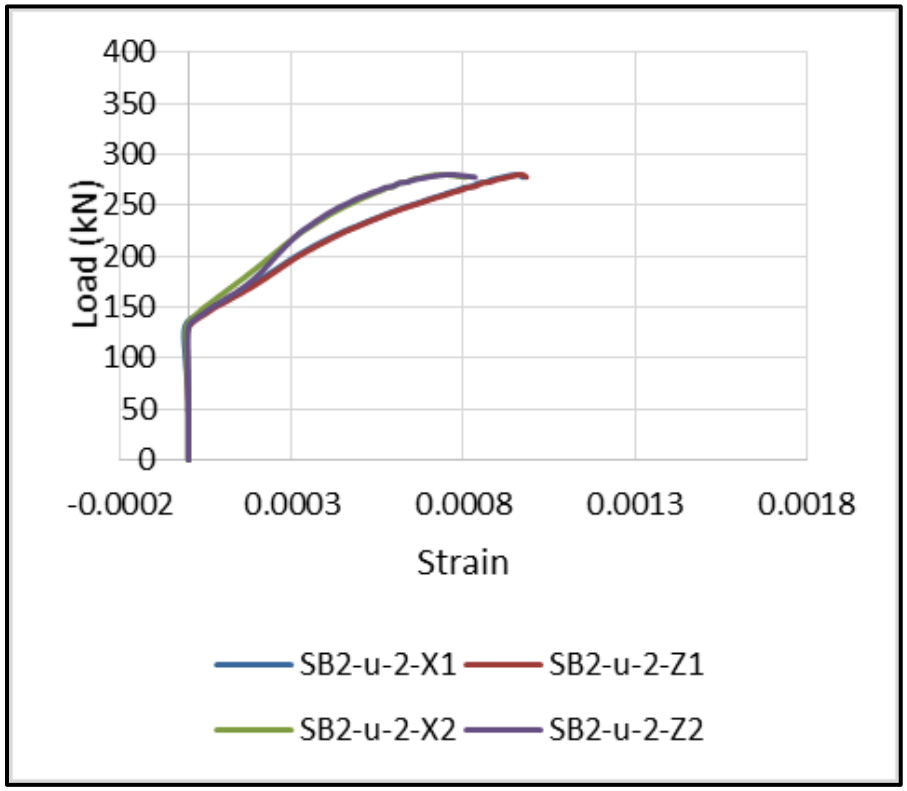

Figure E8: SB2-u-2 Bolt Strain Diagram

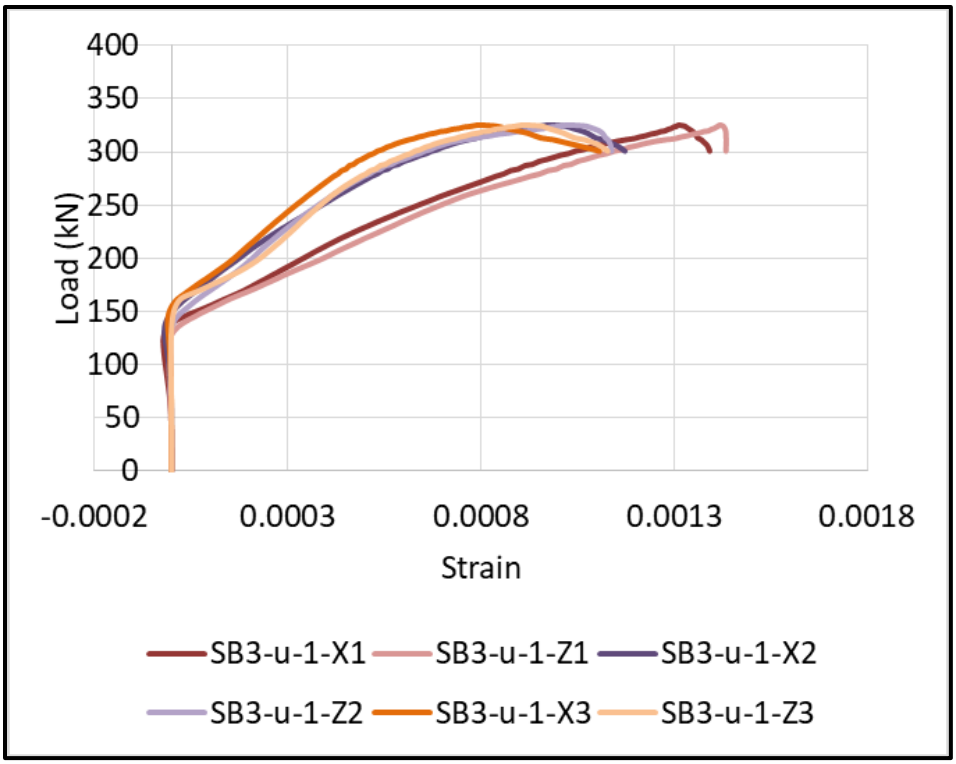

Figure E9: SB3-u-1 Bolt Strain Diagram

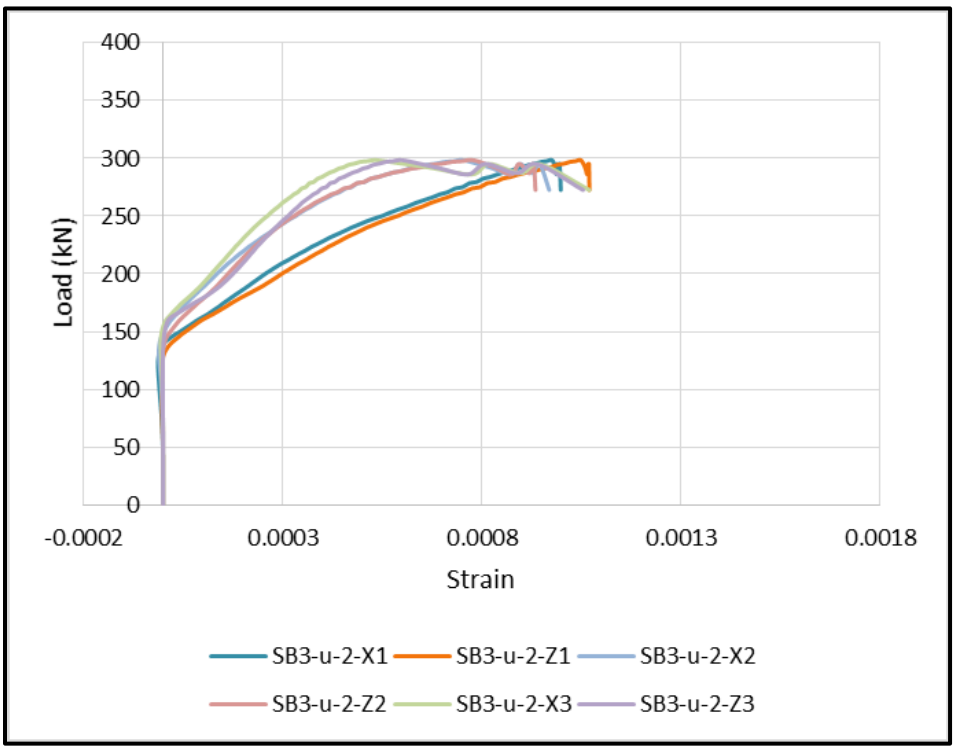

Figure E10: SB3-u-2 Bolt Strain Diagram

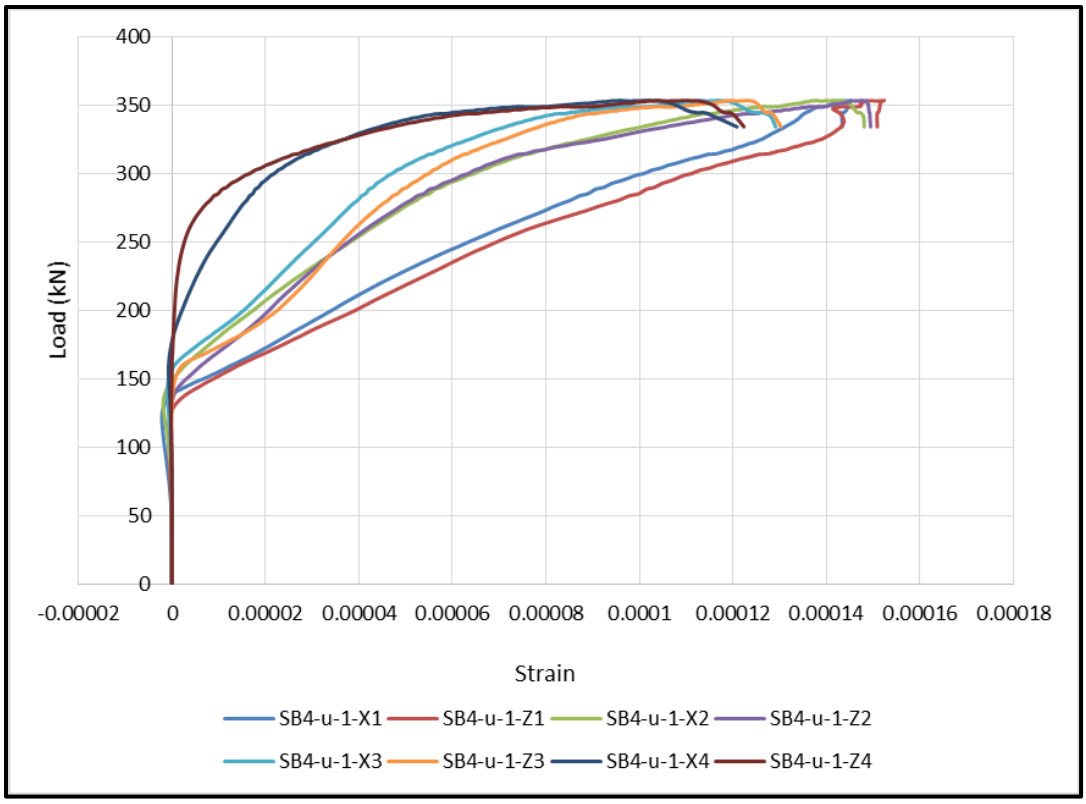

Figure E11: SB4-u-1 Bolt Strain Diagram

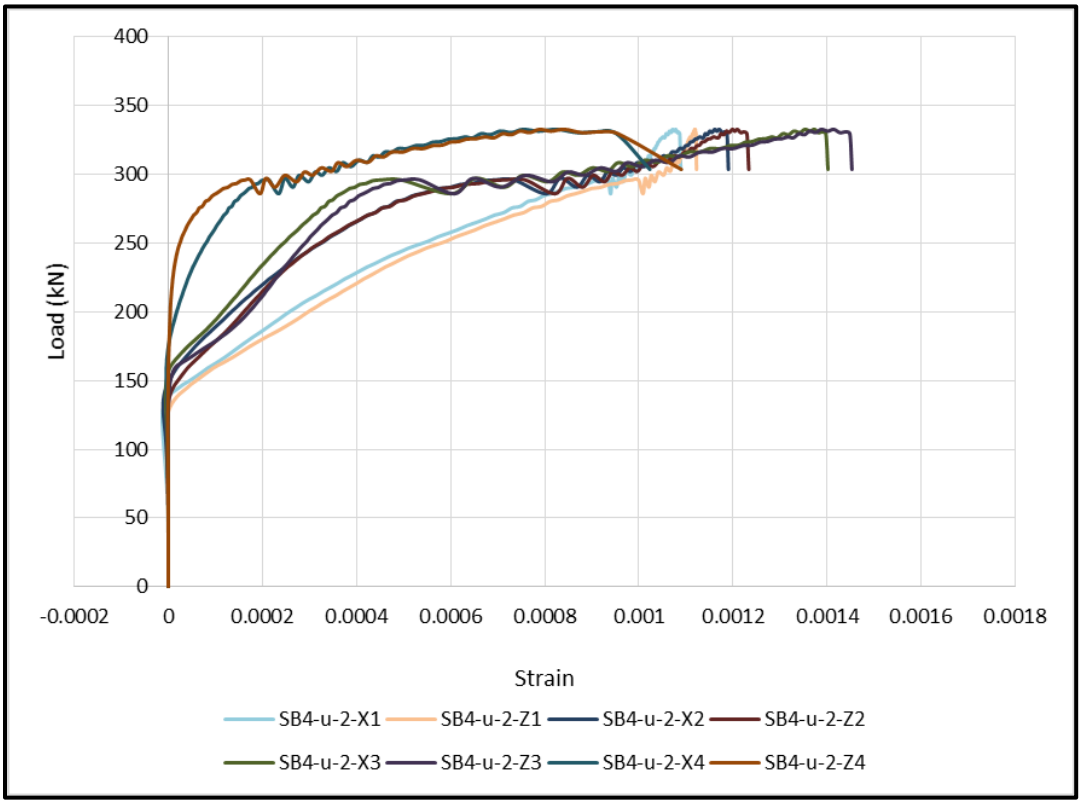

Figure E12: SB4-u-2 Bolt Strain Diagram

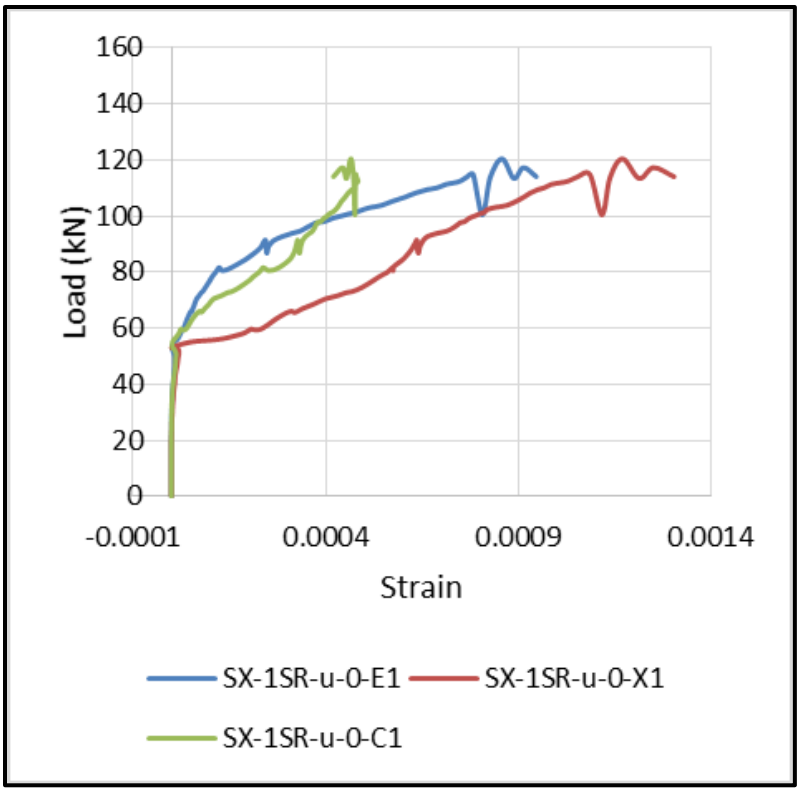

Figure E13: SX-1SR-u-0 Bolt Strain Diagram

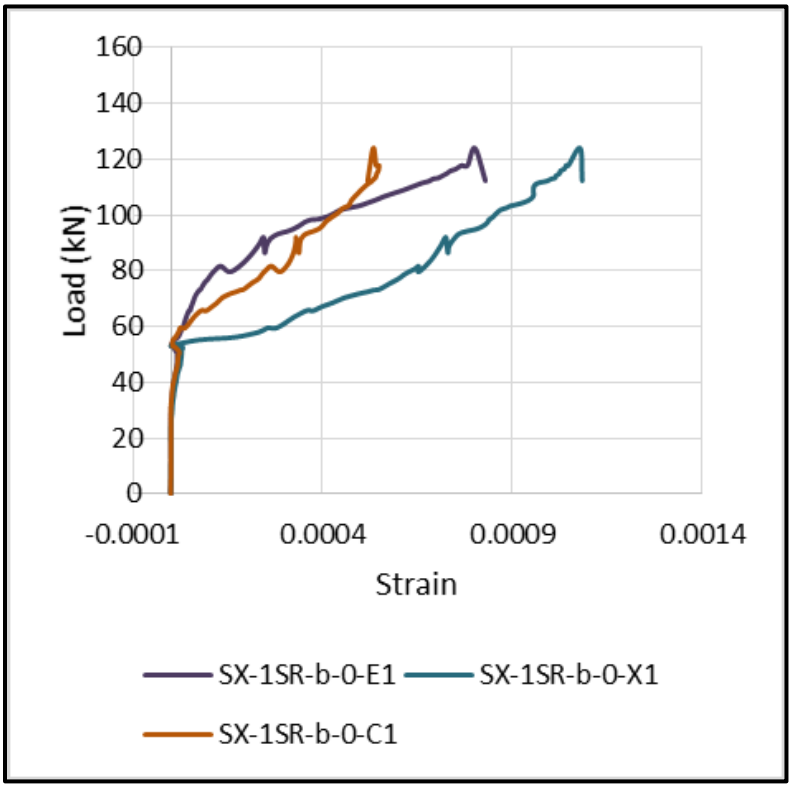

Figure E14: SX-1SR-b-0 Stud Strain Diagram

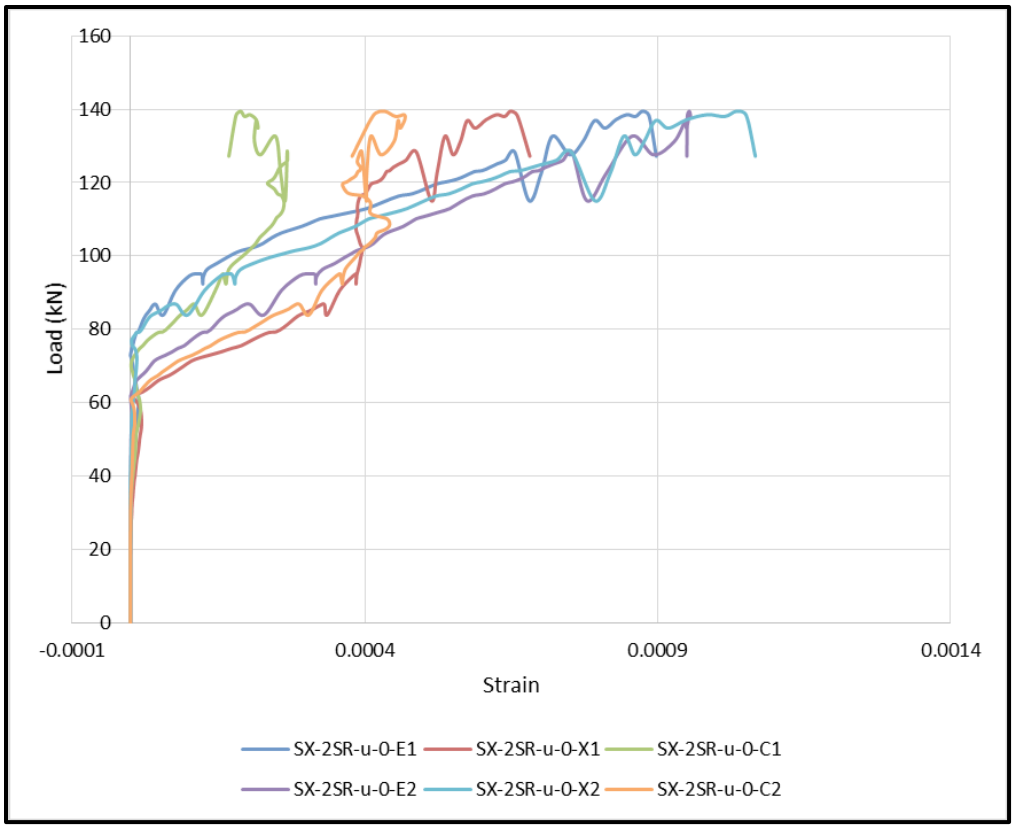

Figure E15: SX-2SR-u-0 Bolt Strain Diagram

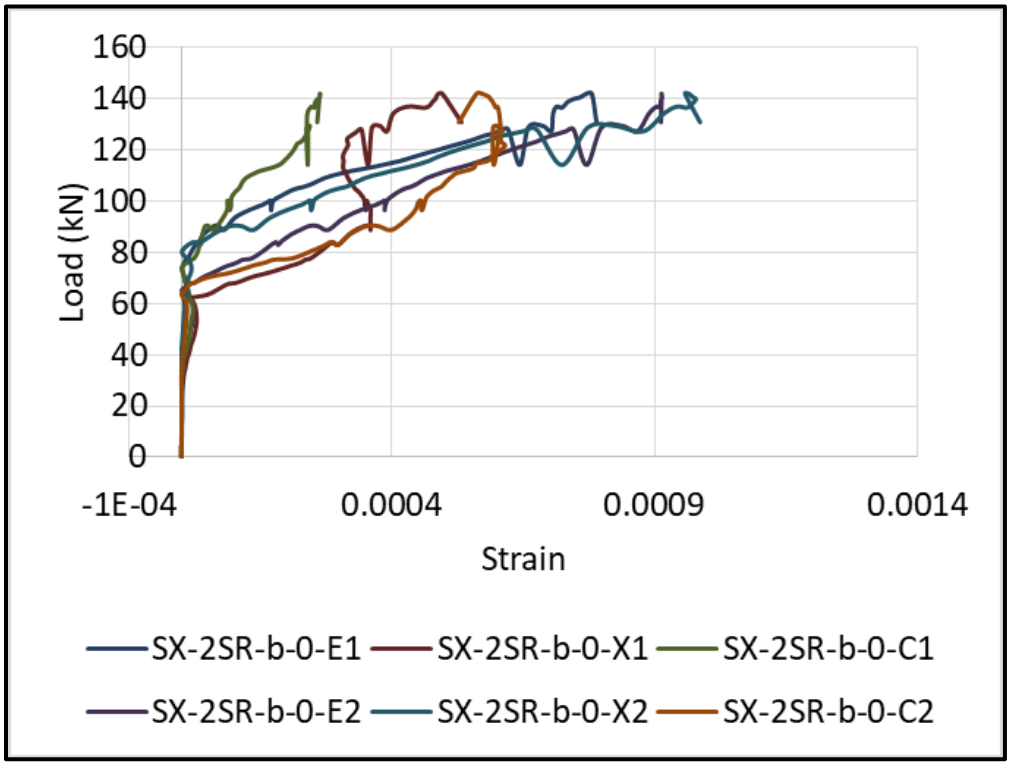

Figure E16: SX-2SR-b-0 Stud Strain Diagram

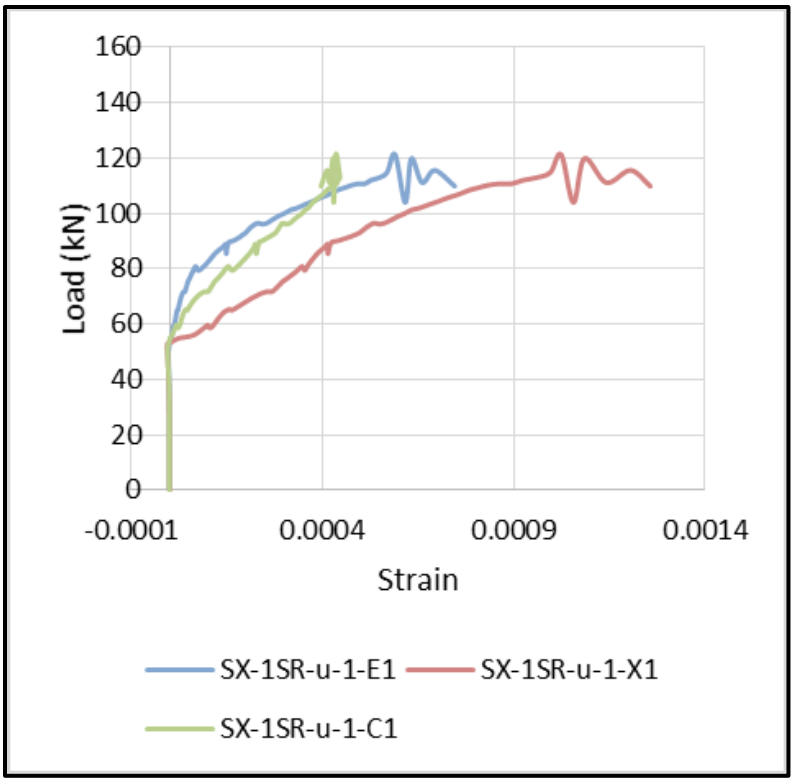

Figure E17: SX-1SR-u-1 Bolt Strain Diagram

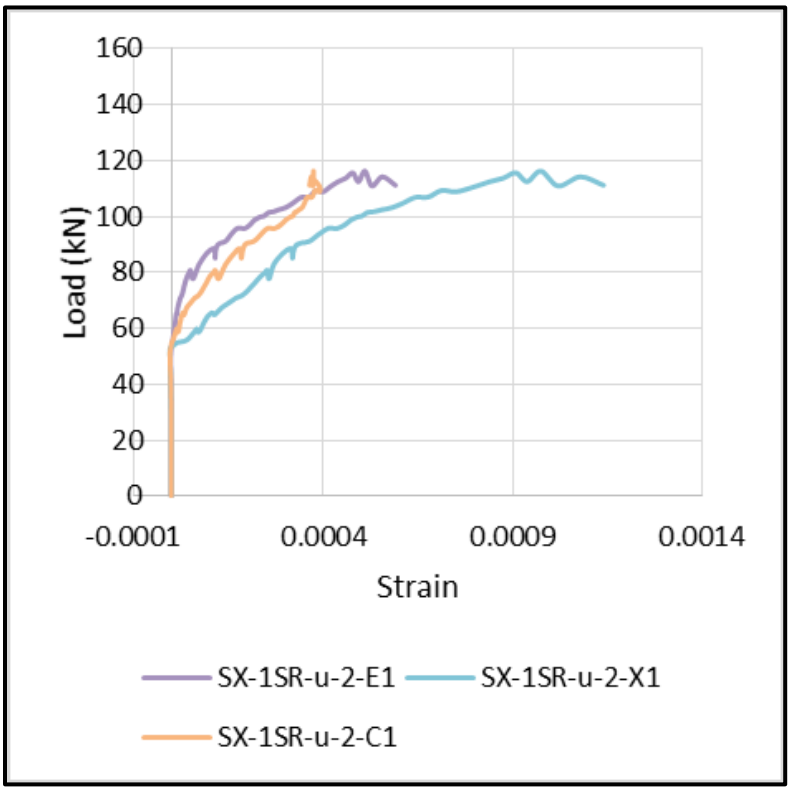

Figure E18: SX-1SR-u-2 Bolt Strain Diagram

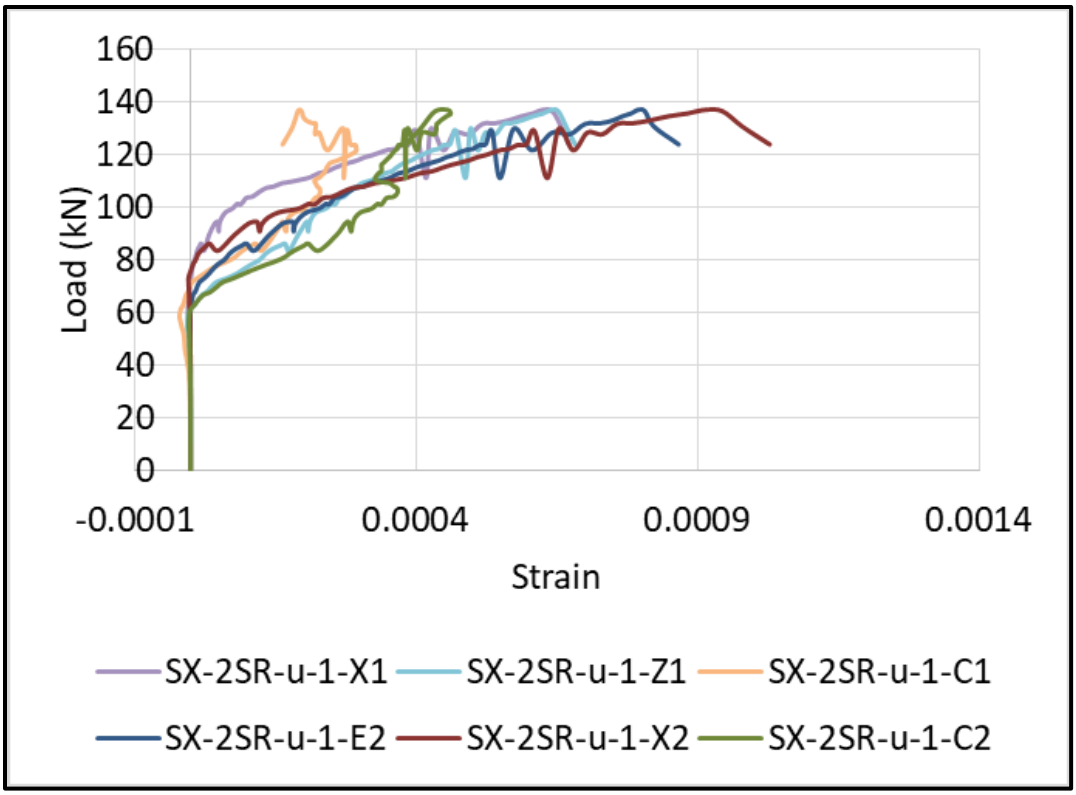

Figure E19: SX-2SR-u-1 Bolt Strain Diagram

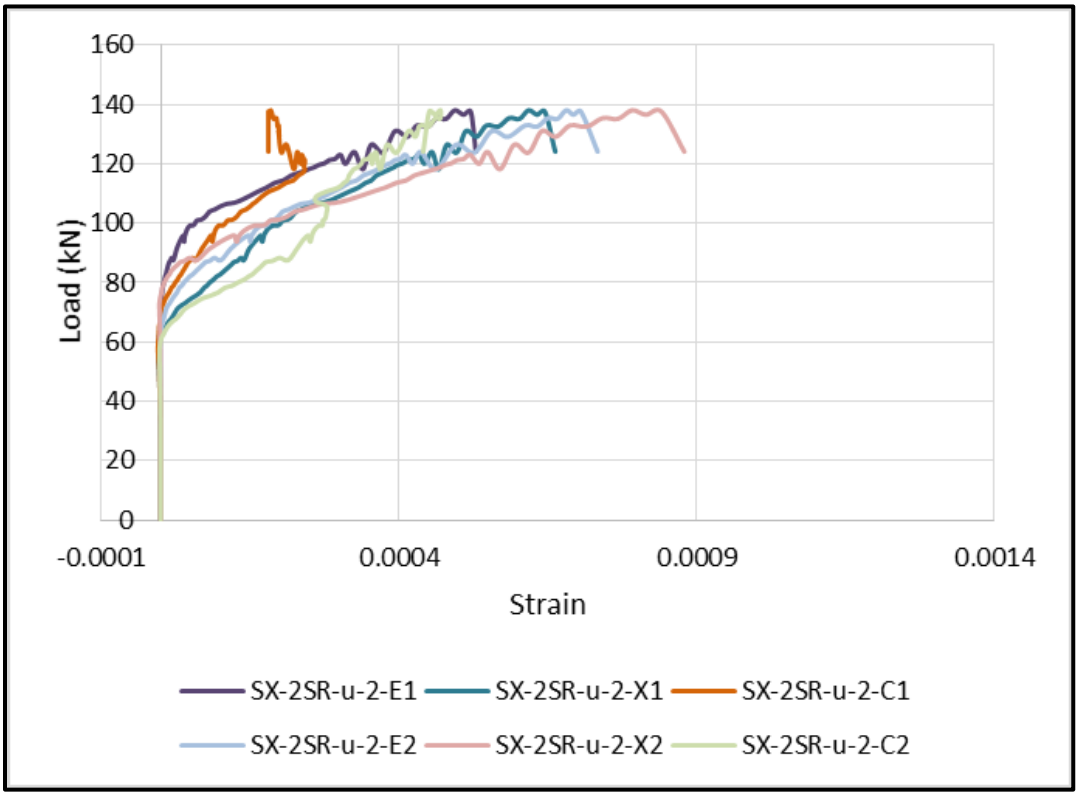

Figure E20: SX-2SR-u-2 Bolt Strain Diagram

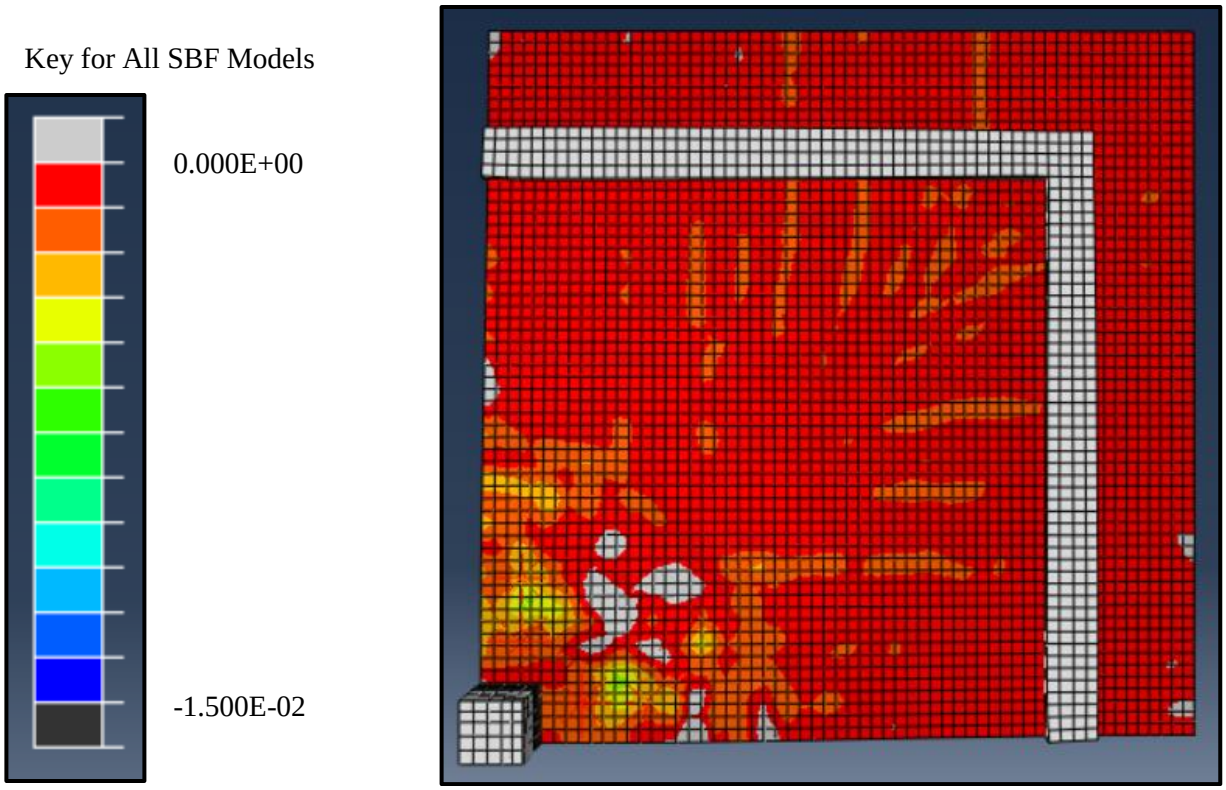

Figure E21: SB2-b-0 Tensile Face Crack Pattern

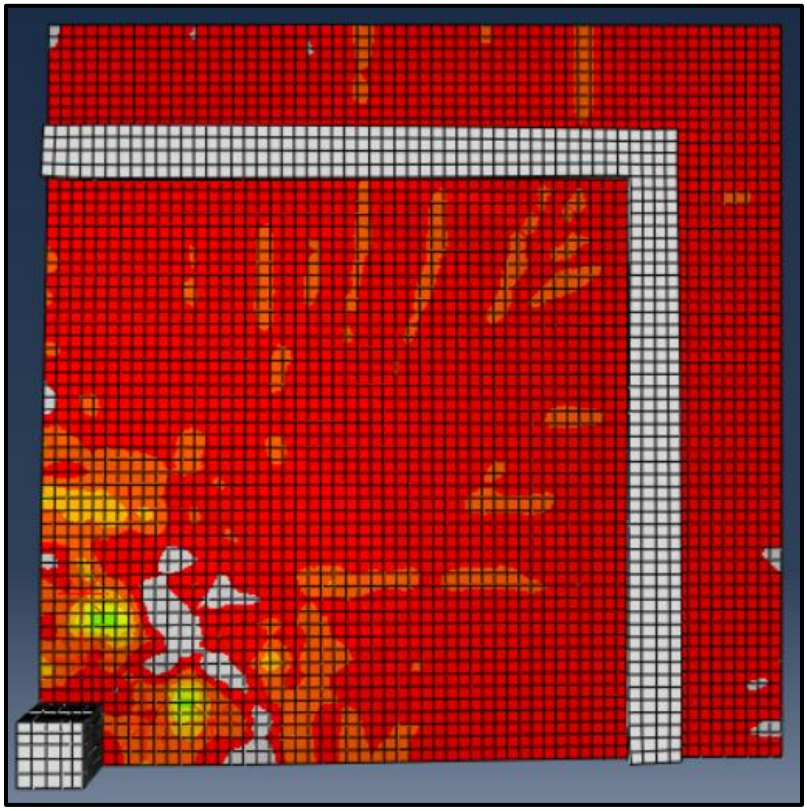

Figure E22: SB2-u-0 Tensile Face Crack Pattern

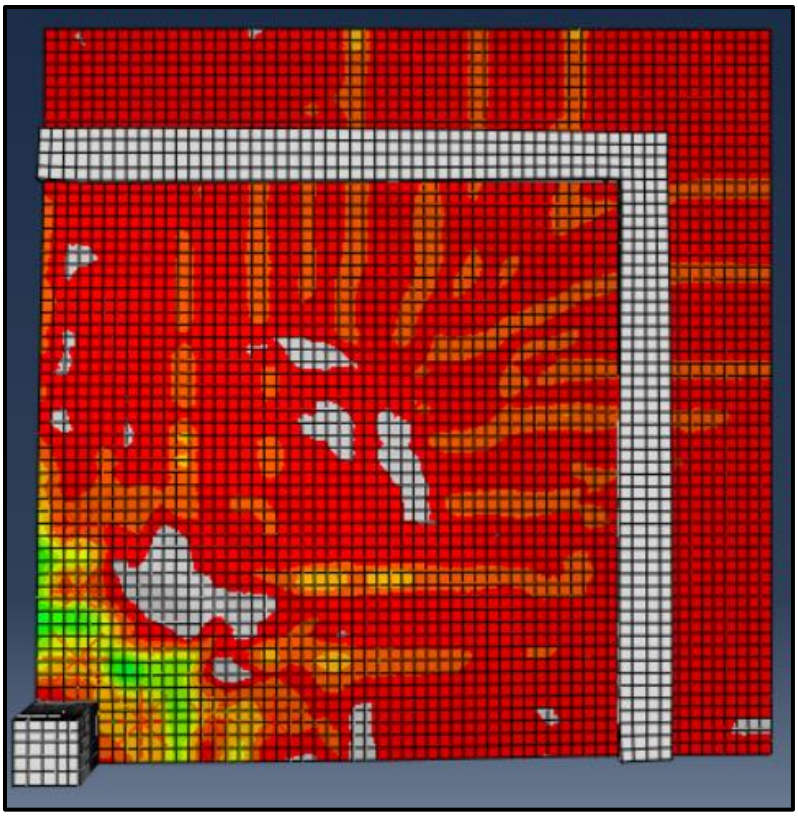

Figure E23: SB3-b-0 Tensile Face Crack Pattern

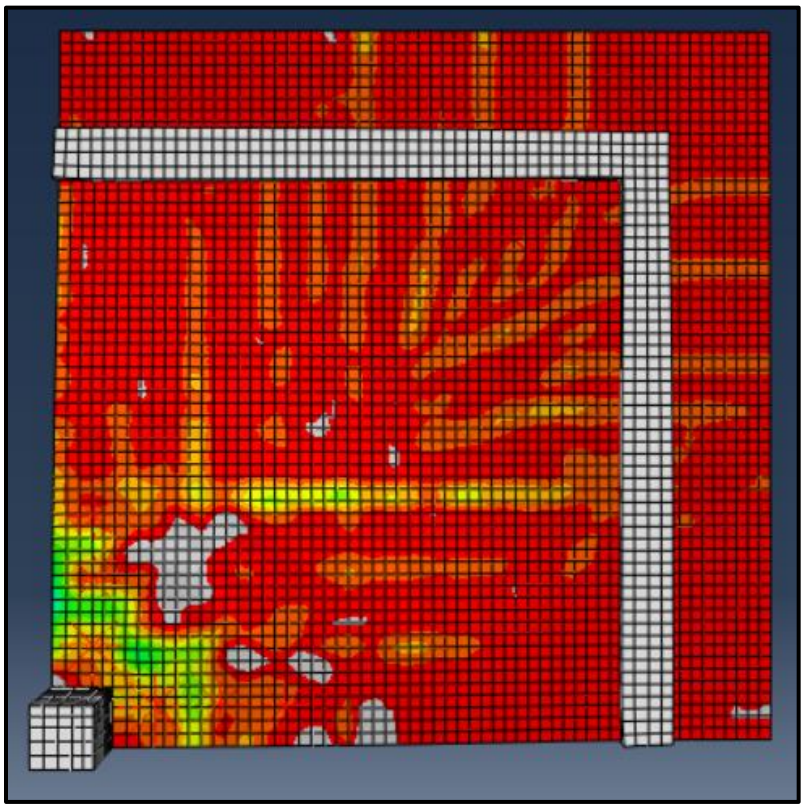

Figure E24: SB3-u-0 Tensile Face Crack Pattern

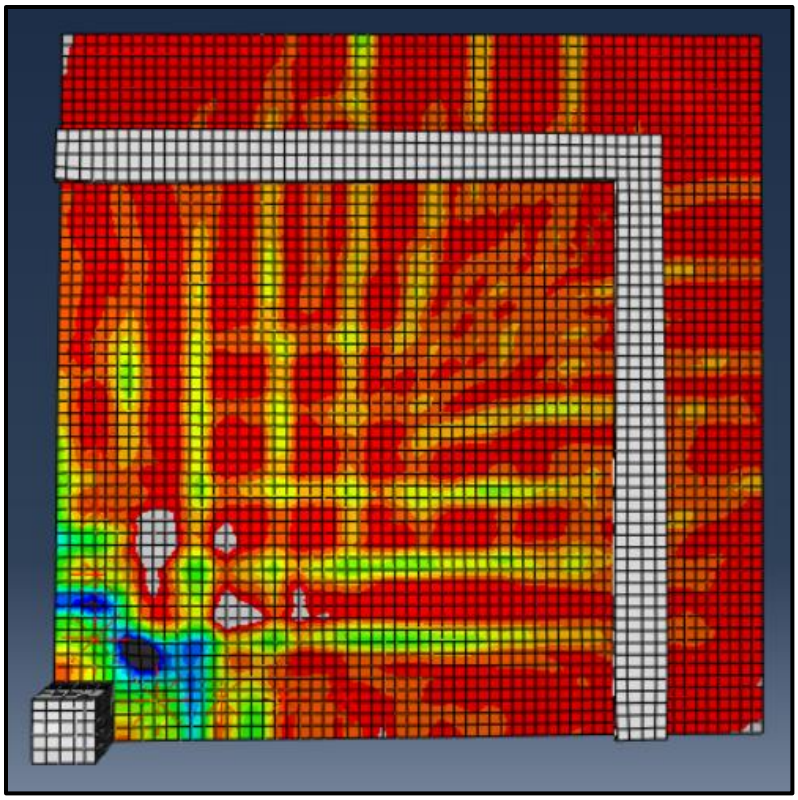

Figure E25: SB4-b-0 Tensile Face Crack Pattern

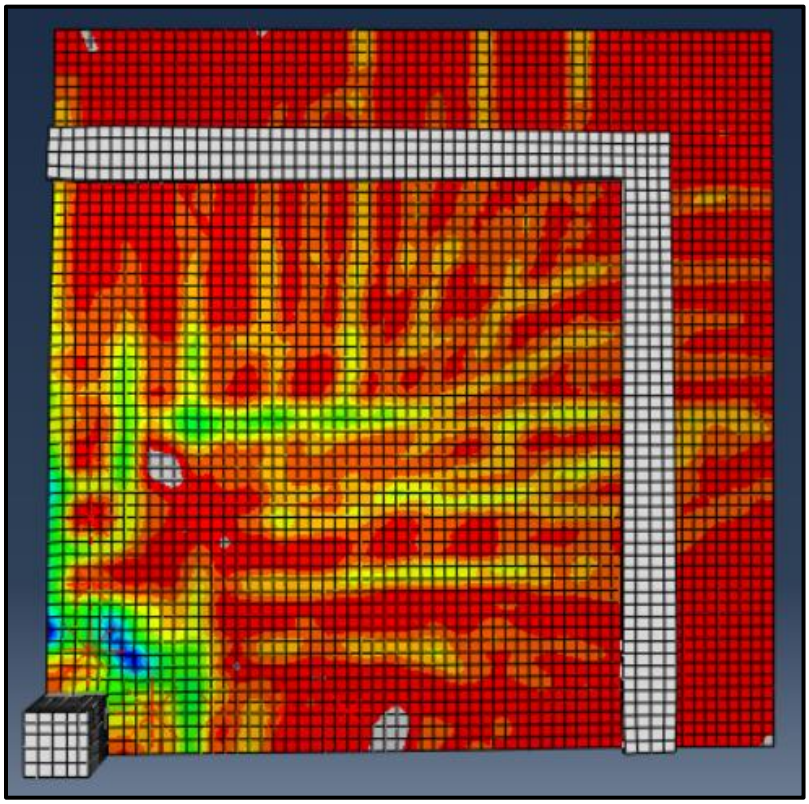

Figure E26: SB4-u-0 Tensile Face Crack Pattern

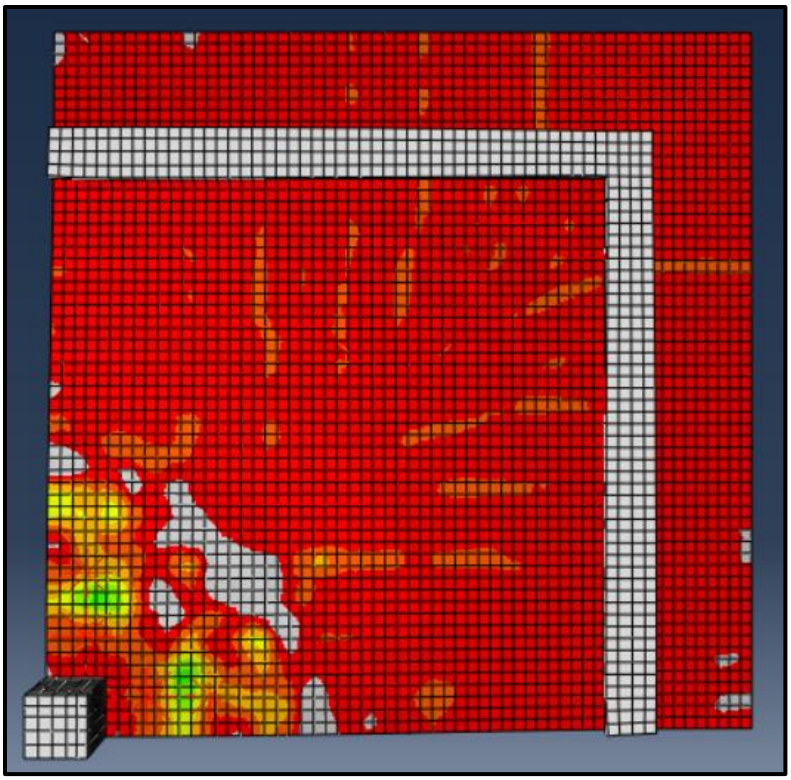

Figure E27: SB2-u-1 Tensile Face Crack Pattern

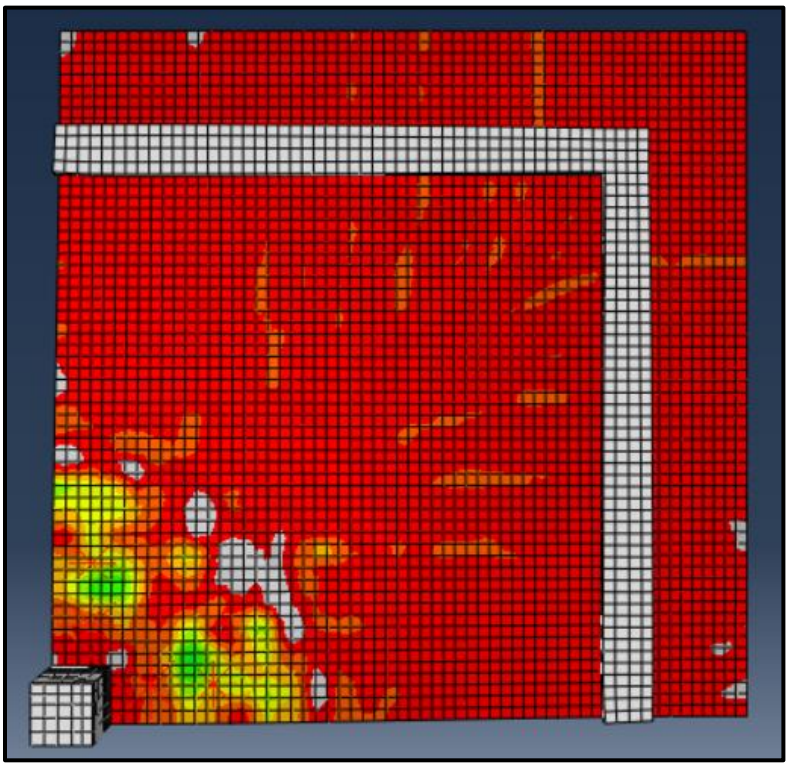

Figure E28: SB2-u-2 Tensile Face Crack Pattern

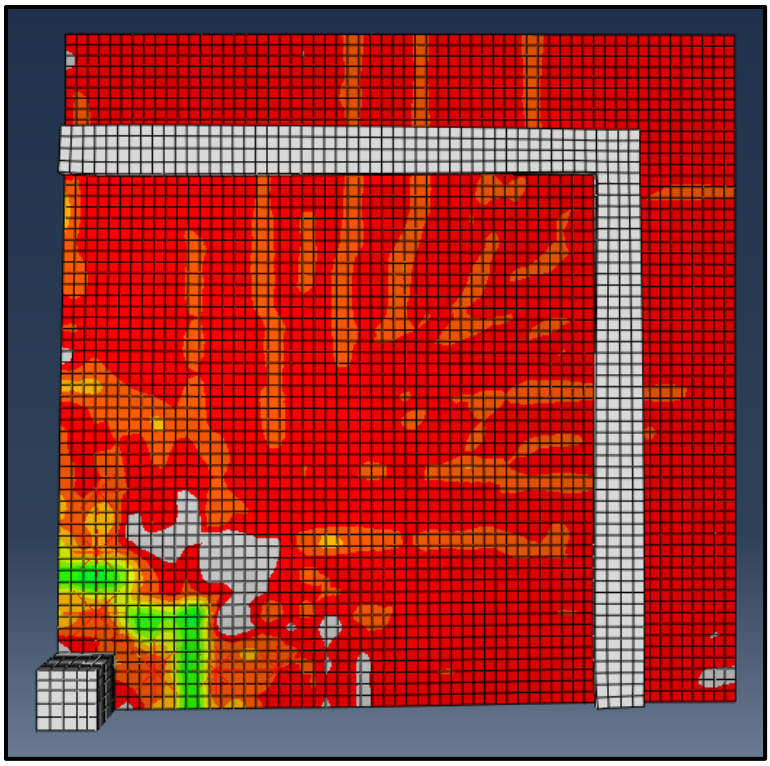

Figure E29: SB3-u-1 Tensile Face Crack Pattern

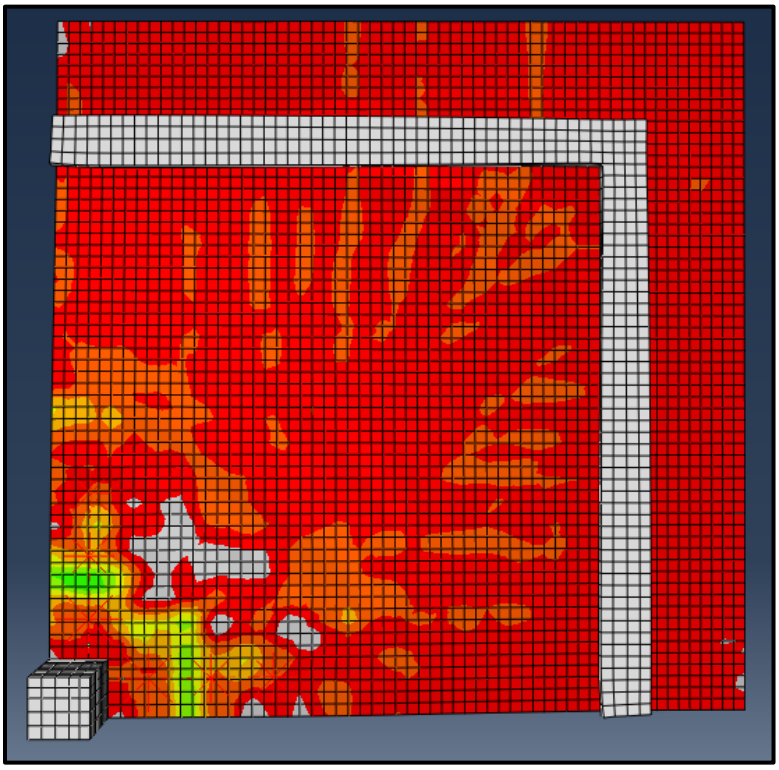

Figure E30: SB3-u-2 Tensile Face Crack Pattern

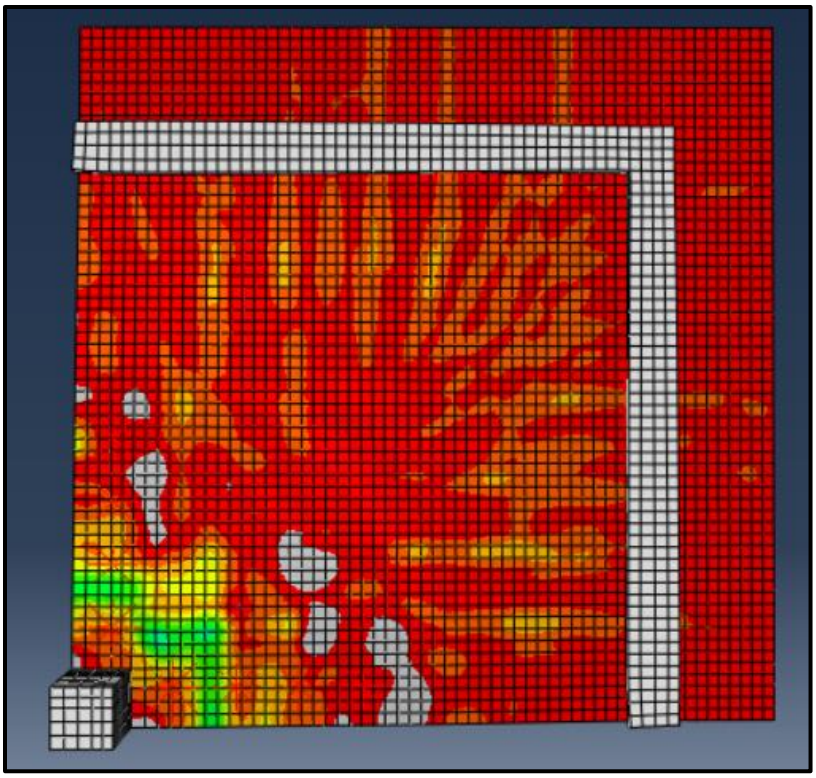

Figure E31: SB4-u-1 Tensile Face Crack Pattern

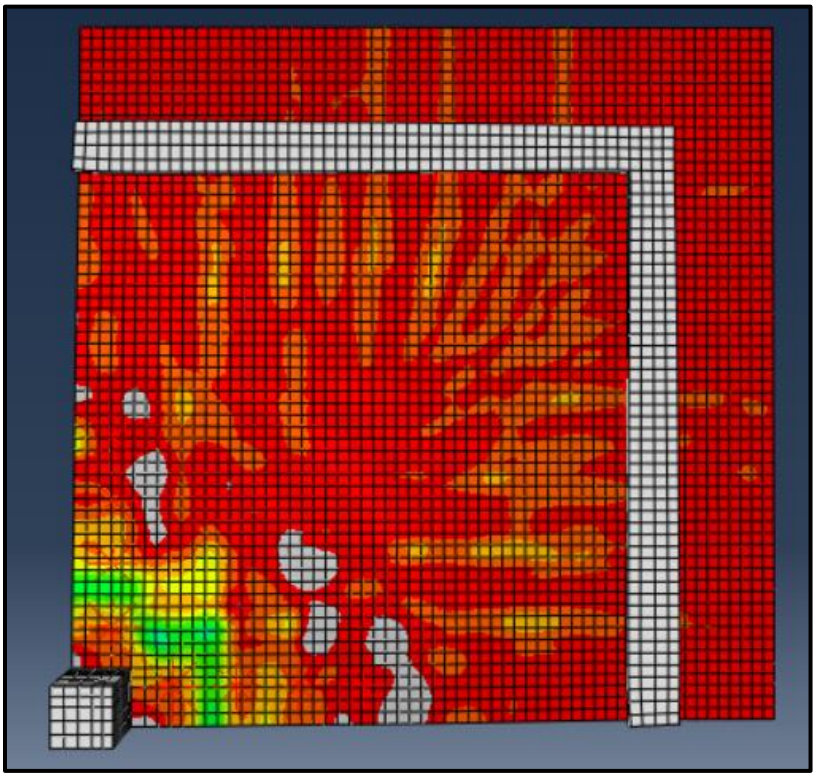

Figure E32: SB4-u-2 Tensile Face Crack Pattern

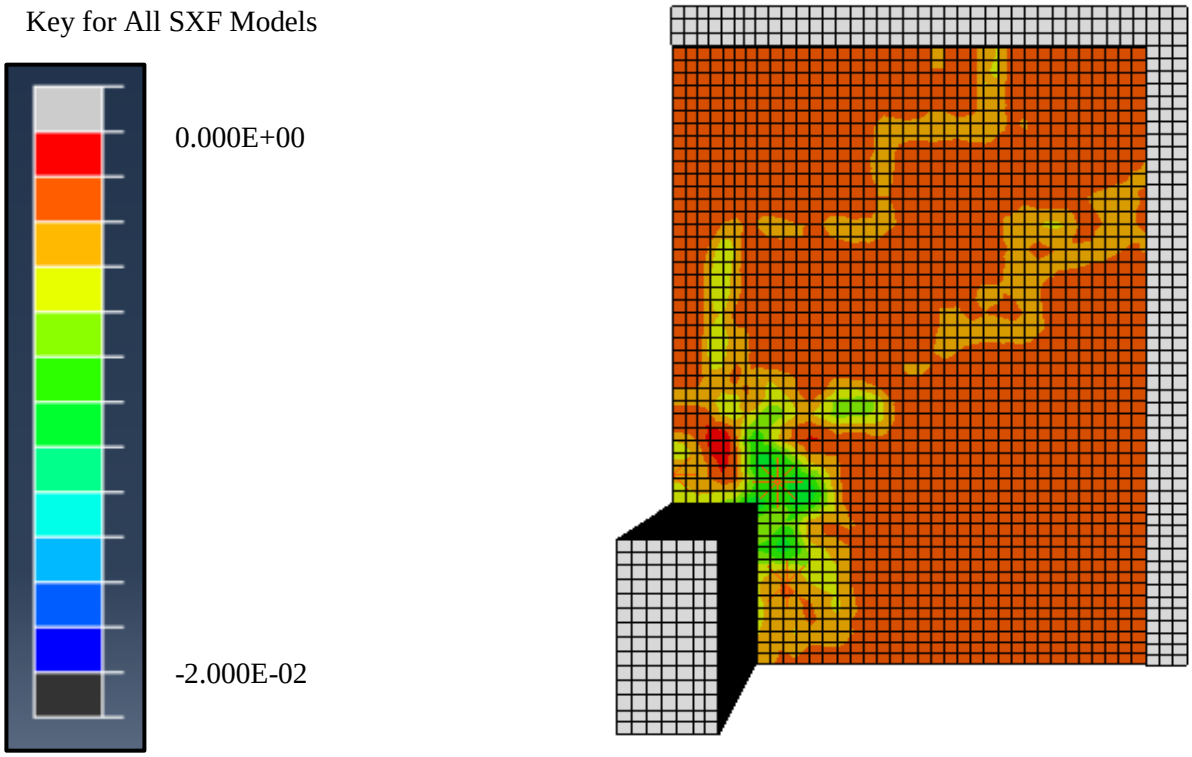

Figure E33: SX-1SR-u-0 Tensile Face Crack Pattern

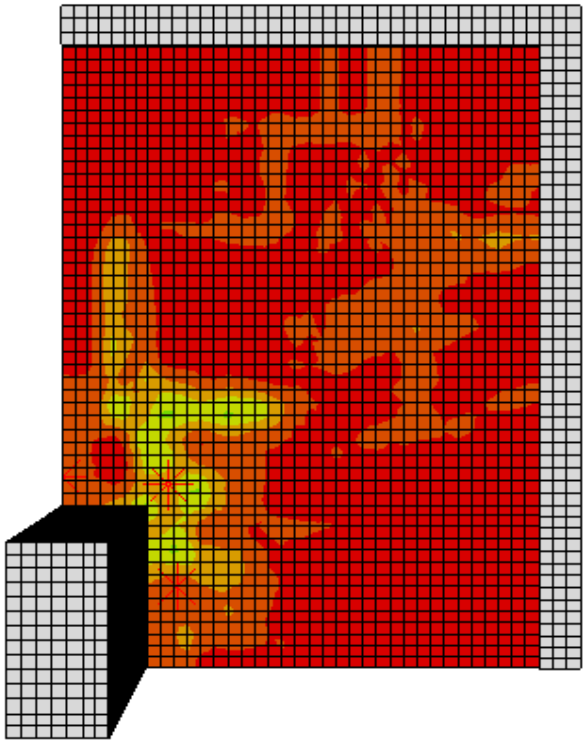

Figure E34: SX-1SR-b-0 Tensile Face Crack Pattern

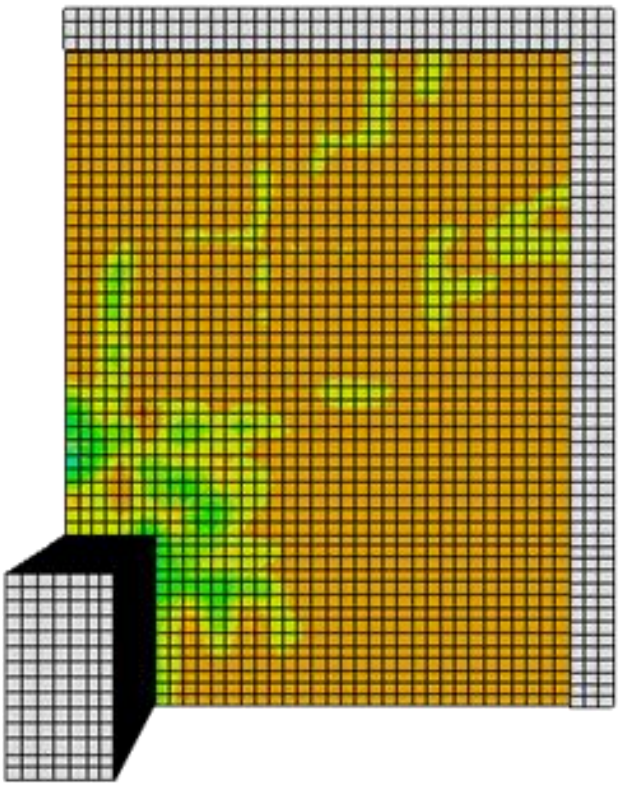

Figure E35: SX-2SR-u-0 Tensile Face Crack Pattern

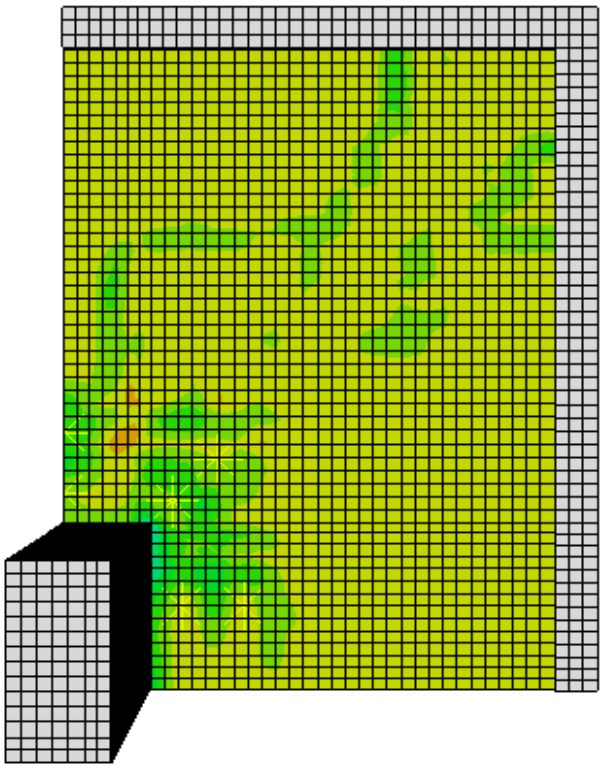

Figure E36: SX-2SR-b-0 Tensile Face Crack Pattern

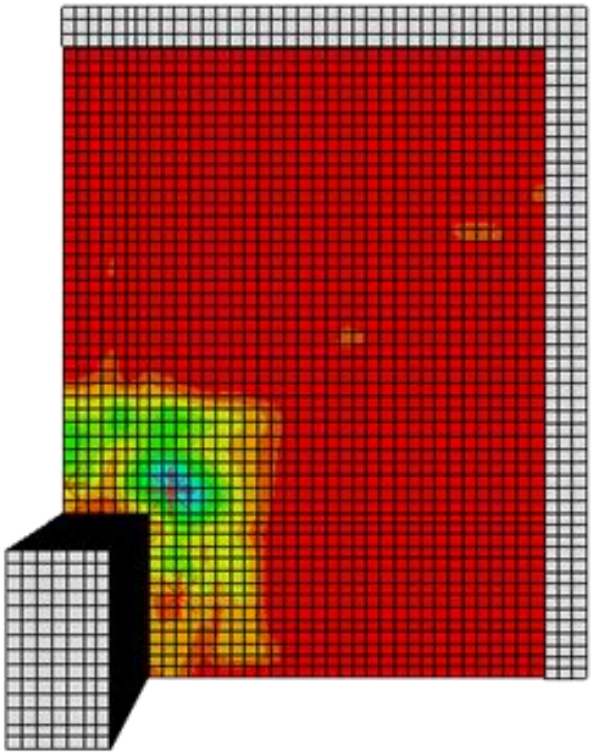

Figure E37: SX-1SR-u-1 Tensile Face Crack Pattern

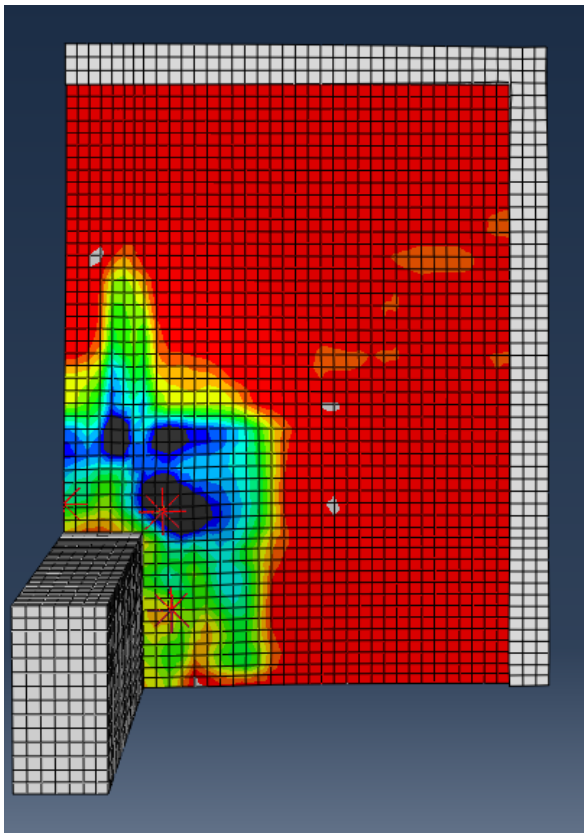

Figure E38: SX-1SR-u-2 Tensile Face Crack Pattern

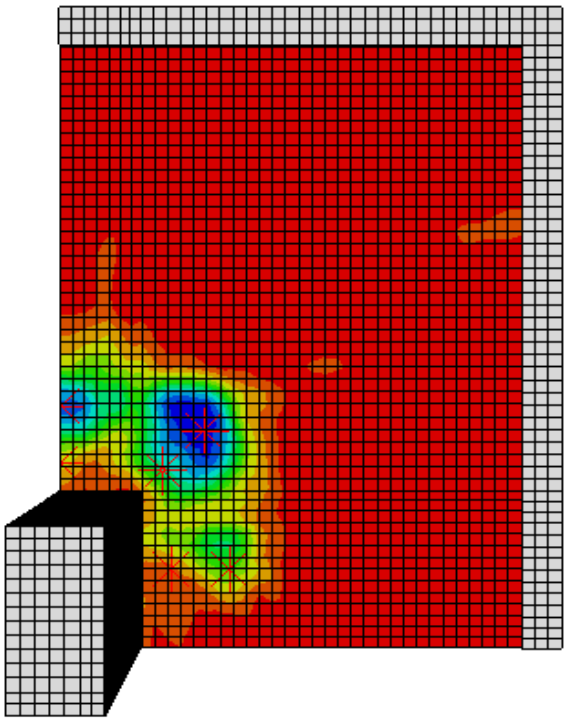

Figure E39: SX-2SR-u-1 Tensile Face Crack Pattern

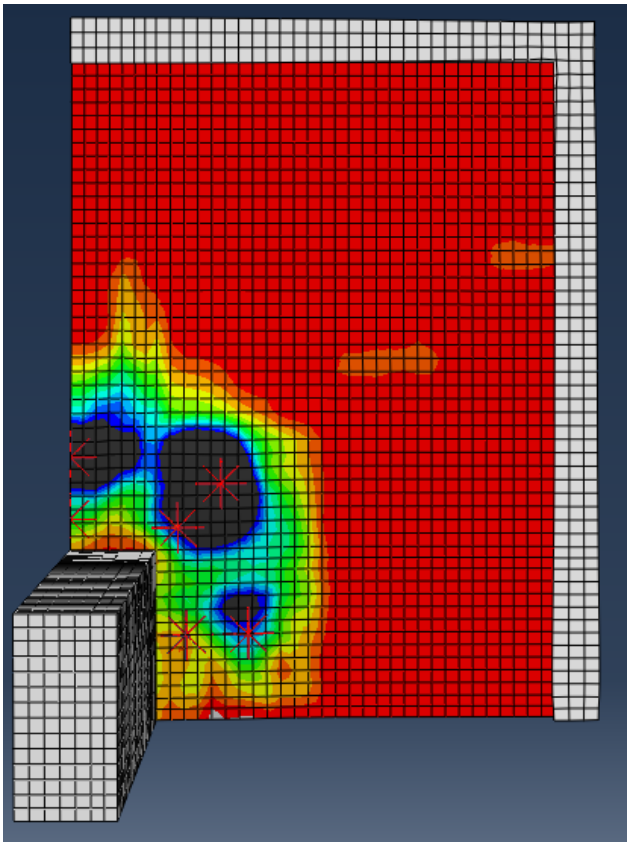

Figure E40: SX-2SR-u-2 Tensile Face Crack Pattern

Key for All SBF Models

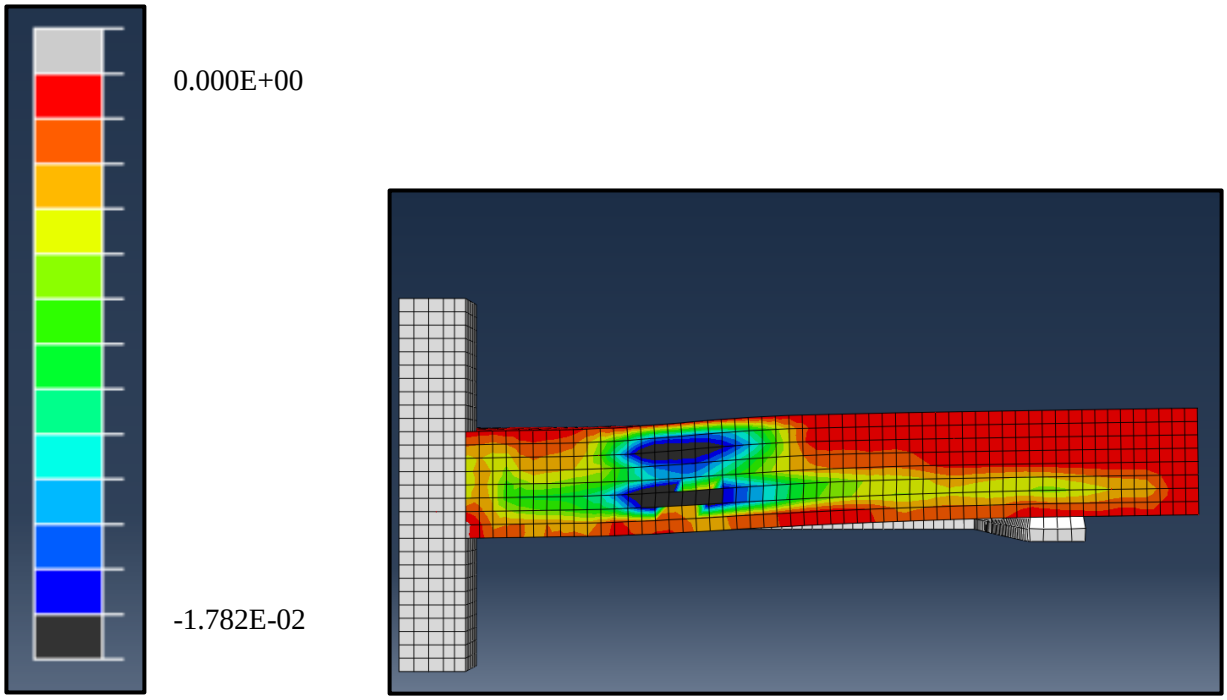

Figure E41: SB2-b-0 Post-Failure Side Crack Profile

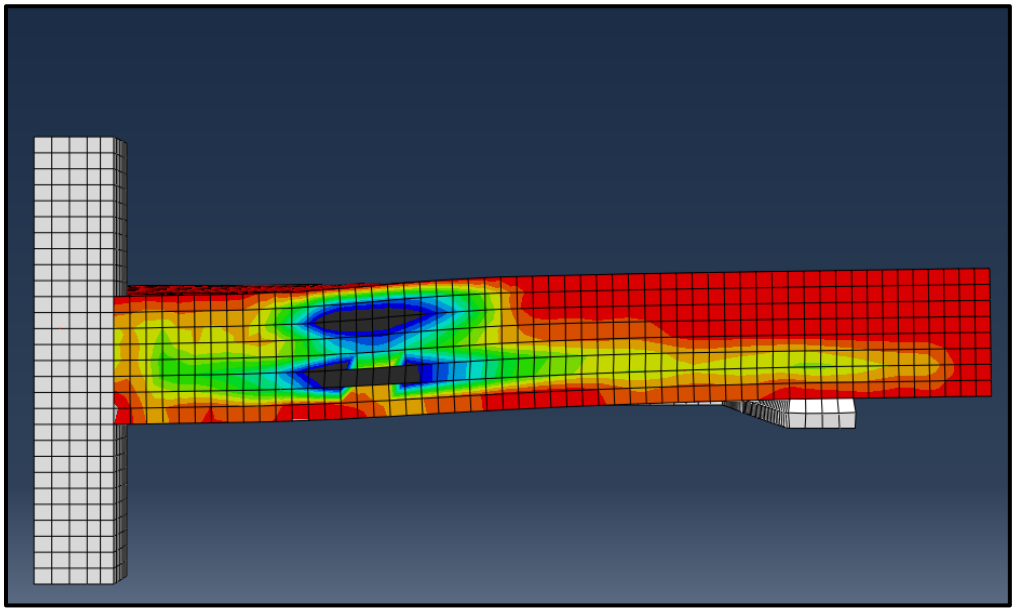

Figure E42: SB2-u-0 Post-Failure Side Crack Profile

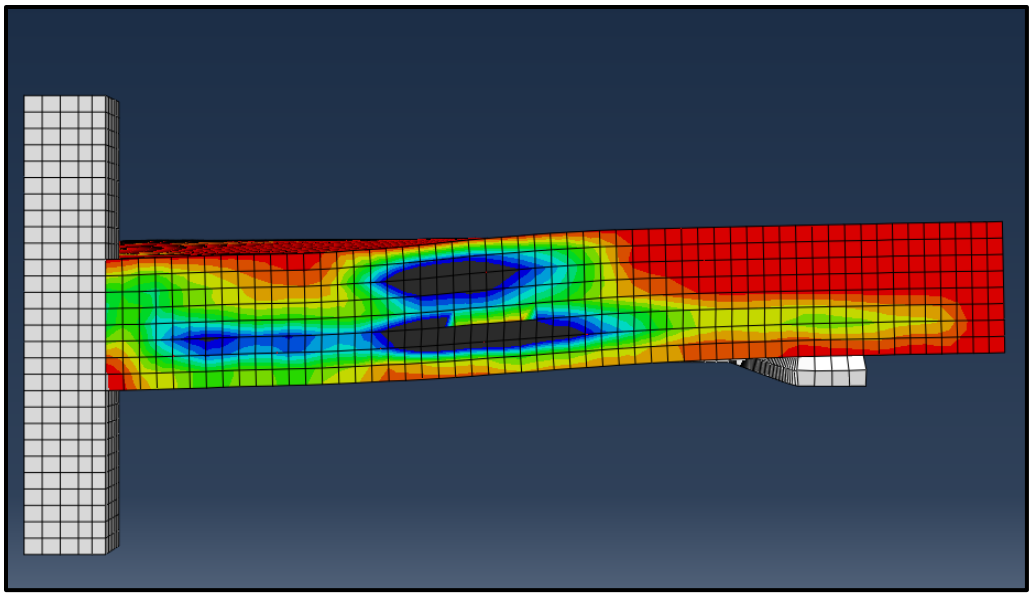

Figure E43: SB3-b-0 Post-Failure Side Crack Profile

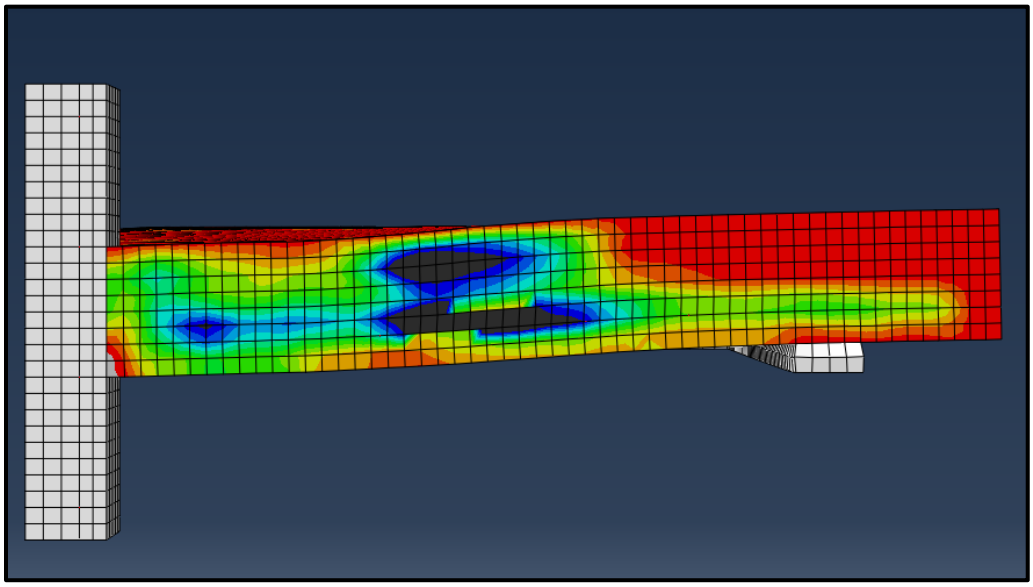

Figure E44: SB3-u-0 Post-Failure Side Crack Profile

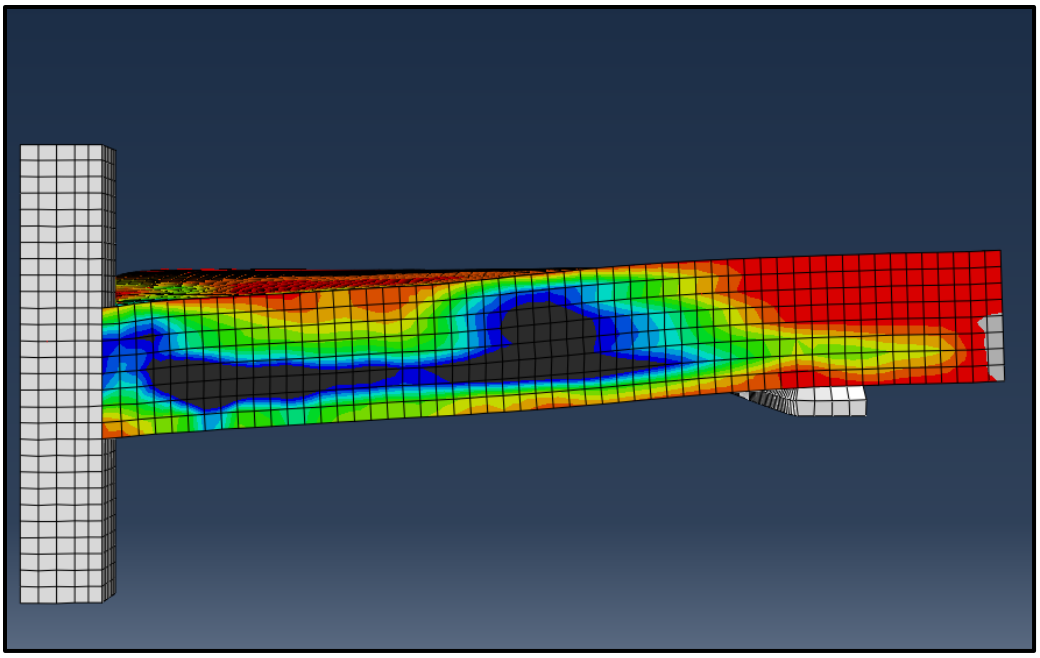

Figure E45: SB4-b-0 Post-Failure Side Crack Profile

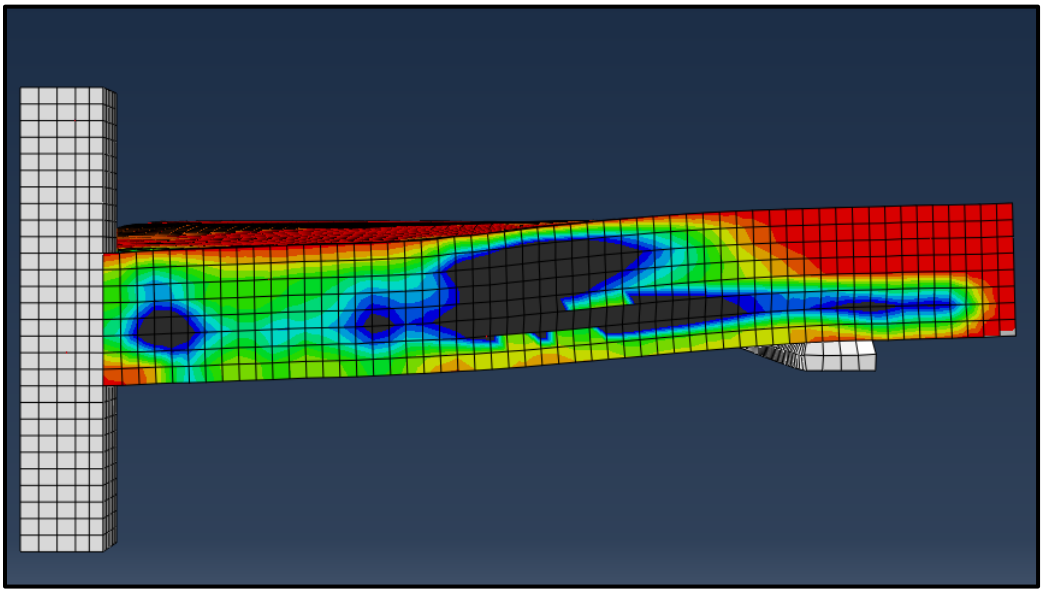

Figure E46: SB4-u-0 Post-Failure Side Crack Profile

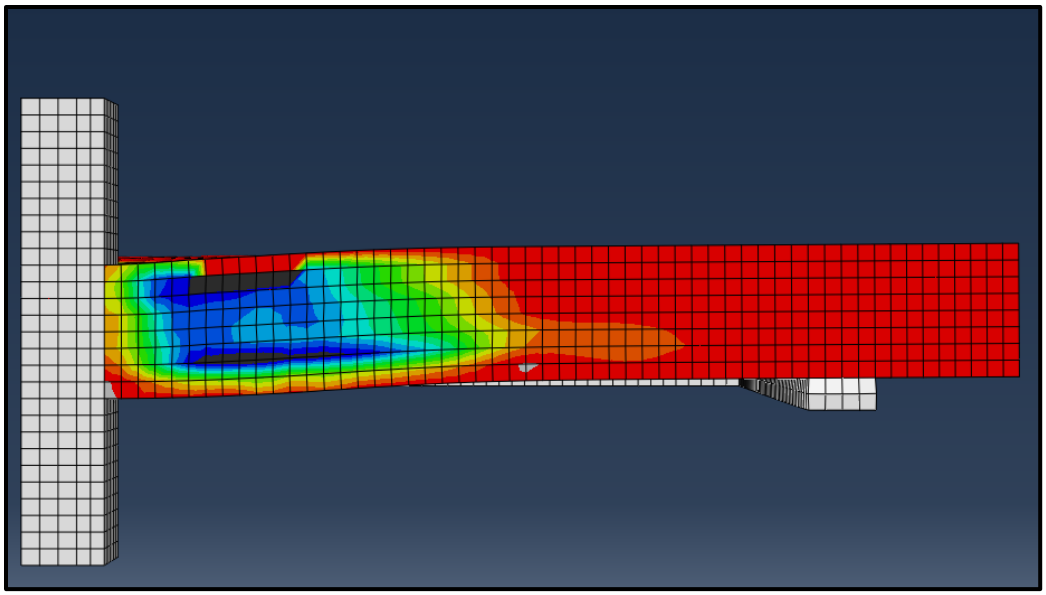

Figure E47: SB2-u-1 Post-Failure Side Crack Profile

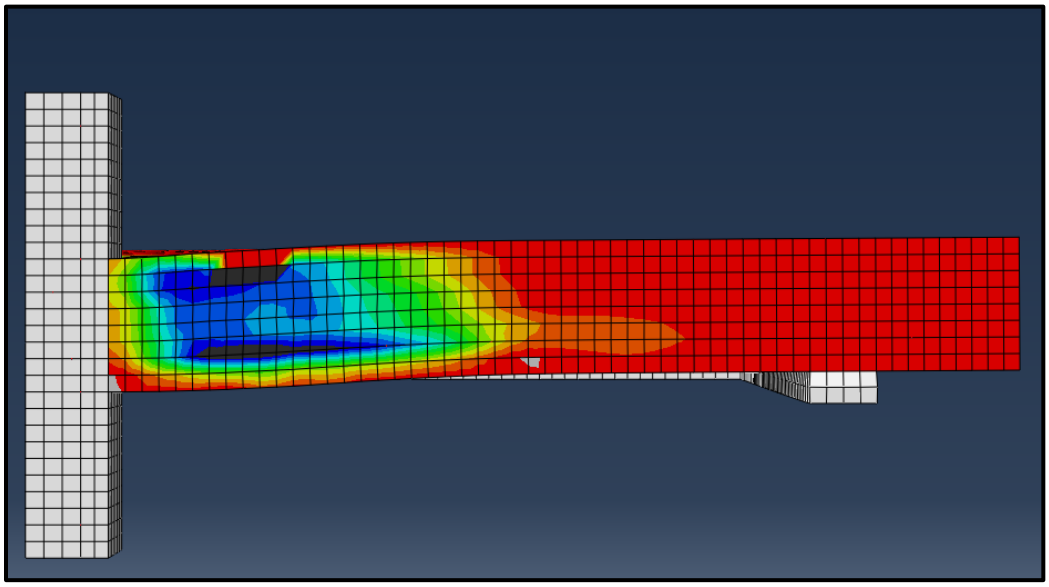

Figure E48: SB2-u-2 Post-Failure Side Crack Profile

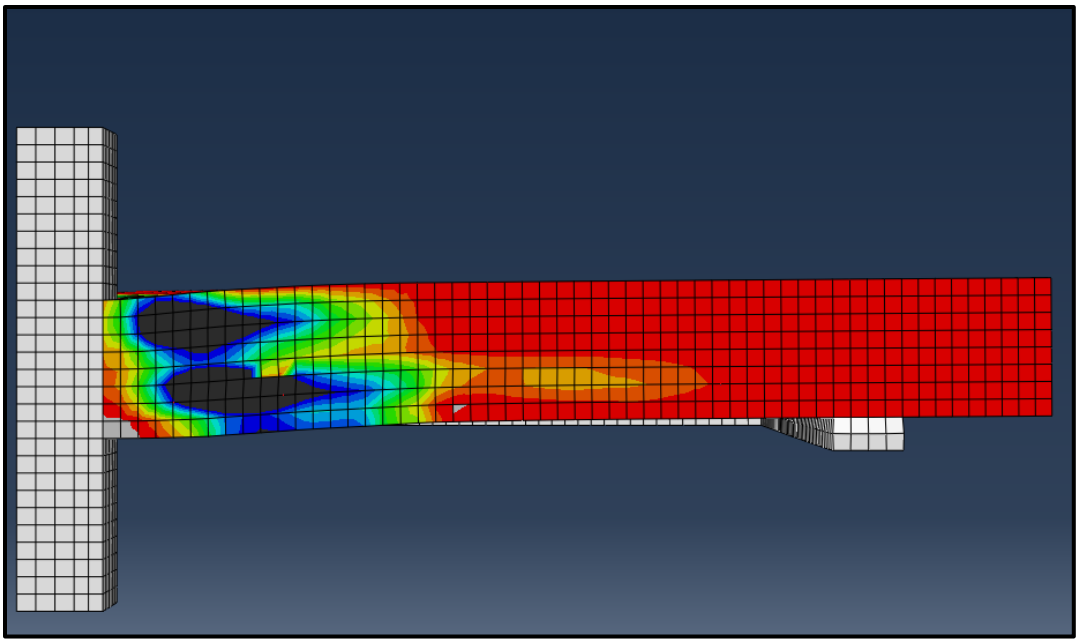

Figure E49: SB3-u-1 Post-Failure Side Crack Profile

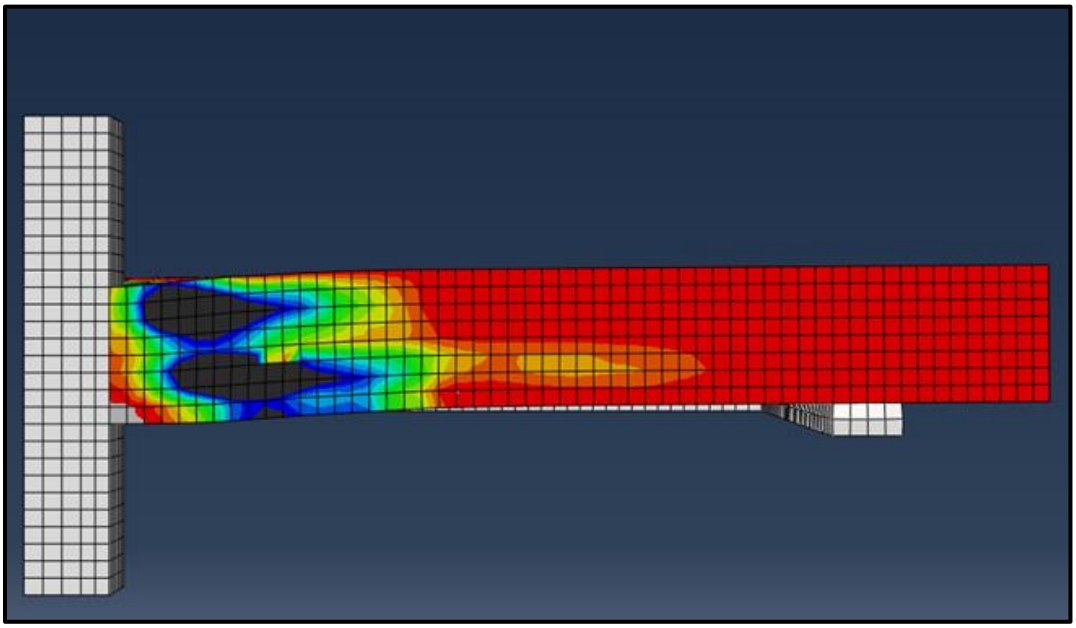

Figure E50: SB3-u-2 Post-Failure Side Crack Profile

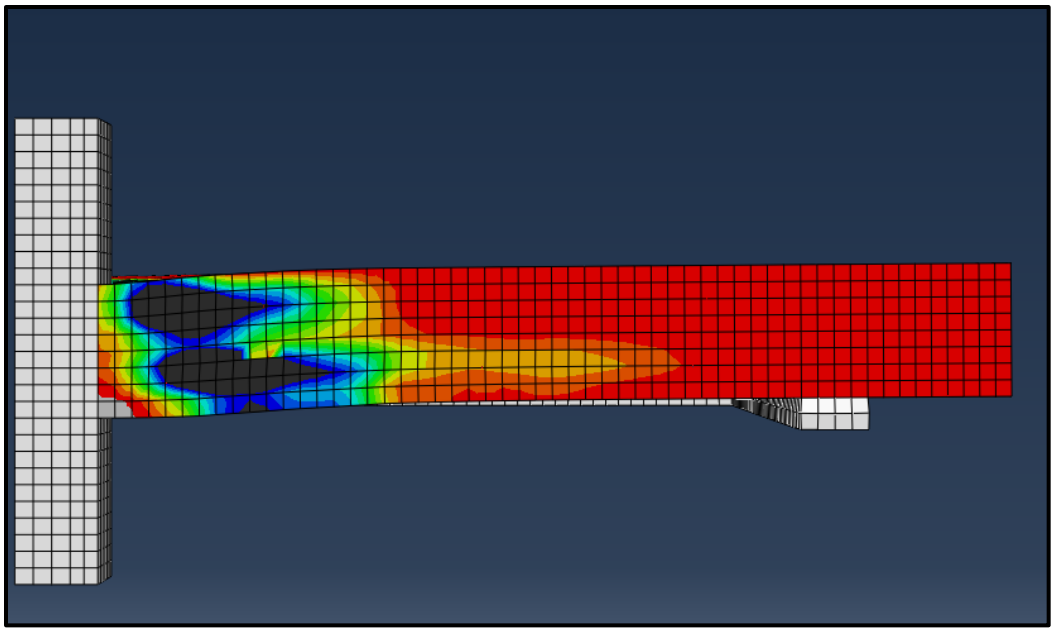

Figure E51: SB4-u-1 Post-Failure Side Crack Profile

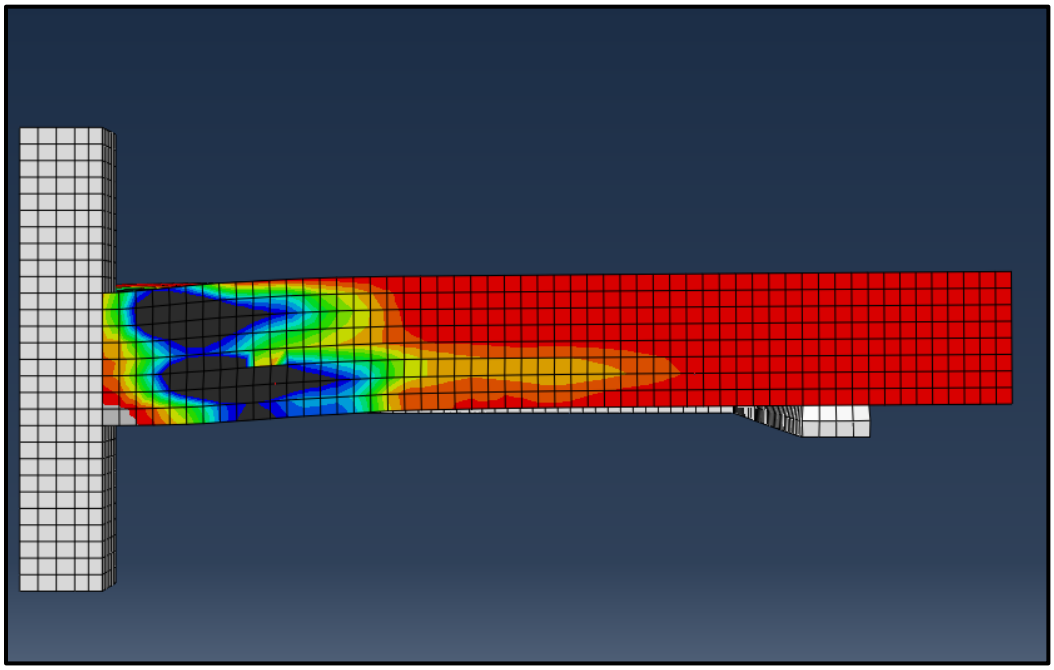

Figure E52: SB4-u-2 Post-Failure Side Crack Profile

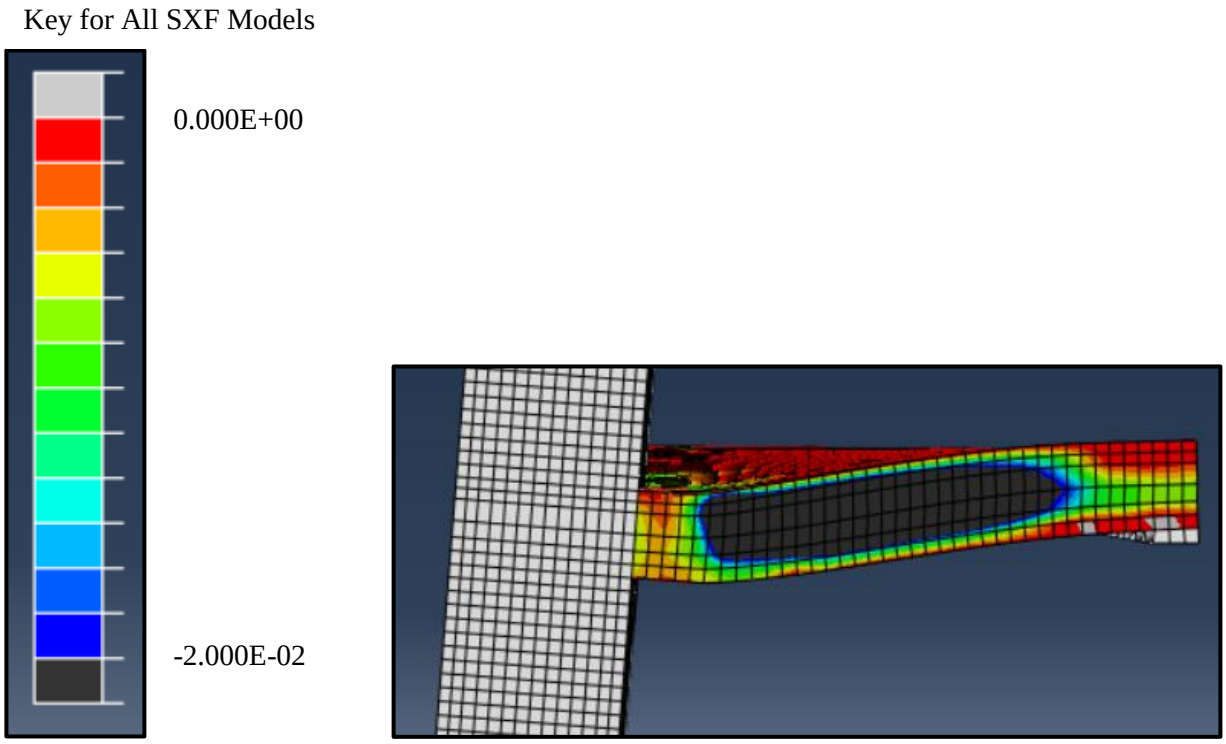

Figure E53: SX-1SR-u-0 Post-Failure Side Crack Profile

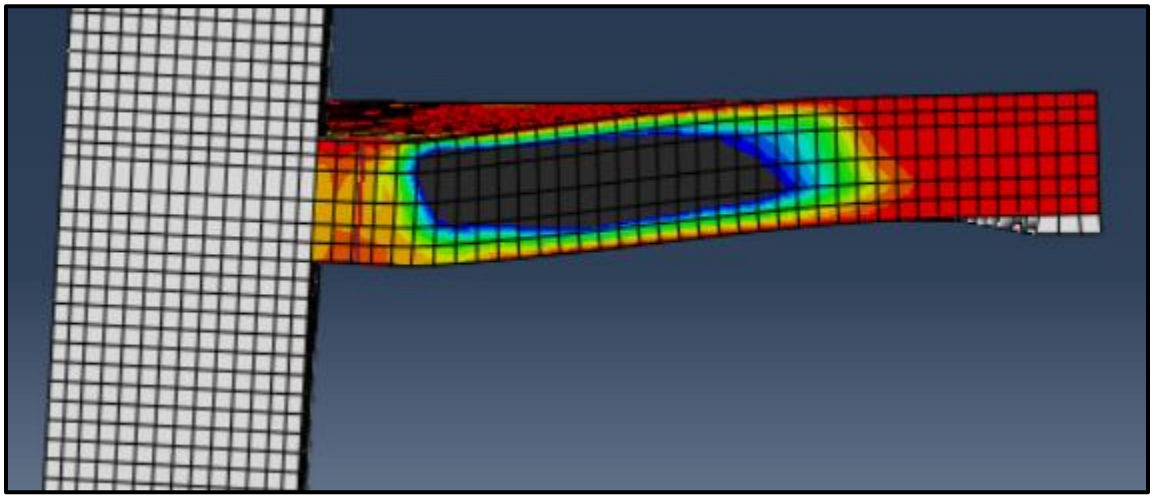

Figure E54: SX-1SR-b-0 Post-Failure Side Crack Profile

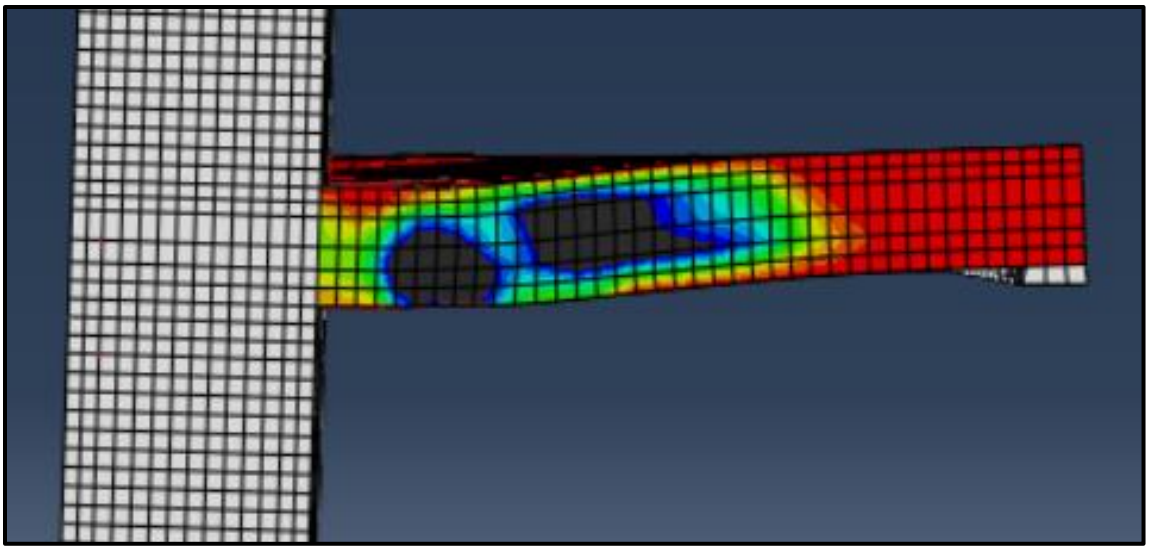

Figure E55: SX-2SR-u-0 Post-Failure Side Crack Profile

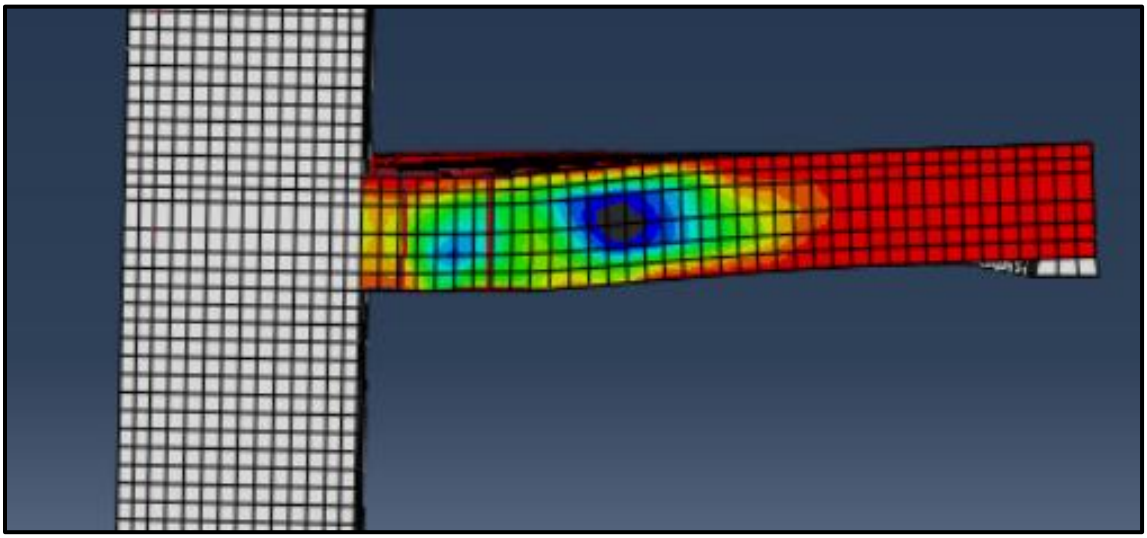

Figure E56: SX-2SR-b-0 Post-Failure Side Crack Profile

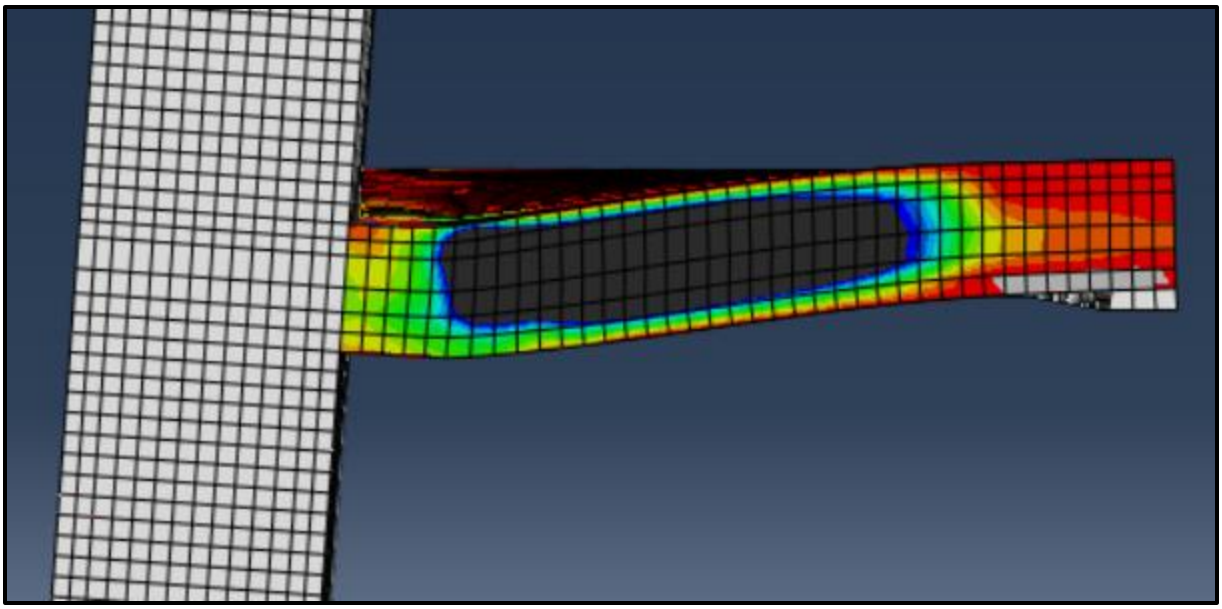

Figure E57: SX-1SR-u-1 Post-Failure Side Crack Profile

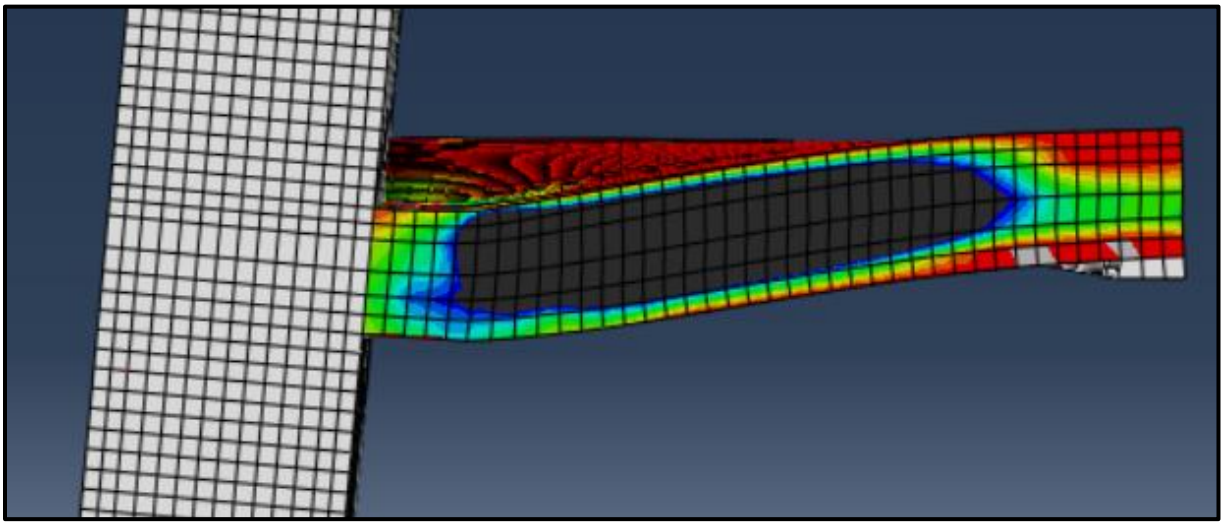

Figure E58: SX-1SR-u-2 Post-Failure Side Crack Profile

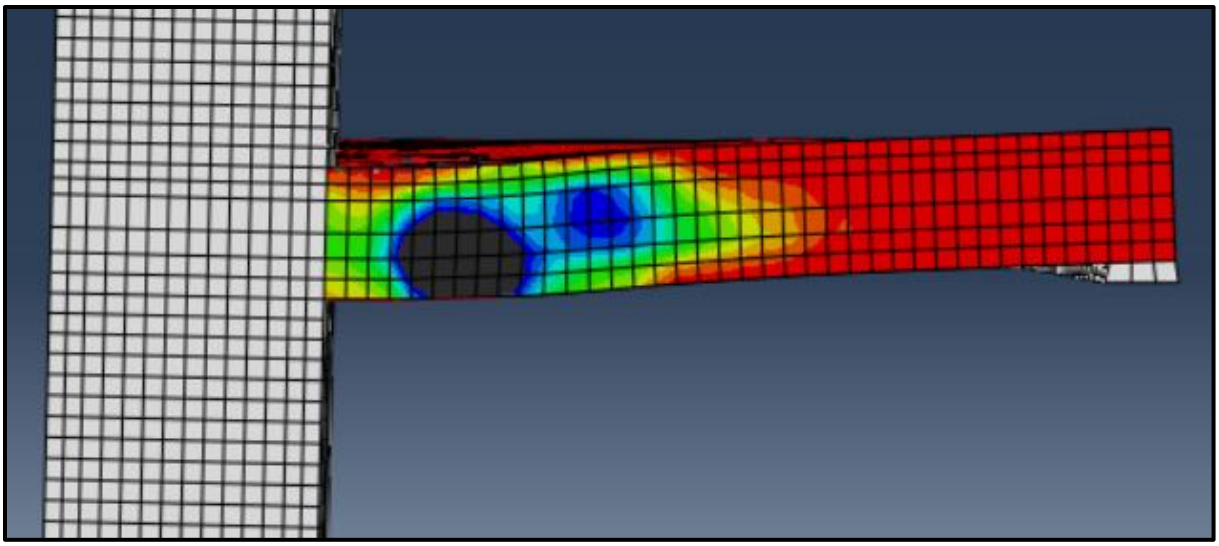

Figure E59: SX-2SR-u-1 Post-Failure Side Crack Profile

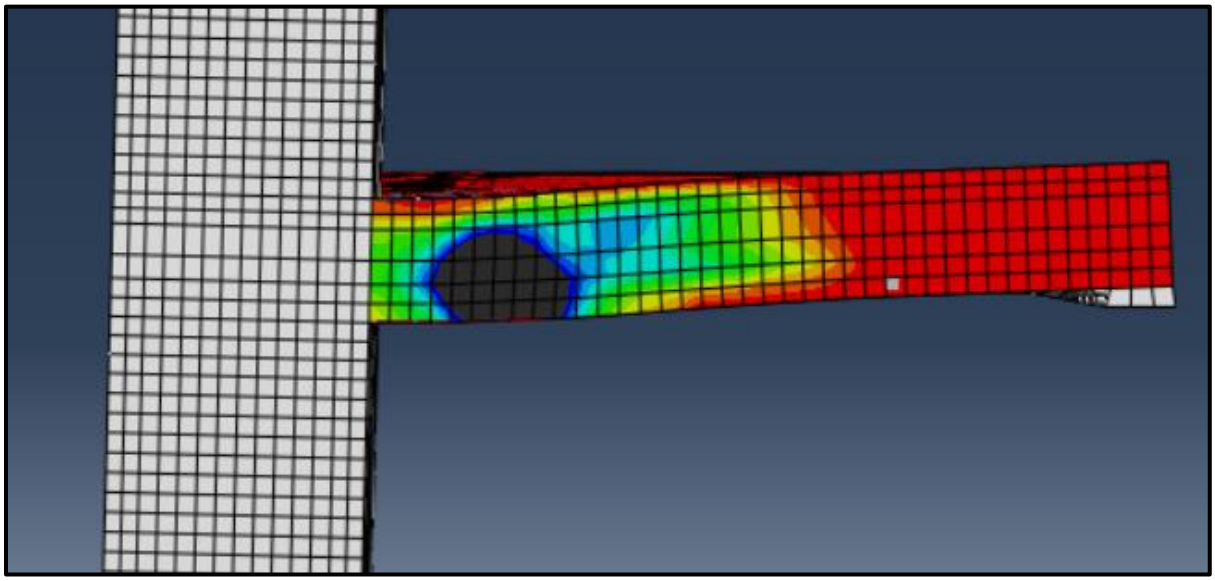

Figure E60: SX-2SR-u-2 Post-Failure Side Crack Profile